



# ROCKET PROPULSION

K RAMAMURTHI



## **ROCKET PROPULSION**



# ROCKET PROPULSION

**K RAMAMURTHI**

*Formerly with Liquid Propulsion Systems Centre,  
ISRO, Thiruvananthapuram  
and*

*Department of Mechanical Engineering  
Indian Institute of Technology Madras  
Chennai*



(An Imprint of Laxmi Publications Pvt. Ltd.)

An ISO 9001:2008 Company

BENGALURU • CHENNAI • COCHIN • GUWAHATI • HYDERABAD  
JALANDHAR • KOLKATA • LUCKNOW • MUMBAI • RANCHI • NEW DELHI  
BOSTON (USA) • ACCRA (GHANA) • NAIROBI (KENYA)

## ROCKET PROPULSION

© by Laxmi Publications Pvt. Ltd.

All rights reserved including those of translation into other languages. In accordance with the Copyright (Amendment) Act, 2012, no part of this publication may be reproduced, stored in a retrieval system, or transmitted in any form or by any means, electronic, mechanical, photocopying, recording or otherwise. Any such act or scanning, uploading, and or electronic sharing of any part of this book without the permission of the publisher constitutes unlawful piracy and theft of the copyright holder's intellectual property. If you would like to use material from the book (other than for review purposes), prior written permission must be obtained from the publishers.

Printed and bound in India  
Typeset at Excellent Graphics, Delhi  
First Edition : 2010; Second Edition : 2016  
ISBN 978-93-85750-00-7

**Limits of Liability/Disclaimer of Warranty:** The publisher and the author make no representation or warranties with respect to the accuracy or completeness of the contents of this work and specifically disclaim all warranties. The advice, strategies, and activities contained herein may not be suitable for every situation. In performing activities adult supervision must be sought. Likewise, common sense and care are essential to the conduct of any and all activities, whether described in this book or otherwise. Neither the publisher nor the author shall be liable or assumes any responsibility for any injuries or damages arising here from. The fact that an organization or Website if referred to in this work as a citation and/or a potential source of further information does not mean that the author or the publisher endorses the information the organization or Website may provide or recommendations it may make. Further, readers must be aware that the Internet Websites listed in this work may have changed or disappeared between when this work was written and when it is read.

All trademarks, logos or any other mark such as Vibgyor, USP, Amanda, Golden Bells, Firewall Media, Mercury, Trinity, Laxmi appearing in this work are trademarks and intellectual property owned by or licensed to Laxmi Publications, its subsidiaries or affiliates. Notwithstanding this disclaimer, all other names and marks mentioned in this work are the trade names, trademarks or service marks of their respective owners.

Branches		
(C)	Bengaluru	080-26 75 69 30
(C)	Chennai	044-24 34 47 26, 24 35 95 07
(C)	Cochin	0484-237 70 04, 405 13 03
(C)	Guwahati	0361-254 36 69, 251 38 81
(C)	Hyderabad	040-27 55 53 83, 27 55 53 93
(C)	Jalandhar	0181-222 12 72
(C)	Kolkata	033-22 27 43 84
(C)	Lucknow	0522-220 99 16
(C)	Mumbai	022-24 91 54 15, 24 92 78 69
(C)	Ranchi	0651-220 44 64

PUBLISHED IN INDIA BY



(An Imprint of Laxmi Publications Pvt. Ltd.)

An ISO 9001:2008 Company  
113, GOLDEN HOUSE, DARYAGANJ,  
NEW DELHI - 110002, INDIA

Telephone : 91-11-4353 2500, 4353 2501  
Fax : 91-11-2325 2572, 4353 2528  
[www.laxmipublications.com](http://www.laxmipublications.com) [info@laxmipublications.com](mailto:info@laxmipublications.com)

C—  
Printed at:

## Preface to the Trinity Edition

The book on **Rocket Propulsion** was first published in 2010 by Macmillan Publishers India Limited and reprinted again in 2011. Subsequently Trinity Press (an imprint of Laxmi Publications (P) Ltd.) acquired the higher education series of textbooks from Macmillan India. I am grateful to Mr. Saurabh Gupta, Managing Director, Laxmi Publications for bringing out the new edition of the book.

While a major part of the book remains the same, additions are made for contour nozzles, rocket plumes, heat transfer in nozzles, cryogenic propellant rockets, pulse detonation rockets and nuclear rockets. The additions were made based on the suggestions of my erstwhile colleagues and students at the Indian Institute of Technology, Madras and the Indian Institute of Space Technology at Thiruvananthapuram. Considering the re-emergence of hybrid rockets, a more detailed discussion of hybrid rockets is provided. The pulsed mode of operation of thrusters in satellites is also dealt with.

Dr. Pramod Kale, formerly Director, Vikram Sarabhai Space Center, Trivandrum and Space Applications Center, Ahmedabad suggested inclusion of sidereal times while discussing geostationary orbits. Professor K. Sudhakar of Indian Institute of Technology, Bombay pointed out to inadequacies in the derivation of the Tsialkowsky's rocket equation. A few misprints in the first edition are also corrected and discussion on monopropellant rockets and electrical thrusters are significantly modified.

April, 2016

**K. Ramamurthi**

## Preface to the First Edition

The book is based on the lecture notes prepared by me for a three credit course in Rocket Propulsion that I have been teaching in the Department of Mechanical Engineering at the Indian Institute of Technology(IIT) Madras. The book deals with the application of the principles of mechanics, thermodynamics, fluid flow, gas dynamics, electrostatics and electromagnetics for rocket propulsion. The theory, operation and performance of the different types of rockets are discussed. Specific examples and exercises are provided to aid the understanding of the subject.

The book is organised in 11 chapters. The first chapter deals with motion in space, the universal law of gravitation, and the requirement of rockets for propelling objects into different orbits or escape from the planets. The basic equation governing rocket propulsion is thereafter derived in Chapter 2 through an analogy of the motion of a sled. The performance parameters of rockets and the staging requirements are brought out. The expansion of high temperature and high pressure gases in nozzles to achieve high jet velocities is discussed in Chapter 3. The different types of nozzles and the efficiency of the nozzles are also deliberated.

Chemical substances used for propellants in rockets, their properties and the methods of estimating their performances are discussed in Chapter 4. A simple procedure is employed for estimating the energy released from the burning of propellants. A more detailed thermodynamic procedure is given in Annexure B.

The solid propellant rockets, liquid bi-propellant, liquid mono-propellant and hybrid rockets are described in Chapters 5, 6, 7 and 8. The elements constituting these rockets, the mechanism of energy release from propellants in solid and liquid phases and parameters influencing the performance and efficiency are discussed. The cycles of operation in liquid propellant rockets are analysed and their relative merits and drawbacks are evaluated.

The large rates of energy release in rockets and the dynamics of interactions of the different sub-systems of a rocket often lead to unstable operation. Chapter 9 deals with this important aspect of combustion instability in solid and liquid propellant rockets. The parameters contributing to instability are illustrated using examples. Methods of stabilising the combustion are also discussed. This chapter is more appropriate for undergraduate honours and post-graduate students and can be skipped for an undergraduate course.

Chapter 10 deals with electrical rockets. Nuclear rockets and other advanced rockets are briefly discussed in Chapter 11.



While the book is primarily intended for the undergraduate and post-graduate engineering students, practicing propulsion engineers would find the book helpful for solving specific problems and anomalies encountered in the development of rockets. It would also assist them in theoretically modelling the rocket propulsion systems. Modelling is the creative side of engineering and is essential for understanding anomalies and instituting corrective steps.

I acknowledge the training and mentoring from Professor John Lee of the Mechanical Engineering Department at McGill University, Montreal, initially as a graduate student and later as a visiting faculty. The motion of a sled in Chapter 3, considered while formulating the theory of rocket propulsion, was an example used by Professor Lee for an undergraduate course in Mechanics in the early 1970s. The work carried out in solid and liquid propellant rockets for launch vehicles and satellites at the Indian Space Research Organisation has been of immense use in the preparation of the class lectures and the writing of this book. Finding solutions to problems during the development of rockets – starting from trivial ones such as zero-gravity based non-ignition of a liquid propellant sustainer rocket to the involved combustion instability and performance – helped in understanding rocket propulsion. Late Professor Satish Dhawan was a driving force in the early years and encouraged an understanding of the basics and modelling the different cycles of operation. I am grateful to Dr. A. E. Muthunayagam for providing the opportunity to work on different problems of rockets and satellite propulsion. The directions received from eminent scientists such as Dr. Vikram A. Sarabhai, Professor U. R. Rao, Dr. A. P. J. Abdul Kalam, Dr. K. Kasthurirangan and Dr. G. Madhavan Nair and the discussions held during the author's tenure at the Indian Space Research Organisation are gratefully acknowledged. I am thankful to Dr Madhavan Nair for inspiring me to organise research laboratories for basic studies in propulsion and also motivating me to develop static and dynamic models of the storable and cryogenic propellant rockets. Working with engineers at the Indian Space Research Organisation and interacting with students, and also having discussions with renowned academicians such as Professor Roger Lo of DLR, Germany and Professor R. N. Kumar of the Jet Propulsion Laboratory have indeed been an enriching experience.

Professor R. Natarajan, former Chairman, All India Council of Technical Education, Delhi and Professor M. S. Ananth, Director, IIT Madras, provided me the opportunity to teach courses on 'Combustion Technology' and 'Combustion Science and Applications' as an Adjunct Faculty at the Indian Institute of Technology Madras during the 1980s and 90s. This paved my way to continue with teaching at IIT Madras subsequently. Talking about rockets to high school teachers and school children and delivering lectures on rocket technology to engineers during their induction training also helped me to organise the contents of the book.

The suggestion to write this book came from Professor M. S. Shunmugam, Head, Department of Mechanical Engineering at IIT Madras. He reviewed the first draft of the book and made suggestions for improvement. My colleagues in the Thermodynamics and Combustion Engineering Laboratory of the Mechanical Engineering Department have been a source of encouragement. I would like to acknowledge the efforts of post-graduate and research students – Mr. Bhadriah Karnam, Mr. V. Nagabhushana Rao, Mr. B. Balaji and Mr Vijay Kumar Cheeda – in making the figures. Mr. Samarjit Mukherjee, an undergraduate student, also helped with some figures. Mr. V. Nagabhushana Rao and Mr. Bhadraiah Karnam checked the manuscript



and suggested changes. The comments and suggestions of the anonymous reviewers helped me to re-organise the text and sharpen the discussions.

I acknowledge the use of some pictures of satellite launch vehicles of Indian Space Research Organisation (ISRO), European Space Agency (ESA) and National Aeronautics and Space Administration (NASA), which appeared in the national dailies, to illustrate the general features of rockets. I also acknowledge the use of pictures of the giant squid and bombardier beetle from National Geographic.

The support received from the Indian Institute of Technology Madras in bringing out the book as a part of the Institute's Golden Jubilee Celebrations is gratefully acknowledged. Professor A. K. Kolar, Head, Centre for Continuing Education, has been a source of encouragement.

**K Ramamurthi**

# Contents

*Preface* (v)

<b>1. MOTION IN SPACE: REQUIREMENTS FOR ORBIT</b>	<b>1–26</b>
1.1 Motion of Bodies in Space .....	1
1.2 Parameters Describing Motion of Bodies .....	4
1.3 Newton's Laws of Motion .....	6
1.4 Universal Law of Gravitational Force .....	7
1.5 Gravitational Field .....	8
1.6 Requirements for Motion in Space .....	9
1.7 Geosynchronous and Geostationary Orbits .....	13
1.8 Eccentricity and Inclination of Orbits .....	14
1.9 Energy and Velocity Requirements to Reach a Particular Orbit .....	17
1.10 Escape Velocity .....	19
1.11 Freely Falling Bodies .....	19
1.12 Means of Providing the Required Velocities .....	20
<i>Solved Examples</i> .....	20
<i>Nomenclature</i> .....	23
<i>Exercises</i> .....	24
<i>References</i> .....	25
<i>Glossary</i> .....	25
<b>2. THEORY OF ROCKET PROPULSION</b>	<b>27–53</b>
2.1 Illustration by an Example of Motion of a Sled Initially at Rest .....	28
2.2 Motion of a Giant Squid in Deep Seas .....	30
2.3 Rocket Principle and the Rocket Equation .....	31
2.4 Mass Ratio of a Rocket .....	33
2.5 Desirable Parameters of a Rocket .....	34
2.6 Rocket Having Small Propellant Mass Fraction .....	35
2.7 Propulsive Efficiency of a Rocket .....	36
2.8 Performance Parameters of a Rocket .....	38
2.9 Staging and Clustering of Rockets .....	39
2.10 Classification of Rockets .....	42



<i>Solved Examples</i> .....	43
<i>Nomenclature</i> .....	49
<i>Exercises</i> .....	50
<i>References</i> .....	52
<i>Glossary</i> .....	52
<b>3. ROCKET NOZZLE AND PERFORMANCE</b>	<b>54–85</b>
3.1 Expansion of Gas from a High Pressure Chamber .....	55
3.2 Shape of the Nozzle .....	58
3.3 Nozzle Area Ratio .....	62
3.4 Performance Loss in a Conical Nozzle .....	65
3.5 Flow Separation in Nozzles .....	66
3.6 Contour or Bell Nozzles .....	68
3.7 Unconventional Nozzles .....	69
3.8 Mass Flow Rates and Characteristic Velocity .....	71
3.9 Thrust Developed by a Rocket; Thrust Coefficient .....	73
3.10 Efficiencies .....	76
3.11 Specific Impulse and Correlation with $C^*$ and $C_F$ .....	76
3.12 General Trends .....	77
<i>Solved Examples</i> .....	78
<i>Nomenclature</i> .....	82
<i>Exercises</i> .....	83
<i>References</i> .....	85
<i>Glossary</i> .....	85
<b>4. CHEMICAL PROPELLANTS</b>	<b>86–123</b>
4.1 Small Values of Molecular Mass and Specific Heat Ratio .....	87
4.2 Energy Release during Combustion of Propellants .....	88
4.3 Criterion for Choice of Propellants .....	95
4.4 Solid Propellants .....	99
4.5 Liquid Propellants .....	104
4.6 Hybrid Propellants .....	108
<i>Solved Examples</i> .....	108
<i>Nomenclature</i> .....	118
<i>Exercises</i> .....	120
<i>References</i> .....	122
<i>Glossary</i> .....	123
<b>5. SOLID PROPELLANT ROCKETS</b>	<b>124–162</b>
5.1 Mechanism of Burning and Burn Rate .....	125
5.2 Choice of Index $n$ for Stable Operation of Solid Propellant Rockets .....	133
5.3 Propellant Grain Configuration .....	135
5.4 Ignition of Solid Propellant Rockets .....	143
5.5 Pressure Decay in the Chamber after Propellant Burns Out .....	149
5.6 Action Time and Burn Time .....	150
5.7 Factors Influencing Burn Rate .....	150
5.8 Components of a Solid Propellant Rocket .....	151



---

<i>Solved Examples</i> .....	152
<i>Nomenclature</i> .....	156
<i>Exercises</i> .....	158
<i>References</i> .....	161
<i>Glossary</i> .....	161
<b>6. LIQUID PROPELLANT ROCKETS</b>	<b>163–214</b>
6.1 Propellant Feed System .....	164
6.2 Thrust Chamber .....	170
6.3 Performance and Choice of Feed System Cycle .....	187
6.4 Turbo-pumps .....	193
6.5 Gas Requirements for Draining of Propellants from Storage Tanks .....	195
6.6 Draining under Microgravity Conditions .....	196
6.7 Complexity of Liquid Propellant Rockets and Simulation .....	198
6.8 Trends in the Development of Liquid Propellant Rockets .....	200
<i>Solved Examples</i> .....	201
<i>Nomenclature</i> .....	208
<i>Exercises</i> .....	210
<i>References</i> .....	212
<i>Glossary</i> .....	213
<b>7. LIQUID MONOPROPELLANT ROCKETS</b>	<b>215–227</b>
7.1 Hydrazine Monopropellant Rockets .....	216
7.2 Catalyst Bed Loading .....	218
7.3 Performance and Applications .....	219
<i>Solved Examples</i> .....	223
<i>Nomenclature</i> .....	226
<i>Exercises</i> .....	226
<i>References</i> .....	227
<i>Glossary</i> .....	227
<b>8. HYBRID ROCKETS</b>	<b>228–236</b>
8.1 Hybrid Propellants .....	229
8.2 Burning Mechanism .....	230
8.3 Turbulators and Other Devices for Better Mixing .....	232
8.4 Initiation of Combustion.....	234
8.5 Multi-port Fuel Grains .....	234
8.6 Promising Feature of Paraffin Wax as Fuel for Hybrid Rockets .....	235
8.7 Advantages of Hybrid Rockets over Solid and Liquid Propellant Rockets.....	235
<i>References</i> .....	236
<i>Glossary</i> .....	236
<b>9. COMBUSTION INSTABILITY</b>	<b>237–285</b>
9.1 Bulk and Wave Modes of Combustion Instability .....	238
9.2 Analysis Procedure for Bulk Mode of Combustion Instability in Liquid Propellant Rockets .....	246
9.3 Bulk Mode of Combustion Instability in Solid Propellant Rockets .....	251
9.4 Wave Mode of Combustion Instability .....	253
9.5 Wave Mode Instability in Solid Propellant Rockets .....	266



9.6	Evaluation of the Growth Constant of Solid Propellant using a T burner .....	268
9.7	Conversion of Growth Constant derived from T Burner for Application in a Solid Propellant Rocket .....	269
9.8	Wave Mode Instability in Liquid Propellant Rockets .....	272
9.9	Non-linear Combustion Instability .....	274
9.10	Process-induced Combustion Instability .....	274
9.11	Pogo Instability due to Interaction of Propulsion and Structure .....	275
9.12	Combustion Instability: Suppression and Control .....	277
	<i>Solved Examples</i> .....	277
	<i>Nomenclature</i> .....	280
	<i>Exercises</i> .....	283
	<i>References</i> .....	283
	<i>Glossary</i> .....	284
<b>10.</b>	<b>ELECTRICAL ROCKETS</b>	<b>286–310</b>
10.1	Electrostatic Force and Electric Field .....	286
10.2	Electromagnetic Force and Magnetic Field .....	287
10.3	Combined Electrical and Magnetic Field .....	288
10.4	Operating Principle and Classification of Electrical Rockets .....	289
10.5	Electro-thermal Thrusters .....	289
10.6	Electrostatic Thrusters .....	290
10.7	Electromagnetic Thruster .....	296
10.8	Power Requirement of the Electrical Thrusters .....	298
10.9	Choice of Parameters for Electrical Thrusters .....	299
10.10	Current Trends .....	303
	<i>Solved Examples</i> .....	304
	<i>Nomenclature</i> .....	307
	<i>Exercises</i> .....	308
	<i>References</i> .....	309
	<i>Glossary</i> .....	309
<b>11.</b>	<b>NUCLEAR ROCKETS AND ADVANCED ROCKETS</b>	<b>311–330</b>
11.1	Nuclear Rockets .....	312
11.2	Radioactive Decay .....	312
11.3	Nuclear Fission .....	313
11.4	Nuclear Fusion .....	314
11.5	Nuclear Electric and Nuclear Thermal Propulsion .....	315
11.6	Feed System Cycles .....	317
11.7	Status of Nuclear Rockets .....	320
11.8	Pulsed Nuclear Rockets .....	321
11.9	Power Generation in Spacecrafts .....	321
11.10	Tri-propellant Rockets .....	322
11.11	Pulsed Detonation Rockets .....	322
11.12	Beamed Rockets and Sail Propulsion .....	326
	<i>Solved Examples</i> .....	327
	<i>References</i> .....	329
	<i>Glossary</i> .....	330



---

<b>ANNEXURE A: SHAPE OF NOZZLES AND PLUMES</b>	<b>331–350</b>
A.1 Design of Conical and Contour Nozzles .....	331
A.2 Method of Characteristic Applied to Contour Nozzle Divergent .....	334
A.3 Contour Nozzle Analysis .....	337
A.4 Plumes from Under-expanded and Over-expanded Nozzles .....	344
<i>References</i> .....	350
<b>ANNEXURE B: DISSOCIATION OF GASES: FROZEN AND SHIFTING EQUILIBRIUM</b>	<b>351–358</b>
B.1 Gibbs Free Energy and Equilibrium .....	351
B.2 Use of Equilibrium Constants to Determine Composition at a given Temperature ....	354
B.3 Use of Equilibrium Constants to Determine Composition in Presence of Dissociation and Temperature of the Dissociated Products .....	355
B.4 Minimization of Gibbs Free Energy .....	357
B.5 Equilibrium and Frozen Assumptions for Performance Prediction .....	358
<b>ANNEXURE C: CRYOGENIC PROPELLANT ROCKETS</b>	<b>359–381</b>
C.1 Introduction .....	359
C.2 Cryogenic Propellants .....	359
C.3 Propellant Tanks and Propellant Supply System .....	362
C.4 Insulation .....	365
C.5 Chill Down of Tanks, Lines and Components before Contact with Cryogenic Propellants .....	366
C.6 Mitigation of Hazards in the Use of Liquid Oxygen and Liquid Hydrogen .....	370
C.7 Use of Cavitating Venturies instead of Orifices for Controlling Flow .....	371
C.8 Choice of Feed System Cycles .....	372
C.9 Injector Configuration .....	373
C.10 Combustion Process .....	376
C.11 Flame Holding and Stabilization .....	377
C.12 Ignition System for Cryogenic Rockets .....	378
C.13 Mass of Thrust Chamber .....	378
C.14 Thrust Chamber Cooling .....	380
C.15 Summary .....	381
<i>References</i> .....	381
<b>INDEX</b>	<b>382–390</b>



## Chapter 1

### Motion in Space: Requirements for Orbit

*“Who are we? We find that we live in an insignificant planet of a ... star lost in a galaxy tucked away in some forgotten corner of a universe in which there are far more galaxies than people.”*

*Carl Sagan, Astronomer*

*“The rocket will free man from his remaining chains, the chains of gravity which still tie him to this planet. It will open to him the gates of heaven.”*

*Wernher von Braun, Rocket Engineer*

The word ‘propulsion’ is derived from the Latin word ‘Propellere’, where ‘pro’ means before or forward and ‘pellere’ means drive or push. Propulsion is about driving forward or pushing the objects, viz., changing the motion of a body. Rocket propulsion is associated with propelling bodies in space. The pushing is done by imparting a change in momentum, i.e. an impulse. In this chapter we first deal with the motion of bodies in space, the parameters, such as, momentum, impulse and force, and the universal law of gravitation which are essential to describe motion in space. This is followed by the requirements for orbit and launching spacecrafts into space.



#### 1.1 MOTION OF BODIES IN SPACE

The space around us is endless and comprises several galaxies moving relative to each other. There are probably more than  $10^{11}$  galaxies in the observable space. The galaxies have their own gravitationally bound system of stars. Our galaxy, ‘The Milky Way’, is some 10,000 light years in diameter (1 light year is the distance traveled by light in one year  $\approx 9.5 \times 10^{12}$  km, the speed of light



in vacuum being  $3 \times 10^5$  km/s) and about 2,500 light years in thickness. In addition to stars, interstellar gas and dust, plasma, unseen dark matter, black holes and quasi-stellar radio sources (Quasars) are present in our galaxy. Stars are massive luminous bodies undergoing nuclear reactions. Black holes have tremendously high values of gravity. Quasars are highly luminous bodies and move at speeds comparable to the speed of light.

The Solar system, which we inhabit, occupies a very tiny fraction of about  $1.5 \times 10^{-8}$  of the Milky Way galaxy. It comprises eight planets orbiting around the star Sun. The planets in the order of increasing distance from the Sun are Mercury, Venus, Earth, Mars, Jupiter, Saturn, Uranus and Neptune. This is shown in Fig. 1.1. Pluto was formerly considered as a planet, but is presently termed as a dwarf planet and considered to be part of the Kuiper belt. The Kuiper belt is a region beyond the planets consisting of asteroids and other remnants leftover during the formation of the Solar system.

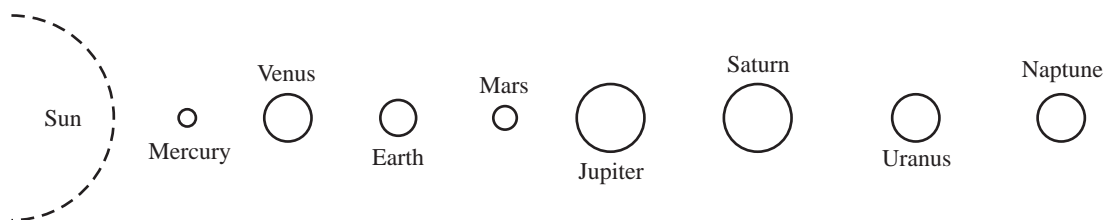


**Fig. 1.1** Planets in the Solar System (not to scale)

Mercury is nearest to the Sun and is the smallest of all planets. It has a mass of  $3.302 \times 10^{23}$  kg and a diameter of 4,880 km. Our planet Earth has a mass of  $5.974 \times 10^{24}$  kg and a mean diameter of about 12,756 km. The details of the mass and diameter of the planets are listed in Table 1.1.

The moon is a natural planetary satellite. There are 31 known moons revolving around the planets. The Earth has a moon at a mean distance of about 30 times the mean Earth diameter (average orbital radius: 3,84,400 km). The mass of Earth's moon is  $7.348 \times 10^{22}$  kg and its diameter is 3,476 km. The Earth's moon travels around the Earth at a mean velocity of 1.02 km/s.

**Table 1.1** Mass and Diameter of Planets

Planet	Mass (kg)	Diameter (km)
1. Mercury	$3.302 \times 10^{23}$	4,880
2. Venus	$4.869 \times 10^{24}$	12,104
3. Earth	$5.974 \times 10^{24}$	12,756
4. Mars	$6.419 \times 10^{23}$	6,805
5. Jupiter	$1.899 \times 10^{27}$	1,42,984
6. Saturn	$5.685 \times 10^{26}$	1,20,536
7. Uranus	$8.683 \times 10^{25}$	51,118
8. Neptune	$1.024 \times 10^{26}$	49,528

The distance of the planets from the Sun and the time taken to go around it once (orbital period) are given in Table 1.2. The Earth is at a mean distance of  $150 \times 10^6$  km from the Sun. This distance



is referred to as an Astronomical Unit (AU) and the distances of the planets from the Sun are given in terms of AU.

**Table 1.2** Period of Revolution and Distance from the Sun

Planet	Period (Years)	Distance from Sun (AU)
1. Mercury	0.241	0.39
2. Venus	0.615	0.72
3. Earth	1.000	1.00
4. Mars	1.880	1.52
5. Jupiter	11.800	5.20
6. Saturn	29.500	9.54
7. Uranus	84.000	19.18
8. Neptune	165.000	30.06

The details of the motion of the planets have been meticulously observed since the ancient times. Johannes Kepler, a mathematician and astronomer, used the observations to formulate the following three basic laws of planetary motion:

1. *Law of Ellipses*: The paths of planets in the solar system about the Sun are elliptical with the centre of the Sun being located at the focus (Fig. 1.2).
2. *Law of Equal Areas*: The imaginary line from the centre of the Sun to the centre of the planets sweeps out equal areas in equal intervals of time (Fig. 1.2).
3. *Law of Harmonies*: The ratio of the square of the orbital period of any two planets is equal to the ratio of the cubes of their average distance from the Sun.

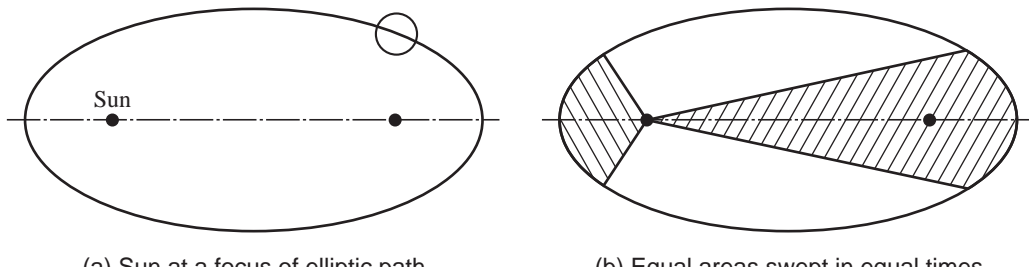


**Fig. 1.2** Kepler's Laws of Ellipses and Equal Areas

Sir Isaac Newton used these laws describing the planetary motions and the experiments of Galileo Galilei regarding freely falling bodies along with his own observations to formulate the universal law of gravitational forces. This universal law of gravitational forces is used to determine the velocities that are to be imparted to bodies such as spacecrafts by a rocket. However, before getting into the details of the universal law of gravitational forces and its application, the parameters used for describing the motion of bodies in space requires to be well understood, and it is addressed in the next section.



## 1.2 PARAMETERS DESCRIBING MOTION OF BODIES

### (a) Fundamental Units of Mass, Length and Time

The motion of bodies is described in terms of fundamental units of mass, length and time. The mass and length are specified by comparison with a standard. The unit of mass is a kilogram and is the mass of a standard made of platinum-rhodium alloy kept at the International Bureau of Weights and Measures at Sèvres in Paris. The unit of length is a meter, for which also a platinum alloy standard is kept at the International Bureau of Weights and Measures.

Time is a more involved unit. It provides the duration of an event or interval between events. Periodic events are used to provide units of time. The unit of time is a second. It is defined as the duration of 9, 192, 631, 770 periods of the radiation corresponding to the transition between two hyperfine levels of the ground state of the Cesium atom (Cs-133).

### (b) Velocity, Momentum and Acceleration

Velocity and acceleration are derived from length and time. Velocity, by itself, is insufficient to characterise the motion. One feels different when hit by a heavy object or a light object traveling at the same velocity. Linear momentum, which is the product of mass and velocity, is therefore more appropriate to describe the motion.

Velocity, momentum and acceleration can take on arbitrary values depending on the way length is defined. If the position of a body can be defined based on a reference frame which is absolutely stationary, then all measurements can be based on it with certainty. However, there is no such absolutely stationary frame of reference in practice. A point on the surface of the Earth moves as the Earth rotates on its axis (Fig. 1.3). The Earth orbits around the Sun. The Sun, the other stars and the galaxies are all in a state of motion. A suitable frame of reference is essential for the measurements.

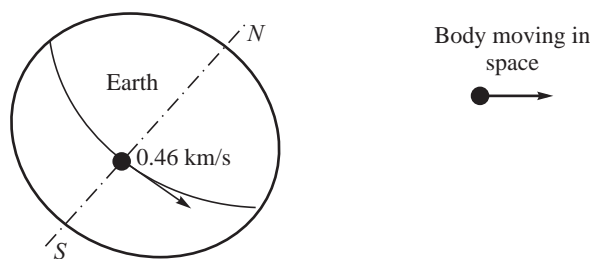


**Fig. 1.3** Need for a Reference Frame for Describing the Motion of a Body

### (c) Inertial Frame of Reference for Describing Motion of Bodies in Space

If the frame of reference, used for defining the position of a body, is either stationary or is moving at constant velocity along a straight line, the changes of the velocity, momentum and acceleration of the body do not depend on the frame of reference used. The laws characterising the motion of a body would then not depend on the frame of reference.



Such a reference frame, which is either stationary or is moving at constant velocity along a straight line, is called inertial frame of reference. A schematic of the inertial frame of reference (stationary and moving at constant velocity along a straight line) is given in Fig. 1.4. If we assume that the points on the surface of Earth move at a constant linear velocity, the reference on Earth can be taken as an inertial frame of reference.

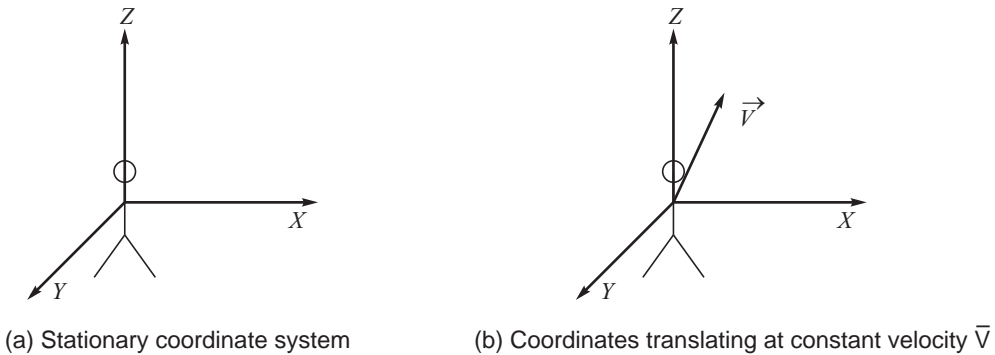


Fig. 1.4 Inertial Frame of Reference

#### (d) Impulse and Force

The concepts of impulse and force are related to momentum. While impulse denotes the change of momentum, the force represents the rate of change of momentum. If we were to consider a body moving with a constant value of momentum  $\vec{p}(t)$  till time  $t$  and the momentum to change due to some interaction over time  $\Delta t$  to  $\vec{p}(t + \Delta t)$  at time  $t + \Delta t$  as shown in Fig. 1.5, the impulse  $\vec{I}$  due to the interaction is:

$$\vec{I} = \vec{p}(t + \Delta t) - \vec{p}(t) \quad \dots(1.1)$$

It is seen in Fig. 1.5 that the change of momentum does not take place uniformly with time over the period of the interaction  $\Delta t$ . The rate of change  $d\vec{p}/dt$  is not constant during the interaction but starts off slowly at time  $t$  and gradually increases to a maximum value when the inflection point A is reached. Thereafter, the rate of change  $d\vec{p}/dt$  decreases and becomes zero at time  $t + \Delta t$ . This is clarified in Fig. 1.6 in which  $d\vec{p}/dt$  is plotted as a function of time. Till time  $t$ , the value of  $\vec{p}$  is a constant and  $d\vec{p}/dt = 0$ . After time  $t + \Delta t$  for which  $\vec{p}$  is a constant,  $d\vec{p}/dt = 0$ . Between time  $t$  and  $t + \Delta t$  during which the momentum changes due to the interaction,  $d\vec{p}/dt$  increases from 0 to a maximum value at A and then falls to 0.

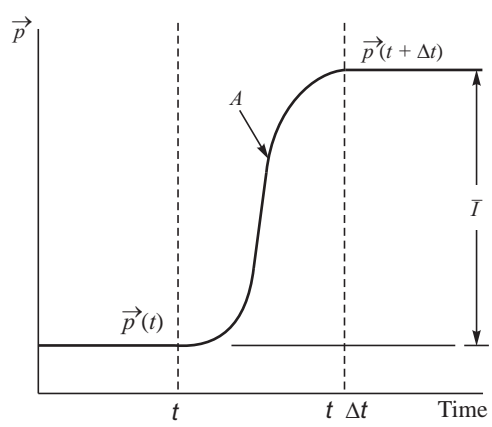
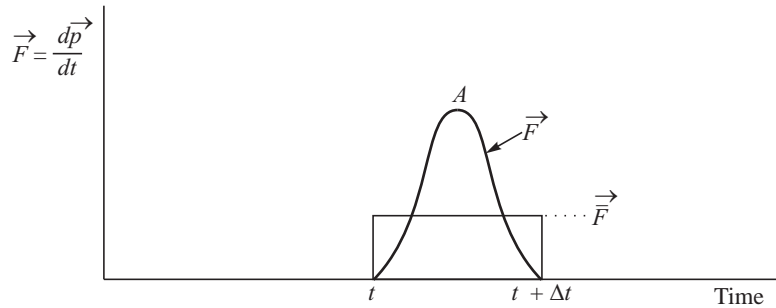


Fig. 1.5 Change of Momentum and Impulse



**Fig. 1.6** Rate of Change of Momentum and Definition of an Average Force

Force is defined as the rate of change of momentum ( $\vec{F} = \frac{d\vec{p}}{dt}$ ). The details of the rate of change of momentum ( $d\vec{p}/dt$ ) during an interaction over which the momentum of a body changes are difficult to measure especially when the interaction is over a short period of time. An average force ( $\vec{\bar{F}}$ ) is therefore defined over the period of interaction  $\Delta t$  as:

$$\vec{\bar{F}} = \frac{\vec{p}(t + \Delta t) - \vec{p}(t)}{\Delta t} \quad \dots(1.2)$$

The average force is related to change in momentum and therefore, to impulse by the following:

$$\vec{I} = \vec{p}(t + \Delta t) - \vec{p}(t) = \int_t^{t + \Delta t} \frac{d\vec{p}}{dt} dt = \int_t^{t + \Delta t} \vec{F} dt = \vec{\bar{F}} \Delta t \quad \dots(1.3)$$



### 1.3 NEWTON'S LAWS OF MOTION

The laws of motion are based on observations at low velocities. The laws are not valid when the velocities of the bodies approach the velocity of light such as the quasars in deep space for which relativistic effects become important.

The three laws of motion are:

1. First law: *Inertia*. Every body continues in its state of rest or of uniform motion unless an external force is impressed on it.
2. Second law: *Force, Acceleration*. The rate of change of momentum is directly proportional to the force acting on the body and the change of momentum takes place in the direction of the force:

$$\vec{F} = \frac{d}{dt} (mv) \quad \dots(1.4)$$

For a given mass  $m$ :

$$\vec{F} = m \frac{dv}{dt} = m\alpha \quad \dots(1.5)$$

where  $\alpha$  is the acceleration.



The acceleration imparted to a body is directly proportional to the force acting on the body and inversely proportional to its mass. With mass in kg and acceleration in m/s<sup>2</sup>, the unit of force is N (kg-m/s<sup>2</sup>).

3. Third law: *Reaction*. Action and reaction are equal and opposite.

In the case of bodies having extremely small dimensions of the order of atomic nuclei, quantum mechanics begins to play a role and the above laws would be inapplicable.



## 1.4 UNIVERSAL LAW OF GRAVITATIONAL FORCE

The universal law of gravitational force was formulated by Newton based on the premise that the falling of apples from a tree to the ground and the motion of the planets in their orbits would be governed by the same principle. All planets in the solar system are in a state of free fall towards the Sun. This will become clear later on in this chapter when we deal with orbits. Newton visualised the commonality of planets going round the sun and the falling of an apple by considering the attraction in the neighbourhood of a large mass. He defined a force ( $\vec{F}_{2-1}$ ) acting on a body of mass  $m_2$  due to a body of large mass  $m_1$  at a distance  $r$  away to be attractive and directed towards the centre of body  $m_1$  as shown in Fig. 1.7. The magnitude of the force was given to be proportional to the product of the masses ( $m_1$  and  $m_2$ ) and inversely proportional to the square of the distance of separation between them ( $r$ ). The force is given by (Fig. 1.7):

$$\vec{F}_{2-1} = -G \frac{m_1 m_2}{|\vec{r}|^3} \vec{r} \quad \dots(1.6)$$

The term  $\vec{r}/|\vec{r}|^3$  in the above equation represents that the force is proportional to  $1/r^2$  and the direction of the force is along  $\vec{r}$ .  $\vec{r}$  is the outward directed vector from the centre of the mass  $m_1$ . The negative sign in the equation is indicative of the fact that the force is attractive, i.e.  $m_2$  being attracted towards  $m_1$ .  $G$  is a constant and is known as the gravitational constant. When  $m_1$  and  $m_2$  are expressed in kg and  $r$  is in meters, the value of  $G = 6.670 \times 10^{-11} \text{ Nm}^2/\text{kg}^2$ .

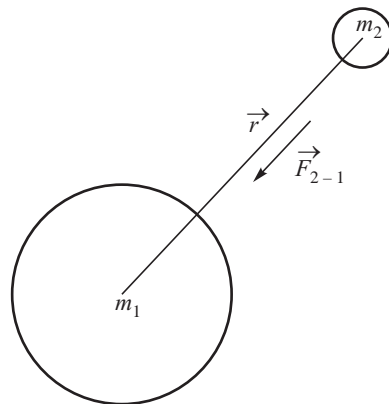
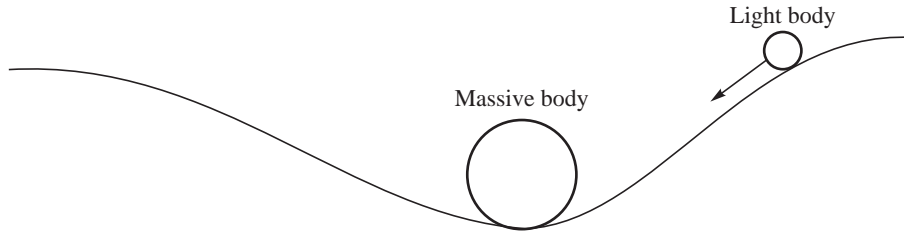


Fig. 1.7 Attraction in the Neighbourhood of the Large Sphere



The law of gravitational force is based on observations. The reason for its existence was brought out by the general theory of relativity by Einstein. The reasoning can be visualised in terms of a massive body distorting the space around it similar to a heavy ball placed on a tightly held rubber sheet and the lighter ball rolling towards it (Fig. 1.8).



**Fig. 1.8** Visualisation of Distortion of Space Around a Heavy Body



## 1.5 GRAVITATIONAL FIELD

Based on the universal law of gravitational force given in eq. (1.6), a body of mass  $m$  at a height  $h$  above the surface of Earth would be attracted towards the centre of the Earth with a force:

$$F = -G \frac{M_E m}{(r_E + h)^2} \quad \dots(1.7)$$

where  $M_E$  is the mass of the Earth and  $r_E$  is its radius. When the height  $h$  is small in comparison with the radius  $r_E$  of the Earth, the above equation can be simplified to give:

$$F = -G \frac{M_E m}{r_E^2} \left(1 - \frac{2h}{r_E} + \dots\right) \quad \dots(1.8)$$

With  $h \ll r_E$ , the above expression becomes:

$$F = -G \frac{M_E m}{r_E^2} \quad \dots(1.9)$$

where  $G$ ,  $M_E$  and  $r_E$  are constants. Writing  $g$  as  $\frac{GM_E}{r_E^2}$ , the force on a body of mass  $m$  becomes:

$$F = -mg \quad \dots(1.10)$$

where  $g$  is spoken of as the gravitational field of Earth. It has units of  $[(\text{Nm}^2/\text{kg}^2)(\text{kg})]/\text{m}^2 = \text{m/s}^2$  viz., acceleration and is therefore referred to as acceleration due to gravity.

Substituting values of  $G = 6.670 \times 10^{-11} \text{ N m}^2/\text{kg}^2$ ,  $M_E = 5.974 \times 10^{24} \text{ kg}$  and  $r_E = 6378 \text{ km}$  we get:

$$g = \frac{6.670 \times 10^{-11} \times 5.974 \times 10^{24}}{6,378,000^2} = 9.8 \text{ m/s}^2 \quad \dots(1.11)$$



Gravitational field of Earth varies with the latitude  $\theta$ , and altitude,  $h$  since the Earth is not a perfect sphere. The radius at the equator is more by about 21 km than at the poles. The variation of the gravitational field of the Earth is given by:

$$g \text{ (m/s}^2\text{)} = 9.780356 [1 + 0.0052885 \sin^2 \theta - 0.0000059 \sin^2(2\theta) - 0.003086h] \quad \dots(1.12)$$

The gravitational field of any planet or heavy body can be found by using eq. (1.9) with the appropriate mass and radius.



## 1.6 REQUIREMENTS FOR MOTION IN SPACE

We had discussed the motion of the planets around the Sun and the moon around the Earth and Kepler's laws of planetary motion at the beginning of this chapter. The trajectory or path of the motion is referred to as orbit. Spacecrafts are made to orbit different planets, or for that matter any celestial body, in a manner similar to the orbit of the planets about the Sun. The universal law of gravitation and a suitable frame of reference are used to find the desired orbits and the requirements of putting up the spacecraft in orbit.

The spacecrafts are launched into space from the surface of the Earth using rockets. Most of the spacecrafts are for communication, remote sensing, scientific and meteorological applications. The orbits could either be elliptic or circular and for simplicity we consider circular orbits in this chapter. The requirements of a body to orbit are derived in the following sections.

### 1.6.1 Motion in a Rotating Frame of Reference – Centrifugal Force

A suitable frame of reference is required to describe the motion of the spacecraft which we assume to have a circular orbit. If a rotational frame of reference which traces the path of the spacecraft is considered, the spacecraft will be stationary in relation to this rotational frame of reference. A simple force balance would then be adequate to describe the motion.

The rotational frame of reference is not an inertial frame of reference (stationary or moving at constant velocity along a straight line) and an additional fictitious force (known as pseudo force) has to be introduced for describing the motion of the body correctly in the rotating frame of reference. The pseudo force and the universal law of gravitational force are used for determining the requirements of orbiting bodies in space.

We consider a body of mass  $m$  revolving at a radius  $R$  with a constant angular velocity  $\omega$  around a point  $O$  (Fig. 1.9). The  $x$  and  $y$  coordinates of the mass at any time  $t$  are:

$$\begin{aligned}x &= R \cos \omega t \\y &= R \sin \omega t\end{aligned} \quad \dots(1.13)$$

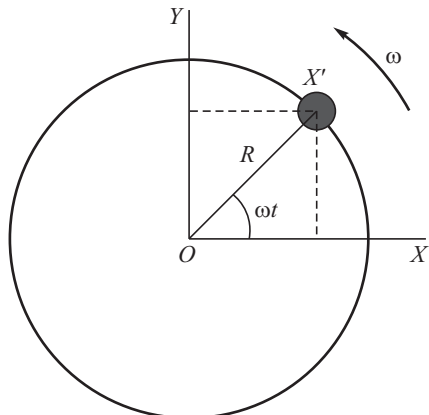


Fig. 1.9 Body of Mass  $m$  Rotating around a Point



The velocity and acceleration of the body along the  $x$  and  $y$  coordinates are:

$$\begin{aligned}\dot{x} &= R \omega \sin \omega t; \ddot{x} = \omega^2 R \cos \omega t \\ \dot{y} &= R \omega \cos \omega t; \ddot{y} = -\omega^2 R \sin \omega t\end{aligned}\dots(1.14)$$

The acceleration  $\ddot{x}$  and  $\ddot{y}$  would cause a force  $m\ddot{x}$  and  $m\ddot{y}$  in the negative  $x$  and negative  $y$  directions as shown in Fig. 1.10. The resultant force is represented by  $F$  and is given by  $\sqrt{(m\ddot{x})^2 + (m\ddot{y})^2}$ .

The value of  $F$  is:

$$\begin{aligned}F &= \sqrt{(m\omega^2 R \cos \omega t)^2 + (m\omega^2 R \sin \omega t)^2} \\ &= m\omega^2 R\end{aligned}\dots(1.15)$$

This force is directed in the negative  $R$  direction. The force is known as centripetal force and is shown in Fig. 1.10. The associated acceleration  $-\omega^2 R$  is the centripetal acceleration.

With respect to the rotating frame of reference  $OX'$ , the body of mass  $m$  is stationary. This rotating frame of reference for the body of mass  $m$  is noninertial as it has changing velocities and acceleration given by eq. 1.14. To be able to describe the stationary state of the body in this frame of reference  $OX'$ , we should have:

$$m \frac{d^2 X'}{dt^2} = 0 \dots(1.16)$$

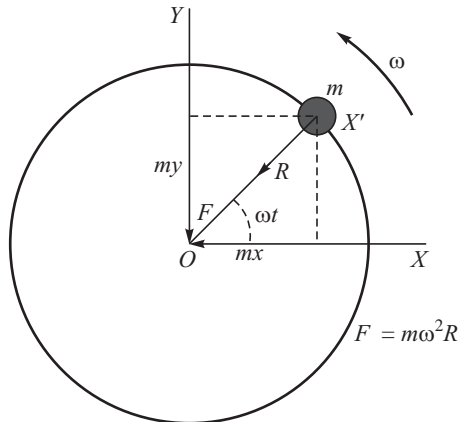


**Fig. 1.10** Centripetal Force

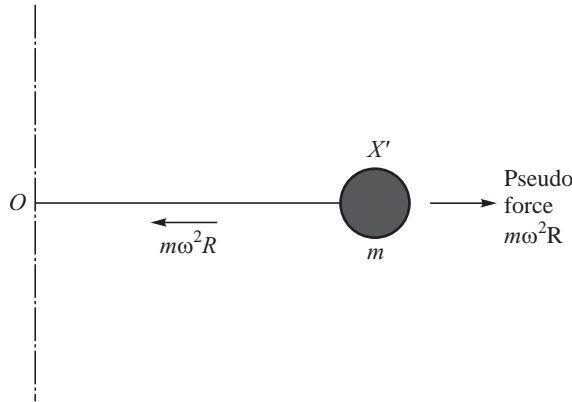


**Fig. 1.11** Pseudo Force to Correct the Non-inertial Frame of Reference

But then a centripetal force  $m\omega^2R$  is present and acting towards the centre  $O$  as shown in Fig. 1.11. A fictitious force (pseudo force) equal and opposite to the above centripetal force must be added in



order to make the body stationary, *i.e.* correctly describe the motion of the rotating body in the rotating frame of reference  $OX'$ . This is the pseudo force that the rotating observer must put in his description of forces to correctly describe the motion (Fig. 1.11). The pseudo force in the rotating frame of reference is called centrifugal force.

### 1.6.2 Orbits, Orbital Velocity and Orbital Period

The requirements to orbit an object can be determined by considering the example of a body of mass  $m$ , circling the Earth  $E$ , at a constant angular velocity  $\omega$ , at a radius  $R$  from the centre of the Earth (Fig. 1.12).

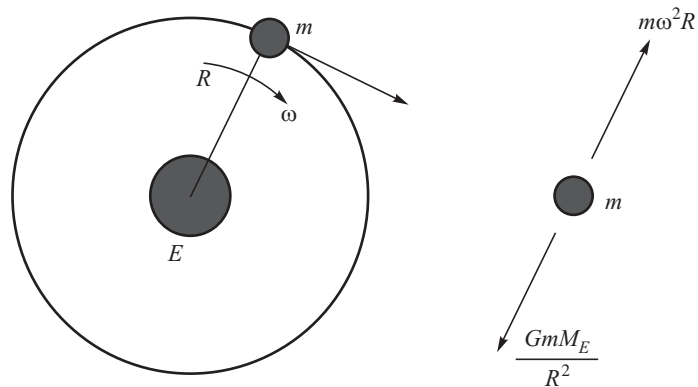


**Fig. 1.12** Forces on the Rotating Body in the Rotating Frame of Reference

The body in the rotating frame of reference will see the force of attraction due to the Earth and the pseudo centrifugal force  $m\omega^2R$ . From the universal law of gravitational force, the force that the body experiences due to the mass of the Earth from eq. 1.6 is seen to be towards the centre of the

Earth  $\vec{F}_{2-1} = -G \frac{mM_E}{|\vec{r}|^3} \vec{r}$ . Here  $M_E$  denotes the mass of the Earth. In the rotating frame of reference,

it also sees the pseudo centrifugal force  $m\omega^2R$ . The two forces must be equal and opposite for the body to be stationary with respect to the rotating frame of reference giving:

$$G \frac{mM_E}{R^2} = m\omega^2R \quad \dots(1.17)$$

The value of angular velocity from the above equation is:

$$\omega = \left( \frac{GM_E}{R^3} \right)^{1/2} \quad \dots(1.18)$$



The velocity along the circular path known as orbit velocity  $V_O$  is given by  $V_O = R\omega$ . Substituting the value of  $\omega$  from eq. 1.18, we get:

$$V_O = R\omega = \left( \frac{GM_E}{R} \right)^{1/2} \quad \dots(1.19)$$

For example, a spacecraft orbiting the Earth at a height ( $h$ ) of 200 km has the orbital velocity:

$$\begin{aligned} V_O &= \left( \frac{GM_E}{R_E + h} \right)^{1/2} = \left( \frac{6.670 \times 10^{-11} \times 5.974 \times 10^{24}}{(6380 + 200) \times 10^3} \right)^{1/2} \\ &= 7760 \text{ m/s} = 7.76 \text{ km/s} \end{aligned}$$

The orbital velocity about the Earth is typically a few km/s. It is seen from eq. 1.20 to decrease as the radius of the orbit increases. Figure 1.13 shows the variation of the orbital velocity as the height of the orbit increases. The orbital velocity is seen to decrease from a value of about 7.9 km/s at the Earth's surface to about 2.66 km/s at a height of 50,000 km.

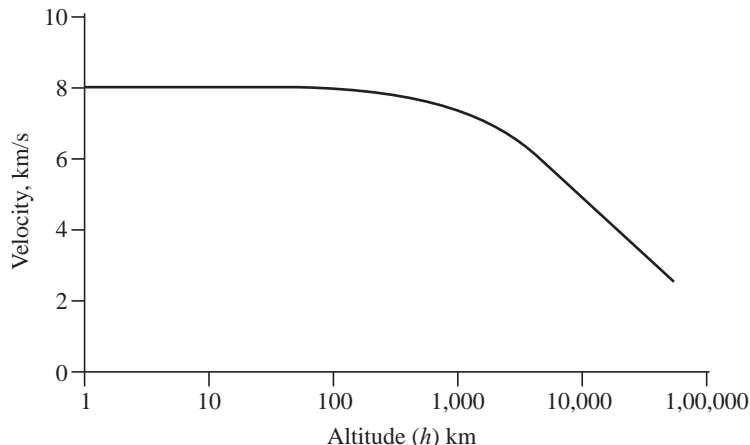


**Fig. 1.13** Variation of Orbital Velocity with Height Above the Earth

The time period of revolution for one orbit is:

$$\tau = \frac{2\pi R}{V_O} = 2\pi \left( \frac{R^3}{GM_E} \right)^{1/2} \quad \dots(1.20)$$

With values substituted for the mass of the Earth in kg, the radius in m and the gravitational constant  $G$  in Nm<sup>2</sup>/kg<sup>2</sup>, the period is:

$$\tau = 0.304 \times 10^{-6} R^{3/2} \text{s} \quad \dots(1.21)$$

The time period for one revolution increases as the height of the orbit increases. The period, in hours, as the height of the orbit above the Earth increases to 50,000 km is shown in Fig. 1.14. The time period increases from about 1.4 hours at a height of 100 km to about 35.7 hours at a height of 50,000 km. At 35,786 km above the Earth, the time for one orbit is 24 hours, viz., one day.

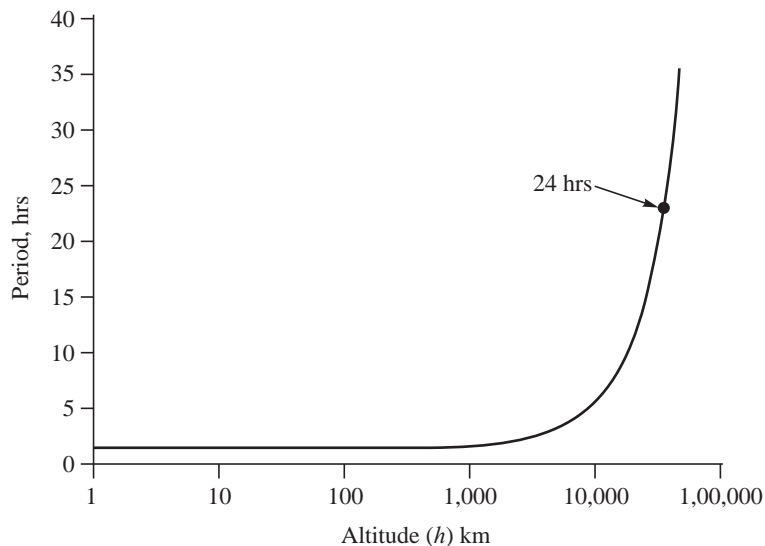


Fig. 1.14 Variation of Orbital Time with Height of Orbit Above the Earth



## 1.7 GEOSYNCHRONOUS AND GEOSTATIONARY ORBITS

The Earth rotates on its axis. The time at a particular point on Earth is determined by the relative position of the Sun with respect to that point. The local noon is defined as the time at which the Sun appears to be at the highest point in the sky. The average period taken for the Sun to return to the highest point is defined as one solar day.

A solar day is made of 24 hours. While the Earth is rotating on its axis, it also revolves around the Sun. The revolution or orbiting of the Earth around the Sun causes the direction between the Earth and the Sun to be additionally influenced compared to the rotation of the Earth on its axis alone. The time corresponding to one complete rotation of the Earth while it is revolving around the Sun is less than one solar day and is known as a sidereal day. This is because during the period of one rotation of the Earth on its axis, it moves a short distance along its orbit by approximately  $1^\circ$ . The Earth therefore moves by a small additional amount for one solar day.

It is this sidereal day which needs to be considered to determine the angular velocity of the rotation of the Earth. The sidereal day is shorter than the solar day by about 4 minutes. The actual duration of the sidereal day is 23 hours 56 minutes and 4.1 seconds which equals 86,164.1 seconds. The angular velocity of rotation of Earth is:

$$\omega_E = \frac{2\pi}{86164.1} = 7.293 \times 10^{-5} \text{ rad/s} \quad \dots(1.22)$$

The angular velocity of the orbit was seen to decrease with an increase of the radius of the orbit. If a body is in circular orbit with an angular velocity equal to that of the Earth and further if it were to rotate in the same direction as that of the Earth, its movement will be synchronous with the rotation of the Earth. The body is then said to be in geosynchronous orbit. It will complete one



rotation in one sidereal day. The radius of the geosynchronous orbit  $R_G$  is found by equating eq. 1.18 for the angular velocity of the orbit with eq. 1.22 for the angular velocity of rotation of Earth to give:

$$\left( \frac{GM_E}{R_G^3} \right)^{1/2} = \omega_E = 7.293 \times 10^{-5} \text{ rad/s} \quad \dots(1.23)$$

The radius of the geosynchronous orbit from the above equation is:

$$R_G^3 = \frac{GM_E}{\omega_E^2} \quad \dots(1.24)$$

Substituting the values of  $G$ ,  $M_E$  and  $\omega_E$ , the value of  $R_G = 42,160.$

With the mean radius of the Earth being 6378 km, the geosynchronous altitude would therefore be  $42,160 - 6378 = 35,782 above the surface of the Earth.$

If the plane of the geosynchronous orbit is in the equatorial plane of the Earth and the body rotates in the same direction as the Earth rotates, the orbiting body will always appear to be stationary to an observer standing on the Earth's surface. It is then said to be in geostationary orbit (Fig. 1.15). The orbiting body will appear to be a fixed point in the sky for an observer on the ground. Arthur Clarke, author of several science fiction books, had put forward this concept of a geostationary orbit in 1945. The orbit is therefore also referred to as Clarke orbit. The first satellite to be placed in the geostationary orbit was Syncor-2 on 26 July 1963.

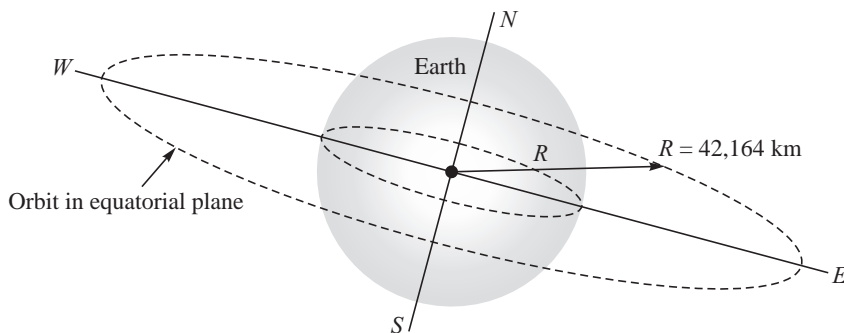


**Fig. 1.15** Geostationary Orbit

Synchronous orbits exist not only for Earth but also for other planets and moons as long as they are rotating about an axis. However, if the rotational speed of a planet or moon is too small, the orbital radius may be too large resulting in undue influence of the gravitational force of the neighbouring planets and stars.



## 1.8 ECCENTRICITY AND INCLINATION OF ORBITS

### 1.8.1 Eccentricity

Orbits are not always circular and in the equatorial plane. An orbit could be elliptic and the departure from a circular orbit is known as eccentricity of the orbit. It is defined as the ratio of the distance



between the foci to the length of the major axis of the ellipse. This is shown in Fig. 1.16. Here  $L_C$  is the distance between the foci and  $2a$  is the length of the major axis giving the eccentricity  $e = L_C/2a$ . In the limit of circular orbit,  $L_C = 0$  and the eccentricity is zero. A body gets into an elliptic orbit when the orbital velocity provided to it is not equal to the orbital velocity required for a circular orbit. Highly elliptic orbits with large inclinations are provided when the spacecraft has to remain over certain restricted zones over long durations.

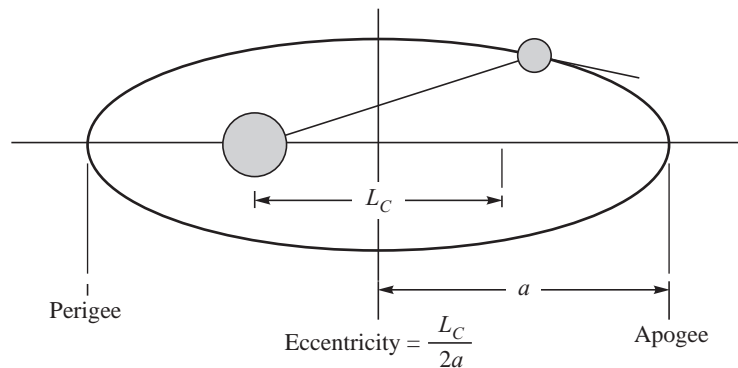


Fig. 1.16 Eccentricity of an Orbit

### 1.8.2 Inclination: Polar and Retrograde Orbits

The inclination of an orbit is the angle between the orbital plane and the equatorial plane of the planet about which the body is orbiting. An orbit at an inclination of  $\theta^{\circ}$  is shown in Fig. 1.17. An inclination of zero denotes that the orbit is in the equatorial plane, *i.e.* the orbital plane and the equatorial plane coincide. An inclination of  $90^{\circ}$  represents the orbit from pole to pole and is known as polar orbit. A circular polar orbit is shown in Fig. 1.18.

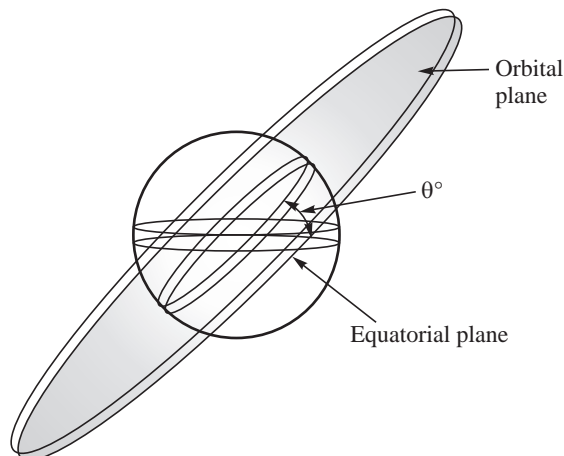


Fig. 1.17 Orbit Inclination



Polar orbits are useful for spacecrafts that carry out mapping or surveillance of the planets. This is because as the planet rotates, the spacecraft has access to every point on the surface of the planet. In the case of polar orbit about the Earth, when the orbital plane precesses at the same period as the Earth precesses in the solar orbit, the Sun would maintain the same inclination. The angle between the line joining the Sun with the Earth and the orbital plane of the satellite remains constant in this case. Such an orbit is known as Sun-synchronous orbit and provides constant illumination by the Sun at a given point on the surface of the Earth as viewed by the spacecraft in polar orbit.

The inclination of the Sun-synchronous orbit is more than  $90^\circ$  and is fixed according to the orbital radius. A constant angle with respect to the Sun-Earth line which rotates at the rate of  $0.985^\circ$  per day is maintained.

An inclination of  $180^\circ$  represents the orbiting body to move in the equatorial plane but in a direction opposite to the direction of rotation of the planet in the equatorial plane. It is known as a retrograde equatorial orbit.

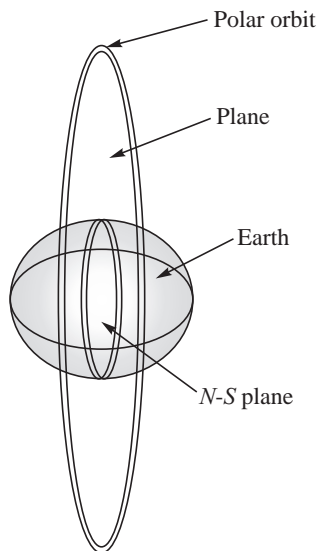


**Fig. 1.18** Polar Orbit ( $\theta = 90^\circ$ )

### 1.8.3 Molniya Orbit

A particular orbit known as Molniya orbit is highly elliptic with the half major and half minor axis being about 46,000 km and 6,800 km respectively. The inclination of the orbit is  $63.4^\circ$ . Spacecrafts in the Molniya orbit remain in the northern hemisphere for as much as 11 hours in an orbit having a time period of 12 hours.

The inclination of  $63.4^\circ$  for the Molniya orbit is based on fact that the Earth is not perfectly spherical but is flatter at the poles and bulges at the equator. The shape of the Earth is an oblate spheroid. This leads to a change in the orientation of the rotational axis, *i.e.* precession as the Earth orbits around the Sun. The major axis which is the line joining the furthest point and the closest point of the spacecraft with respect to the Earth with the center of the Earth (also known as the apsidal line) therefore rotates. There is no rotation of the apsidal line for an orbital inclination of  $63.4^\circ$ .



#### 1.8.4 Transfer Orbit

Instead of directly taking a spacecraft to geosynchronous orbit, the spacecraft is initially placed in an elliptical orbit about the Earth. The orbit is known as the geosynchronous transfer orbit about the Earth and is schematically shown in Fig. 1.19. The farthest point of the spacecraft from the centre of the Earth is called apogee. The point of the spacecraft closest to the Earth is called perigee. The apogee and perigee are shown in Fig. 1.19. The apogee of the elliptic orbit is so chosen that it is near to the radius of the geosynchronous orbit of 42,164 km. The perigee is small at about 6,630 km, the choice being governed such that the drag effects at this altitude will be negligible. The elliptic transfer orbit is circularised to give the geosynchronous orbit.

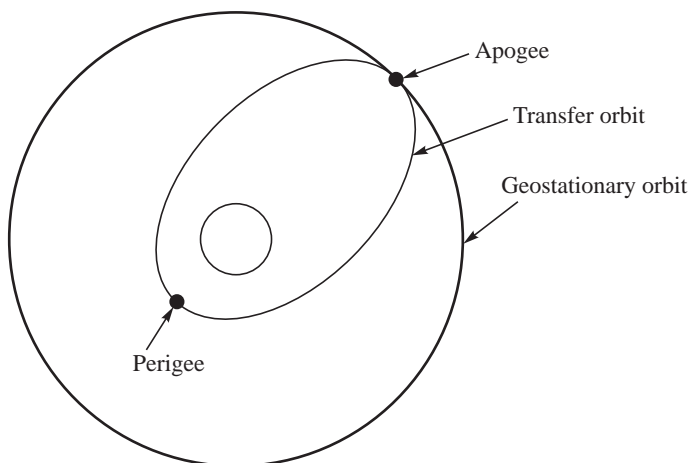


Fig. 1.19 Geosynchronous Transfer Orbit



#### 1.9 ENERGY AND VELOCITY REQUIREMENTS TO REACH A PARTICULAR ORBIT

The orbital velocity of a body at a given radius was discussed in section 1.6.2. In order to reach the given orbit from the surface of a planet, work is required to be done to overcome the attractive force due to the planet. For the particular case of a circular orbit at a radius  $R$  from the centre of the Earth, the work required to be done on a body of mass  $m$  to move from the surface of the Earth at radius  $R_E$  to the radius  $R$  is:

$$\int_{R_E}^R Force \times dr = \int_{R_E}^R \frac{GM_E m}{r^2} dr \quad \dots(1.25)$$

The energy needed to reach the orbit is equal to the above work and can be written as:

$$E = \int_{R_E}^R \frac{GM_E m}{r^2} dr \quad \dots(1.26)$$



This gives:

$$E = GM_E m \left( \frac{1}{R_E} - \frac{1}{R} \right) \quad \dots(1.27)$$

The total energy required to orbit the body must also provide the orbital velocity in addition to reach the orbit. The kinetic energy  $E_0$  corresponding to the orbital velocity  $V_o$  is  $mV_o^2/2$ . The total energy  $E_T$  required to be provided for orbiting the body is therefore:

$$E_T = GmM_E \left( \frac{1}{R_E} - \frac{1}{R} \right) + \frac{mV_o^2}{2} \quad \dots(1.28)$$

Substituting the value of orbital velocity from eq. 1.19, we get:

$$E_T = GmM_E \left( \frac{1}{R_E} - \frac{1}{2R} \right) \quad \dots(1.29)$$

Writing,  $R = R_E + h$ , where  $h$  is the orbiting altitude or height above the surface of the Earth and simplifying,  $E_T$  becomes:

$$E_T = \frac{GM_E m}{2R_E} \left( \frac{R_E + 2h}{R_E + h} \right) \quad \dots(1.30)$$

This is the total energy required to orbit a body of mass  $m$  at an altitude  $h$ . If the total energy given by eq. 1.30 is provided in the form of kinetic energy, the total velocity  $V_T$  required for orbiting the body is obtained by equating  $E_T = mV_T^2/2$ , thus giving:

$$V_T = \sqrt{\frac{GM_E (R_E + 2h)}{R_E (R_E + h)}} \quad \dots(1.31)$$

The velocity requirements for orbiting bodies about any planet or moon or star can be determined from the above expression by suitably considering the mass and radius of the planet, moon or star. The variation in the total velocity for orbiting bodies at different heights above the Earth is shown in Fig. 1.20. Typical values of velocities are about 8 to 10 km/s.

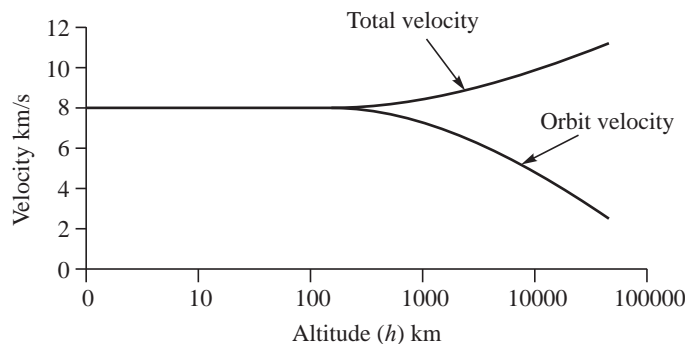


**Fig. 1.20** Velocities for Orbiting Bodies at Different Altitudes



## 1.10 ESCAPE VELOCITY

If a body is provided with sufficient velocity to overcome the gravitational attraction, it would reach infinite radius and escape the attractive force of the planet. This velocity is referred to as escape velocity ( $V_E$ ). The escape velocity can be determined by equating the kinetic energy,  $mV_E^2/2$ , with the work required to move the body from the surface of the planet to infinity. In the case of escape from Earth:

$$\frac{1}{2} mV_E^2 = \int_{R_E}^{\infty} \frac{GM_E m}{r^2} dr \quad \dots(1.32)$$

This gives:

$$V_E^2 = 2GM_E \int_{R_E}^{\infty} \left(\frac{1}{r^2}\right) dr = \frac{2GM_E}{R_E}$$

The escape velocity at the surface of Earth is therefore:

$$V_E = \sqrt{\frac{2GM_E}{R_E}} \quad \dots(1.33)$$

The orbital velocity  $V_O$ , was derived as  $\sqrt{GM_E/R_E}$  at the surface of the Earth for which  $R = R_E$ . The value of escape velocity  $V_E$ , is therefore  $\sqrt{2}$  times the orbital velocity ( $V_O$ ) at the surface of Earth. It decreases with the height above the Earth from which the velocity is provided to escape the Earth's gravitational field. Figure 1.21 shows the escape velocity would decrease from 11.17 km/s at the surface of the Earth to about 3.76 km/s at a height of 50,000 km above the Earth's surface.

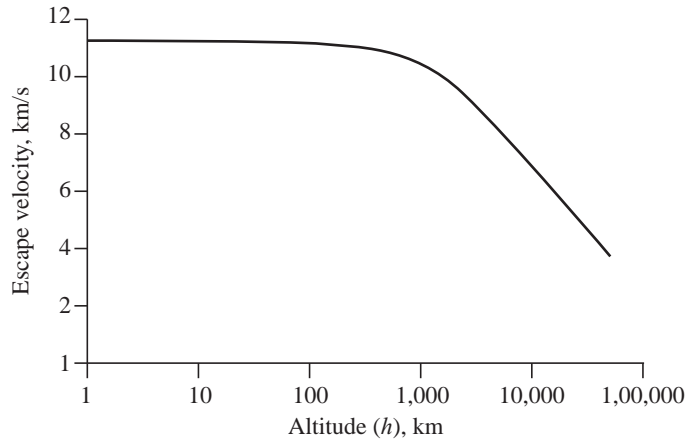


**Fig. 1.21** Variation of Escape Velocity with Height Above the Earth



## 1.11 FREELY FALLING BODIES

### 1.11.1 Orbital and Sub-Orbital Flight

A body in orbit is in a state of free fall. (Free fall means that the body moves freely under the influence of the gravitational field.) A body, provided with an orbital velocity  $V_O$ , tends to move along a straight line in the direction of this velocity. However, the attractive force from the gravitational field of the planet tends to pull it towards its centre. The body therefore falls towards the planet. As



the body falls, the orbit velocity,  $V_O$ , pushes it further away from the planet and the body always misses falling on the planet. As long as the velocity provided to a body is less than the escape velocity, gravitational attraction of the given planet will cause the body to fall towards it. When the body goes into orbit, the motion corresponds to a state of free fall. If the velocity provided is less than the orbital velocity, the body falls on the planet corresponding to a sub-orbital flight.

The motion of different planets in the solar system about the Sun is also in a state of free fall.

### 1.11.2 State of Weightlessness under Free Fall

The free fall is similar to the situation of a stone or an elevator dropping under gravity in the absence of any other external forces. If the frame of reference used for describing the motion of the body is on the freely falling body itself, the frame of reference is subject to a linearly accelerated motion due to the gravity. This frame of reference is accelerating and is not an inertial frame of reference. An observer on the body, however, does not see the motion. A pseudo force equal and opposite to the attractive force of the gravitational field needs to be incorporated in frame of reference of the body in order to correctly describe the absence of motion. The incorporation of the pseudo force provides a state of weightlessness in the frame of reference of the freely falling body. Weightlessness is not because of the absence of the gravitational attraction; it is experienced or a state of zero 'g' exists because of free fall.



## 1.12 MEANS OF PROVIDING THE REQUIRED VELOCITIES

Velocities of several km/s are seen to be necessary for orbiting bodies about the Earth. Velocities required by the bodies to escape from the Earth are even higher. Large values of momentum or impulse are therefore essential. The Greek satirist Lucien de Samosate as early as 180 AD imagined the possibilities of a giant storm over the sea to provide the large impulse to travel to the moon. Jules Verne, the famous science fiction author, in his book *From Earth to the Moon - De la Terra a la Lune* in 1874, suggested the use of a cannon gun. If a velocity of 10 km/s is considered to be provided impulsively to a body of say 1,000 kg over a period of one millisecond, the energy required is  $\frac{1}{2} \times 1,000 \times 10,000^2$  which is  $5 \times 10^7$  kJ and the power is  $5 \times 10^{10}$  kW. This constitutes a large quantity of power. Even if the very high velocities could somehow be provided to the body, frictional heating in the atmosphere would destroy it. The high velocities are therefore achieved by gradually adding velocity to the body by the rocket as the body is being pushed up to the required orbit.

## SOLVED EXAMPLES

**Example 1.1** Frame of reference, momentum, impulse and force:

A ball of mass  $m$  kg is thrown out of a space capsule cruising at a constant velocity  $\vec{V}_i$  m/s in deep space. The ball is thrown over a duration  $\tau$  seconds at a velocity  $\vec{v}_b$  m/s by a sling mechanism. If the mass of the space capsule including the sling mechanism and the ball is  $M$  kg, determine the final velocity of the capsule and the impulse and average force exerted by the sling on the ball.



**Solution:** An observer in the inertial frame of reference (say on the ground) sees the capsule move with a velocity  $\vec{V}_i$  m/s. Let the velocity of the capsule when the ball leaves it be  $\vec{V}_f$  m/s. The observer would therefore see the ball move with a velocity  $(\vec{V}_f + \vec{v}_b)$  m/s.

In the inertial frame of reference of the observer:

Initial momentum of the capsule including the ball  $\vec{p}_i = M \vec{V}_i$  kgm/s.

Final momentum of the capsule and the ball:

$$\vec{p}_f = (M - m) \vec{V}_f + m (\vec{V}_f + \vec{v}_b) \text{ kgm/s}$$

In the absence of any extraneous interaction, the momentum in the inertial frame of reference is conserved giving:

$$(M - m) \vec{V}_f + m (\vec{V}_f + \vec{v}_b) = M \vec{V}_i$$

The final velocity of the capsule is therefore

$$\vec{V}_f = \vec{V}_i - \frac{m}{M} \vec{v}_b$$

The momentum exerted by the sling on the ball  $= m(\vec{V}_f + \vec{v}_b)$  kgm/s.

Impulse provided to the ball  $= m(\vec{V}_f + \vec{v}_b)$  kgm/s.

$$\text{Average force} = \frac{I}{\tau} = \frac{m(\vec{V}_f + \vec{v}_b)}{\tau} \text{ kgm/s}^2 = \frac{m(\vec{V}_f + \vec{v}_b)}{\tau} \text{ N.}$$

### Example 1.2 Force and Impulse:

A momentum of 100 kgm/s is imparted to a projectile over duration of 0.05s. What is (i) impulse and (ii) force provided to the projectile?

**Solution:** Impulse (I) is change of momentum  $= 100$  kgm/s  $= 100$ Ns

$$\text{Force (F) is impulse by time} = \frac{I}{\tau} = \frac{100}{0.05} = 2000 \text{ N.}$$

### Example 1.3 Gravitational attraction:

The space probe ‘Rosetta’ flew by the asteroid ‘Steins’ in the asteroid belt between the orbits of Mars and Jupiter at a distance of about  $400 \times 10^6$  km from Earth. The space probe came within a distance of 800 km of the asteroid.

Determine the force exerted by the asteroid on the probe when the probe was nearest to the asteroid. The mass of the probe can be assumed as 500 kg. The asteroid Steins can be assumed to be spherical with a diameter of 4.6 km. The average density of the asteroid can be taken as  $2370 \text{ kg/m}^3$ . You can neglect the gravitational field of the planets and the Sun.

**Solution:** Mass of asteroid Steins  $= \frac{\pi}{6} \times 4600^3 \times 2370 = 1.208 \times 10^{14} \text{ kg}$

Mass of probe  $= 500$  kg



Distance between probe and asteroid = 8,00,000 m

Force of attraction on probe of mass 500 kg due to asteroid of mass  $1.812 \times 10^{14}$  kg is given by

$$G \frac{m_1 m_2}{r^2} = 6.67 \times 10^{-11} \times \frac{1.208 \times 10^{14} \times 500}{(8 \times 10^5)^2} \text{ Nm}^2/\text{kg}^2 \cdot \text{kg}^2/\text{m}^2 = 6.294 \times 10^{-6} \text{ N}$$

The asteroid is seen to exert a very small attractive force of 6.294  $\mu\text{N}$  on the space probe.

**Example 1.4** Velocity requirements to orbit:

The lunar module Eagle carrying Neil Armstrong and Edwin Aldrin landed on the moon on 20 July 1969 after separating from the mother-ship Columbia, which kept orbiting around the moon. After space walks on the moon were over, Armstrong and Aldrin got back into Eagle and took off from the moon to join the mother-ship Columbia in order to return to Earth. Assuming that Columbia had a circular orbit at an altitude of 150 km above the moon, determine the velocity increment that was provided to Eagle to join Columbia.

**Solution:** The velocity increment must provide the orbital velocity and the kinetic energy to increase the height from moon's surface to 150 km. The velocity is given by eq. 1.31 as:

$$V_T = \sqrt{\frac{GM_m(R_m + 2h)}{R_m(R_m + h)}}$$

The mass of the moon is  $7.348 \times 10^{22}$  kg. The radius of the moon is 1738 km. The required velocity is:

$$V_T = \sqrt{\frac{6.67 \times 10^{-11} \times 7.348 \times 10^{22} \times (2038 \times 10^3)}{1738 \times 10^3 \times (1888 \times 10^3)}} = 1745 \text{ m/s}$$

A velocity increment of 1.75 km/s would have to be provided to Eagle.

**Example 1.5** Launch of space capsule from aircraft:

The space capsule 'Space Ship II' of Sir Richard Branson, meant to ferry tourists from Earth to space, initially rides on a large aircraft known as Whiteknight II. The space capsule is released by the aircraft at an altitude of 15 km after which it climbs vertically to a height of 100 km. Determine the velocity increment to be provided by the spaceship for the vertical manoeuvre.

**Solution:** The velocity increment  $\Delta V$  must provide the kinetic energy to raise the height of the space capsule from  $(R_E + 15)$  km to  $(R_E + 100)$  km, where  $R_E$  is the radius of the Earth in km. We can, therefore, write for a space capsule of mass  $m$ :

$$\frac{1}{2}m\Delta V^2 = \int_{R_E + 15}^{R_E + 100} \frac{GmM_E}{r^2} dr$$

The above expression can be simplified by denoting  $R_1 = (R_E + 15) \times 10^3$  and  $R_2 = (R_E + 100) \times 10^3$  m respectively to reduce the above equation to the form:

$$\frac{1}{2}m\Delta V^2 = \int_{R_1}^{R_2} \frac{GmM_E}{r^2} dr$$

This gives:

$$\Delta V^2 = 2GM_E \left( \frac{1}{R_1} - \frac{1}{R_2} \right)$$



Substituting the values of  $G$ ,  $M_E$ ,  $R_1$  and  $R_2$ , we get  $\Delta V = 1.278$  km/s.

The saving in the velocity increment for this vertical manoeuvre from 15 km height compared to the vertical launch from the surface of Earth is small; the saving works out to be 0.005 km/s. We did not consider the velocity of the aircraft which is available for putting the capsule into orbit. An example of air-launch of a satellite is given in Exercise 5 of this chapter.

Initial velocity can also be provided to the capsule at the surface of the Earth by launching the capsule using a high velocity sled.

**Example 1.6** Escape from geo-stationary orbit:

When the life of a geo-stationary satellite is going to get over, it is desirable to push it into deep space or otherwise, so that the useful orbit does not get crowded and is available for other satellites. Assuming that a geo-stationary satellite is pushed out of Earth's gravitational pull and assuming no attraction from the Sun, moon and other planets, determine the velocity increment to be provided for this purpose.

**Solution:** The escape velocity from the geo-synchronous orbit is derived as:

$$\frac{1}{2} m V_E^2 = \int_{R_{\text{GEO}}}^{\infty} \frac{GmM_E}{r^2} dr = \frac{GmM_E}{R_{\text{GEO}}}$$

giving,

$$V_E = \sqrt{\frac{2GM_E}{R_{\text{GEO}}}}$$

The radius of the circular geo-synchronous orbit  $R_{\text{GEO}}$  is  $(6378 + 35800)$  km.

Substituting, we get:

$$V_E = \sqrt{\frac{2 \times 6.67 \times 10^{-11} \times 5.974 \times 10^{24}}{42178 \times 10^3}} = 4343 \text{ m/s}$$

The velocity increment required is 4.343 km/s.

## NOMENCLATURE

- $F$  : Force (N)  
 $G$  : Gravitational constant defined in eq. 1.6 ( $G = 6.670 \times 10^{-11}$  Nm $^2$ /kg $^2$ )  
 $g$  : Gravitational field; acceleration due to gravity (m/s $^2$ )  
 $h$  : Altitude (m)  
 $I$  : Impulse (Ns or kg m/s)  
 $M, m$  : Mass (kg)  
 $p$  : Momentum (kg m/s)  
 $R, r$  : Radius, distance (m)  
 $t$  : Time (s)  
 $V, v$  : Velocity (m/s)  
 $x$  : Distance (m)



$\alpha$ :	Acceleration ( $\text{m/s}^2$ )
$\rho$ :	Density ( $\text{kg/m}^3$ )
$\tau$ :	Duration (s)
$\omega$ :	Angular velocity (radian/s)
$\Delta$ :	Increment

### Subscripts

$b$ :	Ball
$E$ :	Earth
$f$ :	Final
$G, \text{GEO}$ :	Geo-synchronous orbit
$i$ :	Initial
$m$ :	Moon
$O$ :	Orbital
$T$ :	Total

### Superscript

$X'$  : Rotating frame of reference

## EXERCISES

- The orbit of an unmanned space capsule has to be increased from a circular Low Earth Orbit (LEO) of 350 km to a Medium Earth Orbit (MEO) of 1,500 km without any change of inclination of the orbital plane. Determine the incremental velocity required.
- A particular point on the surface of planet Mars is to be viewed continuously from a spacecraft orbiting Mars. Determine the height of the orbit of this spacecraft above the surface of Mars. You can assume the period of rotation of Mars about its axis to be 24 hours and 40 minutes.
- An astronaut of mass 70 kg moves vertically up by 2 m in a space capsule orbiting Earth at a height of 10,000 km. Find the work done by the astronaut in
  - Inertial frame of reference on the surface of the Earth, and
  - Frame of reference of the space capsule?
- A spacecraft launched from the Earth escapes Earth's gravity and enters into a circular orbit about the moon at a height of 2,000 km above the surface of the moon. Determine the reduction in velocity required to bring down the orbital height to 100 km above the surface of the moon.
- The Pegasus rocket is launched from a jet aircraft at a height of 15 km above the surface of the Earth. Assuming that the rocket is required to place a satellite in circular orbit at a height of 500 km above the surface of the Earth, determine the velocity to be provided by the Pegasus rocket under ideal conditions. You can assume the cruise speed of the aircraft at 15 km altitude as 220 m/s. The velocity required for the different manoeuvres may also be neglected. Are there any additional assumptions made while calculating the required velocity increment?
- Assume that a major explosion occurs on the surface of planet Uranus. What is the kinetic energy required to be imparted in the explosion to a rock of mass 50 kg if the rock is to escape from planet?



## References

1. Clarke, Arthur C., *A Space Odyssey*, G.K. Hall, 1994.
2. Clarke, Arthur C., *The Collected Stories of Arthur C Clark*, Macmillan, 2002.
3. Den Hartog, J.P., *Mechanics*, Dover publications, 1961.
4. Moon, Francis C., *Applied Dynamics*, second edition, Wiley-VCH, Weinheim, 2008.
5. Piscane, Vincent L., *The space environment and its effect on space systems*, AIAA Education series, Joseph A. Schetz, Series Editor-in-chief, AIAA Inc., Reston, 2008.
6. Stuhlinger, E and Mesmer, G., *Space Science and Engineering*, McGraw Hill Book Co., New York, 1965.
7. Verne, Jules, *From Earth to Moon*, Globe Book, 1958.

## Glossary

- AU: Astronomical unit is a measure of distance; equals the mean distance between Earth and Sun ( $= 150 \times 10^6$  km)
- Escape velocity: Velocity required for a body to escape the attractive force of the planet/star
- Frame of reference: Reference based on which the position of a body is described
- Force: Rate of change of momentum
- Free fall: Body moving freely under the influence of the gravitational field. An observer in a freely falling body is in a state of weightlessness
- Geo-synchronous orbit: Orbit having an angular velocity equal to the angular velocity of planet around which orbit takes place
- Geo-stationary orbit (Clarke orbit): An orbit in the equatorial plane of Earth such that the orbiting body appears to be a fixed point for any observer on the surface of Earth
- Gravitational constant  $G$ : The constant in the universal law of gravitational force giving the attractive force between two masses separated by a given distance. When the mass is expressed in 'kg' and the distance in 'm', the gravitational constant is  $6.670 \times 10^{-11} \text{ Nm}^2/\text{kg}^2$ .
- Gravitational field: Force of attraction on a mass ' $m$ ' kg in a gravitational field  $g$  is  $m \times g$  N. Unit of gravitational field is  $\text{m/s}^2$
- Impulse: Change of momentum
- Inclination: Angle between orbital plane and equatorial plane of the planet
- Inertial frame of reference: A frame of reference that is absolutely stationary or moves at constant velocity along a straight line
- Kepler's laws: Laws describing the motion of planets in the solar system
- Molniya orbit: Highly elliptic orbit about the Earth with a large eccentricity and an apogee of about 40,000 km in the northern hemisphere
- Momentum: Product of mass of a body and its velocity
- Orbit: Trajectory or path of motion in space; Path in which a planet, satellite or spaceship moves
- Orbital velocity: Velocity along the path of orbit
- Orbital period: Time to complete one complete circuit or revolution
- Polar orbit: Orbit having an inclination of  $90^\circ$



## 26 Rocket Propulsion

---

Pseudo-force: Fictitious force in a non-inertial frame of reference to correctly describe the motion of the body in the non-inertial frame of reference. In a rotational frame of reference, the pseudo force is the centrifugal force

Spacecraft: Vehicle moving in space including manned or unmanned space stations and artificial satellites of celestial bodies

Sun synchronous orbit: A polar orbit in which the angle between the line joining Sun with Earth and the orbital plane remains constant

Transfer orbit: A temporary orbit in which a satellite is placed before being propelled to the desired orbit

Zero  $g$ : An observer in a body under free fall experiences a state of weightlessness

## Chapter 2

### Theory of Rocket Propulsion

*Consider a cask filled with highly compressed gas. If we open one of its taps the gas will escape through it in a continuous flow, the elasticity of the gas pushing its particles into space will continuously push the cask itself. The result will (be) a continuous change in the motion of the cask. Given sufficient number of taps (say six), we will be able to regulate the outflow of the gas as we liked and the cask (or sphere) would describe any curved line in accordance with any law of velocities.*

*Konstantin E Tsialkovsky, Rocket Pioneer*

*If there is a small rocket on top of a big one, and if the big one is jettisoned and the small one is ignited, then their speeds are added.*

*Herman Oberth, Rocket Pioneer*

Rockets provide the velocities required by spacecrafts for orbiting and for movement in space. The velocities are achieved by ejecting material stored within the rocket. A rocket achieves high values of velocities by the impulse generated on chucking out part of its own mass at high speed. The method is illustrated in this chapter with a simple example of achieving motion by a single large impulse and by a series of smaller impulses. The rocket equation is thereafter derived and the parameters influencing the velocity realised by a rocket are determined. The chapter closes with the classification of rockets according to the method used for generating the impulse.



## 2.1 ILLUSTRATION BY AN EXAMPLE OF MOTION OF A SLED INITIALLY AT REST

The rocket principle can be appreciated through an example of a sled moving over a frictionless surface in the absence of gravitational attraction. Consider a sled on a frictionless surface and two boys standing on the sled. Let the sled be initially at rest. Let each of the boys carry one stone each of mass  $m$ . The total mass of the sled, the boys and the stones is  $M$ .

The sled (including the two boys and the two stones) is initially at rest. In order to move the sled, the boys throw the stones either together or one after the other with a velocity  $v_0$  (Fig. 2.1). The effect of throwing the stone either simultaneously or one after the other is determined in the following sections.

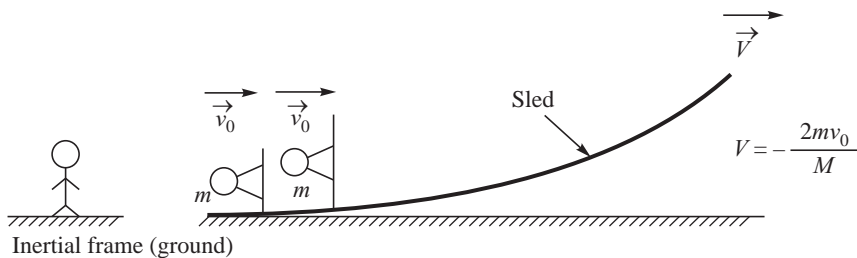


**Fig. 2.1** Motion of Sled with the Two Stones Thrown Together

### 2.1.1 Stones Thrown Together

The initial momentum of the sled, the boys and the stones is zero since all are at rest. The stones are thrown with a velocity,  $v_0$ , relative to the sled. Let us assume that throwing of the stones causes the sled to move with velocity  $V$ . When viewed from a stationary frame of reference on the ground (inertial), the stones have a velocity  $v = V + v_0$  (Fig. 2.1). The final momentum of the sled and the boys and the two stones is:

$$(M - 2m)V + 2m(V + v_0) \quad \dots(2.1)$$

The momentum of the total system is conserved since it is isolated and assumed to be free from extraneous influences. The final momentum is same as the initial momentum giving:

$$(M - 2m)V + 2m(V + v_0) = 0$$

or 
$$V = -\frac{2mv_0}{M} \quad \dots(2.2)$$

The sled, therefore, achieves a velocity of  $-\frac{2mv_0}{M}$ .

The negative sign shows that the direction of motion of the sled would be opposite to the direction of motion of the stones. The velocity of the stones in the frame of reference of the ground is:

$$V + v_0 = \left(1 - \frac{2m}{M}\right) v_0 \quad \dots(2.3)$$



### 2.1.2 Stones Thrown One after the Other

If instead of throwing both the stones together, consider that the boys throw the stones one after the other at the same velocity  $v_0$  relative to the sled. In this case, after the first stone is thrown, the velocity of the sled, following eq. 2.2 is (Fig. 2.2):

$$V' = -\frac{m}{M}v_0 \quad \dots(2.4)$$

The velocity of the first stone  $v_1$  in the frame of reference of the ground (from eq. 2.3) is:

$$v_1 = \left(1 - \frac{m}{M}\right)v_0 \quad \dots(2.5)$$

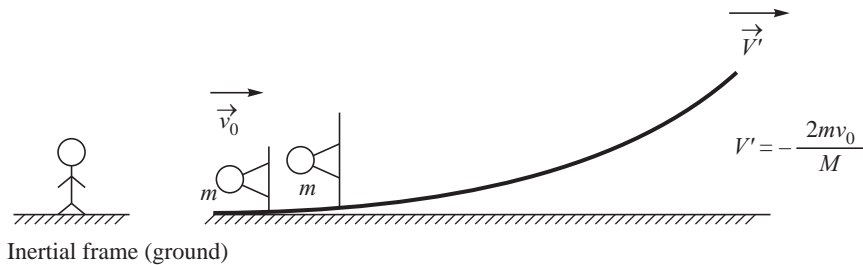


**Fig. 2.2** Motion of Sled with the First Stone Thrown at Velocity  $v_0$

Let the velocity of the sled after the second stone is thrown be  $V''$ . The momentum of the sled and the boys is  $(M - 2m)V''$  in the ground reference frame. The momentum of the second stone is  $mv_2$ , where  $v_2$  is the velocity of the stone in the ground reference frame.

$$v_2 = V'' + v_0 \quad \dots(2.6)$$

After the second stone is thrown (Fig. 2.3), the total momentum is:

$$(M - 2m)V'' + mv_1 + mv_2 \quad \dots(2.7)$$

In the above equation  $mv_1$  is the momentum of the first stone and  $v_1$  is given by eq. 2.5.

Substituting  $v_1$  and  $v_2$  obtained in eqs. 2.5 and 2.6 in the momentum eq. 2.7 and equating the final momentum to the initial momentum of zero, we get:

$$(M - 2m)V'' + mv_0 \left(1 - \frac{m}{M}\right) + m(V'' + v_0) = 0 \quad \dots(2.8)$$

Solving for  $V''$ , we get:

$$(M - m)V'' + mv_0 \left(1 - \frac{m}{M}\right) + mv_0 = 0$$

which gives as shown in Fig. 2.3,

$$V'' = -\left(\frac{m}{M} + \frac{m}{M-m}\right)v_0 \quad \dots(2.9)$$

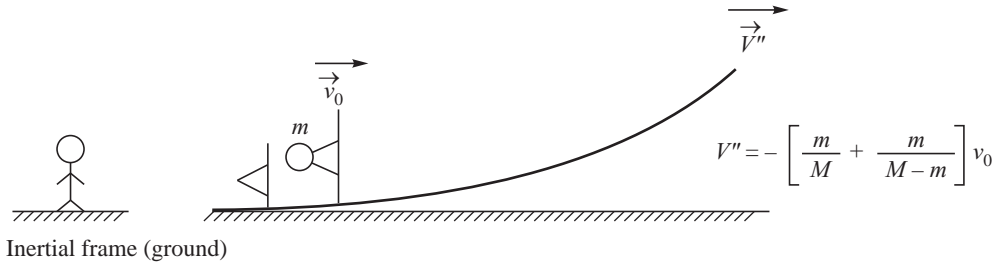


**Fig. 2.3** Motion of Sled with the Second Stone Thrown at Velocity  $v_0$

### 2.1.3 Comparison of the Sled Velocities and Extension to Multiple Stones

The velocity of the sled and the boys when both stones are thrown together ( $V$ ) and when the stones were thrown one after the other ( $V''$ ) are given in eqs. 2.2 and 2.9, respectively. Since the term  $m/(M - m)$  in eq. 2.9 is greater than  $m/M$ ,  $V''$  is greater than  $V$ .

If three stones each of mass  $m$  were considered to be thrown one after the other the velocity of the sled would be:

$$V^m = - \left( \frac{m}{M} + \frac{m}{M-m} + \frac{m}{M-2m} \right) v_0$$

compared to a velocity of  $-3mv_0/M$ , had all the three stones been thrown together. The sled velocity is higher when the stones are thrown one after the other.

The higher sled velocity is achieved as the second stone imparts its momentum to a reduced mass when the stones are thrown one after the other. If we were to consider a total mass  $\Delta M$  to be thrown out of the sled by breaking it up into a large number,  $n$ , of equal fragments, and throwing the fragments one after the other, the net velocity of the sled would be:

$$V = -v_0 \frac{\Delta M}{nM} \left( 1 + \frac{1}{1-\Delta M} + \frac{1}{1-2\Delta M} + \dots + \frac{1}{1-\frac{(n-1)\Delta M}{nM}} \right) \quad \dots(2.10)$$

This is much higher than  $-v_0 \Delta M/M$ , which corresponds to the velocity when the total mass  $\Delta M$  is thrown out in a single shot.

The working principle of a rocket makes use of continual ejection of matter in order to achieve high velocities and is similar in principle to this example of stones being continually thrown out of the sled. A rocket propels forward as the mass is thrown out of it and achieves very high velocities as more and more mass is ejected. The mass which is ejected out is called propellant and could be a gas, a liquid or an electrically charged particle.



## 2.2 MOTION OF A GIANT SQUID IN DEEP SEAS

Certain creatures, found in nature, employ the principle of moving by ejecting mass stored in their bodies and it is pertinent to examine the example of a giant squid before formulating the rocket

principle. The giant squid, shown in Fig. 2.4(a), is a large creature about 10 to 14 m long and is found in the deep oceans. A few have been caught off the coast of Japan or have been washed ashore the New Zealand coast.

The giant squid moves in the deep seas by taking in water by expanding its mantle. It holds the water and pressurises it to about 40 kPa by contracting its mantle. The pressurised water and any other matter that it has gulped, such as, fish, eggs, sand, etc., is squeezed out through a opening, known as a funnel, that can rotate in any direction. The gradual impulse from the squirting out of the water and waste pushes it by as much as 50 m for a single squirt. It is estimated to achieve a velocity of about 7 m/s in a single efflux of the water and waste. A schematic diagram of the squirting is given in Fig. 2.4(b).



**Fig. 2.4 (a)** Giant Squid Found Dead off New Zealand Coast (Source: National Geographic)

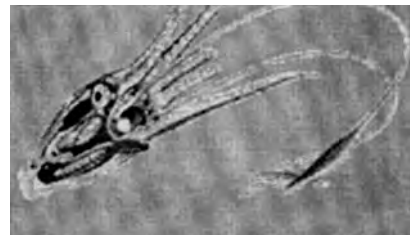


**Fig. 2.4 (b)** Schematic of Squirting of Water (Source: National Geographic)



### 2.3 ROCKET PRINCIPLE AND THE ROCKET EQUATION

The rocket operates on the principle of pushing itself forward by persistently ejecting out material, stored within it. Any type of material can be thrown out, *e.g.* cold gas, hot gas, charged particles, liquid, solid, etc. The rocket is different from a projectile or a canon-ball launched from a gun, wherein the entire momentum is transferred to the projectile or canon-ball in the barrel of the gun or canon itself. The velocity gained by a rocket is by continued efflux of material stored within it and is derived below in a way very similar to that for the sled given in the Sec. 2.1.

We consider a rocket travelling at time  $\tau$  in a drag-free and gravitation-less medium with a velocity  $V$ . The mass of the rocket at any time  $\tau$  is  $M$  and the rocket ejects out mass at a constant rate,  $\dot{m}$ . Over a short duration  $\delta\tau$  the mass,  $\delta M$ , ejected out is  $\dot{m}\delta\tau$ . The velocity of the rocket changes from  $V$  to  $V + \delta V$  due to the ejection of mass,  $\delta M$ . These velocities are in the inertial frame of reference,



viz., with respect to a stationary observer on the ground. A schematic diagram of the changes is shown in Fig. 2.5. The velocity at which the mass  $\delta M$  is ejected out (the efflux velocity) relative to the rocket is denoted by  $V_J$ . The direction of  $V_J$  is opposite to  $V$ .

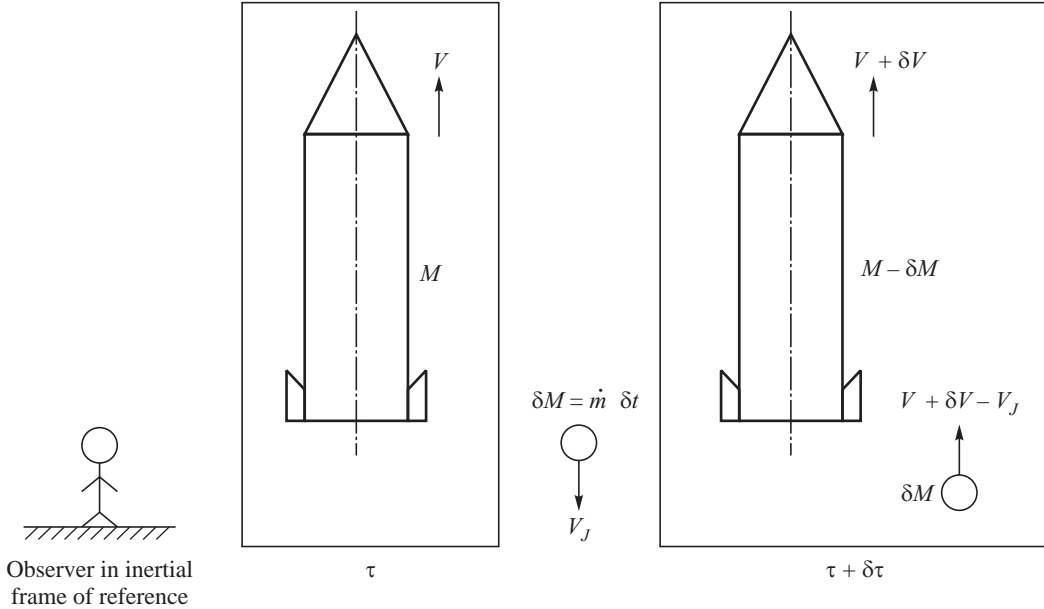


**Fig. 2.5** Mass and Velocity of a Rocket at Time  $\tau$  and  $\tau + \delta\tau$

The momentum of the rocket at time  $\tau$  is  $MV$ . At time  $\tau + \delta\tau$ , the momentum of the rocket is  $(M - \delta M)(V + \delta V)$ . The momentum of the mass ejected out ( $\delta M$ ) is  $[\delta M(V + \delta V - V_J)]$ . Since the momentum of the rocket in the inertial frame of reference is conserved, we have for time  $\tau$  and  $\tau + \delta\tau$ :

$$MV = (M - \delta M)(V + \delta V) + \delta M(V + \delta V - V_J) \quad \dots(2.11)$$

On simplification, the above expression becomes:

$$M \delta V - \delta M V_J = 0 \quad \dots(2.12)$$

This gives  $\delta V = (\delta M/M)V_J$ .

The mass of the rocket  $M$  at time  $\tau$  is the initial mass minus the mass ejected out during the period  $\tau$ . Denoting the initial mass as  $M_i$ , and a constant rate of mass ejection as  $\dot{m}$ , as considered earlier, we have:

$$M = M_i - \dot{m}\tau \quad \dots(2.13)$$

and

$$\delta M = -\dot{m}\delta\tau \quad \dots(2.14)$$

The negative sign for the mass  $\delta M$  indicates that it is leaving the rocket. We have considered this negative sign while denoting the mass of the rocket at time  $\tau + \delta\tau$  as  $M - \delta M$ .

Substituting the values of  $M$  as  $M_i - \dot{m}\tau$  and  $\delta M$  as  $\dot{m}\delta\tau$  from above in the momentum conservation eq. 2.12, we get:

$$\delta V = V_J \frac{\dot{m}\delta\tau}{M_i - \dot{m}\tau}$$



The similarity of this equation with eq. 2.10 for the motion of the sled is evident. Integrating from time  $\tau = 0$ , when the rocket has a mass  $M_i$  and is stationary to a time  $\tau_f$ , when its mass is  $M_f (= M_i - \dot{m} \tau_f)$ , we have the increase in the velocity  $\Delta V$  as:

$$\Delta V = \int_0^{\tau_f} \delta V = \int_0^{\tau_f} V_J \frac{\dot{m} d\tau}{M_i - \dot{m}\tau} \quad \dots(2.15)$$

Here  $\Delta V$  is spoken of as the ideal incremental velocity, ideal because the losses due to gravity, drag or otherwise are not considered in the derivation. Assuming a constant value of the efflux velocity  $V_J$  and integrating the above equation gives:

$$\Delta V = -V_J \ln (M_i - \dot{m} \tau) \Big|_0^{\tau_f} = -V_J \ln \left( \frac{M_f}{M_i} \right)$$

The ideal velocity increment  $\Delta V$  is, therefore, given by:

$$\Delta V = V_J \ln \left( \frac{M_i}{M_f} \right) \quad \dots(2.16)$$

The above equation is known as the rocket equation or Tsialkowsky equation after Konstantin Tsialkowsky who derived it in early 1900s. The equation suggests that a high value of the efflux velocity,  $V_J$ , and a large ratio of the initial mass to the final mass of the rocket are conducive to provide higher velocity to the rocket.  $\Delta V$  needs to be equal to  $V_T$  as given in eq. 1.31 (under ideal conditions) for the rocket to put a body in the desired orbit. Equation 2.16 is general and is applicable for any mode of ejection of the propellant or for any material or medium used for the propellant.



## 2.4 MASS RATIO OF A ROCKET

The ratio of the initial mass to the final mass ( $M_i/M_f$ ) and the efflux velocity  $V_J$  are seen from eq. 2.16 to govern the ideal velocity increment  $\Delta V$  provided by the rocket. The larger the values, the higher would be the velocity increment.

The ratio of the final mass of the rocket after all the propellant has been consumed ( $M_f$ ) to the initial mass before the rocket operation ( $M_i$ ) is called the mass ratio of a rocket and is denoted by  $R_m$ .

$$R_m = \frac{M_f}{M_i} \quad \dots(2.17)$$

The ideal velocity increment,  $\Delta V$ , in terms of the mass ratio from eq. 2.16 is therefore:

$$\Delta V = V_J \ln \left( \frac{1}{R_m} \right) \quad \dots(2.18)$$

The final mass of the rocket consists of the remnant mass after the required quantity of propellants are used up during its operation. This final mass comprises the useful equipments, astronauts, sensors and the other appliances carried by the rocket, the structural and hardware mass of the rocket, the mass of power supplies, guidance and control packages used in the rocket, the inert mass and the mass of the unused propellant if any.



The useful mass carried by the rocket is referred to as payload. If the mass of the payload is denoted by  $M_u$  and the structural mass left over after the functioning of the rocket is denoted as the structural mass  $M_s$ , we have:

$$M_f = M_u + M_s \quad \dots(2.19)$$

The structural mass  $M_s$  in the above expression includes the inert mass in the rocket.

The initial mass  $M_i$  additionally consists of the mass of propellant ejected out ( $M_p$ ) during the operation of the rocket:

$$M_i = M_u + M_s + M_p \quad \dots(2.20)$$

The rocket eq. 2.16 can, therefore, be written as:

$$\Delta V = V_J \ln \frac{M_u + M_s + M_p}{M_u + M_s} \quad \dots(2.21)$$

If the payload mass, structural mass and inert mass and propellant mass are expressed as a fraction of the initial mass  $M_i$ , viz.,,

$$\alpha = \frac{M_u}{M_i}; \beta = \frac{M_s}{M_i}; \gamma = \frac{M_p}{M_i} \quad \dots(2.22)$$

we get,

$$\alpha + \beta + \gamma = 1 \quad \dots(2.23)$$

and

$$\Delta V = V_J \ln \frac{\alpha + \beta + \gamma}{\alpha + \beta} \quad \dots(2.24)$$

Here  $\alpha$ ,  $\beta$  and  $\gamma$  denote the payload, structural and propellant mass fractions in the rocket respectively.



## 2.5 DESIRABLE PARAMETERS OF A ROCKET

We would like to have a rocket which provides large values of payload and velocity increment. From eq. 2.24, it is seen that:

$$\frac{1}{\alpha + \beta} = e^{\Delta V / V_J}$$

This results from the summation of masses which gives  $\alpha + \beta + \gamma = 1$  (eq. 2.23). The payload mass fraction can, therefore, be written as:

$$\alpha = e^{-\Delta V / V_J} - \beta \quad \dots(2.25)$$

The payload mass fraction,  $\alpha$ , is seen from the above equation to decrease as  $\Delta V / V_J$  increases. A given rocket, therefore, yields smaller values of useful payload as the demand for  $\Delta V$  increases. This is illustrated in Fig. 2.6. The value of  $\alpha$  is also seen to decrease as the structural mass fraction,  $\beta$ , increases. The decrease in  $\alpha$  with increase of  $\Delta V / V_J$  and  $\beta$  is shown in Fig. 2.6 for values of  $\beta$  of 0.1, 0.12 and 0.14.  $\alpha$  is observed to increase in the same proportion as the decrease of the structural mass fraction  $\beta$ . In order to achieve higher values of the payload mass fraction,  $\alpha$ ,  $V_J$  needs to be large and  $\beta$  is to be small.

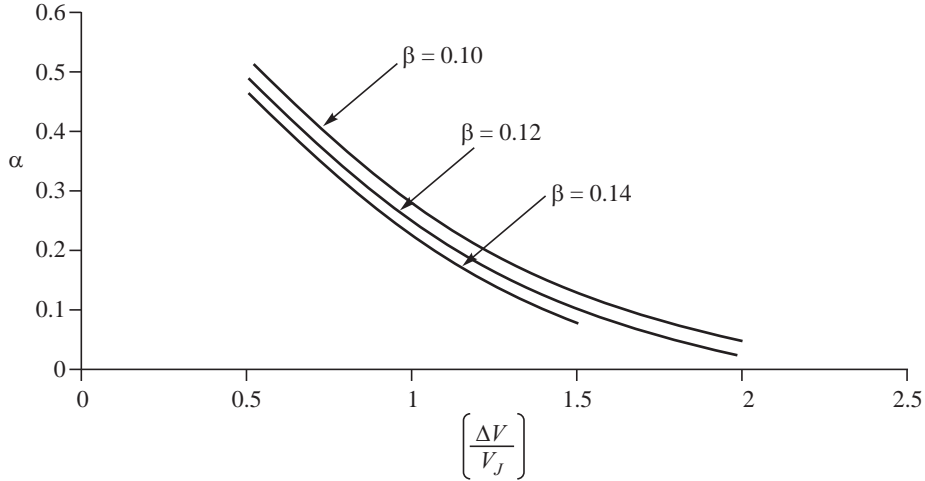


**Fig. 2.6** Variation of Payload Mass Fraction  $\alpha$  with Changes in  $\Delta V/V_J$  and Structural Mass Fraction  $\beta$

For a given rocket, an increase in propellant mass,  $M_p$ , will cause the initial mass,  $M_i$ , to increase. If the structural mass remains the same,  $\beta$  would decrease and the decrease of  $\beta$  would bring about an increase in the useful payload mass fraction  $\alpha$  (Fig. 2.6).

The aim of the rocket designer is to make  $V_J$  as large as possible and  $\beta$  as small as permissible. The different methods of achieving high values of  $V_J$  are considered in subsequent chapters.



## 2.6 ROCKET HAVING SMALL PROPELLANT MASS FRACTION

In case of rockets for which the mass of propellant ejected is less than its structural mass and payload mass:

$$\frac{\gamma}{\alpha + \beta} < 1 \quad \dots(2.26)$$

The ideal velocity increment given by eq. 2.24 can be written as:

$$\Delta V = V_J \ln \left( 1 + \frac{\gamma}{\alpha + \beta} \right)$$

Denoting  $x = \frac{\gamma}{\alpha + \beta}$ , we have the value of  $\ln(1 + x) = x - \frac{x^2}{2} + \frac{x^3}{3} - \dots$  for  $|x| < 1$

The incremental velocity can, therefore, be written for small  $\gamma/(\alpha + \beta)$  as:

$$\Delta V \approx V_J \frac{\gamma}{\alpha + \beta} = V_J \frac{M_p}{M_f} \approx V_J \frac{M_p}{M_i} \quad \dots(2.27)$$



The mass of propellant  $M_p = \rho_p V_p$ , where  $\rho_p$  is the density of the propellant and  $V_p$  is its volume and  $\Delta V$  becomes:

$$\Delta V = \rho_p V_J \frac{V_p}{M_f} \quad \dots(2.28)$$

The volume of propellants,  $V_p$ , which can be contained in a rocket of a given final mass is fairly fixed. The above expression shows that for rockets containing small mass of propellants in relation to the other masses, the incremental velocity is proportional to the product of the efflux velocity,  $V_J$ , and the propellant density  $\rho_p$ . The figure of merit is the product  $\rho_p V_J$ , instead of  $V_J$  as determined earlier.



## 2.7 PROPULSIVE EFFICIENCY OF A ROCKET

The rocket is seen to get its velocity from the momentum of the propellant ejected from it. It is desirable to convert as much of the kinetic energy of the ejected propellant into the useful work for moving the rocket. The efficiency of the conversion of the kinetic energy of the ejected mass into the useful work for moving the rocket is referred to as propulsive efficiency of a rocket ( $\eta_p$ ).

Consider a rocket moving with a velocity,  $V$ , when observed by an observer on the ground, viz., an inertial frame of reference. The velocity of the mass efflux from the rocket is  $V_J$  relative to the rocket and in a direction opposite to the motion of the rocket. The observer sees the mass efflux to follow the rocket with a velocity  $(V - V_J)$  (Fig. 2.7). It may be noted that  $V_J$  here is stated to be opposite to the motion of the rocket as in Fig. 2.5. If the rate of mass efflux is  $\dot{m}$ , the kinetic energy per unit time in the efflux left behind the rocket, as perceived in the inertial frame of reference, is  $\dot{m}(V - V_J)^2/2$ . This amounts to the rate at which energy is left behind by the rocket.

The work done per unit time by the rocket due to the mass efflux is the rate of momentum transferred to it from the mass efflux multiplied by the distance travelled per unit time and is given by  $\dot{m} V_J V$ . The propulsive efficiency of a rocket is given by the ratio of the rate at which work is done by the rocket to the rate of energy supplied to it. The latter equals the sum of the rate of work done by the rocket and the rate of energy left behind in the mass efflux. The propulsive efficiency is, therefore, written as:

$$\eta_p = \frac{\dot{m} V V_J}{\dot{m} V V_J + \frac{1}{2} \dot{m} (V - V_J)^2} \quad \dots(2.29)$$

The above expression can be simplified as:

$$\eta_p = \frac{2 V V_J}{V^2 + V_J^2} = \frac{2 \frac{V}{V_J}}{1 + \left(\frac{V}{V_J}\right)^2} \quad \dots(2.30)$$



By inspection  $\eta_p$  in the above equation is seen to be a maximum of unity when  $V/V_J = 1$ . A plot of the variation of  $\eta_p$  with variation in  $V/V_J$  from eq. 2.30 is shown in Fig. 2.8.

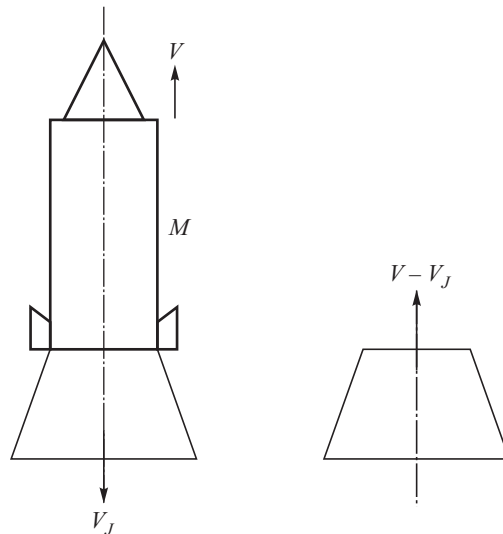


**Fig. 2.7** Mass Efflux Following Rocket with Velocity  $V - V_J$

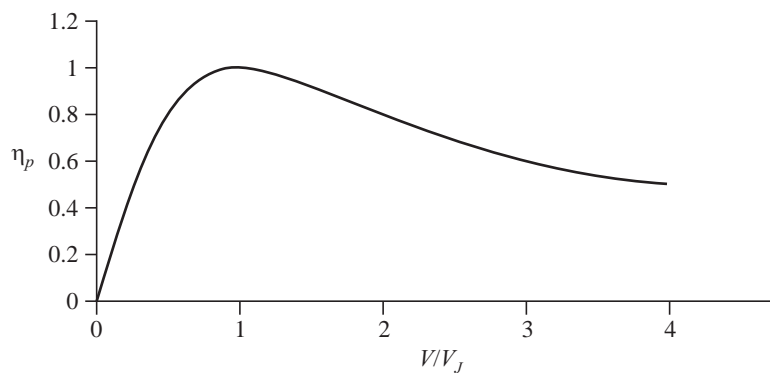


**Fig. 2.8** Variation of Propulsive Efficiency

This condition for maximum propulsive efficiency can also be obtained by differentiating  $\eta_p$  in eq. 2.30 with respect to  $V/V_J$  and equating it to zero as follows.

$$\frac{d\eta_p}{d\left(\frac{V}{V_J}\right)} = \frac{\left[1 + \left(\frac{V}{V_J}\right)^2\right]2 - 4\left(\frac{V}{V_J}\right)^2}{\left[1 + \left(\frac{V}{V_J}\right)^2\right]} = 0 \quad \dots(2.31)$$



On simplifying, we get:

$$1 - \left( \frac{V}{V_J} \right)^2 = 0 \quad \dots(2.32)$$

This gives  $V/V_J = 1$  or  $V - V_J = 0$ . To the observer on the ground, this condition implies that the mass efflux remains motionless. The entire kinetic energy of the efflux under this condition gets transferred into useful work for moving the rocket. In practice, however, it is difficult to match the velocity of the efflux mass ( $V_J$ ) to the velocity of the rocket ( $V$ ) as the rocket is a rapidly accelerating vehicle and its velocity is continually changing.



## 2.8 PERFORMANCE PARAMETERS OF A ROCKET

### (a) Impulse

The momentum associated with the efflux of propellants from the rocket was seen to provide velocity to the rocket. The change of momentum is impulse  $I$ . Denoting the total propellant efflux from the rocket as  $m_p$  and a constant value of the efflux velocity,  $V_J$ , the impulse,  $I$ , is given by:

$$I = m_p V_J \left( \text{kg} \frac{m}{s} = \frac{\text{kg} \cdot \text{m}}{\text{s}^2} \cdot \text{s} = \text{Ns} \right) \quad \dots(2.33)$$

### (b) Specific Impulse

The specific impulse is the impulse delivered per unit mass of propellant. The specific impulse is denoted by  $I_{sp}$  and is:

$$I_{sp} = \frac{I}{m_p} \left( \frac{\text{Ns}}{\text{kg}} \right) \quad \dots(2.34)$$

Substituting the value of  $I$  from eq. 2.33, the specific impulse is seen to be:

$$I_{sp} = V_J \left( \frac{\text{Ns}}{\text{kg}}, \text{m/s} \right)$$

The specific impulse,  $I_{sp}$  and the efflux velocity  $V_J$  are seen to be identical. The units Ns/kg reduces to  $\frac{\text{kgm}}{\text{s}^2} \frac{\text{s}}{\text{kg}} = \frac{\text{m}}{\text{s}}$ .

### (c) Thrust

The force or thrust developed by the rocket is the rate of change of the impulse (eq. 1.3). Denoting the thrust by  $F$ , we have:

$$F = \frac{d}{dt} I = \frac{d}{dt} (m_p V_J) = \frac{dm_p}{dt} V_J = \dot{m}_p V_J (\text{N}) \quad \dots(2.35)$$

Here  $V_J$  is assumed to have a constant value. The specific impulse,  $I_{sp}$ , in terms of thrust becomes:

$$I_{sp} = \frac{F}{\dot{m}_p} = \int \frac{F dt}{\dot{m}_p} = \frac{I}{\dot{m}_p} \quad \dots(2.36)$$



#### (d) Impulse to Mass Ratio

The ratio of the total impulse,  $I$ , divided by the initial mass of the rocket ( $M_i$ ) is spoken of as the impulse to mass ratio.

#### (e) Thrust to Mass Ratio

This represents the initial acceleration of the rocket and is defined as the ratio of the thrust to the initial mass.

$$\text{Thrust to mass ratio} = \frac{F}{M_i} \quad \dots(2.37)$$



## 2.9 STAGING AND CLUSTERING OF ROCKETS

The achievable values of specific impulse ( $I_{sp}$ ) and structural mass fraction,  $\beta$ , encountered in practice are such that it is very difficult for a single rocket to provide the velocities required for orbiting the Earth and for escaping from it. An increase in propellant mass, if provided to give larger value of impulse, makes the rocket unwieldy and heavy and leads to smaller values of the thrust to mass ratio.

If a series of rockets were to be put one on top of the other and operated sequentially in stages one after the other, the total velocity would correspond to the sum of the ideal velocities provided by the operation of each stage of the rocket. Figure 2.9 gives a schematic diagram of a two stage rocket with the first stage rocket taking off from the ground and followed by the operation of the second stage. The second stage gets started when its velocity is equal to the velocity provided by the first stage ( $\Delta V_1$ ), i.e. the velocity at the end of the operation of the first stage. If  $\Delta V_2$  is the velocity contributed by the second stage, the velocity at the end of operation of the second stage is  $\Delta V_1 + \Delta V_2$ .

In general, for a rocket having  $n$  stages, this sequence continues with each successive stage providing an incremental velocity. Denoting the ideal velocity provided by each stage as  $\Delta V_1$ ,  $\Delta V_2$ , ...  $\Delta V_n$  respectively, the total ideal velocity of a  $n$  stage rocket is:

$$\Delta V = \Delta V_1 + \Delta V_2 + \dots + \Delta V_n \quad \dots(2.38)$$

The used rocket stages are discarded once their propellant is consumed in order to reduce the inert mass and hence improve the mass fraction of the upper stages. This procedure of operating a series of rockets sequentially is known as staging of rockets. Since the heavy and unusable parts of a rocket are dropped off once they have functioned, a much lighter rocket is left behind. The lighter rocket would gain higher speeds.

Most of the rockets used for putting spacecrafts into orbit have two to four rocket stages, and are referred to as Satellite Launch Vehicles. The first stage rocket of a satellite launch vehicle, which

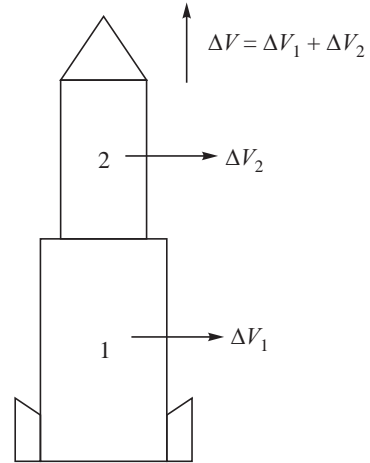


Fig. 2.9 Two Stage Rocket



takes off from the ground, is the heaviest and it carries the upper rocket stages on it. It is known as the booster stage. The payload of the initial rocket stage comprises the upper stage rockets in addition to the actual payload. If the mass ratio of the booster stage is  $R_{m1}$  and the mass ratios of the upper stages are  $R_{m2}, R_{m3}, \dots, R_{mn}$  for a rocket with  $n$  stages in series, the net ideal velocity of the rocket is the sum of the individual velocity increment of each stage, which using eqs. 2.18 and 2.38 give:

$$\Delta V = V_{J1} \ln(1/R_{m1}) + V_{J2} \ln(1/R_{m2}) + \dots + V_{Jn} \ln(1/R_{mn}) \quad \dots(2.39)$$

Here the mass efflux rate for each successive stage is denoted by  $V_{J1}, V_{J2}, V_{J3}, \dots, V_{Jn}$  respectively. If the efflux velocities of all stages are the same and equal to  $\bar{V}_J$ , the above equation becomes:

$$\Delta V = \bar{V}_J \ln \left[ \left( \frac{1}{R_{m1}} \right) \left( \frac{1}{R_{m2}} \right) \dots \left( \frac{1}{R_{mn}} \right) \right] \quad \dots(2.40)$$

Further, if the initial and final mass corresponding to each stage of operations of the multistage rocket is denoted as  $M_i$  and  $M_f$  respectively, eq. 2.40 becomes:

$$\Delta V = \bar{V}_J \ln \left[ \left( \frac{M_i}{M_f} \right)_1 \left( \frac{M_i}{M_f} \right)_2 \dots \left( \frac{M_i}{M_f} \right)_n \right] \quad \dots(2.41)$$

Here the subscripts 1, 2, ...,  $n$  denote the rocket stages.

With  $M_{f,1} = M_{i,2}, M_{f,2} = M_{i,3}, \dots$ , we get:

$$\Delta V = \bar{V}_J \ln \left( \frac{M_{i,1}}{M_{f,n}} \right) \quad \dots(2.42)$$

$M_{i,1}/M_{f,n}$ , which gives the ratio of the initial mass of the rocket to the final mass of the last rocket stage, represents the overall mass ratio of the idealised multi-stage rocket when all stages have the same value of  $\bar{V}_J$ . If the mass ratio of all the stages are the same, viz.,  $R_{m1} = R_{m2} = R_{m3} = \dots = R_{mn} = R_m$  (say),

$$\Delta V = \bar{V}_J \ln \left( \frac{1}{R_m} \right)^n = n \bar{V}_J \ln \left( \frac{1}{R_m} \right) \quad \dots(2.43)$$

As the number of stages  $n$  of a multistage rocket are increased higher values of  $\Delta V$  are obtained. Figure 2.10 shows the earliest satellite launch vehicle SLV-3 developed in India for putting a 40 kg payload in a Low Earth Orbit (LEO). This has four rocket stages, one on top of the other as shown in the following figure.

As the number of stages goes up, the operational complexity and cost of the multi-stage rocket increases. The number of stages

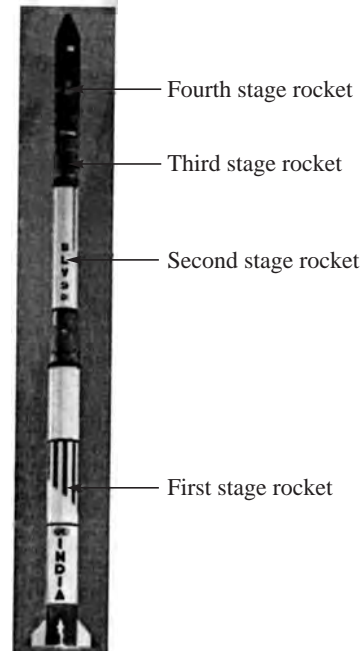


**Fig. 2.10** Satellite Launch Vehicle SLV-3 [Source ISRO]



cannot, therefore, be arbitrarily increased. The aim has been to enhance the value of  $V_J$  and decrease the structural mass fraction,  $\beta$ , keeping the number of stages as small as possible. The present trend is to work towards a Two Stage to Orbit (TSTO) launch vehicle. A Single Stage to Orbit (SSTO) vehicle would perhaps be possible if very advanced materials of construction are devised to reduce the structural and inert mass and have energetic propellants which provide larger values of  $V_J$  than obtainable at present.

The initial mass,  $M_{i,1}$ , of a multi-stage rocket is quite large considering that the mass of all the rocket stages above booster stage have to be carried by it. The thrust of the booster rocket should be sufficient for the vehicle to accelerate and take off from the ground. If the thrust of a single booster rocket is insufficient, a number of rockets are clustered together and operated simultaneously to generate the large values of thrust required. Clustering is like parallel staging. Two booster rockets could also be strapped on either side of the core rocket to get sufficient acceleration for take off. The strapped rockets are known as strap-on rockets. Figure 2.11 shows the Augmented Satellite Launch Vehicle (ASLV) of India in which two rockets are strapped to the core rocket of SLV-3. The Polar Satellite Launch Vehicle (PSLV) of India with six strap-on rockets is shown in Fig. 2.12.



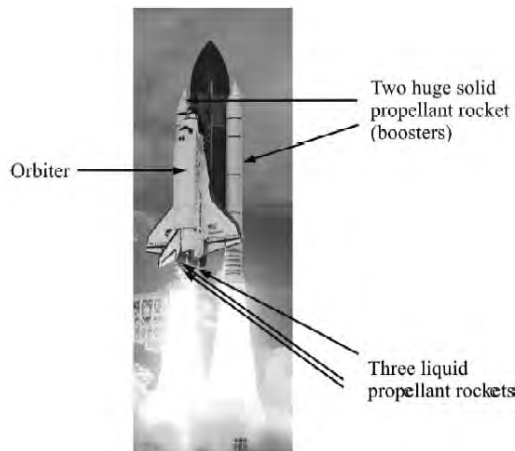
Strap-on  
rockets



Fig. 2.12 Polar Satellite Launch Vehicle  
[Source ISRO]

The space shuttle of USA has two huge strap-on rockets as shown in Fig. 2.13. The core rocket consists of a cluster of three rockets inside the orbiter.

Figure 2.14 shows four rockets clustered around a core in the Geo-synchronous Launch Vehicle (GSLV). The Ariane V satellite launch vehicle having two stages and two strap-on rockets is shown in Fig. 2.15.



**Fig. 2.13** Space Shuttle  
[Source NASA]



**Fig. 2.14** GSLV having a Cluster of Four Rockets Around the Core Booster  
[Source ISRO]

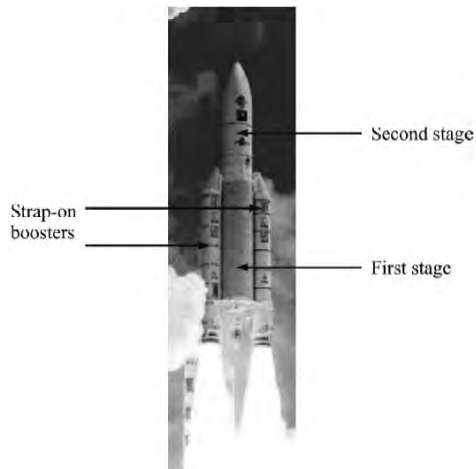


**Fig. 2.15** Ariane V Launch Vehicle  
[Source ESA]



## 2.10 CLASSIFICATION OF ROCKETS

Rockets are classified according to the medium or material (propellant) used for generating the impulse. If a cold gas is used as the propellant, the rocket is known as cold-gas rocket. If water is used as the propellant, it is called a water rocket. If positively charged particles, viz., ions are used, the rocket is called an ion rocket.

A high value of the efflux velocity,  $V_J$ , was seen as desirable to impart the necessary velocity to the rocket. The enthalpy of the gas, used for the propellant, is increased by heating it to high



temperatures in order to get high values of  $V_J$  in a rocket. Heating could be done by chemical reactions (combustion) or by electrical heating or solar heating. Accordingly, the rockets are defined as chemical rockets, electro-thermal rockets and solar rockets respectively. Nuclear energy with fission or fusion reactions or radioactive isotope decay can also be used for heating of the gas in which case the rocket is called a nuclear rocket.

Chemical rockets are most extensively applied for space transportation, launching satellites into the desired orbits and for missile propulsion. The gases, generated from combustion, are expelled at high jet velocities. Chemical rockets need to carry oxygen or oxidiser for the combustion of the fuels. When the fuel and oxidiser are stored in the rocket in the solid phase and burnt, the rocket is called a solid propellant rocket. Liquid propellant rockets use liquid fuels and liquid oxidisers to generate hot combustion gases. In hybrid rockets, the fuel and oxidiser are in different phases.

The word thruster is often used to describe a rocket when the thrust of the rocket is small. For example, a rocket in which the ions are pushed out at high velocities using an electric field is termed as electro-static thruster. Similarly, when electromagnetic forces are used for accelerating the ions, the rocket is termed as electromagnetic thruster. Considerable developments have taken place in electrical thrusters and these are increasingly being applied for spacecraft propulsion.

A high energy beam of laser or microwave radiation from the Sun could also be used to generate the impulse by impinging on an object and moving it. This procedure is termed as beamed propulsion. Photons from the Sun or elsewhere in space can be similarly employed to strike against a huge sail carried in a rocket to generate an impulse.

Any source or mechanism which can generate an impulse can be used for rockets. New methods for achieving very high velocities are being hypothesized by modifying the space and time about a space capsule (viz., shrinking space-time of the dark matter in the universe ahead of space capsule and stretching it behind with the spaceship being contained as it were in a bubble between expanding and shrinking space-time dimensions).

## SOLVED EXAMPLES

### Example 2.1 Water rocket:

A small water rocket is made by pressurising a plastic bottle partially filled with water using compressed air at 0.35 MPa at the ambient temperature and releasing the pressurised water through a vent (Fig. 2.16). The mass of water in the rocket is 0.5 kg. The mass of the empty bottle, which constitutes the mass of the structure and inert components of the rocket, is 0.15 kg. If the useful payload is zero and the ambient pressure is 0.1 MPa, determine the vent diameter required for vertical take off with an initial acceleration of 0.5 g. Neglect the pressure from the height of water in the bottle.

**Solution:** Total take off mass of the rocket

$$= 0.15 + 0.5 = 0.65 \text{ kg}$$

Acceleration at the time of take off = 0.5 g

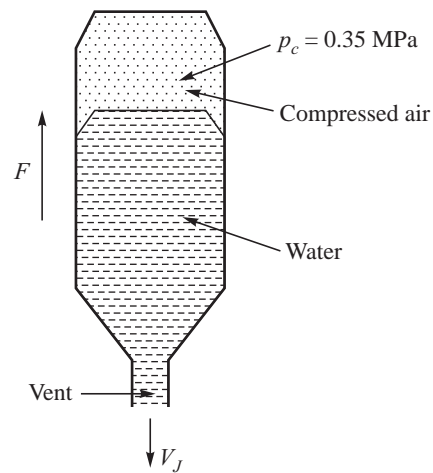


Fig. 2.16 Water Rocket



Thrust at the time of take off

$$\begin{aligned} &= \text{mass} \times \text{acceleration} = 0.65 \times (0.5 g + g) \\ &= 0.65 \times 1.5 \times 9.81 = 9.565 \text{ N} \end{aligned}$$

Thrust is  $F = \dot{m} V_J$ . The pressure of water at the exit of the vent equals the ambient pressure.

But  $\dot{m} = A\rho V_J$ , where  $A$  is the vent area,  $\rho$  is the density of water.

$$F = A\rho V_J^2 = 9.565 \text{ N}$$

In order to determine  $V_J$ , we solve the Bernoulli's equation connecting the pressure and velocity heads, viz.,

$$\frac{p_1}{\rho} + \frac{V_1^2}{2} = \frac{p_2}{\rho} + \frac{V_J^2}{2}$$

Here,  $p_1$  and  $V_1$  denote the pressure and velocity of water in the bottle;  $p_2$  denotes the exit pressure which is same as the ambient pressure. The velocity,  $V_1$ , is small in comparison with the exit velocity,  $V_J$ , and can be neglected. The exit velocity,  $V_J$ , is therefore given by:

$$V_J = \sqrt{\frac{2(p_1 - p_2)}{\rho}} = \sqrt{\frac{2 \times (0.35 - 0.1) \times 10^6}{1000}} = 22.36 \text{ m/s}$$

The density of water is taken as  $1,000 \text{ kg/m}^3$ . Substituting the velocity,  $V_J$ , in the expression for thrust, we get the vent area as:

$$A = \frac{9.565}{1000 \times 22.36^2} = 1.912 \times 10^{-5} \text{ m}^2$$

The vent diameter,  $d$ , is therefore given by:

$$\frac{\pi}{4} d^2 = 1.912 \times 10^{-5} \text{ or } d = 4.935 \times 10^{-3} \text{ m}$$

Vent diameter = 4.9 mm.

### **Example 2.2** Propulsive efficiency:

A rocket used in a satellite launch vehicle increases the velocity of the vehicle from 2,000 m/s to 4,000 m/s. If the efflux velocity of the rocket is constant at 3,000 m/s, determine the propulsive efficiency at the start and end of its operation.

**Solution:** The propulsive efficiency was derived as the ratio of the vehicle power to the power input

to the vehicle and was given by  $\eta_p = \frac{2 \frac{V}{V_J}}{1 + \left( \frac{V}{V_J} \right)^2}$ . Substituting the initial and final velocities as 2,000

and 4,000 m/s and  $V_J = 3,000 \text{ m/s}$ ,  $\eta_p$  at the beginning and end of the stage operation is 0.923 and 0.96 respectively. The propulsive efficiency of the rocket is continuously varying since the residual kinetic energy in the exhaust jet is changing as the rocket velocity changes. It is difficult to describe the performance of a rapidly accelerating rocket in terms of propulsive efficiency. However, a strategy



to achieve maximum propulsive efficiency would be to properly manage the residual kinetic energy of the jet. This has been considered and schemes have been suggested for continually varying the jet velocity. These are somewhat difficult to implement in practice.

In the case of low thrust electrical rockets, whose performance is governed by the power that could be stored in the power system (Chapter 10), varying jet velocities could be incorporated by controlling the power dissipated to generate thrust.

**Example 2.3** Impulse, specific impulse:

The following data is given for a rocket:

Thrust: 9000 kN

Total propellant used: 45,000 kg

Duration of firing of the rocket: 15 s

Assuming constant consumption rate of the propellant and constant thrust, determine the following parameters:

- (a) Impulse provided by the rocket
- (b) Specific impulse of the rocket
- (c) Effective jet velocity.

**Solution:** (a) Impulse ( $I$ ) = Thrust ( $F$ ) × duration ( $t$ ) = 1,35,000 kN-s

$$(b) \text{ Specific impulse } (I_{sp}) = \frac{I}{M_p} = \frac{1,35,000}{45,000} = 3 \text{ kN/kg/s or } 3000 \text{ N/kg/s} (= \text{Ns/kg})$$

$$(c) \text{ Effective jet velocity } (V_J) = I_{sp} = 3,000 \text{ m/s}$$

**Example 2.4** Stage mass ratios, ideal velocities and acceleration:

A four stage rocket is used to put up a satellite of 40 kg mass in a Low Earth Orbit (LEO). The approximate values of mass of the propellant, mass of structure and jet velocity for each stage are given below:

STAGE	I	II	III	IV
Mass of Propellant, (kg)	9,000	3,500	1,700	260
Mass of structure including inerts, (kg)	1,500	550	250	40
$V_J$ , (m/s)	2,200	2,400	2,500	2,750

**Determine:**

- (a) The payload mass fraction of the total rocket (Satellite launch vehicle).
- (b) Structural mass fraction of each stage.
- (c) The ideal  $\Delta V$  provided by each stage and the total  $\Delta V$ .
- (d) If the first stage fires for a period of 50 seconds and the rate of mass depletion can be assumed to be constant, what would be the acceleration of the rocket at take off?

**Soltution:** (a) Payload mass fraction of the satellite launch vehicle

$$= \frac{40}{(9000 + 3500 + 1700 + 260) + (1500 + 550 + 250 + 40) + 40} = \frac{40}{16840} = 2.37 \times 10^{-3}$$



(b) Structural mass fractions:

$$\text{First stage: } \frac{1500}{1500 + 9000} = 0.143$$

$$\text{Second stage: } \frac{550}{550 + 3500} = 0.136$$

$$\text{Third stage: } \frac{250}{250 + 1700} = 0.128$$

$$\text{Fourth stage: } \frac{40}{40 + 260} = 0.133$$

(c) Ideal  $\Delta V$  provided by each stage:

First stage:

$$2200 \ln \frac{(9000 + 3500 + 1700 + 260) + (1500 + 550 + 250 + 40) + 40}{(3500 + 1700 + 260) + (1500 + 550 + 250 + 40) + 40} = 1.682 \text{ km/s}$$

Second stage:

$$2400 \ln \frac{(3500 + 1700 + 260) + (550 + 250 + 40) + 40}{(1700 + 260) + (550 + 250 + 40) + 40} = 1.927 \text{ km/s}$$

Third stage:

$$2500 \ln \frac{(1700 + 260) + (250 + 40) + 40}{(260) + (250 + 40) + 40} = 3.39 \text{ km/s}$$

Fourth stage:

$$2750 \ln \frac{(260) + (40) + 40}{(40) + 40} = 3.979 \text{ km/s}$$

$$\text{Total } \Delta V = 1.682 + 1.927 + 3.39 + 3.979 = 10.978 \text{ km/s}$$

(d) Since the first stage fires for a period of 50 second and the rate of propellant mass depletion is constant, the mass flow rate of propellant

$$\dot{m} = \frac{\text{mass of propellant}}{\text{time}} = \frac{9,000}{50} = 180 \text{ kg/s.}$$

$$\text{Thrust, } F, \text{ of the stage} = \dot{m} V_J = 180 \times 2200 \text{ N}$$

$$\begin{aligned} \text{Total mass at lift off} &= M_i = (9000 + 3500 + 1700 + 260) + (1500 + 550 + 250 + 40) + 40 \\ &= 16,840 \text{ kg} \end{aligned}$$

$$\text{Initial acceleration} = \frac{F - M_i g}{M_i} = \frac{180 \times 2200 - 16840 \times 9.81}{16840} = 13.705 \text{ m/s}^2$$

In the above equation the gravitational field,  $g$ , is  $9.81 \text{ m/s}^2$ .

Hence, net take off acceleration is  $13.705 \text{ m/s}^2$  which is 1.4 times the gravitational field, i.e.  $1.4 \text{ g}$ .

**Example 2.5** Staging, clustering and acceleration:

Saturn V rocket, which launched the first men on the moon, is shown in Fig. 2.17(a) and is the largest rocket ever made. It consists of three stages as shown in Fig. 2.17(b). The first stage is a cluster of five rockets (known as F1) each rocket having a thrust of about 5 MN and a specific impulse of 2980 Ns/kg. The second stage is a cluster of five J2 rockets each with a thrust of 1 MN and specific impulse of 4130 Ns/kg. The third stage has one J2 rocket. If the first, second and third stages burn for a period of 150, 360 and 500 s respectively, determine the impulse provided by each stage of Saturn V and the total quantity of propellant carried in it.

If the total take off mass of Saturn V is  $2.5 \times 10^6$  kg, determine the acceleration at the time of take off.



**Fig. 2.17 (a)** Saturn V used for the Apollo Manned Moon Mission [Source NASA]

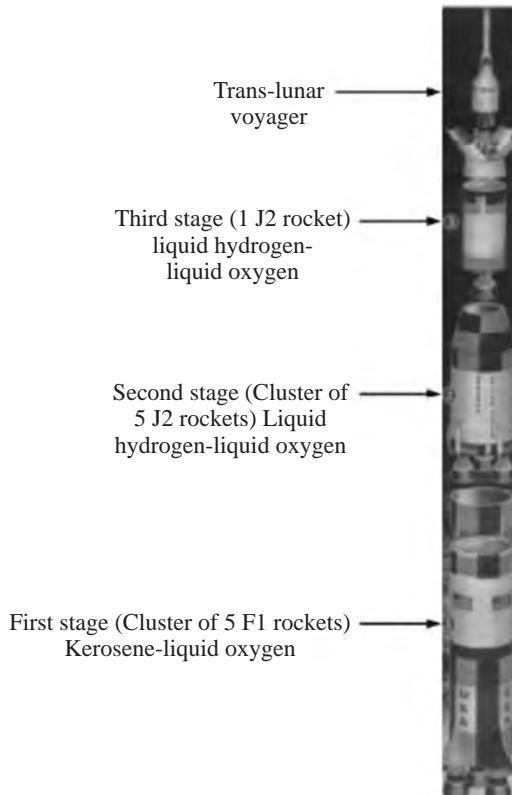


**Fig. 2.17 (b)** Schematic of Stages of Saturn V [Source NASA]

**Solution:** Impulse provided by the first stage consisting of five F1 rockets:

$$I_1 = 5 \times 5 \times 150 \text{ MN s} = 3750 \text{ MN s}$$



Impulse provided by the second stage consisting of five J2 rockets:

$$I_2 = 5 \times 1 \times 360 \text{ MN s} = 1800 \text{ MN s}$$

Impulse provided by the third stage having one J2 rocket:

$$I_3 = 1 \times 1 \times 500 \text{ MN s} = 500 \text{ MN s}$$

$$\text{Total thrust of first stage, } F_1 = 5 \times 5 \text{ MN} = 25 \text{ MN}$$

$$\text{Total thrust of second stage, } F_2 = 5 \times 1 \text{ MN} = 5 \text{ MN}$$

$$\text{Total thrust of third stage, } F_3 = 1 \text{ MN}$$

$$\text{Propellant carried} = \frac{\text{Impulse}}{\text{Specific impulse}}$$

$$\text{Propellant carried in first stage} = \frac{I_1}{I_{sp,1}} = \frac{3750 \times 10^6}{2980} \text{ kg} = 1.26 \times 10^6 \text{ kg}$$

$$\text{Propellant carried in second stage} = \frac{I_2}{I_{sp,2}} = \frac{1800 \times 10^6}{4130} \text{ kg} = 0.44 \times 10^6 \text{ kg}$$

$$\text{Propellant carried in third stage} = \frac{I_3}{I_{sp,3}} = \frac{500 \times 10^6}{4130} \text{ kg} = 0.12 \times 10^6 \text{ kg}$$

$$\text{Total propellant carried} = (1.26 + 0.44 + 0.12) \times 10^6 = 1.82 \times 10^6 \text{ kg}$$

Acceleration at the time of take off = [Thrust at lift off – (mass of rocket  $\times g$ )]/(mass of rocket)  
Here  $g$  is the gravitational field of the Earth.

$$\begin{aligned} \text{Acceleration at the time of take off} &= \frac{F_1 - 2.5 \times 10^6 \times g}{2.5 \times 10^6} \\ &= \frac{25 \times 10^6 - 2.5 \times 10^6 \times 9.81}{2.5 \times 10^6} = 0.19 \text{ m/s}^2 \end{aligned}$$

The acceleration with which the rocket takes off is  $0.19 \text{ m/s}^2$  or  $0.0194 \text{ g}$ .

**Example 2.6** Take off mass of a rocket and upper limit of velocity:

The residual mass of a rocket without payload and propellant is a fraction  $\Phi$  of the initial mass of the rocket including the propellant but without payload. It achieves a velocity  $V$  when all the propellant is consumed. If the payload mass of the rocket is  $M_U$  and the jet velocity of the rocket is  $V_J$ , determine the take off mass of the rocket in terms of parameters  $V$ ,  $V_J$ ,  $F$  and  $M_U$ .

What is the upper limit to the velocity that can be reached by this rocket?

**Solution:** Let the initial mass of the rocket at take off be  $M_i$  and the propellant mass be  $M_p$ . Let the final mass of the rocket be  $M_f$ . If the residual mass of the rocket without the propellant and payload is  $M_0$ , the equations for the initial and final mass are:

$$M_i = M_0 + M_p + M_U$$

$$M_f = M_0 + M_U$$



From rocket equation we have:

$$\frac{V}{V_J} = \ln \frac{M_f}{M_i}$$

Substituting the values of  $M_i$  and  $M_f$  and simplifying, we get:

$$e^{V/V_J} = \frac{M_0 + M_p + M_u}{M_0 + M_u} = M_i \left( \frac{1}{M_0 + M_u} \right)$$

This gives  $M_0 + M_u = M_i e^{-V/V_J}$

It is given that  $\frac{M_0}{M_0 + M_p} = \Phi$ , giving  $M_0 = \frac{\Phi M_p}{1 - \Phi}$ .

Substituting the above in the equation for  $M_0 + M_u$ , we get:

$$M_i e^{-V/V_J} = M_u + \frac{\Phi M_p}{1 - \Phi}$$

But  $M_p = M_i - M_f = M_i \left( 1 - \frac{M_f}{M_i} \right) = M_i (1 - e^{-V/V_J})$ . This gives:

$$M_i e^{-V/V_J} = M_u + \frac{M_i \Phi (1 - e^{-V/V_J})}{1 - \Phi}$$

Simplifying, we have:

$$M_i e^{-V/V_J} (1 - \Phi) = M_u (1 - \Phi) + M_i \Phi (1 - e^{-V/V_J})$$

The take off mass of the rocket is, therefore, given by:

$$M_i (e^{-V/V_J} - \Phi) = M_u (1 - \Phi)$$

$$M_i = M_u \frac{1 - \Phi}{e^{-V/V_J} - \Phi}$$

The upper limit of velocity  $V_{\max}$  is obtained when the payload mass is zero. This condition gives:

$$e^{-V_{\max}/V_J} - \Phi = 0$$

$$V_{\max} = V_J \ln \left( \frac{1}{\Phi} \right)$$

As an example, when the fraction  $\Phi$  is 0.12 and the jet velocity is 2 km/s, the upper limit of velocity of the rocket is  $2 \ln(1/0.12) = 4.24$  km/s.

## NOMENCLATURE

$A$  : Cross sectional area ( $\text{m}^2$ )

$F$  : Thrust (N)

$I$  : Impulse (Ns)



$I_{sp}$  : Specific Impulse (Ns/kg, m/s)  
 $M, m$  : Mass (kg)  
 $p$  : Pressure (Pa)  
 $R$  : Ratio  
 $t$  : Time  
 $V$  : Velocity of rocket (m/s)  
 $V_J$  : Jet (efflux) velocity (m/s)  
 $V_p$  : Volume of propellant ( $m^3$ )  
 $v_0$  : Relative velocity (m/s)  
 $x$  : Variable  
 $\alpha$  : Payload mass ratio  
 $\beta$  : Structural mass ratio  
 $\delta$  : Small quantity  
 $\Delta$  : Increment  
 $\gamma$  : Propellant mass ratio  
 $\eta_p$  : Propulsive efficiency defined by eq. 2.29  
 $\rho$  : Density ( $kg/m^3$ )

### Subscripts

$1, i$  : Initial  
 $2, f$  : Final  
 $1, 2, 3, \dots n$  : Number of stages  
 $J$  : Jet, efflux  
 $m$  : Mass  
 $p$  : Propellant

### Superscripts

$'$  : After one step  
 $''$  : After two steps  
 $'''$  : After three steps  
 $\cdot$  : Rate ( $d/dt$ )

## EXERCISES

1. A satellite in geo-stationary orbit about the Earth has a total dry mass of 1,800 kg. It is provided with rockets having a jet velocity of 3,100 m/s. After about 15 years in orbit when the life of the geo-stationary satellite is tending to be over, due to shortage of the propellant stored in it, it is proposed to push it out into deep space by escaping Earth's gravitational force. In this way the expired satellite will



be prevented from crowding the useful geo-stationary orbit. Assuming no attraction from Sun, moon and other planets, and that all the residual propellant in spacecraft is available for this last manoeuvre, determine the quantity of propellant. Do you suggest this as a feasible means of pushing the satellite out of the geostationary orbit?

2. Consider the launching a satellite from a jet aircraft at a height of 15 km above the Earth into a circular orbit at a height of 500 km above the Earth using a rocket. If the jet velocity of the rocket is 4,500 m/s and the mass of the satellite and the structural mass of the rocket including the inert, which gets into orbit, is 800 kg, determine the mass of propellant required.
3. The following data is reported for a rocket a few seconds after it leaves the launch pad: Thrust is 9 kN; Propellant consumption rate is 3,000 kg/s; Velocity of the rocket is 400 m/s. Calculate, at the particular instant of time for which the data is available:
  - (a) Jet velocity in m/s
  - (b) Propulsive efficiency of the rocket
4. A space mission performed by an electrical rocket requires an incremental velocity of 1.5 km/s. The mass of payload is 1,500 kg. If the efflux jet velocity of the propellant used is 18,000 m/s and the structural mass fraction of the vehicle is 0.2, estimate:
  - (a) The propellant mass required.
  - (b) The overall mass.
5. The attitude and orbit of a satellite are maintained using a number of small rockets housed in the satellite. The attitude and orbit corrections required during the lifetime of a satellite are estimated to be 950 m/s. If the jet velocity of the rocket is 2,500 m/s and the dry mass of the satellite (dry mass is the mass without the propellant being loaded in the satellite) is 800 kg, determine the mass of propellant required for the attitude and orbit corrections.
6. A Satellite Launch Vehicle is used for putting a satellite of mass 1,400 kg in orbit. The launch vehicle has four stages with six strap-on rockets for the first stage. The mass of the structure including inert, the mass of the propellant and the specific impulse of each stage and the strap-on can be assumed to be given by the following:

Stage	Mass of Structure and inert (kg)	Mass of Propellant (kg)	Specific Impulse (Ns/kg)
Strap-on	1,500	9,000	2,570
First stage	25,000	1,40,000	2,640
Second stage	8,200	40,000	2,920
Third stage	1,400	7,000	2,930
Fourth stage	2,200	1,200	3,040

Assume that the six strap-on rockets and the first stage fire together. The thrust of each strap-on rocket can be assumed as 640 kN while the thrust of the first stage is 4,800 kN.

Determine the following:

- (i) Payload fraction ( $\alpha$ ).
- (ii) Initial acceleration of the vehicle.
- (iii)  $\Delta V$  contributed by each stage and the total vehicle.

You can neglect the mass of the different inter-stages. State the assumptions made.

7. If two strap-on rockets and the first stage rocket in the above problem are ignited on the ground, determine the acceleration of the launch vehicle at take-off? What is the acceleration after ignition of the fourth



- stage rocket? The thrust developed by the fourth stage rocket is 14 kN. You can assume a constant value of acceleration field due to Earth's gravity of  $9.81 \text{ m/s}^2$ .
8. A single stage rocket is used as a sounding rocket to make measurements in the Earth's atmosphere. It carries sensors and electronic packages which can withstand a maximum acceleration of 10 g. It develops a constant thrust of 6 kN and has a total impulse of 90 kN-s. It is launched vertically. If the mass of the empty rocket is 40 kg, what is the payload that the sounding rocket can carry so that its acceleration does not exceed 10 g?
  9. A rocket of mass 1,000 kg contains 1,500 kg of propellant. The propellant is consumed at a constant rate of 100 kg/s. Find the acceleration of the rocket at lift-off, 10 s after lift-off and just before burn out. The specific impulse of the rocket is 1500 N-s/kg. Assume vertical flight and no variations in the gravitational field.

## References

1. Barrere, M., Jaumotte, A., Veubeke. B.J. and Vanderkerckhove, J., *Rocket Propulsion*, Amsterdam: Elsevier Publishing Company, 1960.
2. Blasingame, B.P., *Astronautics*, New York: McGraw Hill Book Company, 1973.
3. Colasurdo, G. and Casalino, L., *Energy Management in Rocket Propulsion*, J. Propulsion and Power, vol. 16, 2000, pp. 705-8.
4. Colasurdo, G., Pastrone, D. and Casalino, L., *Mixture Ratio Control to Improve Hydrogen Fuel Rocket Performance*, J. Spacecraft and Rockets, vol. 34, 1997, pp. 214-17.
5. King Jr., M.K., *Rocket Propulsion Strategy based on Kinetic Energy Management*, J. Propulsion and Power, vol. 14, 1998, pp. 270-73.
6. Kleppnar, D., and Kolenkow, R.J., *An Introduction to Mechanics*, New York: McGraw Hill Inc., 1973.
7. Tomita, N., Watanbe, R. and Nebylov, A., *Hands-on Education System Using Water Rocket*, Acta Astronautica, vol. 61, 2007, pp. 1116-20.
8. Sutton, G. P. and Biblarz, O., *Rocket Propulsion Elements*, 7th Ed., Wiley Interscience Publications, New York, 2001.
9. Verne, Jules, *20,000 Leagues Under the Sea*, Hayes Barton Press, 1955.

## Glossary

Booster rocket: High thrust rockets used in lower stages of launch vehicles

Cluster rocket: Assembly of several rockets to increase the thrust

Density specific impulse: Product of specific impulse and density of propellant

Incremental velocity: Increase of velocity of a rocket during its operation

Jet (efflux) velocity: Speed of the stream of working fluid leaving a rocket

Launch vehicle: A multistage rocket for putting up a payload in space

Mass ratio: The ratio of the mass left in the rocket after its operation is over to the initial mass of the rocket.

Multi-stage rocket: Several rockets one on top of the other and operated in sequence one after the other starting from the lowermost rocket.

Payload: The intended application that the rocket carries such as a satellite for a launch vehicle or a warhead for a missile

Payload mass fraction: Fraction of the mass of payload to the total initial mass of the rocket



Propellant mass fraction: Fraction of the mass of propellant used in a rocket to the total initial mass of the rocket

Propulsive efficiency: Efficiency of conversion of the kinetic energy of the efflux gases into useful work for moving the rocket

Specific impulse: Impulse generated per unit mass of propellant in a rocket

Structural mass fraction: Fraction of the mass of the structure of the rockets including the mass of the inert to the total mass of the rocket

Thruster: Rockets having small thrust

Velocity increment: Velocity provided by the rocket.

## Chapter 3

### Rocket Nozzle and Performance

*The Aelopile or “Hero’s engine” named after Aeolus, the Greek God of Wind, had two nozzles situated on opposite sides with steam escaping from them to generate impulse. It was invented by the Greek mathematician and scientist Hero of Alexandria in 200 BC.*



*The Aelopile*

The efflux of propellants from a rocket or the efflux of the products obtained by heating the propellants or burning the propellants provides the required impulse for the motion of the rocket. In a majority of rockets, gases, generated at high pressures from the burning of propellants or otherwise, are ejected out through a vent (opening) to give large values of efflux velocity ( $V_J$ ). The vent or opening is called the nozzle. The efflux of the gas from the nozzle is in the form of a jet and the efflux velocity,  $V_J$ , is spoken of as jet velocity. The performance of nozzles, the magnitudes of jet velocities and characteristics of the different nozzles are dealt with in this chapter.



### 3.1 EXPANSION OF GAS FROM A HIGH PRESSURE CHAMBER

Consider a gas stored in a chamber at pressure  $p_c$  and temperature  $T_c$  and expanded to a lower pressure  $p_e$  through a nozzle as shown in Fig. 3.1. The efflux velocity of the gases on expansion (exit jet velocity) is denoted by  $V_J$  in the figure. Let us assume that the stored gas pressure and temperature are held constant at all times in the chamber. The mass flow through the vent may, therefore, be assumed to be a constant.

If we are to focus our attention on the nozzle in Fig. 3.1, we find a steady mass flow rate enters it from the chamber at pressure  $p_c$  and temperature  $T_c$  and leaves at a lower pressure,  $p_e$ , corresponding to the exit conditions. Considering the nozzle as a control volume, as sketched in Fig. 3.2, we can express the rate of change of enthalpy, kinetic energy and gravitational potential energy between the outlet and the inlet of the control volume as equal to the difference between the rate of heat transfer to the control volume and the rate at which work,  $\dot{W}_e$ , if any, is done by the control volume. This gives the steady flow energy equation for the control volume as:

$$\frac{\dot{Q} - \dot{W}_e}{\dot{m}} = \left( h_e + \frac{V_J^2}{2} + gz_e \right) - \left( h_c + \frac{V_c^2}{2} + gz_c \right) \quad \dots(3.1)$$



**Fig. 3.1** Expansion of Gas through the Nozzle

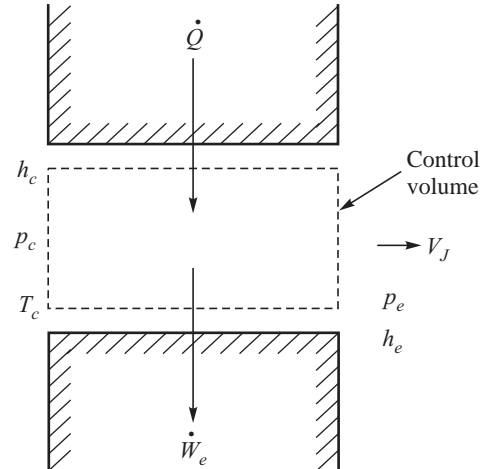


**Fig. 3.2** Control Volume

Here,  $\dot{m}$  is the mass flow rate through the nozzle;  $h_c$  and  $h_e$  are the specific enthalpy of the gas in the chamber and at the exit of the nozzle respectively, and  $z_c$  and  $z_e$  are heights above some datum at the entry and exit. If the nozzle is of fixed construction, the rate at which it does work,  $\dot{W}_e = 0$ . Considering no heat transfer, viz., an adiabatic vent, we have  $\dot{Q} = 0$ . Further, the change of the gravitational potential energy  $g(z_e - z_c)$  is small and could be assumed as negligible. The gas in the chamber could be considered to be stationary ( $V_c = 0$ ). Equation 3.1 for the control volume, therefore, becomes:

$$\frac{V_J^2}{2} = h_c - h_e \quad \dots(3.2)$$

If the gas temperature at the exit of the control volume is denoted by  $T_e$  and further the gas is assumed as a perfect gas, viz., the specific heats of the gas are constant and the gas obeys the ideal gas equation, then eq. 3.2 can be simplified to give:

$$V_J^2 = 2C_p(T_c - T_e)$$



$$= \frac{2\gamma R_0 T_c}{(\gamma - 1) \mathfrak{M}} \left( 1 - \frac{T_e}{T_c} \right) \quad \dots(3.3)$$

This is because the specific heat at constant pressure and at constant volume ( $C_p$  and  $C_v$ ) for a perfect gas are constant and are related by  $C_p - C_v = \frac{R_0}{\mathfrak{M}}$  giving  $C_p = \frac{\gamma R_0}{(\gamma - 1) \mathfrak{M}}$ , where  $R_0$  is the universal gas constant in kJ/(kmol K) [= 8.314 kJ/(kmol K)],  $\mathfrak{M}$  is the molecular mass of the gas in kg/kmol and  $\gamma$  is the specific heat ratio. The units for specific heat in the above is kJ/(kg K).

Considering the expansion of gas in the nozzle to be isentropic, i.e.  $p/p^\gamma = \text{constant}$ , we have:

$$\frac{T_e}{T_c} = \left( \frac{p_e}{p_c} \right)^{(\gamma-1)/\gamma}$$

This gives  $V_J$  as:

$$V_J = \sqrt{\frac{2\gamma R_0 T_c}{(\gamma - 1) \mathfrak{M}} [1 - (p_e/p_c)^{(\gamma-1)/\gamma}]} \quad \dots(3.4)$$

From the above expression, it is seen that to get a high value of  $V_J$ , the quantities  $T_c$  and  $p_c$  must be large while  $\mathfrak{M}$  and  $p_e$  must be small. This implies that propellants which can provide high temperature gases with low molecular mass are required in order to obtain high values of the jet velocity (and hence specific impulse  $I_{sp}$ ). Further, the combustion should take place at high pressures and the gases need to be expanded to low pressures. A low value of the specific heat ratio,  $\gamma$ , is also seen to be desirable.

The variation of  $V_J$  with  $T_c$ ,  $\mathfrak{M}$  and  $\gamma$  at different values of  $p_e/p_c$  is shown in Figs. 3.3, 3.4 and 3.5. Changes in  $T_c$  and  $\mathfrak{M}$  are seen to have a more significant influence at smaller values of  $p_e/p_c$  (i.e. higher expansion) than at larger values of  $p_e/p_c$ . However, a higher expansion (corresponding to small

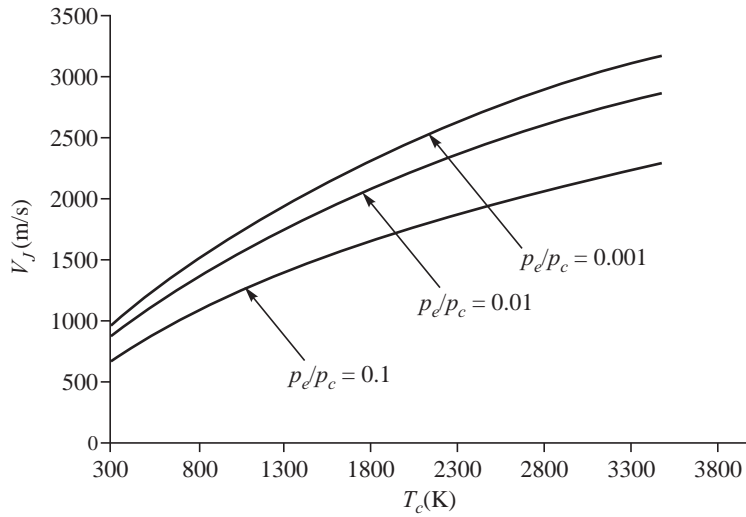


**Fig. 3.3** Variation of  $V_J$  with  $T_c$  for Different  $p_e/p_c$  at  $\gamma = 1.3$  and  $\mathfrak{M} = 20$  kg/kmol



values of  $p_e/p_c$ ) is not seen to give a significant increase of  $V_J$  at the smaller values of  $T_c$  (Fig. 3.3). Changes in  $\gamma$  are seen to be influential only for higher expansion (smaller values of  $p_e/p_c$ ) (see Fig. 3.5).

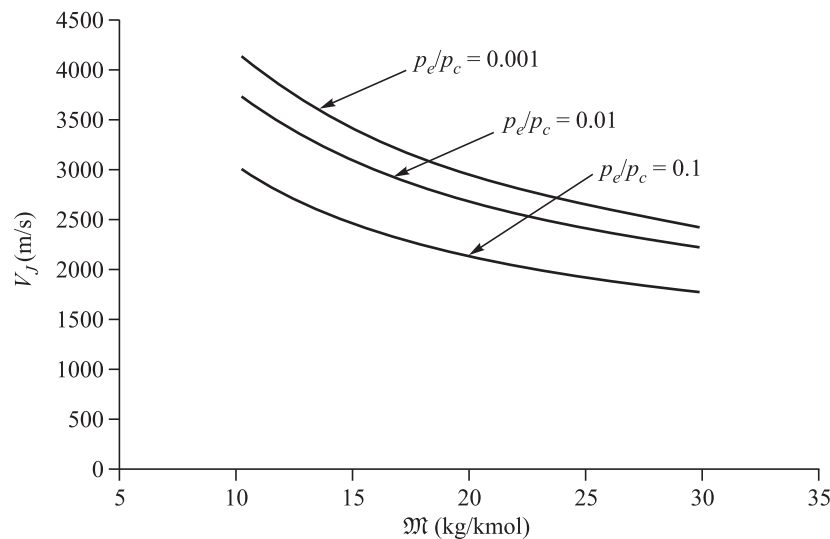


**Fig. 3.4** Variation of  $V_J$  with Molecular Mass for Different  $p_e/p_c$  with  $\gamma = 1.3$  and  $T_c = 3,000$  K

When a cold gas is used for the expansion in the nozzle (*i.e.*  $T_c$  is small) no significant improvement in  $V_J$  is obtained by decreasing the value of  $p_e/p_c$  or equivalently increasing the pressure  $p_c$  (Fig. 3.3). Helium and hydrogen with small values of molecular mass  $M$  give higher values of  $V_J$  and would, therefore, be the desirable cold gases for use. Hydrogen, however, is very reactive and needs to be used with caution. Helium is preferable; the higher value of its specific heat ratio,  $\gamma$ , does not impose a significant loss in  $V_J$  at the values of  $p_e/p_c$  at which these cold gas rockets are used.

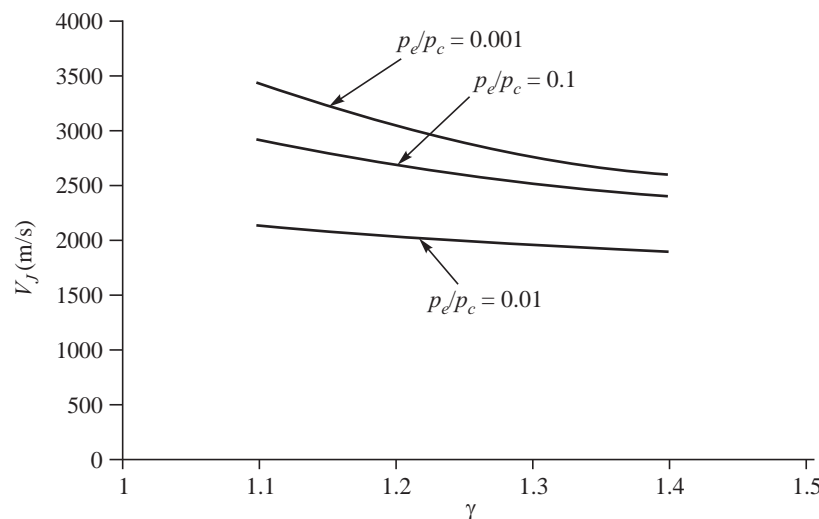


**Fig. 3.5** Variation of  $V_J$  with  $\gamma$  for Different  $p_e/p_c$  with  $T_c = 3,000$  K and  $M = 20$  kg/kmole



## 3.2 SHAPE OF THE NOZZLE

The exhaust velocity  $V_J$  in the nozzle is strongly influenced by its internal configuration and size. In order to determine the shape of the nozzle which would provide high values of  $V_J$ , we consider gas flow over a small area change from  $A$  to  $A + dA$  in the direction of flow over a distance  $\delta x$  from  $x$  to  $x + \delta x$ . This is shown in Fig. 3.6. The pressure ( $p$ ), velocity ( $V$ ) and density ( $\rho$ ) change by small quantities  $dp$ ,  $dV$  and  $d\rho$  during the progress of flow over the distance  $\delta x$  (Fig. 3.6). Considering the flow to be steady and along the  $x$ -axis, the mass and momentum conservation equations are:

$$\dot{m} = \rho A V = \text{constant} \quad \dots(3.5)$$

$$dp + \rho V dV = 0 \quad \dots(3.6)$$

Differentiating the mass conservation relation given in eq. 3.5, we obtain:

$$\frac{d\rho}{\rho} + \frac{dA}{A} + \frac{dV}{V} = 0 \quad \dots(3.7)$$

where  $dA$  is the small change in area of the nozzle as the density and velocity change by  $d\rho$  and  $dV$  respectively.

The variation of velocity with area is of interest for which the term  $d\rho/\rho$  in eq. 3.7 is to be expressed as a function of  $dV/V$ . For this purpose, a relationship between pressure and density is introduced through the velocity of sound  $a$ . A sound wave propagating in a medium causes small perturbations in pressure, density and particle velocity. If the perturbations are represented as  $dp$ ,  $d\rho$  and  $dV$  respectively (Fig. 3.7), we have by considering a frame of reference in which the sound wave is at rest (Fig. 3.8), the mass balance as:

$$Apa = A(\rho + d\rho)(a + dV)$$

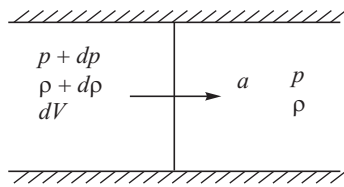


**Fig. 3.7** Propagation of Sound Wave at Velocity  $a$  in a Medium

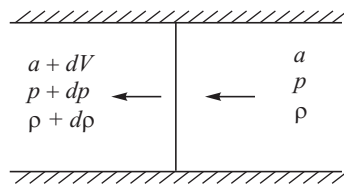


**Fig. 3.8** Properties in Frame of Reference with Sound Wave at Rest

For small values of  $d\rho$  and  $dV$ , the above equation becomes:

$$dV = -a \frac{dp}{\rho} \quad \dots(3.8)$$



The momentum balance (Fig. 3.8) is:

$$dp = -\rho adV \quad \dots(3.9)$$

Combining eqs. 3.8 and 3.9, we get:

$$\frac{dp}{\rho} = a^2 \quad \dots(3.10)$$

Substituting the value of  $dp = a^2 dp$  from the above relation in eq. 3.6 gives:

$$\frac{dp}{\rho} = -\frac{VdV}{a^2} \quad \dots(3.11)$$

Replacing the value of  $\frac{dp}{\rho}$  in eq. 3.7 with the above, we get:

$$-\frac{VdV}{a^2} + \frac{dV}{V} + \frac{dA}{A} = 0 \quad \dots(3.12)$$

which, on simplification yields:

$$\frac{dA}{A} = -\left(1 - \frac{V^2}{a^2}\right) \frac{dV}{V} \quad \dots(3.13)$$

The ratio of the flow velocity to the sound speed  $V/a$  is the Mach number ( $M$ ). The variation of velocity with the area of the nozzle from eq. 3.13 is, therefore:

$$\frac{dV}{V} = -\frac{1}{1-M^2} \frac{dA}{A} \quad \dots(3.14)$$

The above equation shows that for Mach number less than unity, a decrease of the area along the length of the nozzle brings about an increase of velocity. If the Mach number  $M > 1$ , the opposite trend is seen and the area needs to be increased to bring about an increase of the velocity. For  $M = 1$ , the change of area  $dA$  has to be zero for eq. 3.14 to hold and for a meaningful flow to take place.

The above discussions show that if large values of velocities corresponding to  $M \gg 1$  are to be provided by a nozzle, it is necessary to shape it to be initially convergent at the end of which the velocities increase to  $M = 1$ . A constant cross-sectional area is, thereafter, required to have a velocity corresponding to  $M = 1$ . This is to be followed by a diverging section in which the velocity continues to increase for  $M > 1$  as per eq. 3.14.

The minimum area between the convergent and divergent portion at which  $M = 1$  is called the throat. A sketch of the changes in  $dV/V$  as given by eq. 3.14 with changes in area along the length of a convergent divergent nozzle is shown in Fig. 3.9. When  $M = 1$  at the throat,  $dV/V$  increases along the length of the nozzle in both the convergent and divergent portions. However, when  $M < 1$  at the throat, say due to a smaller flow rate, the increasing trend of  $dV/V$  in the convergent portion gets arrested at the throat and begins to decrease after the throat as per eq. 3.14.

The variation of velocity,  $V$ , based on the value of  $dV/V$  determined above is shown in Fig. 3.9. The velocity progressively increases along the length when  $M = 1$  at throat. However, for  $M < 1$  at the throat, velocity decreases along the length of the nozzle in the divergent portion. While the convergent portion accelerates the flow, the divergent part acts as a diffuser.

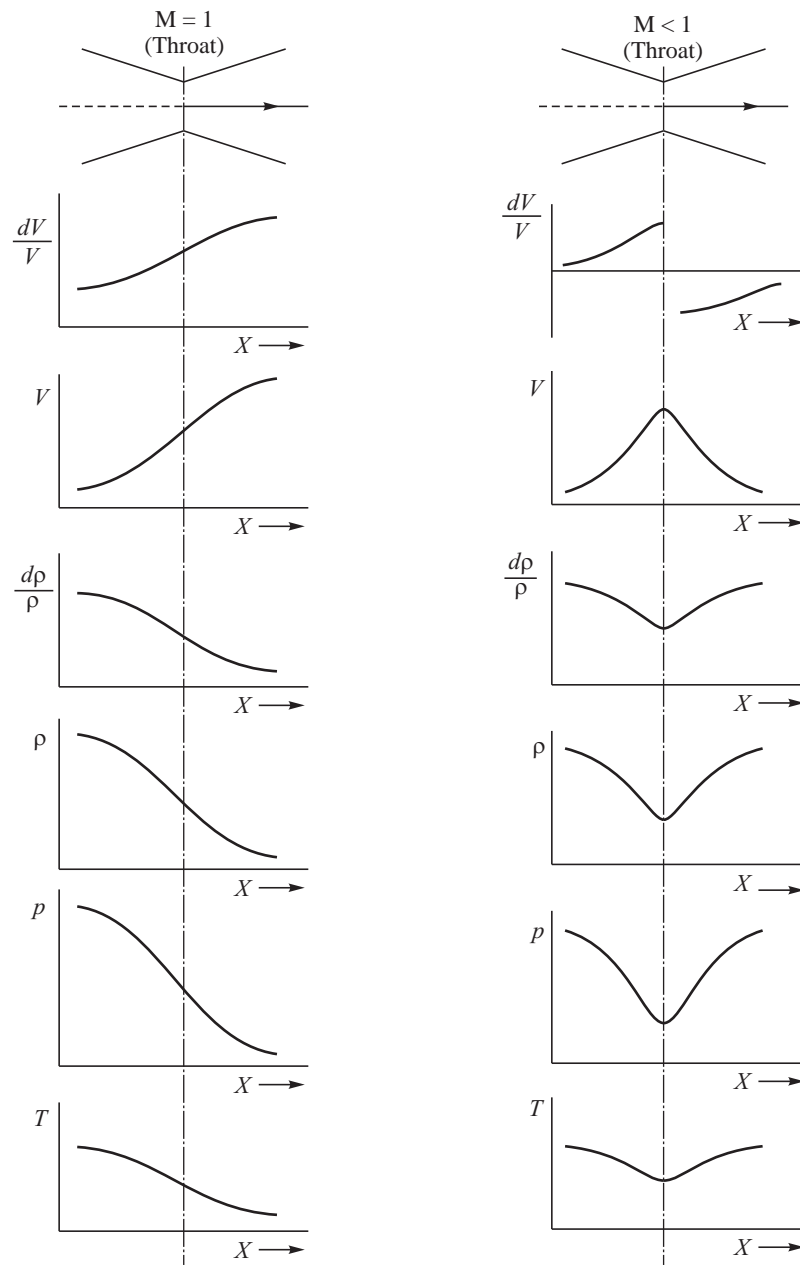


**Fig. 3.9** Variations in Velocity, Density, Pressure and Temperature Along the Nozzle

The observed variations in  $dV/V$  can be used in eq. 3.7 to give the variations of  $dp/\rho$ . From eq. 3.7,  $\frac{dp}{\rho} = - \left( \frac{dA}{A} + \frac{dV}{V} \right)$ . In the convergent portion,  $dA/A$  is negative. The value of  $dV/V$  from eq. 3.14 is positive for  $M < 1$  and further  $\left| \frac{dV}{V} \right| > \left| \frac{dA}{A} \right|$ . The value of  $dp/\rho$ , therefore, would decrease slowly in the convergent portion.



When  $M = 1$  at the throat for which  $M > 1$  in the divergent,  $dV/V$  increases with  $dA/A$  in the diverging portion. The value of  $d\rho/\rho$  will, therefore, continue to decrease in the diverging portion of the nozzle. The variation of  $\rho$  at the throat region would be very steep since  $M \approx 1$ . If, however,  $M < 1$  at the throat, the decrease in  $dV/V$  in the divergent portion will result in an increase in  $d\rho/\rho$ . The density initially decreases up to the throat and increases thereafter in the divergent portion as shown in Fig. 3.9.

The variation in pressure is determined from the density variations using the isentropic expansion process given by  $p/\rho^\gamma = \text{constant}$ . The change in pressure follows the same trend as the density as is seen in Fig. 3.9. The temperature variations along the nozzle can be determined from the isentropic expansion process which gives  $T/(p)^{\gamma-1/\gamma} = \text{constant}$  and gives the same trend as the pressure variations. This is seen in the last set of sketches in Fig. 3.9.

The variations of the sound speed along the length of a convergent-divergent nozzle could be estimated from the temperature variations. Equation 3.10 gave the value of speed of sound as  $dp/d\rho = a^2$ . For the isentropic process under consideration, we have  $p/\rho^\gamma = \text{constant}$ . The value of  $a^2$  is, therefore, given by:

$$\frac{dp}{d\rho} = \frac{\gamma p}{\rho} = \gamma RT = a^2 \quad \dots(3.15)$$

The speed of sound, therefore, varies as  $T^{1/2}$ . It decreases continuously along the length of the nozzle as shown in Fig. 3.10, when  $M = 1$  at the throat. The decrease in the sound velocity will lead to a relatively higher rate of increase of the Mach number as compared to the increase of velocity. This is seen in the region A in Fig. 3.10.

The variations of the speed of sound and Mach number along the length of the nozzle for the case of  $M < 1$  at the throat are also shown in Fig. 3.10. The speed of sound decreases in the convergent portion and increases in the divergent portion, whereas the Mach number increases in the convergent section and decreases in the divergent section. The convergent part accelerates the flow while the divergent part diffuses the flow.

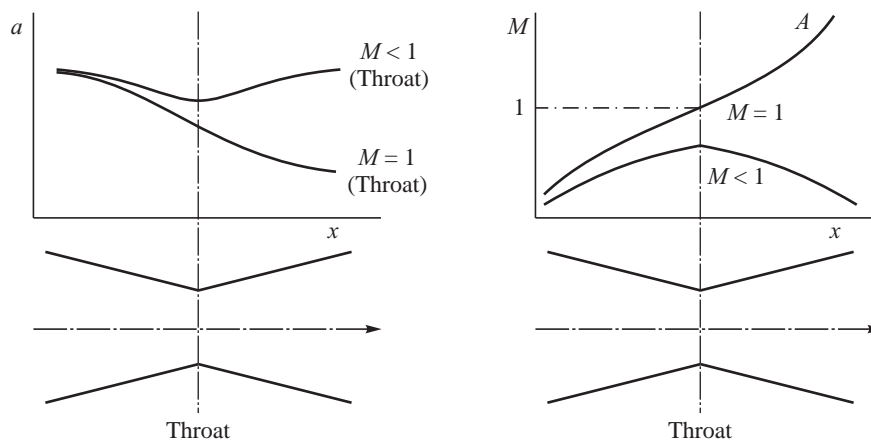


**Fig. 3.10** Variation of Speed of Sound and Mach Number Along the Length of the Nozzle

Convergent-divergent nozzles are used in rockets with  $M = 1$  at the throat in order to accelerate the flow in the divergent portion and achieve high supersonic values of velocity  $V_J$ . The convergent-divergent nozzles are also known as de Laval nozzles. The convergent and divergent portions are



either conical or bell-shaped. It must be remembered that the mass flow rate through the nozzle or equivalently, the temperature and pressure at which the gas is supplied to the nozzle should be such that the Mach number of unity is obtained at the throat. If the mass flow rate gives a Mach number at the throat to be less than 1, the velocity of the gas in the divergent section will be subsonic and would decrease along the length of the nozzle leading to small values of  $V_J$ .

### 3.2.1 Choking of Nozzle

Figure 3.11 shows the variation of mass flow rate ( $\dot{m}$ ) through the nozzle as the pressure downstream ( $p_e$ ) of the nozzle is changed for a given value of chamber pressure and temperature. The mass flow rate ( $\dot{m}$ ) is seen to increase progressively as the nozzle exit pressure ( $p_e$ ) is reduced due to the higher available pressure drop. However, after the velocity has increased to give a Mach number of 1 at the throat, any further decrease of  $p_e$  does not give an increase of  $\dot{m}$ .  $\dot{m}$  remains at the same value as  $p_e$  is further reduced. When the flow through the nozzle reaches a maximum limit, the nozzle is said to be choked. The onset of choking is shown by the dotted line in Fig. 3.11.

Under choked condition, the requirement of additional mass flow rate due to the further decrease in  $p_e$  cannot be communicated to the chamber. In general, pressure waves travelling at the rate of sound velocity communicate the requirement of additional mass flow rate. However, if the flow velocity at the throat equals the sound velocity ( $M = 1$ ), the disturbances (pressure waves) travelling at speed of sound fail to reach the chamber.  $M = 1$  at the throat essentially isolates the downstream portion of the nozzle (divergent) from the upstream convergent portion.

The choking of nozzles places an upper limit of on the maximum possible mass flow rates through the nozzle. Since rockets are configured for achieving maximum jet velocities, the flow through the nozzle is always designed to be choked.



## 3.3 NOZZLE AREA RATIO

The nozzle area ratio ( $\epsilon$ ) is defined as the ratio of the exit area of the nozzle to the throat area ( $\epsilon = A_e/A_t$ , where  $A_e$  = exit area and  $A_t$  = throat area). It depends mainly on the pressure expansion ratio  $p_c/p_e$ . The convergent part of the nozzle ensures a Mach number of unity at the throat and further increase of velocity takes place in the divergent between the throat and the exit. As the ambient pressure ( $p_a$ ) is reduced, as happens at higher altitudes, the pressure ratio ( $p_c/p_e$ ) increases calling for larger values of area ratio ( $\epsilon$ ).

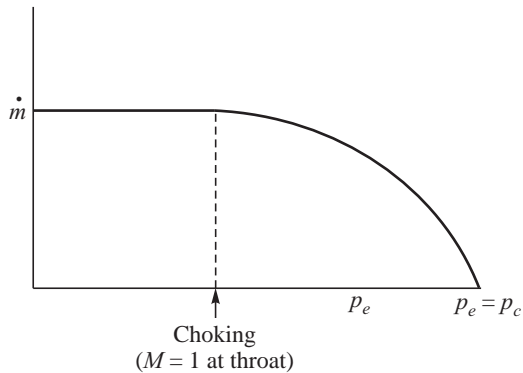


**Fig. 3.11** Choking of Nozzle at Low Backpressures

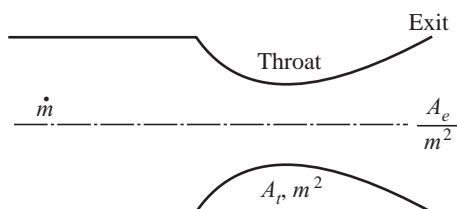


**Fig. 3.12** Convergent Divergent Nozzle



Consider a steady one dimensional mass flow rate  $\dot{m}$  through a nozzle having throat area  $A_t$  and exit area  $A_e$  as shown in Fig. 3.12. The flow rate is given by:

$$\dot{m} = \rho_t A_t V_t = \rho_e A_e V_e \quad \dots(3.16)$$

Here the subscripts  $t$  and  $e$  denote the conditions at the throat and exit respectively. From this equation, we get:

$$\epsilon = \frac{A_e}{A_t} = \frac{\rho_t}{\rho_e} \frac{V_t}{V_e} \quad \dots(3.17)$$

The velocity at the throat  $V_t$  is sonic since the convergent-divergent nozzle for a rocket is always designed for choked flow conditions. If the Mach number at the exit is  $M_e$ , we have:

$$V_t = \sqrt{\gamma RT_t} \quad \dots(3.18)$$

and

$$V_e = M_e \sqrt{\gamma RT_e} \quad \dots(3.19)$$

Assuming the value of the specific heat ratio,  $\gamma$ , and the molecular mass of the gas  $\mathfrak{M}$  to be constant, and substituting eqs. 3.18 and 3.19 in eq. 3.17 and simplifying:

$$\epsilon = \frac{\rho_t}{\rho_e} \frac{1}{M_e} \sqrt{\frac{T_t}{T_e}} \quad \dots(3.20)$$

Using equation of state  $p = \rho RT$ , the above equation reduces to:

$$\epsilon = \frac{\rho_t}{\rho_e} \frac{1}{M_e} \sqrt{\frac{T_e}{T_t}} \quad \dots(3.21)$$

The velocity at the exit of the nozzle has already been calculated earlier (eq. 3.4) in terms of the nozzle exit pressure,  $p_e$ , as:

$$V_e = \sqrt{\frac{2\gamma}{\gamma-1} RT_c} \left[ 1 - \left( \frac{p_e}{p_c} \right)^{\frac{\gamma-1}{\gamma}} \right] \quad \dots(3.22)$$

Here  $R$ , the specific gas constant ( $R = R_0/\mathfrak{M}$ ), is used instead of  $R_0$ . Substituting  $M_e = V_e/a_e$ , where  $V_e$  is given by eq. 3.22 and  $a_e$  is the sound velocity at the exit given by  $\sqrt{\gamma RT_e}$ , in eq. 3.21:

$$\epsilon = \frac{\sqrt{\gamma RT_e}}{\sqrt{\frac{2\gamma}{\gamma-1} RT_c} \left[ 1 - \left( \frac{p_e}{p_c} \right)^{\frac{\gamma-1}{\gamma}} \right]} \frac{p_t}{p_e} \sqrt{\frac{T_e}{T_t}} = \frac{\frac{p_t}{p_c} \frac{p_c}{p_e} \sqrt{\frac{T_e}{T_c}} \sqrt{\frac{T_e}{T_c}} \sqrt{\frac{T_c}{T_t}}}{\sqrt{\frac{2}{\gamma-1} \left[ 1 - \left( \frac{p_e}{p_c} \right)^{\frac{\gamma-1}{\gamma}} \right]}} \quad \dots(3.23)$$

Since  $\frac{T_t}{T_c} = \frac{2}{\gamma+1}$ ,  $\frac{p_t}{p_c} = \left( \frac{2}{\gamma+1} \right)^{\frac{\gamma}{\gamma-1}}$  and  $\frac{T_e}{T_c} = \left( \frac{p_e}{p_c} \right)^{\frac{\gamma-1}{\gamma}}$  (see eq. 3.37 and eq. 3.38 derived subsequently), we get on substituting in eq. 3.23:

$$\epsilon = \frac{\left( \frac{2\gamma}{\gamma+1} \right)^{\frac{\gamma}{\gamma-1}} \left( \frac{p_c}{p_e} \right)^{1/\gamma} \left( \frac{2}{\gamma+1} \right)^{-1/2}}{\sqrt{\frac{2\gamma}{\gamma-1} \left( 1 - \left( \frac{p_e}{p_c} \right)^{\frac{\gamma-1}{\gamma}} \right) \left( \frac{\gamma+1}{\gamma-1} \right)}} \quad \dots(3.24)$$



On simplifying, we get:

$$\epsilon = \frac{\left(\frac{2}{\gamma+1}\right)^{\frac{1}{\gamma-1}} \left(\frac{p_c}{p_e}\right)^{\frac{1}{\gamma}}}{\sqrt{\frac{\gamma+1}{\gamma-1} \left[1 - \left(\frac{p_e}{p_c}\right)^{\frac{\gamma-1}{\gamma}}\right]}} \quad \dots(3.25)$$

The area ratio  $\epsilon$  is seen to be a function of  $\gamma$  in addition to the pressure ratio. The area ratio is plotted as a function of pressure ratio  $p_c/p_e$  for different values of  $\gamma$  in Figs. 3.13 (a) and (b) respectively. As the pressure ratio increases the area ratio increases. A larger area ratio is also seen necessary to give a specified value of the pressure ratio when the value of  $\gamma$  decreases.

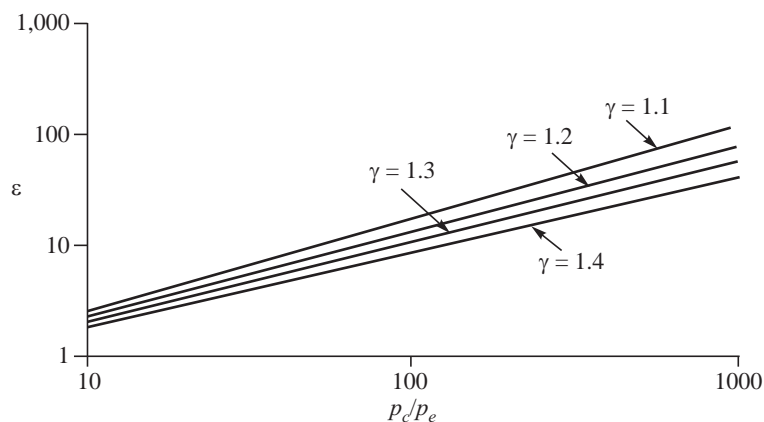


Fig. 3.13 (a) Area Ratio Variations with Pressure Ratios between 10 and 1000

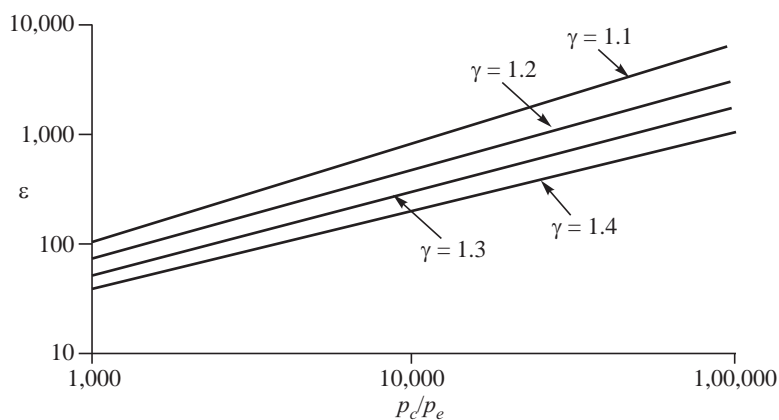


Fig. 3.13 (b) Area Ratio Variations with Pressure Ratios between 1,000 and 1,00,000

Rockets operate at varying altitudes and have area ratios between about 20 and 400. High values of the area ratios are very effective in enhancing the jet velocity and hence the specific impulse of a rocket. However, the area ratio needs to be properly matched to the ambient pressures at the operating altitudes.



### 3.4 PERFORMANCE LOSS IN A CONICAL NOZZLE

Figure 3.14 shows a nozzle having a conical divergent with a semi-divergence angle ( $\alpha/2$ ). The streams in the wall region would leave the nozzle at an angle  $\alpha$  to the axis of the nozzle, while the streams along the centre line leave the nozzle along the axis as shown. The average angle at which the overall stream leaves the nozzle is at an angle  $\alpha/2$  to the axis.

The thrust provided by the nozzle in the axial direction considering the average divergence of the streams to be  $\alpha/2$  is:

$$F = \left( \dot{m} \cos \frac{\alpha}{2} \right) \left( V_J \cos \frac{\alpha}{2} \right) \quad \dots(3.26)$$

$$= \dot{m} V_J \cos^2 \frac{\alpha}{2} \quad \dots(3.27)$$

There is a decrease of thrust from the value of  $\dot{m} V_J$  due to the divergence angle of the nozzle. The ratio of the actual thrust to the ideal thrust had all the streams left the nozzle in the axial direction is known as the divergence loss coefficient. The divergence loss coefficient  $\lambda$  is given by:

$$\lambda = \frac{\dot{m} V_J \cos^2 \frac{\alpha}{2}}{\dot{m} V_J} = \cos^2 \frac{\alpha}{2}$$

In terms of the semi-divergence angle of the nozzle, the coefficient can be written as:

$$\lambda = \frac{1 + \cos \alpha}{2} \quad \dots(3.28)$$

The fractional loss of thrust due to the above loss, denoted by  $\Delta$ , is given by:

$$\Delta = 1 - \lambda \quad \dots(3.29)$$

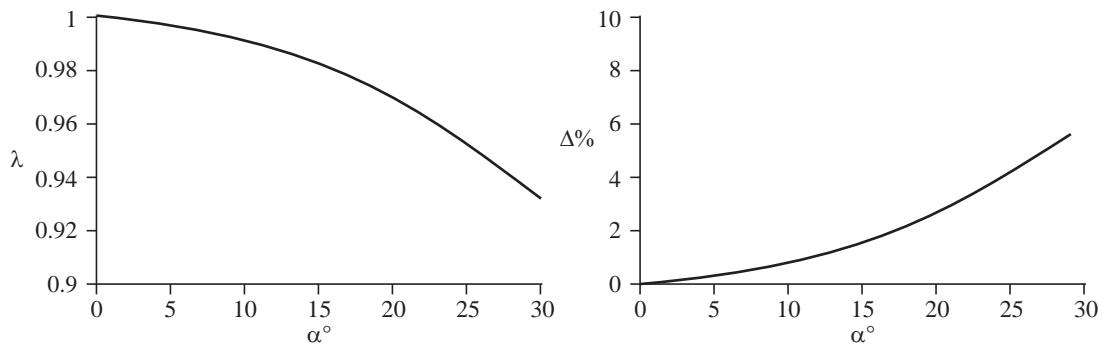


Fig. 3.14 Direction of Streams Leaving a Conical Nozzle

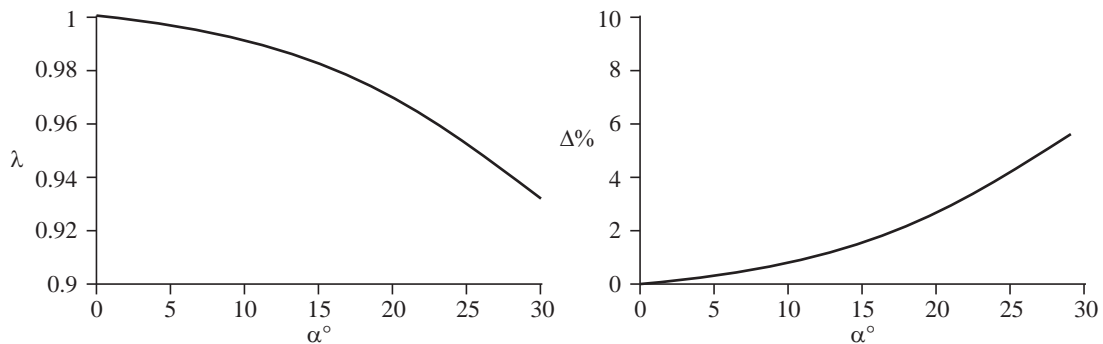


Fig. 3.15 Divergence Loss Coefficient and Fractional Loss of Thrust

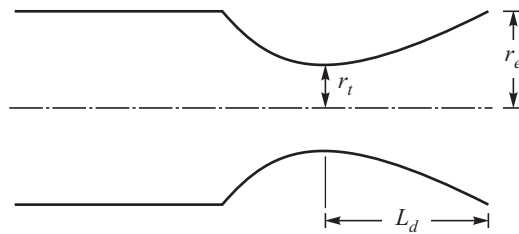


Figure 3.15 shows the variations in divergence loss coefficient  $\lambda$  and the percentage loss in thrust  $\Delta$  as the semi-divergence angles  $\alpha$  of the nozzle increases from 0 to 30°. It is seen that the loss in thrust increases significantly as  $\alpha$  increases. The loss is 6.7% when  $\alpha = 30^\circ$ . A smaller cone angle is, therefore, desirable for the nozzle divergent.

However, as the cone angle decreases, the length of the nozzle divergent part is enhanced for a given area ratio. The divergent length,  $L_d$ , in terms of the angle,  $\alpha$ , is given by (Fig. 3.16):

$$L_d = (r_e - r_t) \cot \alpha \quad \dots(3.30)$$

It is seen from eqs. 3.28, 3.29 and 3.30 that while a smaller divergence angle is preferable from the view of a reduced loss of thrust, the resulting longer nozzle will lead to a heavier mass of the nozzle. The latter would adversely influence the incremental velocity of the rocket. From eq. 3.30, we find that for  $\alpha = 5^\circ$ , the length of the divergent is about three times longer than for an angle of  $\alpha$  of 15°. A 20° nozzle gives a length which is 3/4th of the 15° nozzle (eqs. 3.28, 3.29). The loss in thrust of the 20° nozzle is about 1.75 times that of a 15° nozzle. Considering the disadvantages from the heavier mass with the smaller angles and the loss in thrust for the larger angles, the semidivergence angle for the conical nozzles is typically around 15°.



**Fig. 3.16** Conical Nozzle Divergent



### 3.5 FLOW SEPARATION IN NOZZLES

The exit pressure,  $p_e$ , in a nozzle depends on the area ratio  $\varepsilon$ . When the area ratio of a nozzle is such that pressure at the nozzle exit,  $p_e$ , is greater than the ambient pressure,  $p_a$ , the expansion process to the ambient pressure is incomplete. The nozzle is then said to be an under-expanded nozzle (Fig. 3.17). The opposite conditions prevail when the area ratio of the nozzle is larger than required giving  $p_e < p_a$ . The exit pressure is lower than the ambient pressure and the nozzle is said to be over-expanded. Figure 3.17 shows a schematic of under-expanded and over-expanded nozzles due to area ratio variations for a given chamber pressure and ambient pressure.

A rocket traverses different altitudes, and the ambient pressure decreases as the rocket moves away from the surface of the Earth. If the area ratio of the nozzle is designed for optimum conditions at a given altitude of operation (for which the ambient pressure is  $p_a$ ), it will be operating in an ‘underexpanded’ condition for altitudes higher than the design altitude ( $p_e > p_a$ ) whereas it will function as an ‘over-expanded’ nozzle for the lower altitudes ( $p_e < p_a$ ). Stated differently, if we have a nozzle of a given area ratio which gives a pressure at the nozzle exit of  $p_e$ , which corresponds to the ambient pressure,  $p_a$ , at altitude,  $h_1$ , the nozzle will be over-expanded for altitudes less than  $h_1$  and underexpanded for altitudes greater than  $h_1$  (Fig. 3.18). Because of the under-expansion at the higher altitudes, the momentum generating capacity of a given area ratio nozzle is lower at the higher altitudes than the one designed specifically for the particular altitude. The over-expansion at the lower altitudes also creates a problem and is examined below.

In an over-expanded nozzle, the pressure towards the exit of the nozzle falls below the ambient pressure. The flow within the nozzle divergent being supersonic, cannot sense the conditions ahead of it.

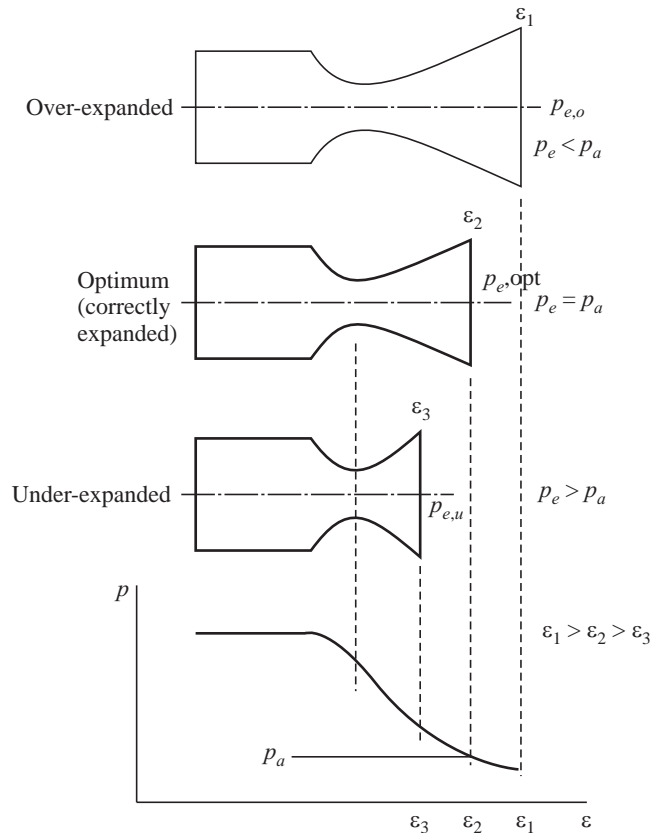


Fig. 3.17 Under-expanded and Over-expanded Nozzles

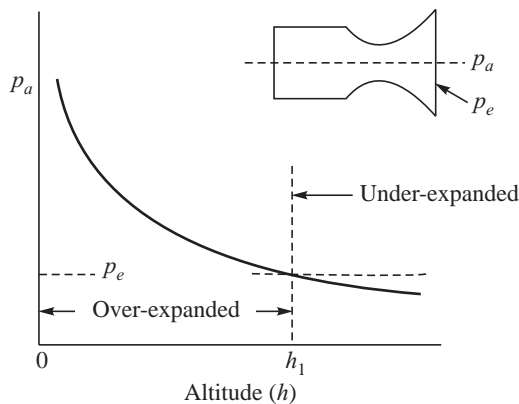


Fig. 3.18 Over-expanded and Under-expanded Nozzles at Different Altitudes

The flow, therefore, abruptly changes through a discontinuity (called shock) and becomes subsonic to match the ambient pressure. The process is shown in Fig. 3.19. A shock is formed at location A so that the pressure at the nozzle exit would be  $p_a$ . The bold line in Fig. 3.19 shows the variation of pressure in the nozzle due to the formation of shock at location A. However, if the exit pressure  $p_e$  is greater than the ambient pressure  $p_a$ , the pressure  $p$  in the nozzle would continue to decrease as indicated by the dotted line in Fig. 3.19.



The sudden compression by the shock and the adverse pressure gradient is associated with separation of flow from the walls. The zone of separation depends on the local pressure and the rate of acceleration and is influenced by the nozzle divergence. In an ideal case, the separated flow would be helpful as it provides higher pressure at the nozzle wall and, therefore, the nozzle can adapt to the altitude. The thrust from a nozzle with flow separation is more than the thrust corresponding to the same area ratio for which flow separation has not taken place. However, in practice, flow separation does not occur symmetrically along the circumference of the nozzle. This causes side forces which are undesirable. Flow separation, thus, has to be avoided.

The inertial forces available in the supersonic flow in the nozzle divergent delay the process of flow separation to pressures much below the ambient pressure. Experiments in conical nozzles have shown the flow to separate at the location where the nozzle pressure ( $p$ ) equals to  $0.4 p_a$ . Denoting the nozzle pressure corresponding to flow separation as  $p_n$ , the criterion  $p_n = 0.4 p_a$  is known as Summerfield criterion for the onset of flow separation. Based on detailed experiments, the criterion for flow separation is seen to additionally depend on the local value of Mach number  $M_e$  and is given as follows:

$$\frac{p_n}{p_a} = (1.88M_e - 1)^{-0.64} \quad \dots(3.31)$$

The area ratio of the nozzle is so selected such that  $p_e \geq (1.88M_e - 1)^{-0.64} p_a$  to avoid flow separation in the nozzle. It is ensured that adverse pressure gradients will not occur at the nozzle wall.

During the start and shutdown transients when the pressure in the thrust chamber is small, the nozzle pressures are small and flow separation invariably takes place. Significant side thrusts are generated in the case of large nozzles during the transient operation.



## 3.6 CONTOUR OR BELL NOZZLES

The divergence loss of a conical nozzle was seen to be brought down by decreasing the semi-divergent angle ( $\alpha$ ). However, this was seen to result in a longer nozzle which is undesirable. In a contour nozzle, the exit angle of a nozzle is brought down by suitably shaping the nozzle in the form of a bell and keeping the length to be small. The initial divergence angle immediately downstream of the throat is enhanced to values between  $20^\circ$  and  $50^\circ$

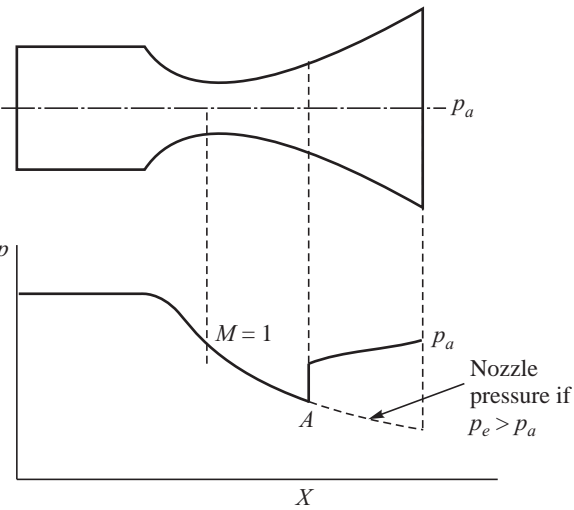


**Fig. 3.19** Formation of Shock from Over-expansion

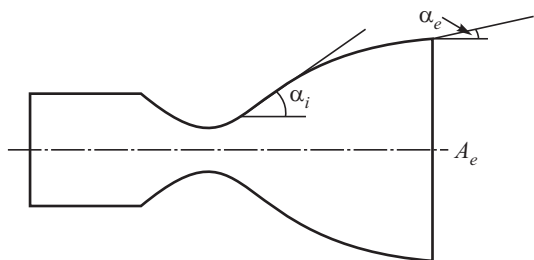


**Fig. 3.20** Bell Nozzle



since the higher values of pressure in this initial region would not allow flow separation at the walls. The final divergence angle is kept between  $2^\circ$  to  $5^\circ$  depending on the nozzle size to reduce the divergence loss. A bell nozzle is shown in Fig. 3.20.

The pressure at the walls of a bell nozzle is higher from the initial lateral expansion than in a conical divergent nozzle. A larger area ratio ( $\epsilon$ ) can, therefore, be used for a bell nozzle. Through a proper selection of the contour, the area ratio can be increased to about twice that of a  $15^\circ$  conical nozzle for the same nozzle length.

The contour of the nozzle is generally chosen to be parabolic and is given by a second degree curve. The length of the nozzle is chosen to be about 80% of the length of a  $15^\circ$  conical nozzle. The nozzle is referred to as 80% bell. It is shorter than the  $15^\circ$  conical nozzle by 20%. Different fractions of length such as 75% or 90% bells are possible. The range of the initial and final divergence angles ( $\alpha_i$  and  $\alpha_e$  in Fig. 3.20) could be varied leading to different possible contours. The optimum choice of  $\alpha_e$  is made to avoid flow separation by having larger values of wall pressures.

The variable ambient pressures encountered during the ascent of a rocket from the ground will lead to flow separation over a much smaller portion of the trajectory of the rocket when a bell-shaped nozzle is used compared to a conical nozzle having the same area ratio. Flow separation, as pointed out earlier, is usually not circumferentially symmetric and causes erratic side forces and needs to be avoided.



## 3.7 UNCONVENTIONAL NOZZLES

### 3.7.1 Extendible Nozzles

The extendible nozzles consist of the bell nozzles in the form of two or three segments. The segments are deployed at low ambient pressures to provide an increase of the area ratio. Figure 3.21 shows an extendible nozzle in which a segment between area  $A_{e1}$  to  $A_{e2}$  is deployed at higher altitudes to increase the area ratio from  $\epsilon_1$  to  $\epsilon_2$ . The deployment of the extension requires special mechanisms.

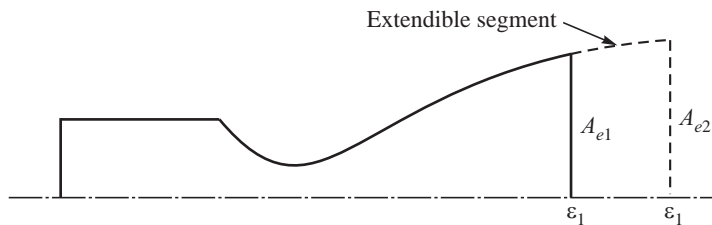
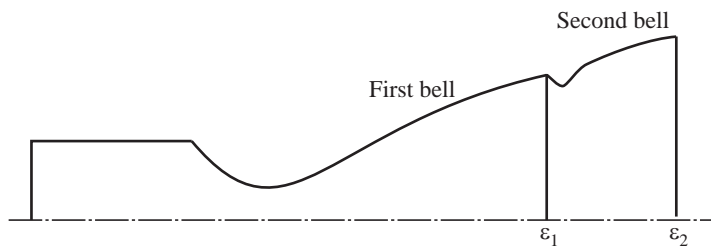


Fig. 3.21 Extendible Nozzle

### 3.7.2 Dual Bell Nozzle

The deployment mechanism necessary for the extendible nozzle can be avoided if the nozzle is made as a dual bell with an inflection point between the two bells. This is shown in Fig. 3.22.



**Fig. 3.22 Dual Bell Nozzle**

At lower altitudes (higher ambient pressure) the first bell functions and the flow from it leaves at area ratio  $\epsilon_1$  without getting attached to the second bell. At higher altitudes (lower ambient pressures) the larger expansion causes the flow to be attached to the second bell allowing a higher area ratio  $\epsilon_2$ .

### 3.7.3 Expansion Deflection Nozzle

The throat of the Expansion Deflection (ED) nozzle has an annular cross-section as shown in Fig. 3.23. The annular throat is formed by a central plug. The nozzle wall (Fig. 3.23) guides the outer boundary of the gas flow from the annular throat while the inner boundary is free. The free inner boundary allows the flow (inner) to expand freely as per the change of the ambient pressure. The expansion deflection nozzle is, therefore, self-adjusting to the varying ambient pressures.

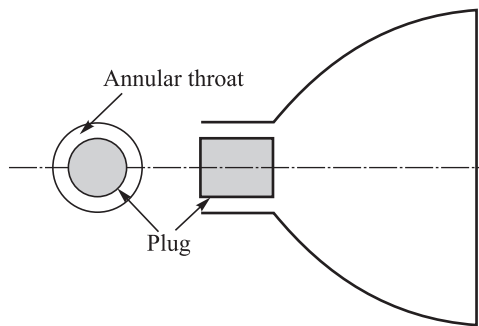


**Fig. 3.23 Expansion Deflection Nozzle**

### 3.7.4 Plug Nozzle

Instead of using the outer boundary of the flow to be guided by the nozzle wall in the expansion deflection nozzle, the inner boundary is guided in the case of a plug nozzle. This is done by the use of a shaped plug which is made to guide the flow. The outer boundary is left free so that it can adjust to the change of the ambient pressure. A schematic diagram of the plug nozzle is shown in Fig. 3.24.

It is necessary that the flow from the annular throat is directed towards the plug. The combustion chamber could as well be housed in the annular region outside the central cylindrical portion of the plug.

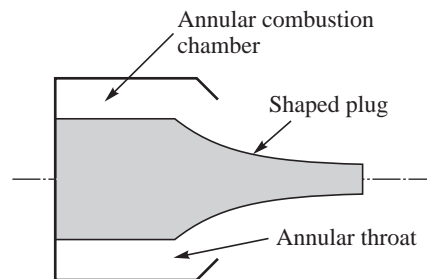


**Fig. 3.24 Plug Nozzle**



The shape of the plug can be in the form of a cone or it could have a parabolic contour or a spike. The nozzle, with the plug in the shape of a spike, is referred to as a spike nozzle.

### 3.7.5 Linear Nozzles

Linear nozzles are similar to the expansion deflection nozzles and plug nozzles with the outer nozzle wall of expansion deflection nozzle and the inner plug surface of the plug nozzle being converted into linear surfaces. The annular throat takes the form of a rectangular slot. The contoured surface is usually a part of the outer surface of a space plane.



## 3.8 MASS FLOW RATES AND CHARACTERISTIC VELOCITY

The mass flow rate,  $\dot{m}$ , through a nozzle having throat area  $A_t$  is:

$$\dot{m} = \rho_t A_t V_t \quad \dots(3.32)$$

Here  $\rho_t$  and  $V_t$  denote the density and velocity at the throat. The density at the throat  $\rho_t$  can be written using the ideal gas equation  $p = \rho RT$  as:

$$\rho_t = \frac{p_t}{RT_t} \quad \dots(3.33)$$

Assuming perfect gas and steady state one-dimensional adiabatic flow in the convergent portion of the nozzle, and following eq. 3.2, we have:

$$C_p T_c = C_p T_t + \frac{V_t^2}{2} \quad \dots(3.34)$$

which gives  $T_c = T_t + \frac{V_t^2}{2C_p} = T_t \left( 1 + \frac{\gamma - 1}{2\gamma R T_t} V_t^2 \right) = T_t \left( 1 + \frac{\gamma - 1}{2} M_t^2 \right) \quad \dots(3.35)$

$M_t$  denotes the Mach number at the throat ( $V_t / a_t = 1$ ) and  $R$  is the specific gas constant given by  $R_0/\mathcal{M}$ . In the above expression, the value of sound speed given by eq. 3.15 as  $a^2 = \gamma RT$  is used.

Equation 3.33 for  $\rho_t$  can be expressed as a function of chamber temperature,  $T_c$ , and chamber pressure,  $p_c$ , as:

$$\rho_t = \frac{p_c}{R T_c} \frac{p_t}{p_c} \frac{T_c}{T_t} \quad \dots(3.36)$$

From eq. 3.35, we have for a Mach number at the throat  $M_t = 1$  corresponding to a choked nozzle:

$$\frac{T_c}{T_t} = \left( 1 + \frac{\gamma - 1}{2} \right) = \frac{\gamma + 1}{2} \quad \dots(3.37)$$

For the isentropic expansion process in the nozzle:

$$\frac{p_c}{p_t} = \left( \frac{T_c}{T_t} \right)^{\gamma/(\gamma-1)} \quad \dots(3.38)$$



Substituting the value of  $\rho_t$  obtained from eq. 3.36 and noting that  $V_t = a_t = (\gamma RT_t)^{1/2}$ , eq. 3.32 on using eq. 3.38, thus, becomes:

$$\dot{m} = \frac{\sqrt{\gamma} p_c A_t}{\sqrt{RT_c}} \left( \frac{T_t}{T_c} \right)^{\frac{\gamma+1}{2(\gamma-1)}} \quad \dots(3.39)$$

Simplifying further by using eq. 3.37, the mass flow rate can be expressed as:

$$\dot{m} = \frac{\sqrt{\gamma} p_c A_t}{\sqrt{RT_c}} \left( \frac{2}{\gamma+1} \right)^{\frac{\gamma+1}{2(\gamma-1)}} \quad \dots(3.40)$$

Denoting:

$$\Gamma = \sqrt{\gamma} \left( \frac{2}{\gamma+1} \right)^{\frac{\gamma+1}{2(\gamma-1)}} \quad \dots(3.41)$$

Equation 3.40 for mass flow rate can be written as:

$$\dot{m} = \frac{\Gamma p_c A_t}{\sqrt{RT_c}} \quad \dots(3.42)$$

The above equation implies that the chamber pressure is  $p_c = \frac{\sqrt{RT_c}}{\Gamma} \frac{\dot{m}}{A_t}$ . The term  $\frac{\sqrt{RT_c}}{\Gamma}$  is a transfer function which represents the relationship between mass flow rate per unit throat area and chamber pressure ( $p_c$ ). It denotes the capacity to generate chamber pressure,  $p_c$ , for a given flow rate

of propellant  $\dot{m}$  when the throat area is  $A_t$ . The units of  $\frac{\sqrt{RT_c}}{\Gamma}$  is:

$$\sqrt{\frac{\text{JK}}{\text{kgK}}} = \sqrt{\frac{\text{Nm}}{\text{kg}}} = \sqrt{\frac{\text{Kg m}}{\text{s}^2} \frac{\text{m}}{\text{kg}}} = \frac{\text{m}}{\text{s}}$$

The parameter  $\sqrt{\frac{RT_c}{\Gamma}}$  has units of velocity and is referred to as characteristic velocity. It is denoted by  $C^*$ . The mass flow rate,  $\dot{m}$ , following eq. 3.42 is written as:

$$\dot{m} = \frac{p_c A_t}{C^*}; \quad C^* = \frac{1}{\Gamma} \sqrt{\frac{R_0 T_c}{\mathfrak{M}}} \quad \dots(3.43)$$

$C^*$  indicates the capacity of propellants to generate hot gases and pressurise the rocket chamber. It is, therefore, an index of performance of a propellant. It has the term  $\sqrt{\frac{R_0 T_c}{\mathfrak{M}}}$  which is common to the jet velocity,  $V_J$ , given in eq. 3.4. The  $C^*$  value is higher as the temperature,  $T_c$ , increases and the molecular mass of the gases,  $\mathfrak{M}$ , reduces.  $C^*$  is weakly dependent on the specific heat ratio,  $\gamma$ , with a smaller value of  $\gamma$  providing somewhat higher  $C^*$  values.

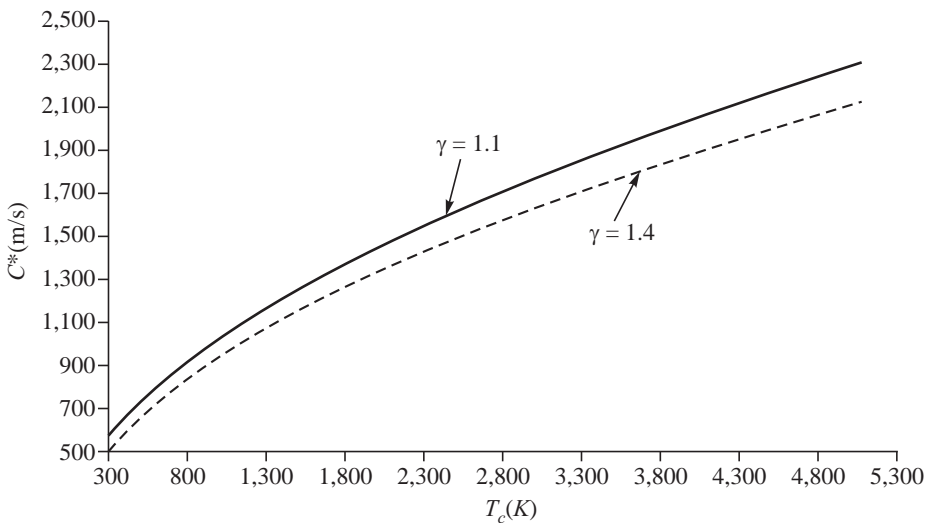


**Fig. 3.25** Variation of  $C^*$  with Temperature and Specific Heat Ratio for a given Molecular Mass  $M = 20 \text{ kg/kmole}$

Figure 3.25 shows the variation of  $C^*$  for variation of  $T_c$  between 300 K and 5,000 K and  $\gamma$  of 1.1 and 1.4 when the molecular mass is kept constant at 20 kg/kmole. It is seen that  $C^*$  varies between about 530 and 2200 m/s as the temperature is increased from 300 K to 5000 K. Change in  $\gamma$  are seen to influence  $C^*$  more significantly at higher values of temperature.



### 3.9 THRUST DEVELOPED BY A ROCKET; THRUST COEFFICIENT

The thrust developed from efflux of propellants was obtained from the rate of change of momentum and was given by eq. 2.35 as  $\dot{m} V_J$ . When gases are expanded in a nozzle to give a jet velocity,  $V_J$ , the ambient pressure and the jet pressure at exit would additionally influence the thrust.

In order to consider the ambient pressure, we consider a control volume in which the rocket is held stationary by a restraining force equal to the thrust,  $F$ , of the rocket as shown in Fig. 3.26. The control volume is bounded by control surfaces AB, BC, CD and DA. The control surface BC is along the exit plane of the nozzle as shown. The jet velocity,  $V_J$ , is normal to the surface BC. The net forces on the control surfaces are along the axis of the jet which is normal to BC. The force  $F_m$  from the rate of change of momentum of the jet is given by:

$$F_m = \dot{m} V_J \quad \dots(3.44)$$

where  $\dot{m}$  is the mass flow rate through the nozzle.

The restraining force, which is keeping the rocket stationary, is the reaction to the thrust,  $F$ , normal to the control surface BC as shown in Fig. 3.26. The forces acting on the control surfaces are those due to pressure acting normal to the surfaces and the reaction thrust  $F$ . The ambient pressure,  $p_a$ , acts over the entire surface and cancels out except over the portion HG on surface AD (pressure =  $p_a$ ) and EF on surface BC (pressure =  $p_e$ ) corresponding to the exit area of the nozzle  $A_e$ . This unbalanced force is  $(p_e - p_a) A_e$ . The sum of the forces acting along the jet axis on the control volume from Fig. 3.26 is:

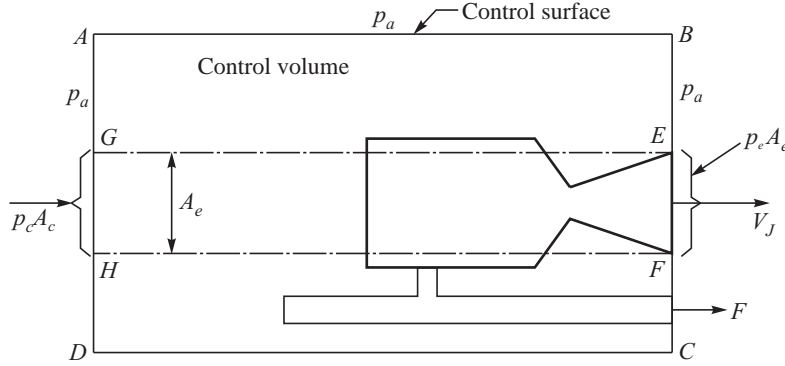


**Fig. 3.26 Control Volume Containing a Stationary Rocket**

$$F_m = F + (p_a - p_e) A_e \quad \dots(3.45)$$

Substituting the value of  $F_m$  from eq. 3.44, we get:

$$F = \dot{m} V_J + (p_e - p_a) A_e \quad \dots(3.46)$$

Using the value of  $\dot{m}$  from eq. 3.40 and  $V_J$  from eq. 3.4 in the above equation, we get:

$$F = \frac{\sqrt{\gamma} p_c A_t}{\sqrt{RT_c}} \left( \frac{2}{\gamma+1} \right)^{\frac{\gamma+1}{2(\gamma-1)}} \left\{ \frac{2\gamma RT_c}{\gamma-1} \left[ 1 - \left( \frac{p_e}{p_c} \right)^{\frac{(\gamma-1)/\gamma}{\gamma}} \right] \right\}^{1/2} + (p_e - p_a) A_e \quad \dots(3.47)$$

On simplification the equation becomes:

$$F = p_c A_t \sqrt{\frac{2\gamma^2}{\gamma-1} \left( \frac{2}{\gamma+1} \right)^{\frac{\gamma+1}{\gamma-1}} \left[ 1 - \left( \frac{p_e}{p_c} \right)^{\frac{\gamma-1}{\gamma}} \right]} + (p_e - p_a) A_e \quad \dots(3.48)$$

The above equation can be rearranged to give:

$$F = p_c A_t \left\{ \sqrt{\frac{2\gamma^2}{\gamma-1} \left( \frac{2}{\gamma+1} \right)^{\frac{\gamma+1}{\gamma-1}} \left[ 1 - \left( \frac{p_e}{p_c} \right)^{\frac{\gamma-1}{\gamma}} \right]} + \left( \frac{p_e}{p_c} - \frac{p_a}{p_c} \right) \frac{A_e}{A_t} \right\} \quad \dots(3.49)$$

The term within the curly brackets denotes the amplification of the force generated by the chamber pressure acting on the nozzle throat. It is called the ideal thrust coefficient and is denoted by  $C_F$ . The equation for thrust can, thus, be written as:

$$F = C_F p_c A_t \quad \dots(3.50)$$

The maximum value of the thrust is obtained for  $p_e = p_a$ , i.e. when the gases are expanded to the ambient pressure. This can be inferred by observing the terms within the square root sign in eq. 3.49, which show that as  $p_e$  decreases the momentum thrust increases, while the pressure thrust term decreases as  $p_e$  decreases. The maximum thrust coefficient obtained for  $p_e = p_a$  is called the optimum thrust coefficient and is denoted by  $C_F^o$ .

$$C_F^o = \sqrt{2} \gamma \left( \frac{2}{\gamma+1} \right)^{\frac{\gamma+1}{2(\gamma-1)}} \frac{1}{\sqrt{\gamma-1}} \sqrt{\left[ 1 - \left( \frac{p_e}{p_c} \right)^{\frac{\gamma-1}{\gamma}} \right]} \quad \dots(3.51)$$



The variation of this optimum thrust coefficient,  $C_F^o$ , with variation in the pressure ratio  $p_e/p_c$  as the specific heat ratio,  $\gamma$ , changes between 1.1 and 1.4 is shown in Fig. 3.27. The value of  $C_F^o$  increases as  $p_e/p_c$  decreases. The increase of  $C_F^o$  is more rapid at the smaller values of  $p_e/p_c$ .

An increase in the value of  $\gamma$  causes a decrease of  $C_F^o$ . The influence of  $\gamma$  is more significant at the smaller values of  $p_e/p_c$ . This aspect is brought out in Fig. 3.28 where  $C_F^o$  is plotted as a function of  $\gamma$  at different values of  $p_e/p_c$ . For a high value of  $p_e/p_c = 0.1$ , there is no perceptible influence of the variation of  $\gamma$  on  $C_F^o$ , whereas for  $p_e/p_c = 0.0001$ , a decrease of  $\gamma$  shows a profound increase of  $C_F^o$ . Higher values of chamber pressures are seen to be desirable in general, while smaller values of  $\gamma$  are to be preferred for smaller values of  $p_e/p_c$  for obtaining higher values of thrust coefficient.

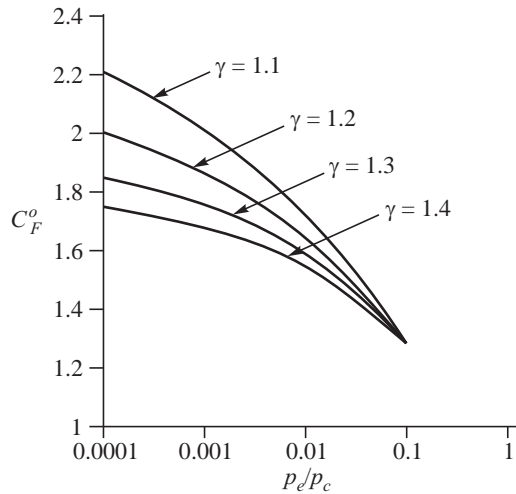


**Fig. 3.27** Dependence of Thrust Coefficient on  $p_e/p_c$

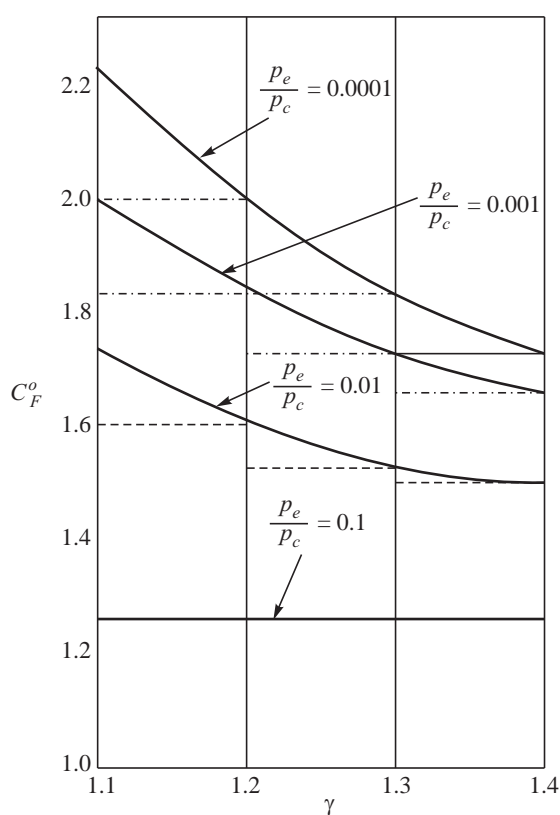


**Fig. 3.28** Variation of Ideal Thrust Coefficient with  $\gamma$



### 3.10 EFFICIENCIES

The jet velocity ( $V_J$ ), mass flow rate ( $\dot{m}$ ), characteristic velocity ( $C^*$ ), thrust ( $F$ ), thrust coefficient ( $C_F$ ) and optimum thrust coefficient ( $C_F^o$ ) were derived assuming perfect gas, steady one dimensional flow and isentropic expansion of the gas in the nozzle. These correspond to idealised conditions and a departure from these ideal conditions would lead to a reduction of these performance parameters. An efficiency factor, called  $C^*$  efficiency ( $\eta_{C^*}$ ) is defined to relate the actual  $C^*$  obtained in a rocket with the theoretical idealised value calculated using eq. 3.43.

$$\eta_{C^*} = \frac{C^*_{\text{actual}}}{C^*_{\text{ideal}}} \quad \dots(3.52)$$

Similarly, a thrust correction coefficient,  $\zeta_F$ , is defined to relate the actual thrust with the thrust determined under idealised conditions. The thrust correction coefficient is given by:

$$\zeta_F = \frac{C_F_{\text{actual}}}{C_F_{\text{ideal}}} \quad \dots(3.53)$$



### 3.11 SPECIFIC IMPULSE AND CORRELATION WITH $C^*$ AND $C_F$

We have seen that  $C^*$ , which indicates the ability of a given mass flow rate of propellant to generate high pressure in the chamber, increases as the temperature of the gas increases and the molecular mass decreases.  $C_F$ , on the other hand, denotes the thrust generating capacity of the nozzle and increases as the pressure ratio ( $p_c/p_e$ ) across the nozzle increases. The thrust developed by a given propellant would depend on the ability to generate high temperature and low molecular mass gases and also the capacity to expand the gases to low values of nozzle exit pressures. The specific impulse,  $I_{sp}$ , would therefore depend on both  $C^*$  and  $C_F$ . The dependence is derived as follows.

Equation 3.43 gives  $C^*$  as:

$$C^* = \frac{p_c A_t}{\dot{m}}$$

while, eq. 3.50 gives the thrust,  $F$ , in terms of  $C_F$  as:

$$F = C_F p_c A_t$$

The specific impulse,  $I_{sp}$ , was defined as the thrust per unit mass flow rate, viz.,

$$I_{sp} = \frac{F}{\dot{m}}$$

Substituting the value of  $F$  and  $\dot{m}$  in terms of  $C_F$  and  $C^*$ , we get:

$$I_{sp} = C^* \times C_F \quad \dots(3.54)$$

The specific impulse,  $I_{sp}$ , is therefore a composite index comprising the transfer function of the propellant to generate high pressure gases and the expansion of the gases in the nozzle. The specific impulse,  $I_{sp}$ , of a given propellant would, therefore, vary depending on the chamber pressure and the nozzle exit pressure. For comparing different propellants, it becomes necessary to specify these



pressures. In the case of rockets operating at ambient sea-level conditions, such as booster rockets and rockets being tested on the ground, the value of  $p_e$  is taken as 1 atm ( $\sim 0.1$  MPa) whereas  $p_c$  is taken as 70 atm (7 MPa). The  $I_{sp}$  is referred to as sea-level specific impulse  $I_{sp, SL}$ . For rockets which operate in deep space, the ambient pressure is zero ( $p_a = 0$ ) and the specific impulse is called the vacuum specific impulse ( $I_{sp, vac}$ ). The thrust obtained for  $p_a = 0$ , from eq. 3.46 is:

$$F = \dot{m} V_J + p_e \times A_e \quad \dots(3.55)$$

The vacuum specific impulse is, therefore:

$$I_{sp, vac} = V_J + \frac{A_e p_e}{\dot{m}}$$

which on simplification gives:

$$I_{sp, vac} = V_J + \frac{A_e}{A_t} \frac{p_e}{p_c} C^* \quad \dots(3.56)$$

The vacuum specific impulse is higher than the sea-level specific impulse.



### 3.12 GENERAL TRENDS

Convergent divergent nozzles with fixed area ratios have been generally applied for solid, liquid and hybrid propellant rockets. The use of adapted nozzles, though promising, has not been applied in the existing rockets of launch vehicles considering the complexity of the deployment mechanisms and the increased mass of the nozzle.

The size of a nozzle depends on thrust and could vary between a few millimeters to a few meters. The flow of hot gases in the nozzle heats up the nozzle especially at the throat region where the heat flux is a maximum. Different methods of cooling the nozzle are, therefore, necessary and we shall consider the various cooling methods in the chapter on Liquid Propellant Rockets.

A conical divergent nozzle of a solid propellant rocket with ablative liners and graphite for thermal protection is shown in Fig. 3.29. Here, ablatives comprising carbon phenolic and silica phenolic composites are used for protecting the metal hardware. Graphite is used at the throat region. The details of ablative materials are discussed in Section 6.2.3.

Metallic and non-metallic materials of construction which can withstand high temperatures such as nickel based alloys, carbon-carbon composites are also employed for the nozzle hardware. Figure 3.30 shows a heated conical divergent portion of a nozzle during a captive ground test of a liquid propellant rocket.

The direction of the thrust needs to be changed during a rocket flight in order to follow a particular trajectory by pitching and yawing the rocket about its axis. This is done by vectoring the thrust by tilting the nozzle. Nozzle with the tilting feature is referred to as gimbal nozzle or flex nozzle. The tilting is done using actuators.

A particular method of thrust vectoring in nozzles, known as Secondary Injection Thrust Vector Control (SITVC), is used in solid propellant rockets to generate side thrust. Here, a secondary fluid is injected in the divergent portion of the nozzle. The injection of the fluid in the supersonic flow creates a shock wave and modifies the symmetric nature of pressure distribution along the circumference of the nozzle. Side forces are generated leading to vectoring of the thrust.



Details on the design of the nozzles and their shapes, the nature of plumes from under-expanded and over-expanded nozzles and heat transfer in nozzles are given in Annexure A.

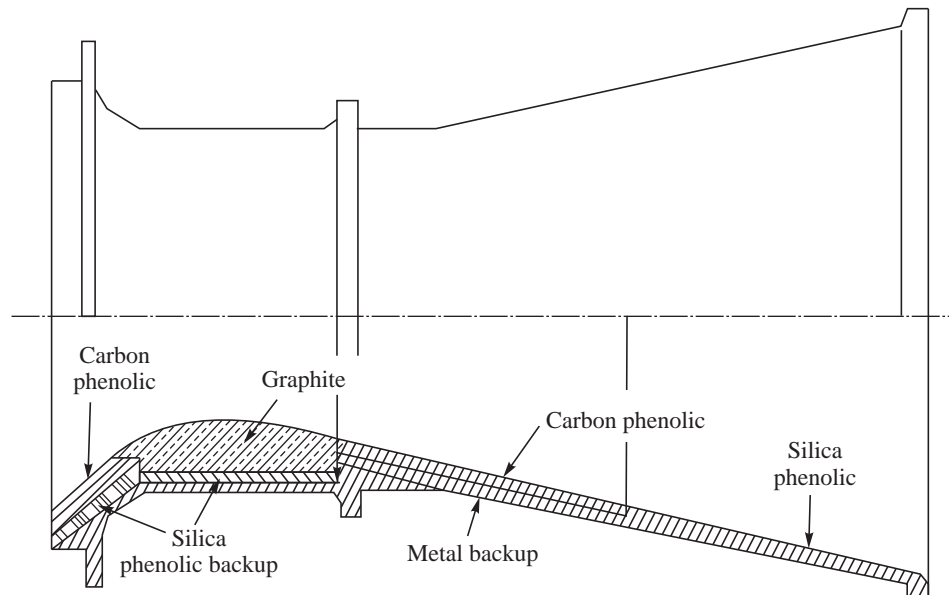


**Fig. 3.29** Ablative Liners for Thermal Protection of Nozzle

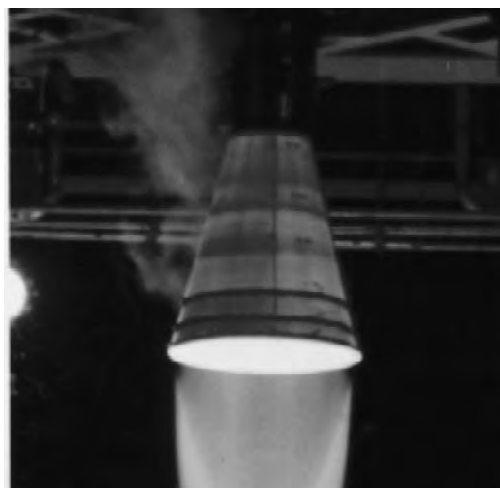


**Fig. 3.30** Conical Nozzle in a Captive Test [Source ISRO]

## SOLVED EXAMPLES

**Example 3.1** Characteristic velocity, specific impulse and thrust:

Hot gases are generated at a temperature of 2,000 K and a pressure of 15 MPa in a rocket chamber. The molecular mass of the gas is 22 kg/kmole and the specific heat ratio of the gas is 1.32.



The gases are expanded to the ambient pressure of 0.1 MPa in a convergent-divergent nozzle having a throat area of  $0.1 \text{ m}^2$ . Calculate: (i) Exit jet velocity, (ii) Characteristic velocity, (iii) Ideal optimum thrust coefficient, (iv) Specific impulse and (v) Thrust generated.

**Solution:** (i) Exit jet velocity:

Assuming the gas to be ideal, we have from eq. 3.4:

$$V_J = \sqrt{\frac{2\gamma R_0 T_c}{(\gamma - 1)\mathfrak{M}} \left[ 1 - \left( \frac{p_e}{p_c} \right)^{\frac{\gamma-1}{\gamma}} \right]}$$

Substituting the values of  $\gamma$ ,  $T_c$ ,  $\mathfrak{M}$  and  $p_c$  and noting that the exit pressure,  $p_e$ , is equal to the ambient pressure of 0.1 MPa, we get the exit jet velocity  $V_J = 2094 \text{ m/s}$ . Here, the value of  $R_0 = 8314 \text{ J/kmole K}$  is used.

(ii) Characteristic velocity:

The characteristic velocity  $C^*$  is given by eq. 3.43:

$$C^* = \frac{1}{\Gamma} \sqrt{\frac{R_0 T_c}{\mathfrak{M}}} \quad \text{where} \quad \Gamma = \sqrt{\gamma} \left( \frac{2}{\gamma + 1} \right)^{\frac{\gamma+1}{2(\gamma-1)}}$$

With  $\gamma = 1.32$ ,  $\Gamma = 0.671$ , the value of  $C^* = 1296 \text{ m/s}$ .

(iii) Ideal optimum thrust coefficient:

The ideal optimum thrust coefficient,  $C_F^o$ , as derived in eq. 3.51 is

$$C_F^o = \sqrt{2} \gamma \left( \frac{2}{\gamma + 1} \right)^{\frac{\gamma+1}{2(\gamma-1)}} \frac{1}{\sqrt{\gamma - 1}} \sqrt{\left[ 1 - \left( \frac{p_e}{p_c} \right)^{\frac{\gamma-1}{\gamma}} \right]}.$$

Substituting the values we get,  $C_F^o = 1.615$ .

(iv) Specific impulse,  $I_{sp}$  = Exit jet velocity =  $2094 \text{ Ns/kg}$

The specific impulse can also be determined as  $I_{sp} = C^* \times C_F^o = 1296 \times 1.615 = 2094 \text{ Ns/kg}$

(v) Thrust generated:

Thrust,  $F = C_F^o p_c A_t = 1.615 \times 15 \times 10^6 \times 0.1 = 2.42 \times 10^6 \text{ N}$  or  $2.42 \text{ MN}$

**Example 3.2** Cold-gas rocket:

A rocket is propelled by the expansion of room temperature hydrogen at 300 K from a pressure of 2 MPa to 0.1 MPa. Calculate the jet velocity, given that the specific heat ratio of hydrogen gas is 1.4 and its molecular mass is 2 kg/kmole.

**Solution:** The jet velocity is given by:

$$V_J = \sqrt{\frac{2\gamma R_0 T_c}{(\gamma - 1)\mathfrak{M}} \left[ 1 - \left( \frac{p_e}{p_c} \right)^{\frac{\gamma-1}{\gamma}} \right]}$$

Substituting the values of  $\gamma$ ,  $T$ ,  $\mathfrak{M}$ ,  $p_c$  and  $p_e$ , we get:



$$V_J = \sqrt{\frac{2 \times 1.4 \times 8314 \times 300}{0.4 \times 2} \left\{ 1 - \left( \frac{0.1}{2} \right)^{\frac{0.4}{1.4}} \right\}} = 2241 \text{ m/s.}$$

It is seen that the low molecular mass hydrogen gas at the ambient temperature of 300 K is able to give a higher jet velocity than the hot combustion products at 2,000 K having a molecular mass of 22 kg/kmole considered in Example 3.1. The molecular mass has a very strong influence on the jet velocity.

**Example 3.3** Area ratio, thrust coefficient and flow separation:

The booster rocket of a satellite launch vehicle operates upto an altitude of 30 km. The rocket has a constant chamber pressure of 7 MPa.

- (i) If the nozzle is designed for optimum expansion at an altitude of 16 km determine the area ratio of the nozzle. The specific heat ratio of the gases can be assumed constant and equal to 1.20. The throat area of the nozzle is 0.1 m<sup>2</sup>. The variation of ambient pressure with altitude is given in the following:

Altitude (km)	0	4	8	12	16	20	30
Pressure (N/m <sup>2</sup> )	101325	61660	35651	19399	10353	5529	1186

- (ii) What would be the thrust coefficient of the nozzle at the altitude of 30 km? What is the percentage reduction from the value corresponding to optimum expansion at 30 km?  
 (iii) Till what altitude would flow separation in the nozzle take place?

**Solution:** (i) Area ratio of the nozzle:

The area ratio of the nozzle is given by eq. 3.25:

$$\epsilon = \frac{\left(\frac{2}{\gamma-1}\right)^{\frac{1}{\gamma-1}} \left(\frac{p_c}{p_e}\right)^{\frac{1}{\gamma}}}{\sqrt{\frac{\gamma+1}{\gamma-1} \left[1 - \left(\frac{p_e}{p_c}\right)^{\frac{\gamma-1}{\gamma}}\right]}}$$

At an altitude of 16 km, the ambient pressure is 0.010353 MPa. The exit pressure,  $p_e$ , for the optimum expansion is, therefore, 0.010353 MPa. Substituting the values of  $p_c$ ,  $p_e$  and  $\gamma$  as 7 MPa, 0.010353 MPa and 1.20 respectively in the above equation, we get,  $\epsilon = 52.5$ .

- (ii) Thrust coefficient of the nozzle:

The thrust was derived in this chapter as:

$$F = p_c A_t \left\{ \sqrt{\frac{2\gamma^2}{\gamma-1} \left( \frac{2}{\gamma+1} \right)^{\frac{\gamma+1}{\gamma-1}} \left[ 1 - \left( \frac{p_e}{p_c} \right)^{\frac{\gamma-1}{\gamma}} \right]} + \left( \frac{p_e}{p_c} - \frac{p_a}{p_c} \right) \frac{A_e}{A_t} \right\}$$

The thrust coefficient for optimum expansion at 30 km corresponds to  $p_e = 0.001186$  MPa. The thrust coefficient is:



$$C_F^o = \sqrt{\frac{2\gamma^2}{\gamma-1} \left(\frac{2}{\gamma+1}\right)^{\frac{\gamma+1}{\gamma-1}} \left[1 - \left(\frac{p_e}{p_c}\right)^{\frac{\gamma-1}{\gamma}}\right]} = 2.246$$

The actual nozzle exit area =  $\epsilon \times 0.1 = 5.25 \text{ m}^2$  and the pressure at the exit = 0.010353 MPa. The actual thrust coefficient is:

$$\begin{aligned} C_F &= \sqrt{\frac{2\gamma^2}{\gamma-1} \left(\frac{2}{\gamma+1}\right)^{\frac{\gamma+1}{\gamma-1}} \left[1 - \left(\frac{p_e}{p_c}\right)^{\frac{\gamma-1}{\gamma}}\right] + \left(\frac{p_e}{p_c} - \frac{p_a}{p_c}\right) \frac{A_e}{A_t}} \\ &= 1.828 + 0.0687 = 1.896 \end{aligned}$$

The reduction from optimum =  $\frac{2.246 - 1.896}{2.246} = 0.156$  or 15.6 per cent.

(iii) The nozzle exit pressure = 0.010353 MPa

Assuming Summerfield criterion for flow separation in a conical nozzle, the ambient pressure for flow separation =  $\frac{p_e}{0.4} = 2.5 \times 0.010353 = 0.0259 \text{ MPa}$ . Flow separation will occur when the ambient pressure exceeds 25900 Pa.

From the given table of ambient pressure at the different altitudes, the altitude corresponding to the above pressure is 10.16 km. Hence, the flow in the nozzle is separated till 10.16 km.

It must be noted that the criterion for flow separation is valid for conical nozzles. In the case of contoured nozzles, as discussed in this chapter, flow separation will occur for higher values of ambient pressures.

**Example 3.4**  $C^*$  efficiency  $\eta_{C^*}$  and thrust correction factor  $\xi_F$ :

The Saturn V rocket considered in Example 2.5 used a cluster of liquid propellant rockets known as F1 for the booster stage. Kerosene and oxygen were used for the propellants in F1. In a variant of this rocket, the thrust generated was about 6800 kN at sea-level with a propellant flow rate of 2,600 kg/s. Assuming the chamber pressure and temperature as 6.65 MPa and 3300 K respectively and the gases to be expanded in the nozzle to the ambient sea-level pressure of 0.1 MPa, determine the  $C^*$  efficiency and the thrust correction factor. You can approximate the throat area as 0.65 m<sup>2</sup>, the average molecular mass of the hot gases generated from combustion of propellants as 22 kg/kmole and the specific heat ratio of the gases as 1.22.

**Solution:**  $C^*$  efficiency:

$$\text{Theoretical } C^* = \frac{1}{\Gamma} \sqrt{\frac{R_0 T_c}{\mathfrak{M}}} \quad \text{where} \quad \Gamma = \sqrt{\gamma} \left(\frac{2}{\gamma+1}\right)^{\frac{\gamma+1}{2(\gamma-1)}}$$

For  $\gamma = 1.22$ ,  $\Gamma = 0.652$  giving:

$$C^*_{\text{Theory}} = \frac{1}{0.652} \sqrt{\frac{8.314 \times 10^3 \times 3300}{22}} = 1713 \text{ m/s}$$

The actual evaluated value of  $C^*$  is given by  $\dot{m}_{\text{act}} = \frac{p_c A_t}{C^*} \Big|_{\text{act}}$ . This gives



$$C_{\text{act}}^* = \frac{6.65 \times 10^6 \times 0.65}{2600} = 1663 \text{ m/s}$$

$$\eta_{C^*} = \frac{C_{\text{act}}^*}{C_{\text{Theory}}^*} = \frac{1663}{1713} = 0.97$$

Thrust correction factor:

The expansion in the nozzle is to 0.1 MPa

The exhaust jet velocity is  $V_J = \sqrt{\frac{2\gamma R_0 T_c}{(\gamma - 1) \mathfrak{M}} \left[ 1 - \left( \frac{p_e}{p_c} \right)^{\frac{\gamma-1}{\gamma}} \right]}$ . Substituting the values gives  $V_J =$

2710 m/s. Since the pressure at the nozzle exit is the ambient pressure, there is no pressure thrust and the specific impulse =  $V_J$ .

$$I_{\text{sp}} = 2710 \text{ N s/kg}$$

Ideal thrust  $F = \dot{m} \times I_{\text{sp}} = 2600 \times 2710 = 7.046 \times 10^6 \text{ N} = 7046 \text{ kN}$

But the actual thrust = 6800 kN

$$\text{Ratio of thrust} = \frac{6800}{7046} = 0.965$$

The above ratio comes from  $\eta_{C^*}$  and thrust coefficient  $\xi_F$ . The thrust coefficient is given by:

$$\xi_F = \frac{0.965}{\eta_{C^*}} = \frac{0.965}{0.97} = 0.995$$

## NOMENCLATURE

- A : Cross-sectional area
- $a$  : Sound speed (m/s)
- $C^*$  : Characteristic velocity (m/s) defined by eq. 3.43
- $C_F$  : Thrust coefficient defined by eq. 3.50
- $C_P$  : Specific heat at constant pressure (kJ/kg K)
- $C_V$  : Specific heat at constant volume (kJ/kg K)
- $F$  : Thrust (N)
- $g$  : Gravitational field; acceleration due to gravity (m/s<sup>2</sup>)
- $h$  : Enthalpy (kJ/kg), also altitude (m)
- $I_{\text{sp}}$  : Specific impulse (Ns/kg)
- $m$  : Mass (kg)
- $M$  : Mach number ( $V/a$ )
- $p$  : Pressure ( $p_a$ )
- $Q$  : Heat (J)
- $r$  : Radius (m)



---

$R_0$	: Universal gas constant (8.314 kJ/kmol K)
$R$	: Specific gas constant ( $R = R_0/\mathfrak{M}$ ; kJ/kg K)
$T$	: Temperature (K)
$V$	: Velocity (m/s)
$W$	: Work (J)
$x$	: Distance (m)
$z$	: Elevation (m)
$\alpha$	: Semi-divergent angle of nozzle
$\varepsilon$	: Nozzle area ratio ( $A_e/A_t$ )
$\gamma$	: Specific heat ratio ( $C_p/C_v$ )
$\eta_{C^*}$	: $C^*$ efficiency defined by eq. 3.52
$\lambda$	: Divergent loss factor defined by eq. 3.28
$\Delta$	: Fractional loss of thrust
$\rho$	: Density (kg/m <sup>3</sup> )
$\zeta_F$	: Thrust correction coefficient defined by eq. 3.53
$\mathfrak{M}$	: Molecular mass (kg/kmole)

### Subscripts

$a$	: Ambient
$c$	: Chamber
$d$	: Divergent part of nozzle
$e$	: Nozzle exit
$i, 1, 2$	: Section at $i, 1, 2$
$n$	: Nozzle
$SL$	: Sea level
$t$	: Nozzle throat
$vac$	: Vacuum (Deep space)

### Superscripts

$^\circ$	: Optimum
$\cdot$	: Rate ( $d/dt$ )

## EXERCISES

1. In a liquid propellant rocket, high temperature and high pressure gases at 3,000 K and 10 MPa are generated in the combustion chamber and expanded in a nozzle to give thrust. The characteristic velocity of the propellant ( $C^*$ ) is 2,000 m/s and the thrust coefficient ( $C_F$ ) is 1.5.
  - (a) What is the specific impulse of the rocket?
  - (b) What must be the throat diameter of the nozzle to give a thrust of 5 kN?



2. (i) A rocket is designed to produce 5 MN of thrust at sea-level. The pressure in the combustion chamber is 7 MPa and the temperature is 2,800 K. If the working fluid is assumed to be an ideal gas with properties of nitrogen at room temperature, determine the following: (a) specific impulse, (b) mass flow rate and (c) throat diameter. The specific heat ratio,  $\gamma$ , for nitrogen can be taken to be 1.4. You can assume that the gases expand in the nozzle to the ambient pressure of 0.1 MPa which is the ambient pressure at sea-level.
- (ii) If the above rocket fires in deep space (ambient pressure is vacuum), what would be the specific impulse? (The exit area of the nozzle corresponds to expansion to a pressure of 0.1 MPa)
3. For an ideal rocket with  $C^*$  of 1500 m/s, a nozzle throat diameter of 18 cm, a thrust coefficient of 1.38 and a mass flow rate of 40 kg/s, determine:
- chamber pressure,
  - thrust and
  - specific impulse.
4. (i) A solid propellant is formulated to generate hot gases at a temperature of 3100 K, a molecular mass of 23 kg/kmol and a specific heat ratio of 1.34. The combustion chamber pressure is 7 MPa. The gases are expanded in the nozzle to the ambient pressure of 0.1 MPa. Determine the following:
- Characteristic velocity ( $C^*$ )
- Thrust coefficient of the rocket ( $C_F$ ).
- Ideal thrust coefficient.
- Ideal Specific Impulse in (Ns/kg) and in (s).
- (ii) Determine the rate in kg/s at which the propellant must burn in order to generate a thrust of  $10^3$  kN. You can assume the  $C^*$  efficiency as 0.97 and the thrust correction coefficient as 0.92.
5. The  $C^*$  of a composite propellant is 2200 m/s. The combustion products of this propellant have a molecular mass of 22 kg/kmole and a temperature of 2600 K. Aluminium powder is added to the above propellant to improve its specific impulse. The molecular mass of the products increases to 24 kg/kmole while the temperature of the combustion products increases to 3200 K on addition of aluminium. If the specific heat ratio of the combustion products of the aluminised and non-aluminised propellants remain the same, determine the  $C^*$  of the aluminised propellant.
- If the above aluminised propellant is used in a solid propellant rocket having a thrust coefficient of 1.2, what is the specific impulse of the rocket?
6. A liquid propellant rocket operates from take-off on ground and fires up to an altitude of 15 km. It uses a conical convergent-divergent nozzle, the half divergence angle being  $15^\circ$ . The nozzle is designed for optimum expansion for an altitude of 5 km for which the ambient pressure is 0.054 MPa. Determine whether flow separates in the divergent portion of the nozzle during take off from the ground when steady state pressure is achieved in the thrust chamber.
- What is the divergence loss of the above conical nozzle?
7. Determine the diameters at the throat and exit of an ideal nozzle designed for optimum thrust at an altitude of 25 km? The thrust generated by the rocket at 25 km altitude is 5 kN. The chamber pressure is 2.07 MPa and the temperature of the hot gases in the chamber is 2880 K. The ambient pressure at 25 km is 2610 Pa. The mean molecular mass and the mean specific heat ratio of the gas are 23.4 kg/kmole and 1.3 respectively.
8. (i) A liquid bipropellant rocket operating at a chamber pressure of 0.8 MPa and having an area ratio of 200 is used for transferring a satellite from an elliptical low Earth orbit to the geosynchronous orbit. The temperature of combustion products is 3050 K and the molecular mass is 20.4 kg/kmole. The specific heat ratio is 1.23.



If the  $C^*$  efficiency is 0.98 and the mass flow rate of propellants is 0.14 kg/s, determine the thrust developed. You can assume the ambient pressure corresponding to the high altitude of operation as zero.

(ii) What is the exit diameter of the nozzle?

## References

1. Hill, P.G. and Peterson, C.R., *Mechanics and Thermodynamics of Propulsion*, 2nd ed., Reading, Massachusetts: Addison Wesley Publishing Company, 1992.
2. Liepmann, H.W. and Roshko, A., *Elements of Gas Dynamics*, 3rd ed., New York: John Wiley and Sons Inc., 1978.
3. Mukunda, H.S., *Understanding Aerospace Propulsion*, Bangalore: Interline Publishing, 2004.
4. Muthunayagam, A.E., Nagappa, R. and Ramamurthi, K., *Development of Composite Nozzle for Solid Rocket Booster*, 30th Int. Astronautical Federation Congress, Munich 1979.
5. Shapiro, A.H., *The Dynamics and Thermodynamics of Compressible Fluid Flow*, vol. 1, New York: John Wiley and Sons Inc., 1953.
6. Sutton, G.P. and Biblarz, O., *Rocket Propulsion Elements*, 7th Ed., New York: Wiley Intescience Publications, 2001.
7. Timnat, Y.M., *Advanced Chemical Rocket Propulsion*, London: Academic Press, 1987.
8. Zucrow, M.J. and Hoffman, J.D., *Gas Dynamics*, vol. 1, John Wiley and Sons, 1976.

## Glossary

Bell nozzle: Inner contour of the divergent part of nozzle in the form of a parabola so that the gas streams leaving the nozzle are guided along the axial direction

Characteristic velocity: The ability of a given mass flow rate of propellant to generate pressure in a rocket chamber of given throat area

Choking: Upper limit of flow rate through a nozzle corresponding to the Mach number at the throat reaching a value of one

Divergent loss coefficient: Ratio of the thrust in a conical nozzle to the thrust had all the streams left the nozzle in axial direction

Extendible nozzles: Nozzles providing variable area ratio

Flow separation: Flow detached from the wall due to adverse pressure gradient; the wall no longer guides the flow

Mach number: Ratio of velocity of the fluid/body to the velocity of sound

Nozzle: Shaped vent or opening to accelerate the flow of gases

Nozzle efficiency: Ratio of actual thrust of a rocket to the theoretically predicted value

Nozzle pressure ratio: Ratio of pressure in the chamber to the pressure at the exit of the nozzle

Nozzle area ratio: Ratio of the nozzle exit area to the throat area

Over-expanded nozzle: The gas flow in a nozzle expanded to a pressure lower than the ambient pressure

Plug nozzle: Adapted nozzle with central plug for variable expansion ratios

Throat: The smallest area at the confluence of the convergent and divergent portions of a nozzle

Thrust coefficient: Amplification of thrust by a nozzle

Under-expanded nozzle: The flow in the nozzle not completely expanded to the ambient pressure.

## Chapter 4

### Chemical Propellants

*The magnitude of atomic weight determines the character of the element, just as the magnitude of the molecule determines the character of a compound body.*

— Dmitri Mendeleev, Chemist

The specific impulse ( $I_{sp}$ ) was seen in Chapter 3 to be proportional to  $\sqrt{T_c/\mathfrak{M}}$ , where  $T_c$  is the gas temperature prior to expansion in the nozzle and  $\mathfrak{M}$  is the molecular mass of the gas. A larger value of temperature,  $T_c$ , and a smaller molecular mass of the gases,  $\mathfrak{M}$ , would give a higher value of  $I_{sp}$ . The heating of the propellant say by electrical power or nuclear energy will increase the temperature,  $T_c$ , and provide high values of specific impulse. Rather than heat propellants, if chemically reactive substances can be used as propellants, and if high temperature gases can be generated at high chamber pressures by the chemical reaction of the propellants, large values of  $I_{sp}$  can be attained. Such reactive propellants, comprising fuel and oxidiser, are termed as chemical propellants and the rockets employing such propellants are known as chemical rockets.

Chemical propellants could be fuels consisting of carbon, hydrogen and nitrogen (e.g., hydrocarbon fuels, hydrazine, polymers, cellulose, etc.) and oxidizers, such as, oxygen, chlorine, fluorine, ammonium perchlorate and nitric acid. The fuel and oxidiser when mixed together and ignited, generate high temperature gases. Chemical propellants could also consist of explosives. Explosives contain inbuilt fuel and oxidiser as a single mass, and undergo spontaneous chemical reaction without the fuel having to find the oxidiser, mix with it and then burn. In this chapter we shall address the factors influencing the choice of chemical propellants.



## 4.1 SMALL VALUES OF MOLECULAR MASS AND SPECIFIC HEAT RATIO

The figure of merit characterising a propellant was given by the characteristic velocity,  $C^*$ , in Chapter 3. Higher values of temperature and smaller values of molecular mass and specific heat ratio of the combustion products, generated by the propellant, were seen desirable in order to achieve large values of  $C^*$ .

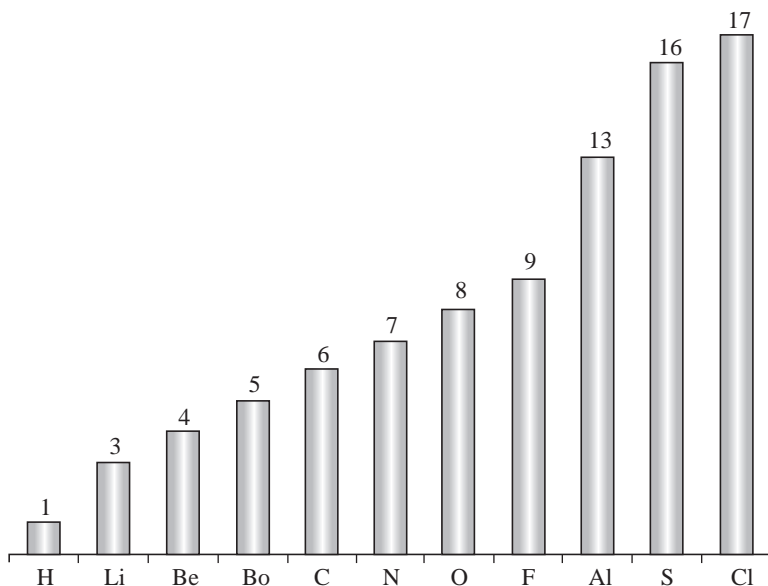


Fig. 4.1 Atomic Number of Light Elements

### (a) Molecular Mass

In order to obtain lower molecular mass of the combustion gases, the propellant needs to be based on elements having low atomic mass. Figure 4.1 gives the atomic number of the different elements constituting chemical propellants. Elements with smaller atomic number and thus smaller molecular mass, such as, hydrogen, lithium, beryllium, boron, carbon, nitrogen, oxygen and fluorine are preferred.

### (b) High Temperatures and Specific Heats

For obtaining higher values of combustion temperature, the energy released by the chemical reactions has to be as large as possible and the specific heat of the combustion gases must be small. We will consider in the next section, a simple procedure to determine parameters contributing to the energy release during burning of propellants. In the following discussion, we address the issue of specific heats.

The specific heat of a gas increases as its molecular structure becomes more complex. The values of specific heat at constant pressure for some of the frequently encountered gases at two typical hot gas temperatures of 2000 K and 3000 K are given in Fig. 4.2. The specific heat in J/mole K does not



change very significantly with change of temperature. It depends on whether the gases are mono-atomic, diatomic, tri-atomic or more complex. The mono-atomic gases, such as, helium (He), hydrogen atom (H) or oxygen atom (O), have the lowest specific heat of about 21 J/mole K. The diatomic gases comprising, typically, hydrogen ( $H_2$ ), oxygen ( $O_2$ ), carbon monoxide (CO), hydroxyl (OH) have higher values of specific heat of about 37 J/mole K. The tri-atomic gases, carbon dioxide ( $CO_2$ ) and water ( $H_2O$ ) have further increased values of specific heats of about 60 J/mole K. Gases having lower specific heats are to be preferred, as they would provide higher combustion temperatures for a given value of energy released in a chemical reaction. Mono-atomic and di-atomic gases in the combustion products are, therefore, to be preferred to gases having more complex molecular structure.

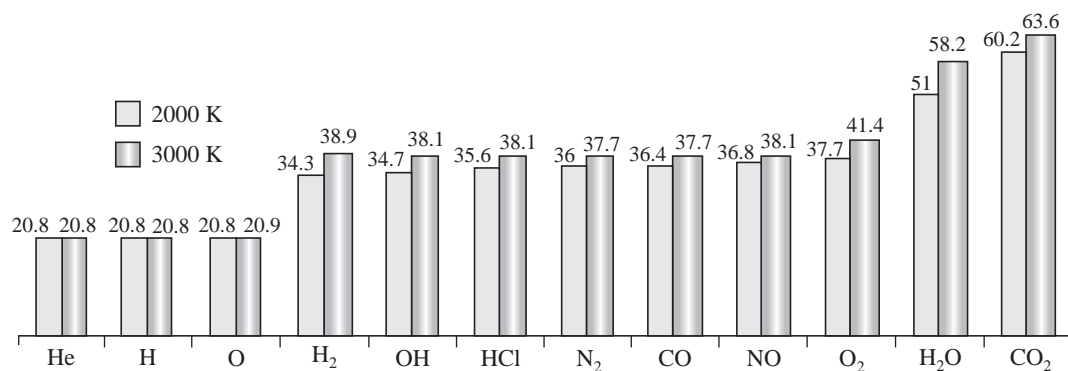


Fig. 4.2 Specific Heat in J/mole K at 2000 K and 3000 K

### (c) Specific Heat Ratio

Substances with a complex chemical structure give smaller values of the specific heat ratio ( $\gamma$ ). The value of  $\gamma$  is, typically, about 1.66 for mono-atomic gases, about 1.4 for di-atomic gases and about 1.33 for tri-atomic gases. A smaller value of  $\gamma$  was seen in the last chapter to be desirable for obtaining higher values of  $C^*$ . Combustion gases having more complex chemical structure are, therefore, to be preferred from the point of view of specific heat ratio. However, this requirement is contradictory to the requirements from the point of view of specific heat and molecular mass. The influence of  $\gamma$  on  $I_{sp}$  was, however, seen to be weaker than the influence of temperature and molecular mass. The general practice is, therefore, to choose propellants which give higher temperatures and lower molecular mass of combustion products.



## 4.2 ENERGY RELEASE DURING COMBUSTION OF PROPELLANTS

The fuel and oxidiser, constituting the propellant, chemically react to form the products of combustion. If the internal chemical energy associated with the chemical structure of the combustion products is less than that of the propellant, the excess energy of the propellants over the products of combustion gets released during the chemical reaction.

The amount of energy released depends on the reactants (propellants) and the nature of the combustion products formed during the chemical reaction. Consider, for example, the following chemical reaction of element carbon in solid phase with gaseous oxygen to form carbon dioxide:



The heat released, if measured, would be 32,800 kJ per kg of carbon burnt. If carbon monoxide were formed during the oxidation process of carbon as per the reaction:



the heat release is much lower at about 9208 kJ per kg of the carbon burnt. This is because the internal chemical energy of carbon monoxide is higher than that of carbon dioxide allowing only a smaller energy to get released in the reaction.

An *a priori* knowledge of the products formed in the combustion process and the value of the internal chemical energy of the products is required in order to determine the heat released during the chemical reaction. In the next two sections, we define a few terminologies and a procedure to determine the products of reaction and the energy released in the combustion of propellants.

#### 4.2.1 Stoichiometry, Mixture Ratio, Moles and Mole Fraction

##### (a) Stoichiometry and Mixture Ratio

The proportion of the reacting substances (viz., fuel and oxidiser) is referred to as stoichiometry. The word stoichiometry is derived from the Greek words stoikheion meaning element and metria meaning amount. In practice, stoichiometry refers to the amount of fuel and oxidiser which leads to the fuel being completely oxidised (*i.e.* forming completely oxidised products). Completely oxidised products are most stable substances with the least internal chemical energies. A stoichiometric chemical reaction, which forms completely oxidized combustion products, therefore, releases maximum amount of energy.

To illustrate the above, the stoichiometric combustion of butane gas ( $\text{C}_4\text{H}_{10}$ ) with oxygen is considered in which completely oxidised products of combustion  $\text{CO}_2$  and  $\text{H}_2\text{O}$  are formed. The reaction is given by:



The combustion of fuel with oxidiser does not always lead to the formation of completed combustion products. When lesser quantities of oxidiser compared to the stoichiometric requirement are available, completely oxidised substances cannot be formed.

A term ‘mixture ratio’ is defined to denote the ratio of the mass of the oxidiser and mass of fuel taking part in the combustion. It is denoted by the symbol  $MR$ .

$$MR = \frac{M_{ox}}{M_f} \quad \dots(4.4)$$

Here  $M_{ox}$  and  $M_f$  denote the mass of oxidiser and fuel taking part in the chemical reaction. The mixture ratio corresponding to stoichiometric composition is referred to as stoichiometric mixture ratio ( $MR_{st}$ ). When  $MR < (MR)_{st}$ , the proportion of fuel is more than stoichiometric, *i.e.* the composition used is fuel rich.

##### (b) Moles and Mole Fraction

While describing chemical reactions, it is more convenient to work with the term moles and mole fractions rather than use the mass of the substances.



Moles, denoted by  $n$ , represent the mass in units of the molecular mass. For example, in the reaction given by eq. 4.3, we say 2 moles of butane reacts with 13 moles of oxygen to form 8 moles of carbon dioxide and 10 moles of water. Two moles of butane are indicative of  $2 \times 58$  g of butane, where 58 g denotes the molecular mass of butane. Similarly, 13 moles of oxygen imply  $13 \times 32$  g of oxygen.

It is important to distinguish between moles and the number of molecules of the substance. By Avagadro's law, we know that the number of molecules in a gas of specified volume, temperature and pressure is the same for all gases and so is independent of the nature of the gas. The number of molecules in a mole of any substance is the molecules contained in the molecular mass of the substance and is the Avagadro's number ( $= 6.023 \times 10^{23}$ ).

Mole fraction of a particular substance, say the  $i^{\text{th}}$  substance in a mixture of several substances is denoted by  $x_i$  and is given by:

$$x_i = \frac{n_i}{n} \quad \dots(4.5)$$

Here  $n_i$  is the number of moles of substance  $i$  and  $n$  is the total number of moles contained in the mixture  $\left( \sum_i n_i \right)$ . From Avagadro's law, stated as equal volumes of all gases at the same temperature and pressure contain the same number of molecules, the mole fraction is the same as the volume fraction for gaseous mixtures.

#### 4.2.2 Heat of Formation

The heat liberated in a chemical reaction was seen to come from the reactants undergoing a change of the chemical structure to form new substances with a different chemical structure and having lower chemical energy. The energy associated with the chemical structure of a substance is, therefore, the required property to determine the heat of a reaction and this property is known as 'Heat of Formation'. We had referred to it as internal chemical energy earlier. It is the enthalpy associated with the chemical structure of the substance and is defined as the enthalpy required to form one mole of the substance at the standard state of  $25^{\circ}\text{C}$  and one atmosphere pressure from its basic elements in the standard state at  $25^{\circ}\text{C}$  and one atmosphere pressure. The basic elements are the naturally occurring elements at the standard ambient conditions ( $25^{\circ}\text{C}$ , one atmosphere pressure), such as, oxygen  $\text{O}_2$  as a gas, carbon C(s) in solid form, hydrogen  $\text{H}_2$  as a gas, etc. The heat of formation is denoted by  $\Delta H_f^{\circ}$ , where  $\Delta H$  indicates enthalpy required to form the substance from the elements, subscript 'f' denotes the formation of the substance from its elements and superscript ' $^{\circ}$ ' denotes that both the elements and the substance formed from the elements are at the same standard state.

In order to illustrate the above, consider the example of carbon dioxide ( $\text{CO}_2$ ).  $\text{CO}_2$  in gaseous state is formed from the elements carbon(s) and oxygen ( $\text{O}_2$ ) which exist in the solid and gaseous state respectively at the standard state of 1 atmospheric pressure and  $25^{\circ}\text{C}$ . The chemical reaction given by eq. 4.1 gave an energy of 32,800 kJ/kg of carbon burnt. For each mole of  $\text{CO}_2$  formed as per reaction, 1 mole of carbon(s) is used. The molecular mass of carbon(s) is 0.012 kg/mole. Hence, the energy release corresponding to one mole of  $\text{CO}_2$  [one mole of  $\text{CO}_2$  is formed from one mole of carbon(s)] is  $0.012 \times 32,800 = 394$  kJ/mol. This energy results in an increase of temperature of  $\text{CO}_2$ .



If the formation of  $\text{CO}_2$  were to be at the standard temperature of  $25^\circ\text{C}$  and one atmosphere pressure, it is essential to remove 394 kJ/mole during the reaction. The heat of formation of  $\text{CO}_2$ , denoted by  $\Delta H_f^\circ, \text{CO}_2$ , is therefore  $-394$  kJ/mole.

If we consider the formation of water [ $\text{H}_2\text{O(l)}$ ] from its elements—hydrogen and oxygen—at the standard state of  $25^\circ\text{C}$  and one atmosphere pressure, the reaction can be written as:



The heat generated during the reaction is 286 kJ per mole of water formed. In order to maintain isothermal conditions ( $25^\circ\text{C}$ ) 286 kJ heat needs to be taken out of the system. The heat of formation of  $\text{H}_2\text{O}$  ( $\Delta H_f^\circ, \text{H}_2\text{O(l)}$ ) is  $-286$  kJ/mole.

If H atoms were generated from the element  $\text{H}_2$ , an energy of 435 kJ is required to be supplied for the reaction:



An amount of energy of  $435/2 = 217.5$  kJ/mole is, therefore, required to be supplied for the formation of 1 mole of H from its element  $\text{H}_2$ . The heat of formation of H ( $\Delta H_f^\circ, \text{H}$ ) is  $+217.5$  kJ/mole.

The heat of formation of different substances in solid, liquid and gaseous phases can be determined by knowing the heat generated or absorbed during their formation from the elements in the standard state. The heat of formation of the elements, *e.g.*, hydrogen, nitrogen and oxygen at  $25^\circ\text{C}$  and one atmospheric pressure, and carbon(s) at  $25^\circ\text{C}$  is, by definition, zero. For liquids and solids the reference state is the real state of the substance at a temperature of  $25^\circ\text{C}$ .

'Heat of formation' is a property characterising the chemical structure of the substance. It is possible to calculate it, based on the nature of atomic bonds which hold the atoms together in the substance. For this purpose we make use of the energy of the bonds in the substance.

Bond energy represents the energy associated with the chemical bonds between the atoms. For a given type of bond between two atoms (*e.g.* O—H, C=O, C—H, etc.) the bond energy is unique. The bond gets weaker as the atomic number increases. Double bonds are stronger than single bonds. In addition to energy between bonds, substances with multiple bond structure, such as, benzene and complex hydrocarbons possess resonance energy associated with vibration between the different structures. The sum of the bond energy and resonance energy is the net internal chemical energy of the substance and constitutes its heat of formation.

The energy of C—H bond per mole is 413 kJ. The bond energy for  $\text{N}_2$  is 945 kJ/mole; for  $\text{O}_2$  and for  $\text{H}_2$ , it is 498 kJ/mole and 436 kJ/mole respectively. The energy of O—H bond is 463 kJ/mole. A bond is said to be a weak chemical bond if the bond energy is less than 200 kJ/mol and average if the bond energy is about 500 kJ/mole. A bond is said to be strong for energy greater than 800 kJ/mole.

Since the heat of formation of a substance is based on the enthalpy required to form the substance from its elements in the same standard state, the heat of formation would correspond to the excess energy of the bonds in the substance over the bond energy of the elements from which it is formed. As an example, the heat of formation of  $\text{H}_2\text{O}$  can be calculated based on the difference in the energies of the two O—H bonds in  $\text{H}_2\text{O}$  and the bond energy of  $\text{H}_2$  and  $\frac{1}{2}\text{O}_2$ . The bond energies of O—H,  $\text{H}_2$  and  $\text{O}_2$  is 463, 436 and 139 kJ/mole respectively. The heat of formation of  $\text{H}_2\text{O(g)}$  would, therefore, be:



$$-\left[2 \times 463 - \left(436 + \frac{1}{2} \times 498\right)\right] = -241 \text{ kJ/mole.}$$

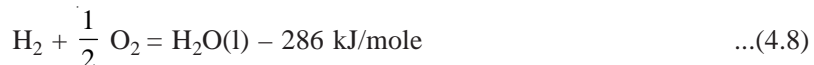
But under the standard condition of one atmosphere pressure and 25°C, H<sub>2</sub>O will be in the form of water, *i.e.* H<sub>2</sub>O(l). We need to consider the heat of vapourisation for H<sub>2</sub>O(g) → H<sub>2</sub>O(l), which is – 40.6 kJ/mole at 100°C to condense the vapour and a sensible heat from 100°C to 25°C of 0.068[kJ/(mole-K)] × 75[K] = – 5.09 kJ/mole. Here 0.068 kJ/(mole K) is the specific heat of water. This gives the heat of formation of water to be, = – [241 + 40.6 + 5.09] = – 286.7 kJ/mole, as given earlier.

The heat of formation can be determined in the above manner using bond energies. The usual practice, however, is by finding out the chemical reactions through which the substance is formed and using the known values of heat of formation of the other substances involved in the reaction.

#### 4.2.3 Heat of Combustion and Temperature of Combustion Products

Heat of combustion refers to the energy liberated in a chemical reaction. It is different from the heat of formation which refers to the energy required to form a particular substance from its stable elements when both are at the standard state. At the standard condition of one atmospheric pressure and 25°C, the heat of combustion corresponds to the negative of the difference between the heat of formation of the products and the heat of formation of the reactants when both the reactants and products are at the same standard state. The excess energy in the reactant above the product is available as heat. The heat of combustion is given by [– (Σ<sub>products</sub> ΔH<sub>f</sub><sup>o</sup> – Σ<sub>reactants</sub> ΔH<sub>f</sub><sup>o</sup>)] and goes to increase the temperature of the combustion products.

In order to illustrate the above through examples, consider the formation of water at 25°C from the elements H<sub>2</sub> and O<sub>2</sub> also at 25°C and one atmospheric pressure. The standard heat of formation of H<sub>2</sub>O(l) is – 286 kJ/mole while H<sub>2</sub> and O<sub>2</sub> being standard elements have zero heat of formation. The heat of combustion for this reaction is – {[ΔH<sub>f</sub><sup>o</sup>]<sub>H<sub>2</sub>O(l)}</sub> – ([ΔH<sub>f</sub><sup>o</sup>]<sub>H<sub>2</sub></sub> + [ΔH<sub>f</sub><sup>o</sup>]<sub>O<sub>2</sub></sub>)} = – {–286 – (0 + 0)} = 286 kJ/mole. The reaction is represented as:



The negative sign shows that the energy must be removed from this reaction for H<sub>2</sub>O(l) to be formed at 25°C and one atmospheric pressure. The reaction is exothermic. This heat goes to increase the temperature of H<sub>2</sub>O.

Similarly, the heat of combustion of the reaction:



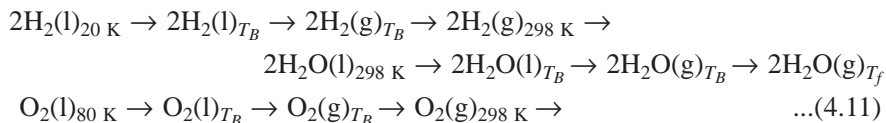
at 25°C and 1 atmospheric pressure can be calculated as – {[ΔH<sub>f</sub><sup>o</sup>]<sub>CO<sub>2</sub></sub> – ([ΔH<sub>f</sub><sup>o</sup>]<sub>CO</sub> +  $\frac{1}{2}$ [ΔH<sub>f</sub><sup>o</sup>]<sub>O<sub>2</sub></sub>)}.

Substituting the values of heats of formation of CO<sub>2</sub>, CO and O<sub>2</sub> as –394, –110 and 0 kJ/mole respectively, we get the heat of combustion as –(–394 – [–110.5 + 0]) = 283.5 kJ for every mole of CO<sub>2</sub> formed. This heat causes an increase in the temperature of CO<sub>2</sub>.

When the reactants and products are not at the standard temperature and pressure conditions, the enthalpy corresponding to the difference between the existing state and the standard state must be accounted for and added to the heat of formation corresponding to the standard state. For example, consider the formation of steam from the combustion of liquid hydrogen at a temperature of 20 K and liquid oxygen at a temperature of 80 K. The overall reaction is given by:



The path considered for determining the heat of combustion can be represented as:



Here  $T_B$  refers to the boiling temperature and  $T_f$  is the final temperature of steam formed.

Liquid hydrogen gets heated as a liquid (sensible heat) from its initial temperature of 20 K to its boiling temperature at which it gets converted into vapour by absorbing latent heat. Thereafter, it gets heated to the standard temperature of 298 K by absorbing sensible heat. Similarly, liquid oxygen gets converted to gaseous oxygen at 298 K by absorbing sensible and latent heats.

Water  $\text{H}_2\text{O}(\text{l})$  is formed at the standard condition of 298 K from hydrogen and oxygen at the standard condition. The heat of combustion raises its temperature to the final temperature of steam,  $T_f$ , by supplying the requisite sensible heats and latent heat. The net heat balance relation for  $2\text{H}_2(\text{l}) + \text{O}_2(\text{l}) = 2\text{H}_2\text{O}(\text{g})$  is:

$$\begin{aligned} 2 \int_{20}^{T_{B1}} C_{p\text{H}_2, L} dt + \int_{90}^{T_{B2}} C_{p\text{O}_2, L} dt + 2H_{v, \text{H}_2} + H_{v, \text{O}_2} + 2 \int_{T_{B1}}^{298} C_{p\text{H}_2, g} dt + \int_{T_{B2}}^{298} C_{p\text{O}_2, g} dt \\ + 2 \int_{298}^{T_{B3}} C_{p\text{H}_2\text{O}, l} dt + 2H_{v, \text{H}_2\text{O}} + \int_{T_{B3}}^{T_f} C_{p\text{H}_2\text{O}, g} dt = 2 \Delta H_f^{\circ, \text{H}_2\text{O(l)}} \end{aligned} \quad \dots(4.12)$$

Here  $\text{H}_2$  and  $\text{O}_2$  are initially at 20 K and 80 K respectively.  $T_{B1}$ ,  $T_{B2}$  and  $T_{B3}$  represent the boiling temperature of liquid hydrogen, liquid oxygen and water respectively.  $H_{v, \text{H}_2}$ ,  $H_{v, \text{O}_2}$  and  $H_{v, \text{H}_2\text{O}}$  represent the latent heat of evaporation of liquid hydrogen, liquid oxygen and water respectively in kJ/mol.  $C_p$  represents the respective specific heat in kJ/(mole K). The heat liberated in the reaction, shown on the right hand side in eq. 4.12, corresponds to 2 moles of  $\text{H}_2$  and 1 mole of  $\text{O}_2$  forming 2 moles of  $\text{H}_2\text{O}$  at the standard state.

The increase of temperature in a given exothermic reaction comes from the heat of combustion, viz., the enthalpy of reaction. The change in enthalpy can be assumed to raise the temperature to  $T_f$ .

#### (a) General Procedure for Calculating Temperature of Combustion Products for any Propellant Combination

Consider the generalised representation of a chemical reaction:

$$\sum_{i=1}^N v_i' M_i = \sum_{i=1}^N v_i'' M_i \quad \dots(4.13)$$

where  $v_i'$  is the mole of species  $M_i$  appearing as a reactant and  $v_i''$  is the mole of species  $M_i$  appearing as a product. The heat of combustion is the net decrease in the heat of formation of the products from that of the reactants:

$$\Delta H_c = - \left[ \sum_{i=1}^N v_i'' \Delta H_{f, M_i}^{\circ} - \sum_{i=1}^N v_i' \Delta H_{f, M_i}^{\circ} \right] \quad \dots(4.14)$$

The exothermic heat is used to raise the temperature of the products from the standard state of 25°C to the final temperature,  $T_f$ . When the enthalpy of the reactants is less than that at the standard



state due to the reactant being at a lower temperature than 25°C or in a different phase, part of the heat of combustion (evaluated based on the standard condition of the reactants and products) has to be apportioned to bring the reactants to the standard state. This results in the final temperature of the combustion products being lower than the temperature when the reactants were at the standard state. If the combustion process is not adiabatic, the heat loss during the chemical reaction results in a lower temperature of the combustion products compared to adiabatic conditions.

#### 4.2.4 Determining the Products of Combustion

The products of combustion,  $M_i$ , and the number of moles of the products,  $v''$ , given in eq. 4.13, must be known in order to determine the net heat of formation of the combustion products and hence the heat of combustion. For the particular case of a stoichiometric reaction or when there is a surplus of oxidiser [ $(MR) \geq (MR)_{st}$ ], completely oxidised products of combustion can be assumed to be formed, e.g. CO<sub>2</sub> from C(s) and H<sub>2</sub>O from H<sub>2</sub>.

When the amount of oxidiser is less than that required for complete combustion [ $MR < (MR)_{st}$ ], under-oxidised products (such as CO) will be formed. Most of the propellants used in practice are fuel rich and we will determine the reasons for this later on in this chapter. In such cases, it is not correct to assume completely oxidised combustion products. The following procedure is used to get an approximate assessment of the products formed with the fuel-rich propellants comprising carbon, hydrogen, nitrogen and oxygen.

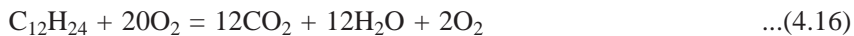
All nitrogen in the propellant is assumed to form N<sub>2</sub> in the products and all hydrogen is assumed to form H<sub>2</sub>O (since hydrogen is more reactive than carbon); the oxygen left in the propellant after forming H<sub>2</sub>O burns carbon to CO and any oxygen still left over burns CO to CO<sub>2</sub>. If the amount of oxygen is not sufficient to convert the hydrogen to H<sub>2</sub>O, only part of the hydrogen is converted to H<sub>2</sub>O and the balance is left as H<sub>2</sub>. Carbon(s) in the propellant remains as Carbon(s) in the products. The method does not take into account the break up (dissociation) of the combustion products at the high temperatures and the formation of oxides of nitrogen.

The procedure is illustrated for oxidiser-rich and fuel-rich combinations by the following example involving chemical reaction between kerosene (C<sub>12</sub>H<sub>24</sub>) and oxygen (O<sub>2</sub>). The stoichiometric reaction for kerosene-oxygen is:

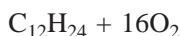


$$\text{The stoichiometric mixture ratio } (MR)_{st} = \frac{18 \times 32}{168} = 3.43.$$

(a) *For oxygen-rich mixture, [(MR) > (MR)<sub>st</sub>]:* If (MR) is say 3.81, the number of moles of oxygen ( $n_{\text{O}_2}$ ) per mole of kerosene is given by  $\frac{n_{\text{O}_2} \times 32}{168} = 3.81$  giving  $n_{\text{O}_2} = 20$ . The oxygen-rich mixture will form completely oxidised products of combustion and the balance oxygen would be available in the products as given below by the reaction:



(b) *For fuel-rich mixture, [(MR) < (MR)<sub>st</sub>]:* If (MR) is say 3.05, we have the number of moles of O<sub>2</sub> as  $\frac{n_{\text{O}_2} \times 32}{168} = 3.05$  or  $n_{\text{O}_2} = 16$ . This gives the reactants as:



In this case, 24H consumes 6O<sub>2</sub> to form 12H<sub>2</sub>O. 12-C reacts with the remaining 10O<sub>2</sub> to form 12CO and 4O<sub>2</sub> is left. Of 12CO formed, 8CO combines with the remaining 4O<sub>2</sub> to form 8CO<sub>2</sub> leaving 4CO as under-oxidised combustion product. The reaction is, therefore, written as:



It must be noted that this method does not take into account the thermodynamic equilibrium and dissociation of the combustion products at the high temperatures (CO<sub>2</sub> and H<sub>2</sub>O break up into CO, OH, H<sub>2</sub>, H and O). An accurate estimation of combustion products must consider chemical equilibrium between the products. The procedure is described in Annexure B.

Once the products of combustion and the number of moles are determined, the heat release in the reaction is found out from the difference between the heat of formation of the products and reactants.



## 4.3 CRITERION FOR CHOICE OF PROPELLANTS

### 4.3.1 Heat Release Considerations

The heat released from combustion of the propellants was seen in the last section as:

$$\Delta H_c = - \left[ \sum_{\text{Products: } i=1}^N v_i'' \Delta H_f^\circ_{f, M_i} - \sum_{\text{Reactants: } i=1}^N v_i' \Delta H_f^\circ_{f, M_i} \right] \quad \dots(4.18)$$

It is seen from the above equation, that the heat of formation of  $\Delta H_f^\circ$  of the products of combustion of the propellants must be large and negative while the propellants themselves (reactants) must have a positive or a small negative value of  $\Delta H_f^\circ$  in order to obtain maximum heat release.

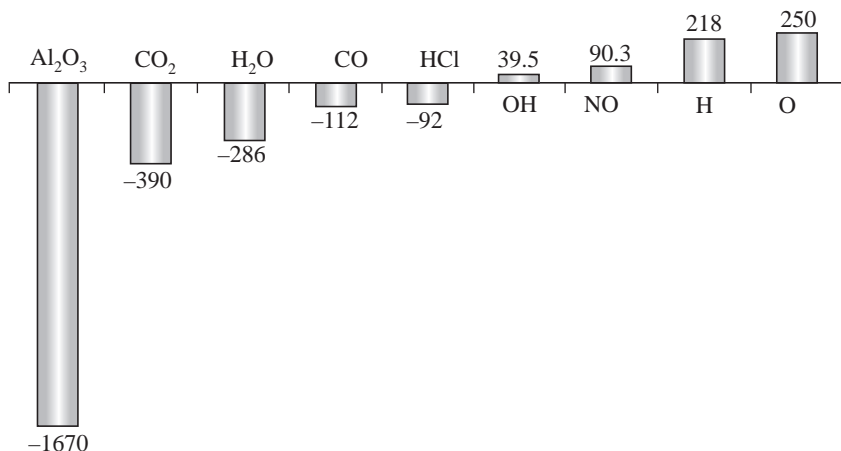


**Fig. 4.3** Heat of Formation in kJ/mole of Some Typical Products of Combustion

The values of  $\Delta H_f^\circ$  for typical products of combustion are given in Fig. 4.3. It is seen that the completely oxidised substances, e.g. CO<sub>2</sub>, H<sub>2</sub>O and Al<sub>2</sub>O<sub>3</sub> have large negative values of  $\Delta H_f^\circ$ . It would, therefore, be desirable that the propellants used and the mixture ratios are such that these



completely oxidised substances are formed during the combustion as against the under-oxidised CO and the dissociated products, such as, OH, H and O.

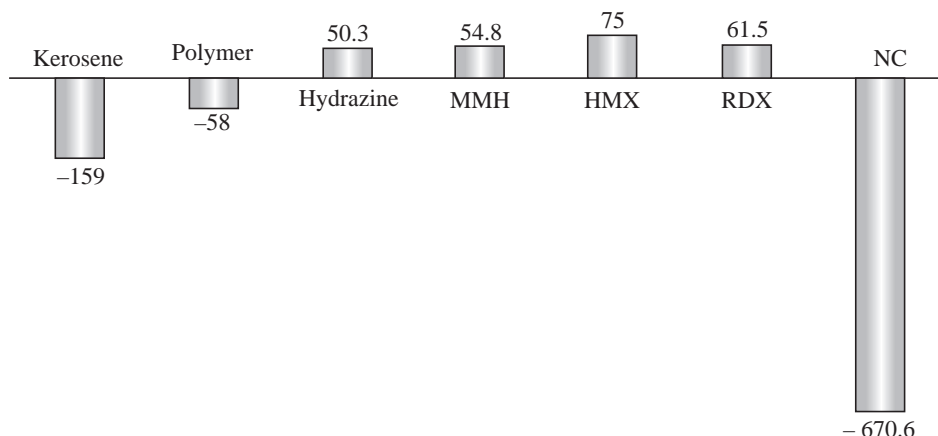


**Fig. 4.4** Heat of Formation in kJ/mole of Some Typical Propellants (Fuels)

The heats of formation of a few propellants comprising fuel, oxidiser or a combination of fuel and oxidiser (explosive) are shown in Figs. 4.4 and 4.5. It is seen that the propellant hydrazine ( $N_2H_4$ ) and explosives, such as, RDX and HMX have positive heats of formation. RDX and HMX are cycloaliphatic compounds. RDX is cyclotrimethylene trinitramine  $[(CH_2)_3(NNO_2)_3]$  while HMX is cyclotetramethylene tetranitramine  $[(CH_2)_4(NNO_2)_4]$ . We shall consider these explosives, which are fuel-rich, while studying solid propellants.

Substances having positive heat of formation, though suited from considerations of energy release, are generally unstable and tend to react spontaneously and are, therefore, hazardous. The trend, therefore, is to choose the reacting propellants with rather small negative values of  $\Delta H_f^\circ$ . Solid oxidisers, such as, ammonium perchlorate (AP) and nitroglycerine (NG), solid fuel consisting of polymers and nitrocellulose (NC), liquid fuels, such as, kerosene and liquid oxidisers, such as, dinitrogen tetroxide ( $N_2O_4$ ) and nitric acid ( $HNO_3$ ), find application as oxidisers and fuels. Substances which are elements at the standard state, such as, hydrogen, oxygen, metal aluminium, metal boron, etc., having  $\Delta H_f^\circ = 0$  are also well suited. Hydrazine ( $N_2H_4$ ) and mono-methyl hydrazine (MMH –  $CH_3N_2H_3$ ) have mildly positive values of  $\Delta H_f^\circ$  and are widely used since they do not spontaneously react.

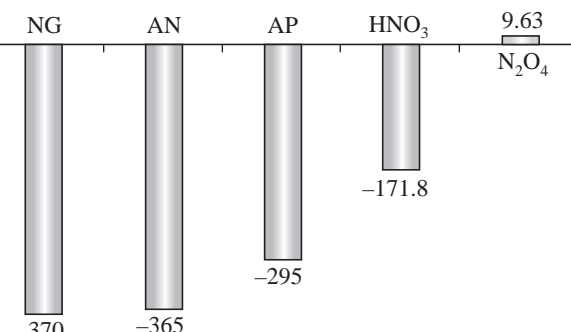


**Fig. 4.5** Heat of Formation in kJ/mole of Some Typical Propellants (Oxidisers)

#### 4.3.2 Molecular Mass Considerations

Lower molecular mass of combustion products is obtainable with fuels having lower atomic mass, such as, fuel hydrogen reacting with oxygen or fluorine. The propellant combination  $H_2/F_2$  has the highest specific impulse followed by  $H_2/O_2$  combination since the molecular mass of the combustion products is very low.



Propellant combinations having fuel-rich mixture ratios ( $(MR) < (MR)_{st}$ ), form combustion products with lower molecular mass. This was seen in the example given in eq. 4.17 wherein CO was formed in addition to  $\text{CO}_2$  for fuel-rich mixture ratios. The use of fuel-rich mixture ratios for propellants is followed in most of the existing rockets. The lower molecular mass of the products also give smaller values of specific heats.

The energy release from the chemical reactions will be maximum at the stoichiometric mixture ratio (since completely oxidised products of combustion with large negative values of heat of formation are obtained). The decrease in the values of specific heats at fuel-rich mixture ratios results in the temperature of a slightly fuel-rich mixture to be very near to that of the stoichiometric mixture ratio. A typical variation of temperature of combustion products, therefore, has a trend as shown in Fig. 4.6. The maximum temperature is obtained in the fuel-rich mixture very near to the stoichiometric mixture ratio. The decrease in the molecular mass for fuel-rich

mixture ratio gives the maximum values of  $\sqrt{\frac{T_c}{M}}$

for fuel rich mixtures. Maximum values of specific impulse would, therefore, be obtained for fuel-rich mixture ratios instead of stoichiometric mixture ratios. This is illustrated in Fig. 4.7.

The method adopted so far for estimating the products of combustion at different mixture ratios was approximate and did not consider the thermodynamic equilibrium and the dissociation of the products at higher temperatures. The energy release from the chemical reactions decreases due to dissociation. The trend of the variations of the temperature of the combustion products  $T_c$  formed from the combustion of LOX and  $\text{LH}_2$  with dissociation taken into account (procedure is given in Annexure B) as the chamber pressure increases from 1 MPa to 1000 MPa is shown in Fig. 4.8. Dissociation is

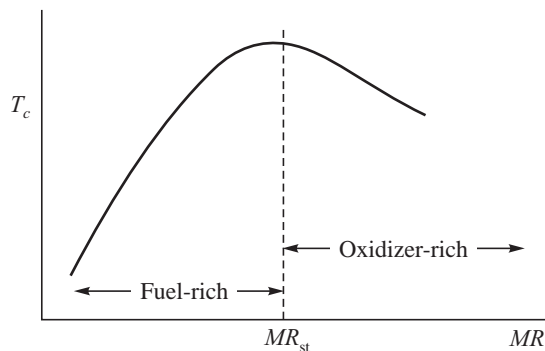


Fig. 4.6 Typical Variation of Temperature of Combustion Products with Mixture Ratio

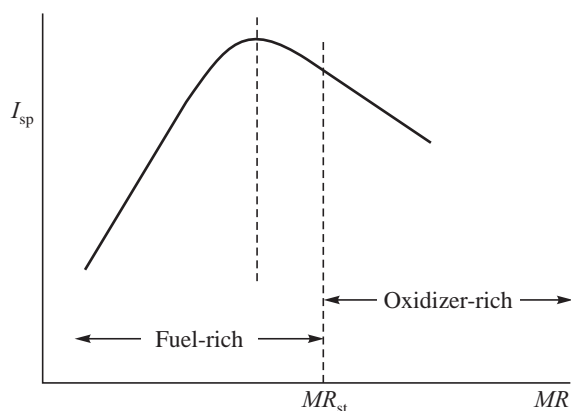


Fig. 4.7 Typical Variation of Specific Impulse with Mixture Ratio

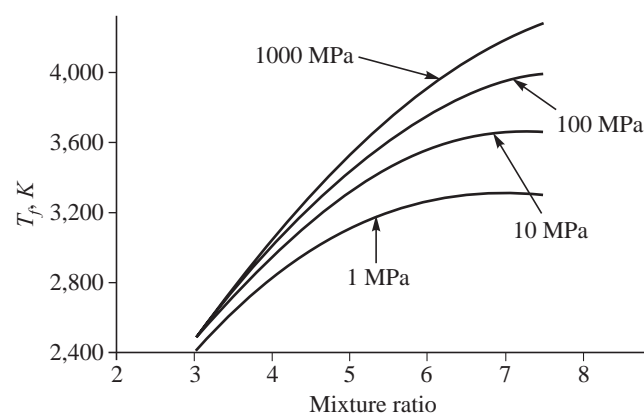


Fig. 4.8 Variation of Temperature of Combustion Products at Different Mixture Ratios and Chamber Pressures for LOX- $\text{LH}_2$



aggravated at lower pressures due to the reduced resistance from the neighbouring molecules. The dissociation results in a reduced temperature at the lower pressures.

The effect of dissociation is to bring down the molecular mass,  $\mathfrak{M}$ , at the lower range of pressures as shown in Fig. 4.9. The specific heat ratio,  $\gamma$ , of the gases, however, increases at the lower chamber pressures due to the formation of the less complex products of combustion. The variation of  $\gamma$  with mixture ratio and chamber pressure is shown in Fig. 4.10.

The net effect of the variations of  $T_c$ ,  $\mathfrak{M}$  and  $\gamma$  on the sea-level specific impulse  $I_{sp, SL}$  for propellants LOX-LH<sub>2</sub> is shown in Fig. 4.11. Here the gases are assumed to be expanded in the nozzle to the ambient pressure of 0.1 MPa corresponding to sea-level. It is seen that the maximum  $I_{sp}$  occurs at fuel-rich mixture ratios much lower than the stoichiometric mixture ratio of 8.0. The peak values of  $I_{sp}$  at the different pressures are joined by the dotted line in Fig. 4.11. The mixture ratio corresponding to maximum  $I_{sp}$  is seen to progressively increase as the chamber pressure increases. At smaller values of pressure for which the dissociation is more significant, the peak value of  $I_{sp}$  occurs at mixture ratios which are considerably fuel-rich. This is due to the combined influence of the temperature, molecular mass and specific heat ratios dealt with in Figs. 4.8 to 4.10.

A fuel-rich mixture ratio would, therefore, be desirable to achieve higher specific impulse. The choice of the optimum value of mixture ratio would vary with the chamber pressure.

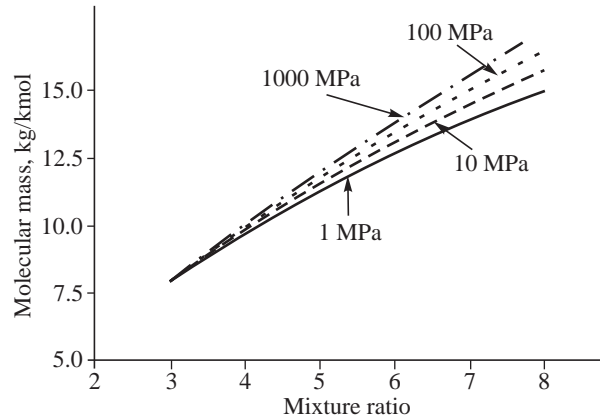


**Fig. 4.9** Variation of Molecular Mass with Temperature of Combustion Products at Different Mixture Ratios and Chamber Pressures for LOX-LH<sub>2</sub>

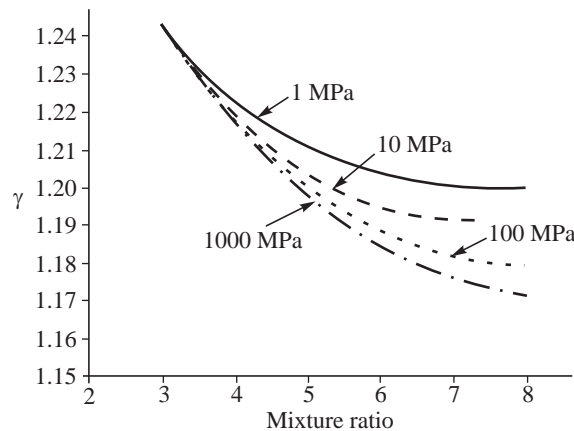


**Fig. 4.10** Variation of Specific Heat Ratio of Combustion Products at Different Mixture Ratios and Chamber Pressure for LOX-LH<sub>2</sub>

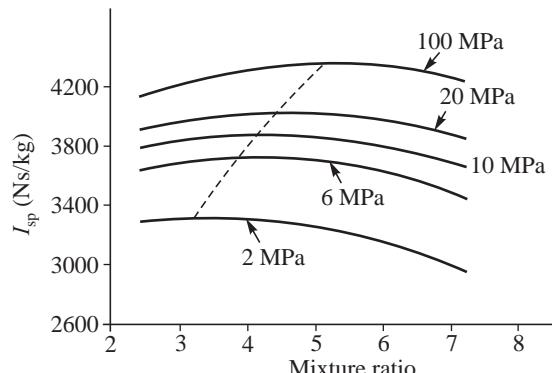


**Fig. 4.11** Variation of Specific Impulse at Different Mixture Ratios and Chamber Pressure for LOX-LH<sub>2</sub>



### 4.3.3 Other Criteria

- (a) **Propellant Density:** The density of a propellant was seen in Chapter 2 to be important and to directly influence the incremental velocity provided by the rocket when the mass of propellant was much smaller than the structural and useful mass of the rocket. This condition applies for the ground stages of a large multistage rocket for which the mass of the upper stages enhances its initial mass. A higher density propellant will also occupy a smaller volume and thus bring down the structural mass of the rocket.
- (b) **Stability of Fuel and Oxidiser:** The stability is important as the propellant should not spontaneously react and explode. Propellants having positive heats of formation are usually less stable.
- (c) **Storability, Corrosiveness and Toxicity:** Propellants, such as, Liquid hydrogen and Liquid oxygen, are required to be stored in specially insulated containers. The storage and use of a propellant, such as, fluorine is difficult as it corrodes almost all metals. Propellants based on the hydrazine family are carcinogenic and call for special precautions in their production, storage and handling. Oxidisers, such as nitric acid and di-nitrogen tetroxide, emit toxic fumes. It would be preferable to choose propellants which are easy to handle and are not harmful to humans and the environment.
- (d) **Cost:** The cost is important for the rocket to be commercially viable. We shall consider the above aspects in addition to the performance while dealing with solid, liquid and hybrid propellants.



## 4.4 SOLID PROPELLANTS

Solid propellants are classified into the following four categories:

- (a) Double-base or homogeneous propellants,
- (b) Composite or heterogeneous propellants,
- (c) Composite modified double-base propellants, and
- (d) Nitramine propellants.

The composition and salient features of these propellants are discussed in the following sections.

### 4.4.1 Double-base Propellants

The propellants comprise nitrocellulose (NC) and nitroglycerine (NG) mixed together at the molecular level to form a homogeneous substance. NC constitutes the fuel. Part of the hydroxyl radicals ( $\text{OH}$ ) in cellulose, which consists of carbon, hydrogen and oxygen in a linear structure  $[\text{C}_6\text{H}_{10}\text{O}_5]_n$  is substituted by the nitrate radical  $\text{ONO}_2$  in NC to give a molecular structure  $[\text{C}_6\text{H}_{10-x}\text{O}_{5-x}(\text{NO}_3)_x]_n$ . The part of hydroxyl radicals, replaced by  $\text{ONO}_2$ , is represented by ' $x$ ' in the above molecular formula and would vary depending on the amount of nitration.

NG, whose chemical formula is  $[\text{C}_3\text{H}_5(\text{ONO}_2)_3]$ , is based on glycerine or propane triol  $[\text{C}_3\text{H}_5(\text{OH})_3]$ . The OH radical of glycerine is replaced by  $\text{ONO}_2$  to form NG. NG is oxidiser-rich. The chemical structure of NG is aliphatic with a straight chain structure shown below:



Both NC and NG can be used singly as propellants since they have both oxidiser and fuel in them. These are known as single base propellants.

When NC and NG are used together, they constitute double-base propellant. NG forms a colloid when properly compounded with NC in the presence of a few additives comprising a plasticiser, such as, diethyl phthalate and triacetin, and stabiliser, such as, diphenylamine. Plasticisers not only increase the fluidity but also make the propellant less sensitive to ignition from impact.

The double-base propellant is also known as ‘homogeneous propellant’, ‘mixed propellant’ or ‘colloidal propellant’. It is also known by the trade name ‘Cordite’.

#### 4.4.2 Composite Propellants

The propellant is heterogeneous with a solid crystalline oxidiser, such as, ammonium perchlorate ( $\text{NH}_4\text{ClO}_4$ ) dispersed in a polymeric fuel. Metal aluminium powder is also added to enhance the energy released during combustion. The polymer binds together the discrete crystalline oxidiser particles and the metal powder to form a tough rubbery mass. The polymeric fuel is, therefore, referred to as binder.

##### (a) Oxidiser

Ammonium Perchlorate (AP) is generally used for the oxidiser. Unlike other solid oxidisers, such as, ammonium nitrate ( $\text{NH}_4\text{NO}_3$ ) and potassium nitrate ( $\text{KNO}_3$ ), AP dissociates easily and is not very hygroscopic, and hence is preferred. There are many energetic perchlorate-containing compounds with lower negative heats of formation, such as, nitronium perchlorate ( $\text{NO}_2\text{ClO}_4$ ), hydrazinium perchlorate ( $\text{N}_2\text{H}_5\text{ClO}_4$ ), and hydrazinium diperchlorate [ $\text{N}_2\text{H}_6(\text{ClO}_4)_2$ ]. However, they have poorer compatibility with the polymeric binder and have lower thermal stability with the result that processing of the propellant and storage becomes problematic. More energetic oxidisers, such as, hydrazinium nitroformate [ $\text{N}_2\text{H}_5\text{C}(\text{NO}_2)_3$ ] are being investigated for high performance composite propellants.

Toxic gases, such as hydrochloric acid formed during combustion of AP and hydrazinium perchlorates with polymeric fuels, pollute the environment. The possibilities of using environmental-friendly energetic oxidiser ammonium dinitramide (ADN) are being studied.

##### (b) Polymeric Fuel

The polymeric fuel called binder consists of H, C and O atoms (sometimes N and S also). The atomic number of sulphur is 16 compared to 6 for carbon and 1 for hydrogen. Sulphur is, therefore, not a desirable constituent since its atomic mass is high and would result in combustion products with larger molecular mass.

Saturated hydrocarbons (alkanes), in which carbon atoms are attached to each other by means of single bonds, have small but negative values of heats of formation and could make good binders. Alkenes with one double bond between carbon atoms, alkadienes with two double bonds, alkynes



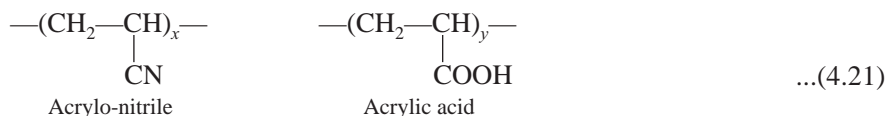
with one triple bond and alkadiynes with multiple triple bonds between carbon atoms are said to be unsaturated. These have large and negative values of heat of formation.

The hydrocarbons could have a straight chain of alkanes, alkenes, alkadienes, alkynes and alkadiynes or could have ring chains in which case they are known as cycloalkanes, cycloalkenes, etc. These straight chain and ring chain hydrocarbons are known as aliphatic compounds and are distinctly different from the aromatic hydrocarbons which have a ring structure of six carbon atoms linked together with three single and three double bonds alternatively (benzene).

The aliphatic compounds especially those with simpler bond structures are to be preferred as they have smaller negative values of heat of formation. However, most of them like methane, ethane, propane and butane are gases. Polymers with multiple cyclo-butadienes in a linear chain structure are, therefore, chosen. These are called Polybutadienes. The butadiene structure comprising alkadienes with four carbon atoms and two alternating double bonds is shown as follows.

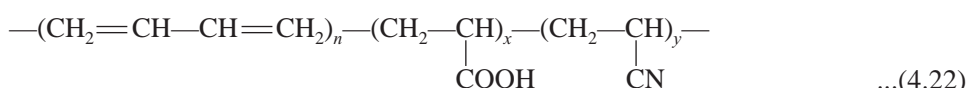


The polybutadiene chain structure is  $-(\text{CH}_2=\text{CH}-\text{CH}=\text{CH}_2)_n-$ . Here  $n$  is the number of butadiene groups. The polybutadiene chain could be attached to poly-acrylo-nitrile group and acrylic acid groups given by:

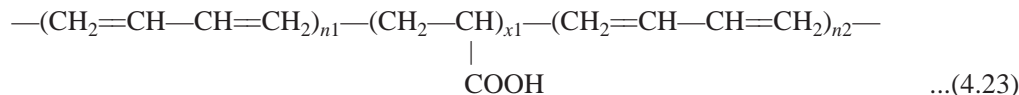


to form polybutadiene acrylic acid acrylonitrile (PBAN).

Carboxy and nitrile groups get attached to the butadiene chain to form a highly cross-linked chain network. The PBAN binder with the linear and cross chains has lower ultimate tensile strength with smaller elongation. It has been used for making propellant grains for large rockets, such as, the solid rocket booster of the Space Shuttle. The structure of the PBAN binder is given below:



The randomness of the cross linking can be reduced by removing the carboxyl groups in PBAN and locating them at the ends of the butadiene chain. This provides better mechanical properties to the binder. The binder with the carboxyl radicals located in a controlled way at the ends of the butadiene chain is known as Carboxy Terminated Poly Butadiene (CTPB).



If the carboxyl radical at the chain ends are replaced by hydroxyl (OH) radical, the binder would give higher performance in a propellant. This is because H in the OH radical has a lower atomic number than C in COOH and the energetics of the hydrogen is superior to carbon. The butadiene chains terminated with OH at the ends is called Hydroxy Terminated Poly Butadiene (HTPB). High performance propellants make use of HTPB.



HTPB and PBAN binders are most widely used for the manufacture of composite propellants.

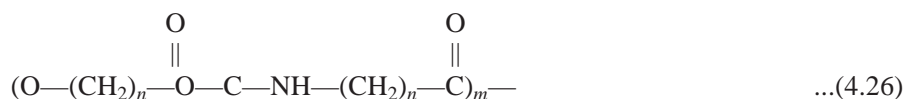
The molecular mass of the binders are large considering the long chain, typical values ranging from 30,000 to 1,00,000 kg/kmole.

Polyvinyl chloride (PVC) was used earlier as the binder. It consists of the chain:



It gives poor performance as it contains less carbon and hydrogen.

Polyurethanes have been used in the past like PVC. They are good energy-wise but contain oxygen and are sensitive to moisture. The chemical structure of polyurethane is given below:



Certain high energy polymers, such as, Glycidyl Azide Polymer (GAP), contain larger percentage of hydrogen and provide higher performance.

### (c) Metals

Metal powders, such as, aluminium are also used as fuel in order to enhance the energy release from combustion since metal combustion is highly exothermic. Aluminium is a light metal and is, therefore, preferable. The aluminium oxide formed as a product of combustion was seen to have a very high negative value of heat of formation (Fig. 4.3).

The use of metal hydrides instead of metals has been thought of with a view to have as much hydrogen in the propellant as possible. The hydrogen, as seen earlier, would contribute to enhancing the specific impulse by lowering the molecular mass of the combustion products. The hydrides are not very compatible with polymeric binders and their use has not been demonstrated in practice.

### (d) Processing of Composite Propellant

The composite propellant, to be concise, consists of solid oxidiser AP, metal powder (aluminium) and a polymer (PBAN, HTPB) which binds the AP crystals and aluminium powder. AP crystals are ground to two different sizes (coarse and fine) to obtain better density of packing and incorporate as much of AP as possible in the propellant. High values of the solid loading in the propellant are desirable. The coarse particle size is typically about 300  $\mu\text{m}$ , while the fine particle size is about 30  $\mu\text{m}$ . The size of the aluminium powder is a few  $\mu\text{m}$ . The ingredients AP and aluminium powder are mixed with the liquid polymer to give viscous slurry. A wetting agent Lecithin is added to ensure proper bonding between the polymer and the solid AP and aluminium powder. Plasticisers are also added as in the double-base propellants. Dioctyl adipate (DOA) is used with HTPB. If the rate of burning of the propellant is to be enhanced or reduced, burn rate modifiers are added. The burning rate accelerators are typically ferric oxide ( $\text{Fe}_2\text{O}_3$ ) and copper chromite ( $\text{Cu}_2\text{Cr}_2\text{O}_5$ ), while an inhibitor for burn rate is lithium fluoride (LiF).

The viscous slurry, so formed, is cured in the rocket chamber at temperatures between 60°C and 150°C to form a tough rubbery mass. The binders are thermosetting substances. Small quantities of



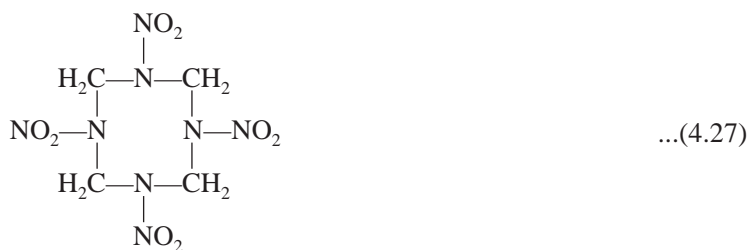
curing agents, such as, Toluene di-isocyanate (TDI), are added which assist in the cross-linking of the polymeric chains and provide structural rigidity to the propellant mass.

The composition of composite propellants is fuel-rich. The solid fraction or solid loading including crystalline AP and aluminium powder is about 80 to 90 per cent with the upper limit of aluminium powder being about 16 to 18 per cent. The binder is generally between 10 to 15 per cent.

#### 4.4.3 Composite Modified Double-base Propellant

The addition of AP crystals to double-base propellants reduces its fuel-richness and improves its specific impulse. The rate of burning of the propellant is also increased as we shall see in the next chapter.

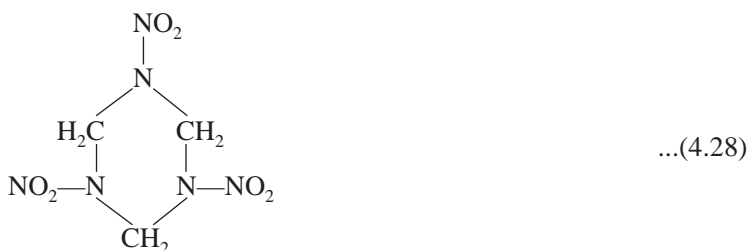
If, instead of adding AP, high explosives, such as, HMX were to be added to the double-base propellants, the energy release could be significantly increased. HMX is an abbreviation for ‘Her Majesty’s Explosive’ and is a ring structure compound—cyclo tetra methylene tetra nitramine [ $C_4H_8N_4(NO_2)_4$ ]. The chemical structure of HMX is given below:



The propellants formed by adding AP or HMX to double-base propellants are known as Composite Modified Double-Base (CMDB) propellants. These are more rugged than the composite propellants and are used for missile propulsion. They have also been used for the upper stage solid propellant rockets.

#### 4.4.4 Nitramine Propellants

High explosives, such as, HMX and RDX are added to fuel binder comprising HTPB or GAP instead of AP and cured to form nitramine propellants. RDX, like HMX is a ring structure compound, but has somewhat lower energy. RDX stands for ‘R&D Explosive’ and is cyclo tri methylene tri nitramine [ $C_3H_6N_3(NO_2)_3$ ]. The chemical structure of RDX is given in the following:



During combustion, the hydrocarbon gases from the polymer combine with the fuel-rich products of HMX and RDX to form low temperature products. Completed products of combustion such as



$\text{CO}_2$  and  $\text{H}_2\text{O}$  will be absent. The polymeric binder acts as a coolant instead of burning the fuel-rich products of HMX and RDX. The infra-red radiation from the products is, therefore, reduced. As much as 85 per cent of HMX and RDX are added to the polymeric binder. The propellant formed by the addition of HMX and RDX to composite propellants having small amounts of oxidiser AP is also referred to as Nitramine propellant. The propellant finds use for strategic applications.



## 4.5 LIQUID PROPELLANTS

Liquid propellants comprise liquid fuels and liquid oxidisers. They are classified according to their energy content, their ignitability and their storage. In the following, we examine the different liquid propellants based on the above classification.

### 4.5.1 Energy Content of Propellant

Energy refers to the heat of combustion. It was seen earlier in this chapter that higher energy release is obtained from fuels and oxidisers having small and negative values of heats of formation or positive heats of formation. The fuels considered were kerosene, hydrazine, mono-methyl hydrazine and hydrogen while the oxidisers consisted oxygen,  $\text{N}_2\text{O}_4$  and  $\text{HNO}_3$ .

Liquid propellants are categorised as per their specific impulse into:

- (a) Low-energy propellants
- (b) Medium-energy propellants, and
- (c) High-energy propellants.

The classification is said to be based on energy though it is actually done on the basis of specific impulse. The specific impulse takes into account the molecular mass of the combustion products in addition to the energy released by the propellant.

#### (a) Low-energy Propellants

The low energy propellants are those which give  $I_{sp}$  at sea-level conditions less than about 3000 Ns/kg. They comprise liquid oxygen ( $\text{LO}_2$ ) and alcohol which was successfully used in the V2 rockets during the Second World War. Liquid oxygen and kerosene, also known as rocket propellant (RP) and certain combinations of oxidisers and fuels, such as, nitric acid with aniline, xylidine or hydrazine and  $\text{N}_2\text{O}_4$  with hydrazine, mono-methyl hydrazine and unsymmetrical di-methyl hydrazine also constitute the low energy propellants. The characteristics of these propellants are discussed in the following:

Aniline ( $\text{C}_6\text{H}_7\text{N}$ ) is an aromatic amine in which the amine radical  $\text{NH}_2$  is attached to the benzene chain. In the case of xylidine ( $\text{C}_8\text{H}_{11}\text{N}$ ) two methyl radicals are additionally attached to the benzene chain.

Both aniline and xylidine react spontaneously with nitric acid ( $\text{HNO}_3$ ) when brought in contact in the liquid phase itself. The combustion products, however, contain a lot of soot considering the aromatic nature of the fuel. The energy release is low since the heats of formation of both the fuels (about  $-100$  kJ/mole) and  $\text{HNO}_3$  (about  $-200$  kJ/mole) are somewhat large and negative. These propellants are used only when high performance is not a requirement.



The oxygen content in  $\text{HNO}_3$  is enhanced by dissolving about 15 per cent  $\text{NO}_2$  in it. Red fumes are obtained from the high  $\text{NO}_2$  content and the mixture is known as Red Fuming Nitric Acid (RFNA). The incorporation of a small quantity of  $\text{NO}_2$  content in  $\text{HNO}_3$  (about 0.5 per cent) is known as White Fuming Nitric Acid (WFNA).

$\text{HNO}_3$  is very corrosive. The addition of about 0.5 to 0.8 per cent of hydrofluoric acid (HF) to RFNA inhibits the corrosion of the storage vessel and the inhibited RFNA is termed as Inhibited Red Fuming Nitric Acid (IRFNA). IRFNA with aniline and xylidine have been extensively used in the past especially for low performing missiles.

Fuel hydrazine ( $\text{N}_2\text{H}_4$ ) has a much simpler molecular structure with bonds as illustrated below:



It has a positive heat of formation and dissociates in the presence of a catalyst to liberate heat. It is, therefore, sometimes used as a single propellant without the need for an oxidiser and is, therefore, called a monopropellant. Similarly, the oxidiser hydrogen peroxide ( $\text{H}_2\text{O}_2$ ) liberates heat during its decomposition and can be used as a monopropellant.  $\text{N}_2\text{H}_4$  combines readily with oxidisers, such as,  $\text{HNO}_3$  and  $\text{N}_2\text{O}_4$  giving much higher heat release than RFNA with aniline and xylidine and forms combustion products with lower molecular mass.

Mono-methyl hydrazine (MMH), which comprises a methyl radical substituted for a hydrogen atom in hydrazine ( $\text{CH}_3\text{N}_2\text{H}_3$ ), is a preferred fuel since its combustion with  $\text{N}_2\text{O}_4$  is more stable than hydrazine and the handling of MMH is also much easier. The fuel, unsymmetrical di-methyl hydrazine (UDMH), in which two of the H atoms, on one side of the  $\text{N}_2\text{H}_4$ , are replaced by methyl radicals  $[(\text{CH}_3)_2\text{N}_2\text{H}_2]$  is also widely used with oxidiser  $\text{N}_2\text{O}_4$ , especially, for boosters. However, the  $I_{sp}$  is lower than that obtained with MMH. A fuel, which is a mixture of 50 per cent  $\text{N}_2\text{H}_4$  and 50 per cent UDMH is known as Aerozene 50 (Az50) and has been used in conjunction with oxidisers  $\text{N}_2\text{O}_4$  and  $\text{HNO}_3$ .

Hydrazine and hydrazine-based fuels MMH and UDMH continue to be used extensively with oxidiser  $\text{N}_2\text{O}_4$ . The sea-level  $I_{sp}$  is less than 3,000 Ns/kg and the propellants fall in the category of low energy propellants.

The fuel kerosene has also been extensively used with  $\text{LO}_2$ . Values of  $I_{sp}$  are higher than obtained with propellant combination MMH/UDMH –  $\text{N}_2\text{O}_4$ . Kerosene, unlike the hydrazine based fuels, is not a chemical compound and consists of several hydrocarbon fractions. It is predominantly paraffin and the chemical structure is approximated by do-decane ( $\text{C}_{12}\text{H}_{26}$ ) with a straight saturated chain structure. It is obtained by refining petroleum crude and depending on the nature of the crude the proportion of straight chain alkane (paraffin) and alkene (olefin) and the ring structured cyclo- and aromatic portions will vary. The presence of aromatics in it makes combustion inefficient.

Pure kerosene, which is a combination of several hydrocarbons, has a flash point of 38°C and is called aviation kerosene. Kerosene mixed (*i.e.* blended) with aviation gasoline, which is the most volatile part of the petroleum, is known as jet mix product (JP) and used for aircraft jet propulsion. In the case of kerosene used for rockets, it becomes essential that the kerosene on heating should not form coke. The typical coking temperature needs to be higher than about 550 K. Kerosene, obtained from petroleum crudes which have high naphthene content, gives higher values of heats of combustion and density and lower levels of aromatics and coking.



Kerosene used for rocket applications has been known as Rocket Propellant (RP). The flash point of RP is above 43°C. Kerosene has also been made synthetically to give higher  $I_{sp}$ . The synthetic kerosene is called 'Sintin'. Efforts continue to enhance the energy level of hydrocarbon fuels, such as, kerosene and, thereby, enhance the  $I_{sp}$  by straining the bonds and effectively decreasing the negative values of the heat of formation.

Kerosene is used with LO<sub>2</sub> in a large number of rockets. LO<sub>2</sub> is a liquid at ambient pressures for temperatures below 90 K. It is, therefore, called a cryogenic liquid. Since kerosene is a liquid at the ambient temperatures while LO<sub>2</sub> is a liquid only at cryogenic temperatures, the propellant combination kerosene-LO<sub>2</sub> is referred to as semi-cryogenic propellant.

### (b) Medium-energy Propellants

The use of UDMH, N<sub>2</sub>H<sub>4</sub> and Az50 with LO<sub>2</sub> gives sea-level  $I_{sp}$  between 3,000 and 3,500 Ns/kg. The use of kerosene with liquid Fluorine, which is an extremely reactive oxidiser also provides the higher sea-level  $I_{sp}$  between 3,000 and 3,500 Ns/kg. Such of the propellant combinations having  $I_{sp}$  in this range are known as medium energy propellants. The medium energy propellants are not popular and only UDMH-LO<sub>2</sub> combination has been used in practice. The use of Fluorine has been difficult in view of its toxicity and reactivity.

### (c) High-energy Propellants

High energy propellants have sea-level  $I_{sp}$  greater than 4000 Ns/kg. Two propellant combinations comprising Liquid Hydrogen (LH<sub>2</sub>) with LO<sub>2</sub> and with Liquid Fluorine (LF) fall in this category. Hydrogen contributes to a significantly reduced molecular mass of the combustion gases. Since LH<sub>2</sub>, LO<sub>2</sub> and LF are liquids only at cryogenic temperatures, these propellant combinations [LH<sub>2</sub>/LO<sub>2</sub>, LH<sub>2</sub>/LF] are known as cryogenic propellants. The boiling point of LF is about 5°C lower than LO<sub>2</sub>. LF is seldom used for reasons of reactivity cited earlier. The only high energy propellant used in practice is LH<sub>2</sub>-LO<sub>2</sub>.

Figure 4.12 classifies the liquid propellants in the categories of low-energy, medium-energy and high-energy propellants. The range of sea level  $I_{sp}$  is also given.

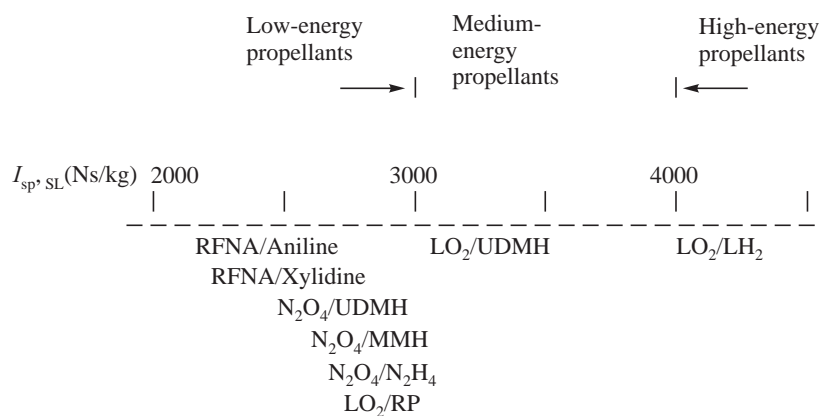


**Fig. 4.12** Propellants Classified as per  $I_{sp,SL}$



Liquefied hydrocarbon gases, such as, liquid methane ( $\text{CH}_4$ ) and liquid propane ( $\text{C}_3\text{H}_8$ ) have lower negative values of heat of formation as compared to kerosene. They give higher  $I_{sp}$  and could be potential propellants for the future.

The addition of metal powders to liquid propellants does not show very significant improvements unlike in the case of solid propellants. This is because with metal addition, the molecular mass of the combustion products increase significantly for liquid propellants. In addition, the metal oxide products that are formed do not solidify and release their energy during the expansion in the nozzle.

#### 4.5.2 Earth-storable and Space-storable Propellants

Rockets are used for launching satellites as satellite launch vehicles, for missile propulsion and for satellite control and propulsion. The conditions of storage and handling of propellants in the rockets of satellite launch vehicles, missiles and satellites are different. In the case of launch vehicles, rockets are used only in the initial phase of mission for putting up the satellite. Storability of the propellants over prolonged periods in the rocket is not essential. The propellants can be filled prior to the launch. In the case of missiles, the missile should be kept ready for the intended application and the propellant should be stored in the rocket for prolonged periods awaiting the mission in silos. In the case of satellites which need to operate in space for several years, the propellants need to be stored at conditions existing in space over the period of operation of the satellite.

Propellants with low boiling and high freezing temperatures are not amenable to storage in space. Consequently, the cryogenic and semi-cryogenic propellants, which call for special storage on the ground in refrigerated or insulated containers, are not well-suited for the rockets used in satellites.

Propellants are categorised based on the storability as:

- (i) Space-storable propellant
- (ii) Earth-storable propellant

The low-energy propellants considered in the last section, except, for the kerosene/ $\text{LO}_2$  propellant combination do not require special conditions of storage on the ground and are said to be Earth-storable. The cryogenic and semi-cryogenic propellants require special refrigerated and/or insulated containers for storage with provision to vent out the vapours, if the pressure in the container increases. These are neither Earth-storable nor space-storable. Space storability demands further strictures on the boiling and freezing temperatures compared to storability on the Earth.  $\text{N}_2\text{O}_4$  has a somewhat high freezing point of  $-9^\circ\text{C}$ . For space applications, a reduced value of the freezing point is desirable. The use of mixed oxides of nitrogen (MON) comprising oxidiser  $\text{N}_2\text{O}_4$  and nitric oxide (NO) provides lower values of freezing temperatures. An amount of 3 per cent by weight of NO in the mixture of NO and  $\text{N}_2\text{O}_4$ , known as MON-3, gives a freezing point of  $-15^\circ\text{C}$ . MON-25, which consists of 25 per cent by weight of NO in the NO and  $\text{N}_2\text{O}_4$  mixture has a freezing point of  $-55^\circ\text{C}$ . The use of MON instead of  $\text{N}_2\text{O}_4$  allows storability under space conditions.

#### 4.5.3 Hypergolic and Non-Hypergolic Propellants

Propellants are said to be hypergolic if spontaneous reaction takes place when the fuel and oxidiser are brought in contact. All Earth and space-storable propellants considered in this chapter are hypergolic. It is the amines with the end group  $\text{NH}_2$  which provide the strong reactivity with  $\text{HNO}_3$ ,  $\text{N}_2\text{O}_4$  and MON.



The semi-cryogenic propellant Kerosene- $\text{LO}_2$  and cryogenic propellant  $\text{LO}_2\text{-LH}_2$  are non-hypergolic and require an ignition device to initiate the combustion. The cryogenic LF-LH<sub>2</sub> propellant combination is hypergolic since fluorine is highly reactive.



## 4.6 HYBRID PROPELLANTS

When fuel and oxidiser are in different phases, the propellant combination is termed as hybrid. Hybrid propellants generally comprise a liquid oxidiser and a solid fuel. The fuel is a polymer as in the case of solid propellants. The liquid oxidiser could be  $\text{LO}_2$ ,  $\text{HNO}_3$  or  $\text{N}_2\text{O}_4$ . Since the boiling temperatures of liquid oxidisers  $\text{LO}_2$  and LF are near to each other, a mixture of 90 per cent  $\text{LO}_2$  and 10 per cent LF, known as FLOX-10, has been used with a solid polymer fuel such as a polybutadiene. Increasing the fluorine content to about 70 per cent (*i.e.* FLOX-70) gives higher values of  $I_{sp}$ . This is due to the formation of HF instead of  $\text{H}_2\text{O}$  and CO instead of  $\text{CO}_2$  in the combustion products both of which contribute to a lower value of the molecular mass.

## SOLVED EXAMPLES

**Example 4.1** Estimation of temperature and molecular mass of combustion products:

A fuel-rich mixture of kerosene and oxygen at a mixture ratio of 2.5 is burnt in a rocket chamber. If the molecular formula for kerosene is given by  $\text{C}_{12}\text{H}_{24}$ , determine:

- (a) Temperature of the combustion products
- (b) Molecular mass of combustion products.

Dissociation of the products could be neglected. The heat of formation  $\Delta H_f^0$  in kJ/mole for kerosene = -159,  $\text{CO}_2$  = -390, CO = -112, and  $\text{H}_2\text{O(l)}$  = -286. The specific heats in J/(mole K) of  $\text{CO}_2$  = 63, CO = 37,  $\text{H}_2\text{O(l)}$  = 90 and  $\text{H}_2\text{O(g)}$  = 58. The boiling temperature of water is 100°C and the latent heat of vaporisation is 40 kJ/mole at 100°C.

**Solution:** Mixture ratio = 2.5:

Let the number of moles of oxygen reacting with 1 mole of kerosene be  $n$ .

The reactants are  $\text{C}_{12}\text{H}_{24} + n\text{O}_2$ , giving mixture ratio as;

$$\frac{n \times 32}{12 \times 12 + 24 \times 1} = 2.5 \quad \text{and} \quad n = 13.125$$

The composition is fuel rich and not all carbon can burn into  $\text{CO}_2$ . We assume all hydrogen to get oxidised to  $\text{H}_2\text{O}$  and the balance oxygen 14.25 O forms 12 moles CO.

However, we find that we are left with 1.125 moles of oxygen (2.25 O) and this can oxidise 2.25 moles of CO to  $\text{CO}_2$ . The balance CO is  $(12 - 2.25 = 9.75)$ . The reaction is, therefore, given by:



- (a) Temperature of combustion products:

The heat liberated in this reaction when the products and reactants are both at the same standard state is:



$$\Delta H_c = - \left( \sum_{\text{Products}} n_i \times \Delta H_{f,i}^{\circ} - \sum_{\text{Reactants}} n_i \times \Delta H_{f,i}^{\circ} \right)$$

Substituting the values of the number of moles and the standard heats of formation, we get:

$$\begin{aligned}\Delta H_c &= - [\{12 \times (-286) + 9.75 \times (-112) + 2.25 \times (-390)\} - \{1 \times (-159) + 13.125 \times 0\}] \\ &= 5242.5 \text{ kJ}\end{aligned}$$

The above heat goes to increase the temperature of the combustion products from 25°C to some temperature say  $T$ . The heat comprises sensible heat and latent heat. We have from heat balance:

$$\begin{aligned}\Delta H_c &= 12 \{C_{\text{H}_2\text{O(L)}}(100 - 25) + H_{L-G} + C_{\text{H}_2\text{O(G)}}(T - 100)\} \\ &\quad + 9.75C_{\text{CO}}(T - 25) + 2.25C_{\text{CO}_2}(T - 25)\end{aligned}$$

Here  $H_{L-G}$  is the latent heat of vaporisation of water in kJ/mole. Substituting the values, we get:

$$\begin{aligned}12 \times [0.090 \times (100 - 25) + 40 + 0.058(T - 100)] + 9.75 \times 0.037 \times (T - 25) \\ + 2.25 \times 0.063 \times (T - 25) = 5242.5\end{aligned}$$

This gives  $T = 3975^\circ\text{C}$ .

The temperature of the combustion products is seen to be 3975°C. However, at this high temperature  $\text{H}_2\text{O}$  and  $\text{CO}_2$  would dissociate into radicals such as OH, H, O, CO, etc. The actual temperature of the products of combustion would be very much lower. The temperature with the dissociation can be estimated by using the procedure outlined in Annexure B.

(b) Molecular mass of combustion products:

$$\begin{aligned}\text{The molecular mass of the products } \mathfrak{M} &= \frac{\sum_{i, \text{Products}} n_i \mathfrak{M}_i}{\sum_{i, \text{Products}} n_i} \\ \mathfrak{M} &= \frac{12 \times 18 + 9.75 \times 28 + 2.25 \times 44}{12 + 9.75 + 2.25} = 24.5\end{aligned}$$

**Example 4.2** Heat release from combustion of cryogenic propellants:

Determine the heat generated from the combustion of liquid hydrogen ( $\text{LH}_2$ ) at a temperature of 20 K and liquid oxygen ( $\text{LO}_2$ ) at 80 K at a mixture ratio of 6. Dissociation of the combustion products could be neglected. The standard heat of formation of  $\text{H}_2\text{O}$  is -286 kJ/mole. The following are the thermophysical properties of  $\text{LH}_2$  and  $\text{LO}_2$ :

Boiling temperature of  $\text{LH}_2$  : 22 K

Specific heat of  $\text{LH}_2$  : 16 kJ/kmole K

Specific heat at constant pressure of  $\text{GH}_2$  : 30 kJ/kmole K

Latent heat of  $\text{LH}_2$  : 892 kJ/kmole

Boiling temperature of  $\text{LO}_2$  : 90 K

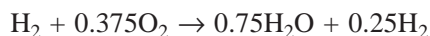
Specific heat of  $\text{LO}_2$  : 54 kJ/kmole K

Specific heat at constant pressure of gaseous oxygen : 29 kJ/kmole K

Latent heat of  $\text{LO}_2$  : 6800 kJ/kmole



**Solution:** The number of moles of O<sub>2</sub> ( $n_{O_2}$ ) required for combustion with 1 mole of H<sub>2</sub> at a mixture ratio of 6 is given by:  $\frac{n_{O_2} \times 32}{2} = 6$  giving  $n_{O_2} = 0.375$ . The reaction can therefore, be written as



It must be noted that we are not considering dissociation of the products.

Since the hydrogen and oxygen are not at the standard gaseous state at a temperature of 298 K, it is necessary to bring them to the standard state prior to evaluating the heat release at the standard state. Once the standard state is reached, the heat from the combustion at the standard state is  $\Delta H_c = -0.75 \times (-286) = 214.5$  kJ for the reaction. This is because the heats of formation for the elements hydrogen and oxygen at the standard state are zero.

Heat in kJ required to bring one mole LH<sub>2</sub> at 20 K to gaseous hydrogen at 298 K is

$$\begin{aligned} C_{LH_2}(22 - 20) + 0.892 + C_{p, GH_2}(298 - 22) \\ = 0.016 \times 2 + 0.892 + 0.030 \times 276 = 9.204 \text{ kJ} \end{aligned}$$

Heat in kJ required to bring 0.375 mole LO<sub>2</sub> at 80 K to gaseous oxygen at 298 K is

$$\begin{aligned} 0.375[C_{LO_2}(90 - 80) + 6.8 + C_{p, LO_2}(298 - 90)] \\ = 0.375[0.054 \times 10 + 6.8 + 0.029 \times 208] \\ = 0.375 \times 13.372 = 5.015 \text{ kJ} \end{aligned}$$

Total heat is required in kJ to bring the given state of LH<sub>2</sub> and LOX to the standard state = 9.204 + 5.015 = 14.22 kJ.

The heat generated in the reaction = 214.5 – 14.22 = 200.28 kJ per mole of H<sub>2</sub>

$$1 \text{ kg of LH}_2 \text{ contains } \frac{1}{2} \text{ kmoles} = 500 \text{ moles}$$

Heat generated per kg of LH<sub>2</sub> burnt =  $500 \times 200.28 = 100,140$  kJ.

**Example 4.3** Mixture ratio and solid loading in a composite propellant:

A composite propellant contains ammonium perchlorate (AP) as oxidiser and hydroxy terminated poly butadiene (HTPB) as binder in stoichiometric proportion. HTPB can be assumed to have a molecular mass of 2734 kg/kmole. Determine:

(a) Mixture ratio

(b) Solid loading in the propellant

**Solution:** (a) Stoichiometric mixture ratio:

The chemical formula for HTPB was seen as

HO – (CH<sub>2</sub> = CH – CH = CH<sub>2</sub>)<sub>n</sub> – OH which can be written as (C<sub>4</sub>H<sub>6</sub>)<sub>n</sub>(OH)<sub>2</sub>. From the value of molecular mass of 2734, the value of ‘n’ in the chemical formula of HTPB is determined to be:

$$(4 \times 12 + 6)_n + (16 + 1)2 = 2734$$

or

$$n = 50$$

The chemical formula for HTPB is, therefore, C<sub>200</sub>H<sub>302</sub>O<sub>2</sub>. Depending on the cross-linking of the polymer the molecular mass and the formula would change.



The chemical reaction between HTPB and AP for stoichiometric combustion would lead to C and H to be completely oxidised by chlorine and oxygen to HCl, H<sub>2</sub>O and CO<sub>2</sub>. The stoichiometric reaction is given by 1 mole of binder reacting with  $a$  moles of AP to form 200 moles of CO<sub>2</sub>,  $a$  moles of HCl,  $b$  moles H<sub>2</sub>O and  $a/2$  moles of N<sub>2</sub>. This is represented by:



Balancing the number of moles of H and O atoms in the reactants and products, we get:

$$\text{H balance: } 302 + 4a = a + 2b$$

$$\text{O balance: } 2 + 4a = 400 + b$$

The equations reduce to:

$$2b = 302 + 3a$$

$$b = 4a - 398$$

On solving we get  $5a = 1098$  or  $a = 219.6$  and  $b = 480.4$ .

The stoichiometric equation is, therefore:



The mixture ratio is given as:  $\text{MR} = \frac{\text{Mass of oxidiser}}{\text{Mass of fuel}}$

$$= \frac{219.6(14 + 4 + 35.5 + 64)}{200 \times 12 + 302 + 32} = 9.44.$$

(b) Solid loading in propellant:

The solid loading in the propellant is the fractional mass of solids in the propellant. In the case of the non-aluminised propellant, it consists of the mass of AP crystals in the propellant. The solid loading is, therefore, given by:

$$\text{Solid loading} = \frac{9.44}{1 + 9.44} = 90\%$$

This example shows that considerable solid AP crystals are required to be dispersed in the HTPB binder to form a stoichiometric mixture. Bonding of the AP crystals with the binder is difficult at these large values of solid loading. The mixture ratio of composite propellants is therefore generally fuel-rich.

**Example 4.4** Fuel-rich composite propellant containing aluminium:

A composite propellant containing 10 per cent aluminium has a solid loading of 90 per cent. The fuel binder is hydroxy terminated polybutadiene (HTPB) as given in the previous example and the oxidiser is ammonium perchlorate (AP). Determine the mixture ratio of the composite propellant and the molar composition of the propellant. Also find whether the composition is fuel-rich or oxidiser rich?

**Solution:** (a) Mixture ratio:

The quantity of plasticiser, curator and burn rate additives in the propellant is small and is neglected. Denoting the mass of AP, HTPB and aluminium in a given mass of propellant as  $m_{AP}$ ,  $m_B$  and  $m_{Al}$  respectively, we have the solid loading as:



$$\text{Solid loading} = \frac{m_{AP} + m_{Al}}{m_{AP} + m_{Al} + m_B} = 0.9$$

Since propellant contains 10 per cent aluminium, we have:

$$\frac{m_{Al}}{m_{AP} + m_{Al} + m_B} = 0.1$$

We, therefore, get:

$$\frac{m_{AP} + m_{Al}}{m_{Al}} = 9 \quad \text{or} \quad \frac{m_{AP}}{m_{Al}} = 8$$

Substituting in the expression for the aluminium fraction, we have:

$$\frac{m_{Al}}{9m_{Al} + m_B} = 0.1 \quad \text{or} \quad \frac{m_B}{m_{Al}} = 1$$

The mass ratios of AP : Al : Binder in the propellant, is, therefore:

$$m_{AP} : m_{Al} : m_B = 8 : 1 : 1$$

The mixture ratio of the propellant is given by:

$$MR = \frac{m_{AP}}{m_B + m_{Al}} = \frac{8}{1+1} = 4$$

(b) Molar composition:

The mass ratios of the three constituents are divided by the molecular mass of each constituent to determine the mole ratios. Denoting the moles of AP, Al and binder by  $n_{AP}$ ,  $n_{Al}$  and  $n_B$  respectively, we have:

$$n_{AP} : n_{Al} : n_B = \frac{m_{AP}}{\mathfrak{M}_{AP}} : \frac{m_{Al}}{\mathfrak{M}_{Al}} : \frac{m_B}{\mathfrak{M}_B}$$

The molecular mass of AP,  $\mathfrak{M}_{AP} = 14 + 4 + 35.5 + 64 = 117.5$  g/mole. The molecular mass of Al,  $\mathfrak{M}_{Al} = 27$  g/mole and the molecular mass of the binder is given as 2734 g/mole. Hence

$$n_{AP} : n_{Al} : n_B = \frac{9}{117.5} : \frac{1}{27} : \frac{1}{2734} \text{ giving}$$

$$n_{AP} : n_{Al} : n_B = 0.672 : 0.325 : 0.003$$

The reactants are, therefore, given by the molar composition:



(c) Fuel-rich/Oxidiser-rich:

The stoichiometric combustion requires that completely oxidised products of combustion to be formed during the reaction. The completed oxidised products are HCl, H<sub>2</sub>O, CO<sub>2</sub> and Al<sub>2</sub>O<sub>3</sub>. The number of O atoms required for the above are determined as follows:

We have a total of  $302 \times 0.003 + 4 \times 0.672 = 3.594$  atoms of hydrogen. Of this, 0.672 is oxidised by Cl to HCl. The remaining H atoms =  $3.594 - 0.672 = 2.922$  would require O atoms for the oxidation to H<sub>2</sub>O. The O atoms required for this purpose are  $2.922/2 = 1.461$ .

The number of C atoms in the reactants is  $200 \times 0.003 = 0.6$ . The O atoms required for oxidation to CO<sub>2</sub> is  $0.6 \times 2 = 1.2$ .



Similarly, the O atoms required for oxidising 0.325 moles of Al =  $0.325 \times 3/2 = 0.4875$ .

The total moles of O<sub>2</sub> required for stoichiometric combustion is  $(1.461 + 1.2 + 0.4875)/2 = 1.574$ . The number of moles of O<sub>2</sub> available in the reactant is  $0.003 + 2 \times 0.672 = 1.347$ . This is very much lower than the requirement of 1.574 moles of O<sub>2</sub> to form completely oxidised products of combustion. The composition of the composite propellant is, therefore, fuel-rich. Only partially oxidised combustion products will be formed.

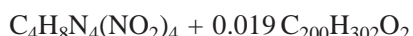
**Example 4.5** Nitramine propellant:

Determine the heat released per kg of a nitramine propellant which consists of 85 per cent HMX added to HTPB binder. The molecular mass of HTPB binder can be assumed to be 2734 kg/kmole, as in the previous problem. Neglect the other small additives to the propellant and dissociation of the combustion products.

**Solution:** The chemical formula for HMX is C<sub>4</sub>H<sub>8</sub>N<sub>4</sub>(NO<sub>2</sub>)<sub>4</sub> and its heat of formation is +74 kJ/mole. The chemical formula for HTPB for the above molecular mass based on the previous problem is C<sub>200</sub>H<sub>302</sub>O<sub>2</sub>. The heat of formation of the binder is - 64 kJ/mole.

The molecular mass of HMX {C<sub>4</sub>H<sub>8</sub>N<sub>4</sub>(NO<sub>2</sub>)<sub>4</sub>} is 296 kg/kmole. The number of moles of HMX in 1 kg of propellant is  $0.85 \times 1000/296 = 2.87$ . The moles of HTPB in 1 kg of propellant =  $0.15 \times 1000/2734 = 0.055$ . The number of moles of HTPB per mole of HMX is  $0.055/2.87 = 0.019$ .

The reactants of the nitramine propellant are, therefore, given as:



The number of O, H, C and N atoms in the composition is:

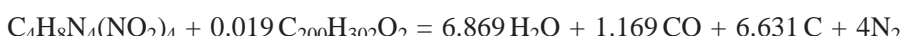
$$\text{O} : 8 + 0.038 = 8.038$$

$$\text{H} : 8 + 5.738 = 13.738$$

$$\text{C} : 4 + 3.8 = 7.8$$

$$\text{N} : 8$$

H is oxidised to form  $13.738/2 (= 6.869)$  moles of H<sub>2</sub>O. This uses up 6.869 of O leaving a balance of  $8.038 - 6.869 (= 1.169)$ . 1.169 moles of CO is, therefore, formed and  $7.8 - 1.169 (= 6.631)$  moles of C are left. The nitramine propellant is very fuel rich and the reactants and products are given as follows:



The heat generated in the above reaction is:

$$-\{6.869 \times (-286) + 1.169 \times (-112) - (74) - (-64)\} = 2168.24 \text{ kJ}$$

In the above equation the heats of formation of H<sub>2</sub>O, CO, C<sub>4</sub>H<sub>8</sub>N<sub>4</sub>(NO<sub>2</sub>)<sub>4</sub> and C<sub>200</sub>H<sub>302</sub>O<sub>2</sub> of -286, -112, +74 and -64 kJ/mole are used.

The total mass of the propellant which contributes to the above energy is  $296 + 0.019 \times 2734 = 347.95$  g.

Heat release per kg of the propellant =  $2168.24/0.348 = 6231$  kJ/kg.

**Example 4.6** Propellant performance neglecting dissociation of combustion products:

Gaseous methane and gaseous oxygen are injected at 25°C in a rocket combustion chamber. The volume flow rates of methane and oxygen are 4 scc/s and 6 scc/s respectively. Determine:

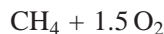


- (a) Mixture ratio of the propellant combination
- (b) The value of  $C^*$  assuming no dissociation of the combustion products.

The specific heats of water, steam and carbon monoxide can be assumed to remain constant over the range of temperatures of interest and equal to 0.09, 0.058 and 0.037 kJ/(mole K) respectively. The standard heats of formation of methane, carbon monoxide and water are  $-75$ ,  $-112$  and  $-286$  kJ/mole respectively. The boiling temperature of water is 373 K and the latent heat of vapourisation of water is 40 kJ/mole.

**Solution:** (a) Mixture ratio:

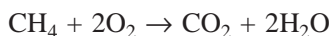
The volume flow rates are proportional to the mole flow rates from Avogadro's hypothesis. The number of moles of oxygen admitted per mole of methane is  $6/4 = 1.5$ . The reactants are, therefore, represented as:



$$\text{Mixture ratio MR} = 1.5 \times 32/(12 + 4) = 3$$

(b) Calculation of products and  $C^*$ :

The stoichiometric composition for methane-oxygen must give completely oxidised products of combustion, viz.,  $\text{CO}_2$  and  $\text{H}_2\text{O}$ . The stoichiometric reaction between methane and oxygen is:

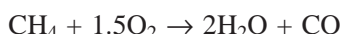


Since the amount of available oxygen in the given composition is less than stoichiometric, CO would be formed. Following the procedure that  $\text{H}_2\text{O}$  is first formed due to the higher reactivity of H and then CO and the balance oxygen if any, converts part of the CO to  $\text{CO}_2$ , we have:



Since we have 3O in the reactants, we are left with 1O. This converts 1 of C to 1CO.

There is no oxygen left to convert CO to  $\text{CO}_2$ . The chemical reaction is, therefore, given by:



The standard heats of formation  $\Delta H_f^\circ$  for  $\text{CH}_4$ ,  $\text{H}_2\text{O}$  and CO are  $-75$  kJ/mole,  $-286$  kJ/mole and  $-112$  kJ/mole respectively. The heat of combustion is:

$$-(2 \times (-286) + 1(-112) - (-75)) = +609 \text{ kJ per mole of CH}_4.$$

The heat converts water to steam and raises the temperature of the combustion products. The specific heat of water is 0.090 kJ/(mole K) and the mean value of specific heat of steam at constant pressure is 0.058 kJ/(mole K). The boiling temperature of water is 373 K and the latent heat of water is 40 kJ/mole. The specific heat of CO at constant pressure over the range of temperature of interest can be assumed as 0.037 kJ/(mole K). Denoting the temperature of the combustion products as  $T_f$ , the energy balance gives:

$$1 \times 0.037 \times (T_f - 298) + 2 \times 0.090 \times (373 - 298) + 2 \times 40 + 2 \times 0.058 \times (T_f - 298) = 609$$

$$\therefore T_f = 3724 \text{ K}$$

In practice the temperature would be lower due to the dissociation of the combustion products.

The mean molecular mass of the combustion products  $\mathfrak{M}$  is:

$$\mathfrak{M} = \frac{2 \times 18 + 28}{8} = 21.33 \text{ kg/kmole}$$



In order to determine the  $C^*$  of the propellant combination, we need to determine the specific heat ratio of the combustion products. The specific heats of the combustion products at constant pressure and constant volume must, therefore, be known. The specific heat of the products at constant pressure  $C_{P, pr}$  is:

$$C_{P, pr} = \frac{2C_{P, H_2O} + 1C_{P, CO}}{3} = \frac{2 \times 0.058 + 0.037}{3} = 0.051 \text{ kJ/mole K}$$

The specific heat at constant volume of the products  $C_{V, pr}$  in kJ/(mole K) is obtained from the relation  $C_p - C_V = R_0$ , where  $R_0$  is the universal gas constant = 8.314 J/(mole K).

$$C_{V, pr} = C_{P, pr} - R_0 = 0.051 - 0.008314 = 0.0427 \text{ kJ/(mole K)}$$

The specific heat ratio of the products  $\gamma$  is

$$\gamma = \frac{C_P}{C_V} = \frac{0.051}{0.0427} = 1.1944$$

The value of  $C^*$  is given by:

$$C^* = \frac{1}{\Gamma} \sqrt{\frac{R_0 T_f}{M}}, \text{ where } \Gamma = \sqrt{\gamma} \left( \frac{2}{\gamma + 1} \right)^{\frac{\gamma + 1}{2(\gamma - 1)}}$$

Substituting the value of  $\gamma = 1.1944$  in the above expression,  $\Gamma = 0.6474$  and

$$C^* = \frac{1}{0.6474} \sqrt{\frac{8.314 \times 3724}{21.33 \times 10^{-3}}} = 1861 \text{ m/s}$$

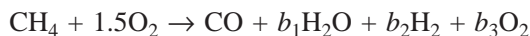
The characteristic velocity of the propellant combination is 1861 m/s.

#### Example 4.7 Propellant performance with dissociation:

If part of the steam formed in the products of combustion in the above problem dissociates into hydrogen and oxygen, determine the fall in temperature of the combustion products and the value of  $C^*$ . The chamber pressure is given as 0.5 MPa. The boiling temperature of water at 0.5 MPa is 425 K and the latent heat of vapourisation is 37.95 kJ/mole.

**Solution:** If we were to consider the dissociation of the products say the dissociation of steam at the high temperature of 3724 K in the previous example into hydrogen and oxygen by the dissociation

reaction,  $H_2O \rightarrow H_2 + \frac{1}{2} O_2$ , the products of combustion become:



We have three unknowns,  $b_1$ ,  $b_2$  and  $b_3$ , in the above equation. From atom balance equations for H and O we have:

$$H : 2b_1 + 2b_2 = 4$$

$$O : b_1 + 2b_3 = 2 \text{ (One O is used in forming CO)}$$

We require one more equation involving  $b_1$ ,  $b_2$  and  $b_3$  to determine their values. This can be done by examining the dissociation reaction  $H_2O \rightarrow H_2 + \frac{1}{2} O_2$ . The equilibrium constant for this reaction is defined as a function of the partial pressures of  $H_2$ ,  $O_2$  and  $H_2O$ :



$$K_P = \frac{p_{H_2} \times p_{O_2}^{1/2}}{p_{H_2O}}$$

The equilibrium constant  $K_p$  is given by eq. B.18 in Annexure B as:

$$\ln K_P = -\frac{\Delta G^\circ}{R_0 T}$$

where  $\Delta G^\circ$  is the change in the standard Gibbs Free Energy for the dissociation reaction  $H_2O \rightarrow H_2 + \frac{1}{2} O_2$ .

Since the equilibrium constant,  $K_p$ , is expressed in terms of partial pressures and the solution required is for the moles  $b_1$ ,  $b_2$  and  $b_3$ , we need to first convert the partial pressures to moles. For this purpose, we need to know the total number of moles in the products. However, this is not known *a priori* and as a first approximation, we assume that the total number of moles equals the moles in the product corresponding to a stoichiometric reaction. The stoichiometric reaction is  $CH_4 + 2O_2 \rightarrow CO_2 + 2H_2O$  giving the total number of moles of products as 3. If the pressure in the chamber is  $p$ , the partial pressures of  $H_2$ ,  $O_2$  and  $H_2O$  are:

$$p_{H_2O} = \frac{p}{3} \times b_1$$

$$p_{H_2} = \frac{p}{3} \times b_2$$

$$p_{O_2} = \frac{p}{3} \times b_3$$

Substituting in the equation for equilibrium constant, we get:

$$K_P = \left(\frac{p}{3}\right)^{1/2} \frac{b_2 \times b_3^{1/2}}{b_1}$$

Once the value of  $K_P$  is given and the chamber pressure is specified, we can find out the values of  $b_1$ ,  $b_2$  and  $b_3$ . This is given in the following. From O balance we had:

$$b_1 = 2(1 - b_3)$$

From H balance:

$$2 \times 2(1 - b_3) + 2b_2 = 4 \text{ giving } b_2 = 2b_3$$

Substituting the value of  $b_1$  and  $b_2$  in the equation for equilibrium constant, we get:

$$\left(\frac{p}{3}\right)^{1/2} \frac{(2b_3)b_3^{1/2}}{2(1 - b_3)} = K_P \quad \text{or} \quad \frac{b_3^{3/2}}{1 - b_3} = \frac{\sqrt{3}K_P}{p^{1/2}}$$

The pressure in the chamber is given as 0.5 MPa. Since the values of pressure in the equilibrium constants are to be expressed in atmospheres, the value of  $p = 5$  atm.

The value of  $K_P$  depends on the temperature and is obtained from the change of the Gibbs Free Energy of the dissociation. A temperature is initially assumed and checked for energy balance if it is the correct value. The temperature in the absence of dissociation was 3,724 K and the temperature should decrease because of the dissociation. Let us assume the temperature  $T_f$  as 3,500 K.



At 3500 K, the Gibbs Free Energy, obtained from standard thermodynamic tables is  $-47,990 \text{ kJ/kg}$  for  $\text{H}_2\text{O}$  and is zero for  $\text{H}_2$  and  $\text{O}_2$ . The value of  $\Delta G^\circ$  for the dissociation reaction,  $\text{H}_2\text{O} \rightarrow \text{H}_2 + \frac{1}{2} \text{O}_2$ , is  $+47,990$  and

$$\ln K_P = -\Delta G^\circ / R_0 T = \frac{-47,990}{8.314 \times 3,500} = -1.6492$$

This gives the value of  $K_P = 0.1922$ .

Substituting the values of  $K_P$  and  $p$  in the equation for  $b_3$ , we have

$$\frac{b_3^{3/2}}{1 - b_3} = \frac{0.1922 \times \sqrt{3}}{\sqrt{5}} = 0.1489$$

Solving iteratively, we get:  $b_3 = 0.234$ .

From the relations between  $b_1$ ,  $b_2$  and  $b_3$

$$b_1 = 2(1 - b_3) = 1.532$$

$$b_2 = 2b_3 = 0.468$$

The chemical reaction with dissociation becomes:



The energy liberated in the above reaction is:

$$\Delta H_C = -\{-112 + 1.532 \times (-286) - (-75)\} = 475.15 \text{ kJ.}$$

Here the values  $-112$ ,  $-286$  and  $-75$  are the heats of formation of  $\text{CO}$ ,  $\text{H}_2\text{O}$  and  $\text{CH}_4$  respectively.

The temperature corresponding to the above heat release must correspond to the assumed temperature of 3,500 K. If it does not agree, the assumed value of temperature is not correct. Denoting the temperature as  $T_f$ , we have:

$$n_{\text{CO}} \times C_{p, \text{CO}} \times (T_f - 298) + n_{\text{H}_2\text{O}} \times [C_{\text{H}_2\text{O(l)}} (425 - 298) + H_V + C_{p, \text{H}_2\text{O}} (T_f - 425)] + n_{\text{H}_2} \times C_{p, \text{H}_2} \times (T_f - 298) + n_{\text{O}_2} \times C_{p, \text{O}_2} \times (T_f - 298) = \Delta H_C = 475.15$$

$H_V$ , in the above expression, is the latent heat of vapourisation of water in kJ/mole. All other symbols were used earlier. The specific heats of  $\text{CO}$ ,  $\text{H}_2\text{O(l)}$ ,  $\text{H}_2\text{O(g)}$ ,  $\text{H}_2$  and  $\text{O}_2$  are  $0.037$ ,  $0.09$ ,  $0.058$ ,  $0.040$  and  $0.042$  kJ/(mole K) respectively. The values can be seen from Fig. 4.2. The heat of vapourisation of water is given as  $37.5$  kJ/mole and the boiling temperature is  $425$  K. Substituting the values we get:

$$0.155(T_f - 298) + 75 = 475.15$$

$T_f = 2880$ . The assumed value of 3500 is an overestimate.

Let us, therefore, redo the problem by assuming the temperature as 3,100 K. At 3,100, the standard Gibbs Free Energy for  $\text{H}_2\text{O}$  from thermodynamic tables is  $-71,467$  kJ/kmole giving  $K_P = -71,467 / (8.314 \times 3100) = -2.773$  or  $K_P = 0.0625$ .

Reworking the values of  $b_1$ ,  $b_2$  and  $b_3$  following the earlier procedure, we get:

$b_3 = 0.122$ ,  $b_2 = 0.244$  and  $b_1 = 1.756$ . This gives the reaction to be:





The heat of reaction works out to be 539.2 kJ instead of 475.15 kJ determined earlier. The temperature  $T_f$  becomes 3,191 K.

We redo the next iteration assuming the temperature as 3,200 K. At 3,200 K,  $\Delta G^\circ$  for the dissociation reaction  $\text{H}_2\text{O} \rightarrow \text{H}_2 + \frac{1}{2}\text{O}_2$  (from the thermodynamic tables) is + 65,604 kJ/kmole giving  $\ln K_P = -65,604/(8.314 \times 3200) = -2.44$  or  $K_P = 0.085$ . This gives  $b_3 = 0.145$ ,  $b_2 = 0.290$  and  $b_1 = 1.71$ .

The reaction becomes:



The heat liberated in the reaction is 526.06 kJ instead of 539.2 kJ calculated in the last iteration. The temperature  $T_f$  is 3,193 K. This is close to the assumed value of 3,200 K.

In the above manner the final temperature and composition is determined. We find the moles of the reactants and products are balanced. With the final temperature as 3,195 K and  $b_3 = 0.145$ ,  $b_2 = 0.29$  and  $b_1 = 1.71$ , the molecular mass of the products is  $\mathfrak{M} = (1 \times 28 + 1.71 \times 18 + 0.29 \times 2 + 0.145 \times 32)/(1 + 1.71 + 0.29 + 0.145) = 20.35 \text{ kg/kmole}$ . The molecular mass due to the dissociation of steam has reduced from 21.33 to 20.35 kg/kmole. The specific heat at constant pressure of the products is 0.049 kJ/(mole K) and the specific heat ratio,  $\gamma$ , becomes 1.204. The specific heat ratio is observed to have increased compared to the calculations without any dissociation.

The value of  $\Gamma = \sqrt{\gamma} \left( \frac{2}{\gamma+1} \right)^{\frac{\gamma+1}{2(\gamma-1)}} = 0.6493$ .

$$C^* = \frac{1}{\Gamma} \sqrt{\frac{R_0 T_f}{\mathfrak{M}}} = \frac{1}{0.6493} \sqrt{\frac{8.314 \times 3195}{20.35 \times 10^{-3}}} = 1760 \text{ m/s}$$

The value of  $C^*$  is seen to have reduced from a value of 1861 m/s to 1760 m/s due to the dissociation of part of the steam in the products of combustion.

## NOMENCLATURE

- Az : Aerozene
- $C_p$  : Specific heat at constant pressure kJ/kmole K
- $d\chi$  : Change in number of moles in a reaction
- $G$  : Gibbs Free Energy (J)
- $g$  : Gas phase
- $H$  : Enthalpy (kJ)
- $H_v$  : Latent heat of vapourisation (kJ/mole)
- $\Delta H_c$  : Heat of combustion (kJ)
- $\Delta H_f^\circ$  : Heat of formation (kJ/mole)
- $I_{sp}$  : Specific Impulse (Ns/kg)
- $K_P$  : Equilibrium constant



---

LF	: Liquid fluorine
LO <sub>2</sub>	: Liquid oxygen
LH <sub>2</sub>	: Liquid hydrogen
<i>l</i>	: Liquid phase
<i>M<sub>i</sub></i>	: <i>i</i> <sup>th</sup> species
MR	: Mixture ratio
<i>N</i>	: Number of species
<i>n</i>	: Moles
<i>S</i>	: Entropy (J/K)
<i>s</i>	: Solid phase
<i>T</i>	: Temperature
<i>T<sub>B</sub></i>	: Boiling temperature
<i>T<sub>f</sub></i>	: Flame temperature
<i>V</i>	: Volume (m <sup>3</sup> )
<i>x</i>	: Mole fraction
$\gamma$	: Specific heat ratio
$\mu$	: Chemical potential
<i>v</i>	: Stoichiometric coefficient for chemical reaction
$\xi$	: Work other than pressure-volume work
$\Sigma$	: Summation
$\mathfrak{M}$	: Molecular mass (kg/kmole)

### Subscripts

<i>c</i>	: Combustion chamber
<i>f</i>	: Fuel, formation
<i>g</i>	: Gas
<i>i</i>	: Species
<i>L</i>	: Liquid
<i>ox</i>	: Oxidiser
<i>st</i>	: Stoichiometric
<i>t</i>	: Total
<i>x, m, n</i>	: Number of molecules in chain

### Superscripts

'	: Reactant
"	: Product of chemical reaction
°	: Standard condition of temperature and pressure (1 atm., 25°C)



## EXERCISES

1. (i) Determine the heat generated during the stoichiometric combustion of kerosene with nitric acid when the initial temperature of kerosene and nitric acid is 25°C. You can neglect dissociation of the combustion products and assume the following. Kerosene is approximated as dodecane with a chemical formula C<sub>12</sub>H<sub>26</sub>. Nitric acid is pure and anhydrous with a chemical formula HNO<sub>3</sub>. The standard heats of formation are given below:

$$\Delta H_f^\circ |_{CO_2} = -390 \text{ kJ/mole}, \quad \Delta H_f^\circ |_{H_2O} = -286 \text{ kJ/mole}, \quad \Delta H_f^\circ |_{CO} = -112 \text{ kJ/mole},$$

$$\Delta H_f^\circ |_{HNO_3} = -171.8 \text{ kJ/mole}, \quad \Delta H_f^\circ |_{\text{kerosene}} = -159 \text{ kJ/mole}.$$

- (ii) What is the mixture ratio corresponding to the stoichiometric composition?  
 (iii) If the molar specific heat of the gases could be assumed constant in the temperature range of interest and are given by the following:

$$CO_2 = 63 \text{ J/mole K}, \quad CO = 37 \text{ J/mole K}, \quad H_2O(g) = 58 \text{ J/mole K}, \quad H_2O(l) = 90 \text{ J/mole K},$$

$$N_2 = 37 \text{ J/mole K},$$

determine the final temperature of the gases. You can assume the combustion process to be adiabatic. The boiling temperature of water can be assumed as 100°C and the latent heat of vapourisation as 40 kJ/mole.

- (iv) What is the molecular mass of the combustion products?  
 (v) Given that the specific heat ratios of CO<sub>2</sub>, CO, H<sub>2</sub>O(g) and N<sub>2</sub> are 1.32, 1.35, 1.33 and 1.4 respectively, determine the value of C\* for the stoichiometric propellant combination of kerosene and nitric acid. The universal gas constant is 8.314 kJ/kmole K.
2. In order to get the advantage of lower molecular mass for improving the specific impulse, a mixture ratio of 4.5 is used for the combustion of kerosene and nitric acid in the rocket. Using the data for the standard heats of formation, specific heats and latent heat given in the previous problem and neglecting dissociation of the combustion products, determine:  
 (a) Molecular mass of the combustion products by the simple procedure that hydrogen is most reactive and all nitrogen in the propellant is converted to N<sub>2</sub>.  
 (b) Energy released from the combustion of 1 kg of kerosene.  
 (c) Adiabatic flame temperature.  
 (d) Sea-level specific impulse ( $I_{sp, SL}$ ) assuming chamber pressure as 7 MPa and the gases to be expanded in the nozzle to the ambient pressure of 0.1 MPa.
3. RDX having molecular formula (CH<sub>2</sub>NNO<sub>2</sub>)<sub>3</sub> and a standard heat of formation of +75 kJ/mole decomposes to form N<sub>2</sub>, CO and H<sub>2</sub>O. Determine the energy release in kJ per kg of RDX and the adiabatic flame temperature of the combustion products. You can use the data of heat of formation and specific heats given in Exercise 1.
4. Most of the geosynchronous satellites use the propellant combination of mono-methyl hydrazine (MMH with molecular formula CH<sub>3</sub>N<sub>2</sub>H<sub>3</sub>) and mixed oxides of nitrogen MON-3 at a mixture ratio of 1.65. The chemical formula for MON-3 can be approximated to be N<sub>2</sub>O<sub>4</sub>. The standard heats of formation of MMH and N<sub>2</sub>O<sub>4</sub> are +54.8 and +9.63 kJ/mole respectively. Determine the following:  
 (a) Is the propellant combination fuel-rich or stoichiometric?



- (b) Determine the energy released in kJ per kg of propellant for MMH and  $N_2O_4$  at a mixture ratio of 2 using the data of standard heats of formation given in Exercise 1. Neglect dissociation of the combustion products. You can assume the initial temperature of the propellants as 25°C.
5. Determine the temperature and the molecular mass of the combustion products in a cryogenic liquid propellant rocket using sub-cooled liquid hydrogen and liquid oxygen at temperatures of 18 K and 80 K respectively at a mixture ratio of 5. You can neglect dissociation of the combustion products and use the thermo-physical properties given in Example 4.2. The thermo-physical properties of  $H_2O$  given in Exercise 1 can be used. The variations of specific heats with temperature need not be considered.
- Determine the specific heat ratio of the combustion products and the characteristic velocity  $C^*$  of this cryogenic propellant combination.
6. A double-base propellant can be assumed to consist 40 per cent NG and 60 per cent NC by mass. The other substances in the propellant, such as, plasticisers, curators and burn rate modifiers are in small quantities and can be neglected. Determine the number of moles of NG per mole of NC in the propellant. The chemical formula for NC can be taken as  $C_6H_7O_4(NO_3)_2$  and the chemical formula for NG is  $C_3H_5(ONO_2)_3$ .
- Is the double-base propellant oxidiser-rich or fuel-rich?
7. A composite modified double base propellant is formed by adding 10 per cent AP by mass to the double-base propellant consisting of 40 per cent NG and 60 per cent NC by mass. Determine the ratio of moles of NC, NG and AP in the composite modified double-base propellant.
8. Aniline ( $C_6H_7N$ ) is used with nitric acid ( $HNO_3$ ) in a liquid propellant rocket at stoichiometric mixture ratio. Determine:
- The mixture ratio
  - If the standard heats of formation of aniline and nitric acid are -30.7 and -172 kJ/mole respectively, determine the temperature of the combustion products. You can use the values of the standard heats of formation and specific heats for the products given in this chapter. The temperature at which aniline and nitric acid are injected can be assumed as 25°C. Dissociation of the combustion products may be neglected.
  - If 3 per cent aluminium powder is added to the above propellant and if all aluminium is converted to  $Al_2O_3$  at the cost of some carbon in the propellant not getting oxidised to  $CO_2$ , determine the heat release per unit mass of propellant. Assume there is no dissociation. The atomic mass of aluminium is 27 and the heat of formation of  $Al_2O_3$  is -1670 kJ/mole.
9. A liquid propellant rocket, used for transferring a satellite from low earth orbit to geosynchronous orbit, uses a propellant combination comprising mono-methyl hydrazine (MMH- $CH_3N_2H_3$ ) and di-nitrogen tetroxide ( $N_2O_4$ ). Equal volumetric flow rates of MMH and  $N_2O_4$  are supplied to the thrust chamber. Given that the density of MMH is 865 kg/m<sup>3</sup> and the density of  $N_2O_4$  is 1400 kg/m<sup>3</sup>, determine the mixture ratio of the propellant combination used.
10. A stoichiometric mixture of hydrogen and oxygen is burnt in a rocket chamber at a chamber pressure of 3 MPa. Both hydrogen and oxygen are admitted as gas at a temperature of 25°C. Determine:
- The heat release from combustion and the temperature of combustion products when there is no dissociation of the products of combustion.
  - The heat release from combustion and the composition and temperature of combustion products when dissociation occurs and the products comprise  $H_2$ , H, OH and  $O_2$  in addition to  $H_2O$ . The standard Gibbs Free Energy for  $H_2O$ , OH and H in kJ/kmole is given in the following Table at 3000, 3200, 3400, 3600, 3800 and 4000 K. The standard values of Gibbs Free energy for  $H_2$  and  $O_2$  is zero at all temperatures:



<i>Chemical Components</i> <i>Temperature</i>	<i>H<sub>2</sub>O</i> <i>G<sup>0</sup></i>	<i>OH</i> <i>G<sup>0</sup></i>	<i>H</i> <i>G<sup>0</sup></i>
3,000 K	-77,326	-4245	46,182
3,200 K	-65,604	-6862	33,928
3,400 K	-53,865	-9457	21,650
3,600 K	-42,110	-12,028	9350
3,800 K	-30,338	-14,576	-2967
4,000 K	-18,458	-17,110	-15,229

11. A hybrid rocket is proposed to be developed using solid hydrogen at a temperature of 8 K and liquid oxygen at a temperature of 80 K. Determine the heat release from combustion of solid hydrogen and liquid oxygen at a mixture ratio of 6 and at atmospheric pressure in the absence of dissociation. The freezing and boiling temperatures of hydrogen may be assumed as 14 K and 20 K and the boiling temperature of oxygen as 90 K at one atmosphere. The heat of vaporisation of liquid hydrogen is 0.89 kJ/mole and the heat of melting of solid hydrogen is 1.004 kJ/mole. The heat of vaporisation of liquid oxygen is 6.8 kJ/mole. The specific heats of solid hydrogen, liquid hydrogen and gaseous hydrogen may be assumed as constant and equal to 5, 20, and 30 J/(mole K) respectively. Similarly, the specific heats of liquid oxygen and gaseous oxygen could also be assumed constant at 29 and 35 J/(mole K) respectively.

The standard heat of formation of water is -286 kJ/mole. The boiling temperature of water at 1 atmosphere is 100°C and the specific heat of water is 90 J/(mole K). The specific heat of steam at constant pressure could be assumed equal to 58 J/(mole K).

## References

- Clark, J.D., *Ignition! An Informal History of Liquid Rocket Propellant*, Rutgers University Press, 1972.
- Glassman, I. and Sawyer, R.F., *The Performance of Chemical Propellants*, AGARDograph 129, Technivision, Slough: England, 1970.
- Bollinger, L.E., Goldsmith, M. and Lemmon Jr., A.W., *Liquid Rockets and Propellants*, vol. 2, Progress in Astronautics and Rocketry, New York: Academic Press, 1960.
- Gordon, S. and McBride, B.J., *Computer Program for Calculation of Complex Chemical Equilibrium Compositions, Rocket Performance, Incident and Reflected Shocks and Chapman Jouguet Detonations*, NASA SP-273, National Aeronautics and Space Administration, Washington, 1971.
- Kubota, N., *Propellants and Explosives: Thermo-chemical Aspects of Combustion*, Weinheim: Wiley-VCH, 2002.
- Kuo, K.K., *Principles of Combustion*, New York: John Wiley and Sons, 1968.
- Mukunda, H.S., *Understanding Aerospace Propulsion*, Bangalore: Interline Publishing, 2004.
- Penner, S.S., *Chemistry Problems in Jet Propulsion*, Pergamon Press, 1957.
- Roy, G.D., *Advances in Chemical Propulsion*, Boca Raton, Florida: CRC Press, 2002.
- Siegel, B. and Schieler, L., *Energetics of Propellant Chemistry*, New York: John Wiley and Sons, 1964.
- Summerfield, M., *Solid Propellant Rocket Research, Progress in Astronautics and Rocketry*, vol. 1, New York: Academic Press, 1960.
- Timnat, Y.M., *Advanced Chemical Rocket Propulsion*, London: Academic Press, 1987.



## Glossary

- Aliphatic compound: Hydrocarbons comprising alkanes, alkenes and alkadienes with straight chains and ring chains
- Aromatic compound: Hydrocarbons having benzene molecular structure with six carbon atoms and three double bonds
- Ammonium perchlorate:  $\text{NH}_4\text{ClO}_4$ ; Oxidiser almost universally used for composite solid propellants
- Aniline: Low performance liquid fuel consisting of aromatic amine in which amine radical is attached to benzene chain
- Az 50: Aerozene 50; a liquid fuel consisting of 50% hydrazine and 50% UDMH
- Composite propellant: Heterogeneous solid propellant with crystalline oxidiser dispersed in a polymeric fuel
- Cryogenic propellant: A propellant used at low temperatures (usually less than  $-150^\circ\text{C}$ ) and requiring suitable storage devices to maintain the low temperatures
- CTPB: Carboxy terminated poly butadiene used as the polymeric fuel for composite propellants
- Dissociation: The breakup of a substance into smaller molecules and atoms
- Double base propellant: Solid propellant having two bases viz., nitroglycerine and nitrocellulose mixed together to form a homogeneous composition
- Equilibrium flow: Chemical reactions go to completion; chemical equilibrium conditions prevail
- Explosive: Substances which contain inbuilt fuel and oxidiser and which burn spontaneously
- Frozen flow: No change in composition of gases as flow progresses
- Heat of formation: Heat required to form a substance from its standard elements when both the substance and the elements are at a standard state of 1 atmosphere pressure and  $25^\circ\text{C}$
- Heat of combustion: Energy liberated in a chemical reaction
- Hydrazine: Liquid fuel having molecular formula  $\text{N}_2\text{H}_4$  which decomposes easily and has a positive heat of formation
- Hypergolic propellant: Fuel and oxidiser spontaneously catch fire when they come into contact with each other
- HTPB: High energy polymeric fuel Hydroxy Terminated Poly Butadiene used widely for composite propellants
- IRFNA: Corrosive nature of RFNA inhibited by adding small quantities of hydrogen fluoride (HF) to RFNA
- Kerosene: Liquid hydrocarbon fuel with molecular structure near to dodecane ( $\text{C}_{12}\text{H}_{26}$ )
- Mixture ratio: Ratio of oxidiser to fuel on a mass basis
- Moles: Mass expressed in units of molecular mass
- Monomethyl hydrazine: Liquid fuel based on hydrazine widely used for upper stages of launch vehicle and spacecraft rockets ( $\text{CH}_3\text{N}_2\text{H}_3$ )
- MON: Liquid oxidiser used for spacecraft rockets; Mixed Oxides of Nitrogen consisting of oxidiser  $\text{N}_2\text{O}_4$  and nitric oxide NO
- Nitramine propellant: Solid propellant containing polymer fuel with explosive HMX or RDX
- PBAN: Polymer polybutadiene acrylic acid acrylo nitrile used for composite propellant in large solid propellant rockets
- Polymer: Hydrocarbons with linear chain structure comprising polybutadienes
- RFNA: Liquid oxidiser red fuming nitric acid comprising 15%  $\text{N}_2\text{O}_4$  added to nitric acid
- Shifting equilibrium: Chemical reaction goes to completion in the flow at each location in the nozzle; composition keeps shifting along the flow
- Sintin: Synthetic kerosene
- UDMH: Unsymmetrical di-methyl hydrazine, a liquid fuel used with oxidizer  $\text{N}_2\text{O}_4$  for booster rockets  $[(\text{CH}_3)_2\text{N}_2\text{H}_2]$

## Chapter 5

### Solid Propellant Rockets

*Solid propellant rockets got started with gunpowder in bamboo tubes in the Fire Arrow of Feng Jishen in 970 AD and solid explosives in steel cases by Tippu Sultan in 1780. Different solid propellants and explosives in different configurations and sizes are used in the present generation of solid propellant rockets for generating thrust levels over a wide range between a fraction of a Newton to several mega Newton.*

In Chapter 4, we discussed solid propellants comprising double base, composite, composite-modified double base and nitramine propellants. These were said to be prepared in the form of solid blocks. Solid propellant blocks are made of different shapes and sizes, and are called propellant grains. Propellant grains are housed in chambers, commonly referred as rocket motor cases. When the propellant grain is formed by directly casting it in the rocket motor case, it is referred as case-bonded grain. If the grain is prepared outside, by an extrusion process or otherwise, and then assembled in the rocket motor case, the propellant grain is referred as free-standing grain. A schematic diagram of solid propellant rocket is shown in Fig. 5.1.

The burning of the propellant's exposed surface generates hot gases which are expanded in a convergent-divergent nozzle to give large values of jet velocities.

The combustion of solid propellants takes place only at the free exposed surfaces of the propellant. The free surface recedes as the burning of the propellant progresses in a direction normal to the surface. The rate at which the surface recedes or regresses is called linear burn rate or the regression

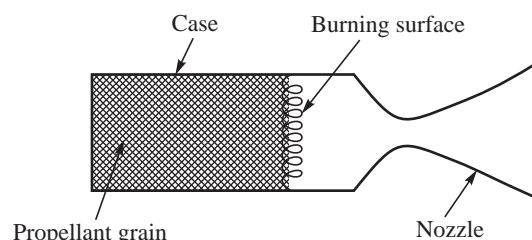


**Fig. 5.1 Solid Propellant Rocket**



rate of the propellant. The rate of mass generation from the burning would depend on the burning surface area and the burn rate of the propellant. In this chapter, we will first address the various parameters, which influence the burning rate of a propellant and then determine the procedure of configuring solid propellant rockets.



## 5.1 MECHANISM OF BURNING AND BURN RATE

An understanding of the burning mechanism is required to determine parameters that influence the rate of burning of propellants. The burning process of double-base propellants would be expected to be distinctively different from composite propellants since the fuel and oxidiser are premixed at molecular level in the double-base propellants; the oxidiser is heterogeneously dispersed in the fuel polymer in the case of composite propellants. The nature of the fuel and oxidiser are also different in the two cases. The composite modified double-base and nitramine propellants would have the combined features of double-base and composite propellants.

### 5.1.1 Double-base Propellants

#### (a) Mechanism of Burning

The burning process of double-base propellants is illustrated in Fig. 5.2. The propellant surface, when heated, degrades exothermally in the solid phase. This zone of decomposition within the solid is known as the ‘foam’ zone. Gases like  $\text{NO}_2$ , NO and aldehydes are liberated during the decomposition. The aldehydes comprise hydrogen attached to the carbonyl group [ $\text{C}=\text{O}-\text{H}$ ] to give compounds such as formaldehyde  $\text{H}-\text{C}=\text{O}-\text{H}$ , acetaldehyde  $\text{CH}_3-\text{C}=\text{O}-\text{H}$ , etc.

The gases mentioned in the previous paragraph ( $\text{NO}_2$ , NO and aldehydes) mix near the surface of the propellant and chemically react to liberate heat. The major reaction is between  $\text{NO}_2$  and the aldehydes, where CO and  $\text{CO}_2$  are formed. The zone of gas phase reaction is known as the ‘fizz’ zone. Temperature increases in this zone and the zone is highly luminescent.

An increase from the surface temperature of the propellant  $T_s$  to  $T_1$  takes place, which is indicated in Fig. 5.2.

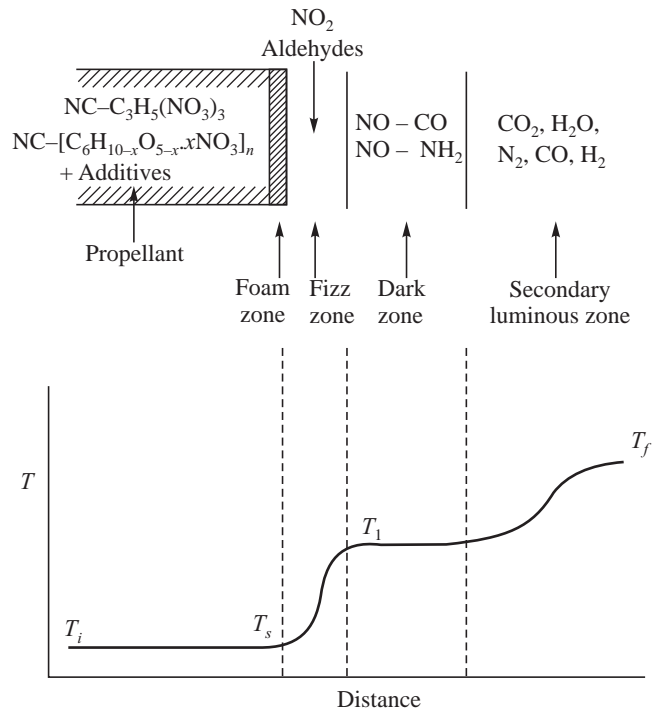
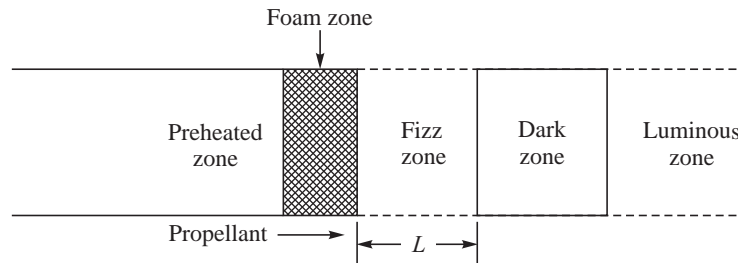


Fig. 5.2 Different Zones of Combustion



In the range of chamber pressures of interest, viz., less than about 10 MPa, the luminous fizz zone is followed by a dark zone in which chemical reactions between NO & CO and NO & NH<sub>2</sub> take place. There is no significant increase in temperature here. This zone is followed by a second luminous flame zone (schematically shown in Fig. 5.3), wherein chemical reactions proceed further with heat-liberation. Temperature rises in this zone from  $T_1$  to the final value  $T_f$  (Fig. 5.2).



**Fig. 5.3** Schematic Diagram of Different Zones of Combustion

The extent of the three zones is very small (order of fraction of mm) and depends very much on pressure. The thickness of the foam zone is much smaller than the fizz zone and dark zone.

The intermediate dark zone is at a lower temperature  $T_1$  than the final temperature  $T_f$ . This causes the overall temperature gradient in the gas phase near the propellant surface to be small and thereby limit the heat transfer from the flame at temperature  $T_f$  to the surface of the propellant. When the pressure exceeds about 10 MPa, the primary fizz zone merges with the second luminous zone, giving rise to increased heating of the propellant from the hot gases.

#### (b) Evaluation of Burn Rate

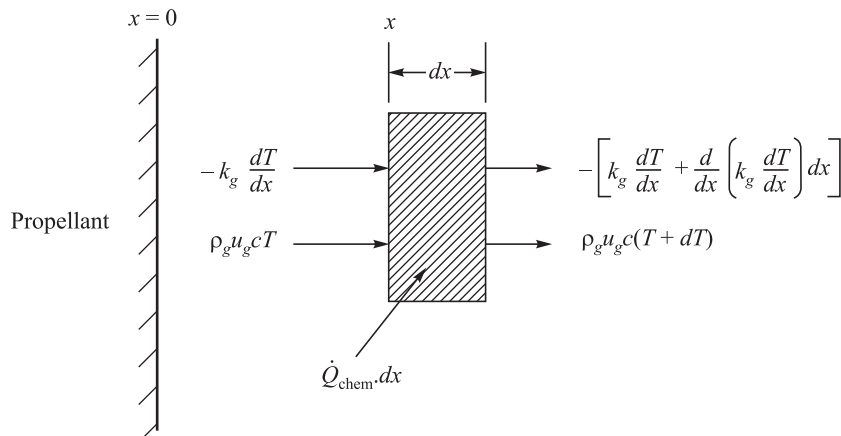


**Fig. 5.4** Energy Balance Across a Control Volume in Fizz Zone

The burn rate of a propellant is derived from the energy balance at the propellant surface by considering a small control volume in the fizz zone of unit cross sectional area and of thickness  $dx$  at a distance  $x$  from the surface of the propellant. The volumetric heat release rate from chemical reactions here is taken as  $\dot{Q}_{\text{Chem}}$  J/(m<sup>3</sup>s). The heat release over a distance  $dx$  is  $\dot{Q}_{\text{Chem}} dx$  J/(m<sup>2</sup>s). This is illustrated in Fig. 5.4.



Heat conduction into the control volume is determined by assuming heat to be conducted along the  $x$ -axis. The heat conducted increases from  $-k_g \frac{dT}{dx}$  at  $x$  to  $-\left\{k_g \frac{dT}{dx} + \frac{d}{dx} \left( k_g \frac{dT}{dx} \right) dx \right\}$  at  $x + dx$ , so that the net heat transfer into the control volume is  $-\left\{ \frac{d}{dx} \left( k_g \frac{dT}{dx} \right) dx \right\}$ . Here,  $k_g$  is thermal conductivity of the gas. The heat transfer to the control volume and the heat generated in it ( $\dot{Q}_{\text{Chem}} dx$ ) go to increase the enthalpy of gases flowing through it.

Enthalpy of the gas flow rate through the control volume increases from  $\rho_g u_g c T$  to  $\rho_g u_g c(T + dT)$ .  $\rho_g$  and  $u_g$  refer to the density of the gases and the one-dimensional velocity in the  $x$  direction.  $c$  is the specific heat of the gas. From the steady flow energy balance for the control volume, we have:

$$-\left\{ \frac{d}{dx} \left( k_g \frac{dT}{dx} \right) dx \right\} + \dot{Q}_{\text{Chem}} dx = \rho_g u_g c(T + dT) - \rho_g u_g c T \quad \dots(5.1)$$

which on simplification becomes:

$$k_g \frac{d^2 T}{dx^2} + \rho_g u_g c \frac{dT}{dx} = \dot{Q}_{\text{Chem}} \quad \dots(5.2)$$

If the edge of the fizz zone is at a distance  $L$  from the propellant surface, the boundary conditions for differential equation given by eq. 5.2 are:

$$\begin{aligned} T &= T_s \text{ at } x = 0 \text{ (Propellant surface)} \\ T &= T_1 \text{ at } x = L \text{ (Edge of fizz zone)} \end{aligned} \quad \dots(5.3)$$

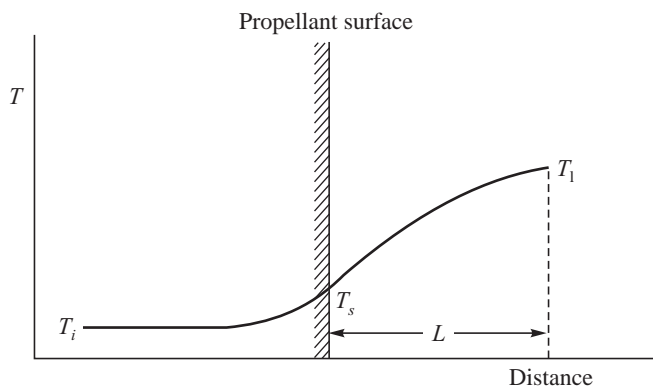


**Fig. 5.5** Distribution of Temperature in the Propellant and Fizz Zone

The temperature distribution can be determined from eqs. 5.2 and 5.3 for a given value of  $u_g$  once  $\dot{Q}_{\text{Chem}}$  is specified. A typical sketch of temperature distribution is shown in Fig. 5.5. Temperature increases from an initial value of  $T_i$  far from the surface to  $T_s$  at the surface and thence to  $T_1$  at the edge of the fizz zone. Heat release rate  $\dot{Q}_{\text{Chem}}$  depends on pressure  $p$  and temperature  $T$  and is proportional to  $A p^m e^{-E/R_0 T}$ , where  $E$  is activation energy for the reaction in J/mole and  $R_0$  is the gas constant in J/(mole k).  $A$ ,  $E$  and  $m$  are constants for the given reaction.



The value of  $u_g$  is decided by the rate at which gases get evolved in the foam zone due to heat transfer from the hot gases at the propellant surface, viz.,  $-k_g \frac{dT}{dx} \Big|_{x=0}$  and also the heat release by the chemical reactions within the foam zone. If the density of the propellant is denoted by  $\rho_p$  and the linear regression (burn) rate of the propellant is denoted by  $r$ , we get from mass balance rate at the surface:

$$\rho_p r = \rho_g u_g \quad \dots(5.4)$$

A unique solution for  $r$  which satisfies the temperature at the boundaries and the heat balance within the foam and fizz zones would give burn rate  $r$  of the propellant. Solution of the set of equations in the fizz and foam zones is somewhat involved. We, however, observe that  $\rho_g$ ,  $u_g$  and  $\dot{Q}_{\text{Chem}}$  depend on pressure  $p$  and, therefore,  $r$  would depend on  $p$ . Temperature  $T_1$  and the initial temperature of the propellant  $T_i$ , the activation energy  $E$  of the chemical reaction and the physical and thermal properties of the propellant and gases would also influence  $r$ . The burn rate is a composite of these parameters and is generally expressed in the form,

$$r = ap^n \quad \dots(5.5)$$

where the constant  $a$  takes care of the initial temperature, composition and other characteristics of the propellant. Index  $n$  brings out the pressure effects, which are dependent of the combustion process. The relation  $r = ap^n$  is known as Vielle's law and also as Saint Roberts' law. The values of  $a$  and  $n$  are generally obtained by fitting the experimentally obtained values of  $r$  at different values of  $p$ .

The existence of the intermediate dark zone at smaller values of temperature  $T_1$  (at pressures below about 10 MPa) causes reduction in heat transfer to the propellant surface. The double-base propellants therefore in general, have lower burn rates than the other types of propellants. At high pressures exceeding about 10 MPa, the secondary reaction zone beyond the dark zone merges with the fizz zone, increasing the temperature of gases from  $T_i$  to the final value  $T_f$  without the intermediate zone at a temperature  $T_1$ . This enhances the heat transfer to the propellant surface and leads to enhanced burn rates.

A typical trend of variations of burn rate of a double-base propellant grain with changes in pressure and initial temperature of the propellant is shown in Fig. 5.6. The pressure and burn rate are plotted in logarithmic scale. The burn rate, which is typically a few mm/s, increases with the increase in pressure and temperature. The index  $n$  also increases at higher values of pressure, as can be seen in Fig. 5.6.

The index  $n$  in the burn rate expression  $r = ap^n$  can be varied by modifying the rate of chemical reactions in the fizz zone. Adding small amounts of lead compounds to the double-base propellants inhibits the pressure dependence over certain ranges of pressure and causes the burn rate to be independent of pressure. A propellant having  $n = 0$  over a certain range of pressure is said to be a plateau-burning propellant. Figure 5.7 shows the trend of burn rate variations for a plateau-burning propellant.

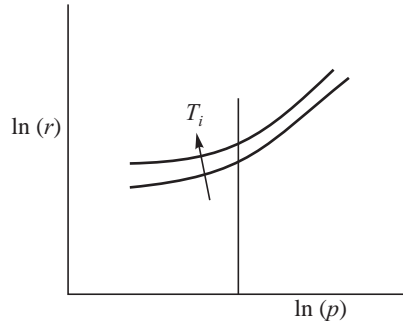


**Fig. 5.6** Burn Rate Variations with Pressure and Temperature



It is also possible to have propellants, in which the burn rate decreases with an increase in pressure (index  $n$  is negative). Such propellants, which exhibit negative values of index  $n$  over a certain range of pressure are known as mesa-burning propellants (Fig. 5.8).

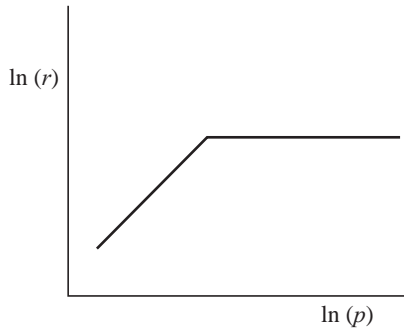


Fig. 5.7 Plateau-burning Propellant

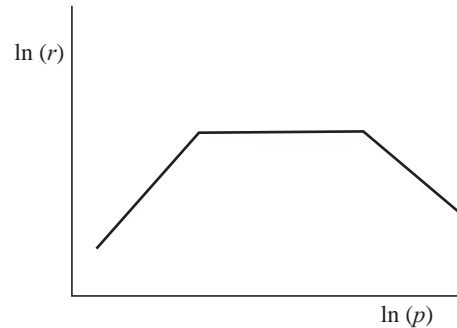


Fig. 5.8 Mesa-burning Propellant

### 5.1.2 Composite Propellants

Due to the heterogeneous nature of the composite propellant, the burning process is distributed spatially. The discrete oxidiser (AP) crystals embedded in the propellant, when heated, decompose to form oxidising gases, whereas fuel hydrocarbon vapours are formed from the pyrolysis of the polymeric fuel binder. The fuel and oxidising vapours mix with each other and form a flame. Aluminium powder, when present in the propellant, burns in the high temperature combustion zone.

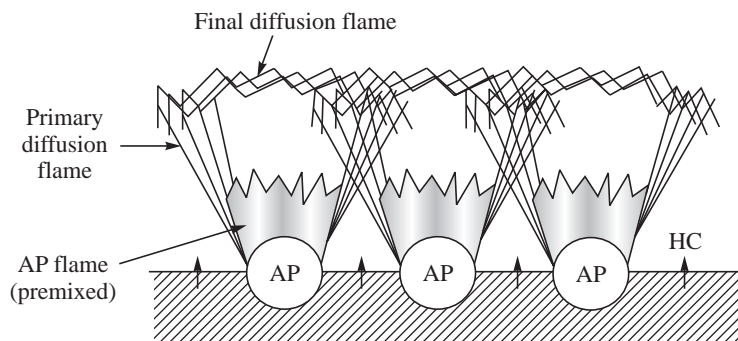


Fig. 5.9 Multiple Combustion Zones

Figure 5.9 gives a simplified scheme of the burning process. AP crystals and fuel binder are shown side-by-side at the propellant surface. AP can burn by itself (decomposition of  $\text{NH}_4\text{ClO}_4$  into  $\text{NH}_3$  and  $\text{HClO}_4$ ) at pressures greater than 1.9 MPa, forming oxidiser-rich gases at about 1300 K. The flame so formed from this decomposition (called premixed flame since no mixing with other constituents is involved), provides the oxidiser-rich gases, which mix subsequently with the hydrocarbon vapour (HC) from the fuel binder. Combustion takes place in the mixing region in the zones, where stoichiometric fuel-oxidiser mixture is formed. The combustion here is controlled by the diffusion process and is called diffusion flame. Typical temperatures achieved in the flame are around 2800 K. The products of combustion from the diffusion flame and the premixed AP flame mix further downstream as shown in Fig. 5.9, giving rise to a final diffusion flame with temperatures up to



3200 K. The net combustion process in this simplistic representation comprises a premixed combustion and two stages of diffusion combustion. The combustion zone is typically about 0.1 mm thick. The thickness of combustion zone decreases as the pressure increases.

Depending on the pressure, the three flames (premixed, initial diffusion and final diffusion flames) have different levels of importance. At low pressures, the chemical reactions are rather slow and take a long time to go to completion. The premixed combustion process governs the time required for combustion to be completed. We, therefore, say that the combustion is controlled by the premixed combustion at the low pressures. At higher values of pressure, the chemical reactions take place much faster, since large number of molecules is available. The diffusion process, however, does not increase with pressure with the result that the diffusion or mixing tends to be slow relative to the rate of chemical reactions. As a result, the diffusion combustion process limits the burning at high pressures.

When the size of the AP crystals is reduced, a larger number of these crystals are available at the surface of the propellant for combustion. Small flames are formed above the surface of the propellant, giving a more uniform temperature distribution near the surface. This enhances the heat transfer to the surface and causes a higher rate of burning.

The mechanism of burning considered in the previous paragraph, could be put together into a simple scheme for describing the combustion process. The three flames are treated to have occurred in a single plane parallel to the surface of the propellant at a distance  $X^*$  from it. This is shown in Fig. 5.10.  $X^*$  is referred to as the stand-off distance of the flame from the surface. The temperature rises from the value  $T_s$  at the propellant surface to the final temperature  $T_f$  at the flame zone.

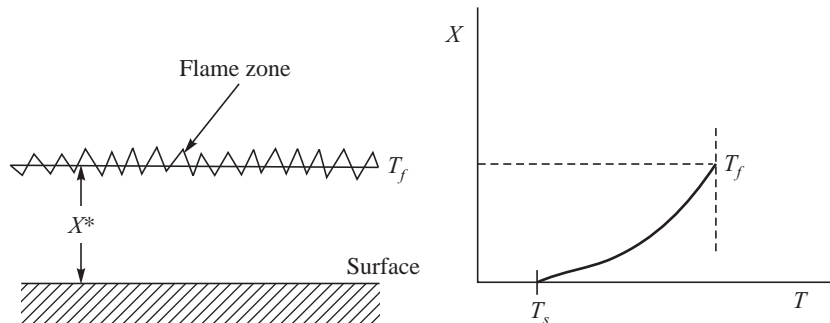


**Fig. 5.10** Simple Interpretation of Combustion of Composite Propellant

Denoting  $k_g$  as the thermal conductivity of the gas in the flame stand-off zone, heat transfer to unit area of surface of the propellant from the flame can be written as:

$$-k_g \frac{dT}{dx} = k_g \frac{T_f - T_s}{X^*} \quad \dots(5.6)$$

The temperature profile is approximated as linear in the above equation. The heat transfer per unit area increases the surface temperature to  $T_s$  from the initial value  $T_i$  and also supplies the energy required for vaporising and pyrolysis of the AP and fuel binder. Denoting the heat required for the endothermic reactions at the surface as  $q$  per unit mass of the propellant, we have the net rate of heat absorption at the surface per unit area as:

$$\dot{m}[c(T_s - T_i) + q] \quad \dots(5.7)$$



Here,  $\dot{m}$  denotes the rate of vapour released from unit surface area of the propellant and corresponds to the mass burn rate of the propellant per unit area. Denoting the density of the propellant as  $\rho_p$ , we have:

$$\dot{m} = \rho_p r \quad \dots(5.8)$$

where  $r$  is the linear burn rate of the propellant.

On substituting the above in eq. 5.7, and equating the heat absorbed per unit area of the surface to the heat flux incident from the flame from eq. 5.6, we get the steady state burn rate  $r$  as:

$$r = \frac{k_g \left[ \frac{(T_f - T_s)}{X^*} \right]}{\rho_p [c(T_s - T_i) + q]} \quad \dots(5.9)$$

The above equation suggests that with increase of flame temperature  $T_f$ , initial temperature  $T_i$  and decrease of flame stand off distance  $X^*$ , the burn rate  $r$  would increase.

The heterogeneity of a composite propellant is characterised by the mean diameter of the AP crystals in it. The stand-off distance  $X^*$  can be assumed to be proportional to this length scale since smaller AP crystals would bring about burning nearer the surface. Smaller AP crystals in the propellant would, therefore, enhance the burn rate. Similarly, as pressure increases, reactions in the gas phase above the propellant take place faster and  $X^*$  decreases, leading to an increase of the burn rate.

In summary, the burning mechanism of composite propellant suggests that as pressure  $p$  increases, burn rate  $r$  increases too. The influence of an increase in the size of AP crystals is to decrease the value of  $r$ . As the initial temperature of the propellant and the final flame temperature increases,  $r$  increases. These influences can be built in Saint Robert's law  $r = ap^n$ , discussed for the double-base propellants, if the effect of the temperature, AP particle size and the composition of propellant can be incorporated in the value of  $a$ .

The pressures of interest in solid propellant rockets typically range between about 3 and 15 MPa. At these pressures, the diffusion flame dominates and the exponent  $n$  varies from about 0.3 to 0.4. At reduced values of pressure below about 1 MPa for which the premixed AP flame controls the burning, exponent  $n$  is higher near to 0.5. The trend of variations of burn rate with pressure, therefore, gives a decreasing rate of increase in the burn rate as pressure increases. This is illustrated in Fig. 5.11 and is different from the double-base propellants. Index  $n$  is also generally smaller for composite propellants than for the double-base propellants.

The burn rate of a propellant can be modified by accelerating or decelerating the rate of chemical reactions, which can be done by adding catalysts or fire retardants. Copper chromite ( $Cu_2CrO_3$ ) or Ferric oxide ( $Fe_2O_3$ ), when added in small quantities to the propellant, enhances the burn rate, while Lithium fluoride ( $LiF$ ) reduces the burn rate. Such substances, added to the propellant to modify the burn rate, are called burn rate modifiers (discussed in Chapter 4).

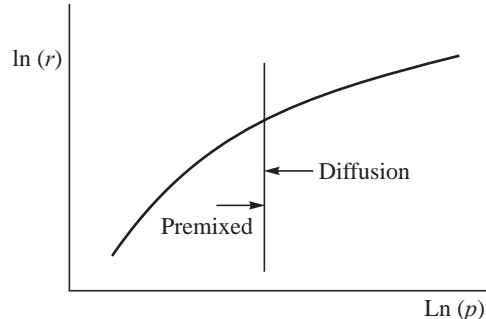


Fig. 5.11 Variations in Burn Rate with Pressure for Composite Propellants



### 5.1.3 Composite Modified Double-base Propellants and Nitramine Propellants

In composite modified double-base propellants, the addition of AP to double-base propellants promotes diffusion combustion between the oxidiser-rich gases from AP with the fuel-rich gases from the double-base propellant. This reduces the higher values of index  $n$  seen in the double-base propellants due to the premixed nature of combustion.

The use of HMX/RDX in nitramine propellants instead of AP for the composite modified double-base propellants causes production of fuel-rich gases from both the polymer and HMX/RDX. The fuel-rich gases do not significantly react further, and the result is that the burning is essentially governed by premixed combustion from the decomposition of HMX/RDX and the binder. This results in higher values of the index  $n$  in the burn rate law  $r = ap^n$  for nitramine propellants.

### 5.1.4 Influence of Initial Temperature of Propellant on Burn Rate

The effect of initial temperature is contained in the coefficient in the burn rate law  $r = ap^n$ . The influence of variations of the initial temperature is expressed by a temperature-sensitivity parameter  $\pi_r$ , defined as the fractional variation in  $r$  due to unit temperature change at constant pressure:

$$\pi_r = \frac{1}{r} \left. \frac{dr}{dT} \right|_p \quad \dots(5.10)$$

Burn rate of the double-base propellants are more sensitive to the changing propellant temperatures due to the chemical reactions within the propellant in the foam zone. Typical values of  $\pi_r$  at a pressure of 7 MPa are about  $5 \times 10^{-3} \text{ }^{\circ}\text{C}^{-1}$  for the double-base propellants and about  $3 \times 10^{-3} \text{ }^{\circ}\text{C}^{-1}$  for composite propellants. The sensitivity-parameter  $\pi_r$  for AP and HMX burning are lower at about  $2 \times 10^{-3} \text{ }^{\circ}\text{C}^{-1}$  at 7 MPa.

The burn rate of a propellant at any temperature  $T$  can be determined from its known value at temperature  $T_0$ , say  $r_{T_0}$ , if  $\pi_r$  is given. Equation 5.10 is written for the specified constant value of  $p$  as:

$$\frac{dr}{r} = \pi_r dT$$

On integrating from the reference value of  $T_0$  at which the burn rate (at given pressure) is  $r_{T_0}$ , we have the value  $r$  at temperature  $T$  at the same pressure  $p$  as:

$$\ln \left( \frac{r}{r_{T_0}} \right) = \pi_r \int_{T_0}^T dT$$

giving

$$r = r_{T_0} \exp[\pi_r (T - T_0)] \quad \dots(5.11)$$

### 5.1.5 Specification of Coefficient $a$ in $r = ap^n$ at Reference Condition of 7 MPa

Burn rate  $r$  has units of (Length/Time) and is generally given in mm/s. The burn rate law  $r = ap^n$  has units of pressure raised to the power of the exponent  $n$  on the right side of the expression. The dimension of the coefficient  $a$  becomes somewhat unwieldy and its magnitude depends on the units of pressure. It is, therefore, more appropriate to express the burn rate by the expression:



$$r = a \left( \frac{p}{p_{\text{ref}}} \right)^n$$

where  $p_{\text{ref}}$  is a reference pressure. In this case, the coefficient  $a$  in the burn rate law will have units of mm/s.

A reference pressure of 7 MPa, which is near to the operating pressure of the high pressure solid propellant rockets, is adopted in practice. Burn rates of different propellants are also generally compared at the reference pressure of 7 MPa. The value of  $a$  is stated as  $a_{70}$  (corresponding to  $7 \text{ MPa} \approx 70$  atmospheres) and  $r$  at 7 MPa is:

$$r|_{7 \text{ MPa}} = a_{70}$$

Using the value of  $a_{70}$ , the burn rate  $r$  at any other pressure  $p$  MPa is determined from the burn rate law as:

$$r = a_{70} \left( \frac{p}{7} \right)^n \quad \dots(5.12)$$



## 5.2 CHOICE OF INDEX $n$ FOR STABLE OPERATION OF SOLID PROPELLANT ROCKETS

A smaller value of the index  $n$  in the burn rate law  $r = ap^n$  is desirable in order to have a stable burning in a solid propellant rocket. The reason for this may be understood by considering the mass generation and mass leaving a rocket having a burning surface area  $S_b$  and a nozzle throat of area  $A_t$ , as shown in Fig. 5.12. The rate of mass generation from the propellant surface  $\dot{m}_{\text{gen}}$  is  $S_b r \rho_p$ , where  $\rho_p$  is the propellant density and  $r$  is the burn rate. The rate at which hot gases leave the nozzle  $\dot{m}_n$  is  $p A_t / C^*$ , where  $C^*$  is the characteristic velocity of the propellant and  $p$  is the chamber pressure. The rate of mass accumulation in the chamber is the difference between the mass generation and the mass leaving through the nozzle; it is represented as:

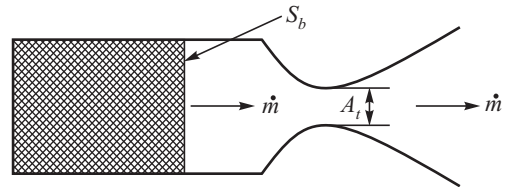


Fig. 5.12 Mass Generation and Mass Depletion

$$\left. \frac{dm}{dt} \right|_{\text{accumulation}} = \dot{m}_{\text{gen}} - \dot{m}_n \quad \dots(5.13)$$

Substituting the values of mass generation and mass leaving, and noting that for steady state conditions there is no mass accumulation in the rocket, we have:

$$S_b r \rho_p - \frac{1}{C^*} p A_t = 0 \quad \dots(5.14)$$

The burn rate law  $r = ap^n$  when incorporated in the above equation, gives the steady state or equilibrium pressure as:



$$p = \left\{ \rho_p a C^* \left( \frac{S_b}{A_t} \right) \right\}^{\frac{1}{1-n}} \quad \dots(5.15)$$

This equilibrium pressure is denoted by  $p_{eq}$ . If  $n$  is near unity, the value of  $1/(1 - n)$  would be very large and any small variation of  $S_b$ ,  $A_t$ ,  $\rho_p$  or a propellant characteristic which influences  $C^*$  and  $a$  would have a significant influence on  $p_{eq}$ .

A value of  $n \ll 1$  would bring about a smaller impact of changes in the burning surface area, nozzle throat area and the characteristics of the propellant on the equilibrium pressure.

In deriving eq. 5.15, we did not consider the change in the gas volume in the chamber due to the regression of the propellant surface. The influence can be incorporated by expressing the mass of gas  $m$  at any instant of time in the chamber in terms of the volume of gas in the chamber ( $V$ ) using the ideal gas equation:

$$m = \frac{pV}{RT} \quad \dots(5.16)$$

$R$  is the specific gas constant and  $T$  is the gas temperature. Substituting in eq. 5.13 and simplifying, we have:

$$\frac{d}{dt} \left( \frac{pV}{RT} \right) = S_b \rho_p a p^n - \frac{p A_t}{C^*} \quad \dots(5.17)$$

The gas temperature does not vary significantly and the left side of the above equation gives:

$$\frac{d}{dt} \left( \frac{pV}{RT} \right) = \frac{V}{RT} \frac{dp}{dt} + \frac{p}{RT} \frac{dV}{dt} \quad \dots(5.18)$$

Noting that  $\frac{dV}{dt} = S_b a p^n$  and  $\frac{p}{RT} = \rho_g$  = density of the gas, we have

$$\frac{V}{RT} \frac{dp}{dt} = S_b a p^n (\rho_p - \rho_g) - \frac{p A_t}{C^*} \quad \dots(5.19)$$

For steady state conditions,  $\frac{dp}{dt} = 0$ .

The equilibrium value of pressure  $p_{eq}$  is:

$$p_{eq} = \left\{ a C^* (\rho_p - \rho_g) \left( \frac{S_b}{A_t} \right) \right\}^{\frac{1}{1-n}} \quad \dots(5.20)$$

Since the density of the gas is less than the density of the propellant (the propellant density of  $\rho_p$  is some three orders of magnitude greater than the gas density  $\rho_g$ ) eq. 5.20 reduces to eq. 5.15.

Equation 5.19 in the limit of  $\rho_g$  being much smaller than  $\rho_p$  is written as:

$$\frac{V}{RT} \frac{dp}{dt} = S_b a p^n \rho_p - \frac{p A_t}{C^*} = \dot{m}_{gen} - \dot{m}_n \quad \dots(5.21)$$

If the terms  $\dot{m}_{gen} = S_b a p^n \rho_p$  and  $\dot{m}_n = \frac{p A_t}{C^*}$  were to be plotted as a function of  $p$  for given values of  $S_b$ ,  $A_t$ ,  $\rho_p$ ,  $C^*$  and  $a$ , we observe that  $\dot{m}_n$  increases linearly with increase of pressure. The mass



generation rate  $\dot{m}_g$ , however, sharply increases with  $p$  when  $n > 1$  while the rate of its increase comes down with increase of  $p$  when  $n < 1$ . These trends are shown in Figs. 5.13 and 5.14 for  $n > 1$  and  $n < 1$  respectively. The point of intersection O of  $\dot{m}_g$  and  $\dot{m}_n$  curves gives the steady state or equilibrium pressure  $p_{eq}$  obtained in eq. 5.15.

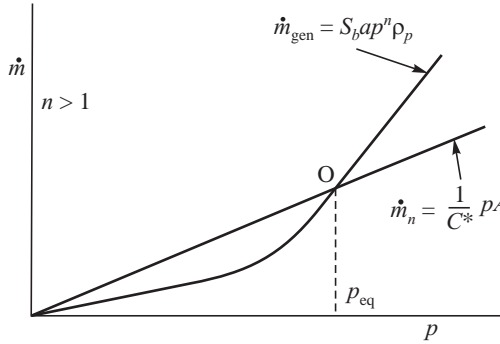


**Fig. 5.13** Unstable Operation for  $n > 1$

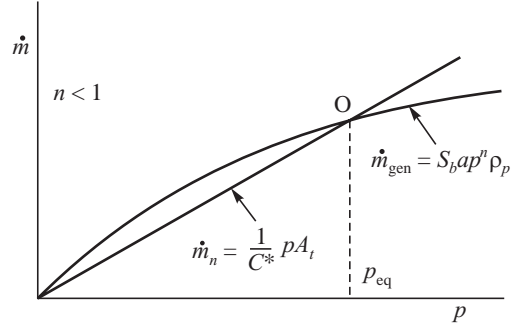


**Fig. 5.14** Stable Operation for  $n < 1$

Consider the operation of rocket at equilibrium pressure  $p_{eq}$  shown by the point O in Figs. 5.13 and 5.14. If for some reason, there is a momentary disturbance, which results in a small increase of  $p$  beyond  $p_{eq}$ , then in case of  $n > 1$  (Fig. 5.13), the rate of mass generation ( $\dot{m}_g$ ) exceeds the rate of mass leaving ( $\dot{m}_n$ ). Since  $\dot{m}_g$  increases with pressure over and above the steady increase of  $\dot{m}_n$ , the pressure continues to increase till the rocket bursts. On the other hand, if the momentary disturbance results in a fall of pressure below  $p_{eq}$ , the pressure continues to fall further since the mass leaving is more than the rate of mass being generated ( $\dot{m}_n > \dot{m}_g$ ). No steady or stable operation is, therefore, possible with  $n > 1$ .

When  $n < 1$ , an increase of  $p$  beyond  $p_{eq}$  causes  $\dot{m}_g < \dot{m}_n$  (Fig. 5.14). This causes  $p$  to decrease and get back to  $p_{eq}$ . Similarly, when  $p$  momentarily falls below  $p_{eq}$ ,  $\dot{m}_g > \dot{m}_n$  which causes  $p$  to increase to the higher value  $p_{eq}$ . Hence for  $n < 1$ , the operation of the rocket is stable.

The condition for stable operation of a solid propellant rocket is  $n < 1$ . If increase in the volume of gas due to consumption of the propellant is to be accounted, we have by comparing eqs. 5.19 and

$$5.21, \text{ the condition for stable operation as: } n < \frac{1}{1 - \frac{\rho_g}{\rho_p}}.$$



### 5.3 PROPELLANT GRAIN CONFIGURATION

Thrust  $F$  developed by a solid propellant rocket is written, using the value of steady state pressure determined in eq. 5.15 and the thrust coefficient  $C_F$  as  $F = C_F p_c A_t$ , to give:

$$F = C_F S_b^{\frac{1}{1-n}} (C^* a \rho_p)^{\frac{1}{1-n}} A_t^{-\frac{n}{1-n}} \quad \dots(5.22)$$



The thrust, as well as the chamber pressure depends on the burning surface area  $S_b$  for the given throat area  $A_t$  of a given solid propellant rocket. The choice of  $S_b$  is, therefore, important. The evolution of  $S_b$  as the burning of the propellant grain progresses will decide the variation of the chamber pressure and thrust.

The burning at the propellant surface is always normal to the surface. If  $S_b$  is maintained constant as the burning progresses, such as in a cylindrical propellant grain burning from the end [Fig. 5.15(a)], the chamber pressure would not vary with time. The burning is referred as ‘neutral’ burning. When  $S_b$  increases as burning of the grain progresses, such as in a hollow cylindrical grain burning radial outward from inside [Fig. 5.15(b)], the pressure and thrust increase as burning proceeds and the configuration is called ‘progressive’ burning. A decrease in  $S_b$  of the propellant grain as the burning proceeds will lead to reduction in pressure and thrust. This can be seen in the case of a cylindrical grain burning radial inward from the outer cylindrical surfaces shown in Fig. 5.15(c). The configuration of burning is known as ‘regressive’ burning.

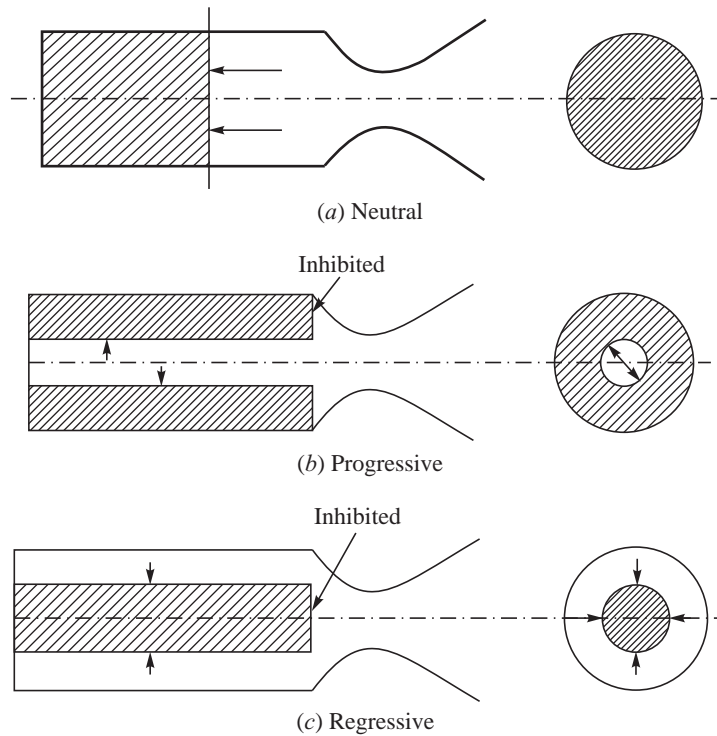


**Fig. 5.15** Neutral, Progressive and Regressive Burning

### 5.3.1 Variation of Chamber Pressure in a Hollow Cylindrical Grain

The variation of chamber pressure with time in a solid propellant rocket, having a hollow cylindrical grain of inner diameter  $D_i$  and outer diameter  $D_O$  and length  $L$  is considered in the following. The burning is progressive from the inner diameter  $D_i$  to the outer diameter  $D_O$ . The initial and final burning surface areas  $S_{bi}$  and  $S_{b0}$  are:



$$S_{bi} = \pi D_i L \quad \dots(5.23)$$

$$S_{b0} = \pi D_O L \quad \dots(5.24)$$

If the throat area of the nozzle is  $A_t$ , the initial chamber pressure in the rocket is obtained from eq. 5.15 as:

$$P_{c,i} = \left( \frac{\pi D_i L C * a \rho_p}{A_t} \right)^{\frac{1}{1-n}} \quad \dots(5.25)$$

The progress of the burning surface is considered in steps of small incremental values of distance  $\delta$ . When the burning surface has regressed over a distance  $\delta$  from the inner diameter  $D_i$  (shown in Fig. 5.16), the diameter of the burning surface is  $(D_i + 2\delta)$  giving the chamber pressure  $p_{c,\delta}$  as:

$$p_{c,\delta} = \left( \frac{\pi L [D_i + 2\delta] C * a \rho_p}{A_t} \right)^{\frac{1}{1-n}} \quad \dots(5.26)$$

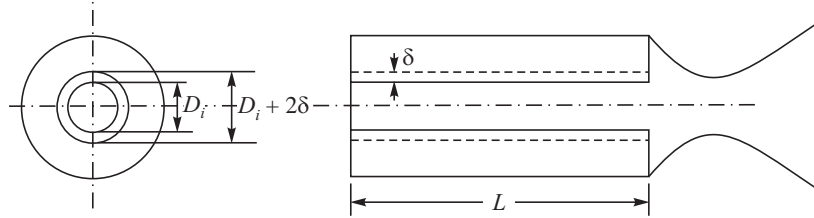


**Fig. 5.16** Calculation of Progressive Radial Burning for a Cylindrical Grain

The time taken to burn through the distance  $\delta$  depends on the mean burning rate over  $\delta$ . The mean burn rate can be estimated considering the average pressure  $\frac{p_{c,i} + p_{c,\delta}}{2}$  for which the burn rate is:

$$\bar{r} = a \left( \frac{p_{c,i} + p_{c,\delta}}{2} \right)^n \quad \dots(5.27)$$

and the time taken  $\Delta t_\delta$  is:

$$\Delta t_\delta = \frac{\delta}{\bar{r}} \quad \dots(5.28)$$

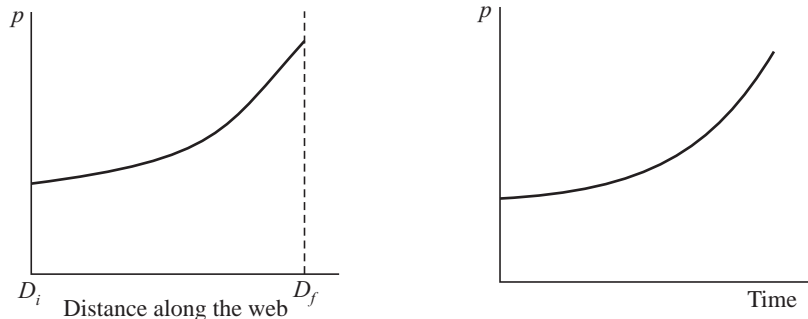


**Fig. 5.17** Pressure Variation as Burning Progresses Radially and with Respect to Time



The time taken for each additional distance  $\delta$  along the diameter is determined till  $D_O$  is reached. The trends of the variation of chamber pressure with distance along the radius of the grain and the variation with time are shown in Fig. 5.17. As  $\delta$  increases, the value of  $p_c$  increases and it reaches the maximum value when the burning surface is at the outer diameter  $D_O$ . The maximum pressure is given by:

$$p_{c,f} = \left( \frac{\pi D_O L C * a \rho_p}{A_t} \right)^{\frac{1}{1-n}} \quad \dots(5.29)$$

### 5.3.2 Burn Time of a Hollow Cylindrical Grain

In case of the hollow cylindrical grain, it is possible to derive a closed form expression for the time taken for the grain to burn and the chamber pressure at any instant of time analytically. The chamber pressure when the burning surface is at a given diameter  $D$  (Fig. 5.18) between the initial and final values of  $D_i$  and  $D_f$  respectively from eq. 5.15 is:

$$p = \left( \frac{\pi LaC * \rho_p}{A_t} \right)^{\frac{1}{1-n}} D^{\frac{1}{1-n}} \quad \dots(5.30)$$

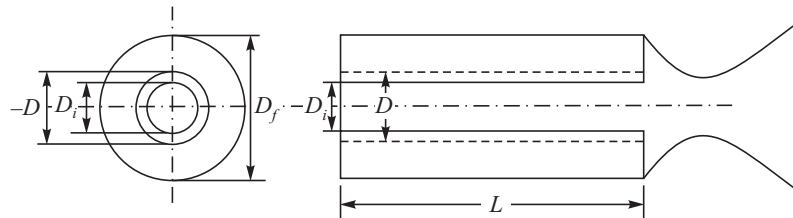


**Fig. 5.18** Cylindrical Grain Burning at a Diameter between Initial and Final Values

Denoting the term  $\left( \frac{\pi LaC * \rho_p}{A_t} \right)^{\frac{1}{1-n}}$  by  $A$ , we have the local burning rate when the burning surface is at diameter  $D$  to be:

$$r = a \left( AD^{\frac{1}{1-n}} \right)^n = aA^n D^{\frac{n}{1-n}} \quad \dots(5.31)$$

The time taken  $dt$  to progress over an infinitesimal distance  $dD$  from diameter  $D$  to  $D + dD$  is:

$$dt = \frac{dD}{2 \left[ aA^n D^{\frac{n}{1-n}} \right]} \quad \dots(5.32)$$

The time required for complete burning of the grain  $t_b$  is determined by integrating the above expression from  $D_i$  to  $D_f$  to give:



$$\int_0^{t_b} dt = \frac{1}{2aA^n} \int_{D_i}^{D_f} \frac{dD}{D^{\frac{n}{1-n}}} \quad \dots(5.33)$$

or

$$t_b = \frac{1-n}{2(1-2n)aA^n} \left[ D_f^{\frac{1-2n}{1-n}} - D_i^{\frac{1-2n}{1-n}} \right] \text{ (for } n \neq 0.5) \quad \dots(5.34)$$

The above expression fails to provide a value of burn rate when  $n \geq 1$  and  $n = 0.5$ . When  $n = 0.5$ , the integration of eq. 5.32 gives:

$$t_b = \frac{1}{2aA^n} \ln \frac{D_f}{D_i} \quad \dots(5.35)$$

We had seen that for  $n \geq 1$ , stable burning of a propellant is not possible and that it is desirable to have as low a value of  $n$  as possible.

### 5.3.3 Grains of Different Configurations

In applications, such as, booster rockets, wherein larger values of thrust are required at the initiation of burning, such as, during take-off of a rocket, the initial burning area is increased by adopting a geometry, which provides large surface area or allowing burning to take place from the ends as well as the inner and outer surfaces. The latter is known as unrestricted burning. The area of cylindrical surfaces is increased by forming creases in a structured way over its surfaces. The creases are formed with shapes, such as, star, dendrite, wagon wheel and slots. Multi-pointed star grain, slotted grain and unrestricted burning grain are illustrated in Fig. 5.19.

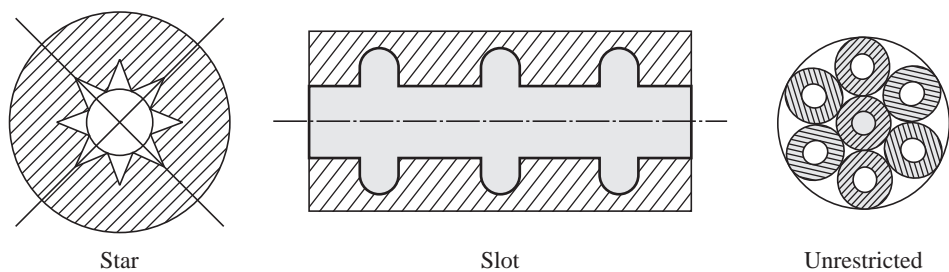
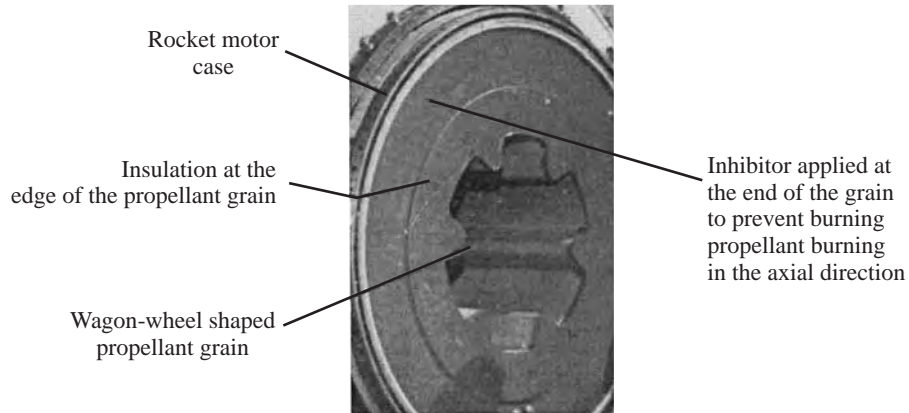


Fig. 5.19 Different Propellant Grain Configurations

The propellant grains, which have the burning taking place only along the radius, are called radial burning grains, while a grain burning along the axis is called end-burning configuration. For the burning to proceed only along the radial direction, the ends are inhibited from burning by coating them with materials, known as inhibitors. When the ends are not inhibited, and the burning progresses in both the radial and axial mode, the burning configuration is referred to as three-dimensional burning. In the case of slotted grain shapes, burning takes place axially and along the radius, giving three-dimensional burning configurations. A view of a radial burning propellant grain in the form of a wagon wheel is shown in Fig. 5.20. The surface of the grain is referred to as port surface and the volume of the cavity in the grain is called port volume.

Various other shapes and configurations of grains are possible. Some configurations include a cone and a fin in a cylinder. These are referred to as 'conocyl' and 'finocyl' grains respectively.



**Fig. 5.20** A Radial Burning Propellant Grain

#### (a) Evolution of Burning Surface; Web Burning and Propellant Sliver

While the evolution of the burning surface area  $S_b$  for the cylindrical and end-burning grains is straightforward, the changes in  $S_b$  for the pointed configurations like the star and slotted grains are more involved. The complexity arises due to the evolution of the surfaces from corners. In order to understand the procedure of determining the evolution of surfaces from a point, the following example of a cylindrical grain having a central square hole along the central axis is illustrated below.

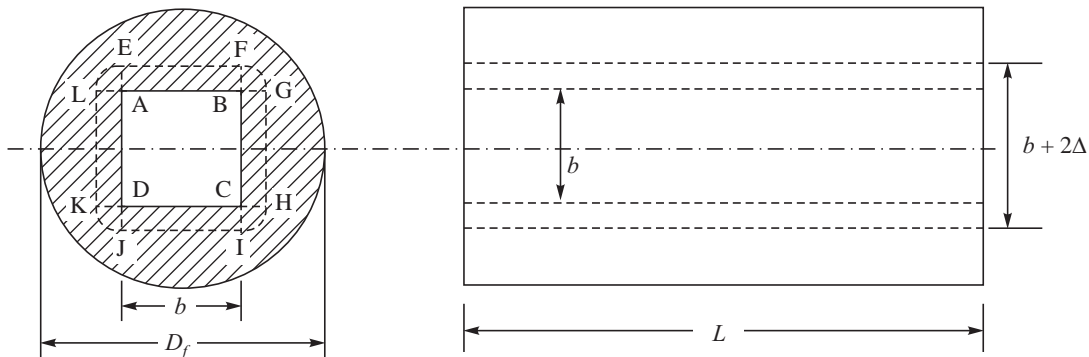


**Fig. 5.21** Evolution of Corner Points

Figure 5.21 shows a grain with the initial burning surface in the form of a square ABCD of sides of length  $b$  placed symmetrically in a cylinder of diameter  $D_f$ . The length of the grain is  $L$ . The initial burning surface area  $S_b$  is, therefore,  $4bL$ . When the burning has progressed over a distance  $\Delta$ , the sides AB, BC, CD and DA progress to EF, GH, IJ and KL as shown since the burning is always normal to the surface. The evolution of the burning from each of the corner points A, B, C and D must also be normal to the point, giving a quadrant of radius  $\Delta$  progressing from the corner point. The burning surface area when burning has progressed by a distance  $\Delta$  is, therefore:

$$S_b = (4b + 2\pi\Delta)L \quad \dots(5.36)$$

Once a part of the perimeter of the evolving surface meets the outer diameter of the grain  $D_f$ , no further increase in the burning surface area is possible. This condition takes place when the flat



surfaces have advanced by  $\Delta_f$  as shown in Fig. 5.22, for which the bisector of the quadrants reaches the outer diameter  $D_f$ . Thereafter, the perimeter decreases for any further burning of the remaining regions of the grain.

The web thickness is the minimum radial width of the propellant grain. It corresponds in this example to the radial distance between the corner of the square and the outer diameter of the propellant grain. The burn time of a radial burning propellant grain is usually referred as the time for burning of the web thickness and is known as the web burn time. The balance of the propellant left after the web burning is called ‘sliver’.

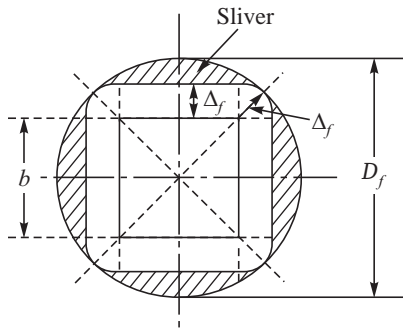


**Fig. 5.22** Decrease of Burning Surface after Web Burning

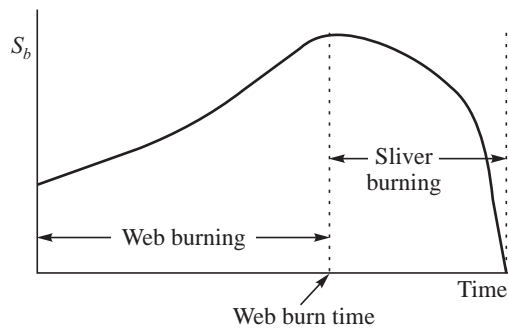


**Fig. 5.23** Evolution of Burning Surface Area and Sliver

Evolution of the burning surface is schematically indicated in Fig. 5.23. The web burn time and time of sliver burning also shown in the figure.

### (b) Evolution of Burning Surface for Star Grain

A star propellant grain with  $n$  vertices, contains  $2n$  flat surfaces. The angle subtended by each of the  $2n$  surfaces of length  $s$  at the center would be  $\pi/n$  as shown in the cylindrical cross-section in Fig. 5.24. The evolution of one particular segment (AB) is illustrated in Figs. 5.24 and 5.25 as it regresses by distance  $\Delta$  normal to its initial surface ( $\Delta = AE = AC$ ). The evolution is between the bisectors of two adjacent points in the star as shown to give a straight line CD and a circular arc EC.

The angle subtended by the arc at A is  $\left(\frac{\pi}{2} + \frac{\pi}{n} - \frac{\theta}{2}\right)$  giving the arc length EC as  $\Delta \left(\frac{\pi}{2} + \frac{\pi}{n} - \frac{\theta}{2}\right)$ .

Here  $\theta$  is the angle between the star segments (Fig. 5.24). The length CD is  $s - \Delta \cot \frac{\theta}{2}$ . The length

ECD is  $\Delta \left(\frac{\pi}{2} + \frac{\pi}{n} - \frac{\theta}{2}\right) + s - \Delta \cot \frac{\theta}{2}$ . The total surface area, considering the  $2n$  segments, when the burning regresses by  $\Delta$  is, therefore, (Fig. 5.25):

$$2n \left[ \Delta \left( \frac{\pi}{2} + \frac{\pi}{n} - \frac{\theta}{2} \right) + s - \Delta \cot \left( \frac{\theta}{2} \right) \right] L \quad \dots(5.37)$$

Here  $L$  is the length of the grain.

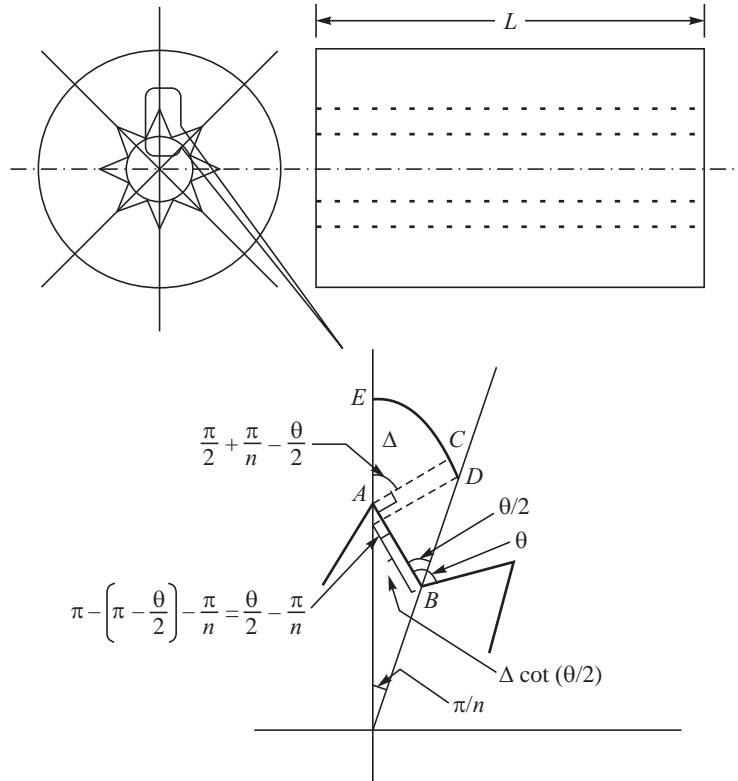
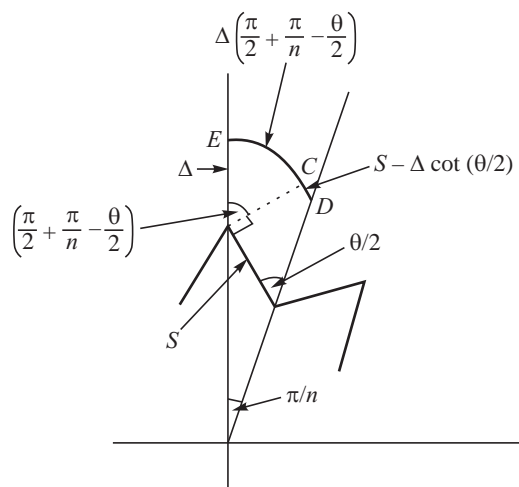


Fig. 5.24 Evolution of Burning Surface Area

Fig. 5.25 Evolution of One Segment of a Star as it Regresses by  $\Delta$ 

Depending on the value of  $\theta$ , it is possible to have either progressive, neutral or regressive burning. To get neutral burning, i.e. constant burning surface:

$$\left( \frac{\pi}{2} + \frac{\pi}{n} - \frac{\theta}{2} \right) = \cot \frac{\theta}{2} \quad \dots(5.38)$$



The above equation when solved iteratively gives  $\theta = 67^\circ$  and  $74.6^\circ$  for a six and eight pointed star respectively. For  $\theta$  greater than the above value, we will get progressive burning since  $\cot \theta/2$  is less than  $\left(\frac{\pi}{2} + \frac{\pi}{n} - \frac{\theta}{2}\right)$ . For lower values of  $\theta$ , regressive burning is achieved. It is, therefore, possible to have neutral, progressive and regressive burning by suitable choice of  $\theta$  in star grains.

The web thickness for the star grain is the radial distance between the upper star point and the outer diameter. The propellant that burns after the web thickness always has a regressive pattern.



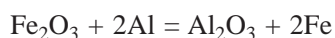
## 5.4 IGNITION OF SOLID PROPELLANT ROCKETS

### (a) Igniter Composition

Ignition is achieved by transferring heat energy to the propellant surface. The heat energy is generated in the igniter by the combustion of an easily burnable mixture such as potassium nitrate with charcoal powder and sulphur. This mixture is known as ‘black powder’ and a typical proportion of potassium nitrate, carbon and sulphur is 0.75 : 0.15 : 0.10. The above composition is used for fireworks and is referred to as pyrotechnic composition. To enhance the energy transfer to the propellant surface, metals, such as, boron and copper are also included. Ammonium perchlorate with polymer and metals is also used.

Adding metals to the igniting mixture enhances the temperature of the products of combustion generated by the igniter. Hot particles of solid and liquid from the igniter have much better heat retention capacity than gases and on coming into contact with the propellant surface, provide good contact and heating of the propellant. Hot gases, though adequate for ignition on the ground, spontaneously expand to low temperatures at low pressures and are not very effective for ignition at high altitudes.

The use of metal oxide of either iron, magnesium, copper or lead with metals such as aluminium as the igniting mixture produce not only high temperatures, but also high concentration of molten products, which are very valuable for ignition. The mixture of the metal oxide and metals used for ignition is known as thermite. The thermite mixture forms high temperature molten products through reactions such as:



### (b) Pyrotechnic Igniter

Combustion of the igniter charge is initiated electrically. A fine electrical resistance wire, such as, nichrome wire is coated with a readily ignitable substance. It is known as a squib and is enclosed in a small quantity of another easily-ignitable substance, such as potassium nitrate. When current is passed through the resistance wire, the rapid combustion of the potassium nitrate initiates the burning of the pyrotechnic composition. In order to prevent accidental ignition by electrostatic discharges and stray electric currents, a threshold value of current is specified only above which ignition can take place. A sketch of the igniter mounted in a solid propellant rocket is shown in Fig. 5.26.



For small rockets, the igniter charge is contained in a bag. The igniter charge is often compressed in the form of pellets like aspirin tablets so that the igniter burns in a controlled manner in a sturdy ignition chamber and the heat release is available over a longer time in order to ensure ignition of the propellant. A number of jets or plumes are formed by the igniter in the form of petals and these are made to impinge on the propellant surface as shown in Fig. 5.26. The igniter is known as pyrotechnic igniter.

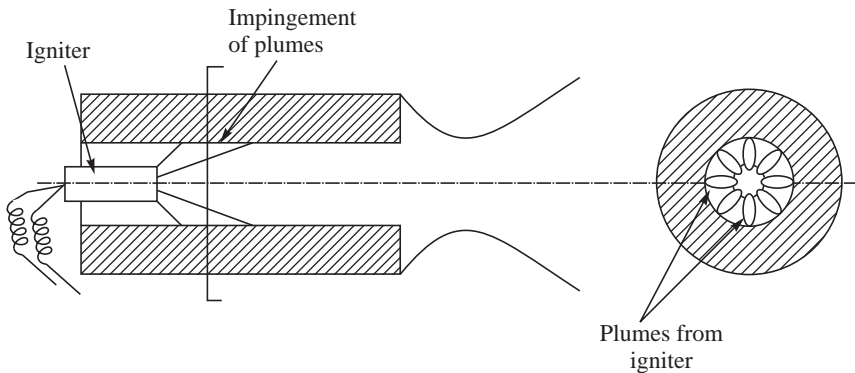


**Fig. 5.26** Schematic of Igniter in a Solid Propellant Rocket

### (c) Pyrogen Igniter

When a solid propellant rocket is very large, the amount of igniter charge required for ignition, goes up significantly. Controlled burning of a large amount of charge is difficult and the practice is to substitute a small solid propellant rocket for the igniter. The plume from the small rocket with a very thin web initiates combustion in the main rocket. Ignition of the small rocket, which is the igniter now, is achieved using the pyrotechnic igniter. The small rocket, used for ignition, is known as a pyrogen igniter. A schematic diagram of the pyrogen igniter is given in Fig. 5.27. It is to be noted that propellants with high metal content are generally not used for the pyrogen igniter since the metal, if condensed in the nozzle throat of the pyrogen igniter, will block the flow.

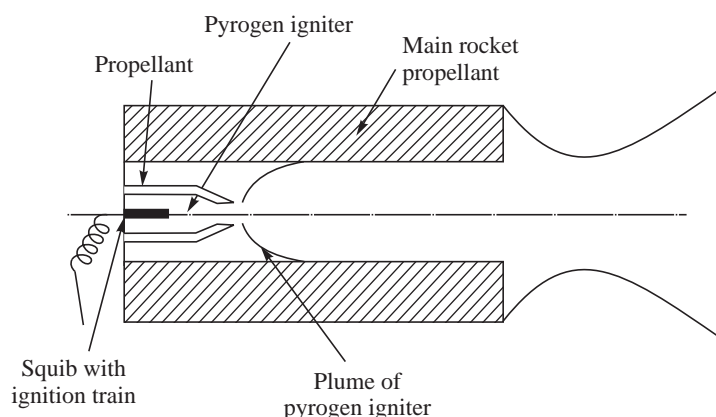


**Fig. 5.27** Pyrogen Igniter Mounted in a Solid Propellant Rocket



A typical thin-web propellant for use in a pyrogen igniter is shown in Fig. 5.28.

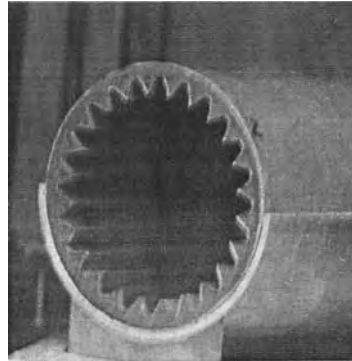


Fig. 5.28 Propellant Grain for a Pyrogen Igniter

#### 5.4.1 Mechanism of Ignition of Solid Propellant Rockets

Ignition is a complex event that involves a number of physical and chemical processes. Heat is transferred to the solid propellant from the igniter by conduction, convection and radiation. Part of the heat is conducted into the propellant. Heat radiation is partially absorbed and partly reflected from the surface of the propellant.

Heating of the propellant leads to the release of volatile vapours of fuel and oxidiser from the surface. Pyrolysis of the propellant and photochemical decomposition also occurs at the surface and in-depth regions of the propellant. Heat is also generated by chemical reactions at the surface and to a small level in the sub-surface region. Ignition occurs when the net heat generated by the different reactions is able to lead to steady state combustion.

#### 5.4.2 Ignition Processes in Solid Propellant Rockets; Local Ignition and Flame Spread

The igniter while heating up a small region of the propellant surface and initiating combustion therein also enhances the pressure in the port volume. The spread of the flame from the locally ignited zone thereafter covers the entire port surface. The spread of the flame from the locally ignited area over the entire surface of the propellant is called flame spread. The pressure continues to increase due to the mass added from the locally ignited zone and from the zones, which gets ignited during the flame spread till the steady state pressure given by eq. 5.20 is reached.

The ignition processes described above are classified into three regimes (Fig. 5.29):

- (a) Port volume pressurisation and local ignition (AB)
- (b) Flame spread (BC)
- (c) Chamber filling to equilibrium pressure (CD).

The processes are shown schematically and in a sketch of pressure buildup in Fig. 5.29. The evolution of pressure can be calculated by solving the mass and energy conservation equations. The flame spread across the propellant surface, can be determined as a series of local ignitions along the surface of the propellant. Considering the gas from the igniter to be at a temperature  $T$  and denoting the mass flow rate from the igniter and propellant surface at any time  $t$  as  $\dot{m}_{ig}$  and  $\dot{m}_p$  respectively, we have the rate of mass accumulation in the port volume at a time  $t$  as:

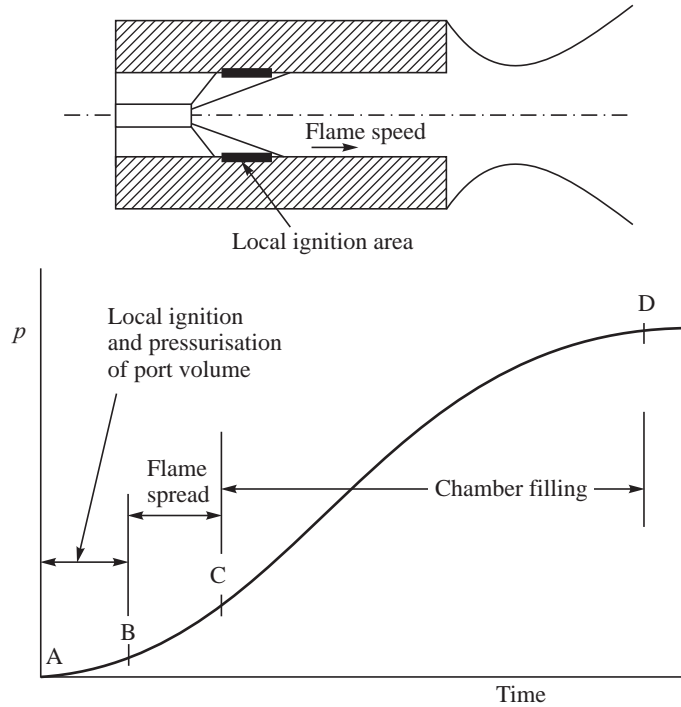


**Fig. 5.29** Processes during Ignition of a Solid Propellant Rocket

$$\frac{dm(t)}{dt} = \dot{m}_{ig}(t) + \dot{m}_p(t) - \dot{m}_n(t) \quad \dots(5.39)$$

Here,  $\dot{m}_n$  denotes the mass flow rate through the nozzle and  $m$  is the instantaneous mass in the chamber. From the ideal gas equation:

$$m = \frac{pV}{RT}$$

$V$ , in the above expression, is the port volume. We have, assuming temperature  $T$  of the gas to be constant:

$$\frac{dm}{dt} = \frac{V}{RT} \frac{dp}{dt} + \frac{p}{RT} \frac{dV}{dt} \quad \dots(5.40)$$

This gives the rate of pressure rise as:

$$\frac{dp}{dt} = \frac{RT}{V} \frac{dm}{dt} - \frac{mRT}{V^2} \frac{dV}{dt} \quad \dots(5.41)$$

The last term in the above equation can also be written as  $\frac{p}{V} \frac{dV}{dt}$ . This is small compared to the other terms since  $dV/dt$  represents the volume rate of regression of the propellant during ignition and can be neglected. Substituting for  $dm/dt$  from eq. 5.39, we get:

$$\frac{dp}{dt} = \frac{RT}{V} (\dot{m}_{ig} + \dot{m}_p - \dot{m}_n) \quad \dots(5.42)$$



The mass flow rate from the igniter  $\dot{m}_{ig}$  is specified. The propellant mass flow rate is  $\dot{m}_p = \rho_p S_b ap^n$  where the burn rate law  $ap^n$  is assumed to be valid. The nozzle flow is given in terms of the characteristic velocity of the propellant  $C^*$  as  $\dot{m}_n = pA_t/C^*$ . This gives the evolution of pressure during the ignition process as:

$$\frac{dp}{dt} = \frac{RT}{V} \left( \dot{m}_{ig} + \rho_p S_b ap^n - \frac{PA_t}{C^*} \right) \quad \dots(5.43)$$

In practice, the local ignition process is alone influential for small rockets. In the case of large solid rockets, the initial phase of ignition and the flame spread process occur at small values of pressure over small times compared to the time required to fill the chamber to the final steady state pressure. Figure 5.30 compares the changes in the nature of ignition transients for rockets with small and large values of the initial port volumes. When port volume is small, the local ignition phase (AB) is dominant with hardly any time for flame spread (BC) due to the small burning surface and a very small period of chamber filling (CD). The rate of the initial pressure rise is rather steep as shown in Fig. 5.30.

Ease of ignition of the solid propellant surface also influences pressure rise rate during the ignition process. If the propellant surface does not spontaneously catch fire, the heat transfer from the igniter heats it up. A delayed ignition of the heated propellant surface is associated with a spurt of mass and energy released into the port volume. The spurt is due to the increased burn rate of a hot propellant and causes a spike in the pressure. This is shown in Fig. 5.31. The pressure spike is spoken of as ignition spike.

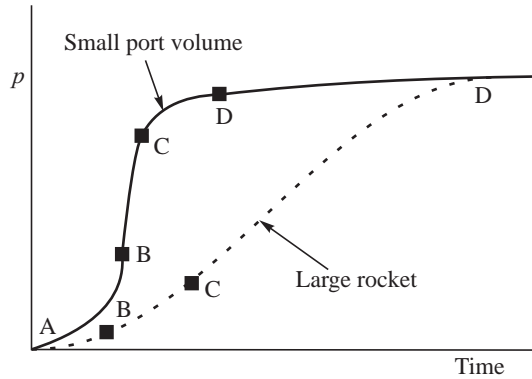


Fig. 5.30 Ignition Transient in a Small and Large Rocket

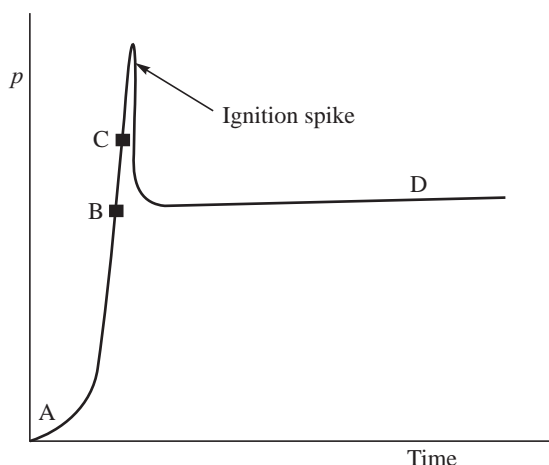


Fig. 5.31 Ignition Pressure Spike



### 5.4.3 Sizing of Igniter

The mass of the igniting mixture (known as charge) that is to be provided depends on burning surface area of the propellant and port volume of the rocket. Since the burning surface area is also dependent on port volume, empirical correlations are given for the igniter charge mass  $m_{ig}$  as a function of the port volume:

$$m_{ig} = f(V) \quad \dots(5.44)$$

The mass of igniter charge  $m_{ig}$  is chosen such that the local ignition process and the flame spread ensure the building of adequate pressure in the rocket chamber for the stable burning of the propellant. For most composite propellants, a pressure of about 1.5 MPa would correspond to stable burning. We shall examine the reason for the existence of a low pressure limit for stable burning in the chapter on combustion instability. A closure disc is generally provided in the nozzle (Fig. 5.32) to contain the igniter gases in the port volume and enhance the pressure in the port volume to values near the stable burning pressure. Once adequate pressure is built up in the rocket, the nozzle closure is forced out.

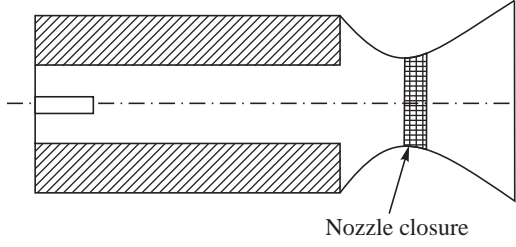


**Fig. 5.32** Nozzle Closure for Ignition

### 5.4.4 Pressure Rise during Ignition

The rate of pressure rise during ignition was given by eq. 5.43. The pressure rise in large solid rockets during the local ignition and flame spreading processes is quite small (Fig. 5.30). The evolution of pressure after the entire port surface  $S_b$  of the propellant is ignited can be determined as follows.

From eq. 5.43, the rate of pressure rise is:

$$\frac{dp}{dt} = \frac{RT}{V} \left( \rho_p S_b a p^n - \frac{PA_t}{C^*} \right) \quad \dots(5.45)$$

The characteristic velocity of the propellant  $C^*$  was given as  $C^* = \sqrt{RT}/\Gamma$  where  $\Gamma$  is a function of  $\gamma$ . Substituting the value  $RT$  from the above and simplifying eq. 5.45, we have:

$$\frac{dp}{dt} = \Gamma^2 C^* \frac{A_t}{V} \left( \frac{S_b \rho_p a p^n C^*}{A_t} - p \right) \quad \dots(5.46)$$

$V/A_t$  has units of length and gives the characteristic length  $L^*$  of the rocket. The term  $V/\Gamma^2 C^* A_t$  in eq. 5.46, therefore, has units of time and is referred to as the characteristic time  $t_{ch}$ . The value of  $S_b \rho_p a C^* / A_t$  was seen from eq. 5.20 to be  $p_{eq}^{1-n}$ , where  $p_{eq}$  is the steady equilibrium pressure in the chamber. Denoting a non-dimensional time  $\bar{t}$  as  $t/t_{ch}$  and a non-dimensional pressure  $\bar{p}$  as  $p/p_{eq}$ , we write eq. 5.44 as:

$$\frac{d \bar{p}}{d \bar{t}} = \bar{p}^n - \bar{p} \quad \dots(5.47)$$

The above equation is to be integrated between the pressure corresponding to the start of the chamber filling after the local ignition and flame spread ( $p_{ig_n}$ ) and any pressure  $p < p_{eq}$  obtained at time  $t$  as:



$$\int_{\bar{p}_{\text{ig}_n}}^{\bar{p}} \frac{d\bar{p}}{\bar{p}^n - \bar{p}} = \bar{t}$$

Here  $\bar{p}_{\text{ig}_n} = p_{\text{ig}_n}/p_{\text{eq}}$  and  $\bar{p} = p/p_{\text{eq}}$ . Integration gives

$$\bar{t} = \ln \left( \frac{1 - \bar{p}_{\text{ig}_n}^{(1-n)}}{1 - \bar{p}^{(1-n)}} \right) \quad \dots(5.48)$$

The pressure rise is logarithmic and the time taken to reach the equilibrium value ( $\bar{p} = 1$ ) is infinity. The equation shows that the approach to equilibrium is gradual in a drooping fashion as schematically indicated by the dotted line CD in Fig. 5.30 for a large solid propellant rocket.



## 5.5 PRESSURE DECAY IN THE CHAMBER AFTER PROPELLANT BURNS OUT

Equation 5.45 can also be used to determine the rate of fall in chamber pressure after the propellant has burnt out by substituting  $S_b = 0$  to give:

$$\frac{dp}{dt} = - \frac{pA_t}{C^*} \frac{RT}{V} \quad \dots(5.49)$$

The equation is valid as long as the flow through the nozzle is choked. If it is also assumed that  $C^*$  does not vary and the temperature of the gases in the chamber do not change, we have on substituting the value of  $RT$  in terms of  $C^*$  and  $\Gamma$  and simplifying:

$$\int_{p_b}^p \frac{dp}{p} = - \frac{\Gamma^2 C^*}{L_b^*} \int_{t_b}^t dt \quad \dots(5.50)$$

Here, the chamber pressure at the instant ( $t = t_b$ ) when all propellant gets burnt out is denoted by  $p_b$  and  $t$  is the time at which the pressure drops to a value  $p$ .

The value of the characteristic length  $L_b^*$  in the above equation corresponds to the final volume of the chamber and is different from the value of  $L^*$  used for the chamber filling during the ignition process. On integrating, the pressure drop is found to be logarithmic with time and is given by:

$$\frac{p}{p_b} = e^{-\frac{\Gamma^2 C^*}{L_b^*}(t - t_b)} \quad \dots(5.51)$$

Figure 5.33 shows the typical variation of the chamber pressure after completion of burning in a solid propellant rocket during the depletion of the hot gases.

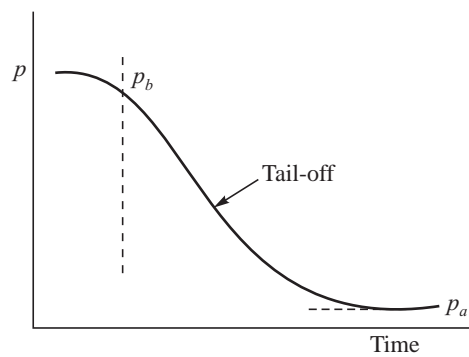


**Fig. 5.33** Exhausting of Chamber Gases



## 5.6 ACTION TIME AND BURN TIME

The logarithmic rate of pressure rise and decay in solid propellant rockets (discussed in the previous sections) makes it difficult to precisely determine the time of ignition or the time corresponding to the burn out. The following empirical procedure is, therefore, used for defining the burn time and time over which thrust is available from the solid propellant rocket.

A burn time  $t_b$  is defined as the time required for the burning of the web of the solid propellant grain. The time corresponding to the intersection of the tangent to the ignition portion and tangent to the web burning portion in the pressure-time plot (shown by A in Fig. 5.34) is taken to correspond to start of web burning. Similarly, the intersection point B between the tangent of the web burn phase and tangent of the tail-off phase is considered completion of burning of the web. The burn time  $t_b$  is the time between A and B and is shown in Fig. 5.34.

Rockets, however, provide impulse before and after the web burn time. An action time  $t_a$  is, therefore, used for rocket missions as the time taken between pressures of 10 per cent of the initial web pressure at A ( $p_{wi}$ ) and 10 per cent of the final web burn pressure at B ( $p_{wf}$ ). This is shown by C and D in Fig. 5.34. Action time  $t_a$  is, therefore, always greater than the burn time.

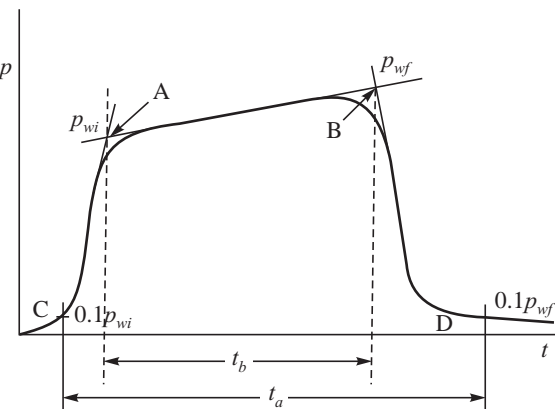


**Fig. 5.34** Action Time and Burn Time



## 5.7 FACTORS INFLUENCING BURN RATE

### 5.7.1 Measurement of Burn Rate using Strands

The simplest method of measuring burn rate of a propellant is to burn small strands of the propellant in the laboratory. The rate of regression of the strand gives the burn rate. Strands of propellant of about 10 mm diameter or 10 mm square cross-section are inhibited from the burning at the sides by applying a restrictor paste. The strands are mounted in a pressure vessel, known as Crawford bomb and ignited at one end. Contact wires are placed along the length of the strand at known distances apart and the burn rate is determined from the time taken for the burning of the known length between the contact wires. Tests are done at different pressures by pressurising the bomb using an inert gas such as nitrogen. The coefficients  $a$  and  $n$  in the burn rate law  $r = ap^n$  over a range of pressures of interest are determined.

### 5.7.2 Variation of Burn Rate from Strand to Rocket

The burn rate in solid propellant rockets is determined as the ratio of the web thickness of the propellant grain to the web burn time. The environment in which the propellant burns in the rocket is different from that of strands in the Crawford bomb. The convection and radiation heat transfer present at the



burning propellant surface in a rocket is different from that in the Crawford bomb. The burn rate of propellant evaluated in a rocket would, therefore, be different from that of propellant strands.

The general practice is, therefore, to measure the propellant burn rate in small rockets called ballistic evaluation rockets. These burn rates are used for designing propellant grains. The Crawford bomb is used only as a laboratory tool to determine the influence of compositional variables in the propellant on the burn rate.

### 5.7.3 Variation of Burn Rate with Size of Rocket

The burn rate measured for a given propellant at the same pressure in rockets of different sizes is not the same. This is primarily due to the changes in radiation and convection heat transfer to the propellant surface. As the port volume increases, the mean beam length of radiation increases resulting in enhanced radiation. Similarly, with a longer propellant grain, the convective heat transfer rate is increased. Using eq. 5.9 and including a term  $q_t$  for the heat transferred to the propellant surface from radiation and convection, the expression for burn rate is written as:

$$\rho_p r [c(T_s - T_i) + q_t] = \frac{k}{X^*} (T_f - T_s) + q_t \quad \dots(5.52)$$

As  $q_t$  increases, the burn rate  $r$  is enhanced. Mechanical properties of the propellant, such as percent elongation, tensile strength and modulus of elasticity would also influence the level of deformation of the grain during the burning and hence the web thickness and the propellant burn rate.

### 5.7.4 Erosive Burning with Long Propellant Grains

Mass flux of hot gas flow in the port volume increases along the length of a propellant grain. The enhanced flow velocities lead to higher shear forces and heat transfer at the propellant surface, resulting in an increase of the burn rate. The increase in burn rate from flow velocity is called 'erosive burning'. The increase of convective heat transfer is suggested as the most dominant mechanism for erosive burning. The dependence on velocity is expressed by the relation:

$$r = k (Mp)^c \quad \dots(5.53)$$

$M$  is the Mach number and  $p$  is the chamber pressure. The exponent  $c$  is between 0.7 and 0.8 for composite propellants.

### 5.7.5 Enhancement of Burn Rate with Acceleration

Rockets are sometimes spun on their axis in order to stabilise their motion along a particular trajectory. The spinning introduces centrifugal forces and for radial burning grains, the centrifugal acceleration moves the flame nearer the surface. This results in enhanced conduction heat transfer and an increase of the burn rate. The increase of burn rate with the increase in acceleration levels between 0 and 50 g is very significant for aluminised composite propellants.



## 5.8 COMPONENTS OF A SOLID PROPELLANT ROCKET

A solid propellant rocket comprises a chamber, known as motor case, made of high strength and light-weight metal or composite material. The motor case houses the propellant grain. The inner



surface of the case is lined with a coating of insulation, so that the case does not get heated unduly by the hot combustion products. Adequate flexibility or relief is provided to the insulation of the case bonded grains to take care of shrinkages and stresses while curing of the propellant in the motor case. The relief is plugged after the grain is cured and cooled down to the ambient temperature. The components of solid propellant rocket are shown in Fig. 5.35.

An igniter is attached preferably at the head-end of the rocket. An insulated convergent-divergent nozzle is provided to expand the hot combustion products to high jet velocities. Nozzles are sometimes submerged in the propellant grain, and in such a case, they are known as submerged nozzles (Fig. 5.35). The nozzle could be tilted or flexed to change direction of the thrust. Such nozzles were called flex nozzles in Chapter 3. The port volume of the propellant grain is initially closed to the ambient by a nozzle closure as shown in Fig. 5.35.

The size of solid propellant rockets depends on the mission that they are required to undertake. The largest solid propellant rocket, presently used for launch vehicles, is the Solid Rocket Booster (SRB) of the Space Shuttle shown in Fig. 2.13. The mass of solid propellants in SRB is about 500 tons. Diameter of the rocket is about 3.7 m, while its length is about 46 m. PBAN propellant, as we had discussed in Chapter 4, comprising PBAN polymer for binder, ammonium perchlorate crystals, and aluminium powder is used in the SRB. Solid propellant boosters used for the Ariane V launch vehicle and the GSLV launch vehicle, shown in Figs. 2.15 and 2.14 respectively, use HTPB propellant with propellant mass of about 280 and 140 tons respectively. The large solid propellant grains are prepared in a few segments up to about five and are then assembled together in the motor case.

Small solid propellant rockets having mass less than a few kilograms are used for applications, such as, spinning of the satellite launch vehicle and retro-rockets while the medium-sized rockets with a mass of a few hundred kilograms to a few tons are used as upper stage rockets and for sounding rockets.

The simplicity and ease of manufacture and storage of the solid propellant rockets make them desirable for launch vehicle and missile propulsion and also for different applications, such as, the Rocket Assisted Take Off (RATO) and Short Take Off and Landing (STOL) of aircrafts. However, once ignited, it is not possible to stop the burning of the solid propellant grain and controllability of the burning and re-ignition, as obtained with liquid and hybrid propellant rockets has not been feasible. Different methods of quenching combustion and re-ignition have been studied, but have generally not been applied in practice.

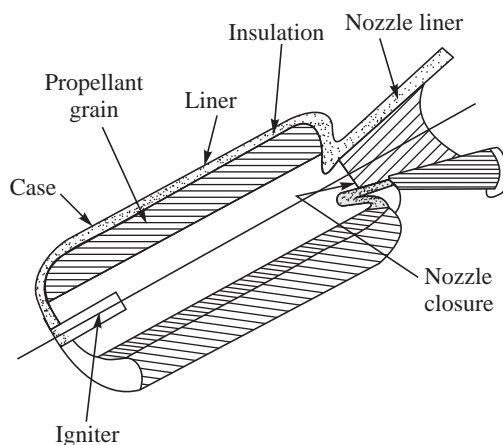


**Fig. 5.35** Components of a Solid Propellant Rocket

## SOLVED EXAMPLES

**Example 5.1** End-burning solid propellant rocket:

An end-burning rocket uses a cylindrical double-base propellant grain with a diameter of 200 mm and generates a thrust of 350 N over a period of 300 s. The thrust coefficient is 1.15. The characteristics of the propellant are:



Density of propellant grain = 1500 kg/m<sup>3</sup>

$$a_{70} = 4 \text{ mm/s}; n = 0.5$$

$$C^* = 1500 \text{ m/s}$$

Determine: (i) the length of the grain

(ii) throat diameter of the nozzle

**Solution:** (i) Length of propellant grain:

$$\text{Burning surface area } S_b = \frac{\pi}{4} \times 0.2^2 = 0.0314 \text{ m}^2$$

$$\begin{aligned} \text{Burn rate law } r &= a_{70} \left( \frac{p}{7 \times 10^6} \right)^n = 4 \times 10^{-3} \left( \frac{p}{7 \times 10^6} \right)^{0.5} \\ &= 1.512 \times 10^{-6} \times p^{0.5} \text{ m/s where the pressure } p \text{ is in Pa.} \end{aligned}$$

The specific impulse  $I_{sp} = C^* \times C_F = 1500 \times 1.15 = 1725 \text{ Ns/kg}$

$$\text{Mass flow rate through the nozzle} = \frac{F}{I_{sp}} = \frac{350}{1725} = 0.203 \text{ kg/s}$$

Mass of propellant =  $0.203 \times 300 = 60.8 \text{ kg}$

$$\text{Volume of propellant} = \frac{60.8}{1500} = 0.0405 \text{ m}^3.$$

$$\text{Length of propellant grain} = \frac{0.0405}{0.0314} = 1.29 \text{ m}$$

(ii) Throat diameter:

$$\text{Burn rate of the propellant} = \frac{1.29}{300} = 4.30 \times 10^{-3} = 4.3 \text{ mm/s}$$

The chamber pressure  $p$  is determined from the above burn rate, using the burn rate law  $1.512 \times 10^{-3} \times p^{0.5} \text{ mm/s}$

$$1.512 \times 10^{-3} \times p^{0.5} = 4.3, \text{ giving } p = 8.09 \times 10^6 \text{ Pa}$$

Thrust  $F = C_F p A_t$ , giving

$$A_t = \frac{F}{C_F p} = \frac{350}{1.15 \times 8.09 \times 10^6} = 37.63 \times 10^{-6} \text{ m}^2$$

$$\text{Hence the diameter of nozzle throat} = \sqrt{\frac{4 \times 37.63 \times 10^{-6}}{\pi}} = 6.92 \times 10^{-3} \text{ m} = 6.92 \text{ mm}$$

We could have calculated the nozzle throat area using  $C^*$  and mass flow rate  $\dot{m} = pA_t/C^*$  to give:

$$A_t = \frac{\dot{m}C^*}{p} = \frac{0.203 \times 1500}{8.09 \times 10^6}$$

=  $37.63 \times 10^{-6} \text{ m}^2$  which is the same as obtained earlier from specific impulse value.



**Example 5.2** Thrust generated after soaking propellant grain to high temperature:

Determine the thrust developed by the solid propellant rocket given in the above example, when the rocket is operated during daytime in a hot desert, wherein the ambient temperature is 50°C and the propellant grain is soaked to the above temperature. The design of the grain in the previous example can be assumed to be for a nominal initial propellant temperature of 25°C. The values of  $C^*$  and  $C_F$  can be assumed not to change with the initial temperature of the grain. The temperature sensitivity coefficient is 0.0035°C<sup>-1</sup>.

**Solution:** Temperature sensitivity coefficient  $\pi_r = \frac{d(\ln r)}{dT} = 0.0035$

The change in burn rate with temperature is given by  $\frac{r_2}{r_1} = e^{\pi_r(T_2 - T_1)}$ , giving the burn rate at 50°C as  $1.512 \times 10^{-6} \times p^{0.5} e^{0.0035(50 - 25)} \text{ m/s} = 1.650 \times 10^{-6} \times p^{0.5} \text{ m/s}$

The equilibrium chamber pressure is obtained from the balance between mass generated and mass flow rate through the nozzle and is:

$$p = \left( \frac{S_b \rho_p a C^*}{A_t} \right)^{\frac{1}{1-n}} = \left( \frac{0.0314 \times 1500 \times 1.650 \times 10^{-6} \times 1500}{37.63 \times 10^{-6}} \right)^{\frac{1}{0.5}} = 9.6 \times 10^6 \text{ Pa. This is higher}$$

than the chamber pressure of  $8.09 \times 10^6 \text{ Pa}$  at 25°C. The thrust would, therefore, be higher and is given by  $F = C_F p A_t = 1.15 \times 9.60 \times 10^6 \times 37.63 \times 10^{-6} = 415.4 \text{ N}$ .

The thrust has gone up from 350 N to 415.4 N, i.e. by about 18.7%.

**Example 5.3** Chamber pressure and propellant sliver:

A solid propellant rocket uses a composite propellant of length 2 m with an outer diameter of 1.2 m. The throat diameter of the nozzle is 60 mm. The burning of the propellant grain starts from an initial port volume, which has a square cross-section (0.4 m × 0.4 m) and proceeds towards the outer diameter of the grain.

If the linear burn rate of the propellant is given in mm/s by the law  $r = ap^n$  and the values of  $n$  and  $a$  for the composite propellants are given as 0.3 and 0.0123 respectively when the pressure is expressed in Pa, determine:

- |  |                               |
|--|-------------------------------|
| (i) Initial equilibrium chamber pressure | (ii) Maximum chamber pressure |
| (iii) Mass of propellant sliver          | (iv) $a_{70}$                 |

The density of the composite propellant is 1700 kg/m<sup>3</sup> and the characteristic velocity of the propellant is 1600 m/s.

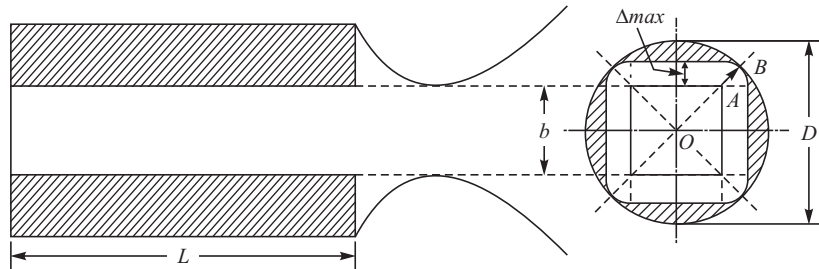
**Solution:** Figure 5.36 shows the initial square port of dimension  $b$  and the diameter of the grain as  $D$ . From the figure the web thickness of the grain (along the radius) is:

$$\text{Web thickness } (\Delta_{\max}) = \text{OB} - \text{OA} = \frac{D}{2} - \frac{1}{2} \sqrt{(b^2 + b^2)}$$

- (i) Initial equilibrium chamber pressure:

$$\text{Throat area } A_t = \frac{\pi}{4} \times 0.06^2 = 2.83 \times 10^{-3} \text{ m}^2$$

$$\text{Initial burning surface area } S_{bi} = 4b^2 = 4 \times 0.4 \times 2 = 3.2 \text{ m}^2$$



$$\text{Web thickness } (\Delta_{\max}) = OB - OA = \frac{D}{2} - \frac{1}{2}\sqrt{(b^2 + b^2)}$$

$$\text{Maximum burning surface area } (S_{b,\max}) = (4b + 2\pi\Delta_{\max})L$$

$$\text{Sliver volume } (V) = \frac{\pi}{4} D^2 L - \left( b^2 L + 4b\Delta_{\max} L + 4 \cdot \frac{\pi}{4} \Delta_{\max}^2 L \right)$$

$$\text{Sliver mass } (m) = \rho_p V$$

**Fig. 5.36** Square Port in Propellant Grain

Initial equilibrium chamber pressure  $p_{c,i}$  is given when the mass generated by the initial burning surface is equal to the mass leaving through the nozzle:

$$\rho_p S_{bi} ap_{c,i}^n = \frac{p_{c,i} A_t}{C^*}, \text{ giving}$$

$$p_{c,i}^{(1-0.3)} = \frac{1700 \times 3.2 \times (0.0123 \times 10^{-3}) \times 1600}{2.83 \times 10^{-3}}$$

This gives the initial pressure  $p_{c,i} = 3.47 \times 10^6 \text{ Pa} = 3.47 \text{ MPa}$

(ii) Maximum chamber pressure:

Maximum chamber pressure is obtained when the burning surface area is a maximum. In this configuration of square cross-section, the corner points evolve as quadrant of a circle with its centre at the initial corner point, while the flat surfaces progress parallel to the initial surface. This is because burning proceeds normal to a surface. The maximum burning surface area is obtained when the quadrant of the circle touches the outer diameter of the propellant grain. Denoting this radius as  $\Delta_{\max}$ ,

the perimeter of the grain corresponding to the maximum surface area is  $4 \times \left( \frac{2\pi\Delta_{\max}}{4} + b \right)$ . The

value of  $\Delta_{\max}$  is seen from the figure to be:

$$\Delta_{\max} = \frac{D}{2} - \frac{1}{2}\sqrt{b^2 + b^2} = \frac{1.2}{2} - \frac{1}{2}\sqrt{0.4^2 + 0.4^2} = 0.317 \text{ m}$$

$$S_{b,\max} = 4 \left( \frac{2\pi\Delta_{\max}}{4} + b \right) L = 4 \left( \frac{\pi \times 0.317}{4} + 0.4 \right) \times 2 = 7.185 \text{ m}^2$$

The maximum pressure  $p_{c,\max}$  is given by:



$\rho_p S_{b,\max} ap_{c,\max}^n = \frac{p_{c,\max} A_t}{C^*}$ , which on substituting the values as done in the last part gives

$$p_{c,\max} = 11.02 \times 10^6 \text{ Pa or } 11.02 \text{ MPa}$$

This maximum chamber pressure corresponds to the web burnout time. Thereafter, the burning surface area and the pressure progressively decrease with time.

(iii) Mass of propellant sliver:

The propellant burning after the web burning (corresponding to the maximum burning surface area) is the sliver. The volume of the propellant sliver is seen from the figure as:

$$\frac{\pi}{4} D^2 L - \left( b^2 L + 4b\Delta_{\max} L + 4 \cdot \frac{\pi}{4} \Delta_{\max}^2 L \right)$$

Mass of propellant sliver =  $\rho_p \times$  volume of sliver

$$= \rho_p \left[ \frac{\pi}{4} D^2 - \left( b^2 + 4b\Delta_{\max} + 4 \times \frac{\pi\Delta^2}{4} \right) \right] L, \text{ which on substituting the}$$

values gives:

$$1700 \times 2 \left[ \frac{\pi}{4} \times 1.2^2 - (0.4^2 + 4 \times 0.4 \times 0.317 + \pi \times 0.317^2) \right] = 500 \text{ kg}$$

$$\text{The total mass of propellant is } \rho_p \left( \frac{\pi}{4} D^2 - b^2 \right) L = 3300 \text{ kg}$$

The fractional mass of propellant sliver is  $500/3,300 = 0.15$ . This shows that 15 per cent of the propellant is burning in the tail-off region which is not desirable. Such grains are not used in practice.

(iv) Value of  $a_{70}$ :

$a_{70}$  is the burn rate at the standard pressure of 70 bars. Taking 70 bars =  $7 \times 10^6$  Pa, we get:

$$a_{70} = ap^n = 0.0123 \times (7 \times 10^6)^{0.3} = 1.39 \text{ mm/s.}$$

## NOMENCLATURE

- $a$  : Coefficient in the burn rate law defined by Vielle's law (eq. 5.5)
- $a_{70}$  : Burn rate at 70 atm. pressure
- $A_t$  : Throat area ( $\text{m}^2$ )
- $b$  : Dimensions of the cross-section of a grain with a square cavity (m)
- $c$  : Specific heat (kJ/kg K); Exponent in eq. (5.53)
- $C^*$  : Characteristic velocity of propellant (m/s)
- $C_F$  : Thrust coefficient
- $D$  : Diameter of propellant grain (m)
- $E$  : Activation energy for a chemical reaction (J/mole)
- $F$  : Thrust developed by a rocket (N)
- $L$  : Length of propellant grain (m)



---

$L^*$	: Characteristic length of the port volume ( $= V_C/A_t$ )
$L_b^*$	: Characteristic length corresponding to burn-out conditions
$m$	: Mass (kg)
$\dot{m}$	: Rate of mass release from burning surface (kg/s)
$M$	: Mach number
$n$	: Exponent of pressure in burn rate law given by eq. 5.5; number of star points
$p$	: Pressure (Pa)
$\bar{p}$	: Non-dimensional pressure given by $(p/p_{eq})$
$q$	: Heat absorption at the propellant surface from endothermic reactions (J/kg)
$\dot{Q}_{\text{Chem}}$	: Volumetric heat release rate from chemical reactions (J/m <sup>3</sup> s)
$r$	: Regression or burn rate normal to propellant surface (m/s)
$r_{T_0}$	: burn rate at temperature $T_0$ (m/s)
$R$	: Specific gas constant (kJ/kg K)
$R_0$	: Universal gas constant (kJ/kmol K)
$s$	: Length of each side in the cross-section of star propellant grain
$S_b$	: Burning surface area of propellant (m <sup>2</sup> )
$t$	: Time (s)
$t_{\text{ch}}$	: Characteristic time
$\bar{t}$	: Non-dimensional time given by $(t/t_{\text{ch}})$
$T$	: Temperature (°C; K)
$u$	: Velocity (m/s)
$V$	: Port volume (m <sup>3</sup> )
$x$	: Coordinate along $x$ -axis
$X^*$	: Flame stand-off distance
$\delta$	: Increment
$\pi_r$	: Temperature sensitivity of propellant burn rate in (°C <sup>-1</sup> ) defined by eq. 5.10
$\theta$	: Angle between star segments of a star propellant grain (°)
$\Delta$	: Increment
$\Gamma$	: Function of specific heat ratio $\gamma$ $\left( \Gamma = \sqrt{\gamma} \left[ \frac{2}{\gamma + 1} \right]^{\frac{\gamma + 1}{2(\gamma - 1)}} \right)$

## Subscripts

$a$	: Action
$b$	: Burn
$c$	: Chamber



eq	: Equilibrium or steady state conditions
f	: Flame; Flat surface
g	: Gas
i	: Initial; inner
ig	: Igniter
gen	: Generated
m	: Maximum
n	: Nozzle
O	: Outer
p	: Propellant
ref	: Reference pressure of 7 MPa
s	: surface
w	: Web

### Superscript

-	: Mean
---	--------

## EXERCISES

1. (a) An end-burning solid propellant rocket, having a throat diameter of 28 mm, is employed as the sustainer of a missile. It needs to provide a constant thrust of 5 KN. If a double-base propellant with a burn rate law  $r = 0.004p^{0.45}$  where  $p$  is in Pa and  $r$  is in mm/s is used, determine the diameter of the propellant grain.

You can assume the specific impulse of the booster to be 1900 N.s/kg. The  $C^*$  and density of the double-base propellant are 1600 m/s and 1540 kg/m<sup>3</sup> respectively.

- (b) In the above problem, if the sustainer has to operate for 200 s, determine the length of the solid propellant grain.

- (c) If the initial temperature of the grain gets reduced to a temperature of -40°C from the nominal value of 30°C due to storage in very cold surroundings, determine the change in the burning duration. You can assume the values of  $C^*$ ,  $C_F$  and density to remain the same. The temperature sensitivity coefficient  $\pi_r = d \ln(r)/dT|_p$  is 0.0020°C<sup>-1</sup>.

2. A radial burning solid propellant rocket has a hollow cylindrical grain. The inner diameter of the grain is 30 mm and the outer diameter is 100 mm. The length of the grain is 0.5 m. The throat diameter of the nozzle is 12 mm.

If the burn rate of the propellant in mm/s is given by the law  $r = 0.019p^{0.38}$ , where  $p$  is the pressure in Pa, determine:

- (a) The thrust soon after ignition (initial thrust) and the thrust at burnout

- (b) The maximum value of chamber pressure

- (c) The burning duration

- (d) The time taken for the chamber pressure to fall from the maximum to 10 per cent of the maximum during tail-off.

You can assume the density of the propellant as 1700 kg/m<sup>3</sup>, the values of  $C^*$  and  $C_F$  as 1400 m/s and 1.1 respectively.



3. An end-burning propellant grain of length 0.6 m takes 100 seconds to burn over its entire length when the ambient pressure is 3 MPa. The burn duration increases by 20 seconds to 120 seconds when it is burnt at an ambient pressure of 2 MPa. Determine the constant  $a$  and index  $n$  in the linear burn rate law:  $r = ap^n$ .
4. A payload of mass 100 kg is launched into orbit from the surface of the Earth, using a four-stage solid propellant rocket. The total mass of the four stages including the propellant put together is 17,000 kg. If the initial acceleration to be provided by the booster rocket is 1.5 g, where g is the gravitational field of Earth, determine for a chamber pressure of 10 MPa in the booster rocket:
  - (a) Throat diameter of the booster rocket
  - (b) Initial value of the burning surface of the booster grainYou can assume the following:  
Burn rate of the propellant used in the booster is given by  $r = 1.5p^{0.3}$  where  $r$  is in mm/s and  $p$  is in atmospheres  
 $C^*$  of the propellant is 1600 m/s  
Density of the propellant is 1750 kg/m<sup>3</sup>  
 $C_F$  for the booster is 1.1.
5. A hollow cylindrical propellant grain of outer diameter 600 mm has the initial propellant surface in the shape of a diverging cone. The axis of the cone coincides with the axis of the cylindrical chamber containing the grain. The port diameter of the conical surface increases from 200 mm at the head end of the grain to 250 mm at the nozzle end. The length of the grain is 750 mm. The throat diameter is 45 mm. The ends of the grain are inhibited from burning.
  - (i) Determine the web thickness
  - (ii) The mass of the propellant sliver
  - (iii) The web burn time assuming that  $a_{70}$  and  $n$  in the burn rate law are  $a_{70} = 5$  mm/s and  $n = 0.3$ . The characteristic velocity  $C^* = 1500$  m/s and the density of the propellant  $\rho_p = 1700$  kg/m<sup>3</sup>.
6. (a) In the simplified model of combustion of a solid composite propellant, you can assume that the final diffusion flame is at a temperature of 3000 K and stands off at a distance of 120 μm from the surface. The steady state temperature of the burning surface is 700 K. The specific heat of the propellant is 800 J/(kg K), the thermal conductivity of the gas above the propellant is 0.05 W/(m K) and the overall heat required at the surface to bring about the pyrolysis and gas release is 50 kJ/kg. Determine the burn rate of the propellant.  
The density of the propellant is 1500 kg/m<sup>3</sup> and the density of the gas above the propellant is 12 kg/m<sup>3</sup>. The temperature of the unburned propellant is 300 K. You can assume a linear profile for the temperature distribution between the flame and the propellant surface.  
(b) If in the above problem, the mean pressure was 1.6 MPa, and if the flame stand-off distance decreases to 100 μm from the surface at a pressure of 4 MPa, determine the exponent  $n$  of the burn rate law. You can assume that the density and thermal conductivity of the gas to be directly proportional to the pressure. The other properties do not change with pressure.
7. The initial burning surface area of a cylindrical propellant grain of outer diameter 300 mm has the configuration of a square hole of dimensions 150 mm. The length of the grain is 400 mm and the grain is inhibited from burning at the ends. If the propellant has a burn rate law given by  $a_{70} = 5$  mm/s;  $n = 0.3$ , determine:
  - (a) initial equilibrium pressure in the rocket chamber
  - (b) chamber pressure after 2 seconds of burning
  - (c) maximum chamber pressure



(d) web thickness, and

(e) propellant sliver.

The  $C^*$  of the propellant is 1680 m/s and the nozzle throat is 35 mm in diameter. The density of the propellant grain is 1700 kg/m<sup>3</sup>.

8. A solid propellant rocket comprises a hollow cylindrical composite propellant grain having an inner diameter of 200 mm and outer diameter of 600 mm. The length of the grain is 1.5 metre. The propellant grain is inhibited from burning at both ends. The burning is radially outward from the inner cylindrical surface. A convergent divergent nozzle, attached at the aft-end of the grain, has a throat diameter of 100 mm. Determine the following:

(a) Maximum chamber pressure

(b) Burn duration of the solid propellant rocket.

The propellant data is given below:

(i)  $a_{70} = 6$  mm/s

(ii) Burn rate index  $n$  in burn rate law  $r = ap^n$  is 0.35

(iii) Characteristic velocity of the propellant is 1400 m/s

(iv) Density of propellant is 1600 kg/m<sup>3</sup>.

9. A long cylindrical hollow propellant grain of density 1700 kg/m<sup>3</sup> with burn rate given by  $r$  (mm/s) =  $0.01p^{0.38}$  where  $p$  is the pressure in Pa is of length 10 m. The characteristic velocity of the propellant is 1600 m/s. The propellant grain has an outer diameter of 0.8 m and is housed in a chamber and integrated with a nozzle. The port diameter is 200 mm. The ends of the grain are inhibited from burning. The throat diameter of the nozzle is 135 mm. Determine:

(a) The static pressure at (i) the head end of the grain and (ii) the nozzle end of the grain at the start of burning.

(b) The static pressure at (i) the head end of the grain and (ii) the nozzle end of the grain at the end of burning.

(c) If the erosive burning in mm/s for the particular propellant is given by the law:  $r$  (mm/s) =  $0.0093(Mp)^{0.7}$ , where  $M$  is the Mach number and  $p$  is the chamber pressure in atmospheres, determine the ratio of the burn rate at the nozzle end to the head end of the grain at the start of burning.

You can assume the specific heat ratio  $\gamma = 1.22$ , molecular mass of the products as 22 kg/kmole and the temperature of the hot gases as 3000 K.

10. A solid propellant rocket used for injecting a spacecraft into orbit is spun on its axis at the rate of 180 rpm while it is burning. The propellant grain, having a burn rate given by  $r = 0.004p^{0.45}$  where  $p$  is in Pa and  $r$  is in mm/s, is of hollow cylindrical configuration. The burning is radial from inside to outside. The inner diameter of the grain is 150 mm and the outer diameter is 450 mm giving a mean diameter to be 300 mm. If the burn rate of the propellant increases linearly from 10% to 30% as the acceleration level increases from 2 g to 6 g, determine the per cent change in the thrust of the rocket due to spinning. State the assumptions made.
11. Determine the time taken during chamber filling portion of the ignition transient in which the chamber pressure increases from a value of 1.2 MPa corresponding to the end of the flame spread to 7.2 MPa. The equilibrium pressure in the rocket at the end of the ignition phase is 8 MPa. The characteristic length of the rocket at ignition is 2 m. The  $C^*$  of the propellant is 1600 m/s and the specific heat ratio of the combustion products  $\gamma$  is 1.3.



## References

1. Barrere, M., Jaumotte, A., Veubeke, B.J. and Vanderkerckhove, J., *Rocket Propulsion*, Elsevier Publishing Company, Amsterdam, 1960.
2. Caveny, L.H. and Kuo, K.K., *Ignition Transients of Large Segmented Solid Rocket Boosters*, NASA Cr-150162, April 1976.
3. Ciepluch, C.C., *Effects of Rapid Pressure Decay on Solid Propellants*, ARS J., Vol. 31, 1961, pp. 1584-1568.
4. Cohen, N.S. and Price, C.F., *Combustion of Nitramine Propellants*, J. Spacecrafts and Rockets, Vol. 12, 1975, pp. 608-612.
5. Glick, R.L. and Brooks, W.J., *Relations Among Temperature Sensitivity Parameters*, J. Propulsion and Power, Vol. 1, pp. 319-320, 1985.
6. Hermance, C.E., *A Model of Composite Propellant Combustion Including Surface Heterogeneity and Heat Generation*, AIAA J., Vol. 4, 1966, pp. 1629-1637.
7. Hugget, C., Bartley, C.E. and Mills, M.M., *Solid Propellant Rockets*, No. 1, Princeton Aeronautical Paperbacks, Donaldson, C.D., General Editor. Princeton University Press, Princeton, 1960.
8. Kuo, K.K. and Summerfield, M., *Fundamentals of Solid Propellant Combustion*, Progress in Astronautics and Aeronautics, Vol. 90, AIAA, New York, 1984.
9. Lenoir, J.M. and Robillard, G., *A Mathematical Model to Predict the Effects of Erosive Burning in Solid Propellant Rockets*, Proc. 6th International Symposium on Combustion, 1957, pp. 663-672.
10. Mukunda, H.S., *Understanding Aerospace Propulsion*, Interline Publishing, Bangalore, 2004.
11. Sutton, G.P. and Biblarz, O., *Rocket Propulsion Elements*, 7th Ed., Wiley Interscience Publications, New York, 2001.
12. Timnat, Y.M., *Advanced Chemical Rocket Propulsion*, Academic Press, London, 1987.
13. Williams, F.A., Barrere, M., and Huang, N.C., *Fundamental Aspects of Solid Propellant Rockets*, AGARDograph, 116, Technivision, Slough, England, 1969.

## Glossary

Action time: Time over which significant impulse is generated in a solid propellant rocket; time between 10 per cent of initial web burn pressure and 10 per cent of pressure at web burn-out

Burn time: Time for burning of the web thickness

Burn rate: Rate at which the propellant surface regresses

Crawford bomb: A pressurised chamber in which strands of solid propellant are burnt at regulated pressures

Equilibrium pressure: Steady value of chamber pressure; Corresponds to rate of mass generated at the propellant burning surface being equal to the mass flow rate leaving through the nozzle

Erosive burning: Increase of burn rate due to axial gas flow over the propellant grain surface

Flame spread: The spread of flame from a small ignited area over the remaining surface of the propellant

Flex nozzle: Nozzle that can be tilted using actuators to provide for vectoring of thrust

Grain: Solid propellant block of given configuration and size

Ignition spike: Sudden jump in chamber pressure during ignition to values much above the equilibrium chamber pressure

Inhibition: Chemical compound coated over propellant surface to prevent the surface from burning



Neutral burning grain: Propellant grain in which the chamber pressure does not change as the burning of the grain progresses

Nozzle closure: Sealing provided for the chamber for containing the hot products of combustion from igniter within the port volume and increasing the pressure in the port volume

Port: Cavity in the propellant grain

Pyrogen igniter: Small solid propellant rocket with thin web used for igniting a large solid propellant rocket

Progressive burning: Propellant grain in which the chamber pressure increases as the burning of the grain progresses

Regressive burning: Propellant grain in which the chamber pressure decreases as the burning of the grain progresses

Sliver: Propellant left after the burning of web

Submerged nozzle: Convergent portion of nozzle countersunk in the propellant grain to decrease the length and mass of the rocket

Temperature sensitivity parameter: Fractional change in burn rate of propellant at a given pressure for unit change of temperature

Tail-off: Decay of thrust of solid propellant rocket after web burn

Thermite: Mixture of metal oxide and metals used for ignition

Vielle law/St Robert's law: Burn rate of a solid propellant ( $r$ ) expressed as a function of pressure  $p$  in the form  $r = ap^n$

Web: Minimum thickness of propellant grain between port surface and case

Web burn time: Time taken to burn through the web; burn time

## Chapter 6

### Liquid Propellant Rockets

*Herman Oberth and Robert Goddard, both considered originator of modern rocketry, designed, built and successfully experimented with liquid propellant rockets independent of each other during the period 1926–30. These were forerunners for the present generation of liquid propellant rockets.*

*“The rockets can be built so powerful that they would be capable of carrying a man aloft.”*

*Herman Oberth, The Rocket into Planetary Space, 1923*

In solid propellant rockets, discussed in the last chapter, the solid propellant grain was contained in the rocket case and the burning at the exposed propellant surface generated a flow of hot gases and hence, the thrust. Liquid propellants cannot be contained in a combustion chamber and burnt like the solid propellants. The liquid oxidizer and liquid fuel need to be vaporised, the fuel vapour mixed with the oxidizer vapour in proper proportion and then burnt. Accordingly, in a liquid propellant rocket, the liquid propellants are metered at the desired flow rates, fragmented and vaporised in the rocket chamber. The purpose of fragmenting the liquid, a process called ‘atomization’, is to increase the surface area of the liquid and hence, enhance its evaporation. This is achieved, using injectors, which also meter the required quantities of the liquid propellants and generate desired flow pattern in the rocket chamber for mixing the vapours.

Liquid propellant rockets comprise tanks containing liquid propellants and suitable propellant feed systems for supplying propellants from the tanks to the combustion chamber at the required flow rates and pressures. The metering of the flow and the atomization is done in an injector. The hot products of combustion are generated in the combustion chamber and ejected through a nozzle. The combination of the injector, combustion chamber and nozzle is known as the ‘thrust chamber’. A schematic diagram of a liquid propellant rocket is shown in Fig. 6.1.

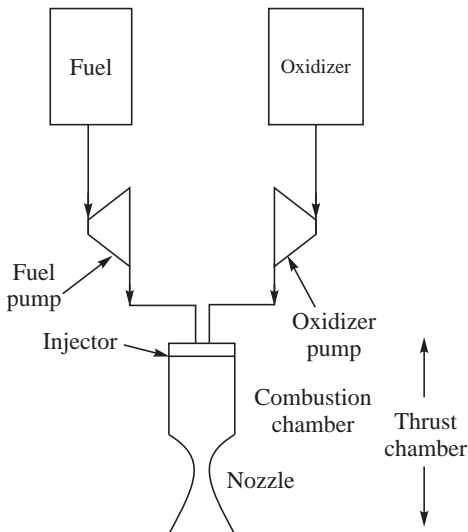


**Fig. 6.1** Schematic of a Liquid Propellant Rocket



**Fig. 6.2** Bombardier Beetle  
[Source National Geographic]

It is of interest to observe that the bombardier beetle shown in Fig. 6.2 stores fuel and oxidizer and forms hot gases in a similar manner. When this beetle is chased by other insects, hydrogen peroxide and hydroquinone are secreted from different chambers in its body to a third chamber coated with enzymes. The enzymes bring about a chemical reaction of hydrogen peroxide and hydroquinone, and hot gases are generated in the third chamber in the body of the bombardier beetle. Hot gases, so formed, are squirted out by the bombardier beetle in an appropriate direction to chase away insects.

In this chapter we shall deal with pressurization systems, thrust chambers and other components of liquid propellant rockets and the mechanism of operation.



## 6.1 PROPELLANT FEED SYSTEM

Liquid fuel and liquid oxidizer need to be supplied to the combustion chamber at specified flow rates from the storage tanks. For this, either pumps are used or the liquid fuel and oxidizer in the tanks are pressurized by a high pressure gas source and forced into the combustion chamber.

### 6.1.1 Blow-down and Regulated Cold Gas Pressurization

Gas at ambient temperature, contained in a gas bottle at high pressure, is supplied to the fuel and oxidizer tanks through a pressure regulator to expel propellants from the tanks. In some cases, the gas or vapour column above the liquid surface in the tank, known as ullage volume, is directly pressurized. These two types of gas pressurization systems are schematically shown in Fig. 6.3 and constitute the regulated mode and blow-down mode of pressurization respectively. In the blow down mode, gas pressure in the propellant tank progressively decreases as the liquid fuel or oxidizer is expelled from the tank.

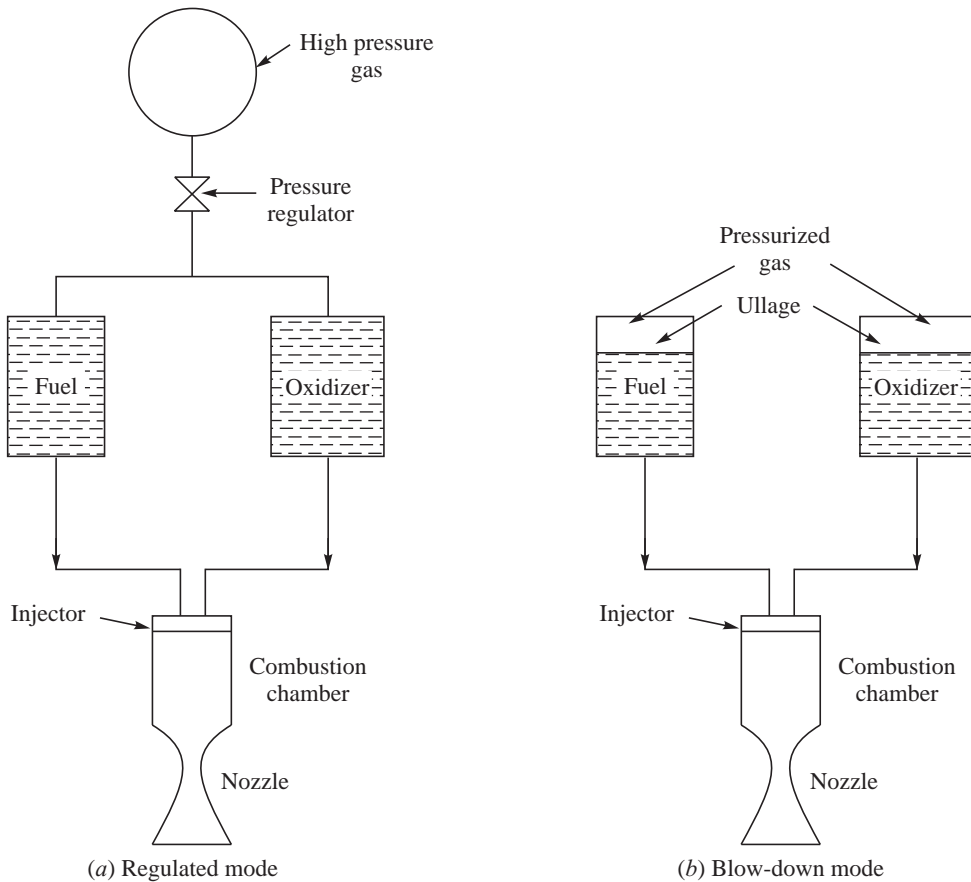


Fig. 6.3 Cold Gas Pressurization

### 6.1.2 Pump-fed Pressurization

Pumps, if used for supplying propellants from the tanks to the combustion chamber, would require a mechanical or electrical drive. The power required is enormous. An order of magnitude of the power can be estimated from the following example. Consider a liquid propellant rocket, having a chamber pressure of 10 MPa, generating a thrust of 600 kN with a specific impulse of 3000 Ns/kg. The supply pressure of the liquid propellants to the chamber should be higher than the chamber pressure and we take a value of the supply pressure to be 11.2 MPa for the chamber pressure of 10 MPa. If the pressure of liquid propellants stored in the tanks is 0.2 MPa, the pressure rise required across the pump would be 11 MPa. The flow rate of the propellants can be determined from the thrust and specific impulse as  $\frac{600 \times 10^3}{3000} = 200 \text{ kg/s}$ . Assuming the mean density of the propellants as  $1000 \text{ kg/m}^3$ , the power requirement of the pump is the product of the volume flow rate and pressure rise and this works out to be  $\left(\frac{200}{1000}\right) \times 11 \times 10^6 \text{ J/s} = 2.2 \text{ MW}$ . This represents a huge amount of power and it is unimaginable to think in terms of an electrical motor and generator for this purpose. The only alternative



seems to run a turbine by the hot gases formed in a gas generator or some other components and use the power output of the turbine to drive the pump. A schematic diagram of the configuration of the pump-fed liquid propellant rocket with turbine driving the pumps is shown in Fig. 6.4.

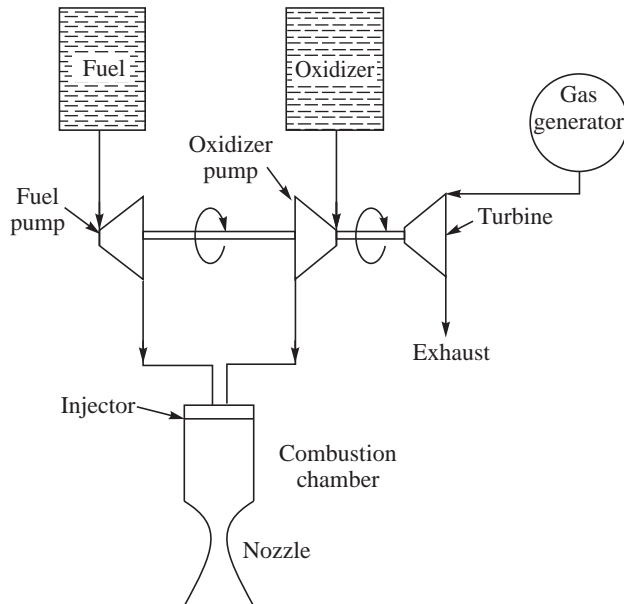


**Fig. 6.4** A Pump-fed Liquid Propellant Rocket

#### (a) Gas Generator Cycle

When power requirements are large for supplying the propellants to the combustion chamber, significant flow rates of hot gases through the turbine are required. Part of the propellants from the fuel and oxidizer tanks is diverted to the gas generator, where hot gases are generated and these hot gases are expanded in the turbine. The turbine drives the pumps.

The turbines cannot operate at high temperatures, considering the material limitations. The mixture ratio of the propellants is chosen such that temperature of the gases in the gas generator is well within the acceptable limits of less than about 1000 K. Auxiliary fluids, such as, water are also sometimes employed to cool hot gases in the gas generator to tolerable levels for use in the turbine.

Exhaust gases from the turbine are at relatively low temperature. They are released to the ambient through an auxiliary nozzle of small area ratio and do not generate any significant thrust. This configuration is known as a pump-fed system operating on Gas Generator (GG) cycle and is sketched in Fig. 6.5.

#### (b) Topping or Staged Combustion Cycle

In order to improve the thrust generation by effectively using the outflow of turbine gases and thus enhancing the net performance of the rocket, exhaust gases from the turbine are sent to the main combustion chamber of the rocket, where they are further mixed with additional quantities of fuel or oxidizer and burnt to high temperatures. A schematic diagram of this arrangement is shown in Fig. 6.6.

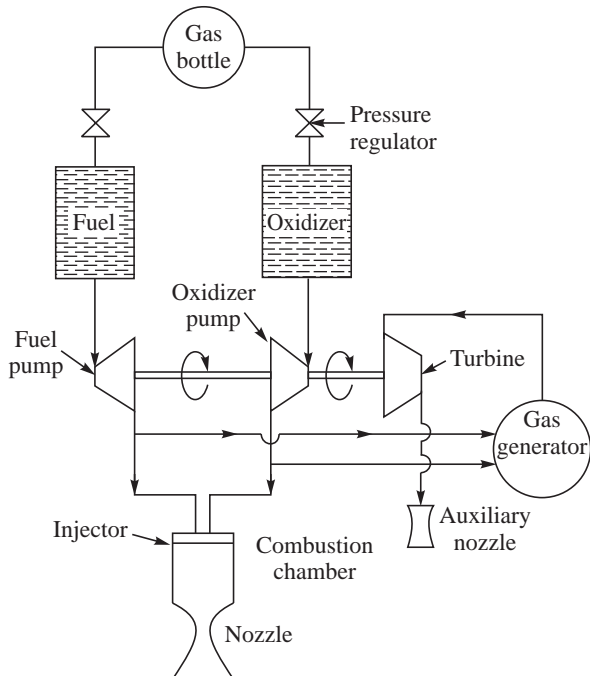


Fig. 6.5 Gas Generator Cycle

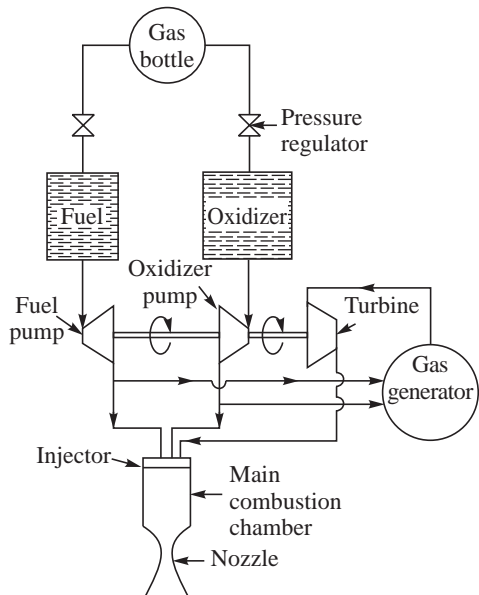


Fig. 6.6 Staged Combustion Cycle

This scheme is similar to the ‘Topping-up’ cycle used in heat engines, wherein heat rejected in one part of the cycle (waste heat) is used to generate work in another part of the cycle. In the thermal power plants using a topping cycle, e.g., a steam turbine power plant, the high pressure steam operates



the turbine and generates power. The left-over exhaust steam is used as a low pressure process steam to heat water or for some other useful purposes. In the case of liquid propellant rockets using the topping cycle, combustion first occurs in the gas generator and the exhaust from the turbine is burnt again in the main combustion chamber. Since the combustion takes place in stages starting in the gas generator and is followed in the main combustion chamber, this mode of operation is also called staged combustion cycle. The gas generator is also referred to as a pre-burner.

The mixture ratio of propellants in the gas generator is either fuel-rich or oxidizer-rich to provide low values of turbine inlet temperatures. The turbine exhaust has to be necessarily at high pressure if it is to be injected into the combustion chamber. Staged combustion cycles generally work at higher pressures and provide higher values of specific impulse. An increased value of chamber pressure was seen to give higher specific impulses in Chapter 4 (Fig. 4.11).

### (c) Expander Cycle

When volatile propellants, such as, liquid oxygen, liquid hydrogen or liquid propane are used, vapour of these substances can be generated while cooling the combustion chamber and nozzle. The vapour could be used to drive the turbine before it is admitted in the combustion chamber for burning. A gas generator would then not be required. This process of driving the turbines with gases obtained during the cooling of the main combustion chamber is illustrated in Fig. 6.7 and is known as expander cycle.

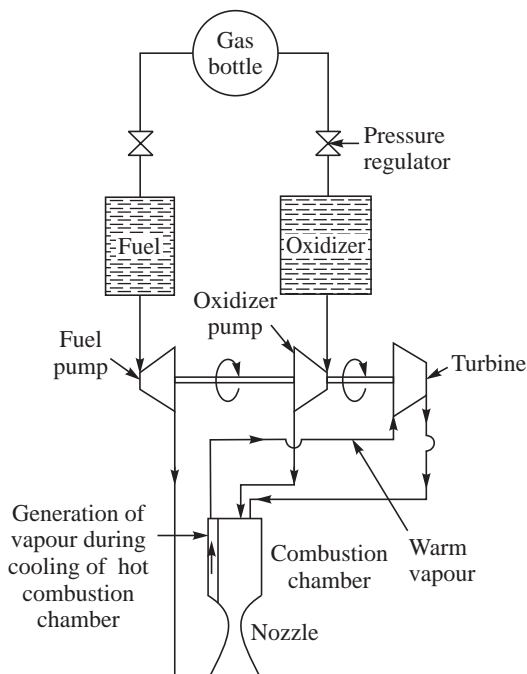


**Fig. 6.7** Expander Cycle

Expander cycle rockets would have limitations in the amount of liquid fuel or oxidizer that can be vaporised using the hot chamber walls. It is used for smaller liquid propellant rockets operating at low chamber pressure for which the demands of power for supplying the propellants are small.



#### (d) Choice of Feed System Cycle

The choice of pressure-fed or pump-fed system and the cycle to be adopted in the pump-fed system significantly influences the efficiency of the liquid propellant rocket. For small thrust rockets operating at low values of chamber pressures, a simple blow-down or regulated gas pressure cold gas system is adequate. As the thrust increases, the quantity of gas required goes up, calling for larger gas bottles and hence increased inert mass of the rocket. In this case, a pump-fed system becomes desirable, especially for larger values of chamber pressures.

Hot gas used for driving the turbine is not available for subsequent combustion and expansion in the main thrust chamber in the gas generator cycle. The efficiency of a liquid propellant rocket using the gas generator cycle would, therefore, be less than the one using the staged combustion and expander cycle. However, for low pressure rockets, for which the quantity of gas required for driving the turbine is insignificant, compared to the total propellant flow rate, the losses are small and the gas generator cycle is still preferred. In Section 6.3 of this chapter, we shall carry out an analysis to determine the conditions for which the gas generator and staged combustion cycle are to be chosen.

#### (e) Miscellaneous Cycles

Variations of the gas generator, staged combustion and expander cycle are possible. Exhaust from the turbine can be admitted in the divergent portion of the nozzle to generate additional thrust in the main thrust chamber instead of exhausting it through an auxiliary nozzle. This practice is known as gas generator with bleed (Fig. 6.8). Split expander cycle can be considered when only a part of the volatile propellant used in the rocket is used to cool the rocket and drive the turbine.

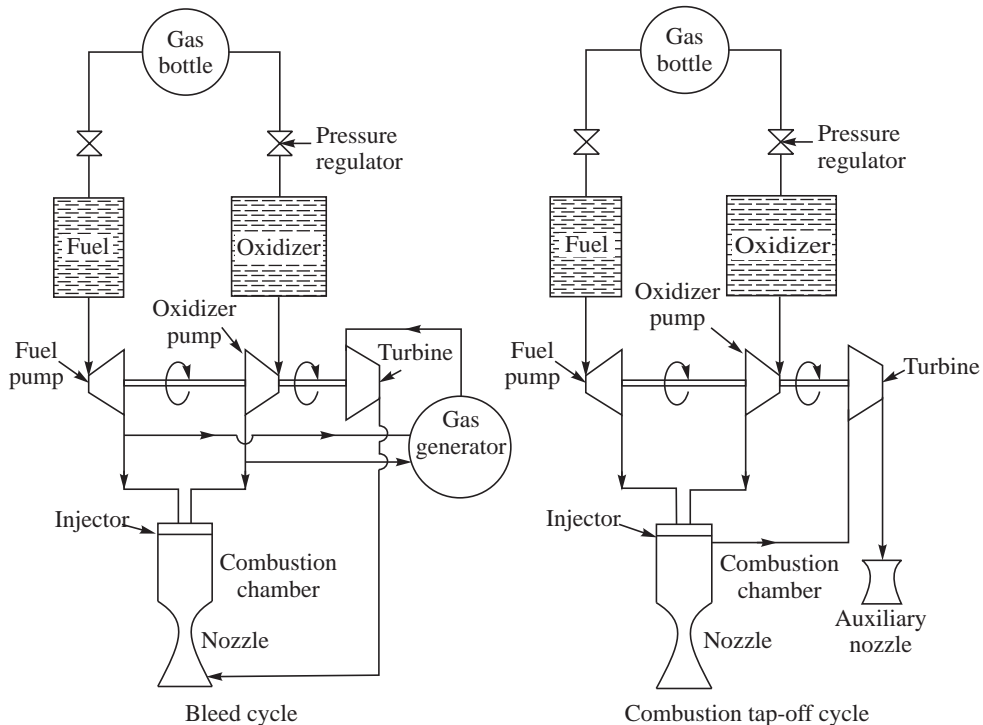


Fig. 6.8 Gas Generator with Bleed and Combustion Tap-off Cycle



Combustion gases could also be taken from the main thrust chamber for driving the turbine. This scheme is spoken of as combustion tap-off cycle and is shown in Fig. 6.8. The use of fuel-rich mixture near the zone of injection in the thrust chamber is preferred. However, it is difficult to have reproducible properties for the fuel-rich gases and the preference would be to bleed the hot gases from the boundary layer in the supersonic portion of the nozzle.



## 6.2 THRUST CHAMBER

The conversion of liquid propellants to the high-velocity jet takes place in the thrust chamber. It consists of injector, combustion chamber and nozzle. We shall deal with these elements in the following:

### 6.2.1 Injector

The injector admits the fuel and oxidizer in proper proportions and at the specified flow rates, for the burning to take place. It breaks up the liquid fuel and liquid oxidizer into fine droplets to facilitate their vaporisation and provides the necessary motion for adequate mixing of the fuel and oxidizer vapours. The energy for the atomization is either derived from pressure or from a high-velocity gas flow and the injectors are accordingly classified as pressure atomizing and gas-assist injectors.

#### 6.2.1.1 Pressure Atomizing Injectors

In the pressure atomizing injectors, liquid fuel and oxidizer are supplied at high pressure to the injector to form high velocity liquid jets or sheets. In some injectors, high-velocity liquid jets are made to impinge on each other and form liquid sheets, which then break up into fine droplets. These are known as impinging injectors and could comprise two jets of liquid impinging on each other (called doublet), three jets of impinging liquid (triplet) or four jets (quadruplet) and so on. Rotational momentum is sometimes provided to the high pressure liquid stream to form a thin hollow conical liquid sheet called swirled annular liquid sheet. The annular sheet breaks up into small droplets. The different configurations are briefly dealt with in the following:

##### (a) Showerhead Injector

Here, a series of slender parallel jets of liquid fuel and liquid oxidizer are formed from a number of holes provided in an injector, very much similar to that of a bath shower. A schematic diagram of a number of orifices for fuel and oxidizer in the injector head is shown in Fig. 6.9. The thin liquid jets of fuel and oxidizer disintegrate into droplets as in a shower.

The configuration of injection holes (orifices) through which the liquid propellant is admitted, significantly influences the atomization. The shape of the entry to the orifice, whether sharp-edged or curved, and the length to diameter ratio of the orifice influences the flow pattern and hence, the velocity profile of the issuing liquid jet. A sharp-edged entry leads to flow separation and formation of a ‘vena contracta’ as shown in

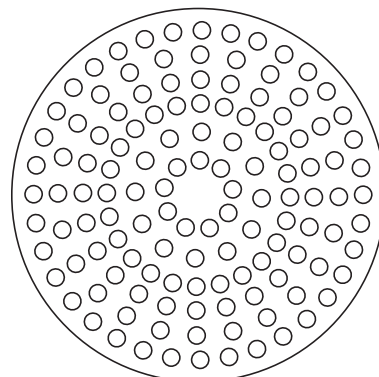


**Fig. 6.9.** Orifices in a Showerhead Injector.



Fig. 6.10. When the length to diameter ratio ( $L/D$ ) of the orifice is small, the separated flow as such, issues out of the orifice. The flow rate is reduced in comparison to full flow through the orifice. In the case of  $L/D$  exceeding about 2, the flow reattaches to the orifice walls [Fig. 6.10(a)]. Given a sufficiently long orifice, full flow is established in the orifice. The velocity profile in the jet leaving the orifice depends on the value of  $L/D$  and conditions of flow at the entry. A near-constant velocity profile along the radius of the jet, such as, in a turbulent flow, gives better atomization.

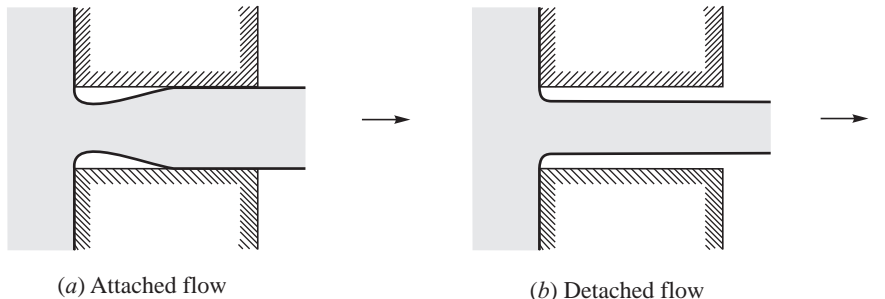


**Fig. 6.10** Attached and Detached Flows in a Sharp-edged Orifice

When the pressure of the liquid in the orifice drops below its vapour pressure, cavities of vapour are formed. The process is known as cavitation. A cavitating flow does not reattach to the orifice walls and the separated flow persists, as shown in Fig. 6.11.

In general, sharp-edged entry orifices having small values of  $L/D$  between 3 and 5 are used. The sharp edges are easier to fabricate reproducibly, compared to shaped entries, especially when a large number of holes are to be made. Small changes in the entry shape lead to significant deviations in the flow. Values of  $L/D$  less than about 2.5 (say between 2 and 3) show both attachment and separation and a flow through the sharp-edged orifice changes during the operation. The change from the attached flow to the separated flow is called ‘hydraulic flip’ and causes unsteady flow and induces disturbances, which are undesirable.

The volumetric flow rate through an orifice can be derived by using Bernoulli's equation. The liquid fuel and oxidizer are assumed to be incompressible. The manifold supplying the liquid fuel and oxidizer to the multiple holes is assumed to have negligible values of velocity. It must be noted that the manifold must ensure near-constant values of pressure for the different orifices which it feeds, very much like the plumbing provided in high-rise apartments to ensure equal pressure of water from a common water tank to the apartments at various floors. Denoting the supply pressure to the orifice as  $p_0$  and the pressure downstream of the orifice as  $p_c$ , we have neglecting the difference in the elevation of the short orifice:

$$\frac{p_0}{\rho} = \frac{p_c}{\rho} + \frac{V^2}{2} \quad \dots(6.1)$$

Here,  $\rho$  is the density of the incompressible liquid and  $V$  is the velocity at the exit of the orifice. The mass flow rate through the orifice is:

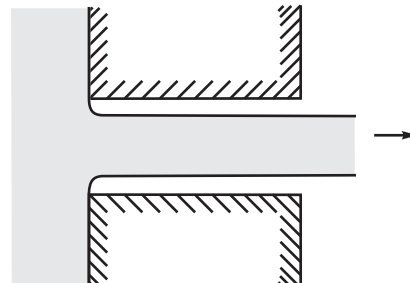


**Fig. 6.11** Cavitated Flow at Higher Flow Velocities in the Orifice



$$\dot{m} = C_d A \sqrt{2(p_0 - p_c) \rho} \quad \dots(6.2)$$

where  $A$  is orifice area.  $C_d$  in the above equation is the discharge coefficient and takes care of the smaller effective area of flow when the flow is separated and for velocity vectors not normal to the cross-sectional area of the orifice ( $A$ ). In the case of long orifices,  $C_d$  takes into account the losses due to friction. The typical value of  $C_d$  for a separated flow is about 0.65, whereas for an attached flow it varies between 0.9 and 0.98.

If we have  $n_{OX}$  number of oxidizer orifices each having an area  $A_{OX}$  in the injector head and if the pressure drop across each of them is  $\Delta p_{OX}$ , the net oxidizer mass flow rate is:

$$\dot{m}_{OX} = n_{OX} C_{d,OX} A_{OX} \sqrt{2\Delta p_{OX} \rho_{OX}} \quad \dots(6.3)$$

$C_{d,OX}$  is the discharge coefficient of the oxidizer orifices and  $\rho_{OX}$  is the density of the liquid oxidizer.  $\Delta p_{OX}$  is the pressure drop across the orifice and is equal to  $(p_0 - p_c)$ . Similarly, the mass flow rate of the fuel through  $n_f$  number of fuel orifices is given by

$$\dot{m}_f = n_f C_{d,f} A_f \sqrt{2\Delta p_f \rho_f} \quad \dots(6.4)$$

The mixture ratio of propellants supplied to the combustion chamber is, therefore, given by

$$MR = \frac{n_{OX} C_{d,OX} A_{OX} \sqrt{\Delta p_{OX} \rho_{OX}}}{n_f C_{d,f} A_f \sqrt{\Delta p_f \rho_f}} \quad \dots(6.5)$$

The mixing of the fuel and oxidizer vapours obtained with the showerhead injector is poor since no differential directions can be provided to the oxidizer and fuel flow. The atomization is also not very efficient.

### (b) Impinging Jet Injectors

Here the liquid jets formed in the sharp-edged orifices are made to impinge one on the other to generate droplets by impact. Doublet, triplet, quadruplet and pentad impinging jets are formed respectively by the impingement of two, three, four or five jets of liquid at a point.

#### b.1. Doublet

In the case of a doublet, the impact of two liquid jets creates a region of high pressure at the point of impact. A thin liquid sheet is formed during the impact and the sheet spreads out from the high pressure zone in a plane at right angles to the plane of the jets. The thin liquid sheet breaks up into small droplets and is called spray fan. Figure 6.12 shows two liquid jets A and B forming a fan

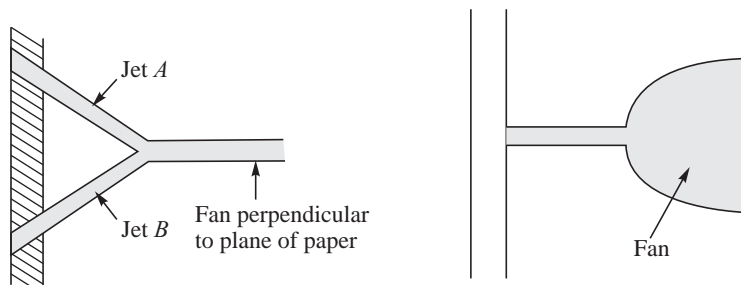


Fig. 6.12 Formation of a Spray Fan from Impingement



perpendicular to the plane of the paper. A photograph of the atomization process in the plane and perpendicular to the plane of impingement of two thin water jets in ambient atmosphere is given in Fig. 6.13 to illustrate the formation of droplets.



Fan in plane of the jets



Fan formed perpendicular to the plane of the jets

**Fig. 6.13** Formation of a Spray Fan in a Doublet

The orientation of the fan, formed by the impinging jets, depends on the impingement angles of the two jets and their respective momentum. Denoting the angle of individual jets with respect to the normal to the injector base as  $\alpha_1$  and  $\alpha_2$  (Fig. 6.14), the resultant angle of the fan  $\beta$  is obtained from the rate of change of momentum (force) along and normal to the injector base to be

$$\tan \beta = \frac{\dot{m}_2 V_2 \sin \alpha_2 - \dot{m}_1 V_1 \sin \alpha_1}{\dot{m}_1 V_1 \cos \alpha_1 + \dot{m}_2 V_2 \cos \alpha_2} \quad \dots(6.6)$$

Here,  $\dot{m}_1$ ,  $\dot{m}_2$ ,  $V_1$  and  $V_2$  are the mass flow rates and velocities of the two jets respectively.

By a judicious choice of the impingement angles  $\alpha_1$  and  $\alpha_2$ , and the momentum of the jets, a distribution of fans and droplets most conducive to good mixing between the fuel and oxidizer is obtained. The thickness of the spray fan depends on the diameter of the two jets, the included impingement angle and the turbulence level in the two jets. By having thin jets impinging at large values of included impingement angles, it is possible to obtain very thin liquid sheet and fine droplets.

The mixing in the spray fan is also influenced by the momentum ratio, the jet diameters and the included impingement angles. Generally, the diameter of the orifices is kept small, with diameters varying between a fraction of millimeter for small thrust rockets to a few mm for large thrust rockets.

When both the impinging jets consist of either the fuel or the oxidizer, the doublet is referred to as like doublet. Fuel fans and oxidizer fans are separately formed and the droplets of fuel and oxidizer evaporate, mix and burn. A number of fans can be formed by improvising doublet elements in the

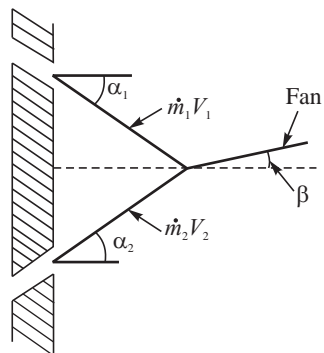


**Fig. 6.14** Orientation of the Fan



injector head as in the shower injector. An injector head with doublet elements is shown in Fig. 6.15. Mixing can be varied by suitably orienting the different fans relative to each other. Secondary impingement of the fans and overlapping of the fans is conducive to good mixing.

If in a doublet element, one of the impinging jets is a fuel while the other is an oxidizer, the doublet is known as an unlike doublet. Chemical reactions take place at the impingement point of the fuel and oxidizer jet when liquid-phase chemical reactions are possible as in hypergolic propellants. The pressure generated from the heat release causes the streams to separate and is known as 'blow-apart'. This creates non-uniformity in the distribution of fuel and oxidizer in the combustion chamber and is not desirable. The phenomenon of blow-apart is present even with non-hypergolic propellants, such as, liquid oxygen and kerosene.

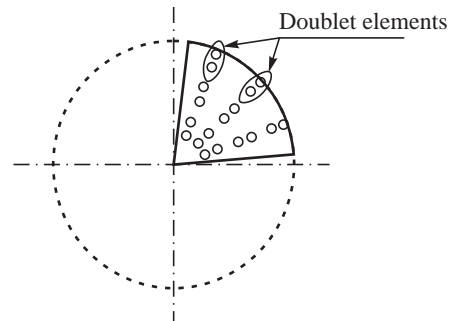
Doublet elements are generally used for small thrust rockets with hypergolic propellants. They are also used for large thrust LO<sub>2</sub>-kerosene rockets. The turbulence and cross winds of the hot gases along the radius of the chamber especially near the injector head, distort the spray fans. The atomization using the doublet is good and the heat from the chemical reactions is released very near the injector head. As a result of the heat release in the vicinity of the injector and the radial winds, the injector tends to heat up and adequate cooling of the injector is required. We shall consider this aspect later in this chapter.

### b.2. Triplet, Quadruplet and Pentad

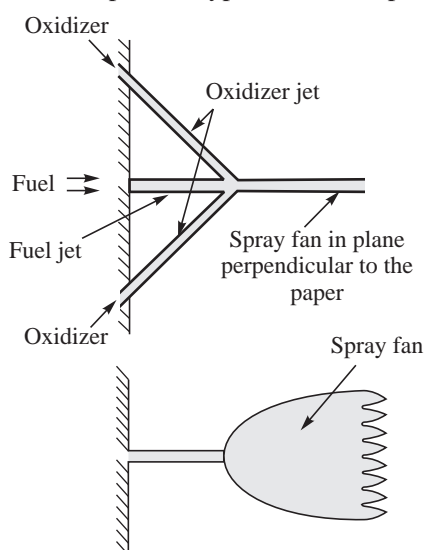
These are used in the unlike mode (injector element consisting oxidizer and fuel jets) and have a distinct advantage over the like and unlike doublet in that the mixing is not influenced by changes in the mixture ratio. They also give a more homogeneous distribution of droplets. A typical unlike triplet injection element is shown in Fig. 6.16. Here, the impingement is between two outer oxidizer jets with an inner fuel jet. It is also possible to have a configuration with the outer jets for fuel and the inner jet for oxidizer.

The net direction of the fan does not change when the mixture ratio is varied. This can be seen from the net force balance of the impinging jets. Unlike triplets are used with hypergolic propellants and have demonstrated extremely good mixing characteristics.

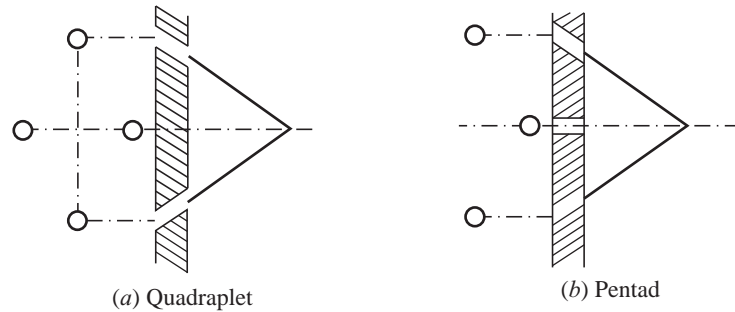
Quadruplet elements are similar to the triplet except that four jets impinge to form a spray fan. A schematic diagram of a quadruplet is shown in Fig. 6.17. The high performance obtained with triplet elements has not been demonstrated in practice with the quadruplets. An unlike pentad consists of five impinging jets, of which four of oxidizer or fuel jets are symmetrically situated about the axial jet of the fuel or oxidizer and is shown in Fig. 6.17.



**Fig. 6.15** Injector Head with a Number of Doublet Elements



**Fig. 6.16** Unlike Triplet

**Fig. 6.17** Quadruplet and Pentad

### b.3 Splash Plate Injector

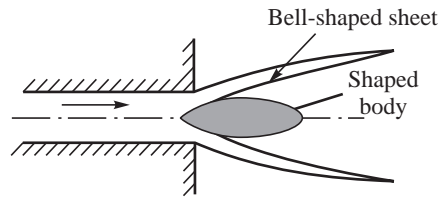
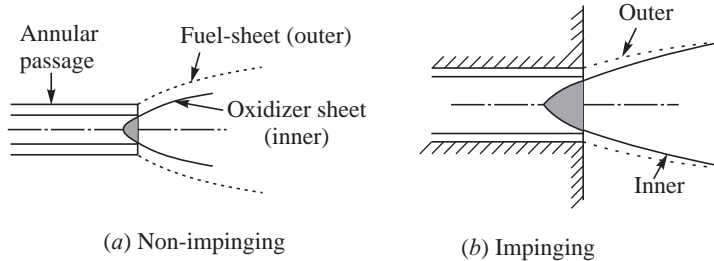
Instead of impinging multiple jets of fuel and oxidizer one on the other, the jets are atomized by impinging them on flat metal surfaces in the combustion chamber. The metal surfaces are known as splash plates.

#### (c) Coaxial Injectors

Here, annular liquid spray fans are formed by injecting the liquid fuel and liquid oxidizer coaxially. Either a shaped body is used to generate a thin annular liquid sheet, or centrifugal forces are used to form annular sheets. Evolution of the annular sheet from impact with a bell-shaped body is shown in Fig. 6.18.

The fuel and oxidizer sheets, formed in coaxial injectors are concentric with the fuel sheet, enclosing the oxidizer sheet or vice versa. We therefore have inner and outer liquid spray fans. Figure 6.19 shows an aerodynamically shaped body—a shaped pintle being symmetrically placed in the path of a high pressure flow in the orifice to form a bell-shaped inner sheet.

The outer sheet is formed using an annular orifice (Fig. 6.19). The inner and outer liquid spray fans either do not impinge, in which case they are known as non-impinging coaxial injection [Fig. 6.19(a)]. When the fans of the oxidizer and fuel impinge on each other, the coaxial injector is called as impinging coaxial injector [Fig. 6.19(b)]. In this case, the divergence of the inner sheet is greater than the outer sheet. Cylindrical and discrete radial sheets have been used as a modification of the impinging co-axial injection. The later has been demonstrated to give extremely good performance over a range of mixture ratios and flow rates.

**Fig. 6.18** Bell-shaped Sheet from Coaxial Injection**Fig. 6.19** Non-impinging and Impinging Coaxial Injection



Instead of using impact to generate the liquid sheet, rotational momentum is generally imparted to the flow of high pressure liquid flow in the injector passage. This is done by incorporating shaped vanes in the form of a helix in the flow passage or else admitting the liquid propellants in the orifice with a tangential velocity component (Fig. 6.20). Ribbons placed along the inner surface of a flow passage in a helical pattern also provide tangential velocity to the flow.

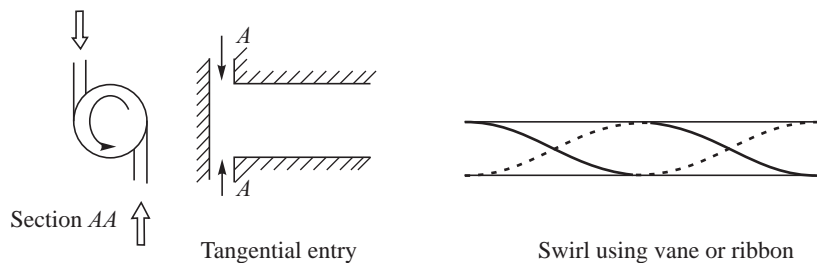


**Fig. 6.20** Generation of Rotational Flow Velocities

The rotational momentum provides centrifugal force in the frame of reference of the rotating liquid and causes an annular film to be formed along the outer radius of the orifice with a gas core in the central region. When this annular liquid film leaves the orifice, the centrifugal forces cause it to spread outward in the shape of a diverging annular bell-shaped liquid sheet. The sheet is known as swirled liquid sheet. As it progresses forward, it becomes thinner and the growth of disturbances on it breaks it up into droplets. The evolution and break up of a swirled liquid sheet in ambient atmosphere is illustrated in Fig. 6.21.

At low values of injection pressure a diverging spray is not formed and a bulbous configuration in the form of a tulip bulb or lotus bud is formed. This is shown in Fig. 6.22. The atomization is not good for such a collapsed shape and is sensitive to disturbances. It is necessary to ensure that a diverging bell-shaped spray is formed through proper choice of injection pressure and rotational velocities.



**Fig. 6.21** Atomization of a Swirled Liquid sheet



Diverging liquid spray



Collapsed liquid sheet

**Fig. 6.22** Collapsed Sheet Instead of the Diverging Spray



The discharge coefficient  $C_d$  of orifices generating the swirled sheets is very much lower than for orifices generating liquid jets. This is due to the formation of a gas core in the central region and the presence of the tangential component of velocities.

A number of coaxial elements are provided in the injector head to meet the required mass flow rate through the injector. The size of elements are kept small, so the characteristic thickness of the sheet is small and finer droplets of the fuel and oxidizer are formed. The elements are assembled in the injector head with suitable fuel and oxidizer supply manifolds. The injector is referred to as multi-element coaxial injector. A sketch of the injector head is given in Fig. 6.23.

The swirled flow is advantageous as it helps in the mixing of the fuel and oxidizer vapours.

#### 6.2.1.2 Gas-assist Injectors

Low temperature boiling fuels, such as liquid hydrogen reach the injector in the gas phase. In applications involving the staged combustion cycle, described in Section 6.1.2, the fuel-rich or oxidizer-rich gaseous products of combustion in the pre-burner, after expansion in the turbine, are admitted into the combustion chamber. The gases, if introduced at high velocities into the injector, could bring about atomization of liquid jets and liquid sheets by shear. These constitute the gas-assist injectors. They make use of high velocity gaseous medium to atomize the liquid fuels or oxidizers. The liquid is introduced as cylindrical jets or thin liquid sheets.

Injectors in which a co-axial flow of gas (or vapour or combustion product) is used for the breakup of the liquid are known as co-axial shear injectors. Figure 6.24 is a schematic diagram of coaxial shear injector used in a cryogenic liquid propellant rocket. Here, the liquid oxygen flows through the central orifice at low velocities, the typical velocities being about 20 to 30 m/s. A jet of liquid oxygen is formed as shown. Gaseous hydrogen is admitted coaxially around the liquid oxygen jet at high velocities of about 200-300 m/s. The gas flow breaks up the liquid oxygen jet into droplets. The central oxygen orifice is recessed in the annular hydrogen orifice, as shown to ensure better interaction of the liquid and gaseous jets.

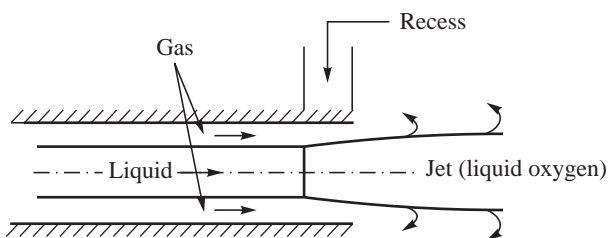


Fig. 6.24 Schematic Diagram of a Shear Coaxial Injector Element

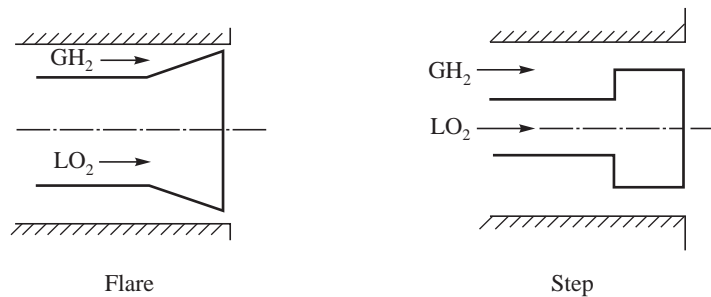
The size of the elements is kept small, as has been discussed earlier, and a number of elements are assembled together in the injector head. Though large values of relative velocities between the



Fig. 6.23 Multi-element Coaxial Injector



liquid and gas are desirable from atomization point of view, the increase of the velocity gradients leads to stretching of the flame and quenching of combustion. The jet velocity of liquid oxygen is sometimes reduced by providing a flare or a step at the exit of the orifice and is shown in Fig. 6.25.



**Fig. 6.25** Flare and Step in the Central  $\text{LO}_2$  Orifice

The use of shear for the gas-assist injector is often combined with the advantage of swirl to provide gas-assist swirl-coaxial injectors. As an example, in the case of liquid oxygen and gaseous hydrogen injection, the central oxygen orifice—sometimes referred to as oxygen post—is provided with rotational momentum to form a swirled liquid oxygen sheet, which meets with the hydrogen gas flow and atomizes the liquid oxygen by shear.

It is also possible to provide rotational motion to the annular gas flow in the swirl injector. The provision of gas swirl would likely change the shear at the interface of the gas-liquid interface and influence the atomization.

#### 6.2.1.3 Manifolds for Injection Elements

The manifold passage in the injector supplies the fuel and oxidizer to the different injection elements, which are housed in the injector head. A large manifold size is desirable for equitable distribution of fuel and oxidizer to all the elements. However, an increase in the volume of the manifold leads to an increase in the time to prime the flow and also causes a gradual decay of flow through the orifices after stopping the flow to the injector.

The volume of propellants in the injector manifold is called ‘dribble’ volume. The propellants from this volume continue the combustion process at reduced pressures and poor efficiencies after the supply of propellants to the injector is terminated. The dribble volume adversely influences the thrust particularly for small rockets, which operate in short pulses.

The flow of propellants in the injector manifolds cools the injector and a smaller manifold volume is conducive to provide the higher velocities for improved cooling. A compromise between efficient distribution (requiring larger area) and cooling (calling for smaller area) is required. Generally, the cross-sectional area of the manifold is kept about four times the flow area of the total group of injection orifices supplied by it. Screens are sometimes placed upstream of the injection orifices in order to achieve pressure drops and obtain uniform distribution of propellants to the different injection orifices.



### 6.2.2 Combustion Chamber and Nozzle

The oxidizer and fuel, metered into the combustion chamber at the required flow rates and at the specified values of mixture ratios by the injector (given by eqs. 6.3, 6.4 and 6.5), are mixed and burned in the combustion chamber. The hot products of combustion are exhausted at high velocities through the nozzle. The chemical reactions continue in the nozzle.

The atomized fuel and oxidizer are distributed spatially in the combustion chamber by the injector and are provided with certain initial velocities. The distribution of the droplet sizes and their velocities depend on the type of injector used. The motion of the droplets, the vaporisation, the mixing of the fuel and oxidizer vapours and subsequent chemical reaction is somewhat complicated. However, the events can be simplified and the progress of combustion can be schematically indicated, as shown in Fig. 6.26.

The droplets formed in the near-injection region move at high velocities in the direction of the spray fan. The flow process here is three-dimensional, with the droplets being formed and their motion being controlled by the injector. The vaporisation of the droplets, the mixing of the vapours and combustion starts here with axial and cross flows viz., a three-dimensional flow field (Fig. 6.26). The vaporisation and combustion progress further in the chamber. At the nozzle throat, the flow is almost one-dimensional and this flow must be established in a stream flow ahead of it, so that we could think in terms of a stream tube flow, essentially one-dimensional, preceding the nozzle flow. The vaporisation and combustion and the expansion can be considered to take place in the stream tubes as a continuation of the three-dimensional zone as is illustrated in Fig. 6.26.

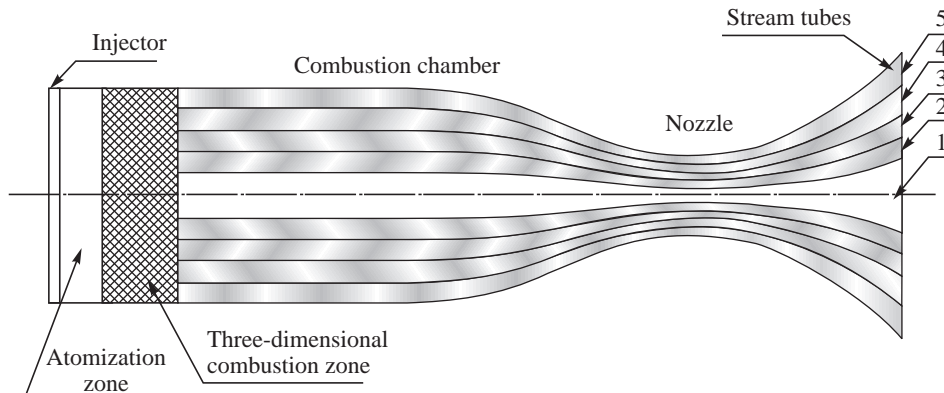


Fig. 6.26 Three-dimensional Zone followed by Stream Tube Flow in Combustion Chamber

#### 6.2.2.1 Progress of Combustion

The relative distribution of the fuel and oxidizer droplets would produce variable mixture ratios in the three-dimensional combustion zone adjacent to the injector (Fig. 6.26). Non-uniform mixture ratios, distinctly different from the overall mixture ratio of the propellants at injection, exist in the transverse direction along the radius of the chamber. These variable mixture ratios feed into the multiple annular stream tubes shown in Fig. 6.26, wherein combustion progresses. The combustion chamber and nozzle are generally not long enough in liquid propellant rockets for turbulence to develop and mixing to take place between the individual stream tubes. Individual stream tubes could be analyzed and the composite performance of all the stream tubes is used for determining the net performance.



### (a) Non-uniform Distribution of Mixture Ratio

Each stream tube, having a unique value of mixture ratio can be considered a miniature rocket of small diameter, expanding to the exit pressure. The stream tube would provide a performance, depending on its mixture ratio. The mixture ratio, it may be recalled, strongly influences the value of  $C^*$  as illustrated in Fig. 6.27 with the maximum  $C^*$  being obtained for a somewhat fuel-rich mixture ratio. If there are  $N$  stream tubes and the fraction of the propellant flow in stream tube  $i$  is  $x_i$  and the characteristic velocity corresponding to its mixture ratio is  $C_i^*$ , we have:

$$\sum_{i=1}^{i=N} x_i = 1 \quad \dots(6.7)$$

and

$$C_{\text{net}}^* = \sum_{i=1}^{N} x_i C_i^* \quad \dots(6.8)$$

Here  $C_{\text{net}}^*$  corresponds to the net mass weighted value of  $C^*$  obtained with all the stream tubes.

The value of  $C^*$  corresponding to the overall mixture ratio say  $(MR)_0$ , which is representative of the fuel and oxidizer injected into the combustion chamber, would be different from the value of  $C^*$  obtained in eq. 6.8. Denoting the  $C^*$  corresponding to the injection conditions as  $C_0^*$  [at mixture ratio  $(MR)_0$ ], the efficiency due to the distribution of mixture ratios is:

$$\eta_{C^*, \text{dist}} = \frac{C_{\text{net}}^*}{C_0^*} = \frac{1}{C_0^*} \sum_{i=1}^{N} x_i C_i^* \quad \dots(6.9)$$

$\eta_{C^*, \text{dist}}$  is the  $C^*$  efficiency due to the distribution of mixture ratios in the combustion chamber. Usually, the overall mixture ratio corresponding to injection is chosen to give maximum value of  $C^*$  and, therefore, the distribution of mixture ratios will lead to  $\eta_{C^*, \text{dist}} < 1$ .

The non-uniformity in mixture ratios is defined by a distribution parameter  $D_R$  given below

$$D_R = 1 - \sum_{i=1}^{N} x_i \frac{|(MR)_0 - (MR)_i|}{(MR)_0} \quad \dots(6.10)$$

where  $N$  refers to the number of stream tubes,  $(MR)_i$  is the mixture ratio in the  $i$ th stream tube,  $(MR)_0$  is the overall mixture ratio and  $x_i$  is the fraction of the mass flow in the  $i$ th stream tube.  $D_R = 1$  refers to uniform distribution. The amount of the departure from unity signifies the non-uniformity.

$\eta_{C^*, \text{dist}}$  from eq. 6.9 can be written as a function of the distribution function  $D_R$  and the overall mixture ratio  $(MR)_0$  as:

$$\eta_{C^*, \text{dist}} = f(D_R, MR_0) \quad \dots(6.11)$$

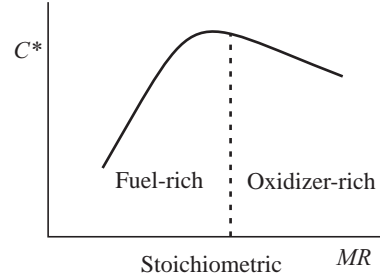


Fig. 6.27 Variation of  $C^*$  with Mixture Ratio

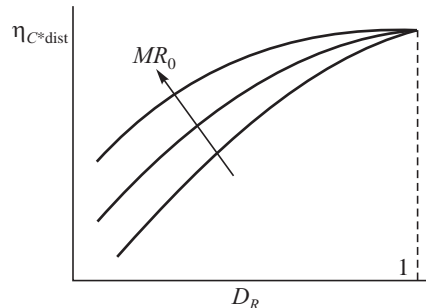


Fig. 6.28 Variation of  $C^*$  Efficiency from Distribution Due to Changes in Distribution Parameter and Overall Mixture Ratio



The  $C^*$  values do not change very rapidly with change of mixture ratios at the higher values of mixture ratios (corresponding to oxidizer-rich conditions) as it does at lower mixture ratios (Fig. 6.27). The influence of the distribution parameter on  $\eta_{C^*,\text{dist}}$  is, therefore, less at the higher overall values of mixture ratios. This is shown in Fig. 6.28. A homogeneous distribution of mixture ratios would provide the maximum  $\eta_{C^*,\text{dist}}$  of one.

#### (b) Incomplete Vaporisation

The size of the droplets formed in the spray and the vaporisation rates of the droplets govern whether the droplets are completely vaporised in the given length of the combustion chamber. Ratio of the vaporised mixture of oxidizer and fuel could also be very different from the overall injected mixture ratio  $(MR)_0$ . As the value of mixture ratio changes,  $C^*$  would also change as indicated in Fig. 6.27. If the injected mixture ratio  $(MR)_0$  is adopted to give the maximum value of  $C^*$ , the value of mixture ratio MR of the vapours being different, could give lower value of  $C^*$ . This is illustrated in Fig. 6.29.

If  $\dot{m}_{\text{OX,vap}}$  and  $\dot{m}_{f,\text{vap}}$  are the rate of formation of the

vapours of the oxidizer and fuel from the droplets and  $\dot{m}_{\text{OX,inj}}$  and  $\dot{m}_{f,\text{inj}}$  are the rates of injection of the oxidizer and fuel into the combustion chamber, the  $C^*$  efficiency due to incompleteness of vaporisation is

$$\eta_{C^*,\text{vap}} = \left\{ \frac{\dot{m}_{\text{OX,vap}} + \dot{m}_{f,\text{vap}}}{\dot{m}_{\text{OX,inj}} + \dot{m}_{f,\text{inj}}} \right\} \left\{ \frac{C^*(MR)_{\text{vap}}}{C^*(MR)_0} \right\} \quad \dots(6.12)$$

Here,  $(MR)_{\text{vap}}$  is the mixture ratio of the vapours formed while  $(MR)_0$  is the mixture ratio corresponding to injection. The first factor on the right side of the above equation represents the fraction of the injected propellants which vaporise. This factor must obviously be less than or equal to unity. The second factor is the ratio of the values of  $C^*$  arising from the changed mixture ratios. This factor could either be less than or greater than unity depending on the choice of mixture ratio adopted for injection and the direction and magnitude of change of mixture ratio from injection to vaporised conditions. The rate of vaporisation  $\dot{m}_{\text{OX,vap}}$  and  $\dot{m}_{f,\text{vap}}$  is determined by considering the motion of droplets in a hot gas with heat and mass transfer effects.

#### (c) Combined Influence of Distribution and Incomplete Vaporisation

The combined influence of distribution of mixture ratios and incomplete vaporisation on  $C^*$  is given by the overall  $C^*$  efficiency:

$$\eta_{C^*} = \eta_{C^*,\text{dist}} \times \eta_{C^*,\text{vap}} \quad \dots(6.13)$$

A homogeneous distribution of mixture ratios and small droplets, which would provide large values of  $\eta_{C^*,\text{dist}}$  and  $\eta_{C^*,\text{vap}}$  respectively, gives maximum  $\eta_{C^*}$ .

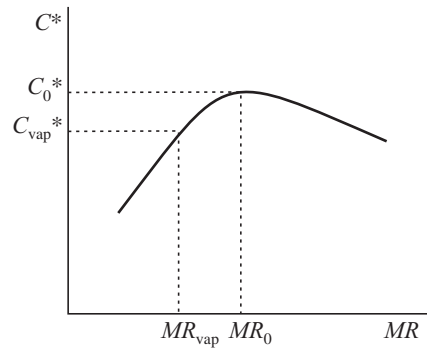


Fig. 6.29 Reduction in  $C^*$  Due to Incomplete Vapourisation



#### (d) Characteristic Length of Thrust Chamber

The length of the combustion chamber needs to be adequate for the vaporisation, mixing and chemical reactions to be completed. A characteristic length  $L^*$  defined as the ratio of the chamber volume to throat area ( $L^* = V_c/A_t$ ), as in the solid propellant rockets, is used to have an indication of the distance and hence, the time available for the processes of evaporation, mixing and chemical reactions to take place.

$L^*$ , in practice varies between 0.8 m and 1.2 m for the different liquid propellant rockets. With smaller values of  $L^*$ , the vaporisation, mixing and reactions do not get completed giving rise to a reduced value of  $\eta_{C^*}$ .

#### (e) Vaporisation, Mixing and Chemical Reactions

A description of these processes can be found in standard textbooks on combustion. For the purpose of understanding the role of vaporisation, mixing and reactions on the  $C^*$  efficiency, we will qualitatively study the processes and identify the controlling parameters.

### Vaporisation of Droplet and Evaporation Constant

Let us consider the time taken for a spherical fuel droplet of diameter  $D$ , having a density  $\rho_l$  to vaporise in the chamber. The mass of the liquid droplet is

$$m = \frac{\rho_l \pi D^3}{6} \quad \dots(6.14)$$

The rate of vapour generated due to evaporation of the droplet is the rate at which its diameter changes with time and is obtained from eq. 6.14 as:

$$\dot{m}_v = \frac{\rho_l \pi D^2}{2} \frac{dD}{dt} \quad \dots(6.15)$$

From eq. 6.15, the change of the square of the diameter with time is

$$\frac{dD^2}{dt} = \frac{4\dot{m}_v}{\rho_l \pi D} = \lambda \quad \dots(6.16)$$

The parameter  $\lambda$  is useful for determining the time required for droplets to vaporise and is dealt with in the following section.

### Evaporation Constant

Consider a fuel droplet to be surrounded by oxidizer vapour. As the fuel droplet vaporises, it gets surrounded by its own vapour (denoted by  $F$ ) in addition to the oxidizer vapour (denoted by  $O$ ) around it. If the droplet radius at any time  $t$  is  $r_s$  as shown in the sketch of a droplet in Fig. 6.30, and considering spherical symmetry, the rate at which the fuel vapour leaves the surface of the drop ( $\dot{m}_F$ ) in terms of the mass flux at the surface  $\dot{m}_F''$  is:

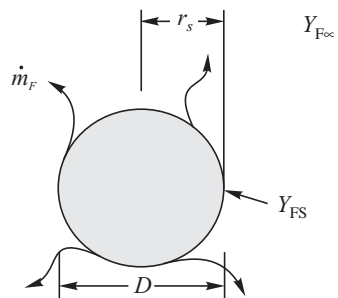


**Fig. 6.30** Vaporization of a Droplet



$$\dot{m}_F = 4\pi r_s^2 \dot{m}_F'' \quad \dots(6.17)$$

Diffusion of fuel vapour takes place in a medium of the fuel vapour and oxidizer vapour. The diffusion takes place by bulk flow and the concentration gradient of the fuel vapour. Denoting the concentration of the fuel vapour by its mass fraction  $Y_F$  ( $Y_F = \frac{m_F}{m_F + m_O}$ ), we can write:

$$\dot{m}_F'' = Y_F(\dot{m}_F'' + \dot{m}_O'') - \rho D_{FO} \frac{dY_F}{dr} \quad \dots(6.18)$$

Here,  $D_{FO}$  is the diffusion coefficient for the fuel vapour in the environment of fuel and oxidizer vapour. It has units of  $\text{m}^2/\text{s}$ . The term  $-\rho D_{FO} \frac{dY_F}{dr}$  gives the mass flux of the fuel vapour due to the concentration gradient  $\frac{dY_F}{dr}$ . The density of the medium comprising fuel and oxidizer vapour is  $\rho$ . Since only the fuel vapour is moving out in an ambience of oxygen, we have  $\dot{m}_O'' = 0$ . Equation 6.18 can, therefore, be rewritten in terms of mass flux at any radius  $r$  as  $\dot{m}_F'' = \frac{\dot{m}_F}{4\pi r^2}$  to give

$$\dot{m}_F = - \frac{4\pi r^2 \rho D_{FO}}{1 - Y_F} \frac{dY_F}{dr} \quad \dots(6.19)$$

If the concentration of fuel vapour at the fuel droplet surface ( $r = r_s$ ) is denoted by  $Y_{FS}$  and if the concentration far from the surface ( $r = \infty$ ) is  $Y_{F\infty}$ , we have on integrating between the surface of radius  $r_s$  and  $\infty$ :

$$\int_{Y_{FS}}^{Y_{F\infty}} - \frac{dY_F}{1 - Y_F} = \int_{r_s}^{\infty} \frac{\dot{m}_F}{4\pi \rho D_{FO}} \frac{dr}{r^2} \quad \dots(6.20)$$

giving:  $\ln \frac{1 - Y_{F\infty}}{1 - Y_{FS}} = \frac{\dot{m}_F}{4\pi \rho D_{FO} r_s}$

The mass flow rate of fuel vapour from the droplet surface is, therefore, given by:

$$\dot{m}_F = 4\pi \rho D_{FO} r_s \ln \frac{1 - Y_{F\infty}}{1 - Y_{FS}} \quad \dots(6.21)$$

The term  $\frac{1 - Y_{F\infty}}{1 - Y_{FS}}$  gives an indication of the transport of the fuel vapour from the surface of the droplet. A transport number  $B$  is defined based on the concentrations at the surface and far from it as:

$$B = \frac{Y_{FS} - Y_{F\infty}}{1 - Y_{FS}} \quad \dots(6.22)$$

Equation 6.21 can be written in terms of the transport number as:

$$\dot{m}_F = 4\pi \rho D_{FO} r_s \ln (1 + B) \quad \dots(6.23)$$

The evaporation parameter  $\lambda$  defined earlier as  $\frac{dD^2}{dt}$  in eq. 6.16 can be obtained by substituting the value of  $\dot{m}_F$  from eq. 6.23 in eq. 6.16 to give



$$\lambda = \frac{8\rho D_{FO}}{\rho_l} \ln(1+B) \quad \dots(6.24)$$

Under steady vaporisation conditions in a particular ambient condition for a given fuel, for which  $\rho$ ,  $\rho_l$ ,  $D_{FO}$  and  $B$  are specified, the value of  $\lambda$  would have a constant value according to eq. 6.24.  $\lambda$  is, therefore, called evaporation constant. The value of  $\lambda$  increases as the temperature of the droplet increases. Droplets of lower molecular mass, in general, have higher values of  $\lambda$  in view of their greater volatility.

The time taken for the evaporation ( $\tau_v$ ) of a droplet of initial diameter  $D_0$  can be determined from eq. 6.16, noting that  $\lambda$  is a constant:

$$\frac{dD^2}{dt} = \lambda$$

as: 
$$\tau_v = \frac{D_0^2}{\lambda} = \frac{D_0^2 \rho l}{8\rho D_{FO} \ln(1+B)} \quad \dots(6.25)$$

The time taken reduces as the droplet diameter decreases. Evaporation of a given droplet at high pressures takes more time. Typical values of vaporisation times are about tens of milliseconds for droplet sizes around 100  $\mu\text{m}$ .

### Burn Rate Constant

When combustion takes place symmetrically around a spherical droplet, a burn rate constant can be determined in a manner very similar to the way, in which the evaporation constant  $\lambda$  was derived. The idealized processes for burning of a droplet are shown in Fig. 6.31. The fuel vapour from the vaporisation of the droplet forms a stoichiometric mixture with the oxidizer vapour at a radius  $r_f$  wherein combustion takes place. The oxidizer vapour stretches to  $\infty$ , where its temperature is  $T_\infty$ . The products of combustion migrate out from the flame at radius  $r_f$ . The droplet gets heated to a steady temperature  $T_f$ . The heat driving the vaporisation of the droplet comes from the enthalpy of the ambient and the heat release in the stoichiometric flame zone, viz.,  $C_p(T_\infty - T_f) + Q_{\text{chem}}$ . If the heat release per unit mass of fuel is  $Q$ , the value of  $Q_{\text{chem}} = Y_F Q = \frac{QY_{0\infty}}{v}$ , where  $Y_{0\infty}$  is the mass fraction of the oxidizer far from the droplet and  $v$  is the stoichiometric mixture ratio. The transport number  $B$ , defined for the vaporisation in terms of the fuel concentration, therefore, gets modified as

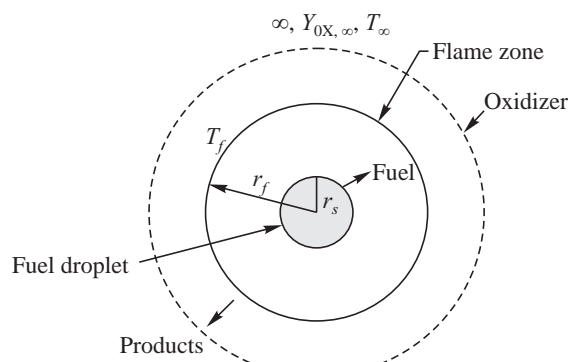


**Fig. 6.31** Combustion of a Droplet



$$B = \frac{C_p(T_\infty - T_l) + QY_{0\infty}/v}{L} \quad \dots(6.26)$$

Here,  $C_p$  is the mean specific heat and  $L$  is the latent heat of vaporisation of the droplet. This expression is used to calculate the burn rate constant in a manner similar to the evaporation constant  $\lambda$  derived from eq. 6.24. The constant depends on the fuel and typically varies between about 1 mm<sup>2</sup>/s for a kerosene droplet and about 21 mm<sup>2</sup>/s for a hydrazine droplet burning in the ambient.

### Transport Number when Droplet is Surrounded by Hot Gas

The transport number when the droplet is surrounded by a hot gas at temperature  $T_\infty$  is seen from eq. 6.26 to be:

$$B = \frac{C_p(T_\infty - T_l)}{L} \quad \dots(6.27)$$

The evaporation constant due to vaporisation of a droplet in a hot surrounding can be determined by substituting the above transport number in eq. 6.24. The vaporisation time of droplets in hot surroundings can be determined once the droplet sizes formed by the injector are known.

### Time for Mixing of Vapours and Chemical Reaction

The time required for mixing the fuel and oxidizer vapours depends on the velocity in the chamber. The time is generally much smaller than the evaporation time of a droplet. The chemical reaction time is also much smaller than the evaporation time, considering the high temperature and high pressure in the combustion chamber. The reaction time also depends on the mixture ratio.

The actual processes of vaporisation, mixing and chemical reactions are more complex, since the ambience of a droplet is not restricted to oxidizer alone. Fuel vapour from the neighbouring droplets and products of combustion are present. The sprays formed by the injector are dense and comprise different droplet sizes moving at different velocities. The simplified scheme, however, helps in understanding and making an overall assessment of the influence of the different parameters on the efficiency of the combustion process.

#### 6.2.3 Cooling of Thrust Chamber

The flow of high temperature gases around 3000 K or higher in the thrust chamber heats up the walls to unacceptable levels. Most of the structural materials either melt or do not retain their strength at these high temperatures. The walls of the thrust chamber are therefore cooled, using one or more of the following methods:

- (i) Film Cooling and Barrier Cooling
- (ii) Regenerative Cooling
- (iii) Ablation Cooling
- (iv) Transpiration Cooling
- (v) Radiation Cooling
- (vi) Heat Sink Cooling



(i) *Film and Barrier Cooling:* A thin film of coolant, comprising either fuel or oxidizer is made to flow along the inner wall surface of the thrust chamber. This is shown in Fig. 6.32. Flow of the coolant along the walls absorbs the heat transferred from the hot combustion gases through sensible and latent heat. The gaseous vapour of the coolant, formed from the vaporisation, is at a temperature lower than the hot core gases and continues to shield the wall from the hot combustion gases.

Instead of using the fuel or oxidizer as coolant, a fuel-rich mixture at the wall would provide a stream of gases at temperatures much below the temperature of combustion products and protect the walls. The provision of low temperature fuel-rich products of combustion is known as barrier cooling. It is readily done by configuring the injector to give the desired fuel-rich streams near the walls. Fuel-rich streams are to be preferred to oxidizer-rich streams since they give lower temperatures than the oxidizer-rich mixtures.

The oxidizer-rich gases also lead to oxidation of the metal walls and need to be avoided.

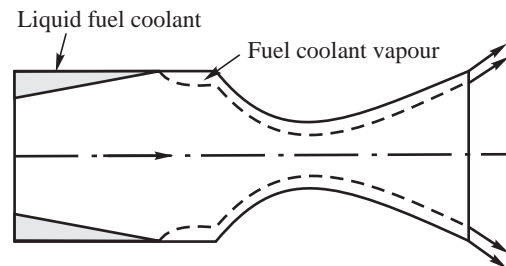


**Fig. 6.32** Film Cooling

(ii) *Regenerative Cooling:* In regenerative cooling, liquid fuel or oxidizer is used to cool the thrust chamber walls externally before being admitted into the thrust chamber through the injector. A schematic diagram of regenerative cooling is given in Fig. 6.33. The heat transferred to the propellant during the cooling process enhances its enthalpy. The heat lost from the chamber is used to heat up the propellants in a manner similar to the regenerative cycle used in power plants, wherein the heat rejected in the exhaust is used for heating the incoming air or water. The cooling is known as regenerative cooling.

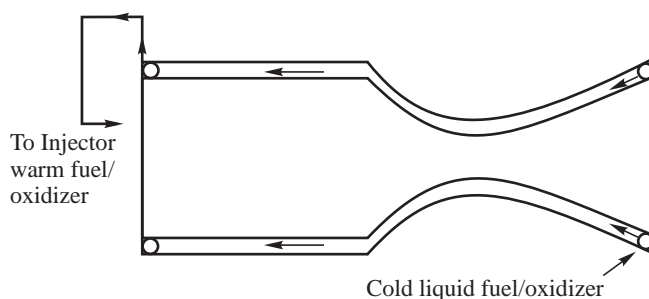


**Fig. 6.33** Regenerative Cooling

Regenerative cooling is widely adopted in liquid propellant rockets. To ensure a homogeneous distribution of temperatures over the surface, regenerative cooling is invariably used in conjunction with film cooling.

(iii) *Ablation Cooling:* Insulating materials, which erode at high temperatures, have been used to protect walls of the thrust chamber from the high temperature products of combustion. The thermal erosion is called ablation. Typical materials that ablate are made of resins (viscous substances like natural gum) such as phenolic resins, epoxies and unsaturated polyesters, which are viscous liquids at room temperature but can be cured by heating to form a tough solid. They are strengthened, using

carbon and silica fibres and are known as composite materials. These resins are thermosetting resins and are distinctly different from thermoplastics, which melt and flow when heated. The thermosetting resins, however, soften at temperatures exceeding a threshold value called the ablation temperature. A high-velocity gas flow at the surface would erode the soft surface. The erosion of the heated soft surface is ablation. The heat incident on the surface is removed through the heat of ablation.

Two types of composite materials comprising carbon phenolic and silica phenolic are used in the high-temperature environment in rockets. Carbon phenolic composites, when heated, initially pyrolyse, release volatiles and then char. They ablate at temperatures exceeding around 1400 K. Similarly, the silica phenolic composites initially form a melt layer of silica. Of these two composite materials, silica phenolic ablative is a better insulator, since silica has lower thermal conductivity than carbon. It can also withstand oxidation unlike the carbon phenolic composite. Improvisation of a liner of a composite ablative insulation over the inner walls of the thrust chamber protects the thrust chamber walls from the high temperature gases. This mode of safeguarding the walls is spoken of as ablative cooling. Figure 6.34 shows a schematic diagram of ablative cooling.

The heat flux at the throat is large compared to that at the chamber and diverging part of the nozzle. The use of ablatives at the nozzle throat leads to significant erosion and change of throat diameter. In order to avoid the erosion, graphite (carbon) and sintered metals are used in the throat region.

(iv) *Transpiration Cooling:* Transpiration cooling is similar to the sweat cooling mechanism, by which the human body regulates its temperature. The liquid propellants are made to ooze through fine pores in a material. This has been used mainly for cooling the injector head in the cryogenic propellant rockets.

(v) *Radiation Cooling:* Instead of protecting the thrust chamber by one of the above methods of cooling, it is possible to employ materials, which can withstand high temperatures. The heated surface can dissipate away the heat by radiation. Materials, such as, columbium and carbon-carbon are used for radiation-cooled liquid propellant rockets.

(vi) *Heat Sink Chamber:* Temperature increase of the thrust chamber would be small during the transient heating, provided that the thermal capacity of the chamber is large and the duration of heating is short. Heavy chambers made of high thermal conductivity materials, such as copper are used for short duration tests that are done on ground to evaluate the performance of the thrust chamber. The chambers are known as heat sink chambers.

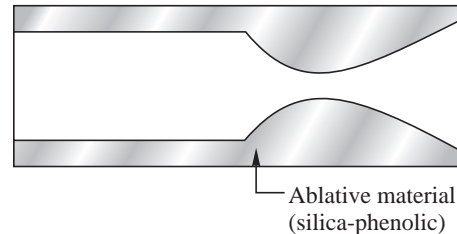


**Fig. 6.34** Ablative Cooling



### 6.3 PERFORMANCE AND CHOICE OF FEED SYSTEM CYCLE

We have seen the different feed systems for liquid propellant rockets and the events taking place in the thrust chamber. In this section, we will illustrate the factors governing the choice of the Gas Generator Cycle (GGC) and the Staged Combustion Cycle (SCC). While the fuel-rich or oxidizer



rich exhaust from the turbine is fed into the main combustion chamber for secondary burning in SCC rockets, the turbine exhaust is expanded through an auxiliary nozzle in GGC rockets. The two cycles are sketched in Fig. 6.35 for a cryogenic liquid propellant rocket using LH<sub>2</sub> and LO<sub>2</sub> as propellants. LH<sub>2</sub> is used for regenerative cooling of the thrust chamber (Fig 6.35). It gets converted to vapour, before being used for combustion in the gas generator and main combustion chamber.

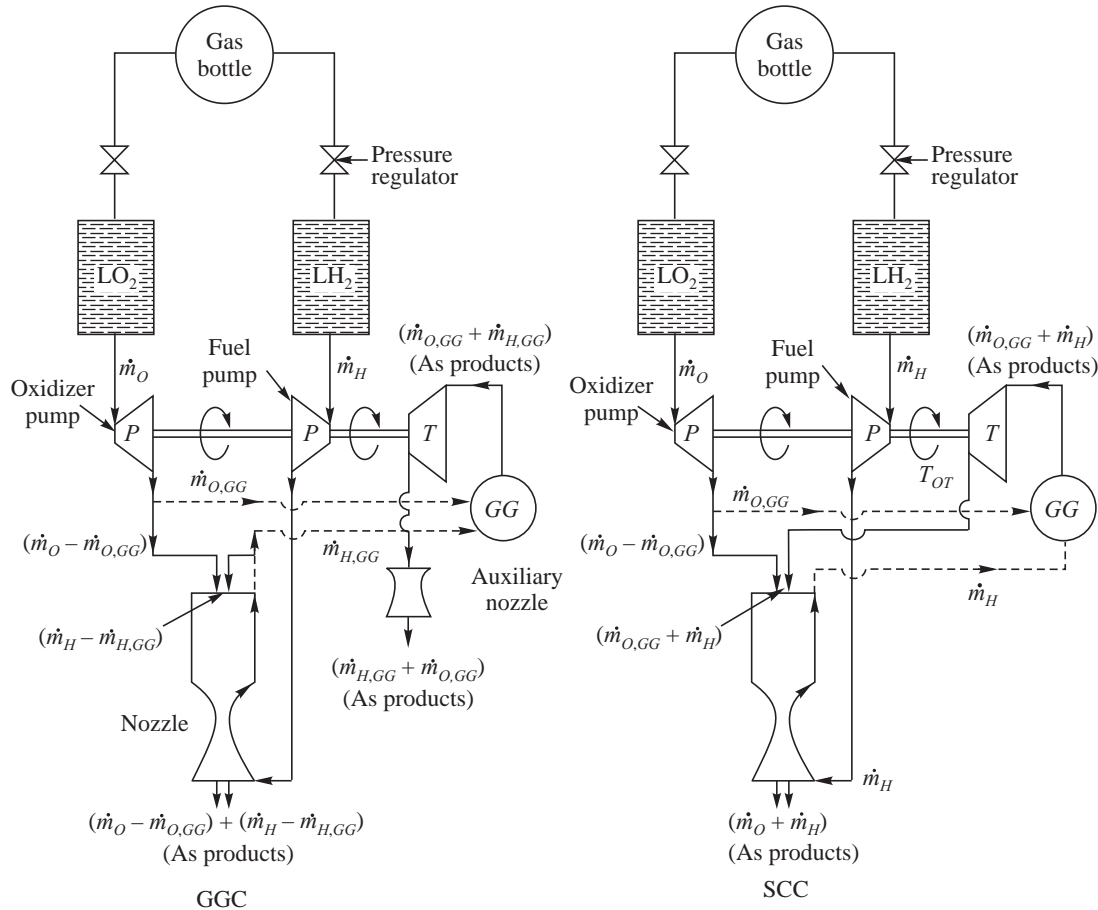


**Fig. 6.35** Flow Processes in GGC and SCC for LH<sub>2</sub>-LO<sub>2</sub> Rocket

The mass flow rate of LH<sub>2</sub> into the gas generator is denoted by  $\dot{m}_{H,GG}$ , while the LO<sub>2</sub> flow rate is  $\dot{m}_{O,GG}$  as shown for GGC in Fig. 6.35. If  $T_{GG}$  is the temperature of the fuel-rich gases generated in the gas generator and  $T_{OT}$  is the temperature of the exhaust gases leaving the turbine after expansion in the turbine, the rate of work done by the turbine is:

$$\dot{W}_T = (\dot{m}_{O,GG} + \dot{m}_{H,GG}) C_p (T_{GG} - T_{OT}) \eta_T \quad \dots(6.28)$$

$\eta_T$  is the turbine efficiency and  $C_p$  is the average specific heat of the gases. The entry temperature to the turbine is  $T_{GG}$ . The above work is supplied to the liquid propellant pumps, where the pressure of the propellant is increased. If the increase of pressure across the pump is  $\Delta p$  for both the fuel and



oxidizer pumps and the combined volumetric flow rate of LH<sub>2</sub> and LO<sub>2</sub> into the pump is  $\dot{Q}$ , the rate of work done on the pump is

$$\dot{W}_P = \frac{\dot{Q}\Delta p}{\eta_P} \quad \dots(6.29)$$

$\eta_P$  is the mechanical efficiency of the pump. Equating the rate of work done on the pump with the turbine work and denoting the composite turbo-pump efficiency  $\eta = \eta_T \times \eta_P$ , gives

$$(\dot{m}_{O,GG} + \dot{m}_{H,GG})C_p(T_{GG} - T_{OT})\eta = \dot{Q}\Delta p \quad \dots(6.30)$$

The above equation can be expressed as a function of mixture ratios in the gas generator and the main thrust chamber. The mixture ratio of the liquid propellant rocket is the ratio of the total mass flow rate of oxidizer to the fuel. This is denoted by  $R$ . If the net mass flow rate from hydrogen and oxygen tank is  $\dot{m}_O$  and  $\dot{m}_H$  as shown in Fig. 6.35,  $R$  is given by:

$$R = \frac{\dot{m}_O}{\dot{m}_H} \quad \dots(6.31)$$

The total propellant flow is  $\dot{m}_H + \dot{m}_O$ . The volumetric flow rate  $\dot{Q}$  through the pump is:

$$\dot{Q} = \frac{\dot{m}_H}{\rho_H} + \frac{\dot{m}_O}{\rho_O} \quad \dots(6.32)$$

Here,  $\rho_H$  denotes the density of LH<sub>2</sub> while  $\rho_O$  is the density of LO<sub>2</sub>. The mixture ratio in the gas generator  $R_{GG}$  is:

$$R_{GG} = \frac{\dot{m}_{O,GG}}{\dot{m}_{H,GG}} \quad \dots(6.33)$$

and the mass flow rate of propellants through it is  $\dot{m}_{O,GG} + \dot{m}_{H,GG}$ .

The mixture ratio of the main combustion chamber  $R_{MC}$  corresponds to the flow of LO<sub>2</sub> and LH<sub>2</sub> into it and for GGC is given by:

$$R_{MC} = \frac{\dot{m}_O - \dot{m}_{O,GG}}{\dot{m}_H - \dot{m}_{H,GG}} \quad \dots(6.34)$$

In the case of SCC:

$$R_{MC} = R \quad \dots(6.35)$$

Substituting the value of  $\dot{Q}$  from eq. 6.32 in eq. 6.30, we get:

$$(\dot{m}_{O,GG} + \dot{m}_{H,GG}) C_p(T_{GG} - T_{OT})\eta = \left( \frac{\dot{m}_H}{\rho_H} + \frac{\dot{m}_O}{\rho_O} \right) \Delta p \quad \dots(6.36)$$

On simplifying, we get:

$$\frac{\dot{m}_H}{\dot{m}_{H,GG}} \left( \frac{1}{\rho_H} + \frac{R}{\rho_O} \right) \Delta p = \eta C_p T_{GG} \left( 1 + R_{GG} \right) \left( 1 - \frac{T_{OT}}{T_{GG}} \right) \quad \dots(6.37)$$



Assuming isentropic expansion in the turbine through a pressure ratio  $r_p$ , the temperature ratio  $\frac{T_{OT}}{T_{GG}}$  is given by:

$$\frac{T_{OT}}{T_{GG}} = \frac{1}{(r_p)^{\gamma-1/\gamma}} \quad \dots(6.38)$$

where  $\gamma$  is the specific heat ratio of the gases in the isentropic expansion process of the gas generator products in the turbine.

Denoting the fraction of the propellant flow rate through the gas generator,  $(\dot{m}_{H,GG} + \dot{m}_{O,GG})$  to the total propellant flow rate  $(\dot{m}_H + \dot{m}_O)$  as  $f$ , we have:

$$f = \frac{\dot{m}_{H,GG} + \dot{m}_{O,GG}}{\dot{m}_H + \dot{m}_O} = \frac{1 + R_{GG}}{1 + R} \frac{\dot{m}_{H,GG}}{\dot{m}_H} \quad \dots(6.39)$$

On substituting in eq. 6.37, we get:

$$f = \frac{\dot{m}_{H,GG} + \dot{m}_{O,GG}}{\dot{m}_H + \dot{m}_O} = \frac{1}{1 + R} \left\{ \frac{\left( \frac{1}{\rho_H} + \frac{R}{\rho_O} \right) \Delta p}{\eta C_p T_{GG} \left( 1 - \frac{1}{r_p^{[\gamma-1/\gamma]}} \right)} \right\} \quad \dots(6.40)$$

The gas generator mixture ratio  $R_{GG}$  is kept significantly fuel-rich such that the turbine entry temperature ( $T_{GG}$ ) is less than about 900 K. This corresponds to  $R_{GG}$  of about 0.6 for LH<sub>2</sub> and LO<sub>2</sub> mixture.

Figure 6.36 shows the variation of the fraction  $f$  as a function of the overall mixture ratio  $R$  for different values of pressure rise across the pump as determined from eq. 6.40. The pressure in the tank is taken as 0.3 MPa. The values of  $\eta$  and  $r_p$  are assumed to be 0.6 and 15 respectively. The pressure-rise across the pumps would be proportional to the chamber pressure. The pressure ratio of a turbine used in a gas generator cycle will be higher than the one used in a staged combustion cycle as the gases in the former are expanded to lower pressures.

It is seen from Fig. 6.36 that fraction  $f$  of the propellant flow through the gas generator increases with pressure-rise across the pump  $\Delta p$ , and hence, would increase with the increase of chamber pressure. This is to be anticipated since pump work increases in order to supply the propellants at the higher pressures. It is also seen that fraction  $f$  is higher at lower values of the overall mixture ratio  $R$ . At the lower mixture ratios, net volume of the propellant is larger in view of the smaller density of LH<sub>2</sub> which leads to an increase of the pump work.

This is also seen from eq. 6.40. If  $\rho_H$  were to be equal to  $\rho_O$  in eq. 6.40,  $f$  will not depend on the mixture ratio  $R$ . However,  $\rho_H$  is generally much lower than  $\rho_O$  and therefore  $f$  decreases with increasing values of  $R$ .

Once the fraction of propellants flowing through the gas generator  $f$  is known, the specific impulse of the liquid propellant rocket ( $I_{sp}$ ) can be calculated. The net  $I_{sp}$  is the mass weighted average of  $I_{sp}$  from the main thrust chamber and the turbine exhaust. Denoting the  $I_{sp}$  corresponding to the main chamber as  $I_{spMC}$  and the specific impulse from the expansion of the turbine exhaust through the auxiliary nozzle as  $I_{spT}$ , the net  $I_{sp}$  is given by:

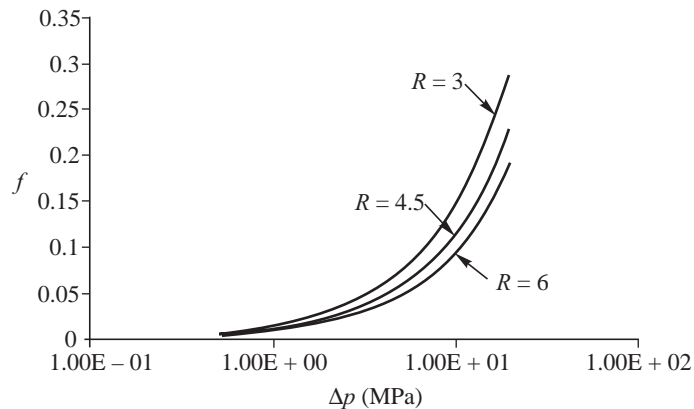


Fig. 6.36 Variation of Propellant Flow Fraction through the Gas Generator

$$I_{sp} = (1 - f) I_{spMC} + f I_{spT} \quad \dots(6.41)$$

In order to determine the value of  $I_{spMC}$  in the main thrust chamber, the mixture ratio must be known. The value of mixture ratio will, however, vary with the fraction  $f$  through the gas generator. Using eq. 6.34, we have:

$$R_{MC} = \frac{\dot{m}_O}{\dot{m}_H} \frac{1 - \frac{\dot{m}_{O,GG}}{\dot{m}_O}}{1 - \frac{\dot{m}_{H,GG}}{\dot{m}_H}} \quad \dots(6.42)$$

Rewriting eq. 6.39 as:

$$\frac{\dot{m}_{H,GG}}{\dot{m}_H} = \frac{1 + R}{1 + R_{GG}} f \quad \dots(6.43)$$

and using eqs. 6.31 and 6.33 for  $R$  and  $R_{GG}$ , we have:

$$\frac{\dot{m}_{O,GG}}{\dot{m}_O} = \frac{R_{GG}}{R} \frac{\dot{m}_{H,GG}}{\dot{m}_H} = \frac{R_{GG}}{R} \frac{1 + R}{1 + R_{GG}} f \quad \dots(6.44)$$

Substituting values of  $\frac{\dot{m}_{H,GG}}{\dot{m}_H}$  and  $\frac{\dot{m}_{O,GG}}{\dot{m}_O}$  from eqs. 6.43 and 6.44 in eq. 6.42, the value of  $R_{MC}$

is obtained as follows:

$$R_{MC} = R \frac{\frac{1 - \frac{R_{GG}}{R} \frac{1 + R}{1 + R_{GG}} f}{1 - \frac{1 + R}{1 + R_{GG}} f}}{1 - \frac{1 + R}{1 + R_{GG}} f} \quad \dots(6.45)$$

The above equation implies that for  $f = 0$ , i.e. there is no gas generator as in the expander cycle,  $R_{MC} = R$ . As  $f$  increases, the denominator in eq. 6.45 decreases more than the numerator causing the value of  $R_{MC}$  to be higher than  $R$ . This is because  $R_{GG} \ll R$ . This trend for the thrust chamber



mixture ratio to increase to values higher than the overall mixture ratio is shown in Fig. 6.37 for values of  $R$  of 3, 4 and 5 for  $R_{GG} = 0.6$ .

The main combustion chamber should operate at mixture ratios, which give maximum  $I_{sp}$ . The overall mixture ratio  $R$  of the gas generator cycle would, therefore, be lower than this optimum ratio.

Using the values of  $I_{spMC}$  determined at different chamber pressures for a nozzle expanding to an ambient pressure of 0.1 MPa (sea-level), the effective  $I_{sp}$  for a GGC is determined. The fraction of the total propellant flow through the gas generator for the different chamber pressures and overall mixture ratio  $R$  is first determined. This is shown in Fig. 6.38 for chamber pressures of 2, 10 and 20 MPa and mixture ratios between 3 and 7. The data used is the same as for Fig. 6.36. The higher chamber pressure of 20 MPa is seen to demand a very large fraction of the total propellant flow. Increase of the mixture ratio in the main combustion chamber  $R_{MC}$  with the increase of the chamber pressure and the overall mixture ratio  $R$  is given in Fig. 6.39. The chamber mixture ratio  $R_{MC}$  increases to extremely large ratios as the chamber pressure is increased.

Using the  $I_{sp}$  of the main combustion chamber obtained at different values of  $R_{MC}$  and chamber pressures and considering expansion in the nozzle to sea level, the net  $I_{sp}$  for a GGC is determined and plotted in Fig. 6.40. Here, the specific impulse from turbine exhaust  $I_{spT}$  is taken as 2000 Ns/kg. The  $I_{sp}$  for SCC is the value obtained in the main chamber ( $I_{spMC}$ ). The values of  $I_{sp}$  for GGC and SCC are compared in Fig. 6.40 at different chamber pressures for different values of mixture ratio  $R$ . It is seen that at small values of chamber pressures of 2 MPa, there is hardly any difference between  $I_{sp}$  in a GGC and SCC. As the chamber pressure increases, the difference in  $I_{sp}$  becomes greater and for a chamber pressure exceeding about 10 MPa, the SCC gives much higher values of  $I_{sp}$  than GGC. The mixture ratio at which  $I_{sp}$  is a maximum for the SCC is also higher than for GGC. This is an advantage since the density of liquid oxygen is very much higher

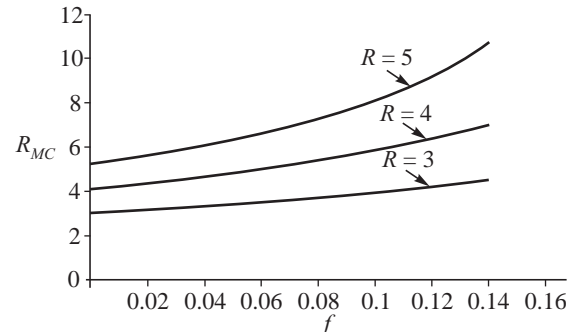


Fig. 6.37 Variation of  $R_{MC}$  with Fraction  $f$

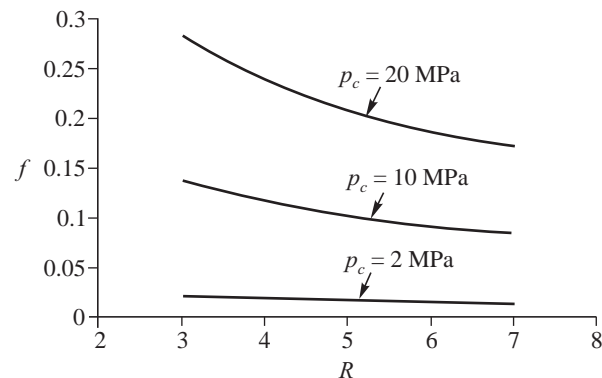


Fig. 6.38 Fraction of Flow through Gas Generator at Different Chamber Pressures and Mixture Ratios

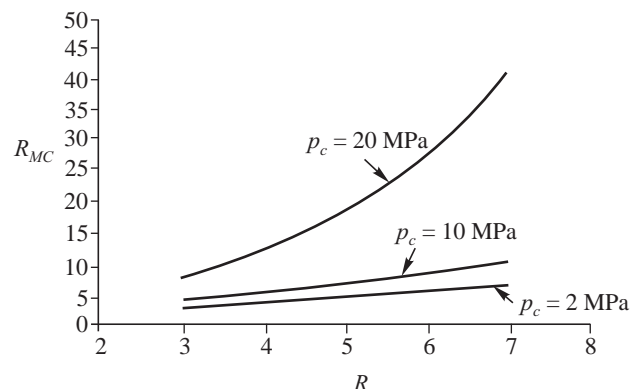


Fig. 6.39 Variation of Mixture Ratio of the Main Combustion Chamber with Change of the Overall Mixture Ratio and Chamber Pressure



than liquid hydrogen, resulting in much smaller total volume of the propellant tanks. The decrease in the performance of GGC at higher chamber pressures is due to the larger fraction of flow through the gas generator, which is not effectively burned and exhausted.

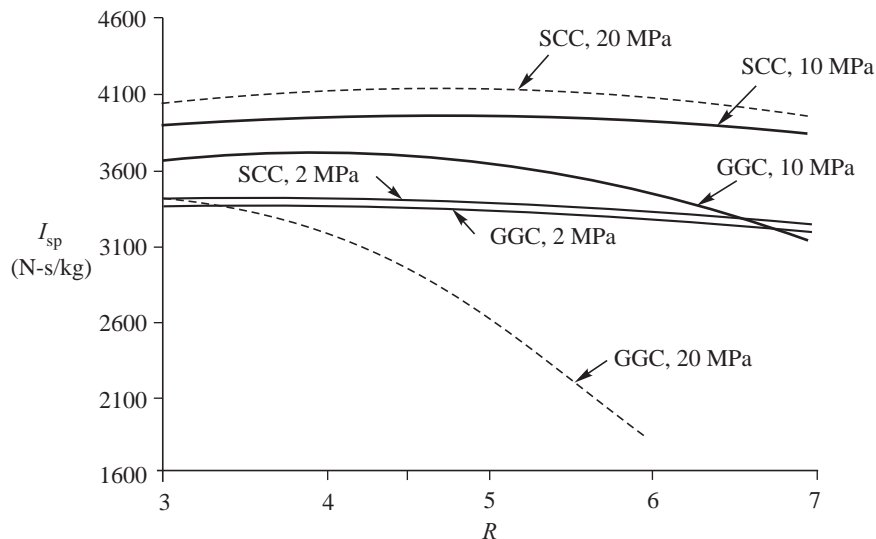


Fig. 6.40  $I_{sp}$  of GGC and SCC at different Chamber Pressures

The performance of the different feed cycles can be determined using a similar analysis. In general, the staged combustion cycle and the expander cycle rockets give much higher performance than the gas generator cycle engines especially at higher values of chamber pressure. SCC is preferable for high-chamber pressure rockets, while GGC is adequate for low-chamber pressure rockets.



## 6.4 TURBO-PUMPS

The choice of pumps and turbines depends on the propellant used, feed system cycle, combustion chamber pressure and thrust generated by the rocket. Centrifugal, axial and a combination of these pumps are used. For high pressure applications, such as in SCC, multiple stages of compression is necessary. Axial pumps have more number of stages than the centrifugal pumps. In the case of turbines, the expansion is similarly done in a number of stages, especially in GGC, for which the gases are expanded to lower pressures in the auxiliary nozzle. The turbines are generally of the impulse type.

The rotational speeds of the turbines and pumps are high, typical values being about 20,000 to 50,000 and more, since the dimensions and mass of the turbo-pump need to be as small as possible.

For more details about turbines and pumps, the reader should consult standard textbooks in turbo-machines. However, in order to have an overall assessment of the choice of parameters, we note that the parameters of interest in the choice of the turbo-pumps are the flow rate through the pump ( $\dot{Q}$ ,  $\text{m}^3/\text{s}$ ), the pressure increase ( $\Delta p$ , Pa), the density of the propellant ( $\rho$ ,  $\text{kg}/\text{m}^3$ ), the rotational speed of the pump ( $N$ , rps) and the characteristic diameter of the pump viz., diameter of pump impeller ( $d_i$ , m). The increase of pressure  $\Delta p$  can be expressed as a function of the above parameters:



$$\Delta p = f(N, \dot{Q}, \rho, d_i) \quad \dots(6.46)$$

The rotational speed  $N$  rps can be expressed in radians per second  $\omega = 2\pi N$ . The five parameters in eq. 6.46 are  $\Delta p$ ,  $\omega$ ,  $\dot{Q}$ ,  $\rho$ , and  $d_i$ . Denoting the units of mass, length and time as M, L and T, the units of  $\Delta p$  is  $M/(LT^2)$ ,  $\omega$  is  $1/T$ ,  $\dot{Q}$  is  $L^3/T$ ,  $\rho$  is  $M/L^3$  and  $d_i$  is L. Of these five parameters, two have independent dimensions. The number of non-dimensional groups that can be formed as per the Buckingham's  $\Pi$  theorem is, therefore, three. From dimensional considerations, the three non-

dimensional parameters are  $\frac{\Delta p}{\rho \omega^2 d_i^2}$ ,  $\frac{\omega \sqrt{\dot{Q}}}{(\Delta p/\rho)^{3/4}}$  and  $\frac{d_i (\Delta p/\rho)^{1/4}}{\dot{Q}^{1/2}}$ . They represent the non-dimensional

pressure rise, non-dimensional speed and non-dimensional impeller diameter respectively. The functional form between the non-dimensional parameters can be represented as:

$$\frac{\Delta p}{\rho \omega^2 d_i^2} = f \left( \frac{\omega \sqrt{\dot{Q}}}{(\Delta p/\rho)^{3/4}}, \frac{d_i (\Delta p/\rho)^{1/4}}{\dot{Q}^{1/2}} \right) \quad \dots(6.47)$$

The non-dimensional speed  $\frac{\omega \sqrt{\dot{Q}}}{(\Delta p/\rho)^{3/4}}$  is called specific speed ( $N_s$ ) while the non-dimensional

impeller diameter  $\frac{d_i (\Delta p/\rho)^{1/4}}{\dot{Q}^{1/2}}$  is called specific diameter ( $d_s$ ). The operation of a given configuration

of a pump for a given propellant is restricted to a narrow range of parameters  $N_s$  and  $d_s$ , making the non-dimensional parameters useful.

Cavitation is a major cause of worry for the pumps. The supply pressure of propellants from the tanks is restricted to about 2 to 5 atmospheres, since higher tank pressures call for large thicknesses of the tank walls, thus making them unacceptably heavy with higher structural mass. With smaller values of supply pressure to the pumps, high velocities induced in the pump would result in very low values of static pressure. Cavitation would occur when the pressure falls below the vapour pressure of the propellant. Cavitation is avoided by placing an inducer pump (also called booster pump) prior to the main pump to increase pressure and prevent cavitation. A parameter Net Positive Suction Head (NPSH) is defined which is the difference between the stagnation pressure of the propellant at the entry to the pump ( $p_0$ ) and the vapour pressure of the propellant ( $p_v$ ). This is given by:

$$NPSH = \frac{p_0 - p_v}{\rho g} \quad \dots(6.48)$$

NPSH is required to be high enough to prevent cavitation. It can be increased by increasing the tank pressure. However, this is difficult considering the increase of the structural mass. Sub-cooling of the propellant is done to reduce its vapour pressure. Inducers are also used.

A specific speed parameter corresponding to the above suction pressure is defined as suction specific speed  $N_{ss}$ :



$$N_{ss} = \frac{\omega\sqrt{\dot{Q}}}{(NPSH g)^{3/4}} \quad \dots(6.49)$$

Here, the net positive suction head NPSH replaces the head developed by the pump  $\Delta p/\rho$  in the expression for specific speed  $N_s$ . The non-dimensional parameters are useful for determining the choice of speeds and overall dimensions of the pump.



## 6.5 GAS REQUIREMENTS FOR DRAINING OF PROPELLANTS FROM STORAGE TANKS

The propellant tanks are pressurized using high pressure inert gas contained in gas bottles. The pressurized propellants are supplied either directly to the combustion chamber in pressure-fed rockets or else to the pump in the pump-fed rockets. The mass of gas required to be stored in the gas bottles at a given pressure for expelling a known mass of the propellants in the tank is determined in this section.

A schematic diagram of the pressurization and expulsion of propellants from the tanks is shown in Fig. 6.41. The high-pressure of the stored gas in the bottle is reduced by a regulator to a lower value, corresponding to the supply pressure of the propellants. This pressure acts on the propellant surface in the tanks and expels the propellant from it at a constant regulated value of pressure.

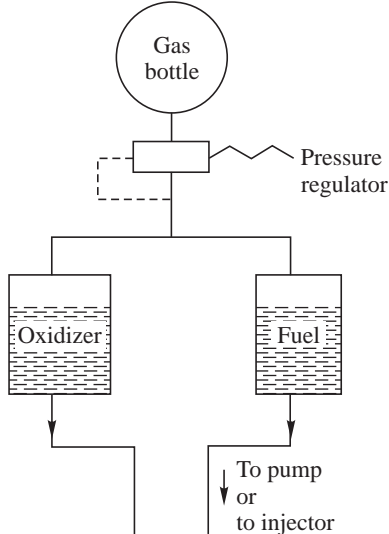


Fig. 6.41 Expulsion of Propellants using Gas Pressurization

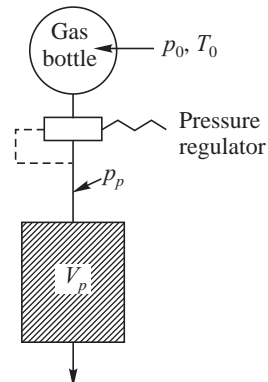


Fig. 6.42 Simplified Scheme of Expulsion

In order to simplify the analysis, we consider the expulsion of a single propellant at pressure  $p_p$  from a tank of volume  $V_p$ , completely filled with propellants. The pressurizing gas is contained in a high-pressure gas bottle at pressure  $p_0$  (Fig. 6.42). The pressure regulator maintains a constant value of pressure  $p_p$  in the propellant tank.



The expansion of gases in the bottle during depletion of the propellant causes fall in temperature. Let the initial value of the gas temperature be  $T_0$ . Once all the propellants are expelled from the tank, the gas expands to the additional volume  $V_p$  at pressure  $p_p$ . If final temperature of the remaining gas in the gas bottle is  $T_r$ , we have assuming an adiabatic process:

$$\text{Change of internal energy of gas} (-dU) = \text{Work done} (dW) \quad \dots(6.50)$$

The initial internal energy of the high pressure gas is  $m_0 C_v T_0$ , while the final internal energy of the expanded gas is given by  $m_r C_v T_r + m_p C_v T_p$ . Here,  $m_p$  is the mass of gas occupying volume  $V_p$  at pressure  $p_p$  and temperature  $T_p$ .  $m_r$  is the residual mass of the gas in the gas bottle at pressure  $p_r$  and temperature  $T_r$ . The gas is assumed to be perfect.

Substituting the values in eq. 6.50, we get:

$$-(m_r C_v T_r + m_p C_v T_p) - m_0 C_v T_0 = p_p V_p \quad \dots(6.51)$$

The value of  $m_0$  from the above equation, considering that  $m_p = \frac{p_p V_p}{R T_p}$  and  $m_r = \frac{p_r V_0}{R T_r}$  is:

$$m_0 = \frac{p_p V_p}{C_v T_0} + \frac{p_p V_p}{R T_0} + \frac{p_r V_0}{R T_0} \quad \dots(6.52)$$

Here,  $V_0$  is the volume of the gas bottle and  $R$  is the specific gas constant. Further, with  $C_v = \frac{R}{\gamma - 1}$ , where  $\gamma$  is the specific heat ratio, we have:

$$m_0 = \frac{p_p V_p}{R T_0} + (\gamma - 1) \frac{p_p V_p}{R T_0} + \frac{p_r V_0}{R T_0}$$

The volume  $V_0 = m_0 \frac{R T_0}{p_0}$ . Substituting in the above equation and simplifying gives:

$$m_0 = \frac{p_p V_p}{R T_0} \left\{ \frac{\gamma}{1 - p_r/p_0} \right\} \quad \dots(6.53)$$

The term  $p_p V_p / R T_0$  represents the mass of gas required if the propellants were expelled, using isothermal expansion of high pressure gas. The term in brackets represents the change due to the adiabatic expansion process. In practice, there would be heat transfer and the process is not adiabatic.

A gas stored at high pressure  $p_0$ , reduced molecular mass  $\mathfrak{M}$  (which gives higher value of the specific gas constant  $R = R_0/\mathfrak{M}$ ) and high temperature  $T_0$  is advantageous, as smaller mass of gas would be required. The use of low molecular mass gas, such as helium at high pressures of about 20 to 25 MPa is adopted in practice. Hot gas pressurization is also seen to be advantageous.



## 6.6 DRAINING UNDER MICROGRAVITY CONDITIONS

Zero  $g$  conditions would be experienced by components in a satellite under free fall conditions, such as during orbit (See Chapter 1). If a liquid propellant rocket is to be used for orbit maneuvers of a satellite, liquid propellants in the tanks in the satellite would be in a state of weightlessness and float



randomly in the propellant tank instead of settling at the bottom of the tank due to gravity. A stream of pressurized gas used for pressurizing the liquid could squirt out instead of the propellant. It becomes essential to device different methods to ensure that liquid propellant is always available at the drain port of the tank to be supplied to the thrust chamber.

#### (a) Positive Expulsion System

The simplest procedure is to separate the propellant from the pressuring gas and contain the propellant in a flexible material such as a bladder, bellow or diaphragm. The outside portion of the flexible container is pressurized to force out the propellants into the thrust chamber. This method of containing the propellant is known as positive expulsion system, illustrated in Fig. 6.43.

The flexible containment, such as the bellow or bladder, cannot expel all the propellants enclosed in it. Expulsion efficiency, which denotes the fraction of propellants expelled to the propellants stored in the flexible containment, is typically between 0.95 and 0.97 for the positive expulsion system. The value of expulsion efficiency depends on the configuration of the containment and materials of construction used. Flexible materials usually used are Teflon and EPDM rubber (Ethylene Propylene Diene Monomer). These are not only flexible, but also do not react with fuel hydrazine used for spacecraft rockets. We shall deal with the influence of small quantities of dissolved materials of the containment in poisoning the catalysts in mono-propellant rockets in the next chapter.

#### (b) Surface Tension Expulsion System

The expulsion efficiencies can be increased to over 99% by using the surface tension principle. When a liquid is in contact with a surface, the force of adhesion at the surface smears the liquid over the surface, whereas the force of cohesion within the liquid causes the formation of a bead of liquid and prevents the surface from getting wet. Surfaces that get wet by a given liquid, viz., the force of adhesion over the surface is more than the force of cohesion are said to be hydrophilic.

A mesh or screen, which can be made wet by the propellant, if placed at the drain port, would ensure supply of liquid propellant to the thrust chamber. The size of the pores in the screens/mesh can be configured in such a way that the pressure from surface tension will prevent the gas from permeating the screen. If the mean radius of the pores in the screen is  $R$ , the surface tension pressure  $\Delta p_{ST}$  in  $P_a$  is:

$$\Delta p_{ST} = \frac{2\sigma}{R} \quad \dots(6.54)$$

where  $\sigma$  is the surface tension coefficient in N/m and  $R$  is in m. This must be greater than the gas pressure.

Once the propellant reaches the thrust chamber and thrust is generated, the local acceleration resulting from the thrust, would settle the propellants to the bottom of the tank. The wetting does not depend on the state of weightlessness since it depends only on the surface forces, i.e. surface tension. Surface tension has units of surface energy per unit area or equivalently force per unit length.

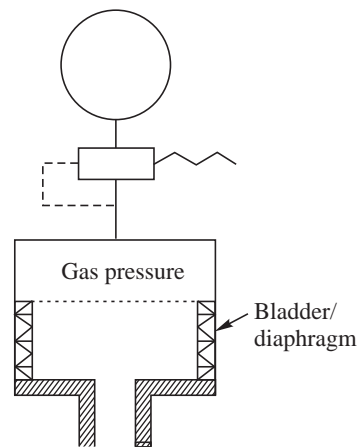
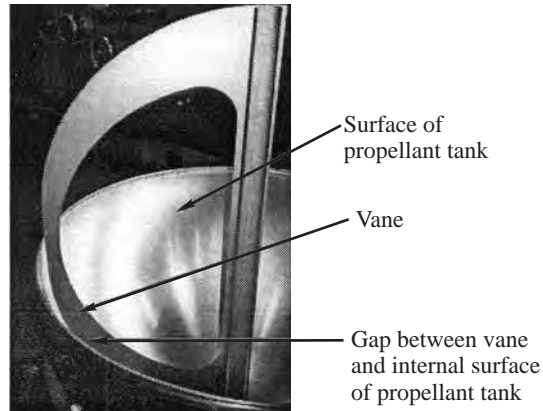


Fig. 6.43 Positive Expulsion



Vanес are provided at the inner surface of the tank along the length of the tank in the recent configurations of the surface tension feed system. Any liquid floating freely under zero g conditions, as and when it comes in contact with the vanes, is captured by the gap between the vane and the propellant tank surface and is brought to the draining port of the tank by surface tension forces. This is done by proper shaping of the vane surfaces and the gap between the vane and the wall of the tank. A schematic diagram of the vane and the bottom surface of a tank is shown in Fig. 6.44. The vanes are known as propellant acquisition vanes.



**Fig. 6.44** Illustration of a Vane Close to the Hemispherical Bottom Part of Propellant Tank



## 6.7 COMPLEXITY OF LIQUID PROPELLANT ROCKETS AND SIMULATION

The liquid propellant rocket is seen to consist of several elements like gas bottles, propellant tanks, propellant feed lines, pumps, turbines, gas generator, injector, combustion chamber and nozzle. In addition, pressure regulators, vent and relief valves are required to maintain constant gas pressures in tanks and ensure safe limits of operating pressures. Flow control valves and start valves to initiate the flow of propellants from the tanks to the gas generator and thrust chamber and shut down valves to terminate the operation of the rocket are also necessary.

The mixture ratios and mass flow rates of propellants in the thrust chamber and gas generator have to be maintained within certain range of values so that the temperatures and pressures do not exceed the safe operating limits and the required performance and thrust is achieved. Suitable control systems or controllers for mixture ratios and flow rates are therefore incorporated in the liquid propellant rocket. The combination of these different components and systems makes the liquid propellant rocket complex as compared to a solid propellant rocket.

When the propellants used are non-hypergolic, an igniter is required for both the gas generator and the thrust chamber as in the solid propellant rocket. A slug of hypergolic chemicals is also used to initiate the combustion.

The principles governing the operation, as seen in this chapter, are simple even though the liquid propellant rocket comprises a large number of components and a suitable control system. The principles are based on the basics of fluid flow, combustion, thermodynamics and gas dynamics. It is, therefore, possible to develop a theoretical procedure to simulate the total liquid propellant rocket and predict its performance under steady state, transient and dynamic conditions. For the steady state performance, also known as static performance, the pressure drops and gains in the different components and the steady combustion processes in the gas generator and thrust chamber (in presence of the control) are considered. In the case of transient performance, the inertial terms for flow and torque and power for the turbo-pumps are additionally included. The equations for flow and combustion processes are



solved together with the force, torque and energy balance conditions for determining the performance. The dynamic performance, in addition to the inertial terms, takes into account the delayed feedback in the interactions of the different elements, the processes and the control. This could lead to the instability of a liquid propellant rocket. Instability in liquid propellant rockets is considered in Chapter 9 on combustion instability. In the following, a simple procedure of computing the performance is illustrated by putting together some of the elements like feed-lines, pumps, turbine, gas generator and thrust chamber.

The pressure drop across a fluid line consists of the resistive drop due to friction and the drop due to acceleration. It can be represented as:

$$\Delta p_{\text{Loss}} = R \dot{m}^2 + L \frac{d\dot{m}}{dt} \quad \dots(6.55)$$

Here  $\dot{m}$  is the mass flow rate through the feed line,  $R$  is the frictional resistance term and  $L$  is the reactance (resistance due to mass flow rate variations).

The pressure rise in a pump depends on the type of the pump and the number of stages, blade configurations, their dimensions, the pump speed  $N$  and the mass flow rate through the pump  $\dot{m}$ . The following equation represents the pressure increase across a pump:

$$\Delta p_{\text{Pump}} = K_1 N^2 + K_2 N \dot{m} + K_3 \dot{m}^2 \quad \dots(6.56)$$

Here  $K_1$ ,  $K_2$  and  $K_3$  are constants for a given pump and their values can be determined from cold flow experiments of the pump. The pump speed  $N$  is usually specified in revolutions per minute (RPM). The form of eq. 6.56 is derivable from theory of pumps.

The turbine, being generally of the impulse type, converts the pressure head to velocity by expansion. The pressure drop across a turbine is:

$$\Delta p_{\text{Turbine}} = R_T \dot{m}^2 \quad \dots(6.57)$$

Here  $R_T$  is the resistive constant for the turbine.

The torque imbalance between the turbine and the pump goes to accelerate the rotational parts of the pump and turbine. The difference between the torque developed by the turbine  $\tau_{\text{Turbine}}$  and the torque used by the pumps  $\Sigma \tau_{\text{Pump}}$  is  $(\tau_{\text{Turbine}} - \Sigma \tau_{\text{Pump}})$ . Denoting the moment of inertia of the moving parts of the turbine and pumps as  $I$  and the angular speed in radians per second as  $\omega$ , we get:

$$I \frac{d\omega}{dt} = \tau_{\text{Turbine}} - \Sigma \tau_{\text{Pump}} \quad \dots(6.58)$$

The torque of the turbine  $\tau_{\text{Turbine}}$  and of the pumps  $\Sigma \tau_{\text{Pump}}$  is determined from their power divided by their angular speed. Considering the pump speed and turbine speed to be the same, we have:

$$\tau_{\text{Turbine}} = \eta_T \dot{m} C_p T_{\text{in}} [1 - (p_{\text{out}}/p_{\text{in}})^{(\gamma-1)/\gamma}] / \omega \quad \dots(6.59)$$

$$\tau_{\text{Pump}} = \Delta p_{\text{pump}} \frac{\dot{Q}}{(\omega \eta_P)} \quad \dots(6.60)$$

In the above expressions,  $\eta_T$  and  $\eta_P$  are the efficiencies of the turbine and pumps respectively.  $T_{\text{in}}$  is the temperature at the inlet to the turbine which is same as the temperature of the products of combustion in the gas generator. This temperature is known from the mixture ratio of the gas generator



which is available from the calculated mass flow rates of the fuel and oxidizer into it.  $\dot{Q}$  is the volume flow rate through the pumps.

The rates of mass accumulation in the gas generator and the thrust chamber are used to determine rates of pressure rise in them as:

$$\frac{V_{GG}}{RT_{GG}} \frac{dp}{dt} = \dot{m}_{in,GG} - \dot{m}_{out,GG} \quad \dots(6.61)$$

$$\frac{V_C}{RT_C} \frac{dp}{dt} = \dot{m}_{in,C} - \dot{m}_{out,C} \quad \dots(6.62)$$

The mass flow rates  $\dot{m}_{out}$  for both the gas generator and the thrust chamber are given in the form:

$$\dot{m}_{out} = \frac{pA_t}{C^*} \quad \dots(6.63)$$

Values of  $C^*$  of the gas generator and the thrust chamber are known from their mixture ratio of operation. The above set of equations (eqs. 6.55 to 6.63) is put together for the different feed-lines and components of the liquid propellant rocket including the control system which regulates either the flow or the mixture ratio. The mass flow rates, the mixture ratios, turbo-pump speeds and the other parameters such as variations in pressure at the different locations are determined.



## 6.8 TRENDS IN THE DEVELOPMENT OF LIQUID PROPELLANT ROCKETS

Liquid propellant rockets are versatile, have higher values of specific impulse compared to solid propellant rockets and are controllable unlike the solid propellant rockets. They are, therefore, widely used for the boosters and upper stages of satellite launch vehicles. Liquid propellant rockets using higher density propellants such as fuel kerosene with liquid oxygen and unsymmetrical dimethyl hydrazine (UDMH) with oxidizer di-nitrogen tetroxide ( $N_2O_4$ ) are applied for the booster stages. This is because the density specific impulse is more relevant for the initial booster stage (see Chapter 2). The Saturn rocket, which was used in the Apollo missions for landing men on moon, used five F-1 rockets burning kerosene (called Rocket Propellant RP-1) and liquid oxygen for the booster stage. The thrust was about 6.8 MN and the gas generator cycle was used. The chamber pressure was 7 MPa. Similarly, the Atlas Centaur launch vehicle used kerosene-liquid oxygen propellant rockets in the gas generator cycle with a thrust of about 1.8 MN for the booster. The RD-170 rocket, which has about the highest thrust level among all available liquid propellant rockets, has a staged combustion cycle with kerosene and liquid oxygen for the propellants. RD-170 is used for the booster of Zenith launch vehicle. It has a thrust of about 7.25 MN. The chamber pressure of the rocket is very high at 24.5 MPa.

The UDMH- $N_2O_4$  propellant rockets are used for the booster in earlier versions of the Ariane launch vehicles and in the Proton launch vehicle. The launch vehicle GSLV, shown in Fig. 2.14 also used this propellant combination in the gas generator cycle. Considering the higher cost of the hydrazine based fuels and its carcinogenic nature calling for special efforts in handling and production, the



propellant combination kerosene-liquid oxygen is advantageous. However, the development of the kerosene-liquid oxygen rockets has been plagued with combustion instability problems. The aspect of combustion instability in rockets is discussed in Chapter 9.

High performance cryogenic rockets employing liquid hydrogen and liquid oxygen have been applied for the different stages of launch vehicles in the gas generator, staged combustion and the expander cycles. The Space Shuttle Main Engine (SSME shown in Fig. 2.13) uses a staged combustion cycle at a chamber pressure of 19 MPa and a thrust of 1.8 MN. The Ariane-V launch vehicle uses for its booster the cryogenic propellants hydrogen and oxygen in a gas generator cycle along with solid propellant rockets. The cryogenic propellant rocket, known as Vulcain, operates at a chamber pressure of 11 MPa with a thrust of about 1 MN. Expander cycle rockets are used in upper stages such as the cryogenic rocket RL-10 in the Titan and Delta launch vehicles. RL-10 has a thrust of about 70 kN and a chamber pressure of between 3 and 4 MPa. An expander cycle cryogenic rocket Vinci having a chamber pressure of about 6 MPa and a thrust of about 180 kN is being developed to replace the HM-7 liquid hydrogen-liquid oxygen rocket which employs a gas generator cycle at a chamber pressure of about 3.5 MPa and a thrust of 65 kN for the upper stages of Ariane-V launch vehicle. A notable feature of Vinci is the very high pump speed of approximately 90,000 revolutions per minute.

Details of cryogenic propellant rockets are given in Annexure C.

The Earth storable and space storable propellant combinations comprising mono-methyl hydrazine (MMH) and  $N_2O_4$  are widely used in a pressure-fed mode for upper stages of launch vehicles, orbital transfer applications and for satellite propulsion and control. While the thrust levels for the Attitude and Orbit Control System (AOCS) for satellites is typically between about 10 and 20 N, the thrust of the upper stage rockets varies between a fraction of a kN and few tens of kN. The low thrust satellite rockets operate in small pulses generating small impulses as against long durations of operation of rockets in the upper stages including orbit transfer applications.

Liquid propellant rockets have come a long way from the early A-4 rockets developed for the V-2 missile using alcohol for fuel and liquid oxygen for the oxidizer. Efforts continue towards improvement of injectors which was seen in this chapter to control the atomization and distribution of fuel and oxidizer and their mixing in the combustion chambers. The developments of high temperature resistant materials such as refractory materials, ceramics and carbon-carbon have helped to decrease the losses associated with cooling of the combustion chamber and the nozzle. Improvements in performance of high speed turbo-pumps and control systems are an integral part of the development of the large thrust liquid propellant rockets. The quest for reducing the number of stages in a satellite launch vehicle has prompted work on adapted and extendable nozzles dealt with in Chapter 3 and investigation of multiple propellants for a liquid propellant rocket. We shall consider the tripropellant rockets in Chapter 11.

## SOLVED EXAMPLES

**Example 6.1** Profiling mixture ratio across injector face:

The mixture ratio in a thrust chamber is distributed by the injector in three concentric zones around a core. The propellants used are  $LH_2$  for fuel and  $LO_2$  for oxidizer. The core has a stoichiometric mixture ratio. The three annular zones surrounding the core have successively decreasing values of mixture ratios of 7, 5 and 3 so that the gases in contact with the wall are fuel-rich. The mixture ratio of 3 at the wall provides barrier cooling. If the mass flow rates of the propellants comprising  $LH_2$  and



$\text{LO}_2$  are the same in each of the four zones starting with the core and moving towards the wall, find the overall mixture ratio and the specific impulse of the rocket?

The specific impulse corresponding to the mixture ratios of 8, 7, 5 and 3 corresponding to the chamber pressure and expansion ratio of the rocket are 4500, 4540, 4500 and 4300 Ns/kg respectively.

**Solution:** We assume the net performance to be a composite of the performance in the four stream tubes of mixture ratios of 8, 7, 5 and 3. If the total propellant flow in the chamber is  $\dot{m}_p$ , the propellant flow rate in each of the four zones of stratified mixture ratios is  $\dot{m}_p/4$ , since the combined mass flow rates of  $\text{LH}_2$  and  $\text{LO}_2$  in all the four stream-tubes are the same. Denoting the core by subscript '1' and the surrounding annular zones by subscripts 2, 3, and 4 respectively, we have for the core:

$$\frac{\dot{m}_{O,1}}{\dot{m}_{H,1}} = 8 \quad \text{giving} \quad \frac{\dot{m}_{O,1} + \dot{m}_{H,1}}{\dot{m}_{H,1}} = 9$$

$$\text{This gives: } \dot{m}_{H,1} = \frac{\dot{m}_p}{4} \frac{1}{9} \quad \text{and} \quad \dot{m}_{O,1} = \frac{\dot{m}_p}{4} \frac{8}{9}$$

Similarly, for the surrounding annular zones 2, 3, and 4 which have mixture ratios of 7, 5 and 3 respectively, we have:

$$\dot{m}_{H,2} = \frac{\dot{m}_p}{4} \frac{1}{8} \quad \text{and} \quad \dot{m}_{O,2} = \frac{\dot{m}_p}{4} \frac{7}{8}$$

$$\dot{m}_{H,3} = \frac{\dot{m}_p}{4} \frac{1}{6} \quad \text{and} \quad \dot{m}_{O,3} = \frac{\dot{m}_p}{4} \frac{5}{6}$$

$$\dot{m}_{H,4} = \frac{\dot{m}_p}{4} \frac{1}{4} \quad \text{and} \quad \dot{m}_{O,4} = \frac{\dot{m}_p}{4} \frac{3}{4}$$

$$\text{The total hydrogen flow is: } \dot{m}_H = \frac{\dot{m}_p}{4} \left( \frac{1}{9} + \frac{1}{8} + \frac{1}{6} + \frac{1}{4} \right)$$

$$\text{The total oxygen flow rate is: } \dot{m}_O = \frac{\dot{m}_p}{4} \left( \frac{8}{9} + \frac{7}{8} + \frac{5}{6} + \frac{3}{4} \right)$$

$$\text{The overall mixture ratio } R_{m,0} \text{ is: } \frac{\dot{m}_O}{\dot{m}_H} = \frac{\frac{8}{9} + \frac{7}{8} + \frac{5}{6} + \frac{3}{4}}{\frac{1}{9} + \frac{1}{8} + \frac{1}{6} + \frac{1}{4}} = \frac{241}{47} = 5.13$$

The net specific impulse is:

$$\begin{aligned} I_{sp} &= 0.25 \times 4500 + 0.25 \times 4540 + 0.25 \times 4500 + 0.25 \times 4300 \\ &= 4460 \text{ Ns/kg} \end{aligned}$$

The value of  $I_{sp}$  interpolated at the overall mixture ratio of 5.13 from the values given at mixture ratios of 5, 7 and 8 is 4503 Ns/kg. This is much higher than the value of 4460 Ns/kg obtained, because of the distribution in mixture ratio. The efficiency associated with the distribution is  $4460/4503 = 0.99$ .

Profiling of mixture ratio leads to a loss in specific impulse, though it is required to bring down the temperature of the combustion chamber walls and nozzle.

**Example 6.2** Gas generator cycle:

A high pressure pump-fed liquid propellant rocket based on the gas generator cycle has a vacuum thrust of 735 kN and a burn duration of 180 sec. The propellants used are N<sub>2</sub>O<sub>4</sub> and UDMH. The specific impulse is 2950 N-s/kg. The mixture ratio is 1.87.

The pressure in the thrust chamber of the rocket is 6 MPa and the propellant supply pressure to the chamber is 7 MPa. N<sub>2</sub>O<sub>4</sub> is stored in the propellant tank at a pressure of 0.4 MPa and UDMH is stored at 0.32 MPa. The densities of N<sub>2</sub>O<sub>4</sub> and UDMH are 1400 kg/m<sup>3</sup> and 790 kg/m<sup>3</sup> respectively, at the temperatures used in the rocket. Determine:

- (i) Power required to drive N<sub>2</sub>O<sub>4</sub> and UDMH pump.
- (ii) If the efficiency of the pump is 60% and the turbine efficiency is 80%, determine the mass flow rate through the turbine. The gas generator pressure and temperature can be assumed to be 3.5 MPa and 670 K respectively. The exit pressure of the turbine can be taken as 0.18 MPa. You can assume the molecular mass of the combustion products from the gas generator to be 20.19 kg/kmole, the specific heat of the gas at constant pressure as 1.9 kJ/kg K and the specific heat ratio of the gases  $\gamma$  as 1.264.
- (iii) What would be the speed in RPM of the N<sub>2</sub>O<sub>4</sub> pump and the UDMH pump if the specific speed ( $N_s$ ) of the N<sub>2</sub>O<sub>4</sub> pump is 0.66 and of the UDMH pump is 0.44.
- (iv) If the oxidizer N<sub>2</sub>O<sub>4</sub> is stored in the propellant tanks at a temperature of 25°C, and the vapour pressure of N<sub>2</sub>O<sub>4</sub> at 25°C is 0.12 MPa, determine the net positive suction head of the N<sub>2</sub>O<sub>4</sub> pump and its suction specific speed?

**Solution:** A simplified schematic diagram is illustrated in Fig. 6.45.

- (i) Power required for driving the pumps:

$$\text{Thrust} \quad F = 735 \text{ kN}$$

$$\text{Specific Impulse} \quad I_{sp} = 2950 \text{ Ns/kg}$$

$$\text{Propellant mass flow rate} \quad \dot{m}_p = \frac{F}{I_{sp}} = \frac{735000}{2950} = 249.15 \text{ kg/s}$$

$$\text{Mixture ratio} \quad R = 1.87$$

$$\text{Fuel (UDMH) mass flow rate} \quad \dot{m}_U = \frac{\dot{m}_p}{1+R} = \frac{249.15}{2.87} = 86.81 \text{ kg/s}$$

$$\text{Oxidizer (N}_2\text{O}_4\text{) mass flow rate} \quad \dot{m}_N = \frac{R\dot{m}_p}{1+R} = \frac{1.87 \times 249.15}{2.87} = 162.34 \text{ kg/s}$$

$$\text{Volumetric flow rate of UDMH} \quad \dot{Q}_U = \frac{\dot{m}_U}{\rho_U} = \frac{86.81}{790} = 0.11 \text{ m}^3/\text{s}$$

$$\text{Volumetric flow rate of N}_2\text{O}_4 \quad \dot{Q}_N = \frac{\dot{m}_N}{\rho_N} = \frac{162.34}{1400} = 0.115 \text{ m}^3/\text{s}$$

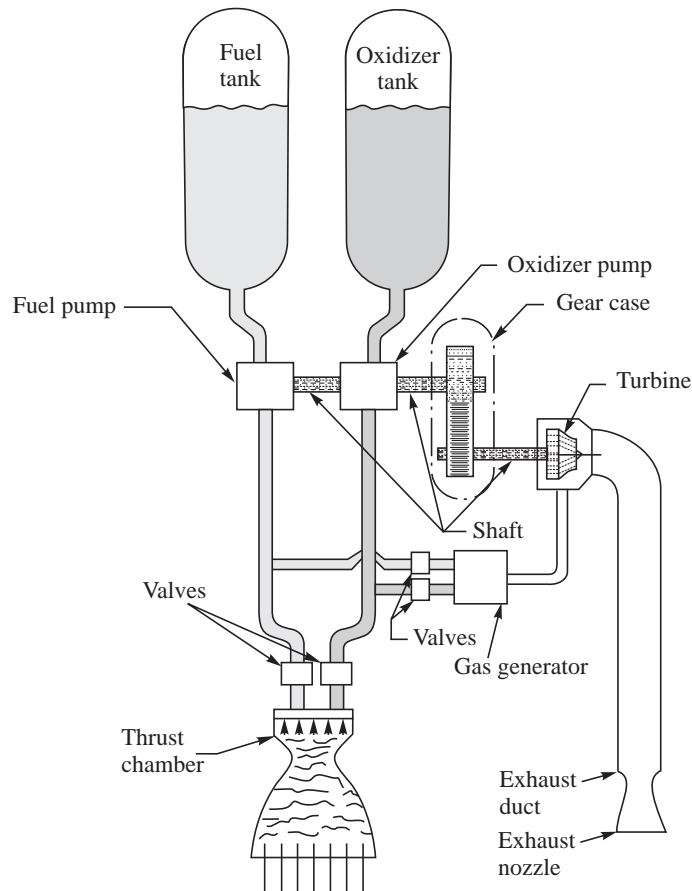


**Fig. 6.45** Simplified Schematic Diagram

The pressure increase in the pump is from the propellant tank supply pressure to the injection pressure of 7 MPa.

$$\text{Pressure rise across UDMH pump } \Delta p_U = 7 - 0.32 = 6.68 \text{ MPa}$$

$$\text{Pressure rise across N}_2\text{O}_4 \text{ pump } \Delta p_N = 7 - 0.4 = 6.6 \text{ MPa}$$

$$\text{Power of UDMH pump} = \dot{Q}_U \Delta p_U = 0.11 \times 6.68 \times 10^6 \text{ W} = 0.735 \times 10^6 \text{ W}$$

$$\text{Power of N}_2\text{O}_4 \text{ pump} = \dot{Q}_N \Delta p_N = 0.115 \times 6.6 \times 10^6 \text{ W} = 0.765 \times 10^6 \text{ W}$$

(ii) Mass flow rate through the turbine:

$$\text{Total power to be supplied to the pumps} = \frac{\dot{Q}_U \Delta p_U + \dot{Q}_N \Delta p_N}{\eta_p}$$

With a pump efficiency of 0.6, the power to be supplied to pumps

$$= \frac{(0.735 + 0.765)10^6}{0.6} = 2.5 \times 10^6 \text{ W}$$



$$\text{The power input to the turbine} = \frac{2.5 \times 10^6}{\eta_T}$$

where  $\eta_T$  is the efficiency of the turbine = 0.8

$$\text{Power input to the turbine} = \frac{2.5 \times 10^6}{0.8} = 3.125 \times 10^6 \text{ W}$$

Considering a mass flow rate through the gas generator to be  $\dot{m}_{GG}$ , the power input to the turbine from the expansion of hot gases in it is:

$$\dot{m}_{GG} C_p T_{GG} \left[ 1 - \left( \frac{P_{e,T}}{P_{i,T}} \right)^{\frac{\gamma-1}{\gamma}} \right]$$

Here  $C_p$  is the specific heat of the gases,  $T_{GG}$  is the entry temperature to the turbine which is the gas generator temperature,  $p_{i,T}$  is the pressure at the inlet to the turbine and  $p_{e,T}$  is the pressure at the exit of the turbine. Substituting the values, we get:

$$\dot{m}_{GG} \times 1900 \times 670 \times \left[ 1 - \left( \frac{0.18}{3.15} \right)^{\frac{0.264}{1.264}} \right] = 0.6 \times 10^6 \dot{m}_{GG}$$

Equating to the power supply determined earlier, we get:

$$0.6 \times 10^6 \dot{m}_{GG} = 3.125 \times 10^6$$

giving the mass flow rate through the turbine = 5.21 kg/s.

(iii) Pump speed:

$$\text{Specific speed of UDMH pump } N_S \text{ (from eq. 9.47)} = \frac{\omega \sqrt{\dot{Q}_U}}{(g \Delta h_U)^{3/4}}$$

$$\Delta h_U = \frac{\Delta p_U}{\rho_U g} = \frac{6.68 \times 10^6}{790 \times 9.81} = 862 \text{ m}$$

$$N_S = \frac{\omega \sqrt{0.11}}{(9.81 \times 862)^{3/4}} = 3.76 \times 10^{-4} \omega$$

The specific speed is given as 0.44.

$$\text{Hence } \omega = \frac{0.44}{3.76 \times 10^{-4}} = 1170 \text{ rad/s}$$

$$\text{The speed in RPM } N = \frac{1170 \times 60}{2\pi} = 11,172 \text{ RPM}$$

$$\text{Similarly for the N}_2\text{O}_4 \text{ pump } \Delta h_N = \frac{\Delta p_N}{\rho_N g} = \frac{6.6 \times 10^6}{1400 \times 9.81} = 480.6 \text{ m, and}$$

$$N_S = \frac{\omega \sqrt{0.115}}{(9.81 \times 480.6)^{3/4}} = 5.96 \times 10^{-4} \omega$$



The specific speed is given as 0.66 so that  $\omega = \frac{0.66}{5.96 \times 10^{-4}} = 1107$  rad/s, which is about the same as  $\omega$  determined for the UDMH pump. The speed of the pumps is about 10570 RPM.

(iv) NPSH and  $N_{SS}$  of  $\text{N}_2\text{O}_4$  pump:

The Net Positive Suction Head (NPSH) at the  $\text{N}_2\text{O}_4$  pump inlet

$$\begin{aligned} &= (\text{pressure available} - \text{vapour pressure}) \text{ expressed in m} \\ &= \frac{(0.4 - 0.12) \times 10^6}{9.81 \times 1400} = 20.4 \text{ m} \end{aligned}$$

$$\text{The suction specific speed } N_{SS} = \frac{\omega \sqrt{\dot{Q}_N}}{(g \text{ NPSH})^{3/4}} = \frac{2\pi(10570/60)\sqrt{0.115}}{(9.81 \times 20.4)^{3/4}} = 7.06$$

**Example 6.3** Design of a liquid propellant thrust chamber:

A film-cooled rocket for application in a satellite needs to develop a thrust of 10 N. The propellant to be used is MMH for fuel and MON-3 for oxidizer. A mixture ratio of 1.65 is to be adopted, since it provides about the same volumetric flow rates and the same propellant tanks can be used for both MMH and MON-3. A cold-gas regulated pressure-fed system is to be used, considering the requirements of small mass for the propulsion system of the satellite. The value of chamber pressure is, therefore, kept low at 0.7 MPa. Design the 10 N thrust chamber.

**Solution:** From thermo-chemical calculations described in Chapter 4 and Annexure B, the properties of the combustion products of MMH-MON-3 at mixture ratio of 1.65 are

$$T_C = 3028 \text{ K}$$

$$\mathfrak{M} = 20.39 \text{ kg/Kmole}$$

$$\gamma = 1.235$$

$$C^* = 1737 \text{ m/s}$$

We need to convert the theoretical value of  $C^*$  into a realizable value of  $C^*$ . Being a film-cooled thruster, the mixture ratio at the walls would be fuel-rich. The variations in mixture ratio across the injector will lead to a drop in  $C^*$ . Further, being a small thruster, significant heat losses would also be present. The satellite thrusters are generally required to be used for short durations since very small impulse values are necessary for correcting the attitude and orbit of a satellite. The operation in pulses, compared to a steady state mode of operation, further reduces the  $C^*$  efficiency. We choose a  $\eta_{C^*} = 0.9$ .

$$C_{\text{actual}}^* = 0.9 \times C_{\text{ideal}}^* = 0.9 \times 1737 = 1563 \text{ m/s}$$

(i) **Nozzle:** The ambient pressure  $p_a$  is zero. We would like to choose a large value of the expansion ratio of the nozzle. Choosing an area ratio (exit area/throat area) of 200, we have the relation between area ratio  $\epsilon$  and nozzle exit pressure as (Chapter 3):

$$\epsilon = \frac{\left(\frac{2}{\gamma+1}\right)^{\frac{1}{\gamma-1}} \left(\frac{p_c}{p_e}\right)^{\frac{1}{\gamma}}}{\sqrt{\frac{(\gamma+1)}{(\gamma-1)} \left\{1 - \left(\frac{p_e}{p_c}\right)^{\frac{\gamma-1}{\gamma}}\right\}}}$$



This gives the value of  $p_e = 157$  Pa for  $p_c = 0.7$  MPa and  $\gamma = 1.235$ .

The theoretical thrust coefficient  $C_F$  is given by:

$$C_{F,\text{theo}} = \sqrt{\frac{2\gamma^2}{\gamma-1} \left( \frac{2}{\gamma+1} \right)^{\frac{\gamma+1}{\gamma-1}} \left\{ 1 - \left( \frac{p_e}{p_c} \right)^{\frac{\gamma-1}{\gamma}} \right\} + \epsilon \left( \frac{p_e - p_a}{p_c} \right)}$$

For  $p_a = 0$ ,  $p_e = 157$  Pa and  $p_c = 0.7 \times 10^6$  Pa,  $C_{F,\text{theo}} = 1.95$

Taking a nozzle thrust correction parameter  $\zeta_F = 0.95$ ,  $C_{F,\text{actual}} = 0.95 \times 1.95 = 1.85$

Thrust  $F = C_F P_c A_t$ . For a thrust of 10 N at  $p_c = 0.7$  MPa

$$A_t = \frac{10}{1.85 \times 0.7 \times 10^6} = 7.72 \times 10^{-6} \text{ m}^2$$

This gives the throat diameter  $d_t = 3.14$  mm.

The nozzle exit diameter  $d_e = d_t \sqrt{\epsilon} = 44.4$  mm.

Length of the nozzle divergent portion for a conical nozzle with a half divergent conical angle of

$$15^\circ \text{ (see Chapter 3)} = \frac{d_e - d_t}{2} \frac{1}{\tan 15} = 77 \text{ mm}$$

A contour nozzle of shorter in length by about 80% is to be chosen, as given in Chapter 3 and Annexure A.

(ii) **Combustion Chamber:** The diameter of the chamber  $d_c$  is chosen about 4 times the throat diameter giving  $d_c = 13$  mm.

The  $L^*$  for this thruster using MMH-MON-3 is similar to the value recommended for MMH-N<sub>2</sub>O<sub>4</sub> propellant combination. Being a low pressure and in small pulses, we choose from literature a value of  $L^* = 900$  mm. The volume of chamber up to the throat  $V_c = L^* \times A_t$  giving  $V_c = 6948$  mm<sup>3</sup>.

The length of the convergent portion of the nozzle  $L_n = \frac{d_c - d_t}{2 \tan \theta}$ , where  $\theta$  is the semi-convergent cone angle. The value of  $\theta$  is typically 30°, giving the convergent length as 8.6 mm.

Volume of the convergent portion of the nozzle =  $\frac{L_n(A_c + A_t + \sqrt{A_c A_t})}{3}$ , where  $A_c$  is the cross-

sectional area of the chamber and  $A_t$  is the throat area. Substituting value of  $A_c = \frac{\pi}{4} \times 13^2 = 133$  mm<sup>2</sup> and  $A_t = 7.72$  mm<sup>2</sup>, we get nozzle convergent volume = 495 mm<sup>3</sup>.

$$\begin{aligned} \text{Volume of cylindrical portion} &= \text{Total chamber volume} - \text{Volume of nozzle convergent} \\ &= 6948 - 495 = 6453 \text{ mm}^3 \end{aligned}$$

$$\text{Length of the chamber} = \frac{6453}{133} \text{ mm} = 48.5 \text{ say } 50 \text{ mm}$$

The achieved specific impulse  $I_{sp} = C_{F,\text{actual}} \times C_{actual}^* = 1.85 \times 1563 = 2892$  Ns/kg



$$\text{The propellant flow rate} = \frac{\text{Thrust}}{I_{\text{sp}}} = \frac{10}{2892} = 3.46 \times 10^{-3} \text{ kg/s} = 3.46 \text{ g/s}$$

Since the mixture ratio is 1.65, the mass flow rate of MMH =  $\frac{3.46}{2.65} = 1.31 \text{ g/s}$

$$\text{The mass flow rate of MON-3} = \frac{3.46 \times 1.65}{2.65} = 2.15 \text{ g/s}$$

(iii) **Injector:** Let the choice be a triplet—with two oxidizer jets impinging on a single fuel jet injected along the axis of the chamber. We would like to maintain a pressure drop across the injection orifices  $\Delta p$  of about half the chamber pressure  $p_c$  from combustion instability considerations given in Chapter 9. This gives  $\Delta p = 0.35 \text{ MPa}$ . Taking separated flow in the fuel and oxidizer orifices, which would give a discharge coefficient of about 0.66, we calculate the area of the MMH orifice  $A_f$  and the MON-3 orifice  $A_o$  as:

$$\dot{m}_f = C_d A_f \sqrt{2\rho_f \Delta p}$$

$$\dot{m}_o = C_d A_o \sqrt{2\rho_o \Delta p}$$

Substituting the density of MMH as  $864 \text{ kg/m}^3$  and the density of MON-3 as  $1420 \text{ kg/m}^3$ , we get  $A_f = 8.07 \times 10^{-8} \text{ m}^2$  and  $A_o = 5.17 \times 10^{-8} \text{ m}^2$ . The diameter of the MMH orifice is, therefore, 0.32 mm and that of the MON-3 orifice is 0.26 mm.

## NOMENCLATURE

$A$ :	Area of injection orifice (m)
$A_t$ :	Throat diameter (m)
$B$ :	Transport number defined by eqs. 6.22, 6.26 and 6.27
$C_d$ :	Coefficient of discharge defined by eq. 6.2
$C^*$ :	Characteristic velocity of propellant (m/s)
$C_p$ :	Specific heat at constant pressure (kJ/kg K)
$C_V$ :	Specific heat at constant volume (kJ/kg K)
$D$ :	Diameter (m)
$D_0$ :	Initial droplet diameter (m)
$D_R$ :	Mixture ratio distribution parameter defined by eq. 6.10
$D_{FO}$ :	Diffusion coefficient for fuel vapour in fuel and oxidizer environment ( $\text{m}^2/\text{s}$ )
$d_i$ :	Diameter of impeller (m)
$f$ :	Fractional flow rate through the gas generator
GCC :	Gas generator cycle
$I_{\text{sp}}$ :	Specific impulse (Ns/kg)
$I_{\text{sp},MC}$ :	Specific impulse of main combustion chamber (Ns/kg)
$I_{\text{sp},T}$ :	Specific impulse from expansion of turbine exhaust (Ns/kg)



---

$K$ :	Constant
$L$ :	Length (m); Latent heat of vaporisation (kJ/kg); Inductance in eq. 6.55
$m$ :	Mass (kg)
$\dot{m}$ :	Mass flow rate (kg/s)
$n$ :	Number of orifices of fuel and oxidizer in injector
$N$ :	Number of stream tubes; pump speed in revolutions per second
$N_s$ :	Specific speed given by eq. 6.48
$N_{ss}$ :	Suction-specific speed given by eq. 6.49
NPSH :	Net-positive suction head (m)
$p$ :	Pressure (Pa)
$p_0$ :	Stagnation pressure at pump inlet (Pa)
$p_r$ :	Residual pressure in the tank after expulsion of propellant
$p_v$ :	Vapour pressure of the liquid propellant at the given temperature (Pa)
$Q$ :	Heat release per unit mass of fuel (J/kg)
$Q_{\text{chem}}$ :	Heat release during the reaction per unit mass of fuel and oxidizer (J/kg)
$\dot{Q}$ :	Volumetric flow rate ( $\text{m}^3/\text{s}$ )
$r$ :	Radial distance (m)
$r_p$ :	Pressure ratio across the turbine
$r_s$ :	Droplet radius (m)
$R$ :	Overall mixture ratio; Radius (m); Frictional resistance; Specific gas constant
SCC :	Staged combustion cycle
$T$ :	Temperature (C, K)
$T_{\text{OT}}$ :	Outlet temperature of gases in the turbine (K)
$U$ :	Internal energy (J)
$V$ :	Velocity (m/s)
$V_C$ :	Chamber volume ( $\text{m}^3$ )
$V_P$ :	Volume of propellant in tank ( $\text{m}^3$ )
$W$ :	Work (J)
$x$ :	Fraction
$Y$ :	Mass fraction
$Y_{O\infty}$ :	Mass fraction of oxidizer far from droplet surface
$\alpha$ :	Angle made by liquid jet with respect to axis of chamber ( $^\circ$ )
$\beta$ :	Spray fan angle ( $^\circ$ )
$\gamma$ :	Specific heat ratio
$\eta$ :	Efficiency



$\lambda$ :	Evaporation constant defined by eqs. 6.16, 6.24
$v$ :	Stoichiometry
$\rho$ :	Density ( $\text{kg}/\text{m}^3$ )
$\sigma$ :	Surface tension ( $\text{N}/\text{m}$ )
$\tau$ :	Torque ( $\text{N m}$ )
$\omega$ :	Angular speed (radians/s)
$\Delta p$ :	Pressure drop (Pa)
$M$ :	Molecular mass ( $\text{kg}/\text{Kmole}$ )

### Subscripts

$C$ :	Chamber
dist :	Distribution of mixture ratio
$f, F$ :	Fuel
$l$ :	Liquid
$O$ :	Oxygen, supply conditions for injection
OX :	Oxidizer
$p$ :	Propellant tank
$r$ :	Residual
$S$ :	Surface
$ST$ :	Surface tension
$T$ :	Turbine
$vap$ :	Vaporisation

### Superscript

$''$ :	Per unit area
--------	---------------

## EXERCISES

1. A cryogenic rocket, called Vinci, working on the expander cycle is proposed for the upper stage of the Ariane launch vehicle. In this rocket, hot hydrogen gas, generated in the regenerative cooling passage of the thrust chamber, drives two turbines installed in series. The first turbine drives the liquid hydrogen pump, while the second turbine drives the liquid oxygen pump. The two separate turbopumps, each equipped with an inducer, pressurize the propellants. Assuming the power of the hydrogen and oxygen turbo-pumps as 2500 kW and 400 kW, and their speeds as 90,000 RPM and 19,000 RPM respectively, determine the specific speed of the pumps. You can assume the efficiencies of the both pumps as 0.6. The thrust developed by the rocket in vacuum is 180 kN and the vacuum specific impulse is 4560 Ns/kg. The mixture ratio in the thrust chamber can be taken as 5.8. You can assume the density of liquid hydrogen as  $75 \text{ kg}/\text{m}^3$  and the density of liquid oxygen as  $1150 \text{ kg}/\text{m}^3$ .
2. Determine the heat to be transferred in the regenerative coolant passages of a cryogenic rocket, using liquid hydrogen and liquid oxygen and operating in the expander cycle, given the following data. A



single turbine is configured to drive both the LH<sub>2</sub> and LOX pumps:

Thrust: 10 kN

Mixture ratio: 5

Specific impulse: 4500 Ns/kg

Temperature of liquid hydrogen in storage tank: 20 K

Supply pressure of LH<sub>2</sub> and LOX to the pumps from the tanks: 0.25 MPa

Outlet pressure of LH<sub>2</sub> pump: 4.6 MPa

Outlet pressure of LOX pump: 3.6 MPa

Temperature at hydrogen injection into thrust chamber = temperature of hydrogen at outlet from turbine: 150 K

Efficiency of the turbo-pump system: 0.65

Specific heat of liquid hydrogen: 9.7 kJ/kg K

Specific heat of gaseous hydrogen: 14.9 kJ/kg K

Density of liquid hydrogen: 75 kg/m<sup>3</sup>

Density of liquid oxygen: 1150 kg/m<sup>3</sup>

Latent heat of vaporisation of liquid hydrogen: 446 kJ/kg

Boiling temperature of liquid hydrogen in coolant passage: 23 K

State any assumptions made.

3. A cryogenic liquid propellant rocket using liquid hydrogen for fuel and liquid oxygen for oxidizer works on a gas generator cycle. The overall mixture ratio of the rocket is 4.0 while the mixture ratio in the gas generator is 0.6. The temperature of the hot gases in the gas generator (corresponding to the mixture ratio of 0.6) is 700 K. The pressure ratio across the turbine is 3. Find the fraction of the propellants required to be supplied to the gas generator and the mixture ratio in the main thrust chamber. You can assume the efficiency of the turbo-pump system as 0.6. The specific heat ratio and molecular mass of the products of combustion of the gas generator are 1.35 and 3.3 kg/kmole. The densities of liquid hydrogen and liquid oxygen are 75 and 1140 kg/m<sup>3</sup> respectively. The pressure rise across the liquid hydrogen pump and liquid oxygen pump can be taken to be 5 MPa.
4. In the above problem, if the specific impulse in the main thrust chamber is 4450 Ns/kg and the specific impulse of the gases expanded from the turbine exhaust is 2500 Ns/kg, what is the specific impulse of the gas generator fed cryogenic rocket?
5. Determine the volume of gas bottle required to pressurize the propellant tanks containing UDMH and N<sub>2</sub>O<sub>4</sub> in a high thrust liquid propellant rocket operating in a gas generator cycle. The gas used is helium and is stored in the gas bottle at a pressure of 32 MPa and a temperature of 300 K. The volume of the UDMH tank and N<sub>2</sub>O<sub>4</sub> tank is the same and is 15,400 liters. Both fuel and oxidizer are supplied to the pumps at a rate of 110 liters/s. The supply pressure of UDMH is 0.37 MPa, while that of N<sub>2</sub>O<sub>4</sub> is 0.34 MPa. Two separate pressure regulators are used, which reduce the pressure of the helium gas from the gas bottle pressure to 0.37 MPa for UDMH tank and 0.34 MPa for the N<sub>2</sub>O<sub>4</sub> tank. You can assume the UDMH and N<sub>2</sub>O<sub>4</sub> tank to be completely filled with propellants. The pressure loss in the feed-lines and flow control components can be neglected.
6. (a) Calculate the combustion volume of a thruster burning Liquid Oxygen (LO<sub>2</sub>) and Kerosene at a pressure of 5 MPa and generating a thrust of 60 kN. The actual thrust coefficient can be taken as 1.4 and the characteristic velocity C\* as 2800 m/s. The characteristic length (L\*) for a kerosene – LO<sub>2</sub> thruster can be assumed as 1.7 m.



- (b) If the mixture ratio in the thruster is 2, determine the volumetric flow rates of LO<sub>2</sub> and kerosene. You can take the specific gravity of LO<sub>2</sub> and kerosene as 1.14 and 0.8 respectively.
- (c) If like doublet injection elements with sharp-edged orifices of diameters of 1 and 1.14 mm are used for LO<sub>2</sub> and kerosene, find the number of injection elements required. You can assume the discharge coefficient of the orifices as 0.64 and the supply pressure to the injector as 6 MPa.
7. (a) A liquid propellant rocket uses hydrazine for fuel and N<sub>2</sub>O<sub>4</sub> for oxidizer. The rate of hydrazine injection is 4 g/s and that of N<sub>2</sub>O<sub>4</sub> is 6 g/s. If the mean diameter of hydrazine and N<sub>2</sub>O<sub>4</sub> droplets formed in the spray is 0.3 mm and the mean axial velocity of droplets is 50 m/s, determine:
- (i) Mixture ratio at injection
  - (ii) Mixture ratio of the vaporised propellant
- You can take the length of the combustion chamber as 50 cm. The evaporation of the droplets can be assumed to be given by the law:  $d^2 = d_0^2 - \lambda t$ , where the evaporation constant  $\lambda$  is 3 mm<sup>2</sup>/s for hydrazine droplets and 5 mm<sup>2</sup>/s for N<sub>2</sub>O<sub>4</sub> droplets.
- (b) If the characteristic velocity  $C^*$  in m/s is expressed in terms of mixture ratio  $R$  by the expression:
- $$C^* = 2000 - 100(|R - 1.4|),$$
- find the  $C^*$  efficiency due to incomplete vaporisation.
- (c) In the above problem, if the distribution of mixture ratio in the combustion chamber provides four streams with a core having 40% of the propellant flow and surrounded with annular streams having 30%, 20% and 10% of the total propellant flow, determine the mixture ratio of the stream adjacent to the chamber walls? The mixture ratio of the core is 1.6. The mixture ratio of the streams conveying 30% and 20% of the flow is 1.5 and 1.4 respectively.
- Determine the  $C^*$  efficiency due to mixture ratio distribution.
- (d) What is the net  $C^*$  efficiency?
8. A liquid propellant rocket developing a thrust of 500 N uses MMH and N<sub>2</sub>O<sub>4</sub> for the propellant at a mixture ratio of 1.65. The chamber pressure is 0.7 MPa. The value of the characteristic velocity  $C^*$  of the propellant at the above chamber pressure and mixture ratio of 1.65 is 1800 m/s. The thrust coefficient  $C_F$  of the rocket is 1.5.
- Determine the following:
- (i) Throat area of the nozzle
  - (ii) Mass flow rate of MMH and N<sub>2</sub>O<sub>4</sub>
  - (iii) The diameter of the injection holes to be provided in the injector for the MMH and N<sub>2</sub>O<sub>4</sub> if 10 doublet injector elements are used. The injection pressure of MMH and N<sub>2</sub>O<sub>4</sub> is 1 MPa. The discharge coefficient of the orifices is 0.95.
- The density of MMH is 868 kg/m<sup>3</sup> and the density of N<sub>2</sub>O<sub>4</sub> is 1400 kg/m<sup>3</sup>.

## References

1. Altman, D., Carter, J.M., Penner, S.S. and Summerfield, M., *Liquid Propellant Rockets*, Princeton Aeronautical Paperbacks, Donaldson, C.D., General Editor. Princeton University Press, Princeton, 1960.
2. Barrere, M., Jaumotte, A., Veubeke, B.J. and Vanderkerckhove, J., *Rocket Propulsion*, Elsevier Publishing Company, Amsterdam, 1960.
3. Bollinger, L.E., Goldsmith, M. and Lemmon Jr., A.W., *Liquid Rockets and Propellants*, Vol. 2, Progress in Astronautics and Rocketry, Academic Press, New York, 1960.
4. Dunning, J.E.P., *The Optimum Size of a Rocket Engine*, The Journal of the Royal Aeronautical Society, Vol. 64, 1960, pp. 717-742.



5. Huzel, D.K. and Huang, D.H., *Modern Engineering for Design of Liquid Propellant Rocket Engines*, Progress in Astronautics and Aeronautics, Vol. 147, AIAA Washington, December 1992.
6. Oates, G.C., *Aircraft Propulsion Systems Technology and Design*, Vol. 3 of AIAA Education Series, AIAA Inc., Washington, 1989.
7. Manski, D., *Effect of Engine Cycle Type on Payload Delivery of Future European Launcher*, IAF-85-127, 36th Congress of International Astronautical Federation, Stockholm, Sweden, October 7-12, 1985.
8. Mattingly, J., Elements of Propulsion: *Gas Turbines and Rockets*, AIAA Education Series, AIAA, 2006.
9. Mukunda, H.S., *Understanding Aerospace Propulsion*, Interline Publishing, Bangalore, 2004.
10. Ramamurthi, K. and Jayashree, A., *Optimization of Mixture ratio Distribution in Liquid Propellant Rocket Thrust Chamber*, J. Propulsion and Power, Vol. 8, 1992, pp. 605-608.
11. Riebling, R.W., *Criterion for Optimum Propellant Mixing in Impinging Jet Injection Elements*, J. Spacecrafts and Rockets, Vol. 4, 1967, pp. 817-819.
12. Rossini, C., Attygalle, A.B., Gonzalez, A., Smedley, S.R., Eisner, M., Meinwald, J. and Eisner, T., *Defensive Production of Formic Acid (80%) by Carabid Beetle (Galerita lecontei)*, Proc. National Academy of Science, USA, Vol. 94, 1997, pp. 6792-6797.
13. Ryan, R.S. and Townsend, J.S., *Fundamental Issues in Launch Vehicle Design*, J. Spacecrafts and Rockets, Vol. 34, 1997, pp. 192-198.
14. Sutton, G.P. and Biblarz, O., *Rocket Propulsion Elements*, 7th Ed., Wiley Interscience Publications, New York, 2001.
15. Timnat, Y.M., *Advanced Chemical Rocket Propulsion*, Academic Press, London, 1987.
16. Valentine, R.S., Dean, L.E. and Pieper, J.L., *An Improved Method for Rocket Performance Prediction*, J. Spacecrafts and Rockets, Vol. 3, 1966, pp. 1409-1413.
17. Yang, V., Habiballah, M., Hulka, J. and Popp, M., *Liquid Rocket Thrust Chamber: Aspects of Modeling, Analysis and Design*, Vol. 200, Progress in Astronautics and Aeronautics, AIAA Inc., Washington, 2004.
18. Zucrow, M.J., *Aircraft and Missile Propulsion: Vol. 1, Thermodynamics and Fluid Flow in Applications and Propulsion Engines*, Wiley, Chapman & Hall, New York, 1958.

## Glossary

- Ablation cooling: Protection of metal walls from hot combustion gases by sacrificial ablation of insulating materials
- Blow-apart: Separation of impinging liquid jets due to chemical reactions; leads to mal-distribution of mixture ratios in combustion chamber
- Blow down pressurization: Pressurized gases contained in the ullage volume above the liquid propellant in the propellant tank supplies the propellant into the thrust chamber
- Cavitation: Formation of cavities or gas bubbles in a liquid flow due to vapour pressure of the liquid falling below the pressure in the liquid
- Characteristic length of chamber: Ratio of the chamber volume to the throat area which gives an indication of the length over which combustion processes take place and hot gases are generated
- Coaxial injector: Injector in which fuel is injected concentrically over the oxidizer or vice versa
- C\* efficiency: Ratio of realizable characteristic velocity to the theoretical value
- Discharge coefficient: Coefficient correcting for the mass flow rate by considering the reduced effective area of flow, non-axial flow velocities and friction
- Distribution parameter: Parameter used for describing the level of non-uniform distribution of mixture ratio in thrust chamber



Dribble volume: Volume of propellant locked-up in the injector manifold

Evaporation constant: Rate of change of surface area of a spherical droplet with time due to evaporation

Expander cycle: Turbo-pump driven by gases generated from heating of volatile liquid fuel in the regenerative cooling passages of thrust chamber

Gas-assist atomization: Gases at high velocities used for breaking up liquid propellant into droplets

Gas generator cycle: Hot gases from a gas generator drive the turbo-pump and the exhaust from the turbine is expanded in an auxiliary small area ratio nozzle

Film cooling: Cool thrust chamber walls by a thin film of liquid fuel coolant or vapour coolant

Hydraulic flip: Unsteady flow through injection orifice due to flow getting periodically attached and separated from the walls of the orifice

Impinging jets: Impacting high velocity liquid jets on one another to break up the liquid into droplets; they could be doublets, triplets, quadruplets and pentads, depending on whether two, three, four or five jets are used

Injector: Element of liquid propellant rocket which injects liquid fuel and oxidizer at desired flow rates into the combustion chamber, breaks up the liquid into droplets and distributes them suitably for burning

Manifold: Supply passages for orifices in injector

Microgravity: Near-zero weightless conditions

Net positive suction head: Available head at pump inlet over and above the vapour pressure (NPSH)

Positive expulsion: Liquid propellant contained in a flexible medium such as a bladder and separated physically from the gas used to expel it

Radiation cooling: Transferring the heat from heated walls by radiation

Regenerative cooling: Heat gained from cooling of thrust chamber used beneficially to generate energy in combustion

Regulated cold gas pressurization: A constant gas pressure, obtained using a pressure regulator, is impressed over the liquid propellant surface for supplying the propellant to the thrust chamber

Showerhead injector: Parallel streams of thin high velocity liquid jets formed by small orifices in injector

Specific speed: Non-dimensional speed of turbo-pump expressed as a combination of the parameters pump speed, flow rate and head developed by the pump

Staged combustion cycle: Hot gases from a gas generator/pre-burner drive the turbo-pump and the exhaust from the turbine is fed into the thrust chamber for further burning

Stream tube combustion: Individual performance of annular stream-tubes of vaporised propellant at different mixture ratios integrated together to determine net performance due to stratification of mixture ratios and mass flow rates in thrust chamber

Suction specific speed: Specific speed of pump in which the net positive suction head replaces the head developed by the pump

Swirl: Axial flow with rotation

Thrust chamber: Thrust generating device of a liquid propellant rocket consisting of injector, combustion chamber and nozzle

Transpiration cooling: Sweat cooling

Transport number: Indicates transport of vapour from the surface of a droplet. It is defined either as a function of concentration of vapour at the droplet surface and far from it, or as the ratio of enthalpy of hot gases surrounding the droplet and the latent heat of vaporisation

Ullage: Gas volume above the liquid propellant in the propellant tank

## Chapter 7

# Liquid Monopropellant Rockets

*The development of a rational view on the nature of catalysis was ... absolutely dependent on the creation of the concept of the rate of chemical reaction.*

*Wilhelm Ostwald, Nobel Prize in Chemistry for work on catalysis, chemical equilibria and reaction velocities*

Propellants hydrazine ( $\text{N}_2\text{H}_4$ ) and hydrogen peroxide ( $\text{H}_2\text{O}_2$ ), which are liquids at the ambient temperature of  $25^\circ\text{C}$  and have the standard heats of formation of +50.3 and -187.8 kJ/mole respectively, can be readily decomposed either by a catalyst or by applying heat. Catalyst iridium decomposes hydrazine, while silver decomposes hydrogen peroxide and heat is released during the decomposition. The hot gases, generated from decomposition of hydrazine or hydrogen peroxide, can be expanded in a nozzle to generate thrust. Rockets which use a single propellant (monopropellant), such as hydrazine or hydrogen peroxide for generating hot gases and hence the thrust are known as ‘monopropellant rockets’.

The temperature of the decomposition products in monopropellant rockets is significantly lower than the combustion products in solid and liquid propellant rockets considered earlier. The specific impulse of the monopropellant rockets is, therefore, lower than the solid and liquid propellant rockets. However, since a single propellant is involved, the construction of the rocket is simpler than the bipropellant rocket. Monopropellant rockets have been used in a pressure-fed mode to generate low thrust levels typically between 0.5 N and 50 N for spacecraft propulsion and for auxiliary rockets of satellite launch vehicles.



## 7.1 HYDRAZINE MONOPROPELLANT ROCKETS

Hydrazine has higher values of heat of decomposition compared to hydrogen peroxide and, is generally preferred for monopropellant rockets. Hydrazine is stored in a tank, and is supplied using regulated gas pressure to the thrust chamber as shown in Fig. 7.1. This is similar to the cold gas regulated pressure fed system dealt with in the last chapter.

The catalyst, activated iridium, is adsorbed in small spherical granules of porous alumina of diameters between 1.5 mm and 3 mm. A number of such alumina granules are packed together in an assembly, known as catalyst bed, which is contained in the thrust chamber. Hydrazine flows through the catalyst bed and decomposes to form hot gases, which are expanded in the nozzle. The combustion chamber pressures are typically between 0.7-1 MPa and are much lower than in the bipropellant rockets.

The porous nature of the alumina ensures the presence of activated iridium catalyst not only on its surface, but also in the pores of the alumina globules. This ensures that the catalyst is maximally in contact with hydrazine.

Hydrazine is injected into the catalyst bed, using showerhead-type of injectors. The orifice diameters are smaller than those in liquid bi-propellant rockets considering the reduced flow rates of the hydrazine. Typical orifice diameters are about a fraction of a millimeter. Cylindrical screens or porous discs are sometimes incorporated downstream of the injector and embedded in catalyst bed to distribute the hydrazine homogeneously in the catalyst bed.

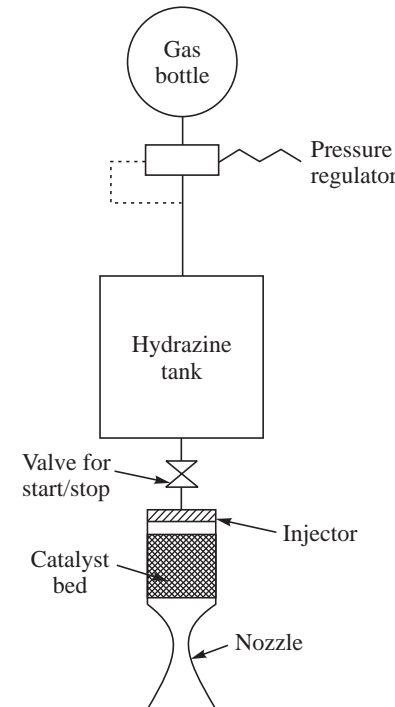


**Fig. 7.1** Hydrazine Monopropellant Rocket

### 7.1.1 Decomposition of Hydrazine: Degree of Dissociation and $C^*$

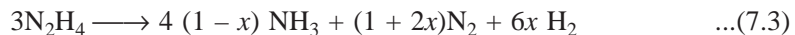
Hydrazine is decomposed by catalyst iridium in two steps. Hydrazine first decomposes to ammonia and nitrogen.



This reaction is exothermic, the heat release being  $-(4 \times -45.9 - 3 \times 50.3) = 334.5 \text{ kJ}$ . Here, 50.3 and  $-45.9 \text{ kJ/mole}$  are the standard heats of formation of  $\text{N}_2\text{H}_4$  and  $\text{NH}_3$  respectively. The ammonia further dissociates into nitrogen and hydrogen as per the reaction:



The heat from this reaction is  $-(0 - 4 \times (-45.9)) = -183.6 \text{ kJ}$  and is endothermic. The overall reaction, depending on the degree of ammonia dissociation, can be written as:





Here,  $x$  denotes the degree of ammonia dissociation. It depends on the residence time over which the hydrazine is in contact with the catalyst, the size and configuration of the catalyst bed and the nature of pores in the alumina globules.

The temperature of gases decreases when the degree of ammonia dissociation increases due to the heat absorbed during the dissociation of ammonia. This is shown in Fig. 7.2.

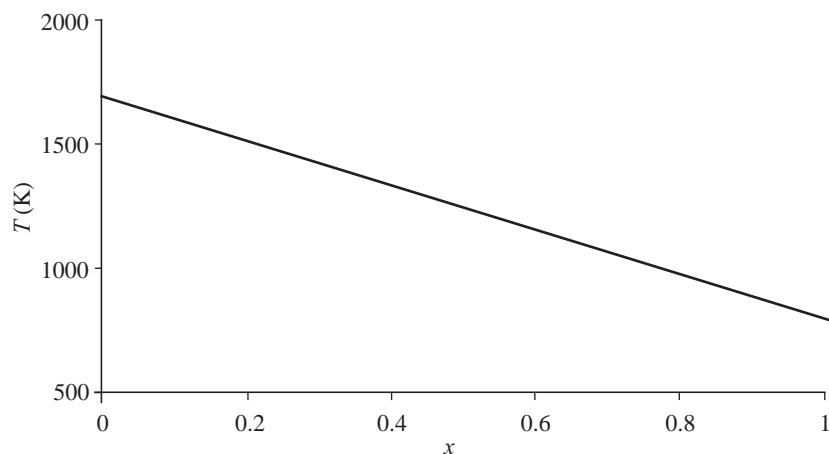


**Fig. 7.2** Temperature of the Decomposition Products

The molecular mass of hot gases also decreases from about 19.2 kg/kmole to 10.7 kg/kmole. This is seen from eq. 7.3 due to the lower molecular mass of hydrogen formed as the degree of ammonia dissociation increases from 0 to 1 (Fig. 7.3). Since  $C^*$  is proportional to  $\sqrt{T_c/\mathfrak{M}}$ , net effect of the decrease of the temperature and molecular mass is to give rise to very small variation of  $C^*$  for degree of dissociation between about 0 and 0.4. The maximum  $C^*$  is obtained for a degree of dissociation of about 0.2 as shown in Fig. 7.4.

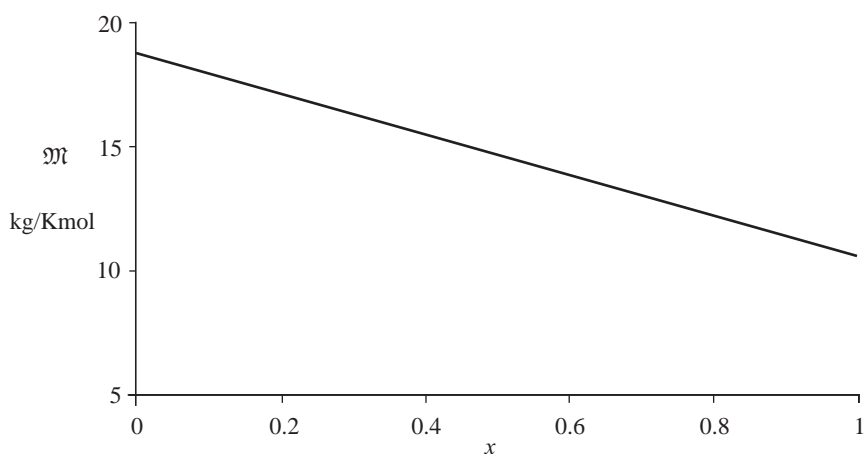


**Fig. 7.3** Molecular Mass of the Decomposition Products

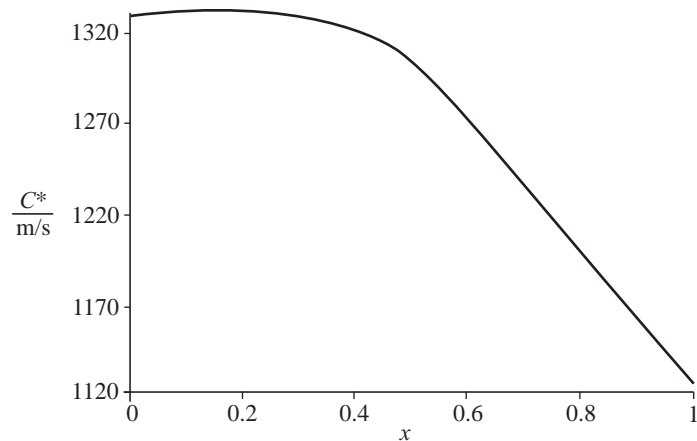


**Fig. 7.4** Variation of Characteristic Velocity with Degree of Dissociation



## 7.2 CATALYST BED LOADING

A single, double or layered bed of the alumina granules, impregnated with activated iridium is used for the catalyst bed. Finer granules have more of the activated iridium to interact with hydrazine; however, the pressure drop across a bed containing fine granules increases. The practice is to have finer granules in the top layers of the bed and coarse granules in the remaining part of the catalyst bed.

The passage of the hydrazine into the pores of the alumina provides the contact with iridium for the decomposition of hydrazine. The permeability of the alumina is, therefore, important. The overall catalyst bed is characterized by the ratio of the mass flow rate of hydrazine to the cross-sectional area of the catalyst bed and is known as the bed loading of the catalyst. For very small thrust levels of the monopropellant rocket, the bed loading is about  $1 \text{ g/cm}^2\text{s}$ , whereas for the larger thrust, the bed loading increases to about  $50 \text{ g/cm}^2\text{s}$ .

Since the catalyst is impregnated in the pores of the porous alumina pellets, hydrazine as it seeps into the pores comes in contact with the catalyst. It also comes in contact with the catalyst at the surface of the pellets. The porosity and permeability of the alumina pellet decide the ability of hydrazine within the pores to be in contact with the catalyst.

The flow rate of hydrazine vapor in the pores of alumina in  $\text{m}^3/\text{s}$  is given by the continuum Darcy law:

$$\dot{Q} = - \frac{K_m A}{\mu} \frac{dp}{dx} \quad \dots(7.4)$$

where  $K_m$  is the permeability of hydrazine vapor in  $\text{m}^2$ ,  $A$  is the cross-sectional area of the pore in  $\text{m}^2$  and  $\mu$  is the viscosity in  $\text{kg}\cdot\text{m}/\text{s}$ .  $dp/dx$  is the pressure gradient in  $\text{Pa}/\text{m}$ . Permeability denotes the ease with which flow takes place in the given porous medium and depends on the pore structure and the nature of the vapor.



There would also be diffusion of hydrazine from the concentration gradient, which is given by the Fick's law of diffusion:

$$\dot{m} = -DA \frac{d\rho}{dx} \quad \dots(7.5)$$

Here  $D$  is the diffusion coefficient in  $\text{m}^2/\text{s}$ ,  $A$  is the area in  $\text{m}^2$  and  $d\rho/dx$  is the density gradient in  $\text{kg/m}^4$ . Assuming hydrazine vapor to be an ideal gas, we have:

$$\rho = \frac{p}{RT} \quad \dots(7.6)$$

For a given temperature of the hydrazine vapor:

$$\dot{m} = -DA \frac{dp}{dx} \frac{1}{RT} = \frac{DA\rho}{p} \frac{dp}{dx} \quad \dots(7.7)$$

giving

$$\dot{Q}_{Diff} = -\frac{DA}{p} \frac{dp}{dx} \quad \dots(7.8)$$

The ratio of the transport by flow in the pores to that by diffusion is therefore:

$$\frac{\dot{Q}}{\dot{Q}_{Diff}} = \frac{K_m p}{D\mu} \quad \dots(7.9)$$

Generally this ratio is large and it is adequate to consider Darcy flow alone to determine the quantity of fluid in contact with the catalyst. The hydrazine vapor is drawn into the pores and generates hot gases by combustion in presence of the catalyst. The pressure so generated expels the hot gases. The surface tension which holds the gas therefore becomes important.

A higher value of temperature promotes a faster reaction rate within the pore. The catalyst bed is therefore extraneously heated to a temperature of about  $120^\circ\text{C}$ . The heat generated by the catalytic reaction with hydrazine subsequently maintains the temperature of the catalyst bed at the high value. If the catalyst be is initially cold, it takes some time for the chemical reaction of decomposition to heat the bed and the transient of the pressure rise is longer till a steady state temperature is reached in the bed. Cold starts, such as the above, would also lead to a reduction in the life of the catalyst bed.



### 7.3 PERFORMANCE AND APPLICATIONS

The degree of ammonia decomposition influences the performance as seen in Fig. 7.4. The amount of decomposition is influenced by bed loading. A warm catalyst bed favours the quick start of decomposition. The general practice is to keep the bed warm by using electrical heating. A hot bed of catalyst is, however, not desirable as the heat conducted from the bed to the injector can result in the heating up of the hydrazine in the injector, leading to flow problems from vaporisation of hydrazine. The hydrazine, if overheated, could explode and explosions have been observed during the development of these thrusters. The heat transfer from the catalyst bed would also cause high temperatures in the injector and the other upstream elements, such as, flow control valves, particularly in the pulsed



mode of operation. This is because the cooling effect from the propellant flow is not present during the time in which the rocket is not firing. Heat conduction paths are provided to keep the injector cool. The volume of the hydrazine in the injector manifold (dribble volume) discussed in Chapter 6, is also kept as small as possible.

### 7.3.1 Catalyst Loss and Poisoning

Loss of activated iridium occurs from the breaking up of the alumina granules due to pressure from the decomposing hydrazine within the pores and thermal expansion of the alumina being restricted in the catalyst bed. The loss of catalyst activity results in incomplete decomposition of hydrazine and loss of performance.

Traces of contaminants, such as, polymer from the positive expulsion system in the tank and impurities such as aniline, mono-methyl hydrazine and iron in hydrazine, poison the catalyst and degrade the performance of the rocket.

### 7.3.2 Pulsed Operation

The monopropellant thruster readily admits to an intermittent or pulsed mode of operation. The intermittent operation is associated with a duty cycle which is the nominal burn time of the thruster with respect to the total duration of a cycle of events. The duration of the total cycle of events in a pulse consists of the time over which thrust is developed and the time over which no thrust is developed. As an example, if a single pulse of operation is over a period of  $t_p$  s, and the actual duration of the thrust or burning is over a time  $t_b$  s, the duty cycle is  $t_b/t_p$ . This is illustrated in Fig. 7.5.

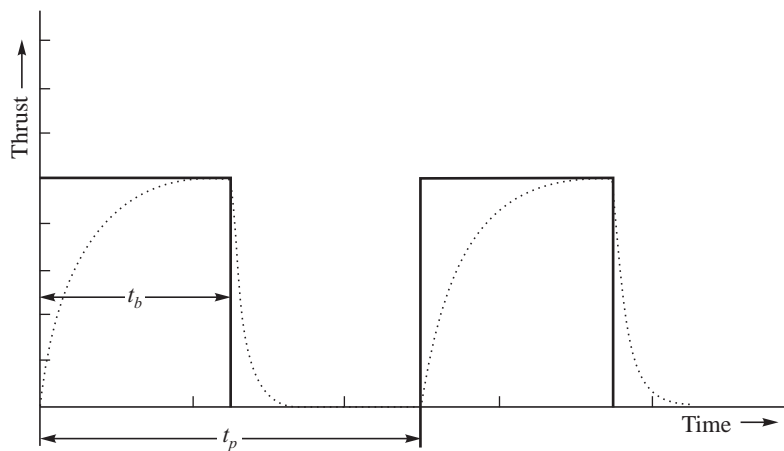


**Fig. 7.5** Time of pulse and burn time in an intermittent mode of operation

(Dark lines show an ideal pulse whereas the dotted lines show the pulse due to delays in the response of the system.)

The shape of the thrust time profile, shown in Fig 7.5, will depend on the total pulse time and the duty cycle. The valve which supplies the hydrazine to the catalyst bed will take some time to supply the design value of hydrazine to the fuel line depending on its response time. There will be a further



delay in the hydrazine reaching the catalyst bed depending on the feed line length and the injector volume. After the hydrazine comes in contact with the catalyst bed, some additional time is required to generate the hot gases and hence the thrust. This depends on the rate of the catalytic reactions with delays being of the order a one to two milliseconds when the catalyst is hot whereas for a cold catalyst bed, the reactions are slow giving a value to be very much larger than 2 milliseconds. Figure 7.6 shows the time taken to supply the design value hydrazine fuel to the catalyst bed and the thrust transient in the thruster.

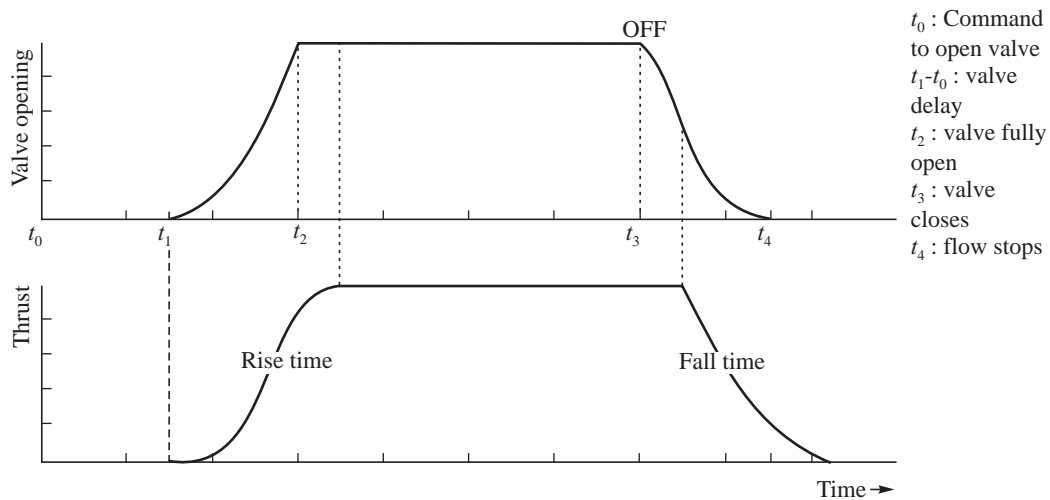


Fig. 7.6 Delayed Response

When the valve is given a signal to open and start a pulse of operation, it takes some time ( $= t_1$ ) for the valve to respond. It thereafter takes another period of time [ $= (t_2 - t_1)$ ] to admit the design value of hydrazine. When the valve is closed to finish one pulse of operation, the flow of hydrazine to the catalyst does not immediately stop but persists for some time depending on the valve response, the fuel line, injection system and the catalyst bed. The hydrazine flow therefore starts after a delay, gradually builds up to the maximum flow rate and when the valve is switched off, the flow gradually reduces to zero. The chamber pressure and the thrust would also follow the same trend and is shown in Fig. 7.6.

For long enough pulses the pressure and hence the thrust can reach a plateau corresponding to steady state of operation. However, if the pulse is of shorter duration, the plateau could vanish. The shortest pulse duration would consist of rise time and fall time of the pulses such that the plateau in the thrust is just reached. It corresponds to the minimum impulse bit that the thruster could deliver. Figure 7.7 shows the duration of the minimum impulse bit corresponding to the rise time and fall time of the thrust.

When the pulse duration is less than the pulse duration for the minimum impulse bit, pressure or equivalently the thrust corresponding to the value at the plateau is not reached, the specific impulse of the thruster rapidly falls. A schematic of the pressure rise and decay for very short pulses is shown in Fig. 7.7 and compared with the minimum impulse bit. The specific impulse of the thruster drastically reduces for such short pulses of operation.

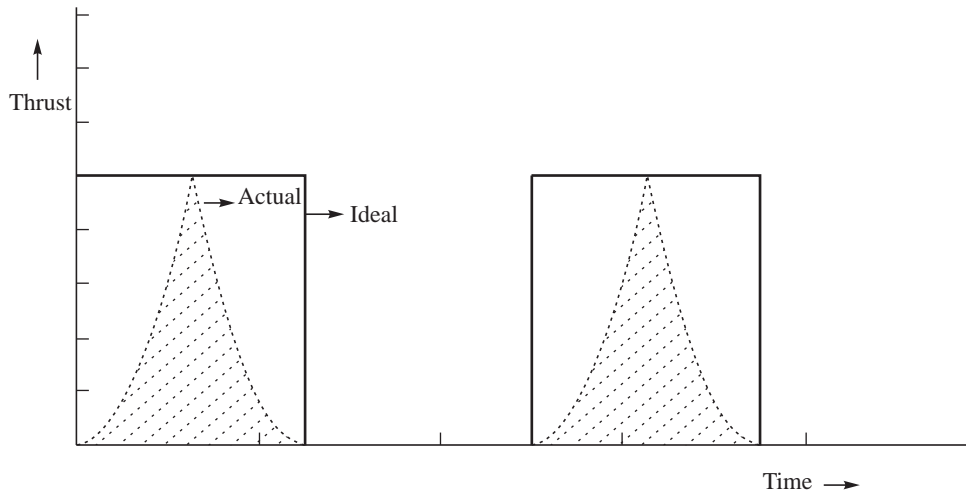


Fig. 7.7 Minimum Impulse Bit

The certainty of obtaining repeatable values of impulses also reduces from one pulse to the other as the incomplete catalytic reaction from the previous pulse provides higher pressure and thrust in the next pulse. As the pulse width reduces, the uncertainty in obtaining reproducible impulse bit increases. At very low duty cycles, giving short duration of the catalytic decomposition times, the specific impulse of the thruster rapidly declines. The uncertainty in the pressure and specific impulse varies not only from one pulse to the other but also from one thruster to the other. A schematic of the variations is shown in Fig. 7.8.

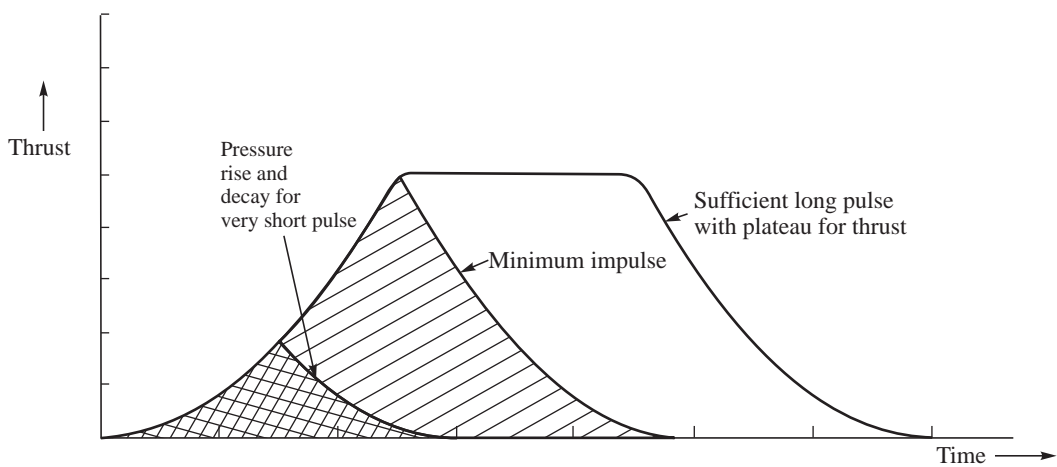


Fig. 7.8 Very Short Duration Pulses

Impulse bits for hydrazine thrusters depend on the size of the thruster, the bed loading, the temperature of the bed and the size of the catalyst pellets. Impulse bits as low as  $10^{-3}$  N-s have been achieved with a 1 N hydrazine thruster. As the thrust rating of the thruster increases, the minimum impulse bit also increases. Typical variation of the impulse bits from cycle to cycle of operation i.e., from pulse to pulse and from one hardware to the other of the same thrust rating are shown in Fig. 7.9

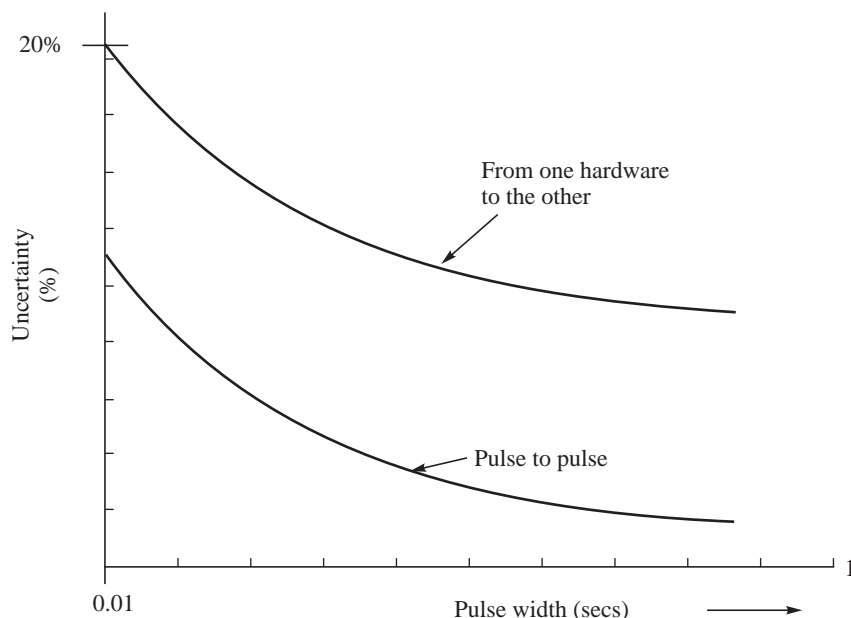


Fig. 7.9 Uncertainty in Impulse Bit as a Function of Pulse Time

### 7.3.3 Applications

The use of monopropellant rocket has considerably reduced in favour of bipropellant rockets as the latter give much higher performance. The requirements of small values of impulse required for spacecraft orbit control can, however, be readily obtained with the low thrust monopropellant rockets operating in pulses. An unified propulsion system, comprising bipropellant rockets using hydrazine and  $N_2O_4$  for propelling the spacecraft from transfer orbit to the final orbit and thereafter, using hydrazine in monopropellant rockets with low impulse bits for spacecraft attitude and orbit corrections has been actively considered. The burning of hydrazine with  $N_2O_4$  is not very smooth and gives rise to combustion instabilities and is dealt with in Chapter 9. The unified propulsion system, comprising monopropellant and bipropellant rockets with hydrazine holds promise for the future.

## SOLVED EXAMPLES

**Example 7.1** Performance of a hydrazine mono-propellant rocket:

Hydrazine ( $N_2H_4$ ) at a temperature of  $25^\circ C$  is decomposed in a catalytic bed in a monopropellant thruster, using activated iridium adsorbed in alumina. The catalyst bed is designed to give 30% dissociation of the ammonia ( $NH_3$ ). Determine the following:

- (i) Heat release per kg of hydrazine
- (ii) Temperature of the products of decomposition
- (iii) Molecular mass of the products
- (iv) Characteristic velocity of the monopropellant rocket



The following data is to be used:

Property	Hydrazine (liquid)	Ammonia (vapour)	Hydrogen (gas)	Nitrogen (gas)
Standard heats of formation $\Delta H_f^\circ$ in kJ/mole	+55	- 46	—	—
Average specific heat $C_p$ in kJ/mole K	—	0.04	0.03	0.035

**Solution:** (i) *Heat release per kg of hydrazine:* If the fractional dissociation of ammonia is denoted by  $x$ , the decomposition of hydrazine is given by:



The degree of ammonia dissociation  $x$  is given as 0.3. The equation describing the formation of products of the decomposition is:



$$\begin{aligned} \text{Heat release during the reaction} &= \Delta H_c = -(\sum \Delta H_f, \text{products} - \sum \Delta H_f, \text{reactants}) \\ &= -[2.8 \times (-46) + 1.6 \times (0) + 1.8 \times (0) - 3 \times (55)] \\ &= 293.8 \text{ kJ for every 3 moles of hydrazine} \end{aligned}$$

$$\text{Heat released per kg of hydrazine} = \frac{293.8}{3 \times (2 \times 14 + 4 \times 1) \times 10^{-3}} = 3060 \text{ kJ}$$

(ii) *Temperature of products of decomposition:* Denoting the temperature of the products of decomposition by  $T$ , we have the heat released in the chemical reaction:

$$\Delta H_c = 2.8C_{p,\text{NH}_3}(T - 298) + 1.6C_{p,\text{N}_2}(T - 298) + 1.8C_{p,\text{H}_2}(T - 298)$$

which on substituting the values of the specific heat and heat release gives:

$$293.8 = (2.8 \times 0.04 + 1.6 \times 0.035 + 1.8 \times 0.03) \times (T - 298) \text{ giving}$$

$$T = 1621 \text{ K}$$

(iii) *Molecular mass of products:* Denoting the molecular mass of products of dissociation as  $\mathfrak{M}$ , we have:

$$\mathfrak{M} = \frac{\sum n_i \mathfrak{M}_i}{\sum n_i}$$

$$\therefore \mathfrak{M} = \frac{2.8 \times (14 + 3 \times 1) + 1.6 \times (14 \times 2) + 1.8 \times (1 \times 2)}{2.8 + 1.6 + 1.8}$$

$$= 15.5 \text{ kg/mole}$$

(iv) *Characteristic velocity:* We know the temperature and molecular mass of the products of dissociation. However, we do not know the value of the specific heat ratio  $\gamma$ . We first calculate the value of the specific heat of the products  $C_p$ , from which we determine the specific heat ratio.



$$C_p = \frac{\sum_i n_i C_{pi}}{\sum_i n_i} = \frac{2.8 \times 0.04 + 1.6 \times 0.035 + 1.8 \times 0.03}{2.8 + 1.6 + 1.8} = 0.0358 \text{ kJ/mole K}$$
$$= 35.8 \text{ J/mole K}$$

Assuming the products as perfect gas and using the relation:  $C_p - C_v = R_0$ , we get:

$$C_v = C_p - R_0 = 35.8 - 8.314 = 27.49 \text{ kJ/mole K.}$$

$$\text{The specific heat ratio } \gamma = \frac{C_p}{C_v} = \frac{35.8}{27.49} = 1.302$$

The characteristic velocity  $C^* = \frac{1}{\Gamma} \sqrt{\frac{R_0 T}{M}}$  where  $\Gamma = \sqrt{\gamma} \left( \frac{2}{\gamma + 1} \right)^{\frac{\gamma + 1}{2(\gamma - 1)}}$ . Substituting the values of  $\gamma$ ,  $M$ ,  $T$  and  $R_0$  we get  $C^* = 1398 \text{ m/s}$ .

### Example 7.2 Sizing of a hydrazine monopropellant rocket:

Determine the diameter of the catalyst bed of a monopropellant hydrazine rocket to provide a thrust of 11 N given that the bed loading, based on the permeability of the alumina granules, is specified as 2 g/(cm<sup>2</sup>s). The specific impulse is 2000 Ns/kg. What would be the throughput of hydrazine for which the bed needs to be designed if the total duration of operation of the rocket is 6 hours.

**Solution:** Diameter of catalyst bed:

$$\text{Mass flow rate of hydrazine} = \frac{F}{I_{sp}} = \frac{11}{2000} = 0.0055 \text{ kg/s} = 5.5 \text{ g/s}$$

$$\text{Cross-sectional area of catalyst bed} = \frac{\text{Mass flow}}{\text{Bed loading}} = \frac{5.5 \text{ g/s}}{2 \text{ g/(cm}^2\text{s)}} = 2.75 \text{ cm}^2$$

$$\text{Diameter of bed} = \sqrt{\frac{2.75 \times 4}{\pi}} = 1.9 \text{ cm}$$

**Throughput:** This is the total quantity of hydrazine, which can flow through the bed. Since the total duration of operation is  $6 \times 3600 = 2.16 \times 10^4$  s and the flow rate per second is 5.5 g/s, the throughput of hydrazine =  $2.16 \times 10^4 \times 5.5 \text{ g} = 118.8 \text{ kg}$ .

### Example 7.3 Hydrogen Peroxide thruster: Bell Rocket Belt

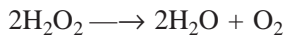
Hydrogen peroxide monopropellant rockets have been used in the early satellites. Considering the environment-friendly nature of hydrogen peroxide, interest continues in the development of the hydrogen peroxide monopropellant rockets.

A belt with a stabilization device in which a hydrogen peroxide monopropellant thruster is integrated is known as a ‘bell rocket belt’. It is worn by people for being propelled in air. The ‘bell rocket belt’ has been used to fly individuals during the opening ceremonies of some Olympic games.

Determine the specific impulse of a monopropellant thruster used in a bell rocket belt assuming no dissociation of the products when pure hydrogen peroxide is injected into a catalyst chamber at a temperature of 25°C. The chamber pressure is 0.5 MPa and the nozzle is designed to expand the combustion products to the ambient pressure of 0.1 MPa.



**Solution:** Hydrogen peroxide decomposes to form steam and oxygen. In the absence of any dissociation, the chemical reaction is represented by:



The standard heat of formation is  $-187.8 \text{ kJ/mole}$  for  $\text{H}_2\text{O}_2$  and is  $-286 \text{ kJ/mole}$  for water. The heat liberated in the above reaction is:

$$-\{2(-286) - (2(-187.8))\} = 196.4 \text{ kJ}$$

The heat raises the temperature of water and oxygen from  $298 \text{ K}$  to the high temperature say  $T_C$ . Denoting the specific heat of water as  $C_W \text{ kJ/mole K}$ , the specific heats of steam and oxygen at constant pressure as  $C_{P,\text{H}_2\text{O}}$  and  $C_{P,\text{O}_2} \text{ kJ/mole K}$  respectively and the latent heat for evaporation as  $H_V \text{ kJ/mole}$ , we have from the energy balance:

$$196.4 = 2 \times [C_W(T_B - 298) + H_V + C_{P,\text{H}_2\text{O}}(T_C - T_B)] + 1 \times C_{P,\text{O}_2}(T_C - 298)$$

$T_B$  in the above equation is the boiling temperature of water. At  $0.5 \text{ MPa}$ ,  $T_B = 152^\circ\text{C}$  ( $425 \text{ K}$ ) and  $H_V = 37.95 \text{ kJ/mole}$ . The values of  $C_W$ ,  $C_{P,\text{H}_2\text{O}}$ , and  $C_{P,\text{O}_2}$  are assumed constant and equal to  $0.09$ ,  $0.058$  and  $0.036 \text{ kJ/mole K}$  respectively. Substituting in the energy balance relation, we have  $T_C = 1044 \text{ K}$ .

The molecular mass of the products  $\mathfrak{M} = (2 \times 18 + 32)/3 = 22.67 \text{ g/mole}$ . The mean specific heat at constant pressure for the products is  $C_p = (2 \times 0.058 + 1 \times 0.036)/3 = 0.051 \text{ kJ/mole K}$ . The specific heat at constant volume of the products  $C_V = C_p - R_0 = 0.051 - 0.008314 = 0.0427$ . The specific heat ratio  $\gamma$  is, therefore,  $0.051/0.0427 = 1.195$ .

The specific impulse assuming frozen expansion in the nozzle is determined by substituting the values of temperature, molecular mass, specific heat ratio and the pressures in the expression of the jet velocity in eq. 3.4 of Chapter 3 on nozzles. The specific impulse is:

$$\begin{aligned} I_{sp} &= \sqrt{\frac{2\gamma R_0 T_C}{(\gamma - 1)\mathfrak{M}} \left[ 1 - \left( \frac{p_e}{p_c} \right)^{(\gamma - 1)/\gamma} \right]} \\ &= \sqrt{\frac{2 \times 1.195 \times 8.314 \times 1044}{0.195 \times 22.67 \times 10^{-3}} \left[ 1 - \left( \frac{0.1}{0.5} \right)^{(0.195)/1.195} \right]} \\ &= 1041 \text{ Ns/kg} \end{aligned}$$

The above value does not consider the dissociation of products and is greater than an achievable value of about  $1010 \text{ Ns/kg}$ .

## NOMENCLATURE

$x$  : Degree of ammonia dissociation

## EXERCISES

1. The catalyst bed of a hydrazine monopropellant rocket gives the degree of dissociation of ammonia to be  $0.2$ . Determine the proportion of ammonia, nitrogen and hydrogen in the products of dissociation



and the heat liberated per kg of hydrazine. The standard heats of formation of hydrazine and ammonia are + 50.3 kJ/mole and – 45.9 kJ/mole respectively. You can assume the hydrazine to be injected into the catalyst bed at the standard state of 25°C.

What is the characteristic velocity corresponding to the above degree of decomposition of 0.2. You can take the specific heats of ammonia, hydrogen and nitrogen as 0.04, 0.03 and 0.035 kJ/mole K respectively?

2. A hydrogen peroxide ( $H_2O_2$ ) rocket is made by the decomposition of  $H_2O_2$  at a pressure of 0.5 MPa using heated silver wire-mesh as the catalyst. Assuming that  $H_2O_2$  is injected into the catalyst chamber at a temperature of 298 K and is decomposed by the catalyst to steam and oxygen, determine the characteristic velocity of the  $H_2O_2$  rocket. You can use the following data:

Standard heat of formation of  $H_2O_2$  = – 188 kJ/mole

Standard heat of formation of  $H_2O$  = – 286 kJ/mole

Specific heat of water = 90 J/mole K

Specific heat of steam = 58 J/mole K

Boiling temperature of water = 150°C

Latent heat of steam = 38 kJ/mole

## References

1. Altman, D., Carter, J.M., Penner, S.S. and Summerfield, M., *Liquid Propellant Rockets*, Princeton Aeronautical Paperbacks, Donaldson, C.D., General Editor, Princeton University Press, Princeton, 1960.
2. Dithienne, N. and Cornu, N., *Design and Development of Propulsion Subsystem for Small Satellite Application*, ESA SP-398, edited by Perry, M., European Space Agency, Paris, 1997, pp. 77-84.
3. Mukunda, H.S., *Understanding Aerospace Propulsion*, Interline Publishing, Bangalore, 2004.
4. Sutton, G.P. and Biblarz, O., *Rocket Propulsion Elements*, 7th Ed., Wiley Interscience Publications, New York, 2001.

## Glossary

Catalyst: Substance which accelerates the speed of a chemical reaction without itself getting consumed in the reaction

Poisoning of catalyst: Loss of activity of the catalyst due to contamination

## Chapter 8

### Hybrid Rockets

*The early hybrid rocket of Sergei Korolev in 1933 used gelled gasoline suspended in a metal screen and liquid oxygen. Herman Oberth experimented with wax and also carbon with liquid oxygen. The number of fuels experimented are very diverse and include cryogenic solid fuels such as pentane, methane and solid hydrogen.*

Solid propellant rockets, liquid bipropellant and monopropellant rockets were discussed in the last three chapters. While the solid propellant and liquid bipropellant rockets employed the combustion between fuels and oxidizers for generating hot gases, monopropellant rockets used the catalytic decomposition of substances such as hydrazine or hydrogen peroxide to generate hot gases. The hot gases were expanded in a convergent divergent nozzle to generate thrust.

Hybrid propellant rockets are rockets in which the propellants comprising the fuel and oxidizer are in different phases. The oxidizer could be a liquid while the fuel could be a solid or vice versa. Similarly gaseous fuels or oxidizers could be used with solid and liquid oxidizers or fuels. Considering the low density of gases and the requirement of large volumes to store the mass of gas required, hybrid propellant rockets using gaseous fuels or oxidizers are not usable in practice. Generally, liquid oxidizers and solid fuels are used. It is possible to use a solid oxidizer with a liquid fuel; however, solid oxidizers are generally crystalline in nature like ammonium perchlorate or are powders such as potassium nitrate. It is difficult to make them into a solid oxidizer block with adequate mechanical properties. The hybrid rockets developed so far invariably make use of a solid fuel block and a liquid oxidizer for the propellants.

The configuration of a hybrid propellant rocket would therefore be a queer combination of solid propellant rocket and liquid bipropellant rocket in that a solid fuel block as in a solid propellant rocket would be present while the liquid oxidizer is injected through an injector as in a liquid propellant rocket. The solid fuel block or grain regresses as in the solid propellant grain.



A schematic of a hybrid propellant rocket is shown in Fig. 8.1. Liquid oxidizer is injected at high pressures as a spray over the surface of a solid fuel block kept in the combustion chamber. The liquid oxidizer is contained in a tank and is pressurized using high pressure gas from a gas bottle or by a pump. Hot gases are generated by the chemical reaction between the fuel and the oxidizer and the hot products of combustion are ejected at high velocities through a nozzle to generate thrust.

The different hybrid propellants, the characteristics of hybrid propellant rockets and their advantages and disadvantages over solid and liquid propellant rockets are addressed in this chapter. There is a revival of interest in hybrid propellant rockets with the Stage Composites company in US developing them for use in space tourism.

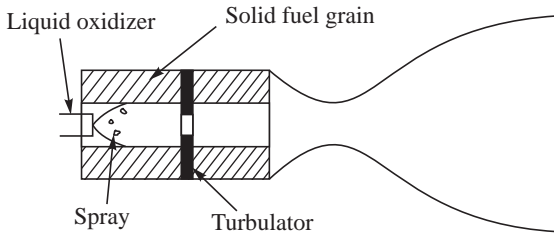


**Fig. 8.1** Hybrid Rocket



## 8.1 HYBRID PROPELLANTS

### 8.1.1 Liquid Oxidizers

Liquid oxidizers are similar to those used in liquid propellant rockets. Cryogenic oxidizers, Liquid Oxygen or a combination of liquid oxygen and liquid fluorine viz., FLOX are energetic oxidizers. Di-nitrogen tetroxide  $N_2O_4$  and the red fuming nitric acid (RFNA) are also viable oxidizers. Hydrogen peroxide  $H_2O_2$ , which is neither toxic nor corrosive unlike RFNA and  $N_2O_4$  is also usable. Oxidizers  $N_2O_4$ , RFNA and  $H_2O_2$  do not require special refrigerated storage requirements such as liquid oxygen or FLOX.

Hydrogen peroxide could also be used after its catalytic dissociation in a catalyst bed. Silver is a catalyst for hydrogen peroxide. The dissociated  $H_2O_2$  ( $H_2O_2 \rightarrow H_2O + \frac{1}{2}O_2$ ) contains oxygen and can initiate combustion of solid fuel at the high temperatures of dissociation.

Nitrous oxide ( $N_2O$ ), a gas at normal ambient temperatures and pressures liquefies at a pressure of 5.4 MPa. The density of  $N_2O$  liquid is  $670 \text{ kg/m}^3$  at the room temperature of  $20^\circ\text{C}$ . At atmospheric pressure, it boils at a temperature of  $-59^\circ\text{C}$ .  $N_2O$  gas is colorless, stable and is inert with a sweet smell. It is known as laughing gas. The gas is non-flammable though it could detonate at a temperature exceeding  $650^\circ\text{C}$ .

$N_2O$  if stored at high pressure as a liquid could be directly fed into the chamber containing the solid fuel as a gas. This is due to the self pressurization characteristics from the saturated conditions at atmospheric temperatures. There would be no requirements of pumps to supply the nitrous oxide from its liquid state at pressures exceeding 5.4 MPa in the oxidizer tank nor would inert high gas pressure be required. The ullage volume above the liquid could be suitably heated, if necessary, to supply the gas at the saturated vapor condition.

Liquid  $N_2O$  has been used as an oxidizer in hybrid sounding rockets SERI-3. It has also been used in the hybrid rockets developed by Scaled Composites and Virgin Galactic for space tourism.



Stanford University and Space Propulsion Group in US developed a modified nitrous oxide by absorbing liquid oxygen in it. The resulting liquid known as Nytox, which is a combination of  $\text{N}_2\text{O}$  and  $\text{O}_2$  has a boiling temperature of  $-45^\circ\text{C}$ . The Nytox can be readily self pressurized and supplied to the combustion chamber of a hybrid rocket as a spray.

### 8.1.2 Solid Fuels

Solid fuels could be carbon or hydrocarbons. Hydrocarbons are to be preferred since the hydrogen in the fuel forms low molecular mass species in the products of combustion. The first hybrid rocket developed in early 1930's by the Russians used gelled kerosene. Carbon, poly vinyl-chloride (PVC), poly ethylene (PE), poly methyl methacrylate (PMMA –  $[\text{C}_6\text{H}_{10}\text{O}_x]_n$ ) also known as plexi-glass, rubber, hydroxyl terminated poly butadiene (HTPB) are typical solid fuels which have found applications.

Unlike the solid composite propellants which contain the above fuels and ammonium perchlorate (AP) mixed together and bonded, the pure fuels in the hybrid rocket have a very low regression rate. This is a drawback in the use of HTPB and other fuels listed earlier. The low regression rate arises from the heat transfer from the burning which drives the volatilization of the fuel. The mass of volatiles from the surface blocks the heat transfer process and this aspect will be considered later in this chapter. There have been studies on doping HTPB with AP to enhance the regression rate of the solid fuels; however, the safety of using the pure HTPB is then lost.

Addition of aluminium hydride ( $\text{AlH}_3$ ) also known as Alane to HTPB improved the regression rate and also the performance of the hybrid rocket. The improvement in performance from the addition of Alane to HTPB is also dealt with subsequently.

Compared to polymeric solid fuels discussed in the above, paraffin fuels such as paraffin wax is an alkane with a straight chain of saturated single bonds. Paraffins containing more than 15 carbon atoms are solids. The chemical formula for paraffin wax is  $\text{C}_{31}\text{H}_{64}$ . It is neither toxic nor hazardous. Tests at the Space Propulsion Group at Stanford University show its regression rate to be about three times that of HTPB. Aluminium powder or else Alane could be added to it to make it more energetic.



## 8.2 BURNING MECHANISM

The liquid oxidizer is injected as a spray of droplets or else as a gaseous oxidizer in the port volume of the solid fuel grain. When injected as a spray, the droplets evaporate forming oxidizer vapor. In either case, gaseous oxidizer moves at high velocities over the solid fuel surface.

Once a flame is initiated between the oxidizer vapor and the fuel vapor above the solid fuel surface, heat transfer from the flame will further pyrolyse the solid fuel and blow fuel vapor from the surface of the fuel grain into the free stream flow of the oxidizer. A coating of a hypergolic fuel is provided above the fuel surface or else the oxidizer vapor is initially heated to initiate the chemical reaction and the flame. A schematic of the flame and the regions of the oxidizer and fuel vapor are shown in Fig. 8.2.

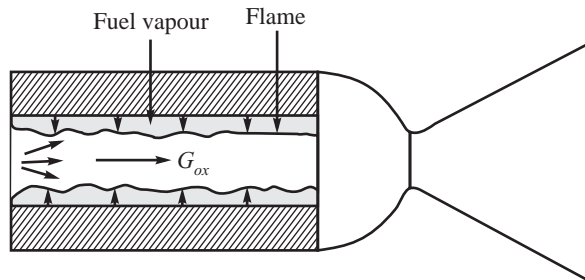


Fig. 8.2 Flame above Solid Fuel Surface

The fuel vapor moves outward from the fuel surface and mixes with the gaseous oxidizer flowing from the injector. A stoichiometric mixture of fuel and oxidizer vapor is formed in the mixing region at the boundary layer over the solid surface. Combustion takes place in this stoichiometric zone. The combustion zone in the boundary layer is sketched in Fig. 8.3. The fuel vapor blows into the boundary layer and thickens it.

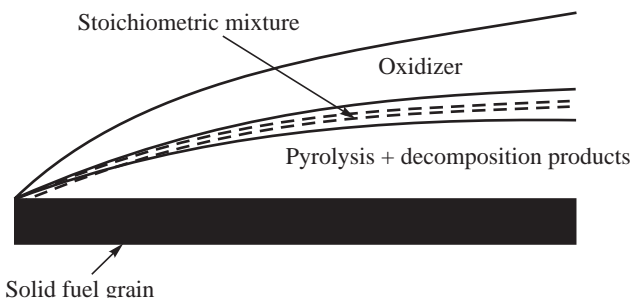


Fig. 8.3 Boundary Layer Combustion

The blowing of fuel vapor into the boundary layer from the fuel surface blocks the heat transfer from the zone of combustion to the fuel surface. This blocking of heat transfer does not permit adequate vaporization of the fuel at the surface with the result that the regression of the solid fuel remains low. In the case of a solid propellant, which contains oxidizer AP in the fuel matrix, oxidizer rich and fuel rich zones and a series of premixed and diffusion flame regions are formed. The regression rate is dominantly a function of pressure and could be modeled in terms of St. Robert's law  $r = ap^n$ . The regression rate for the fuel in the hybrid rockets is a function of the mass flux of the gaseous oxidizer flow which decides the boundary layer thickness. The regression rate  $r$  is given by:

$$r = C \left( \frac{\dot{m}_{ox}}{A_p} \right)^n = C G_{ox}^n \quad \dots(8.1)$$

In the above expression  $\dot{m}_{ox}$  is the oxidizer flow rate in kg/s,  $A_p$  is the port area in  $m^2$  and  $G_{ox}$  is the oxidizer mass flux in  $kg/(m^2 s)$ .  $C$  is a constant.

The heat transfer to the solid fuel surface is expected to be turbulent. The value of exponent ' $n$ ' would therefore be near to 0.8.

In addition, as the distance along the axis of the port increases, the oxidizer gets consumed and for a constant port area its mass flux decreases while the boundary layer thickness increases. Denoting the axial distance by  $X$ , the regression rate with respect to  $X$  would have the dependence:



$$r \sim X^{-0.2} \quad \dots(8.2)$$

similar to the heat transfer on a flat plate over which the boundary layer grows.

The dependence of the regression rate on  $G_{ox}$  and  $X$  therefore gives the dependence of the regression rate as:

$$r = aG_{ox}^n X^{-m} \quad \dots(8.3)$$

Here  $a$  is a constant. The values of  $n$  and  $m$  are 0.8 and 0.2 respectively.

The regression rate for a given oxidizer flow rate is therefore dependent on the size of the fuel grain used. As the port area of the grain increases, the regression rate will decrease if the mass flow rate of the injected oxidizer is a constant.

The mixture ratio as a function of the diameter “ $d$ ” of a port of a cylindrical grain length “ $L$ ” can be written as:

$$MR = \frac{\dot{m}_{ox}}{\dot{m}_F} = \frac{\dot{m}_{ox}}{(\pi dL)\rho_F a(4\dot{m}_{ox}/\pi d^2)^n X^{-m}} \quad \dots(8.4)$$

following Eqs. 8.1 and 8.3. On simplification the mixture ratio gives the following dependence:

$$MR \approx d^{2n-1} (\dot{m}_{ox})^{1-n} / \rho_p a L X^{-m} \quad \dots(8.5)$$

With  $n \sim 0.8$ , the mixture ratio increases with diameter and becomes fuel rich. This causes the value of the characteristic velocity  $C^*$  to continually change as the regression progresses. The performance of a hybrid propellant rocket will therefore be continually varying unlike a solid propellant rocket or a liquid propellant rocket.

The mixture ratio will also change along the length of the port.



### 8.3 TURBULATORS AND OTHER DEVICES FOR BETTER MIXING

The mixture ratio unlike in a solid or liquid propellant rocket is seen to continually vary not only along the axis but also as the diameter of the solid fuel port diameter changes as the regression proceeds. In addition, if we could model the combustion to progress along stream tubes like in the liquid propellant rocket, the stream tubes along the axis consists of pure oxidizer while the annular stream-tube at the fuel surface has pure fuel vapor. The drastic variations of mixture ratio in the combustion volume would lead to poor burning and the  $C^*$  efficiency would be small.

The mixing of the fuel and oxidizer vapor is improved by placing a diaphragm in the upstream portion of the fuel grain as shown in Fig. 8.4. It squirts the oxidizer and fuel vapor as a jet and brings about better mixing downstream of it.

Turbulence generating devices, known as turbulators, in the form of a petal nozzle or in the shape of a cruciform which lead to recirculation flow downstream of it and contributes to better mixing and flame holding. The turbulator is placed in the downstream portion of the solid fuel grain ahead of the nozzle compared to the diaphragm placed upstream. A schematic of the turbulator is shown in Fig. 8.5. Both the diaphragm and the turbulator contribute to enhance the  $C^*$  efficiency in the hybrid rocket.

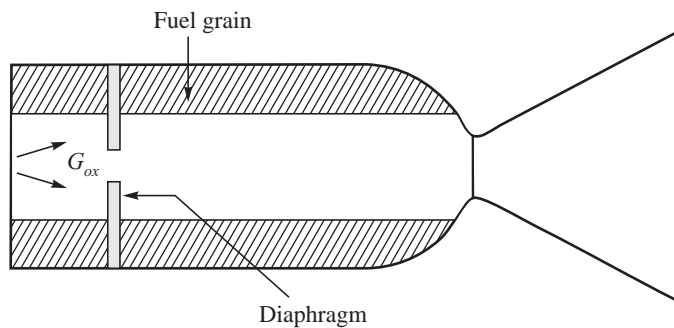


Fig. 8.4 Diaphragm Placed Upstream for Mixing

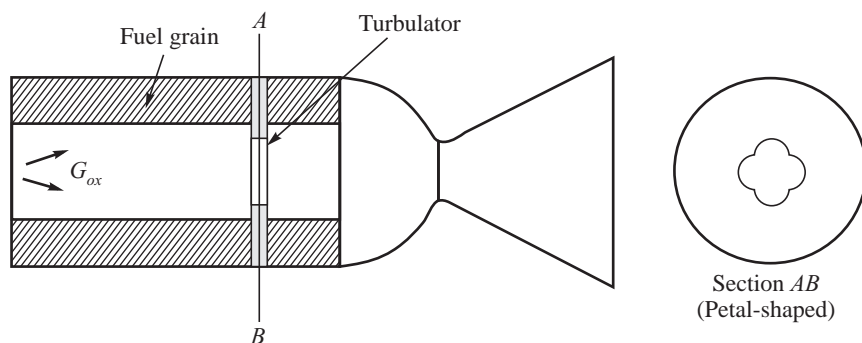


Fig. 8.5 Turbulator

The placement of a heated tube in the port volume enhances the vaporization of the oxidizer droplets and supplies ignition energy for the initiation of the reaction between the fuel and oxidizer vapor. The schematic of a heated tube in the port is shown in Fig. 8.6.

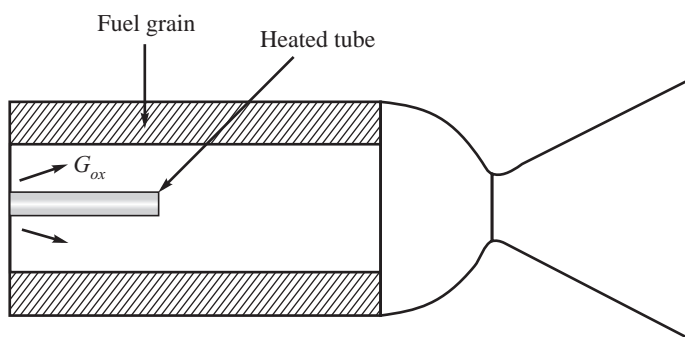


Fig. 8.6 Heated Tube for Improving Mixing and Combustion

Swirl injectors, discussed in liquid propellant rockets, provide rotational momentum to the oxidizer vapor and better mixing with the fuel vapor. However, maintenance of swirl over the entire length of the fuel grain is not possible with the result it is not very effective.



## 8.4 INITIATION OF COMBUSTION

### 8.4.1 Solid Propellant Cartridge as an Igniter

A solid propellant charge placed in a pre-chamber could initiate combustion by providing a jet of hot gases which not only heat up the oxidizer vapor but also pyrolyses the fuel vapor from the surface of the fuel grain. The hot igniter gases heat up the fuel-oxidizer mixture to the ignition temperature. Once combustion is initiated, the heat transfer from the zone of combustion sustains further vaporization of the fuel vapor and its combustion with the oxidizer vapor.

### 8.4.2 Hypergolic Ignition

A thin layer of a solid which is hypergolic with the oxidizer is coated over the solid fuel grain. When the oxidizer vapor comes in contact with it during the injection of the oxidizer into the port volume, it spontaneously ignites and sustains the combustion thereafter.

### 8.4.3 Monopropellant Pre-chamber

Hydrogen peroxide decomposed by a catalyst bed generates hot steam and oxygen. The hot gases can initiate the combustion between the oxidizer and the fuel as done by a solid propellant cartridge. The monopropellant rocket when used in conjunction with a hybrid rocket enhances the specific impulse of the hydrogen peroxide monopropellant rocket. It operates like the Augmented Electrothermal Hydrazine Thruster (AEHT).

### 8.4.4 Electrical Sparks for Ignition

The oxidizer injected into the chamber, if heated by powerful electrical sparks, could be heated up significantly. The flow of hot gases over the solid fuel grain would pyrolyze it and the mixture of the hot oxidizer and fuel would ignite in the boundary layer wherein a stoichiometric mixture is formed.



## 8.5 MULTI-PORT FUEL GRAINS

We have discussed so far about the use of a fuel grains with a single port along the centre line of the hybrid rocket chamber. Considering the poor heat transfer due to its blocking by the fuel vapor from the grain surface, the low regression rates of the fuel are not generally conducive to generate the significant values of mass flow rates required in the large thrust rockets. Wrinkling the grain surfaces is an option (such as star, wagon wheel and other configurations) but is not as effective as in the solid propellant rockets. If a large number of ports could be used and each port could be provided with injector for admitting the oxidizer, it is possible to significantly enhance the thrust. A schematic of a multi-port fuel grain is shown in Fig. 8.7.

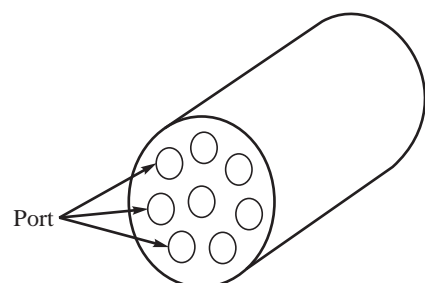


**Fig. 8.7** Multi-port Fuel Grain



However, the thickness of the grains especially at near burnout conditions should be able to withstand the pressure created in each of the ports. The structural integrity of the fuel grain is thereby compromised. The volumetric loading of the grain also gets drastically reduced. Though theoretically feasible, the application of multi-port fuel grain does not appear to be readily justifiable for larger values of thrust to be provided by the rocket.



## 8.6 PROMISING FEATURE OF PARAFFIN WAX AS FUEL FOR HYBRID ROCKETS

The low regression rate of the fuel grains was seen to be a limitation in the development of hybrid rockets. Investigations at the Space Propulsion Group and Stanford University have shown that alkanes such as solid paraffin wax form a melt layer during the combustion process in a hybrid rocket. The formation of the molten layer can be visualized by considering the formation of flame in a candle. The molten layer has low values of viscosity and surface tension.

The oxidizer gases injected at high velocities will shear off the molten layer and form droplets of the paraffin wax. The process of pyrolysis which was constrained by the blockage of heat transfer by the blowing of the pyrolyzed gases is not a limitation any more in the rate at which the solid fuel is removed from the surface. The entrained droplets of the paraffin fuel evaporate and mix with the oxidizer gases to form stoichiometric mixtures for combustion. The formation of a diffusion flame between the oxidizer vapor and the vaporized paraffin in the boundary layer is sketched in Fig. 8.8.

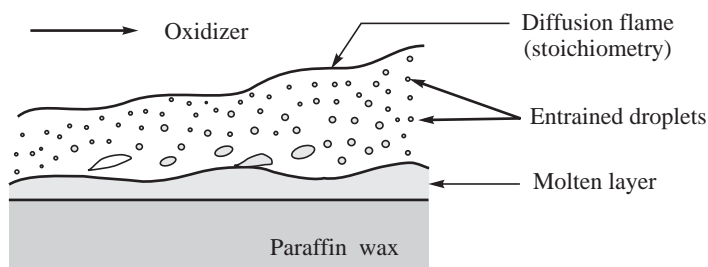


**Fig. 8.8** Modified Process of Combustion with use of Paraffin Fuel Grains

The critical pressure of paraffin is 1.2 MPa. Since the operating pressures of a hybrid rocket would be much higher than 1.2 MPa, the liquid layer would be in a supercritical state without any distinct difference between the liquid phase and the gaseous phase of its own vapor.



## 8.7 ADVANTAGES OF HYBRID ROCKETS OVER SOLID AND LIQUID PROPELLANT ROCKETS

Hybrid rockets have the solid fuel totally isolated from the liquid oxidizer and are therefore safer and less hazardous than solid and liquid propellant rockets. In a solid propellant grain, the fuel and oxidizer are intimately mixed and any accidental fire or an ignition source can lead to its burning. In the case



of liquid propellant rockets, a mixture of fuel and oxidizer can be generated and an explosion could occur from the spill of propellants from the tanks unlike with hybrid rockets. The handling and transportation of hybrid rockets especially when large thrusts are involved is definitely less hazardous.

The thrust in a hybrid rocket can be throttled unlike in a solid propellant rockets. The thrust could be terminated at will by stopping the supply of the liquid oxidizer. The throttling, thrust termination and restart features of the hybrid rocket along with its simple constructional features makes it particularly easier to develop than solid and liquid propellant rockets.

The stringent requirements of defect-free fuel grains as with solid propellant grains are not a requirement for the hybrid rockets. Cracks, pores, de-bonds and other imperfections in solid propellant rockets lead to a drastic increase in the burning surface area and an uncontrolled pressure increase leading to an explosion. In hybrid rockets, any increase in chamber pressure due to an enhancement of the burning surface area will decrease the injector pressure drop and reduce the flow of oxidizer. This would reduce the chamber pressure and stabilize the combustion process.

While the positive attributes of the hybrid rocket comprising safety, good performance, throttling, restart and thrust termination encourages their application, the problems of low frequency instability and the poor regression rates of fuels are points of concern. We shall deal with the subject of combustion instability in the next chapter.

## References

1. Chiaverini, M.J., and Kuo K.K., *Fundamentals of Hybrid Rocket Combustion and Propulsion*, Vol. 218, Progress in Astronautics and Aeronautics, Frank K. Lu, editor-in-chief, AIAA Inc., Washington, 2007.
2. Marxman, G.A., *Combustion in the Turbulent Boundary Layer on a Vaporizing Surface*, Proc. 10th Int. Symposium on Combustion, Pittsburg, 1965, pp. 1337-1349.
3. Smoot, L.D., and Price C.F., *Regression Rates of Metalized Hybrid Fuel System*, AIAA J., Vol. 4, 1966, pp. 910-915.
4. Wolfhard, H.G., Glassman I., and Green L. Jr., *Heterogeneous Combustion*, *Progress in Astronautics and Rocketry*, Vol. 15, Academic Press, New York, 1964.

## Glossary

Spaceship: A vehicle for manned flight in space

## Chapter 9

### Combustion Instability

*Whatever has overstepped its due bounds is always in a state of instability*

*Lucius Annaeus Seneca, Roman Philosopher, 1st century AD*

The combustion process in any system is never perfectly smooth. Disturbances or fluctuations occur in pressure, temperature, velocity and species comprising the combustion products. The fluctuations are not only caused by combustion but also by turbulence, flow separation and other fluid mechanical processes. The fluctuations or disturbances, under certain conditions, grow with time to form limit cycle oscillations with large amplitudes. The growth is due to the interaction between the fluctuations and the unsteadiness associated with the energy released by the combustion process. The growth of the oscillations due to interaction of the disturbances with the combustion process is spoken of as combustion instability.

The rate of energy release per unit volume in chemical rockets from the combustion process, viz., the power density is very much higher than in the other propulsive devices. This is indicated in Fig. 9.1. The power density of the combustion chamber in a high pressure and high thrust rocket is about  $10^3$  kW/cm<sup>3</sup>. This is about four to five orders of magnitude greater than the power density of an automobile engine and about two to three orders of magnitude greater than in a gas turbine combustor. The power density is of the same order of magnitude as in an explosion. If a minuscule part of this large energy release rate (from the combustion process) goes into increasing the amplitude of the fluctuations, it would result in very large amplitudes of oscillations. Large amplitude oscillations are undesirable since they could lead to rapid enhancement in heat transfer and excessive vibrations and to thermal and mechanical failure of components, high levels of noise, and unacceptably high burn rates of the propellants. Combustion instability must, therefore, be avoided. The different ways in which combustion instability could manifest in rockets, the parameters influencing instability and methods of controlling and preventing their occurrence are dealt with in this chapter.

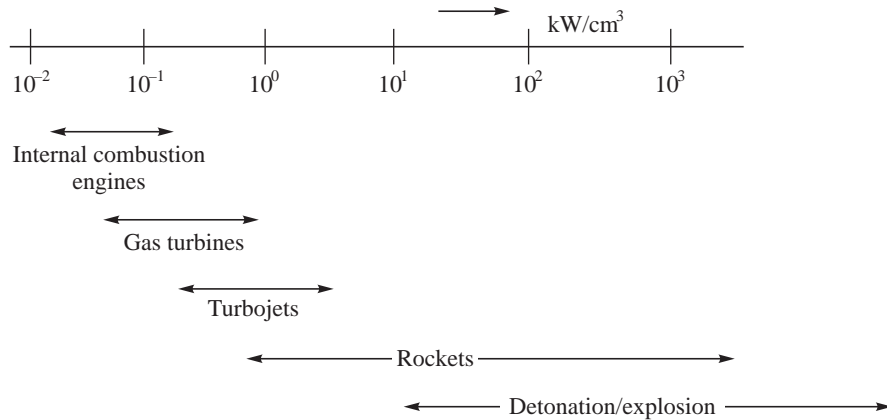


**Fig. 9.1 Power Density of Different Propulsive Devices**



## 9.1 BULK AND WAVE MODES OF COMBUSTION INSTABILITY

The oscillations or disturbances which originate in the combustion chamber could either occur in unison over the entire volume of the chamber or with different amplitudes and phases in different locations in the chamber. When the entire volume or bulk of the gas in the combustion chamber oscillates in unison as a lumped mass, the combustion instability is said to be in the bulk mode. When the oscillations at the different locations of the combustion chamber are not in phase and the fluctuations are transmitted by motion of waves, the instability is said to be in the wave mode. We shall illustrate these two modes through typical examples before analyzing the causes and determining the procedures to avoid the occurrence of combustion instability.

### 9.1.1 A Simple Example Illustrating the Bulk Mode of Instability

We follow a simple example discussed by Summerfield. A hypothetical liquid propellant rocket using a single propellant, shown schematically in Fig. 9.2, is considered. For a given area of injection ( $A_0$ ), density of the propellant ( $\rho$ ) and discharge coefficient for flow through the injection orifices ( $C_d$ ), the mass flow rate of the propellant  $\dot{m}_p$  into the combustion chamber is:

$$\dot{m}_p = C_d A_0 \sqrt{2\rho (p_{\text{inj}} - p_C)}$$

Here,  $p_{\text{inj}}$  is the pressure at which the liquid is supplied to the injector and  $p_C$  is the chamber pressure. If the injection pressure  $p_{\text{inj}}$  is maintained constant, the chamber pressure  $p_C$  can be determined from the steady state mass flow conservation conditions, viz., the injected flow rate  $\dot{m}_p$  equals the flow rate through the nozzle  $\dot{m}_n$  giving the relation:

$$\dot{m}_p = C_d A_0 \sqrt{2\rho (p_{\text{inj}} - p_C)} = \dot{m}_n = \frac{p_C A_t}{C^*} \quad \dots(9.1)$$

In the above expression,  $A_t$  is the nozzle throat area and  $C^*$  is the characteristic velocity. For a given rocket  $C_d$ ,  $A_0$ ,  $\rho$  and  $C^*$  are constants and the value of  $p_C$  is proportional to  $\dot{m}_p$ . We shall, in the following, deal with the possibilities of achieving oscillations of chamber pressure by varying the injection pressure.

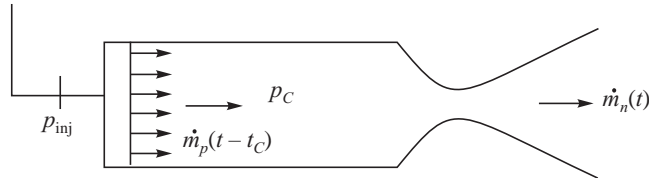


Fig. 9.2 Simplified Scheme of Propellant Injection and Mass Efflux

#### (a) Constant Amplitude Oscillations

Let us consider an example in which the chamber pressure is 5 MPa and the pressure at which the liquid is supplied to the combustion chamber is 7.5 MPa. The mass rate of injection  $\dot{m}_p$  is proportional to  $\sqrt{(7.5 - 5)}$  since the other parameters  $C_d$ ,  $A_0$  and  $\rho$  are constants. Let this steady mass flow rate be indicated as  $\bar{m}$ . The values of  $\dot{m}_p$  and  $p_C$  are steady at  $\bar{m}$  and 5 MPa respectively, and are shown in Fig. 9.3 for the initial time till  $t_0$ .

If there is a sudden drop in chamber pressure from 5 to 4.5 MPa at time  $t_0$  (shown by AB in Fig. 9.3) due to some perturbation in the system, an additional pressure drop of 0.5 MPa becomes available at  $t = t_0$  for the injection of the propellant. The mass flow rate through the injector becomes proportional to  $\sqrt{(7.5 - 4.5)}$  instead of  $\sqrt{(7.5 - 5)}$ . The flow rate, therefore, increases in the proportion  $\sqrt{3/2.5} \approx 1.1$  times the original steady state flow rate as shown in Fig. 9.3. This flow gets converted to hot gases after a certain time delay ( $t_C$ ) which corresponds to the time required to vaporize and burn the propellant. The time delay  $t_C$  depends on the type of propellant used and the atomization, vaporisation and mixing of the propellant vapours.

Since the chamber pressure is proportional to the mass flow rate, the value of  $p_C$  becomes 5.5 MPa after the time delay ( $t_C$ ). This is shown by the line CD in Fig. 9.3. The higher flow rate of 1.1 times the nominal flow  $\bar{m}$  through the injector precedes the increase in  $p_C$  and is shown by the line B' C'.

Once the chamber pressure is 5.5 MPa (D in Fig. 9.3), the mass injected becomes proportional to  $\sqrt{7.5 - 5.5}$  which is  $\sqrt{2/2.5}$ , i.e. 0.9 times the flow rate corresponding the steady flow  $\bar{m}$  for a  $p_C$  of 5 MPa. The reduced flow rate, shown by D' E' in Fig. 9.3, reduces the chamber pressure to  $0.9 \times 5 = 4.5$  MPa (point F). The sequence of changes continues with chamber pressure oscillating between 4.5 and 5.5 MPa (Fig. 9.3).

#### (b) Increasing Amplitude of Oscillations

Consider a different scenario of a steady state chamber pressure of 5 MPa but with an injection pressure of 7 MPa. A sudden drop in the chamber pressure from 5 to 4.5 MPa (as in the previous

discussion) causes the mass flow rate to increase by a fraction  $\sqrt{\frac{7 - 4.5}{7 - 5}} = 1.12$ . This results in the chamber pressure jumping to 5.59 MPa after a delay of time  $t_C$  (Fig. 9.4). The increased value of  $p_C$  of 5.59 MPa reduces the mass flow rate to  $\sqrt{\frac{7 - 5.59}{7 - 5}} = 0.84$  of the steady value corresponding to  $p_C$  of 5 MPa. The chamber pressure, therefore, drops to 4.2 MPa. The reduced value of  $p_C$  of 4.2 MPa

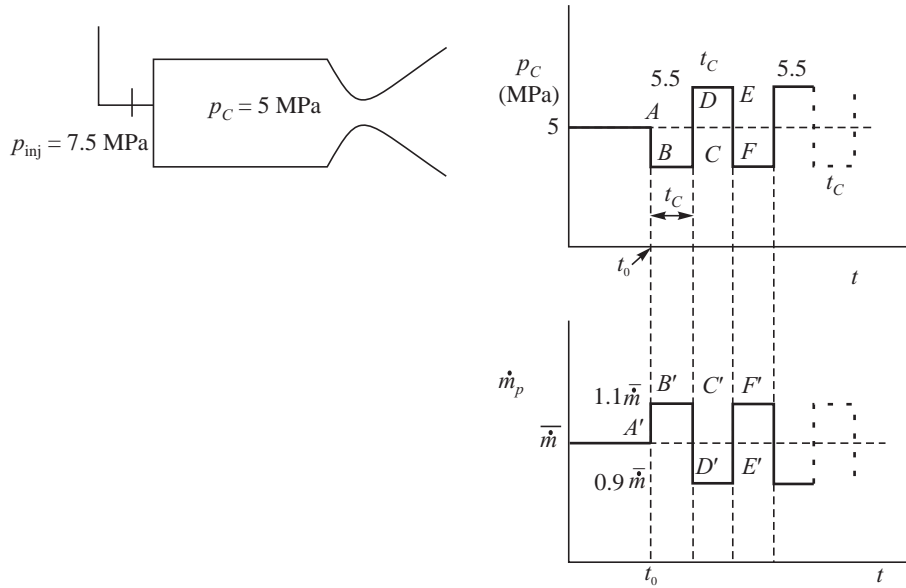


Fig. 9.3 Changes of Chamber Pressure and Mass Flow Rate with Time

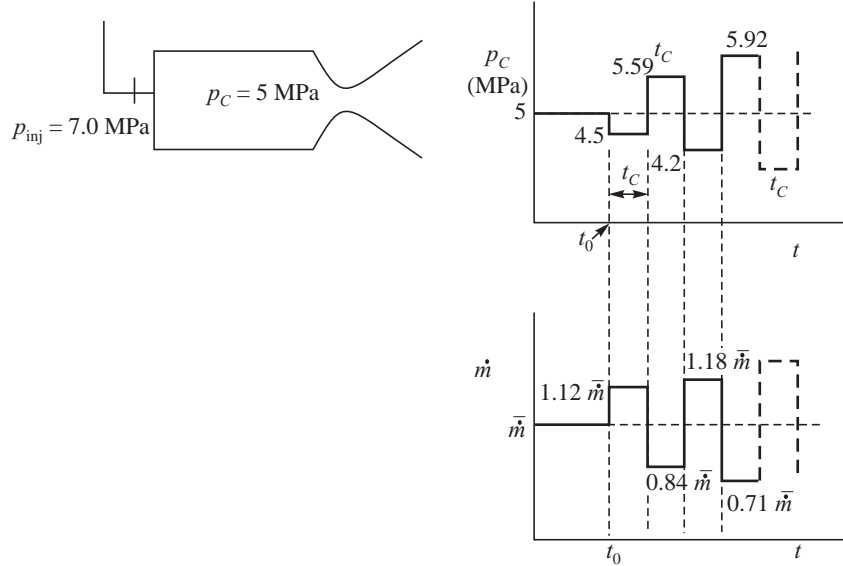


Fig. 9.4 Increasing Amplitudes of Oscillations

causes an increase in the mass flow rate by a factor  $\sqrt{\frac{7-4.2}{7-5}} = 1.18$ . The value of  $p_C$  accordingly

becomes 5.92 MPa. The sequence of changes of the chamber pressure and mass flow rates is shown in Fig. 9.4. It is seen that the amplitude of oscillations progressively increases with time.

### (c) Decaying Amplitudes

For a third scenario of chamber pressure of 5 MPa and a propellant injection pressure of 9 MPa, the sequence of changes in the mass flow rates and chamber pressure after the chamber pressure falls



suddenly to 4.5 MPa is shown in Fig. 9.5. The fall in chamber pressure to 4.5 MPa increases the flow rate by a factor  $\sqrt{\frac{9-4.5}{9-5}} = 1.061$ . This causes the chamber pressure to increase to 5.3 MPa after a delay of time  $t_C$ . The increased chamber pressure of 5.3 MPa reduces the mass flow rate by  $\sqrt{\frac{9-5.3}{9-5}} = 0.962$  with a consequent reduction of  $p_C$  to 4.8 MPa. The reduced value of  $p_C$  enhances the mass flow rate by  $\sqrt{\frac{9-4.8}{9-5}} = 1.025$  causing  $p_C$  to become 5.12 MPa. The amplitudes of the oscillations are seen to decay (Fig. 9.5).

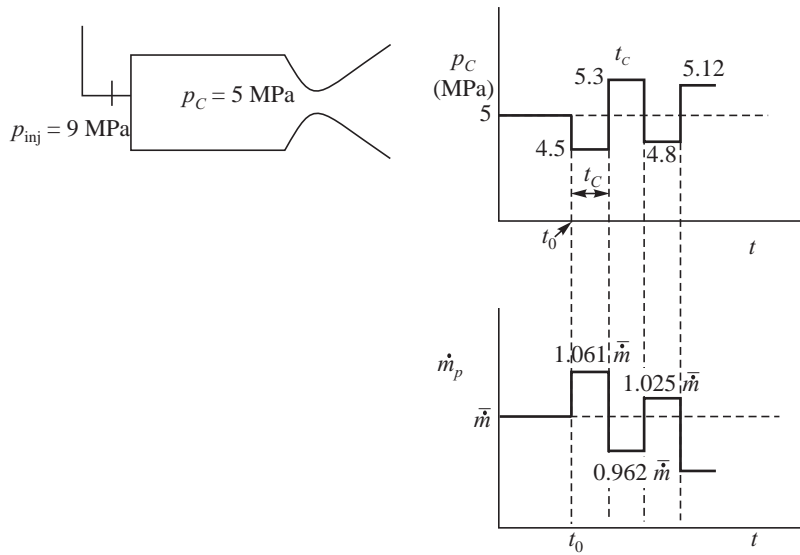


Fig. 9.5 Decaying Amplitudes of Oscillations

#### (d) Bulk Mode of Instability

The chamber pressure was observed to oscillate with constant amplitude when  $p_{\text{inj}} = 7.5$  MPa (Fig. 9.3). For  $p_{\text{inj}} = 9$  MPa, the amplitude of the oscillations decayed (Fig. 9.5) whereas for  $p_{\text{inj}} = 7$  MPa, the amplitude of the oscillations increased (Fig. 9.4). Changes in the pressure drop across the injector, caused a proportional variation in mass flow rate which, after the combustion delay of time  $t_C$ , gave rise to a change of chamber pressure and a cycle of disturbances. Figure 9.6 is a block diagram illustrating the process. Mass  $\dot{m}_p$  is injected into the chamber. The chamber pressure responds after a time delay  $t_C$ . It is the feedback of the change of chamber pressure with a delayed response which causes the oscillations. The oscillations are termed as bulk mode of combustion instability since the entire volume or bulk of the gases in the combustion chamber oscillates.

If the calculations are repeated for different values of injection pressures, it will be seen that combustion instability results when  $(p_{\text{inj}} - p_C) < p_C / 2$ . A detailed analysis of the bulk mode of oscillations and factors controlling it are given in Sections 9.2 and 9.3 of this chapter.

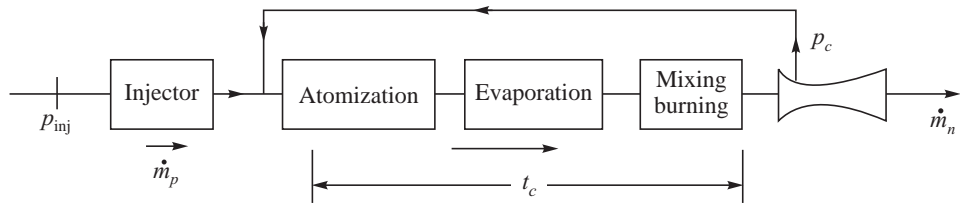


Fig. 9.6. Block Diagram of the Feedback

### 9.1.2 Standing Waves in Combustion Chamber

The combustion chamber of a rocket, whether solid propellant or liquid propellant, is in the form of a cavity. Any disturbance generated in a cavity at some local zone, such as the flame zone will travel in the cavity. Let us consider the motion of a sinusoidal pressure wave travelling along the axial length  $X$  of a cavity with velocity  $a$ , as shown in Fig. 9.7(a). The waveform is shown in Fig. 9.7(b). Over a duration  $t$ , the wave moves by a distance  $at$  to occupy the dotted position shown in Fig. 9.7. The pressure fluctuations in the travelling wave can be represented by:

$$p' = A \sin \frac{2\pi}{\lambda} (x - at) \quad \dots(9.2)$$

Here  $A$  denotes the maximum pressure amplitude of the wave.  $\lambda$  is the wavelength. For weak pressure waves such as sound waves, the wave velocity  $a$  is the sound speed.

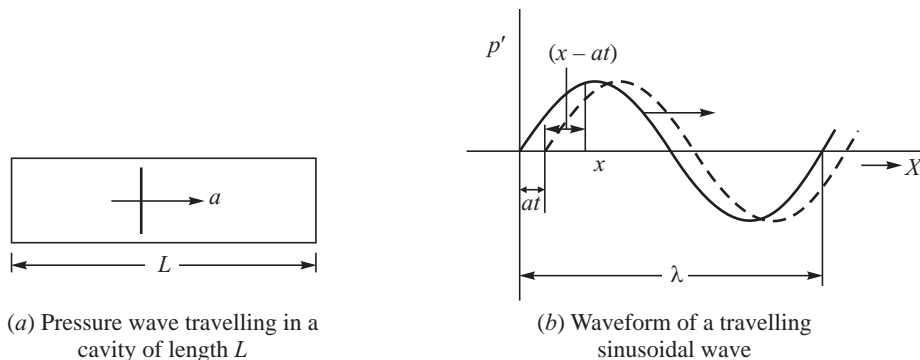


Fig. 9.7 Travelling Pressure Waves

The wave gets reflected at the end of the cavity. Let us consider the ends of the cavity to be closed with perfect reflecting surfaces. The wave would get reflected without any attenuation of the amplitude. The equation of the reflected wave, which travels in a direction opposite to the incident wave, is given by:

$$p' = A \sin \frac{2\pi}{\lambda} (-x - at) = -A \sin \frac{2\pi}{\lambda} (x + at) \quad \dots(9.3)$$

The interaction of the incident and reflected wave gives the resulting wave as:

$$p' = A \sin \frac{2\pi}{\lambda} (x - at) - A \sin \frac{2\pi}{\lambda} (x + at) \quad \dots(9.4)$$



Denoting the time taken by the wave to travel one wavelength as the time period  $T$ , we have:

$$T = \frac{\lambda}{a} \text{ or frequency } f = \frac{1}{T} = \frac{a}{\lambda} \quad \dots(9.5)$$

The circular frequency  $\omega$  can be written as  $\omega = 2\pi f$ , giving

$$a = \frac{\lambda}{2\pi}\omega \quad \dots(9.6)$$

Defining a term wave number as  $K = \frac{2\pi}{\lambda}$ , eq. 9.4 is written as:

$$p' = A \sin (Kx - \omega t) - A \sin (Kx + \omega t) \quad \dots(9.7)$$

Expanding  $\sin (Kx - \omega t)$  and  $\sin (Kx + \omega t)$  and simplifying, the above expression becomes:

$$p' = -2A \cos Kx \sin \omega t \quad \dots(9.8)$$

This is seen from the expansion of  $\sin (A - B) = \sin A \cos B - \cos A \sin B$  and  $\sin (A + B) = \sin A \cos B + \cos A \sin B$ , giving  $\sin (A - B) - \sin (A + B) = -2 \cos A \sin B$ .

Equation 9.8 for the resulting wave does not contain the traveling component  $at$ . Instead of moving, as in the incident and reflected wave of eqs. 9.2 and 9.3, it is stationary. At locations where  $\cos Kx = 0$ , the pressure perturbations are zero. At locations where  $\cos Kx = 1$ , the pressure perturbations are maximum. The zero pressure disturbances are known as pressure nodes while the maximum pressure disturbances are called pressure antinodes. The resulting wave has fixed locations of maximum and minimum amplitudes and is called a stationary wave or standing wave.

The combustion chamber of a rocket is in the form of a cylindrical cavity and has one closed and one open end. The open end is the nozzle. The rapid acceleration of the gas at the throat region of the nozzle causes large density gradients which reflect the waves as if it were a closed end. The rocket chamber essentially, therefore, conforms to a cavity with both ends closed. The velocities behind the wave are brought to zero at the closed ends. The pressure disturbance is, therefore, a maximum here. If we denote the length of the chamber up to the nozzle throat as  $L$ , we have, considering the resulting eq. 9.8, the condition at the closed end  $x = L$  as:

$$\cos KL = 1 \quad \dots(9.9)$$

giving

$$KL = n\pi \text{ with } n = 1, 2, 3, \dots \quad \dots(9.10)$$

Substituting the value of wave number  $K = 2\pi/\lambda$  in the above equation, we get:

$$\lambda = \frac{2L}{n}$$

This gives the frequency of oscillations as:

$$f = \frac{a}{2L/n} = \frac{na}{2L} \quad \dots(9.11)$$

$n = 1$  corresponds to the basic or fundamental mode of oscillation. The frequency is  $a/2L$ . The wave form is shown in Fig. 9.8. The pressure antinodes are at the ends, viz.,  $x = 0$  and at  $x = L$ . At  $x = L/2$ , the amplitude of the pressure perturbations is proportional to  $\cos 2\pi/2$ , which for  $n = 1$  is zero. The amplitude of the pressure oscillation is, therefore, zero giving a pressure node at  $x = L/2$  as shown.

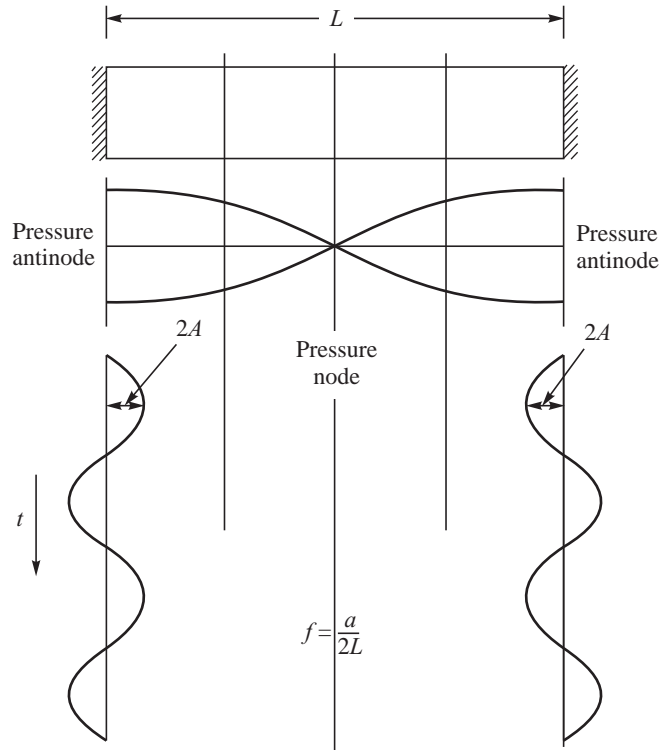


**Fig. 9.8** Standing Wave in Fundamental Mode

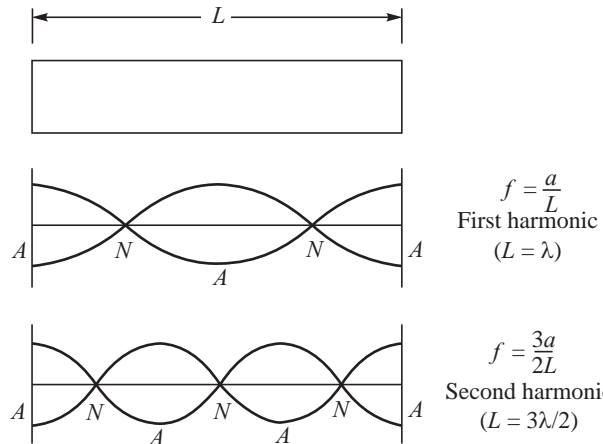
The stationary waves corresponding to  $n \geq 2$  are the harmonics. The first harmonic is  $n = 2$  and has a frequency  $f = a/L$ . The waveforms are shown for the first harmonic and second harmonic in Fig. 9.9. Three pressure antinodes and two pressure nodes are seen for the first harmonic. The second harmonic is for  $n = 3$  with a frequency of  $f = 3a/2L$  (Fig. 9.9) for which there are four pressure antinodes and three pressure nodes.

The velocity perturbations in the chamber can be derived from the above pressure perturbations by relating the velocity and pressure through the momentum equation  $\frac{dv}{dt} = -\frac{1}{\rho} \frac{dp}{dx}$ . We get the

functional form of the velocity perturbation  $v'$  from the pressure perturbation  $p'$  given by eq. 9.8, by differentiating it with respect to  $x$  and integrating with respect to  $t$  to give the form of velocity perturbation as:

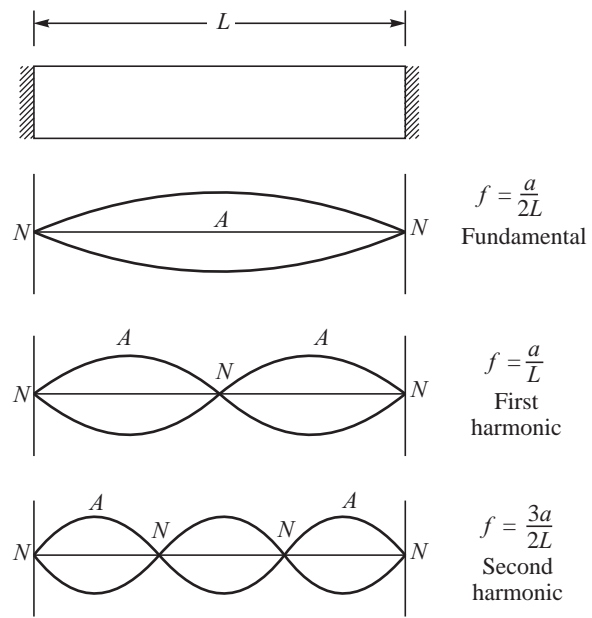
$$v' = -B \sin Kx \cos \omega t = B \sin Kx \sin \left( \omega t - \frac{\pi}{2} \right) \quad \dots(9.12)$$

Here  $B$  is the maximum amplitude of the velocity perturbation. The velocity perturbation is seen to lag the pressure perturbations by  $\pi/2$ . From eq. 9.12, the velocity perturbations are seen to be zero at  $x = 0$  and at  $x = L$  for which the pressure perturbations are maximum. At the closed ends of the cavity we, therefore, have velocity nodes. The velocity antinode is at  $x = L/2$  for  $n = 1$ . The positions of the velocity nodes and antinodes for the fundamental and the first and second harmonics are shown in Fig. 9.10. The frequency, as determined earlier, is  $f = na/2L$ .



(N: Pressure node; A: Pressure antinode)

**Fig. 9.9** Pressure Nodes and Antinodes for the First and Second Harmonic



(N: Velocity node; A: Velocity antinode)

**Fig. 9.10** Velocity Nodes and Antinodes in the Fundamental, First and Second Harmonic

### 9.1.3 Wave Mode of Combustion Instability

Combustion in an end-burning solid propellant rocket takes place at the location of the pressure antinode, corresponding to the fundamental as well as the higher harmonics. For a liquid propellant rocket, the combustion of the injected mass of propellants, if very rapid, also takes place at the zone of the pressure antinode. This is shown in Fig. 9.11. If the interactions of the higher levels of the



amplitude of pressure perturbations, present at the antinodes of the standing wave, bring about an enhancement of energy release during the combustion process, and the energy release in-turn augments the amplitude of pressure oscillations, growth of amplitude of the oscillations takes place. The process of enhancement of the amplitude of the standing waves by energy released from combustion is the wave mode of combustion instability. The nature of the standing wave formed in the combustion chamber and the interaction of the combustion process with the standing wave govern the combustion instability of the wave mode. Details are given in Section 9.4.

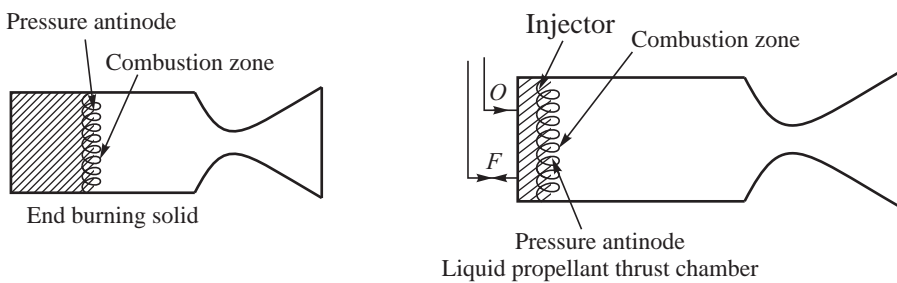


**Fig. 9.11** Burning Zones at Pressure Antinode



## 9.2 ANALYSIS PROCEDURE FOR BULK MODE OF COMBUSTION INSTABILITY IN LIQUID PROPELLANT ROCKETS

The accumulation of propellants in the chamber during the combustion delay period ( $t_C$ ) was seen to be responsible for the oscillations, in the example cited for the bulk mode of combustion instability in Section 9.1.1. If the rate of mass of the hot gas getting generated in a combustion chamber is  $\dot{m}_g$ , and the rate of mass leaving is  $\dot{m}_n$ , the rate of accumulation of mass in the chamber is:

$$\frac{dm}{dt} = \dot{m}_g - \dot{m}_n \quad \dots(9.13)$$

The mass flow rate of propellant injected into the chamber  $\dot{m}_p$  gets converted into hot gas only after a combustion delay  $t_C$ . The parcel of gas leaving the nozzle  $\dot{m}_n$  and the mass of hot gases which accumulate in the chamber  $dm/dt$  would therefore correspond to the propellant injected at time  $t_C$  earlier. The mass balance given by eq. 9.13 is therefore written in terms of mass flow rate of propellant injected  $\dot{m}_p$  as:

$$\frac{dm}{dt} = \dot{m}_p (t - t_C) - \dot{m}_n \quad \dots(9.14)$$

Following the discussions in Section 9.1.1, the rate of propellant injection is given by  $\dot{m}_p = C_d A_0 \sqrt{2\rho(p_{\text{inj}} - p_C)}$ . The mass flow rate through the nozzle  $\dot{m}_n = \frac{1}{C^*} p_C A_t$ . The mass of gas in the chamber  $m$  in Eq. 9.14 is given as  $p_C V_C / RT_C$ , where  $V_C$  is the chamber volume,  $T_C$  is the temperature of the hot gases in the chamber and  $R$  is the specific gas constant. Substituting these values in eq. 9.14 for a fixed chamber volume  $V_C$ , gives:



$$\frac{dp_C}{dt} = \frac{RT_C}{V_C} \left[ C_d A_0 \sqrt{2\rho(p_{inj} - p_C)} \right]_{(t-t_c)} - \frac{1}{C^*} \frac{RT_C}{V_C} p_C A_t \quad \dots(9.15)$$

Here the temperature of the gas in the chamber  $T_C$  is taken as a constant. Noting that the characteristic velocity  $C^* = \frac{1}{\Gamma} \sqrt{RT_C}$  and the characteristic length of the motor  $L^* = V_C/A_t$ , the term

$\frac{1}{C^*} \frac{RT_C}{V_C} p_C A_t$  in eq. 9.15 reduces to:

$$\frac{1}{C^*} \frac{RT_C}{V_C} p_C A_t = \frac{\Gamma \sqrt{RT_C}}{V_C/A_t} p_C = \frac{\Gamma^2 C^*}{L^*} p_C \quad \dots(9.16)$$

The term  $\frac{RT_C}{V_C} \left[ C_d A_0 \sqrt{2\rho(p_{inj} - p_C)} \right]_{(t-t_c)}$  in eq. 9.15 is to be determined when the chamber pressure fluctuates. For this purpose, we introduce a perturbation in chamber pressure  $p_C = \bar{p}_C + p'$ , where  $\bar{p}_C$  is the steady state value of chamber pressure and  $p'$  is the pressure fluctuation and substitute in eq. 9.15, to give:

$$\frac{RT_C}{V_C} \left[ C_d A_0 \sqrt{2\rho(p_{inj} - p_C)} \right]_{(t-t_c)} = \frac{RT_C}{V_C} C_d A_0 \sqrt{2\rho(p_{inj} - \bar{p}_C)} \left( 1 - \frac{p'}{p_{inj} - \bar{p}_C} \right)^{1/2} \Big|_{(t-t_c)}$$

But  $C_d A_0 \sqrt{2\rho(p_{inj} - \bar{p}_C)}$  corresponds to the steady state flow which equals  $\frac{1}{C^*} \bar{p}_C A_t$ . Equation 9.15 can, therefore, be simplified to give:

$$\frac{dp_C}{dt} = \frac{\Gamma^2 C^*}{L^*} \bar{p}_C \left( 1 - \frac{p'}{p_{inj} - \bar{p}_C} \right)^{1/2} \Big|_{(t-t_c)} - \frac{\Gamma^2 C^*}{L^*} p_C \quad \dots(9.17)$$

The term  $\frac{L^*}{C^* \Gamma^2}$  has dimensions of time. It represents the stay time or residence time of the propellants in the chamber. This can be seen as follows. The residence time  $t_{res}$  is given by the ratio of the volume of the chamber ( $V_C$ ) to the volume flow rate of the propellants ( $\dot{V}$ ):

$$t_{res} = \frac{V_C}{\dot{V}} \quad \dots(9.18)$$

Expressing the volume flow rate in terms of mass flow rate and expressing the density of the gases as a function of the chamber pressure and temperature, we get:

$$t_{res} = \frac{V_C}{\dot{m}_g / \rho} = \frac{V_C p_C}{\dot{m}_g RT_C} \quad \dots(9.19)$$

Under steady state flow conditions  $\dot{m}_g = \frac{1}{C^*} p_C A_t$ . Substituting the value of  $\dot{m}_g$  in the expression for  $t_{res}$  gives:



$$\frac{t_{\text{res}}}{V_C p_C} = \frac{C^*}{RT_C} \frac{C^*}{p_C A_t} = \frac{L^*}{C^* \Gamma^2} \quad \dots(9.20)$$

Simplifying eq. 9.17 using the above value of residence time and assuming the pressure fluctuation  $p'$  to be small compared to the steady state value of injection pressure drop ( $p_{\text{inj}} - \bar{p}_C$ ) we have:

$$\frac{dp_C}{dt} = \frac{\bar{p}_C}{t_{\text{res}}} \left[ 1 - \frac{1}{2} \left( \frac{p'}{p_{\text{inj}} - \bar{p}_C} \right) \right] - \frac{p_C}{t_{\text{res}}} \quad \dots(9.21)$$

Expressing the pressure perturbation  $p'$  non-dimensionally as  $\phi = \frac{p'}{\bar{p}_C}$ , and denoting  $\frac{\bar{p}_C}{2(p_{\text{inj}} - \bar{p}_C)}$  as  $\beta$ , we have:

$$\frac{dp_C}{dt} = \frac{\bar{p}_C}{t_{\text{res}}} [1 - \beta \phi(t - t_c)] - \frac{p_C}{t_{\text{res}}} \quad \dots(9.22)$$

With  $p_C = \bar{p}_C(1 + \phi)$ , the above expression becomes:

$$\frac{d\phi}{dt} + \frac{\phi}{t_{\text{res}}} = -\frac{\beta}{t_{\text{res}}} \phi(t - t_c) \quad \dots(9.23)$$

The growth of the amplitude of the pressure perturbations can be expressed as:

$$\phi = Ae^{(\alpha + i\omega)t} \quad \dots(9.24)$$

where  $\omega$  is the circular frequency ( $= 2\pi f$ ) and  $\alpha$  denotes the growth of the perturbations.  $\alpha$  is known as the growth constant. If  $\alpha > 0$ , the perturbation in pressure grows with time. If  $\alpha < 0$ , the pressure perturbation decays as the time progresses. For  $\alpha = 0$ , the amplitude of the oscillations remain constant.

Substituting eq. 9.24 in eq. 9.23 and separating the real and imaginary parts, we get:

$$\alpha + \frac{1}{t_{\text{res}}} = -\frac{\beta}{t_{\text{res}}} e^{-at_c} \cos \omega t_c \quad \dots(9.25)$$

$$\omega = \frac{\beta}{t_{\text{res}}} e^{-at_c} \sin \omega t_c \quad \dots(9.26)$$

Here  $\phi(t - t_c)$  in eq. 9.23 is expressed as  $Ae^{(\alpha + i\omega)(t - t_c)}$  and  $e^{-i\omega t_c}$  is written as  $\cos \omega t_c - i \sin \omega t_c$ .

Solving eqs. 9.25 and 9.26 for  $\alpha = 0$ , which is the boundary between a stable ( $\alpha < 0$ ) and unstable process ( $\alpha > 0$ ), we have:

$$\frac{1}{t_{\text{res}}} = \frac{\beta}{t_{\text{res}}} \cos \omega t_c \quad \dots(9.27)$$

$$\omega = \frac{\beta}{t_{\text{res}}} \sin \omega t_c \quad \dots(9.28)$$

This gives

$$\cos \omega t_c = -\frac{1}{\beta} \quad \dots(9.29)$$

and

$$\sin \omega t_c = \frac{\omega t_{\text{res}}}{\beta} \quad \dots(9.30)$$



Solving the above two equations, we get:

$$(\omega t_{\text{res}})^2 + 1 = \beta^2 \text{ giving } \omega^2 = \frac{\beta^2 - 1}{t_{\text{res}}^2} \text{ or } \omega t_{\text{res}} = \sqrt{\beta^2 - 1} \quad \dots(9.31)$$

and

$$\sec \omega t_C = -\beta \text{ i.e., } \tan \omega t_C = \sqrt{\beta^2 - 1} \text{ giving:}$$

$$\omega t_C = \pi - \tan^{-1} \sqrt{\beta^2 - 1} \quad \dots(9.32)$$

The frequency is seen to be inversely proportional to the combustion time delay  $t_C$  for a given value of the injection pressure drop parameter  $\beta$ . As  $\beta$  increases the frequency decreases as per eq. 9.32.

Dividing eq. 9.32 by eq. 9.31, we have:

$$\frac{t_C}{t_{\text{res}}} = \frac{\pi - \tan^{-1} \sqrt{\beta^2 - 1}}{\sqrt{\beta^2 - 1}} \quad \dots(9.33)$$

The above condition holds good for  $\alpha = 0$ , i.e. the amplitude of oscillations do not grow or decay. The condition for  $\alpha < 0$ , for which the waves will not grow, can be deduced from the above expression by noting that  $\alpha$  decreases for given values of  $\beta$ ,  $\omega$  and  $t_C$  as  $t_{\text{res}}$  increases (eq. 9.26). The condition for  $\alpha < 0$  from eq. 9.33 is, therefore:

$$\frac{t_C}{t_{\text{res}}} \leq \frac{\pi - \tan^{-1} \sqrt{\beta^2 - 1}}{\sqrt{\beta^2 - 1}} \quad \dots(9.34)$$

A plot of  $t_C/t_{\text{res}}$  as a function of  $\beta$ , given by eqs. 9.33 and 9.34, is shown in Fig. 9.12. As  $\beta$  tends to unity,  $t_C/t_{\text{res}} \rightarrow \infty$ . When  $\beta \rightarrow \infty$ ,  $t_C/t_{\text{res}}$  tends to zero. The variation of  $\beta$  for which  $\alpha < 0$  is shown shaded in Fig. 9.12. It is seen that for small values of combustion delay  $t_C$ , or large values of residence time  $t_{\text{res}}$ , the combustion is stable ( $\alpha \leq 0$ ) even for a large value of  $\beta$ .

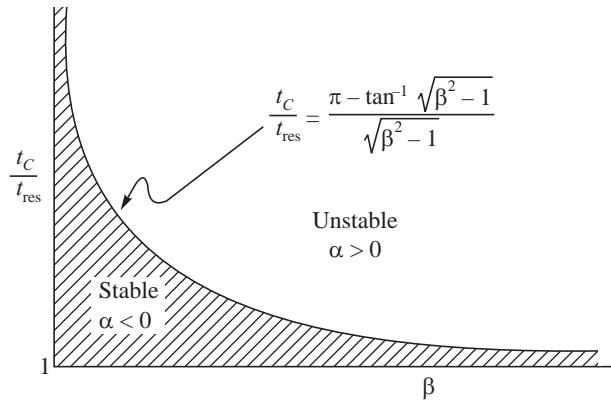


**Fig. 9.12** Stable and Unstable Zones

The analysis shows combustion instability to occur when  $\beta \approx 1$  in the limit of large combustion delays or very small residence times. For other values of the characteristic times,  $\beta$  has to exceed a

threshold value (greater than 1) for combustion instability to occur. As the ratio of  $\frac{t_C}{t_{\text{res}}}$  decreases, the



threshold value of  $\beta$  increases.  $\beta$  was defined as  $\frac{\bar{p}_C}{2(p_{\text{inj}} - \bar{p}_C)}$  in eq. 9.22. If the pressure drop across the injector ( $p_{\text{inj}} - \bar{p}_C$ ) is denoted by  $\Delta p_{\text{inj}}$ , we observe that for large combustion delays ( $t_C \rightarrow \infty$ ) or for small residence times ( $t_{\text{res}} \rightarrow 0$ ), combustion instability will occur for  $\frac{\bar{p}_C}{2\Delta p_{\text{inj}}} > 1$ . This is equivalent to stating that combustion instability will occur when:

$$\frac{\Delta p_{\text{inj}}}{\bar{p}_C} < \frac{1}{2} \quad \dots(9.35)$$

The injection pressure drop should, therefore, exceed a threshold value of half the chamber pressure for combustion to be stable in the bulk mode of oscillations. This is the same result which was stated in the illustrative example given in Section 9.1.1.

The criterion for stability can be readily extended for a bipropellant rocket having a mixture ratio  $R$  as:

$$\frac{\Delta p_{\text{inj}} |_{\text{oxidizer}}}{p_C} > \frac{R}{1+R} \quad \dots(9.36)$$

and

$$\frac{\Delta p_{\text{inj}} |_{\text{fuel}}}{p_C} > \frac{1}{1+R} \quad \dots(9.37)$$

for oxidizer injection and fuel injection respectively. This criterion is known as Summerfield criterion.

It is valid for large values of  $\frac{t_C}{t_{\text{res}}}$ , i.e., large combustion delay times or small residence times. When combustion delay times are small or the residence time is large, a much lower value of injection pressure drop is adequate to ensure stability of combustion.

A less reactive propellant or a small combustion chamber is more likely to exhibit the bulk mode of instability, based on the above analysis. Since the injection pressure drop plays a major role in causing this bulk mode of combustion instability, and the injection pressure drop depends on the supply pressure from the feed system, this instability is also known as feed system coupled combustion instability.

The pressure perturbation  $p'$  causes perturbations in the mass flow rate of oxidizer  $\dot{m}_{\text{ox}}$  and in the mass flow rate of the fuel  $\dot{m}_f$  as shown in the block diagram in Fig. 9.13. This provides fluctuations in the quantities of vapour formed after an evaporation time for the fuel and oxidizer respectively. The mass of gas formed from the mixing and reaction of the vapours further delays the generation of the perturbed combustion products. The delay is associated with injection, vaporisation, mixing and chemical reaction; the total of which is  $t_C$ .

A delayed rate of hot gas produced from an oscillation in chamber pressure leads to an increase in the chamber pressure oscillation after a time  $t_C$ . An overall response function is defined as:

$$\frac{\dot{m}'/\dot{m}}{p'/\bar{p}_C} \quad \dots(9.38)$$

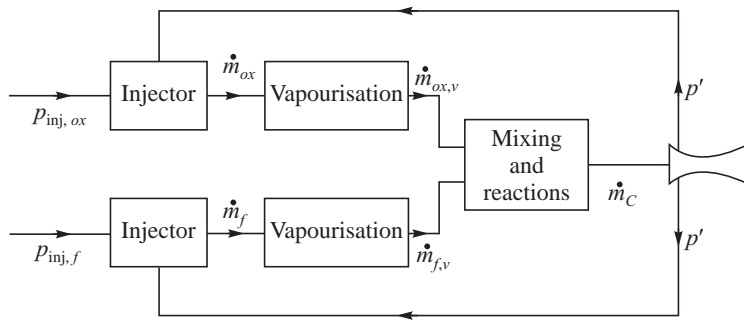


Fig. 9.13 Feedback

to give the changes in mass perturbation as a function of the steady mass flow rate  $\bar{m}$  for pressure perturbation  $p'$ . The phase difference between the mass injected and the mass generation rate (corresponding to time  $t_C$ ) plays an important role in augmenting the growth of the oscillations.



### 9.3 BULK MODE OF COMBUSTION INSTABILITY IN SOLID PROPELLANT ROCKETS

The mechanism governing the combustion instability in bulk mode in solid propellant rockets is influenced by the combustion time delay, as in liquid propellant rockets. The combustion delay  $t_C$  and a lag in the heating of the solid propellants from the reduced heat flux corresponding to the pressure ( $\bar{p}_C - p'$ ) following a pressure perturbation  $p'$  leads to fluctuations in the rate of mass generation  $\dot{m}_g$ . The phenomenon can be seen as follows: Consider a solid propellant rocket operating at a steady value of chamber pressure  $\bar{p}_C$ . Let there be a sudden drop in the chamber pressure by  $p'$  from A to B as shown in Fig. 9.14. In view of the reduced pressure in the chamber ( $\bar{p}_C - p'$ ), the density of the gases and the rate of chemical reactions slow down, leading to an increase of the chemical delay  $t_C$ . The heating rate of the surface of the solid propellant at the reduced pressure is also lower; however, the thermal inertia of the heated propellant corresponding to the higher value of pressure  $p_C$  persists for some time causing the rate of mass generation from the propellant to remain at the higher value (during the characteristic thermal time) than at the value corresponding to the lower chamber pressure.

The reduced rate of chemical reactions from a decrease in pressure results in smaller values of gas flow rates and an increase in the residence time. The increased residence time provides an opportunity for the chemical reaction to progress further and generate more heat release. The combined influence of the increased residence time and the existing thermal inertia of the propellant results in increased mass generation and causes the chamber pressure to increase from B to C as shown in Fig. 9.14.

The increased pressure at C brings about the opposite effect, viz., a smaller residence time and a reduced thermal depth corresponding to a lower pressure. The mass generation drops and the pressure falls to D (Fig. 9.14). The process of oscillations, therefore, continues as shown by the dashed line in Fig. 9.14.



A rocket with a small value of  $L^*$  has a small residence time  $t_{\text{res}}$ , which may not be adequate for the combustion to reach completion. Changes in the chemical delay time  $t_C$  will adversely influence the degree of completion of the reaction when the residence time is small, and cause significant changes in the value of  $\dot{m}_g$ . However, if the residence time of the rocket is large such that  $t_{\text{res}} \gg t_C$ , a small change in  $t_C$  will not change the amount of completion of the reaction and  $\dot{m}_g$  will not be significantly influenced by  $t_C$ . Solid propellant rockets having small values of  $L^*$  are, therefore, more prone to fluctuations of  $\dot{m}_g$  and hence are more likely to exhibit the bulk mode of instability. Since  $L^*$  is an important parameter influencing the instability, the bulk instability is also referred to as  $L^*$  instability.

As the chamber pressure of a rocket decreases, the combustion delay time increases, which could approach the residence time. A rocket would therefore exhibit  $L^*$  instability preferably at a low chamber pressure. The main parameters influencing the instability are  $L^*$  and chamber pressure  $p_C$ . As chamber pressure decreases, the rocket becomes more susceptible to the instability at a given value of  $L^*$ . The domain of  $L^*$  instability is sketched in Fig. 9.15 for a particular composite propellant.

The thermal depth of a propellant would depend on the rate at which heat is absorbed by it. The thermal diffusivity of the propellant ( $\alpha_d$ ) quantifies the diffusion of heat into the propellant and has units of  $\text{m}^2/\text{s}$ . The ratio of the diffusion coefficient to the mean burn rate of the propellant ( $\bar{r}$ ) gives an indication of the thermal depth  $\delta_{\text{th}}$ , viz.,

$$\delta_{\text{th}} = \frac{\alpha_d}{\bar{r}} \quad \dots(9.39)$$

The possibilities of expressing the parameters controlling  $L^*$  instability using non-dimensional parameters have been studied for composite propellants. The value of  $L^*$  was made dimensionless using the thermal depth  $\delta_{\text{th}}$ . The frequency of oscillation  $\omega$  was made dimensionless by dividing it either by  $\bar{r}^2/\alpha_d$  or  $\bar{r}/a$  where  $a$  is the value of the larger value of oxidizer particle size used in the composite propellant. It may be recalled that two sizes of oxidizer AP crystals were added to the binder in the composite propellant to enhance the solid loading. The terms  $\bar{r}^2/\alpha_d$  and  $\bar{r}/a$  have units of frequency (1/s). The experimental results obtained with non-aluminized propellants showed that the non-dimensional plot of  $L^*/\delta_{\text{th}}$  versus  $\omega/(\bar{r}/a)$  gave a systematic variation of the dependence.

When the solid composite propellants contained large amounts of aluminium, say about 16%, such as used in the present generation of rockets, the heterogeneity in the propellant characterized by

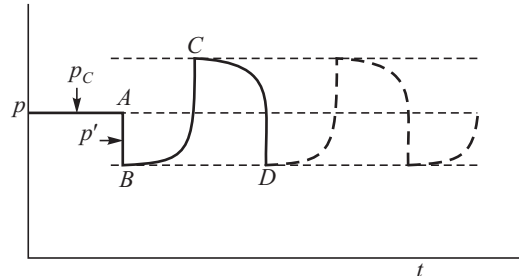


**Fig. 9.14** Bulk Mode Oscillation in Solid Propellant Rocket

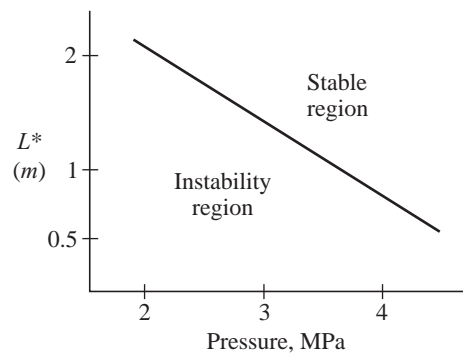


**Fig. 9.15** Domain of  $L^*$  Instability of a Solid Propellant



oxidizer particle  $a$  no longer played a role. The frequency of oscillations scaled as the term  $\bar{r}^2/\alpha_d$  instead of  $\bar{r}/a$ . This is because in aluminized propellants, a molten layer of aluminium forms over the burning surface of the solid propellants causing the heterogeneity to be less influential.

### 9.3.1 $L^*$ Burner

The burner in which the  $L^*$  instability is studied is known as  $L^*$  burner. The combustion volume (and hence  $L^*$ ) is varied using a movable piston as shown in Fig. 9.16. The propellant is attached to the piston. The throat area is varied to give different  $p_C$ . Experiments are conducted for different values of  $L^*$ , and the parameters  $p_C$  and  $L^*$  at which instability occurs is determined.

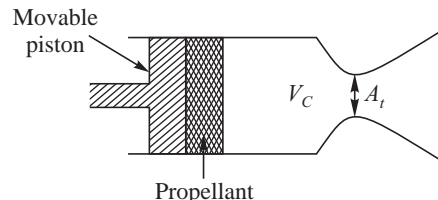


Fig. 9.16  $L^*$  Burner

### 9.3.2 Instability and Chuffs

$L^*$  instability is to be distinguished from the periodic pressure surges which occur when the ignition is not effective, such as during a hang-fire, which is manifested by periodic ignition followed by extinction. The pressure surges are known as chuffs. The pressure during the chuffs falls to the ambient pressure and is illustrated in Fig. 9.17. This is in contrast to  $L^*$  oscillations for which the mean pressures are much above the ambient pressure. The frequencies of the chuffs are much lower than those for  $L^*$  oscillations.

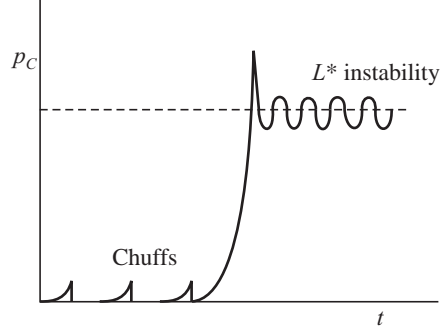


Fig. 9.17 Chuffs and  $L^*$  Instability



## 9.4 WAVE MODE OF COMBUSTION INSTABILITY

The bulk mode of combustion instability assumed that the entire gas in the combustion chamber oscillates in unison. This assumption holds good when the wavelength of the oscillations  $\lambda$  is much greater than the dimensions of the chamber, *i.e.*  $\lambda \gg L$ . A large value of  $\lambda$  implies lower frequencies and the bulk mode of oscillations are generally obtained at frequencies less than about 200 Hz.

When the wavelength of the oscillations is smaller than the characteristic dimensions of the chamber (higher frequencies of the oscillations), and waves propagate in the chamber, it becomes necessary to consider the variations of the perturbations at the different locations in the chamber. The pressure variations are functions of both the spatial coordinates and time, *viz.*,  $p'(x, t)$  instead of  $p'(t)$  dealt with in the bulk mode of combustion instability. This is done by taking into account the motion of waves in the chamber which results in the formation of standing waves. The burning process could respond to the different amplitudes of the pressure at the different locations of the standing wave and form large amplitude waves. Such type of wave growth is called combustion instability in the wave mode.



The amplitude of the standing wave increases under the following conditions:

- (i) Periodic mass addition in phase with pressure fluctuations. (Mass addition increases pressure)
- (ii) Periodic heat release in phase with temperature fluctuations. (Heat release provides enhancement of temperature)
- (iii) Periodic body force in phase with velocity fluctuations. (Body force provides momentum and hence velocity)

While a periodic mass release creates a time dependent change in pressure, the periodic heat release creates a change in the temperature. The pressure disturbance or temperature disturbance augments the existing pressure or temperature fluctuation resulting in an increase in the amplitude of the disturbance. A periodic body force, in phase with velocity disturbance, provides additional power leading to a higher value of a velocity disturbance. A rate of energy addition term for the mass, heat and body force per unit volume is represented by a parameter  $\sigma$  which is defined as:

$$\sigma = \frac{\dot{m}' p'}{\rho_0} + \frac{\dot{Q}' T'}{T_0} + \bar{F}' \cdot V' \quad \dots(9.40)$$

Here  $p'$ ,  $T'$  and  $V'$  denote the pressure, temperature and velocity fluctuations, while  $\dot{m}'$ ,  $\dot{Q}'$  and  $\bar{F}'$  denote the mass, heat and body force fluctuations per unit volume arising from the combustion process.  $\rho_0$  and  $T_0$  are the undisturbed density and temperature. The unit of  $\sigma$  is J/s per unit volume = W per unit volume. If the energy release during a cycle of oscillation is positive, then the amplitude of the standing wave grows and leads to combustion instability in the wave mode. The condition is represented by:

$$\oint dt \int \sigma dv > 0 \quad \dots(9.41)$$

The integration in time is over a cycle of the oscillation. The integration over volume is over the entire combustion volume. In practice, there would be dissipative processes in the chamber such as viscosity, radiation, etc. If we were to denote the rate of energy dissipation by  $\Omega$  Watts per unit volume, we can infer that waves would be enhanced when:

$$\oint dt \int (\sigma - \Omega) dv > 0 \quad \dots(9.42)$$

The parameters  $\sigma$  and  $\Omega$ , given above, have been suggested by Chu for a physical understanding and modeling of the growth and decay of waves.

#### 9.4.1 Rayleigh Criterion

For small pressure disturbances associated with an acoustic wave, the compression and expansion process can be assumed as isentropic, i.e.  $p/\rho^\gamma$  is a constant. Further, from the equation of state, we have  $p/\rho T = \text{constant}$ . The variations of pressure and temperature for the disturbance is, therefore,

given by  $p^{\frac{\gamma-1}{\gamma}} / T = \text{constant}$ . This on differentiating gives  $T' = \frac{\gamma-1}{\gamma} p' \frac{T}{p}$

$$\text{and} \quad \frac{\dot{Q}' T'}{T_0} = \frac{\gamma-1}{\gamma} \frac{\dot{Q}' p'}{p_0} \quad \dots(9.43)$$

Here the undisturbed pressure is  $p_0$ .



Adding energy  $\dot{Q}'$  in phase with pressure fluctuation  $p'$  is similar to adding  $\dot{Q}'$  to  $T'$  and leads to an increase of parameter  $\sigma$  given in eq. 9.40. This causes an increase of the wave amplitude. The phenomenon was determined by Lord Rayleigh and is known as the Rayleigh criterion. It states that 'if heat is supplied at the moment of greatest compression or removed at the moment of greatest rarefaction, the oscillation will be encouraged'. The heat addition and heat removal in phase with the larger amplitude compression and rarefaction respectively at the antinodes of the standing waves will lead to significant amplification of the pressure wave forms and hence combustion instability.

#### 9.4.2 Wave Modes in a Chamber

The interaction of the standing waves with perturbations in mass (or concentration), energy (or temperature) and momentum (or force) in the combustion process was seen in the last section as contributing to intensification of the waves. The identification of the standing wave modes is, therefore, the first step in understanding the wave mode of combustion instability. The formation of standing waves was discussed in Section 9.1.2 for wave motion along the length of the chamber, i.e. longitudinal mode of oscillations. It is also possible to have standing waves moving in the circumferential and radial directions of the combustion chamber.

The frequencies and waveforms of the different standing wave modes can be determined from the wave equation which describes the perturbations in the limit of small amplitudes and small values of mean flow velocities in the chamber. The wave equation is derived from mass and momentum conservation equations assuming an inviscid gas and homentropic flow. A homentropic flow implies that the gas particles, which are processed by the wave, undergo isentropic expansion and compression. The mass and momentum conservation equations for a three-dimensional geometry are:

$$\frac{\partial \rho}{\partial t} + \vec{\nabla} \cdot (\rho \vec{V}) = 0 \quad \dots(9.44)$$

$$\rho \frac{D}{Dt} \vec{V} = - \vec{\nabla} p \quad \dots(9.45)$$

Here  $\vec{V}$ ,  $\rho$ , and  $p$  denote the velocity, density and pressure.  $\vec{\nabla} \cdot (\rho \vec{V})$  denotes the divergence, i.e. change of mass flow while  $\vec{\nabla} p$  represents the gradient of pressure.  $\partial/\partial t$  is the partial derivative while  $D/Dt$  is the total derivative. The inviscid assumption is used in the momentum equation (eq. 9.45). The homentropic assumption gives:

$$\frac{D}{Dt} s = 0 \quad \dots(9.46)$$

where  $s$  is the entropy. For the particular case of small amplitude of pressure oscillations ( $p = \bar{p} + p'$ ,  $p'$  small) and negligible mean velocity, eqs. 9.44, 9.45 and 9.46 reduce to:

$$\frac{\partial^2 p'}{\partial t^2} = a^2 \nabla^2 p' \quad \dots(9.47)$$

$a$  in the above equation is the velocity of sound and  $p'$  is the pressure perturbation.  $\Delta^2 p'$  is the Laplacian of the scalar pressure which in the cylindrical polar coordinate system ( $r, \theta, x$ ) is

$\frac{1}{r} \frac{\partial}{\partial r} \left( r \frac{\partial p'}{\partial r} \right) + \frac{1}{r^2} \frac{\partial^2 p'}{\partial \theta^2} + \frac{\partial^2 p'}{\partial x^2}$ . In the Cartesian coordinates ( $x, y, z$ ),  $\nabla^2 p'$  is  $\frac{\partial^2 p'}{\partial x^2} + \frac{\partial^2 p'}{\partial y^2} + \frac{\partial^2 p'}{\partial z^2}$ .

Equation 9.47 is known as the linear wave equation.



The solution of this equation for the specified boundaries of the chamber provides the wave modes of oscillation and hence the characteristic frequencies of the pressure oscillations in the chamber. In the case of a chamber having cylindrical geometry, the wave given by eq. 9.47 in the polar cylindrical coordinate system ( $r, \theta, x$ ) reduces to:

$$\frac{\partial^2 p'}{\partial t^2} = a^2 \left[ \frac{\partial^2 p'^2}{\partial x^2} + \frac{1}{r} \frac{\partial}{\partial r} \left( r \frac{\partial p'}{\partial r} \right) + \frac{1}{r^2} \frac{\partial^2 p'}{\partial \theta^2} \right] \quad \dots(9.48)$$

The equation can be solved using the method of separation of variables. Denoting:

$$p' = p'(x) \cdot p'(r, \theta) \quad \dots(9.49)$$

Equation 9.48 becomes:

$$\begin{aligned} \frac{d^2 p'(x)}{dt^2} &= a^2 \frac{d^2 p'(x)^2}{dx^2} \\ \frac{d^2 p'(r, \theta)}{dt^2} &= a^2 \left[ \frac{1}{r} \frac{d}{dr} \left( r \frac{dp'(r, \theta)}{dr} \right) + \frac{1}{r^2} \frac{d^2 p'(r, \theta)}{d\theta^2} \right] \end{aligned} \quad \dots(9.50)$$

The time dependence of the oscillatory pressure can be expressed in the form  $e^{i\omega t}$ . The above equations, therefore, reduce to:

$$\begin{aligned} -\omega^2 p' &= a^2 \frac{d^2 p'(x)}{dx^2} \text{ giving} \\ \frac{d^2 p'(x)}{dx^2} + \frac{\omega^2}{a^2} p' &= 0 \end{aligned} \quad \dots(9.51)$$

and  $\frac{1}{p'(r, \theta)} \frac{d^2 p'(r, \theta)}{dr^2} + \frac{1}{r} \frac{1}{p'(r, \theta)} \frac{dp'(r, \theta)}{dr} + \frac{1}{r^2} \frac{1}{p'(r, \theta)} \frac{d^2 p'(r, \theta)}{d\theta^2} = -\frac{\omega^2}{a^2} \quad \dots(9.52)$

With  $p'(r, \theta) = p'(r) \times p'(\theta)$ , eq. 9.52 can be simplified to give:

$$\frac{r^2}{p'(r)} \frac{d^2 p'(r)}{dr^2} + \frac{r}{p'(r)} \frac{dp'(r)}{dr} + \frac{\omega^2}{a^2} r^2 = \frac{1}{p'(\theta)} \frac{d^2 p'(\theta)}{d\theta^2} \quad \dots(9.53)$$

The left side is a function of  $r$  while the right side is a function of  $\theta$ . This is possible only if both the sides are equal to a constant independent of  $r$  and  $\theta$ . Denoting the constant as  $m^2$ , we get:

$$r^2 \frac{d^2 p'(r)}{dr^2} + r \frac{dp'(r)}{dr} + \left( \frac{\omega^2}{a^2} r^2 - m^2 \right) p'(r) = 0 \quad \dots(9.54)$$

and  $\frac{d^2 p'(\theta)}{d\theta^2} + m^2 p'(\theta) = 0 \quad \dots(9.55)$

The solutions to  $p'(x)$ ,  $p'(r)$  and  $p'(\theta)$  from eqs. 9.51, 9.54 and 9.55 when put together in the form given by eq. 9.49 give:

$$p' = A \cos \left( \frac{n\pi x}{L} \right) \cos (m\theta) \left[ B J_m \left( \frac{\beta_{m,l} r}{R} \right) + C Y_m \left( \frac{\beta_{m,l} r}{R} \right) \right] \sin (\omega t) \quad \dots(9.56)$$



This is the general solution of the wave equation for a cylindrical chamber of length  $L$  and radius  $R$ .  $J_m$  and  $Y_m$  are the Bessel functions of the first kind and second kind respectively. The order of the Bessel function is  $m$ . A, B and C are constants.  $n$  gives the mode of oscillation in the  $x$  (longitudinal) direction while  $m$  and  $l$  give the modes of oscillation in the  $r$  (radial) and  $\theta$  (circumferential) directions. Since  $Y_m(r)$  tends to infinity as  $r$  tends to 0, and the pressure  $p'$  cannot be infinity, the constant C would be 0. The equation for the standing waves in the chamber is, therefore, given by:

$$p' = A \cos\left(\frac{n\pi x}{L}\right) \cos(m\theta) J_m\left(\frac{\beta_{m,l} r}{R}\right) \sin(\omega t) \quad \dots(9.57)$$

where  $A$  is a new constant.

$\beta_{m,l}$  is the non-dimensional frequency for the standing wave modes in the  $r$  and  $\theta$  directions and can be written as:

$$\beta_{m,l} = \frac{2\pi R f}{a} \quad \dots(9.58)$$

Standing waves with nodes and antinodes are formed in the radial and tangential directions in a manner similar to the standing waves in the longitudinal direction (given by eq. 9.11) corresponding

to the term  $\cos\left(\frac{n\pi x}{L}\right)$  in eq. 9.57. The standing wave pattern in the tangential and radial directions

is given by:

$$p'(r, \theta) = \hat{p} \cos(m\theta) \begin{pmatrix} J_m\left(\frac{\beta_{m,l} r}{R}\right) \\ \frac{J'_m(\beta_{m,l})}{J_m(\beta_{m,l})} \end{pmatrix} \sin(\omega t) \quad \dots(9.59)$$

Here  $\hat{p}$  denotes the maximum pressure perturbation at  $\theta = 0$  and  $r = R$ . The non-dimensional frequency  $\beta_{m,l}$  is determined from the above equation using the condition of zero velocity at the wall of the cylindrical chamber, viz.,  $r = R$  :

$$\frac{d}{dr} \left[ J_m\left(\frac{\beta_{m,l} r}{R}\right) \right] \Big|_{r=R} = 0 \quad \dots(9.60)$$

Equation 9.60 can be simplified at  $r = R$  to give:

$$J_{m-1}(\beta_{m,l}) + J_{m+1}(\beta_{m,l}) = 0 \quad \dots(9.61)$$

Values of  $\beta_{m,l}$  are determined for the different tangential modes  $m$  and radial modes  $l$  of the standing wave from the above equation using values of standard Bessel functions. Table 9.1 gives the values of  $\beta_{m,l}$ , so obtained, for different tangential modes and radial modes. The value of  $m = 0$  with  $l = 2, 3, \dots$  imply only radial modes. The first tangential mode is for  $m = 1$  and  $l = 1$ . The second tangential mode corresponds to  $m = 2$  and  $l = 1$ . A combined tangential and radial mode, viz., a second tangential and first radial corresponds to  $m = 2$  and  $l = 2$ .



**Table 9.1** Non-dimensional Frequencies  $\beta_{m,l}$  of Standing Waves in Tangential, Radial and Combined Tangential Radial Modes

	$l = 1$	$l = 2$	$l = 3$	$l = 4$
$m = 0$	0	3.832(1 <sup>st</sup> radial)	7.016(2 <sup>nd</sup> radial)	10.173(3 <sup>rd</sup> radial)
$m = 1$	1.841 (1 <sup>st</sup> tangential)	5.331 (combined 1 <sup>st</sup> tangential and 1 <sup>st</sup> radial)	8.526 (combined 1 <sup>st</sup> tangential and 2 <sup>nd</sup> radial)	11.706 (combined 1 <sup>st</sup> tangential and 3 <sup>rd</sup> radial)
$m = 2$	3.054 (2 <sup>nd</sup> tangential)	6.707 (combined 2 <sup>nd</sup> tangential and 1 <sup>st</sup> radial)	9.970 (combined 2 <sup>nd</sup> tangential and 2 <sup>nd</sup> radial)	13.170 (combined 2 <sup>nd</sup> tangential and 3 <sup>rd</sup> radial)
$m = 3$	4.200 (3 <sup>rd</sup> tangential)	8.014 (combined 3 <sup>rd</sup> tangential and 1 <sup>st</sup> radial)	11.348 (combined 3 <sup>rd</sup> tangential and 2 <sup>nd</sup> radial)	14.586 (combined 3 <sup>rd</sup> tangential and 3 <sup>rd</sup> radial)

The tangential and radial frequencies ( $f$ ) in Hz. are calculated for the different modes using the above values of  $\beta_{m,l}$  in eq. 9.58. Figures 9.18 to 9.20 show the pressure amplitudes  $p'/\hat{p}$  and waveforms corresponding to the first tangential mode ( $m = 1, l = 1$ ), second tangential mode ( $m = 2, l = 1$ ), and third tangential mode ( $m = 3, l = 1$ ) respectively in a cylindrical chamber of radius  $R$ . The first tangential mode is shown in Fig. 9.18. The pressure amplitude varies in the circumferential direction (perpendicular to the radius) and is shown along the cross-section of a cylinder. There are two antinodes at the opposite ends of the diameter and the node is at the centre. One of the antinodes is seen to have the maximum positive amplitude whereas the other has the maximum negative amplitude (Fig. 9.18).

The number of antinodes at the outer radius increases to four and six for the second and third tangential modes respectively (Figs. 9.19 and 9.20).

The first radial mode ( $m = 0, l = 2$ ) and the second radial mode ( $m = 0, l = 3$ ) are shown in Figs. 9.21 and 9.22 respectively. Here the direction of the oscillations is along the radius and the nodes and antinodes are along concentric circles. For the first radial mode, the antinodes are at the centre and at the outer radius as shown in Fig. 9.21, with a node in between. In the case of the second radial mode, a third antinode is formed at an intermediate location between the center and the outer antinodes. There are two nodes. This is seen in Fig. 9.22.

A combination of the first radial mode with the first tangential mode ( $m = 1, l = 2$ ) is shown in Fig. 9.23. Here, the combined tangential and radial oscillations are seen to lead to non uniform pressures at the outer radii with the maximum pressure oscillations at the location of the tangential pressure antinode. Spatial variations in the pressure amplitudes also take place along the radii. The variations in pressure get more complicated for the combined modes of higher order in the radial and tangential directions. This is illustrated in Fig. 9.24, where the combined second tangential and first radial mode of the standing wave is shown.

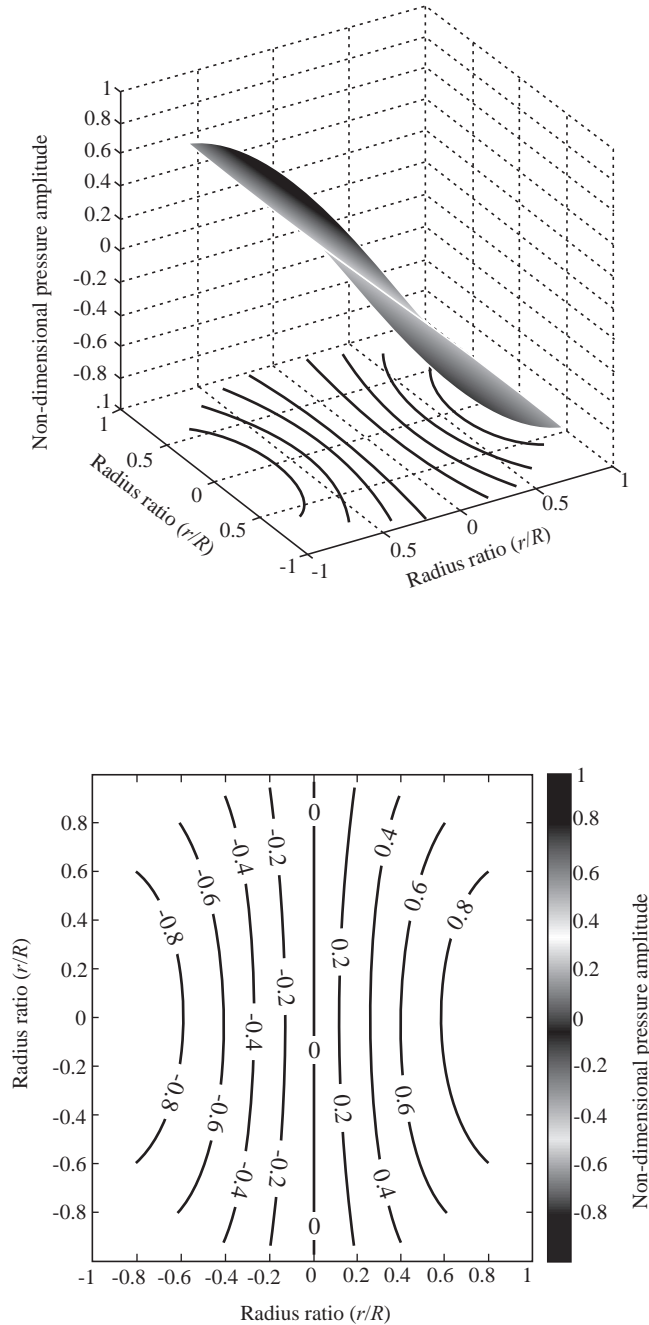


**Fig. 9.18** First Tangential Mode ( $m = 1, l = 1$ )

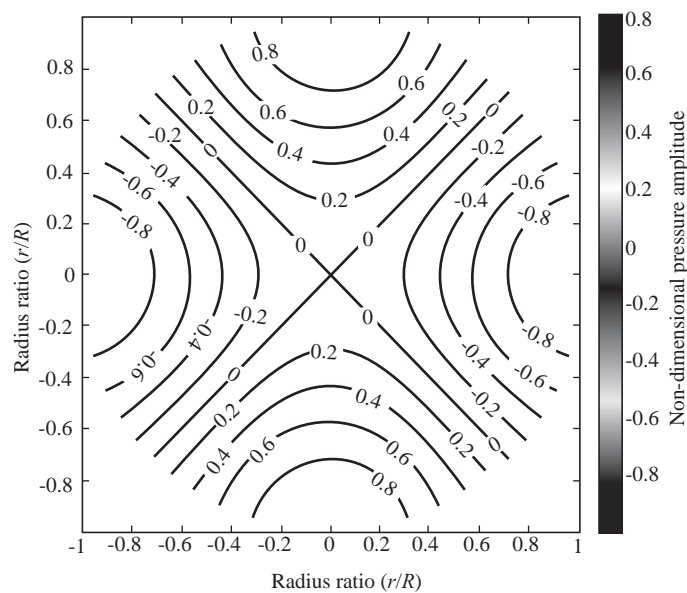
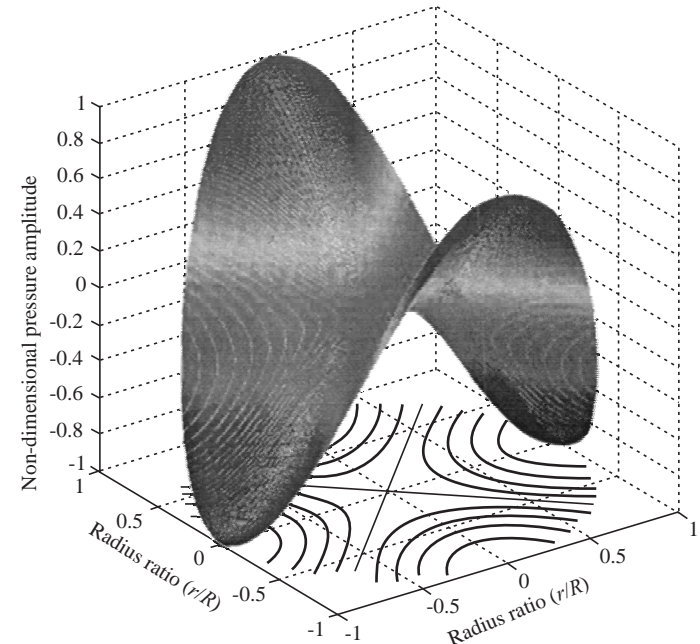


**Fig. 9.19** Second Tangential Mode ( $m = 2, l = 1$ )

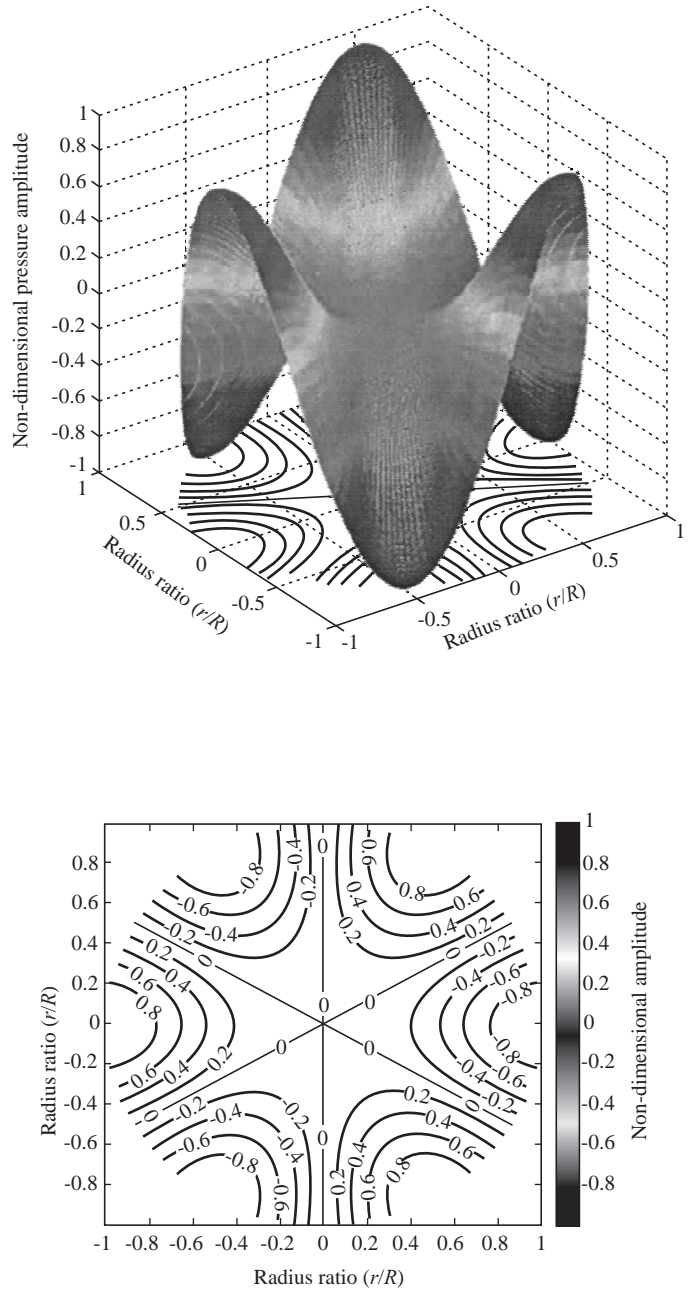


**Fig. 9.20** Third Tangential Mode ( $m = 3, l = 1$ )

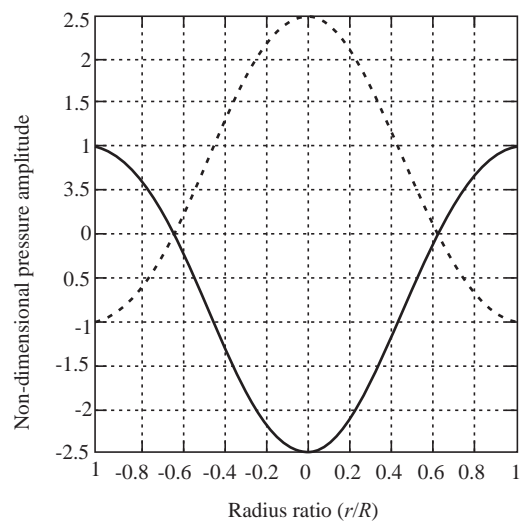
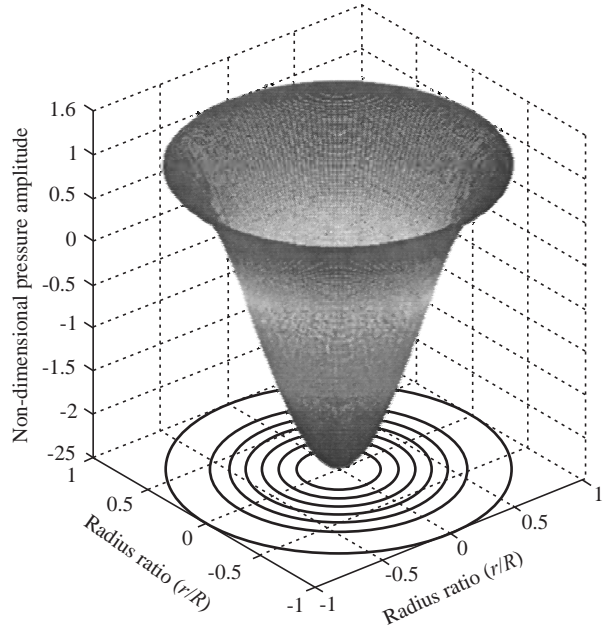


**Fig. 9.21** First Radial Mode ( $m = 0, l = 2$ )

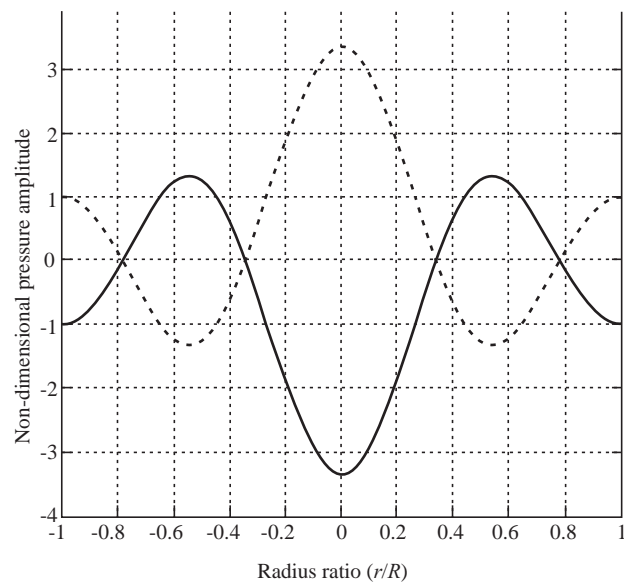
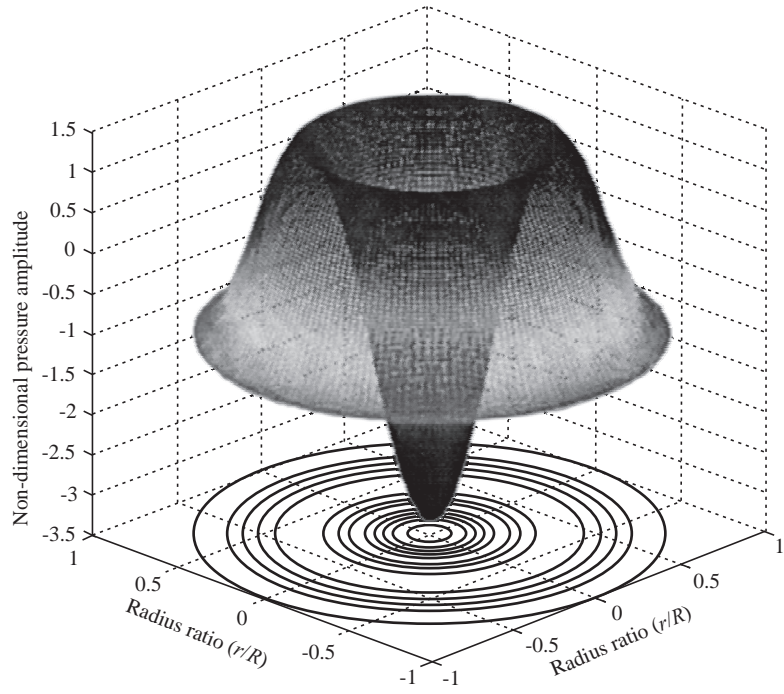


**Fig. 9.22** Second Radial Mode ( $m = 0, l = 3$ )

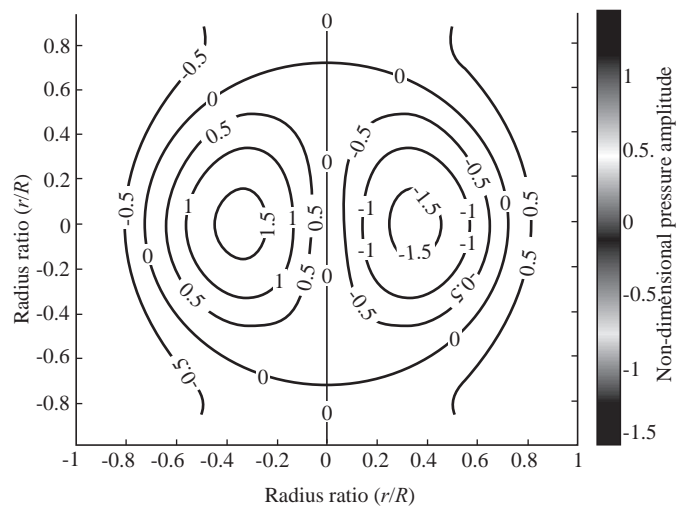
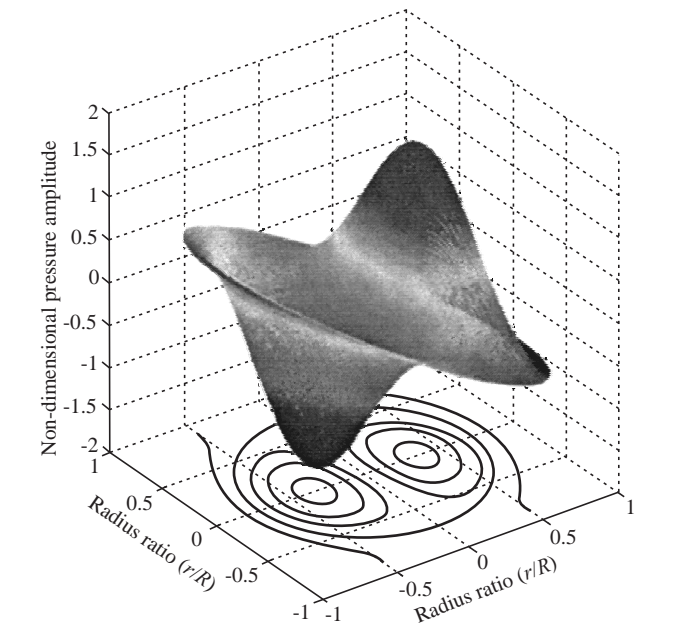


**Fig. 9.23** Combined First Tangential and First Radial Mode ( $m = 1, l = 2$ )

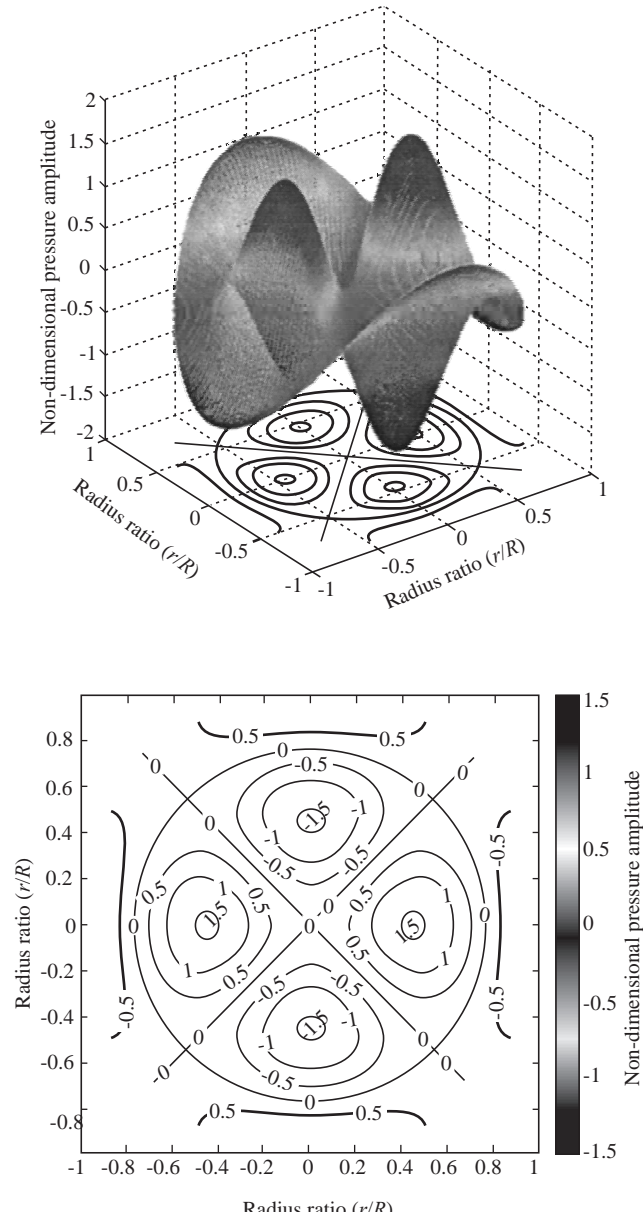


Fig. 9.24 Combined Second Tangential and First Radial Mode ( $m = 2, l = 2$ )

### 9.4.3 Longitudinal, Tangential, Radial and Mixed Wave Modes of Combustion Instability

The frequencies and form of the standing waves formed in a cylindrical cavity, closed at both ends, were determined in Section 9.1.2 for the longitudinal direction (along the axis of the cylindrical cavity) and in Section 9.4.2 for the tangential and radial directions. A combination of the wave motion in the three directions could give rise to mixed modes. When the pressure perturbation in the standing



wave, corresponding to the longitudinal, radial or tangential modes or a combination of these, is in phase with the energy release from the combustion process at a particular location, then the amplitude of the standing wave increases. Large amplitude standing waves are formed and combustion instability occurs.

The typical frequencies associated in the wave mode type of combustion instability are greater than about 1500 Hz and the combustion instability is also referred to as high frequency combustion instability. In general, the radial modes have frequencies which are much higher in view of the relatively small diameters of the rocket chambers. Combustion instability in the wave mode is generally encountered in tangential and coupled radial and tangential modes.



## 9.5 WAVE MODE INSTABILITY IN SOLID PROPELLANT ROCKETS

The combustion of solid propellants takes place essentially at the surface of the propellants as discussed in Sections 5.1.1 and 5.1.2 of Chapter 5. The interaction of the pressure perturbations in the standing wave at the propellant surface with the combustion process therein could lead to an increase of the amplitude of standing waves and combustion instability.

The response of the burning surface of a propellant to pressure perturbations is defined as the surface acoustic admittance of the burning surface. It is defined as:

$$Y = \frac{V' \bar{V}}{p' \bar{p}} \quad \dots(9.62)$$

Here  $V'$  is the velocity perturbation normal to the propellant surface caused by the pressure perturbation  $p'$ .  $\bar{V}$  and  $\bar{p}$  are the mean values of velocity and pressure. Following eq. 9.12 and denoting the phase difference between the pressure and velocity perturbations during the burning process  $p'$  and  $V'$  by  $\delta$ , we have:

$$\begin{aligned} p' &= \Delta p \sin \omega t \\ V' &= \Delta V \sin (\omega t + \delta) \end{aligned} \quad \dots(9.63)$$

The value of  $\delta$  was seen to be equal to  $-\pi/2$  for the small amplitude isentropic wave (Section 9.1.2).  $\Delta p$  and  $\Delta V$  in eq. 9.63 are the maximum amplitudes of pressure and velocity. The acoustic admittance of the burning propellant surface therefore reduces to:

$$Y = \frac{\Delta V \bar{V}}{\Delta P \bar{P}} e^{i\delta} \quad \dots(9.64)$$

The mean velocity  $\bar{V}$  and the velocity perturbation  $\Delta V$  are proportional to the mass release at the solid propellant surface. The admittance  $Y$  can, therefore, be expressed as  $\frac{\Delta m \bar{m}}{\Delta P \bar{P}} e^{i\delta}$ , where  $\Delta m$  is the fluctuation in mass release and  $\bar{m}$  is the mean value. When the admittance  $Y$  is positive, mass is added over and above the steady value due to a positive pressure perturbation. This results in the increase of the average energy of the wave. The amplitude of the standing wave would, therefore, increase if this energy is not dissipated by other mechanisms present in the rocket chamber.

The nozzle radiates away part of the acoustic energy. The visco-elastic nature of the solid propellant also absorbs some energy. Loss of acoustic energy also occurs due to flow turning in the combustion



chamber and viscous dissipation from particulates, such as burning aluminium. Of the above factors governing the losses, the contribution from the nozzle is most dominant. If the real part of the acoustic admittance  $Y$  of the burning propellant surface is represented by  $\beta_c$  and similarly the real part of the nozzle admittance is represented as  $\beta_n$ , the wave equation given by eq. 9.47 can be solved to determine whether the pressure amplitudes would grow subject to these two conditions at the boundaries of the propellant surface and nozzle. Combustion instability would occur when the amplitude of the pressure disturbances grow.

Values of admittance  $\beta_c$  and  $\beta_n$  are required for predicting the combustion instability. Both theoretical and experimental procedures are available for determining the admittance values. Devices such as the T burner, which generate standing waves at specific frequencies, have been applied, for experimentally determining the value of  $\beta_c$ . The T burners are discussed subsequently.

The growth of the amplitude of the oscillations in the standing wave due to combustion can be represented by:

$$p' = \Delta p e^{\alpha_g t} \sin \omega t \quad \dots(9.65)$$

where  $\Delta p$  is the initial maximum pressure amplitude of the standing wave and  $\alpha_g$  is the growth constant in  $s^{-1}$ . During the initial period ( $t \approx 0$ ),  $\alpha_g$  does not vary significantly and a plot of  $\log(p')$  vs.  $t$  gives a straight line. This is schematically illustrated in Fig. 9.25. Since the energy of the wave is proportional to  $p'^2$ , we see from eq. 9.65

that  $2\alpha_g = \frac{dE/dt}{\bar{E}}$ . The growth constant  $\alpha_g$ ,

therefore, denotes the ratio of the rate at which energy is added to the standing wave and twice the mean energy of the standing wave. If the rate of energy addition to the standing wave by combustion is denoted by  $\dot{E}$  and the mean wave energy by  $\bar{E}$ , then  $\alpha_g = \dot{E}/(2\bar{E})$ .

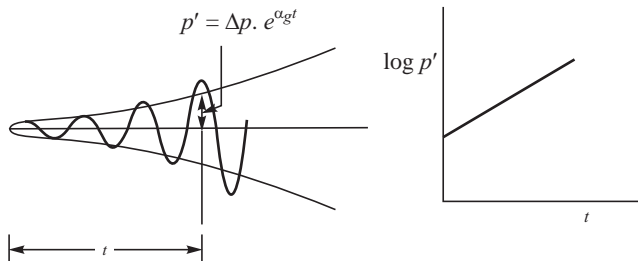


Fig. 9.25 Growth Constant in a Solid Propellant Rocket

The energy in the standing wave is partially radiated out of the nozzle. Part of the energy is dissipated by the viscous drag over the solid and liquid particulates present in the flow, the flow turning and the visco-elastic damping by the solid propellant. Similar to the growth constant  $\alpha_g$ , a decay constant  $\alpha_d$ , due to dissipation of energy by the nozzle, particulate damping, flow turning, etc., is defined ( $\alpha_d = \dot{E}_{Loss}/2\bar{E}$ ). It represents the ratio of the rate at which energy is removed from the standing wave and twice the mean energy of the wave.

When the rate of energy that gets into the wave mode is greater than the rate of its dissipation for the particular frequency  $\omega$  of the standing wave, the growth of the wave at frequency  $\omega$  takes place. Pressure perturbations grow and combustion instability is said to occur at that particular frequency. If the decay constants, due to losses of the wave energy arising from the interaction of the standing wave with the nozzle, particulates in the gas, flow turning, etc., are denoted by  $\alpha_n$ ,  $\alpha_p$ ,  $\alpha_{ft}$  ..., the condition for which combustion instability occurs is:

$$\alpha_g - (|\alpha_n + \alpha_p + \alpha_{ft} + ...|) > 0 \quad \dots(9.66)$$



The decay constants are available in literature as semi-empirical expressions involving geometrical and flow parameters. The growth constants, however, are sensitive to the physical and chemical characteristics of the solid propellant and are dependent on the raw materials used in the propellant, the composition and the processes involved in manufacturing the propellant. They are generally determined experimentally for the particular frequencies of interest in small burners and scaled up for the particular configuration of burning of the solid propellant rocket. This aspect is dealt with in the next two sections.



## 9.6 EVALUATION OF THE GROWTH CONSTANT OF SOLID PROPELLANT USING A T BURNER

A *T* burner is used to determine the growth constant of solid propellant at different frequencies. It consists of a straight cylindrical tube of variable lengths to get the different frequencies of oscillation in the fundamental longitudinal mode. Two thin solid propellant discs of diameter equal to the diameter of the tube, inhibited from burning over the cylindrical surfaces and identical to each other are placed at the ends of the tube which correspond to pressure antinodes. The tube has a vent at the central location corresponding to a pressure node. The vent is connected to a pressurized surge tank as shown in Fig. 9.26. The pressure in the tube can be varied by changing the pressure in the surge tank.

Since the ends are closed, the fundamental longitudinal frequency of the tube is:

$$f = \frac{a}{2L} \quad \dots(9.67)$$

Here  $a$  is the sound velocity of the gas in the tube and  $L$  is the length of the tube. The length  $L$  is varied to obtain frequencies of interest, typically between a few hundred and a few thousand Hertz. The diameter of the tube varies between 35 and 150 mm.

The propellant discs at both the ends are simultaneously ignited using either a pyrotechnic charge or electrical resistance heating. The burning surface of the propellant is at the antinodes and is subjected to the maximum pressure amplitude of the standing wave. If the burning propellant surface responds to the pressure oscillations at the given frequency, the amplitude of the pressure oscillations increase and reach a limiting value as shown in Fig. 9.27. After burning ceases, the amplitude of the oscillation decays to zero.

The growth of the pressure oscillations and the subsequent decay, such as shown in the above figure, are curve-fitted with the expression  $p' = \bar{p} e^{(\alpha + i\omega)t}$  to obtain values of growth constant  $\alpha_g$  and decay constant  $\alpha_d$  during the initial phase of the growth and towards the end of the decay. The pressure amplitudes in the initial and final phases are small and an exponential growth and decay can be assumed. Since the growth and decay of the oscillations take place in a similar environment in the tube and the dissipative processes during the decay are operative during the combustion, the contribution of the burning propellant to growth of the pressure amplitude in a *T* burner  $\alpha_c|_T$  is:

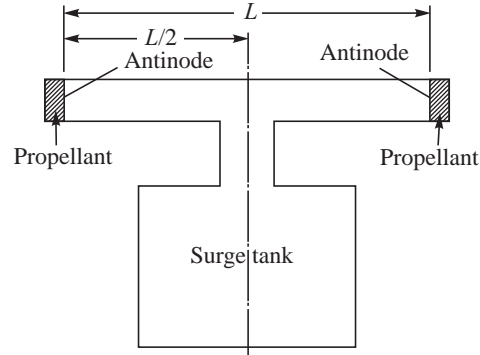


**Fig. 9.26** *T* Burner

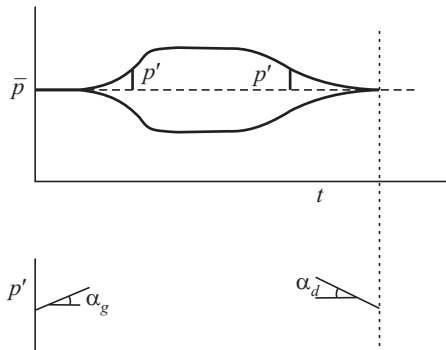


**Fig. 9.27** Growth and Decay of Pressure in a T Burner

$$\alpha_c |_T = \alpha_g + |\alpha_d| \quad \dots(9.68)$$

When the solid propellants contain a large percentage of aluminium (typically 12 to 18%) or when a melt layer is formed over the surface of the propellant during the combustion process, it is difficult for oscillations to grow in the *T* burner. Additional modifications, such as increased area with a cylindrical burning surface or inducing oscillations through pressure pulses, become necessary.

The value of  $\alpha_c |_T$  determined in a *T* burner cannot be directly used for a solid propellant rocket. This is because in a *T* burner, the interaction of the wave and burning is at the location of pressure antinodes alone whereas in a rocket having radial or unrestricted burning, the burning propellant surface interacts with the standing wave at all regions. The conversion of the growth constant measured in the *T* burner to the growth constant in a rocket is discussed in the next section.



## 9.7 CONVERSION OF GROWTH CONSTANT DERIVED FROM *T* BURNER FOR APPLICATION IN A SOLID PROPELLANT ROCKET

In a *T* burner, the propellants burn at the pressure antinodes whereas in a solid propellant rocket, the different amplitudes of pressure in the standing wave interact with the burning surface. We review some terms used in the analysis prior to applying the results obtained in a *T* burner to a rocket motor.

The wave motion in a medium is characterized by the specific acoustic impedance  $z$  of the medium which is defined as:

$$z = \frac{p'}{u'} \quad \dots(9.69)$$

Here  $p'$  is the pressure fluctuation associated with a velocity fluctuation  $u'$ . The unit of specific acoustic impedance is  $(Pa - s)/m$ .

For acoustic waves,  $\frac{\partial p}{\partial \rho} = a^2$  or equivalently  $\frac{p'}{\rho'} = a^2$ . Considering the continuity equation for

small amplitude waves [ $\rho_0 a = \sqrt{\rho_0 + \rho'} (a - u')$ , where  $u'$  is the particle velocity behind the wave and  $\rho_0$  is the undisturbed value of density], the specific acoustic impedance of the medium (given by eq. 9.69) becomes  $\rho_0 a$  which represents the product of its density and the sound speed.



The acoustic admittance (conductance) is the reciprocal of the impedance and is given by:

$$y = \frac{u'}{p'} = \frac{1}{\rho_0 a} \quad \dots(9.70)$$

The response of the burning surface to pressure disturbances is defined by using the admittance of the burning propellant surface. Since the properties of the burning surface are different from the medium, its acoustic admittance is taken as:

$$\frac{u'}{p'} = \frac{\kappa}{\rho_0 a} \quad \dots(9.71)$$

where  $\kappa$  is called the acoustic conductance ratio of the burning surface of the propellant.

The rate of energy release at a burning surface of area  $S$  is

$$\dot{E}_s = \frac{1}{2} \int_S p' u' dS \quad \dots(9.72)$$

which using eq. 9.71 becomes:

$$\dot{E}_s = \frac{1}{2\rho_0 a} \int_S \kappa p'^2 dS \quad \dots(9.73)$$

The growth constant was seen to be equal to one-half of the ratio of the rate of energy added, to the average energy of the wave, viz.,  $\frac{\dot{E}_s}{2\bar{E}}$ . The energy in the wave per unit time per unit volume is

$\frac{1}{2} \rho_0 u'^2$ . Using eq. 9.70 and simplifying, the mean acoustic energy in the volume  $V$  of the combustion chamber is:

$$\bar{E} = \int_V \frac{1}{2} \frac{p'^2}{\rho_0 a^2} dV \quad \dots(9.74)$$

where  $V$  represents the combustion volume or port volume. The value of the growth constant is determined from eqs. 9.73 and 9.74 as:

$$\alpha = \frac{1}{2} \frac{\frac{1}{2} \frac{1}{\rho_0 a} \int_S \kappa p'^2 dS}{\frac{1}{2} \frac{1}{\rho_0 a^2} \int_V p'^2 dV} \quad \dots(9.75)$$

This on simplification gives:

$$\alpha = \frac{a}{2} \frac{\int_S \kappa p'^2 dS}{\int_V p'^2 dV} \quad \dots(9.76)$$

Taking the acoustic conductance ratio of the burning surface as constant, the above equation simplifies to:



$$\alpha = a \Phi \frac{\int_S p'^2 dS}{\int_V p'^2 dV} \quad \dots(9.77)$$

Here  $\Phi$  is known as burning surface parameter. If this parameter is known, the growth constant for the particular mode of the stationary wave can be obtained.

The value of  $\alpha_c|_T$  determined in a  $T$  burner is used to evaluate the value of  $\Phi$ . The standing wave mode in the  $T$  burner has the form:

$$p' = \hat{p} \cos \frac{\pi x}{L} \quad \dots(9.78)$$

where  $L$  is the length of the  $T$  burner and  $x$  is the distance from one end. The burning surfaces are at the antinodes (corresponding to  $x = 0$  and  $x = L$ ) for which  $p' = \hat{p}$ . The value of  $\int_S p'^2 dS$  in eq. 9.76

is, therefore,  $2\hat{p}^2 S$  where  $S$  is the area of cross-section of the burner tube. The propellants at both ends of the tube have the same surface area as the cross-sectional area of the tube. The integral

$$\int_V p'^2 dV \text{ becomes:}$$

$$\int_V \hat{p}^2 \cos^2 \frac{\pi x}{L} dV = \frac{1}{2} \int_L S p'^2 \left(1 + \cos \frac{2\pi x}{L}\right) dx = SL \frac{\hat{p}^2}{2} \quad \dots(9.79)$$

Substituting values of  $\int_S p'^2 dS$  and  $\int_V p'^2 dV$  in eq. 9.77, we get for a  $T$  burner:

$$\alpha_c|_T = \frac{4a\Phi}{L} \quad \dots(9.80)$$

$$\text{or } \Phi = \frac{\alpha_c|_T L}{4a} \quad \dots(9.81)$$

The frequency of the  $T$  burner is  $\alpha/2L$ . Denoting this frequency as  $f$ , we get:

$$\Phi = \frac{\alpha_c|_T}{8f} \quad \dots(9.82)$$

The above value of the burning surface parameter  $\Phi$  corresponding to frequency  $f$  is used to determine the growth constant of the burning propellant in a solid propellant rocket. Equation 9.77 is used for the particular standing wave mode occurring at the same value of  $f$ .

The following illustrates the procedure for an internal cylindrical burning propellant grain of length  $L_m$  and diameter  $D_m$ . The standing wave in longitudinal mode of oscillation corresponding to the fundamental mode is considered for simplicity.



The value of  $\int_S p'^2 dS$  is

$$\int_0^{L_m} \hat{p}^2 \cos^2 \frac{\pi x}{L_m} \pi D_m dx = \frac{\hat{p}^2 \pi D_m L_m}{2} \quad \dots(9.83)$$

while the volume integral  $\int_V p'^2 dV$  is

$$\int_0^{L_m} \hat{p}^2 \left( \cos^2 \frac{\pi x}{L_m} \right) \frac{\pi D_m^2}{4} dx = \frac{\hat{p}^2 \pi D_m^2 L_m}{8} \quad \dots(9.84)$$

Substituting the values of surface and volume integrals from eqs. 9.83 and 9.84 in eq. 9.77, we obtain the growth constant  $\alpha_m$  in the rocket chamber for this particular standing wave mode as:

$$\alpha_m = \frac{4\Phi a}{D_m} \quad \dots(9.85)$$

The value of  $\Phi$  at the frequency  $f$  is given in terms of the growth constant measured in the  $T$  burner from eq. 9.82. Substituting this value in eq. 9.85 gives:

$$\alpha_m = \frac{a \alpha_c |_T}{2f D_m} \quad \dots(9.86)$$

It must be noted that the frequency  $f$  at which  $\alpha_c |_T$  is evaluated should be the same as the frequency of the rocket chamber. The value of sound speed in the above equation corresponds to the sound speed in the chamber, which would be different from the sound speed in the  $T$  burner.

The value of the above growth constant, if in excess of the sum of the damping terms in eq. 9.66 implies combustion instability in the particular standing wave mode.



## 9.8 WAVE MODE INSTABILITY IN LIQUID PROPELLANT ROCKETS

The mechanism is similar to that discussed in Section 9.5 for solid propellant rockets. The instability occurs when the rate of energy release from the combustion of liquid propellants reinforces the standing waves in the chamber. When the combustion energy release occurs in the region of pressure nodes, no energy can be added to the wave, since there is no wave motion at the node. If, however, the energy release from the combustion of the liquid fuel and oxidizer is located in the region of the pressure antinodes, wherein the pressure perturbations are a maximum and the pressure wave and heat release fluctuation have the same phase, the standing wave amplitudes could be readily enhanced as per the Rayleigh principle. This leads to combustion instability. Injectors of liquid propellant rockets, which produce high intensity of combustion in the region of pressure antinodes, would, therefore, be more susceptible to instability. Distributing the energy release away from the pressure antinodes is one way of reducing the instability.

The mixed modes involving tangential and radial wave motions are particularly important for liquid propellant rockets. This is because the injector can cause localized burning at different radial and circumferential locations and excite standing waves in the radial, tangential and mixed modes. Localized regions of heat release are schematically indicated in Fig. 9.28.

Analysis of combustion instability in liquid propellant rockets could be done by solving the wave equation, (which predicts the standing waves), subject to the boundary conditions at the injector, where energy is supplied to the wave and the boundaries of the chamber walls and nozzle, wherein the energy is dissipated from the wave. An admittance function  $Y$  is specified at the boundaries corresponding to the injector, chamber walls and nozzle. The admittance function provides for the response from combustion, friction at the walls and energy loss from the nozzle to pressure perturbation  $p'$ .

### 9.8.1 Gain Stabilization and Detuning

Since the wave mode of combustion instability is caused by the energy added to the standing wave at the frequency of the wave, a measure of the energy contributed to the wave from the combustion process and the frequency of the standing wave are the relevant parameters to describe combustion instability in liquid propellant rockets. The rate of energy ( $\dot{E}$ ) gained by the standing wave from the combustion if greater than that lost by dissipation at the frequency of interest would lead to instability.

An energy or heat release parameter proportional to the rate of burning is defined as a measure of the energy added to the standing wave of a given mode. An increase in the rate of chemical reactions enhances the heat release parameter. The rate of reactions is described for a combustion process through a non-dimensional parameter called Damkohler number (Da) and this parameter is used to signify the heat release. The energy dissipated is essentially by viscous dissipation. A dissipation parameter is characterized by the reciprocal of Reynolds number (Re) since Reynolds number is the ratio of the inertial force to the viscous force. The boundary between the stable and unstable region is based on the relative magnitudes of the viscous dissipation parameter ( $1/Re$ ) and a heat release rate parameter Da. Stability is obviously enhanced by an increase of the dissipation parameter ( $1/Re$ ) and a decrease of the heat release parameter (Da), as indicated in Fig. 9.29. The practice of addressing the energy gains and losses and ensuring stable operation of a rocket by verifying that the gains are lower than the losses is spoken of as ‘gain’ stabilization.

The possibility of whether combustion can respond by being in tune with the standing wave modes is the procedure adopted in the frequency or tuning method of addressing the wave mode of instability. The fraction of energy from combustion which is required to increase the amplitude of the wave motions is very small. It therefore becomes necessary to prevent even a small transfer of energy from the combustion into the wave motion. For this purpose it is necessary to avoid any frequency match between the different standing wave modes and the combustion process. The general practice

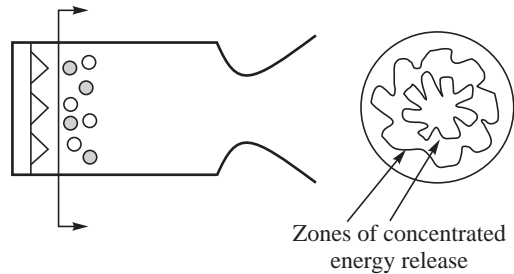


**Fig. 9.28** Localized Regions of Heat Release

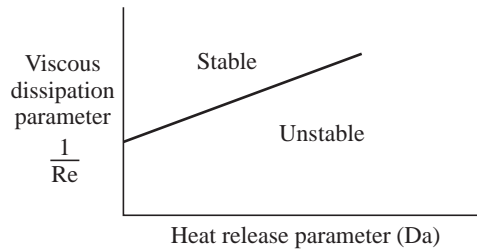


**Fig. 9.29** Stability Boundary



is to keep the frequency of combustion much lower than the frequencies of the standing wave modes in the chamber so that energy is not transferred to the wave. This procedure is known as 'Detuning'.

In addition to detuning, the energy release rates from the combustion can be made slow; thereby ensuring that the rate of energy augmenting the waves is much lower than the rate of dissipation of energy. Both detuning and gain stabilization procedures are used to prevent the occurrence of instability.

In general, the likelihood of occurrence of the wave mode of combustion instability in liquid propellant rockets can be lessened by the following:

- (i) Distribute combustion over a wider region instead of being concentrated near the antinodes,
- (ii) Modify frequency of the wave modes to be higher than the frequency of the combustion process by incorporating baffles in the chamber,
- (iii) Improvise resonators in the chamber which would modify the characteristic frequency of the chamber and make it different from the combustion process,
- (iv) Have relatively large droplet sizes in the spray formed by the injector and make the combustion slow and inefficient,
- (v) Add additives to the propellant, which would decrease the energy release rates,
- (vi) Enhance viscous damping, and
- (vii) Have a gradually shaped convergent nozzle so that the waves are partially radiated out instead of being totally reflected back into the chamber to form standing waves.



## 9.9 NON-LINEAR COMBUSTION INSTABILITY

The bulk and the wave mode of combustion instability have been considered so far. In the wave mode, the standing waves formed from the small amplitude pressure waves (acoustic waves) were considered. These are, therefore, referred to as acoustic modes of instability.

In some instances the combustion process in the rocket motor does not respond to the small amplitude disturbances associated with the acoustic modes; however, combustion instability is obtained when the amplitude of disturbances are large, such as during the ignition pressure spikes or during certain anomalies in the burning of the rocket. The instabilities, associated with finite amplitude waves, are termed as non-linear modes of combustion instability.

There is a threshold value of the perturbations only beyond which the combustion becomes unstable. These non-linear instabilities occur both in solid propellant and liquid propellant rockets. Miniature bombs or pulse guns are used to create finite amplitude disturbances (such as, a blast wave) in the combustion chamber to evaluate the non-linear combustion instability.



## 9.10 PROCESS-INDUCED COMBUSTION INSTABILITY

There are several processes occurring with distinct frequencies during the combustion in solid and liquid propellant rockets, which contribute towards its combustion instability. A few of these are given in the following.



### 9.10.1 Heterogeneity of Composite Propellant

The composite solid propellant is heterogeneous, with solid particles of ammonium perchlorate dispersed in the binder. If the mean burning rate of the propellant is  $r$  and the mean size of ammonium perchlorate crystal in the propellant is  $a$ , the characteristic frequency (periodicity) associated with this heterogeneity is  $r/a$ . This frequency, if in resonance with some wave mode or process, could lead to the enhancement of the perturbations.

### 9.10.2 Vortex Shedding at Protrusions of Segment Joints

In large solid propellant rockets, several grains are bonded together to form a large propellant grain. The material used to bond the grain segments does not burn at the same rate as the propellant, and projections or protrusions are formed between the grain segments as the burning progresses. The flow of the combustion gases over the protrusions causes vortices to be shed. The frequencies of vortex shedding, if similar to frequencies associated with some other process of combustion or wave modes, could lead to amplification of the disturbances arising from the segment joint.

### 9.10.3 Periodicities, Mixture Ratio Fluctuations and Popping

In the case of liquid propellant rockets, the periodicities associated with the atomization process involving disintegration of jets and unsteady flows through the injector (hydraulic flip) could couple with the wave modes or other processes during the combustion and cause instability. When hypergolic propellants are used, the impingement of the fuel and oxidizer sometimes create a reactive intermediate, which spontaneously explodes to form localized blast waves. Localized explosions and overpressure could also be obtained in the flammable regions of a stratified mixture in the combustion chamber. These finite amplitude disturbances help trigger combustion instability. The instability is known as popping instability.

### 9.10.4 Entropy Waves

Mal-distribution of fuel and oxidizer in the combustion chamber can cause changes in the mixture ratios and temperature fluctuations. Local zones of heat release bring about a change of entropy and heat release zones could progress along the combustion chamber at the mean flow velocity. The propagation of the heat release zone is, therefore, spoken of as entropy wave. Entropy waves are material waves and are distinctly different from the acoustic waves. On being reflected from the throat, they cause a pressure wave to travel back into the chamber which could also excite the formation of standing waves and combustion instabilities. Considering that the propagation of entropy waves are at the flow velocities, the frequencies associated with entropy waves are small.



## 9.11 POGO INSTABILITY DUE TO INTERACTION OF PROPULSION AND STRUCTURE

A liquid propellant rocket consists of propellant tanks, feed lines, pumps and a combustion chamber (Chapter 6). The propellants are fed to the combustion chamber through the feed lines and pumps. A liquid propellant rocket carries considerable quantities of propellants in large slender tanks as in Fig. 9.30.



The propellant tank structure can vibrate during the ascent of the rocket when unsteady loads are imposed on it, such as by unsteady aerodynamics or otherwise. The structural oscillations are usually at low frequencies from the large mass of propellants in the tanks. The oscillation of the structure can induce a variable head (pressure oscillation) at the inlet to the pump. The amplitude of the pressure oscillations at the pump outlet is increased according to the pressure ratio of the pump. The resulting large oscillatory propellant flow to the thrust chamber results in the modulation of thrust at the same frequency of oscillation. A schematic diagram of the process is given in Fig. 9.31.

The oscillatory thrust leads to an increase in the amplitude of structural vibrations, essentially along the thrust axis. The elasticity of the propellant feed system further responds to these oscillations. The interactions between the flow fluctuations magnified by the pump, the resulting thrust oscillations and the structural vibrations during the flight of the rocket makes the rocket go up in jerks, very much like a Pogo stick. This instability is known as pogo instability. The Pogo stick, it may be recalled, consists of a stick with a T bar handle at one end and spring-loaded footpad at the other end (Fig. 9.32). When a person mounts on the footpad and compresses it and thereafter lifts off his weight, the stick lifts off the ground and he is able to hop.



**Fig. 9.30** Liquid Propellant Rocket with Propellant Tanks (Source ISRO)

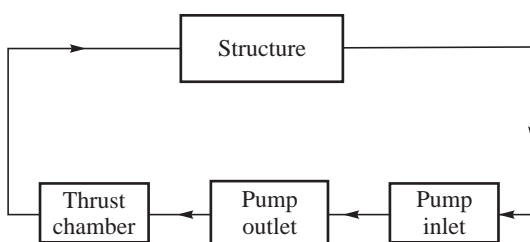


**Fig. 9.31** Feedback Loop for Pogo Instability

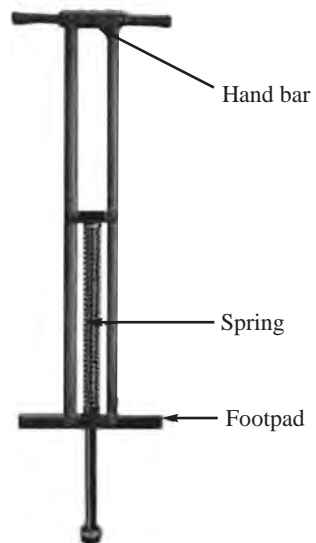


**Fig. 9.32** Pogo Stick

The processes responsible for the Pogo instability are distinctly different from other forms of combustion instabilities given earlier. To prevent the occurrence of the pogo instability, the response



of the feed system at the characteristic structural frequencies is brought down. This is done by introducing gas bubbles in the fluid line. A mixture of gas and liquid has net lower sound velocity, and this reduces the characteristic frequency of the propulsion system and dampens the oscillations in the fluid line. A Pogo corrector is employed to inject the gas into the fluid line. This is a detuning device which ensures enough separation between the structural and propulsion system frequencies, thereby preventing an interaction.



## 9.12 COMBUSTION INSTABILITY: SUPPRESSION AND CONTROL

The different processes contributing to combustion instability have been discussed in this chapter. The instability is seen to occur at low frequencies in the bulk mode of oscillations and at high frequencies in the wave mode. While for feed system coupling, combustion delay time and residence time of the propellant in the chamber are the main parameters governing the bulk mode of combustion instability in liquid propellant rockets, the propellant composition, chamber pressure and  $L^*$  influence the occurrence of the instability in solid propellant rockets. The wave mode of instability arises from the interaction of the standing waves in the longitudinal, radial, tangential or a combination of these with the combustion process.

In addition to the bulk and wave modes of combustion instabilities, non-linear instabilities and process induced instabilities are also seen to be possible. In particular, popping instability from mixture ratio stratification in liquid propellant rockets, oscillations from vortex shedding in large segmented solid propellant rockets and pogo instability from structural interactions in liquid propellant rockets were examined. In all cases, the feedback associated with perturbations in the rocket chamber and its interaction with combustion or a related process contributes to the occurrence of combustion instability.

Considerable efforts have been devoted to overcome the instability when encountered in the development of rockets. The practice has been to adopt a passive type of control involving detuning of either the chamber or a process and reducing the gains associated with the energy exciting the oscillations. These were discussed in this chapter. Since the combustion instabilities are associated with feedback, the possibilities of actively controlling the instability by modifying the feedback as and when instability gets triggered is being studied. The application of active control to prevent the occurrence of combustion instability in rockets is yet to be demonstrated.

## SOLVED EXAMPLES

**Example 9.1** Characteristic frequencies in a thrust chamber:

A thrust chamber has an inner diameter of 0.25 m and a length of 0.9 m between the injector and the nozzle throat. It operates at a pressure of 10 MPa. The temperature of the hot gases in the chamber is 3200 K. The molecular mass and specific heat ratio of the gases are 22 kg/kmole and 1.22 respectively. Determine the fundamental frequency of the oscillations in the longitudinal, tangential and radial modes.

If a quarter wave tube of diameter 5 mm and length 0.11 m is connected to the chamber at the head end and the composition and temperature of the gas in this tube are the same as in the thrust



chamber, determine the frequencies of the fundamental and first harmonics of the quarter wave tube.

**Solution:** Longitudinal, tangential and radial frequencies:

For the longitudinal mode of oscillations, the chamber can be approximated as a tube of length equal to the distance between the injector and the nozzle throat. The nozzle throat is taken as a closed end, since rapid changes in density occur here and functions as a reflecting surface. For tangential and radial modes, the diameter of the chamber is the relevant parameter.

$$\text{The sound speed in the chamber} = \sqrt{\frac{1.22 \times 8314 \times 3200}{22}} = 1215 \text{ m/s}$$

$$\text{The fundamental frequency in the longitudinal mode} = \frac{a}{2L} = \frac{1215}{2 \times 0.9} = 675 \text{ Hz}$$

The fundamental frequency in the tangential and radial modes are the first tangential and first radial modes and are found from eqs. 9.61 as:  $\beta_{m,l} \times a/2\pi R$ , where  $R$  is the radius of the chamber and  $\beta_{m,l}$  gives the non-dimensional frequency for the different modes (Table 9.1). In the case of the first tangential  $m = 1$  and  $l = 1$ ,  $\beta_{m,l} = \beta_{1,1}$ , the value of which is 1.841. In the case of the first radial mode  $m = 0$  and  $l = 2$  and the value of  $\beta_{0,2}$  is 3.832. With the radius of the chamber as 0.125 m and  $a = 1215$  m/s the frequencies of the first tangential mode  $f_{1t}$  and the first radial mode  $f_{1r}$  are:

$$f_{1t} = \frac{1.841 \times 1215}{2 \times \pi \times 0.125} = 2848 \text{ Hz}; f_{1r} = \frac{3.832 \times 1215}{2 \times \pi \times 0.125} = 5927 \text{ Hz}$$

Frequencies of the quarter wave tube:

The quarter wave tube is closed at one end and open at the other. The open end is a pressure node while the closed end is a pressure antinode so that for the fundamental and first harmonic, the length of the tube corresponds to 0.25 of the wavelength and 1.25 of the wavelength respectively. This gives the frequencies of the fundamental and first harmonic as  $a/4L$  and  $5a/4L$  respectively. With  $L = 0.11$  m and  $a = 1215$  m/s, the frequencies are 2761 Hz and 13,807 Hz.

**Example 9.2** Mode of combustion instability and fixes for a liquid propellant rocket:

The initial version of the Viking liquid propellant rocket got into the problem of combustion instability during the second flight of the Ariane launch vehicle. High amplitude pressure oscillation at a dominant frequency of about 2300 Hz were observed. It is required to determine the mode of oscillation.

**Solution:** The diameter of the thrust chamber is about 0.50 m and the length of the chamber up to the throat is about 0.6 m. The temperature of the combustion products is about 3100 K and the specific heat ratio is 1.19. The mean molecular mass is 20.70 kg/Kmol. The sound speed in the chamber  $a$  is,

$$\text{therefore, } \sqrt{\frac{1.19 \times 8314 \times 3100}{20.7}} = 1217 \text{ m/s.}$$

The frequencies of the oscillations in the longitudinal, tangential, radial and mixed tangential cum radial modes calculated as per Example 9.1 are given in the Table 9.2.

**Table 9.2** Mode and Frequency of Oscillations

Sl. No.	Mode of Oscillation	Frequency (Hz)	Formula Used
1.	Longitudinal (Fundamental)	1014	$\frac{a}{2L}$
2.	Longitudinal (First harmonic)	2028	$\frac{a}{L}$
3.	First tangential	1426	$\frac{\beta_{1,1} \times a}{2\pi R}; \beta_{1,1} = 1.841$
4.	First radial	2968	$\frac{\beta_{0,2} a}{2\pi R}; \beta_{0,2} = 3.832$
5.	First tangential cum first radial	4130	$\frac{\beta_{1,2} \times a}{2\pi R}; \beta_{1,2} = 5.331$
6.	Second tangential	2366	$\frac{\beta_{2,1} \times a}{2\pi R}; \beta_{2,1} = 3.054$
7.	Second radial	5196	$\frac{\beta_{0,3} \times a}{2\pi R}; \beta_{0,3} = 7.016$
8.	Second tangential cum first radial	5171	$\frac{\beta_{2,2} \times a}{2\pi R}; \beta_{2,2} = 6.707$

It is seen from the Table 9.2 that the second tangential mode is very near to the frequency observed in the instability. The calculations of the sound speed would not be precise as adiabatic conditions were assumed in the calculations. The frequencies obtained in the other modes are far removed from the observed frequency. Hence it is likely that combustion instability has occurred in the second tangential mode.

The propellants used in this rocket were N<sub>2</sub>O<sub>4</sub> for the oxidizer and UDMH for the fuel. The following procedure was employed for preventing the occurrence of instability.

The energy release from combustion was decreased by reducing the heat value through addition of hydrazine hydrate to UDMH. The rate of energy release was also reduced by enhancing the droplet sizes formed by the injector. The diameter of the injection holes were increased for this purpose. A decrease of the energy release rates contributed to stabilizing the combustion.

In addition, an annular slot was placed at the nozzle end which would have its own characteristic frequency and detune the chamber. The fixes used for the stabilization were a combination of gain stabilization and detuning.

**Example 9.3** Characteristic frequency of L\* instability in a solid propellant rocket:

A non-aluminized composite solid propellant rocket uses ammonium perchlorate (AP) having particle sizes of 300 and 30 μm. If the mean burn rate at which L\* instability is observed is 3 mm/s, what is the likely frequency of L\* oscillations?

**Solution:** L\* instability is a low frequency bulk mode of oscillation. The periodicity of the consumption of the heterogeneity is the ratio of the burn rate to the size of the AP =  $\frac{3}{300 \times 10^{-3}} = 10$  Hz. The larger particle size is used since it represents the most significant heterogeneity in the propellant.



The other characteristic length scale is the thermal depth of the propellant. If the thermal diffusivity of the propellant is  $\alpha(\text{m}^2/\text{s})$  and the burn rate of the propellant is  $r(\text{m/s})$ , then the thermal depth  $\delta = \alpha/r$ . The thermal diffusivity of a non-aluminized composite propellant  $\approx 20 \times 10^{-4} \text{ cm}^2/\text{s}$ . For a burn rate of 3 m/s,  $\delta = \frac{20 \times 10^{-4}}{0.3} = 0.0067 \text{ cm}$ . The frequency based on the thermal depth is  $\frac{r}{\delta} = \frac{3 \times 10^{-1}}{0.0067} \approx 45 \text{ Hz}$ .

The thermal depth may be more relevant for aluminized composite propellants since a melt layer is formed over the burning surface. The thermal diffusivity of aluminized composite propellants is typically about  $14 \times 10^{-4} \text{ cm}^2/\text{s}$ .

For the non-aluminized propellant,  $L^*$  instability is likely from the coarse crystals of AP and the frequency would be 10 Hz.

**Example 9.4** Prediction of bulk mode instability in a liquid propellant rocket and the frequency of oscillations:

A pressure-fed liquid propellant rocket with radiation and film-cooling of the thrust chamber operates at a chamber pressure of 0.8 MPa. The pressure drop across the injector is 0.3 MPa. If the residence time of the propellants within the chamber is 3 ms and the combustion delay time of the propellants is 10 ms, is it likely that the bulk mode of oscillations would occur in the thrust chamber?

**Solution:** From eq. 9.34, we have for bulk mode of instability:

$$\frac{t_c}{t_{\text{res}}} \geq \frac{\pi - \tan^{-1} \sqrt{\beta^2 - 1}}{\sqrt{\beta^2 - 1}}$$

$$\text{With } \beta = \frac{P_c}{2\Delta p} = \frac{0.8}{0.6} = 1.33, \tan^{-1} \sqrt{\beta^2 - 1} = \frac{41.25}{180} \times \pi = 0.23\pi$$

$$\frac{t_c}{t_{\text{res}}} \geq \frac{0.77\pi}{0.88} = 2.75 \text{ for instability to occur}$$

The given data yields  $\frac{t_c}{t_{\text{res}}} = 3.33$ . This is larger than 2.75 and hence instability in the bulk mode is likely to occur.

The frequency of the oscillations is obtained from eq. 9.32 as:

$$\omega t_c = \pi - \tan^{-1} \sqrt{\beta^2 - 1} \text{ giving}$$

$$\omega = \frac{0.77\pi}{0.01} = 242 \text{ rad/s. This gives the frequency to be 39 Hz.}$$

## NOMENCLATURE

$a$  : Sound speed (m/s); oxidizer particle size ( $\mu\text{m}$ )

$A_0$  : Injection area ( $\text{m}^2$ )



---

$A_t$	: Throat area ( $\text{m}^2$ )
$C_d$	: Discharge coefficient
$C^*$	: Characteristic velocity of propellant (m/s)
$D$	: Diameter (m)
$Da$	: Heat release parameter
$E$	: Energy (J)
$\dot{E}$	: Rate of change of energy ( J/s)
$f$	: Frequency (Hz)
$J_m$	: Bessel function of order m
$K$	: Wave number $\left( = \frac{2\pi}{\lambda} \right)$
$l$	: Mode of oscillation in tangential (azimuthal) direction
$L$	: Length of chamber (m)
$L^*$	: Characteristic length of chamber $\left( = \frac{V_C}{A_t} \right)$
$m$	: Mass (kg); mode of oscillation in radial direction
$\dot{m}$	: Mass flow rate (kg/s)
$\dot{m}'$	: Fluctuation in mass flow rate (kg/s)
$n$	: Mode of oscillation in longitudinal direction
$p_C$	: Chamber pressure (Pa)
$p'$	: Pressure fluctuation (Pa)
$\dot{Q}$	: Heat release rate (J/s)
$r$	: Radius (m)
$R$	: Mixture ratio; Inner radius of chamber (m); Specific gas constant (kJ/kg K)
$Re$	: Reynolds number
$S$	: Surface area ( $\text{m}^2$ )
$t$	: Time (s)
$t_C$	: Combustion delay (s)
$t_{\text{res}}$	: Stay time of gases in chamber (s)
$T$	: Time period for one oscillation (s)
$T_C$	: Temperature of gases in chamber (K)
$u$	: Velocity (m/s)
$V$	: Velocity (m/s); Volume ( $\text{m}^3$ )
$V_C$	: Volume of chamber ( $\text{m}^3$ )
$v'$	: Velocity fluctuation in chamber (m/s)



- $x$  : Distance along longitudinal axis of chamber  
 $y$  : Acoustic admittance of medium  
 $Y$  : Admittance defined by eq. 9.62  
 $Y_m$  : Modified Bessel function of order m  
 $z$  : Specific acoustic admittance defined by eq. 9.69 (Pa – s/m)  
 $\alpha$  : Growth rate of oscillations (1/s); Thermal diffusivity ( $\text{m}^2/\text{s}$ )  
 $\beta$  : Non-dimensional pressure ratio  $\left( \frac{\bar{p}_C}{2(p_{\text{inj}} - \bar{p}_C)} \right)$ ; Real part of admittance  $Y$   
 $\beta_{m,l}$  : Non-dimensional frequency of standing wave in  $r, \theta$  directions  
 $\delta_{th}$  : Thermal depth (m)  
 $\delta$  : Phase delay  
 $\phi$  : Non-dimensional pressure perturbation  $\left( \frac{p'}{\bar{p}_C} \right)$   
 $\gamma$  : Specific heat ratio  
 $\kappa$  : Acoustic conductance ratio of burning surface  
 $\lambda$  : Wavelength (m)  
 $\theta$  : Azimuthal angle  
 $\rho$  : Density ( $\text{kg}/\text{m}^3$ )  
 $\sigma$  : Rate of energy addition defined by eq. 9.40  
 $\tau$  : Time (s)  
 $\omega$  : Angular frequency (rad/s)  
 $\Delta p$  : Maximum amplitude of pressure perturbation (Pa)  
 $\Delta V$  : Maximum amplitude of velocity perturbation (m/s)  
 $\Phi$  : Burning surface parameter  
 $\Gamma$  : Function of  $\gamma$   $\left( \Gamma = \sqrt{\gamma} \left[ \frac{2}{\gamma + 1} \right]^{\frac{\gamma + 1}{2(\gamma - 1)}} \right)$

## Subscripts

- $C$  : Chamber  
 $d$  : Decay  
 $ft$  : Flow turning  
 $g$  : Gas generated in chamber; growth  
 $\text{inj}$  : Injection conditions  
 $m$  : Solid Propellant grain



- 
- $n$  : Nozzle  
 $O$  : Steady state  
 $p$  : Propellant  
 $T$  :  $T$  burner

### Superscripts

- ' : Fluctuation  
- : Steady state

## EXERCISES

1. The thrust chamber of a liquid propellant rocket measures 1.5 m between the injector and the nozzle throat. Considering the nozzle throat to be equivalent to a closed end, determine the frequencies of the standing waves in the fundamental, first and second harmonics for wave modes along the axis of the chamber.  
You can assume the temperature of the hot gases in the chamber to be 3200 K, the specific heat ratio of the gases as 1.2 and the mean molecular mass of the gas as 20 kg/kmole.  
Show the wave forms of the standing waves and the locations of the pressure nodes and antinodes in the fundamental, first and second harmonics.
2. (i) The growth constant of a solid propellant is to be determined in a  $T$  burner at a frequency of 600 Hz. Determine the length of the  $T$  burner given that the sound velocity of the gases in the  $T$  burner is 500 m/s.  
(ii) Determine the growth constant of the propellant, if the maximum amplitude of pressure oscillations measured in the  $T$  burner at two instants of time of 0.3 and 0.6 seconds are 0.02 and 0.025 MPa respectively.
3. The amplitude of pressure perturbation behind a wave in ambient atmosphere (pressure and temperature of 0.1 MPa and 27°C) is 50 Pa. The specific heat ratio of air is 1.4. Determine the temperature perturbation in °C due to the pressure perturbation assuming isentropic process.
4. A vertically-held tube, open at both ends generates oscillatory pressures at the fundamental frequency of the tube when heat is released in the tube. This configuration of the tube, generating sound by heat release, is known as Rijke tube. Show that the amplitude of the oscillations is a maximum when the heat source is located at one-fourth the length of the tube, from the lower end.

### References

1. Barrere, M., Jaumotte, A., Veubeke B.J. and Vanderkerckhove J., *Rocket Propulsion*, Elsevier Publishing Company, Amsterdam, 1960.
2. Brownlee, W.G., *Nonlinear Axial Combustion Instability in Solid Propellant Motors*, J. AIAA, vol. 2, 1964, pp. 275-284.
3. Chu, B.T., *On Energy Transfer to Small Disturbances in Fluid Flow (Part-I)*, Acta Mechanica, vol.1, 1965, pp. 215-234.
4. Coates, R.L. and Horton, M.D., *Design Considerations for Combustion Stability*, J. Spacecraft and rockets, vol. 6, 1968, pp. 296-302.



5. De Luca,+ L., Price E.W., and Summerfield M., *Non-steady Burning and Combustion Stability of Solid Propellants*, Progress in Astronautics and Aeronautics, vol. 143, AIAA Inc., Washington, 1992.
6. Harrje, D.T., and Reardon F.H., *Liquid Propellant Rocket Combustion Instability*, NASA SP-194, NASA Washington, 1972.
7. Kinsler, L.E., Frey A.R., Coppens D.B., and Sanders J.V., *Fundamentals of Acoustics*, 4th ed., John Wiley and Sons, New York, 2000.
8. Kumar, R.N., and McNamara R.P., *Some Experiments related to L Star Instability in Rocket Motors*, AIAA Paper 73-1300, 1973.
9. Lawver, B.R., *A Model of the Hypergolic Propellant Phenomenon*, J. Spacecraft and Rockets, vol. 9, 1972, pp. 225-226.
10. Mukunda, H.S., *Understanding Aerospace Propulsion*, Interline Publishing, Bangalore, 2004.
11. Oefelein, J.C. and Yang, V., *Comprehensive Review of Liquid Propellant Combustion Instabilities in F-1 Engine*, J. Propulsion and Power, vol. 9, 1993, pp. 657-677.
12. Schoyer, H.R.R., *Results of Experimental Investigation of L Star Phenomenon*, J. Spacecraft and Rockets, vol. 17, 1980, pp. 200-207.
13. Seghal, R. and Strand, L.D., *A Theory of Low Frequency Combustion Instability in Solid Rocket Motors*, AIAA J., vol. 2, 1964, pp. 696-702.
14. Summerfield, M., *A Theory of Unstable Combustion in Liquid Propellant Rocket Systems*, J. American Rocket Society, vol. 21, 1951, pp. 108-114.
15. Yang, V., and Anderson, W., *Liquid Rocket Engine Combustion Instability*, Progress in Astronautics and Aeronautics, vol. 169, AIAA Inc., Washington, 1995.

## Glossary

- Acoustic admittance of propellant: The ratio of the non-dimensional velocity perturbation resulting from a nondimensional pressure perturbation
- Acoustic conductance ratio: Ratio of acoustic admittance of burning surface to acoustic admittance of the medium in which burning takes place
- Antinodes: Locations in standing wave wherein amplitude of oscillations are a maximum
- Bulk mode of combustion instability: Entire volume oscillates in unison; low frequency instability
- Chuff: Periodic ignition followed by extinction
- Circular frequency: Frequency of oscillations in radians per second
- Combustion delay: Time taken for heat release to take place after propellant injection considering the processes of atomization, evaporation, mixing and chemical reactions
- Chemical delay: Time taken for chemical reactions to take place
- Detuning: Making the frequency of the combustion process to be different from the frequency of the wave modes and the other characteristic frequencies in the chamber
- Damping: Reduction of energy in the oscillation by viscosity, radiation of acoustic pressure, heat losses, friction, etc.
- Gain stabilization: Reducing the rate of energy supplied to the oscillations from the combustion process
- Entropy waves: Progress of zone of heat release in combustion chamber
- Frequency: Number of oscillations per unit time
- Growth constant: Rate of increase of the amplitude of the waves



Harmonics: Modes higher than the fundamental

Hydraulic flip: Unsteady flow through injection orifice from attached and separated flows

Longitudinal modes: Oscillations along the axial length of the chamber

L\* instability: Low frequency bulk mode of oscillations

Mixed modes of oscillations: Combination of tangential, radial and/or longitudinal modes

Non-linear instability: Combustion instability triggered only with finite amplitudes of the disturbances

Nodes: Locations in standing wave wherein the amplitude of oscillation is zero

Phase difference: Shift or offset between waves expressed as a fraction of a complete cycle of oscillation

Popping instability: Oscillations from localized explosions in stratified regions in combustion chamber

Pogo instability: Low frequency oscillation in liquid propellant rockets due to structural oscillations being amplified in turbo-pump and causing oscillations in thrust

Power density: Energy per unit volume per unit time

Radial modes: Oscillations in the radial direction of the cylindrical chamber

Rayleigh criterion: The addition of heat to a pressure wave when the amplitude of the wave in compression is a maximum and the removal of heat from the wave in rarefaction when the amplitude is a maximum lead to growth of oscillations

Reynolds number: Ratio of the inertial forces to the resisting viscous forces

Residence time: Time spent by the medium in the device

Specific acoustic impedance: The ratio of pressure fluctuation in a medium associated with a given velocity perturbation (Pa·s/m)

Standing wave: Interaction between an incident traveling wave and its reflection leads to the formation of a standing wave. The standing wave has maximum amplitudes of oscillation (antinodes) at certain locations and no oscillations (nodes) at some locations

T burner: A small diameter straight tube with propellant grains at the ends and a vent at the centre for measuring growth constant of the propellant in the fundamental standing wave mode along the length of the tube

Tangential modes: Oscillations along the circumferential direction of a cylindrical chamber

Thermal depth of propellant: Depth over which the propellant gets heated during the burning process

Vortex shedding: Vortices formed from protrusions at segment joints between grains

Wave mode of combustion instability: Standing waves formed from the interaction of incident and reflected waves interact with unsteady combustion processes; high frequency instability

Wave number: Angular or circular wave number inversely proportional to wavelength and given by  $2\pi/\lambda$  where  $\lambda$  is the wavelength

## Chapter 10

### Electrical Rockets

*The rocket pioneers Konstantin E Tsialkovsky, Herman Oberth and Robert Goddard addressed the development of high performance of electrical rockets from the acceleration of charged particles in electric and magnetic fields. Valentin Petrovich Glushkov constructed the first electrical rocket from electrically vapourised liquid metals. Ernst Stuhlinger designed ion propulsion for planetary missions.*

**C**hemical rockets using solid and liquid propellants provide exhaust jet velocities between 2000 and 4800 m/s. The requirements of a high combustion temperature and low molecular mass of the combustion products for obtaining high exhaust jet velocities impose a limitation on the achievable jet velocities. The use of electrical energy permits the heating of propellants of low molecular mass to achieve jet velocities higher than obtainable in chemical rockets. Further the electrostatic and electromagnetic forces also permit the acceleration of charged particles and plasmas to very high velocities. Electrical rockets, depending on the availability of power, can therefore, offer very high values of specific impulse and are dealt with in this Chapter. The electrostatic and electromagnetic forces, central to the generation of high efflux velocities in electrical rockets, are first discussed. Different types of electrical rockets are thereafter discussed and their performance assessed.



#### 10.1 ELECTROSTATIC FORCE AND ELECTRIC FIELD

Forces exist between electrically charged particles. Coulomb gave the law for such forces in a form similar to the Newton's law for gravitation. The law states that the force ( $\vec{F}$ ) between a pair of point charges is directly proportional to the product of the charges ( $q_1, q_2$ ) and inversely proportional to the square of the distance ( $\vec{r}$ ) separating them (Fig. 10.1).



$$\vec{F} = K \frac{q_1 q_2}{|\vec{r}|^3} \vec{r} \quad \dots(10.1)$$

In the above expression  $q_1$  and  $q_2$  are measured in Coulomb, force  $F$  is in Newton and distance  $r$  is in meter. The constant  $K$  is:

$$K = 9 \times 10^9 \text{ Nm}^2/\text{Coulomb}^2 \quad \dots(10.2)$$

The constant  $K$  is often written as  $1/(4\pi\epsilon_0)$ , where  $\epsilon_0$  is defined as the electrical permittivity of free space. Permittivity denotes the ability to store a charge in the medium. The unit of permittivity is

$$\frac{1}{K} = \frac{\text{C}^2}{\text{Nm}^2} = \frac{\text{C}}{(\text{Nm/C})\text{m}} = \frac{\text{C}}{\text{Vm}} = \frac{\text{F}}{\text{m}} \quad \dots(10.3)$$

The potential difference in Volts (V) which corresponds to the work done in transporting unit charge, viz., (Nm/C) and Farad (F) which denotes the charge in Coulomb per volt (C/V) have been used in the above expression. The permittivity of free space  $\epsilon_0$  is determined from the constant  $K$  in eq. 10.2 as  $8.852 \times 10^{-12} \text{ F/m}$ .

The permittivity of any medium ( $\epsilon$ ) is expressed as a function of the permittivity of free space ( $\epsilon_0$ ) and is given as:

$$\epsilon = \epsilon_r \epsilon_0 \quad \dots(10.4)$$

where  $\epsilon_r$  is called relative permittivity.

In a manner similar to a gravitational field about a heavy body, the region around a charged particle can be defined to have an electrical field if a unit charge placed therein experiences a force. The electric field is obtained from eq. 10.1 as:

$$\vec{E} = \frac{K q_1}{|\vec{r}|^3} \vec{r} \quad \dots(10.5)$$

If a charge  $q_2$  is placed in this field, the force acting on it is given by:

$$\vec{F} = \vec{E} q_2 \quad \dots(10.6)$$

The unit of electrical field is:

$$\frac{\text{N}}{\text{C}} = \frac{\text{Nm}}{\text{Cm}} = \frac{\text{V}}{\text{m}} \quad \dots(10.7)$$

$\vec{E}$  is expressed in units of Volt/meter.

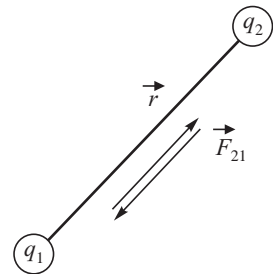


**Fig. 10.1** Force between Charged Particles



## 10.2 ELECTROMAGNETIC FORCE AND MAGNETIC FIELD

If a charge experiences a force moving in space but does not experience it when at rest, then the region in space is said to have a magnetic field. The magnetic field is denoted by  $\vec{B}$ . A charge in the field is at rest and a 'dipole' aligns along the field. A charge  $q$  moving with velocity  $v$  experiences a force perpendicular to the direction of  $\vec{v}$  and  $\vec{B}$ . The force  $\vec{F}$  is given by:



$$\vec{F} = q\vec{v} \times \vec{B} \quad \dots(10.8)$$

If the charge is moving in the direction of the magnetic field, the force is zero. The unit for magnetic field from eq. 10.8 is:

$$\frac{\text{Ns}}{\text{Cm}} = \frac{\text{N}}{\text{Am}} = \text{T} \quad \dots(10.9)$$

The unit [N/(Am)] is known as Tesla (T). It is also called Weber/m<sup>2</sup>. The Earth's magnetic field is about  $0.5 \times 10^{-4}$  T.

The ability of a material to magnetize in a magnetic field is called permeability. The permeability of free space is denoted by  $\mu_0$  and is related to the permittivity of free space ( $\epsilon_0$ ) through the velocity of light in vacuum ( $C_0$ ), viz.,

$$\mu_0 = \frac{1}{C_0^2 \epsilon_0} \quad \dots(10.10)$$

The velocity of light in vacuum  $C_0$  is  $3 \times 10^8$  m/s. The unit of permeability is Henry/meter (H/m) and from eq. 10.10 is:

$$\frac{1}{(\text{m}^2/\text{s}^2)(\text{C}^2/\text{Nm}^2)} = \frac{\text{Ns}^2}{\text{C}^2} = \frac{\text{N}}{\text{A}^2} \quad \dots(10.11)$$

The permeability of free space is  $1.257 \times 10^{-6}$  H/m.

Similar to relative permittivity  $\epsilon_r$ , given in eq. 10.4, relative permeability of a medium, ( $\mu_r$ ), is defined to give the permeability of the medium as  $\mu = \mu_0 \mu_r$ . The induced magnetic field  $\vec{B}$ , in Tesla, in a medium of permeability,  $\mu$ , from an auxiliary magnetic field of strength  $\vec{H}$ , [formed by a given amount of charge per unit area, traveling at a given velocity  $\left( \frac{\text{C}}{\text{m}^2} \times \frac{\text{m}}{\text{s}} \right)$ ], is  $\mu \vec{H}$  Tesla

$$\left[ \frac{\text{C}}{\text{m}^2} \times \frac{\text{m}}{\text{s}} \times \frac{\text{N}}{\text{A}^2} = \frac{\text{N}}{\text{Am}} = \text{T} \right].$$



### 10.3 COMBINED ELECTRICAL AND MAGNETIC FIELD

In the presence of both the electric field  $\vec{E}$  and magnetic field  $\vec{B}$ , the net force experienced by a charge of  $q$  Coulomb is a combination of electrostatic and electromagnetic forces given by eqs. 10.6 and 10.8, and is:

$$\vec{F} = q\vec{E} + q\vec{v} \times \vec{B} \quad \dots(10.12)$$



## 10.4 OPERATING PRINCIPLE AND CLASSIFICATION OF ELECTRICAL ROCKETS

Electrical rockets are classified into electro-thermal, electrostatic and electromagnetic rockets depending on whether electrical heating or electrostatic or electromagnetic forces are used for achieving the high jet velocities. The electrical rockets generally have much lower thrust than the chemical rockets and are referred to as thrusters. We shall briefly consider the operating principle of the different types of electrical thrusters in the following.



## 10.5 ELECTRO-THERMAL THRUSTERS

The propellants in electro-thermal thrusters are heated to high temperatures using electrical power, and the hot gases are expanded in a convergent-divergent nozzle to provide the thrust. There are two different configurations of electro-thermal thrusters. In one, heat is transferred to the propellant from electrically heated surfaces. The mode of heating of the surfaces is by electrical resistance and the thrusters are, therefore, known as resistojets. In the other mode, known as arcjet, electrical arc discharge is used to heat the propellants. The propellant flows through the electrical arc discharge. Schematic diagrams of the resistojet and arcjet are given in Figs. 10.2 and 10.3, respectively.

Hydrogen, ammonia and nitrogen have been used as propellants for the electro-thermal thrusters. Hydrogen, having lower molecular mass, yields the highest performance. The gases are heated to higher temperatures in the electrical arc discharge compared to resistance heating. As the gas temperature increases, the specific impulse increases. The overall efficiency and reliability of the thrusters, however, decreases with the use of higher temperatures, thus imposing a limit on the achievable specific impulse. The losses are also higher with arc heating, since in the region of the arc discharge, ionization and dissociation of the gases take place.

The arc discharge and the initiation of thrust can be automatically started in the arc jet thrusters by commencing the flow of gases into the arc discharge chamber. The voltage, at which the arc forms, is given by Paschen's law which states the dependence of the breakdown voltage as a function of the product of the arc gap and the gas pressure. The arc breakdown voltage is minimum at a critical value of this product. In the vacuum conditions of space, the value of the product of pressure and arc gap is near zero which is much lower than the critical value at which the arc discharge can spontaneously occur. As the gas flow is initiated, the enhanced pressure in the arc gap causes a

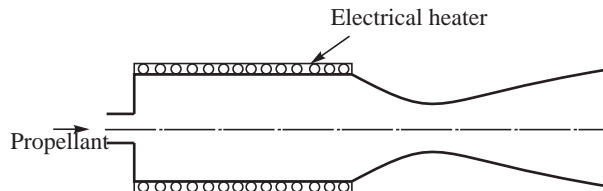


Fig. 10.2 Schematic Diagram of Resistojet

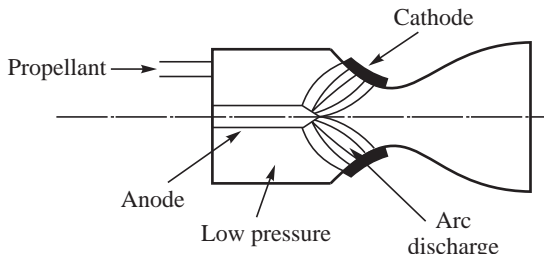


Fig. 10.3 Schematic of Arcjet



reduction in the breakdown voltage, and a spontaneous arc discharge takes place for a given impressed voltage. Other configurations of starting electrical arc discharge have been attempted, such as using a mechanical starter and forming an arc at small distance, and then stabilizing it for larger distances.

The highest temperature in the arc jet is in the region of the arc-core. The gases, comprising plasma of neutral particles and high energy charged particles, are not in thermodynamic equilibrium. The arc generated radio noises and the ionized wake formed by the arc jet thrusters are points of concern in their application.

The ionized gases of the arc jet can also be accelerated using magnetic fields. Such arc jet thrusters are known as arc jets with accelerator.

#### **10.5.1 Chemical Arc Jet Thruster and Augmented Electro-thermal Hydrazine Thruster**

Monopropellant rockets using hydrazine and hydrogen peroxide can also be used in conjunction with the arc jets and resisto-jets. Here the chemical energy of the propellant is released in addition to the electrical heat. The arc jet, using a monopropellant, is known as chemical arc jet thruster. In a resistojet configuration, hydrazine is dissociated using electrical heating and the temperature of the dissociated products is further enhanced by resistive heating. The thruster is referred to as Augmented Electrothermal Hydrazine Thruster (AEHT). Heat is transferred from electrically heated surfaces to the dissociated products of combustion by conduction and convection. Adequate residence time is provided for the heat transfer. The increase in the temperature of the gases provides higher values of the specific impulse. The use of very high temperatures, however, introduces problems of compatibility with the materials of construction of the thruster.



### **10.6 ELECTROSTATIC THRUSTERS**

#### **10.6.1 Principle and Choice of Propellants**

The propellant is electrically charged in an ionization chamber and then accelerated to high velocities using an electrostatic field. If a given mass of propellant is electrically charged to  $q$  (Coulomb), the electrostatic force that it experiences in an electric field  $\vec{E}$  (Volts/m) was seen earlier this chapter to be  $\vec{F} = q\vec{E}$  (N). If the mass of the charged particle is  $m$  (kg) and if the particle is accelerated to a velocity  $V_J$  (m/s) by the electrostatic field, the kinetic energy achieved is  $\frac{1}{2} mV_J^2$  (J). This kinetic energy comes from the work received by the charge  $q$  due to the potential difference  $V$  volts to which it is subjected in the electric field  $\vec{E}$ . Noting that the potential difference is the work done in moving a unit charge from the lower to the higher potential ( $V$  volts), we have under ideal conditions:

$$\frac{1}{2} mV_J^2 = qV \quad \dots(10.13)$$



This gives the efflux velocity as:

$$V_J = \sqrt{\frac{2qV}{m}} \quad \dots(10.14)$$

Large values of velocity  $V_J$ , typically between 30 and 200 km/s, are obtained with high voltages. As the mass of the propellant particle reduces, the velocity  $V_J$  increases.

The thrust generated is:

$$F = \dot{m}V_J$$

Here,  $\dot{m}$  is the rate of efflux of the charged particles which can be written as  $mI/q$ .  $I$  is the current in Amperes associated with the motion of the charge  $q$  Coulomb as it is being accelerated, i.e. the beam current associated with motion of the charge. This gives the thrust  $F$  as:

$$F = \frac{mI}{q}V_J \quad \dots(10.15)$$

Substituting the value of  $V_J$  from eq. 10.14 in the above equation and simplifying, we have:

$$F = I \sqrt{\frac{2Vm}{q}} \quad \dots(10.16)$$

A larger mass of the charged propellant is seen to be required to get a higher value of thrust based on the above equation. Positive ions, which have larger mass than the negative ions (electrons), are used and the electrostatic thrusters are referred to as ion thrusters.

Typical propellants which have been used in ion rockets have high atomic mass, such as xenon (atomic number: 54, atomic mass: 132), cesium (atomic number: 55, atomic mass: 133) and mercury (atomic number: 80, atomic mass: 200). Though mercury has the highest mass among the above three elements, the contamination problems of the optical surface of the spacecrafts by mercury vapours have been a problem and its use has been discontinued. Cesium is readily ionized by heated tungsten and has been used for spacecraft propulsion. However, it is very reactive. The current trend is to use xenon, which is a noble gas having atomic mass near to cesium. The atomic number and atomic mass of the heavy propellants xenon, cesium and mercury are compared with hydrogen and nitrogen in Table 10.1.

**Table 10.1** Atomic Mass

Sl. No.	Substance	Mass Relative to Hydrogen Atom	Mass of an Atom
1.	Nitrogen	14	$2.32 \times 10^{-26}$ kg
2.	Hydrogen	1	$0.167 \times 10^{-26}$ kg
3.	Mercury	200	$33.2 \times 10^{-26}$ kg
4.	Cesium	133	$22.1 \times 10^{-26}$ kg
5.	Xenon	131	$21.8 \times 10^{-26}$ kg

It is also possible to use charged particles of some colloidal substances or dust particles instead of ions, and these could be either positively or negatively charged. The use of charged colloidal particles to produce thrust in an electrostatic field is known as colloidal propulsion.



### 10.6.2 Acceleration of Charged Particles—Gridded Ion Thruster

The acceleration of the charged particles to velocity  $V_J$  is done in the electric field between two perforated plates or grids placed adjacent to each other. The first grid extracts or takes in the charged particles (ion). The second grid, maintained at a high potential difference with respect to the first, and of opposite polarity to the charge, accelerates the charge to a high velocity. The first grid is therefore called the extractor grid while the second grid is called the acceleration grid (Fig. 10.4). Since grids are used for the extraction and acceleration of the ions, the thruster is known as a gridded ion thruster. High potential difference is maintained between the extractor and acceleration grids to provide the necessary acceleration to the charged particle.

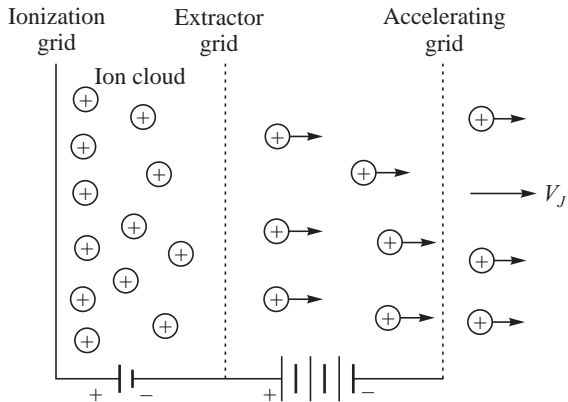


**Fig. 10.4** Acceleration of Charged Particles

### 10.6.3 Maximum Thrust

The accelerated flow of the charge between the extractor and acceleration grids causes a beam current. As the number density of the charge increases, the voltage which extracts the charge at the charge emitting surface decreases. The electric field of the ion cloud basically opposes the accelerating electric field. As the current density increases, a stage is reached when the extracting voltage gradient ultimately reduces to zero, and no flow of ions becomes possible. Thus there exists a limit to the beam current density, beyond which the acceleration of the charged particles by the acceleration grid is not possible. This limiting value of the beam current density is known as the space charge-limited current density ( $j$ ) and is given by the Child-Langmuir law:

$$j = \frac{4\epsilon_0}{9} \sqrt{\frac{2q}{m}} \frac{V^{3/2}}{L^2} \quad \dots(10.17)$$

Here,  $\epsilon_0$  is the permittivity of free space in F/m,  $L$  is the distance between the extractor and acceleration grid in m,  $V$  is the voltage across the grids in Volts,  $q$  is the charge in Coulomb and  $m$  is the mass of the charged particle in kg. Since the thrust given by eq. 10.16 is proportional to the current, the limitation of the current density imposes a ceiling on the maximum possible thrust.

The maximum thrust  $F_{\max}$  based on the limiting value of current density  $j$  can be obtained from the limiting current  $I$  beyond which acceleration of the charged particles is not possible, viz.:

$$I = jA = \frac{4\epsilon_0 A}{9} \sqrt{\frac{2q}{m}} \frac{V^{3/2}}{L^2} \quad \dots(10.18)$$

Substituting the above in eq. 10.16, the value of maximum thrust  $F_{\max}$  is obtained as:

$$F_{\max} = \frac{8\epsilon_0}{9} \frac{V^2}{L^2} A$$

If the diameter of the current beam is  $d$  and the aspect ratio of the beam  $R = d/L$ , the maximum thrust is:

$$F_{\max} = \frac{2\pi}{9} \epsilon_0 V^2 R^2 \quad \dots(10.19)$$



The strong dependence of the thrust on the potential difference between the extractor and accelerator grids is seen from the above equation. It is also seen necessary to reduce the spacing between the extractor grid and the accelerating grid to as small a value as possible. The spacing is about 0.5 mm and the accelerating potentials are between 1.5 and 2.5 kV. The space-charge limitation can be partly overcome and the beam current increased by placing a deceleration grid downstream of the acceleration grid.

The impact of the charged particles on the grids leads to their erosion. The erosion, known as sputtering, is to be avoided if the ion thruster has to operate over a long period of time. Molybdenum is used as the material of the grids due to its low sputter.

#### 10.6.4 Ionization of Propellant – Bombardment Ion Thruster and Radio Frequency Ion Thruster

Different methods of ionization of the propellant, such as, thermionic emission and radio frequency ion generation, have been employed. In thermionic emission, propellant xenon or cesium is passed in gaseous form over a high temperature base grid comprising low work function metals like tungsten, molybdenum, silver or some alkali metals. The grid has a porous structure. Work function denotes the minimum amount of energy needed to remove an electron from a metal. The heated metal releases electrons (thermionic emission) into the propellant gas. The interaction of the electrons and the propellant gas forms ions. The motion of the electrons is controlled by a magnetic field, so that it interacts with the propellant gas for a longer period. Propellants cesium and xenon have low ionization potentials and are ionized readily. Ions are, thus, generated and the bombardment of the surface by the ions produces secondary electron emission, viz., field emission. Ion thrusters employing this principle of generating ions by secondary electron emission are known as bombardment ion thrusters.

The propellant can be ionized by increasing its temperature, by impinging radio frequency waves on it. This is done by containing the propellant at low pressures in an inductively coupled self-sustaining radio frequency discharge unit. Xenon and cesium have low ionization potential and ions of these elements are readily formed due to heating. Thrusters using radio frequencies for generating ions are known as Radio frequency Ion Thrusters (RIT).

The thrust levels of the ion thrusters are generally between 20 and 100 mN and the efflux velocities are about 25,000 m/s.

#### 10.6.5 Neutralization

Charged particles, such as positive ions, while leaving the thruster, cause the opposite charge to be accumulated in the thruster. The positive ions escaping the thruster leave behind excess electrons, making the thruster negatively charged. The negatively charged thruster attracts back the ions leaving the thruster and prevents the generation of thrust. The returning ions also aggravate the space-charge effect discussed earlier. The ions leaving the thruster, therefore, require to be neutralized. This is done by supplying electrons into the accelerated beam of ions leaving the thruster. The electrons are generated from a heated cathode comprising a filament or a plate emitter placed downstream of the accelerator. A schematic diagram of the neutralization process is shown in Fig. 10.5.

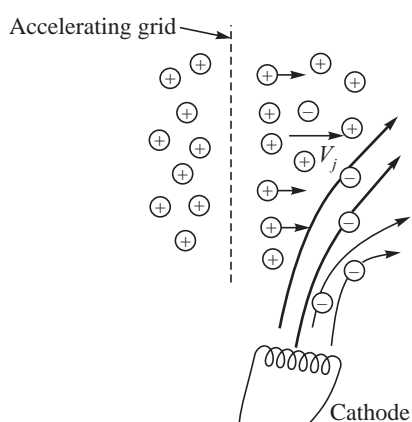


Fig. 10.5 Neutralization



### 10.6.6 Deceleration Grid

The electrons added during the neutralization should not travel upstream of the acceleration grid as these would be accelerated upstream by the same field which accelerates the ions in the downstream direction. If a grid is placed downstream of the acceleration grid at a higher potential than the acceleration grid, it will attract the electrons and prevent them from moving upstream. The space charge limitation and the limiting beam current density will not get aggravated. However, the higher potential in this downstream grid will reduce the velocity of the acceleration ion and act as a decelerating grid. A variation of the potential in the region of the acceleration and deceleration grids is shown in Fig. 10.6.

Though the deceleration grid reduces the ion velocity, it enhances the maximum beam current and hence effectively increases the maximum thrust for the ion rocket. A schematic of the three grids in the ion thruster is shown in Fig. 10.7

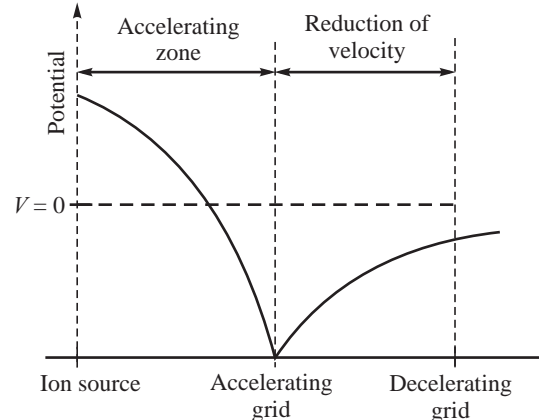


**Fig. 10.6** Voltage Variation Across the Grids

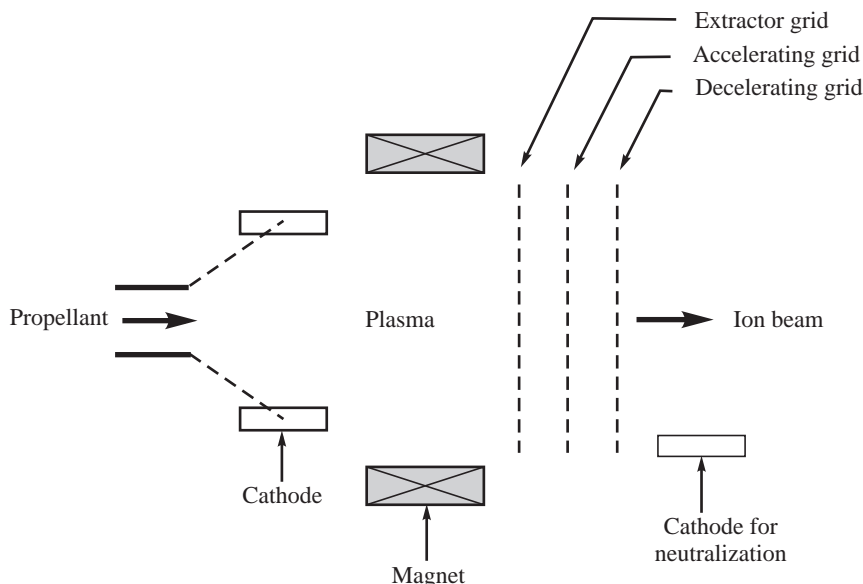


**Fig. 10.7** Schematic of the Three Grids

### 10.6.7 Hall Effect Thruster

We have seen that the two major drawbacks of the ion thruster are the space charge limitation and the sputtering. These two limitations are overcome by use of the Hall Effect, described in the following. Hall Effect states that when the current flows in a conductor in the presence of a magnetic field



perpendicular to the flow of current, the combination of the current and the magnetic field generates a voltage perpendicular to both the current and the field.

An annular chamber is used and electrons generated in the cathode are allowed to be attracted by an anode along the length of the annulus as shown in Fig. 10.8. A radial magnetic field is introduced across the annulus by suitably positioning magnets between the annulus. When electrons travel through the annulus towards the anode, they get deflected by the Hall Effect along the circumferential direction. The electrons, therefore, proceed in the annular space in a spiral path towards the anode.

The propellant gas (usually xenon) is admitted in the annular chamber from the anode as shown in Fig. 10.9. The spirally moving electrons collide with xenon and ionize it efficiently considering the larger values of residence time available from the spiraling electrons for the interaction with xenon.

Electrons are generated using a thermionic cathode as shown in Fig. 10.9. The Hall Effect essentially traps the electrons in the annular passage and uses them effectively to ionize the propellant.

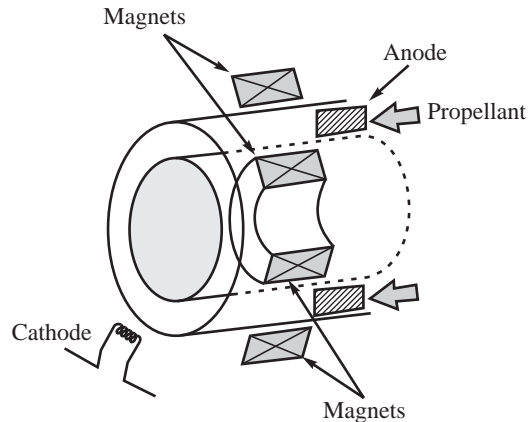


**Fig. 10.8** Schematic of Hall Effect Thruster.

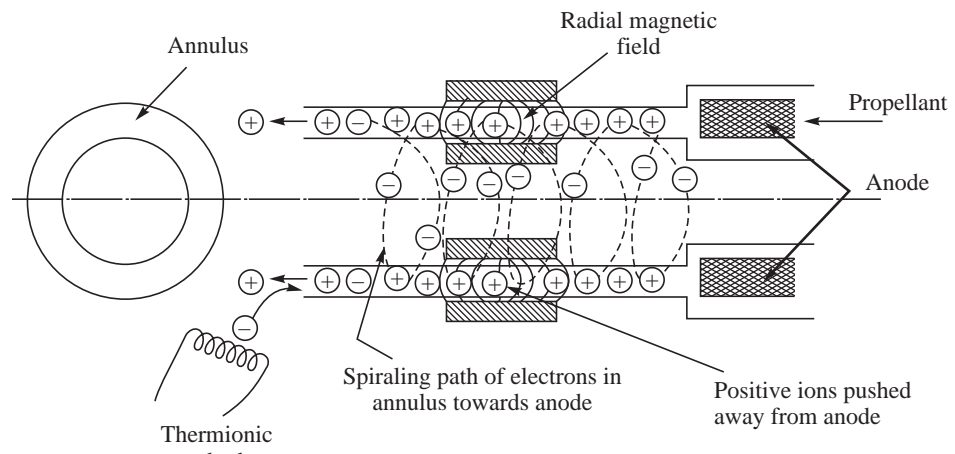


**Fig. 10.9** Hall Effect for Generating and Expelling Ions

While the electrons, being much lighter than the ions, are easily deflected by radial magnetic field to form the swirl flow, the ions continue to be pushed by the electrostatic field away from the anode along the length of the annulus. In this way thrust gets generated.

The acceleration of the ions takes place in neutral plasma and the drawbacks of the space charge limited current observed with ion thrusters no longer exist. The charge of the efflux of the ions is neutralized with the necessary quantity of the negatively charged electrons from the cathode.

The exit velocity of the ions is between 12,000 and 18,000 m/s. The magnetic field is about 0.04 Tesla and the discharge current is about 4 A. The voltages are much lower than those used in the bombardment thruster and are typically around 300 V. The flow rate of the propellants is a few mg/s. Since the electrons do not contribute to the thrust, the efficiency of the thruster is about 70%.



The Hall Effect thrusters are also known as Stationary Plasma Thrusters (SPT). Ceramic material is used for the construction of the annular chamber.

The efflux of the ions from this thruster has higher divergence as compared to a gridded ion thruster and results in contamination and heating of the spacecraft surfaces. An Anode Layer Thruster (TAL) which uses a shorter length of the acceleration chamber gives smaller divergence of the efflux plume.

#### **10.6.8 Field Emission Electric Propulsion**

The surface of liquids exposed to strong electric field can form charged liquid droplets and these could be accelerated in the same electrostatic field. This thrust generation system is referred to as Field Emission Electric Propulsion (FEEP).



### **10.7 ELECTROMAGNETIC THRUSTER**

The ions are accelerated in the electromagnetic thruster by the Lorentz force generated by the charge moving in the magnetic field ( $\vec{F} = q\vec{v} \times \vec{B}$ ). The field could either be an externally applied magnetic field or else it could be an induced magnetic field due to a current ( $B = \mu H$ ). Since the ion must have a velocity in order to generate the thrust, the electromagnetic thrusters are known as dynamic thrusters. The flow consists of ions, electrons and neutral atoms of the propellant which is called as plasma. The electromagnetic thrusters are therefore called as Magneto Plasma Dynamic (MPD) thrusters.

When permanent magnets or stationary electrical coils are wound to generate the required magnetic field, the electromagnetic thruster is known as Applied Field MPD thruster. If a current discharge for the flow of ions also induces the magnetic field, the thruster is known as a Self-induced MPD thruster. We shall examine these two types of MPD thrusters in the following.

#### **10.7.1 Applied Field MPD Thruster**

In this thruster the applied magnetic field  $B$  is orthogonal to the beam current  $I$  which arises from the motion of the ions. A simplified configuration is sketched in Fig. 10.10. The current  $I$  is in the radial direction and is normal to the applied magnetic field  $B$  which is in the tangential direction. The Lorentz force is generated perpendicular to the direction of  $I$  and  $B$  as shown in Fig. 10.10 and this force accelerates the ions in the axial direction.

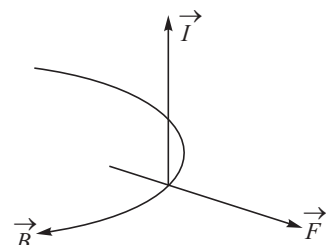


**Fig. 10.10** Principle of Applied Field MPD Thruster

The induced magnetic field could either be steady or it could be applied in pulses such as by periodic electrical discharge. The application of a steady induced magnetic field for the MPD thruster is similar to way the applied field is applied. A simple configuration would be a cross field thruster illustrated in Fig. 10.11. Here, the induced field  $B$  is in a direction into the paper (in the direction Z) and is generated by the electric field  $E$  in the positive Y direction. The plasma traveling in the X direction gets accelerated from the Lorentz force normal to the directions of  $B$  and  $E$ .

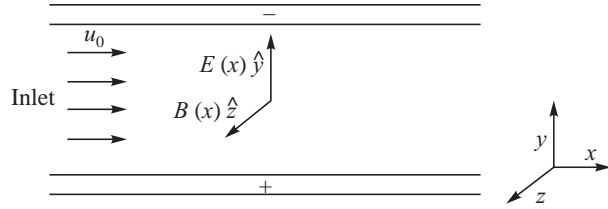


Fig. 10.11 Cross Field Acceleration

The magnetic field generated by the current flowing in the plasma would also have an influence but this would be much smaller than the induced field from the current discharge across the electrode.

The induced field MPD thruster actually grew out of the arc jet thruster. The arc jet thruster uses an electric discharge between the anode and cathode to heat the neutral propellant gases to a high temperature and these hot gases are expanded in a convergent divergent nozzle to high velocities. The induced magnetic field created by the electric discharge could also accelerate the heated plasma produced from the arc heating. In fact, the genesis of the MPD thrusters came about accidentally while conducting tests of the arc jet thrusters at very low pressures i.e., at low mass flow rates of the propellant gas. At these low flow rates, the thrust was found to increase as the mass flow rate diminished and prompted the recognition of the role of the induced field in driving a more strongly ionized plasma at the lower values of pressure. A schematic of the induced field MPD thruster based on arc discharge is shown in Fig. 10.12.

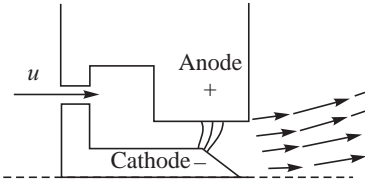


Fig. 10.12 Induced Field MPD Thruster

In the case of an unsteady or pulsed induced field such as produced by a pulsed discharge field, thrust is generated in pulses. A schematic of the configuration of such Pulsed Plasma Thruster (PPT) is shown in Fig. 10.13. Here we consider a rectangular geometry with the current density ( $J$ ) applied between the top and bottom of two electrodes, a magnetic field  $B$  generated into the paper as shown. The plasma in the region of the field  $B$  and the current density  $J$  gets accelerated in the axial direction.

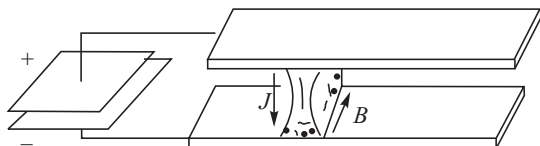


Fig 10.13 Principle pf a Pulsed Plasma Thruster

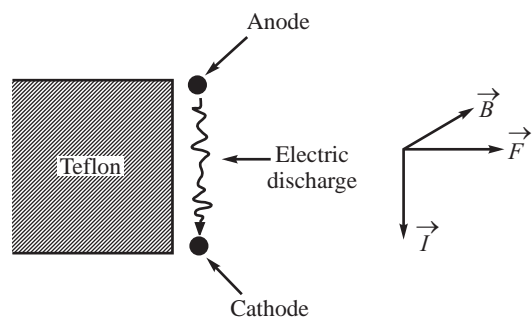


Fig. 10.14 Pulsed Plasma Thrusters

A solid propellant like Teflon is used for the Pulsed Plasma Thruster (PPT). A rapid electrical discharge over the surface of Teflon ablates it and creates plasma of carbon and chlorine ions and atoms. The current in the discharge induces a magnetic field. The plasma is accelerated by this induced field to generate thrust. A schematic of this PPT is shown in Fig. 10.14.

While the ions are accelerated by the induced field, the neutral atoms could be expanded in a convergent divergent nozzle. The magnetic field accelerates the ions just as the convergent divergent nozzle accelerates the neutral gases and is spoken of as a magnetic nozzle. The pulse duration is



typically a few microseconds and both the magnetic and the gas dynamic nozzles are used with the PPT. PPTs hold promise for application in small satellites. The thrust level of a PPT is in the range of a milli-Newton to about 0.1 Newton. The required power levels are about 10 to 100 W while the specific impulse is between  $10^4$  and  $10^5$  N-s/kg.

### 10.7.3 Combined Applied and Induced Magnetic Fields

The applied and induced magnetic fields could be combined to generate high values of acceleration of the ions and hence the thrust. In the Variable Specific Impulse Magnetoplasma Rocket (VASIMR) an applied field of around 0.1 T and an induced field between  $10^{-4}$  and  $10^2$  T has been proposed to provide thrust between 0.1 and 10 N. The specific impulse claimed for VASIMR ranges between  $10^5$  and  $10^6$  N-s/kg.

It is dependent on the induced field and the thrust. The requirement of large values of the induced magnetic field results in abnormally large power levels of a few MW. A schematic of VASIMR is shown in Fig. 10.15. The neutral gas is turned into plasma and then electromagnetically accelerated. A gas dynamic nozzle is also used as shown. It is essential for the ions which are accelerated in the magnetic field to detach from the magnetic field in order to generate the thrust.

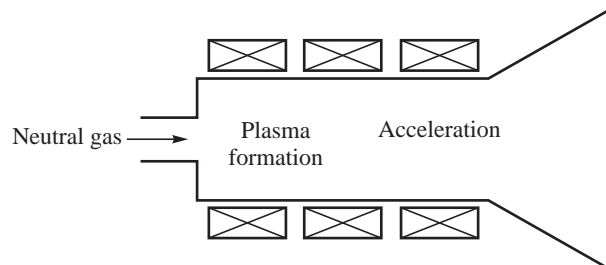


**Fig. 10.15** Schematic of VASIMR



## 10.8 POWER REQUIREMENT OF THE ELECTRICAL THRUSTERS

The order of magnitude of power required for the different electrical thrusters is given as a function of their specific impulse in Fig. 10.16. While a pulsed plasma thruster and resistojet require less than a kW of power, the pulsed plasma thruster has a much higher value of specific impulse than the resistojet. However its thrust levels are much lower. The electrostatic ion thruster has higher specific impulse than the pulsed plasma thruster; however, it requires a few kW of power for its operation. The arcjet demands more power than the resistojet but has higher specific impulse. The power levels of magnetoplasma thrusters are much higher up to about a MW and the specific impulses are about those obtained in the electrostatic ion thrusters. The role of power in the choice of the electrical thrusters is examined in the next section.

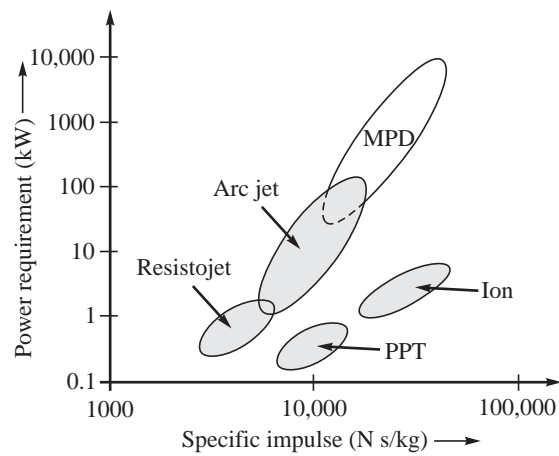


**Fig. 10.16** Power Requirements



## 10.9 CHOICE OF PARAMETERS FOR ELECTRICAL THRUSTERS

The electrical power, used for heating the propellant to high temperatures, or for generating charged particles of the propellant and accelerating it to high velocities in an electric or magnetic field, is stored and conditioned in a power unit in the rocket. The mass and power rating influence the performance of the electrical thruster and are dealt with as follows:

### 10.9.1 Mass of Electrical Power Unit

In electro-thermal thrusters, a mass flow rate of propellant  $\dot{m}$  kg/s is heated by electric power of  $P$  Watts and the heated propellant on expansion in a nozzle attains a jet velocity  $V_J$  m/s. In electrostatic and electromagnetic thrusters, the power of  $P$  Watts induces electrical charge in a propellant mass flow rate of  $\dot{m}$  kg/s and provides the necessary field to accelerate the charged propellant to a velocity  $V_J$  m/s. In both categories of electrical rockets, the electrical power  $P$  is used to provide an efflux velocity of  $V_J$  m/s. If the efficiency of conversion of the power to the kinetic energy of the efflux is  $\eta$ , we have from energy balance:

$$\frac{1}{2} \dot{m} V_J^2 = \eta P \quad \dots(10.20)$$

High values of power  $P$  would provide large efflux velocity  $V_J$  for a given flow rate of the propellant  $\dot{m}$  kg/s. The power is either stored in a battery or is generated in a fuel cell or an electrical power plant housed in the rocket. The electrical power is converted to the required voltage and current in a Power Processing Unit (PPU). The initial and final mass of the electrical rocket will therefore include an additional mass due to the power source and PPU.

The larger the power, higher would be the mass of the power source and the PPU. The power plant and the PPU are supported by the structure of the rocket and a larger power source will demand a larger structural weight to support it. The sum of the mass of the power unit  $M_{PP}$  and the structural mass  $M_S$  of the rocket would therefore be expected to scale as power  $P$ . For the total power generated by the power unit  $P$ , if  $M_{PP} + M_S$  is the sum of mass of the power unit and structure, the specific mass of the power  $\chi$  is defined as:

$$\chi = \frac{M_S + M_{PP}}{P} \text{ kg/W} \quad \dots(10.21)$$

The value of  $\chi$  depends on the type of power source used.

An increase of the power not only leads to higher values of velocity  $V_J$  (eq. 10.20) but also to higher values of mass  $M_{PP} + M_S$ . While the higher  $V_J$  gives an increase of the velocity increment  $\Delta V$  of the rocket, the increased mass will lead to a reduction of  $\Delta V$ . An increase of power  $P$  could, therefore, adversely influence the  $\Delta V$  of the rocket or for a given value of  $\Delta V$  severely reduce the useful payload of the rocket. This aspect is considered in the next section.

### 10.9.2 Choice of $V_J$ with Changes in Specific Mass $\chi$

The additional mass  $M_{PP} + M_S$  in electrical rockets modifies the expressions for initial mass and final mass of a rocket given in Chapter 2 (eq. 2.20) as:



$$M_i = M_U + M_S + M_P + M_{PP} \quad \dots(10.22)$$

$$M_f = M_U + M_S + M_{PP} \quad \dots(10.23)$$

Here  $M_U$  is the mass of the useful payload and  $M_P$  is the mass of the propellant.  $M_i$  and  $M_f$  are the initial and final mass of the rocket.

Substituting the value of  $M_{PP} + M_S$  in terms of power  $P$  from eq. 10.21 and using eq. 10.20, we get:

$$M_{PP} + M_S = \frac{\chi \dot{m} V_J^2}{2\eta} \quad \dots(10.24)$$

If the mass of propellant  $M_P$  is assumed to be ejected at a constant rate over a time period ( $\dot{m} = M_P/t$ ), then:

$$\frac{\chi V_J^2}{2\eta t} = \frac{M_{PP} + M_S}{M_P} \quad \dots(10.25)$$

Noting from eq. 10.23 that  $M_{PP} + M_S = M_f - M_U$ , we get:

$$\frac{\chi V_J^2}{2\eta t} M_P = M_f - M_U$$

The above equation can be written as:

$$\frac{\chi V_J^2}{2\eta t} (M_i - M_f) = M_f - M_U \quad \dots(10.26)$$

Dividing by  $M_i$  and simplifying, we get:

$$\frac{M_U}{M_i} = \frac{M_f}{M_i} \left( 1 + \frac{\chi V_J^2}{2\eta t} \right) - \frac{\chi V_J^2}{2\eta t}$$

Further, substituting  $\frac{M_f}{M_i} = e^{-\Delta V/V_J}$  from the rocket equation 2.16, we get:

$$\frac{M_U}{M_i} = \left( 1 + \frac{\chi V_J^2}{2\eta t} \right) e^{-\Delta V/V_J} - \frac{\chi V_J^2}{2\eta t} \quad \dots(10.27)$$

The term  $\frac{\chi V_J^2}{2\eta t}$  has units of (kg/W) (m<sup>2</sup>/s<sup>2</sup>) (1/s) and is dimensionless.

It is difficult to explicitly visualize the dependence to the useful mass ratio  $M_U/M_i$  on velocity  $V_J$ , specific mass  $\chi$  and efficiency  $\eta$  from eq. 10.27 and the above dimensionless parameter  $\frac{\chi V_J^2}{2\eta t}$ .

Rewriting eq. 10.27 as:

$$\frac{M_U}{M_i} = e^{-\Delta V/V_J} - \frac{\chi V_J^2}{2\eta t} (1 - e^{-\Delta V/V_J}) \quad \dots(10.28)$$



and splitting  $\frac{\chi V_J^2}{2\eta t}$  into two dimensional parts comprising  $\frac{\chi}{\eta t}$  and  $V_J$ , we observe from eq. 10.28

that for given values of  $\Delta V$  and  $V_J$ , an increase in the value of  $\frac{\chi}{\eta t}$  brings about a decrease in  $M_U/M_i$ .

A higher specific mass ( $\chi$ ), a reduced efficiency ( $\eta$ ) and a decrease of the duration of the operation of the rocket ( $t$ ) leads to a reduction of the useful payload. Further, for a given value of  $\Delta V$  and  $\frac{\chi}{\eta t}$ , as

$V_J$  increases the first term on the right side of the above equation increases contributing to an increase of  $M_U/M_i$ . The second term leads to a decrease of  $M_U/M_i$  as  $V_J$  increases. The values of the parameters

$\frac{\chi}{\eta t}$  and  $V_J$  are such that the first term initially dominates bringing about an increase of  $M_U/M_i$  as  $V_J$

increases. For further increases of  $V_J$ , however, the second term dominates and causes  $M_U/M_i$  to decrease. This dependence is indicated in Fig. 10.17 for different values of  $\chi/\eta$ . Here, arbitrary values of  $\chi/\eta$  of  $5 \times 10^{-3}$ ,  $10^{-2}$ ,  $20 \times 10^{-3}$  and  $30 \times 10^{-3}$  kg/W are taken based on the realizable weights of power packages and overall efficiencies. The time ( $t$ ) of operation would depend on the mission. It is assumed for Fig. 10.17 that the time  $t$  is 10 days and the mission is to use the electrical rocket to take a payload from a low Earth orbit to a geosynchronous orbit by providing ideal velocity requirement  $\Delta V$  of 4 km/s.

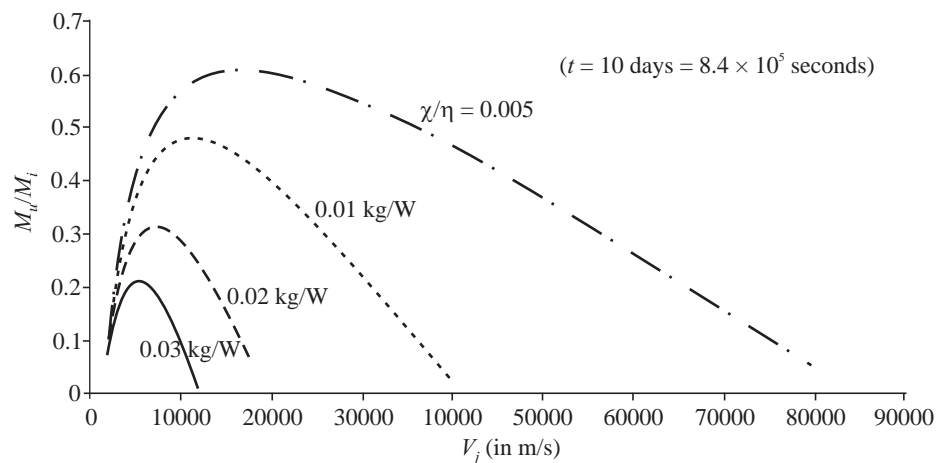


Fig. 10.17 Variation of Mass Ratio with Changes in Efflux Velocity ( $t = 10$  days)

It is seen from Fig. 10.17 that the useful mass fraction decreases as the specific mass  $\chi$  increases or the efficiency  $\eta$  of the power transformation decreases. Further, for a given value of the ratio  $\chi/\eta$ , there is an optimum value of  $V_J$  which gives a maximum value of the useful mass ratio. This optimum value of  $V_J$  increases as the ratio  $\chi/\eta$  decreases. The observed trend implies that, heavier power plants, and electrical rockets with lower efficiency of transformation of electric power to kinetic energy in the efflux, should not be designed to provide larger efflux velocities.

The thrust is given by the rate of change of momentum of the mass efflux:

$$F = \dot{m}V_J$$



The ratio of thrust to the power is:

$$\frac{F}{P} = \frac{\dot{m}V_J}{P} = \frac{2\eta}{V_J} \quad \dots(10.29)$$

Here, eq. 10.20 relating the kinetic energy of the mass efflux to the power has been used. It is seen from eq. 10.29 that the thrust developed for a given power decreases as  $V_J$  increases. This is because a given value of power will accelerate only smaller mass flow rates to higher velocities leading to smaller values of thrust. However, if a higher value of thrust is sought by adopting a lower value of  $V_J$ , the increased  $\dot{m}$  will result in an enhanced propellant consumption. The storage volume of the propellants would increase, resulting in a larger value of the structural mass fraction.

Figure 10.18 shows the influence of increasing the duration of operation of the electric rocket for which the mass ratio was plotted in Fig. 10.17 to 20 days from 10 days. The mass ratio and the optimum efflux velocity are observed to increase. The choice of  $V_J$  would therefore depend on the duration of the mission. This is further clarified in Fig. 10.19 wherein the duration of the rocket operation is brought down to 5 days. The optimum value of  $V_J$  is seen to decrease.

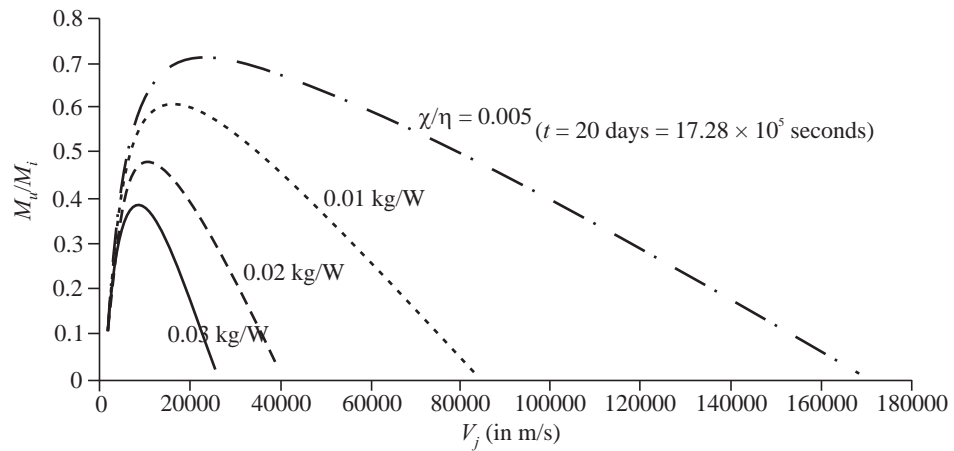


**Fig. 10.18** Variation of Mass Ratio with Changes in Efflux Velocity ( $t = 20$  days)

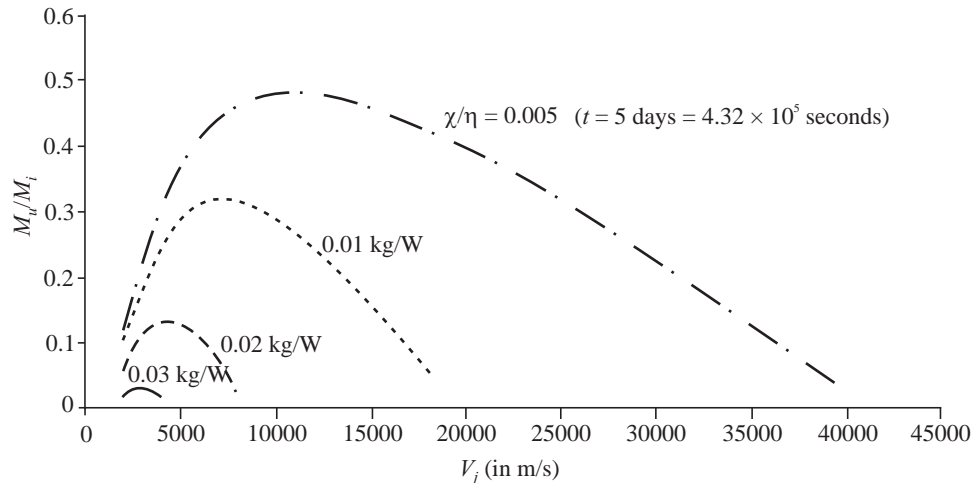


**Fig. 10.19** Reduction of Period of Operation to 5 Days



### 10.9.3 Power Limitations

An increase of power not only leads to an increase of the inert mass of the rocket with an adverse influence on the useful payload ( $\chi = (M_S + M_{PP})/P$ ), but also to an increase of  $V_J$  which does not contribute effectively to the mission beyond an optimum value. The performance of electrical rockets is therefore limited by power. In the case of chemical rockets, considered in previous chapters, the requirements of high  $V_J$  called for high values of temperature  $T_C$ . The high temperatures were obtained by releasing energy from chemical reaction of the propellants. However, there is a limit to which  $T_C$  can be increased, since a gas begins to dissociate at high temperatures. Further, the hardware of a rocket cannot withstand very high temperatures. Chemical rockets are therefore energy-limited unlike the electrical rockets which are limited by power.



## 10.10 CURRENT TRENDS

Electrical propulsion finds increasing applications for satellite propulsion and control. Electro thermal, electrostatic and electromagnetic thrusters have all been used for satellites. The resistojets using the electro-thermal hydrazine thrusters were applied for the small satellites in the Iridium Communication Constellation for attitude control and de-orbit. Ammonia arc jet thrusters have been used for Telstar satellite, the radio amateur satellite, and the Lockheed Martin Astrospase (LMAS) series of satellites. They were demonstrated for orbit control of the Advanced Research and Global Observation Satellite (ARGOS) at a power level of 30 kW. The specific impulse of ammonia is about half, obtained from using hydrogen.

Ion thrusters have been employed in several communication satellites. These include the Application Technology Satellite (ATS-6), Eureca, Artmis and ETS-6 satellite of Japan. The ion thrusters could also be used for compensating the effects of atmospheric drag of small satellites in Low Earth Orbit. Operation at high voltages with small gap between the grids and supply and the control of small flow rates of cesium and xenon for the ion thruster are particularly challenging. Specially configured orifices which provide small values of discharge coefficients have been used. The sputtering of the grids imposes a reduced life to the thruster.

The pulsed plasma electromagnetic thrusters using Teflon have also been demonstrated in flight and used in the Nova satellite. Since Teflon gets eroded during the operation, the thruster is also referred to as the erosion pulsed plasma thruster. Gaseous propellants and other solids such as carbon could also be used for the pulsed plasma thruster.

Hall Effect thrusters, also termed as Stationary Plasma Thrusters (SPT), have been traditionally used in the Cosmos and Molniya family of satellites. They are finding increased applications world wide for station keeping of large geosynchronous satellites. This is due to the simplicity, low voltage of operation and effectiveness of ionization in the Hall Effect thrusters. Higher values of thrust can also be generated in these thrusters compared to ion thrusters. The higher thrust would be an advantage for transferring satellites from low Earth orbit or a transfer orbit to the final orbit. During the passage of the satellite in the Van Allen belt during the orbit transfer, the components of the satellite could get damaged from the harmful radiation. With enhancement of thrust, the time spent by the satellite in the harmful Van Allen belt is smaller and the damage from radiation therefore gets reduced.



In the case of interplanetary missions, the operation of electrical thrusters with power derived from nuclear power plants appears promising. Nuclear propulsion would be briefly dealt with in the next chapter.

## SOLVED EXAMPLES

### **Example 10.1** Electrostatic force:

A stream comprising of 0.001 kg of positively charged xenon gas, charged to an average charge density of  $2 \times 10^4$  Coulomb/kg, is placed in a linear electrostatic field of 1 kV/mm. Determine the acceleration force experienced by the stream.

$$\text{Solution: Electrostatic force} = q\vec{E} = 2 \times 10^4 \times 0.001 \times 1 \times 10^6 \text{ C/kg} \times \text{kg} \times \text{V/m}$$

The potential difference in Volt is the work done in carrying a unit charge from the lower to the higher potential. The unit of Volt (V) is Joule/Coulomb = Nm/C

$$\text{The electrostatic force is } 2 \times 10^7 \text{ C Nm/C m} = 2 \times 10^7 \text{ N}$$

Significant force is exerted by a high voltage field on a charge. In this example, if the distance over which the charge is accelerated is 4 mm, the potential difference accelerating the charge is 4 kV. The work done on the charge is  $2 \times 10^7 \times 4 \times 10^{-3} = 8 \times 10^4$  J. This work goes into increasing the kinetic energy of the charge. If the initial velocity of the charge is negligibly small and the final velocity is  $v$  m/s, the increase of kinetic energy is  $mv^2/2$  and equals the work done on the charge, viz.,

$$\frac{mv^2}{2} = 8 \times 10^4 \text{ J}$$

With  $m = 0.001$  kg, the increase of velocity of the charge is  $1.265 \times 10^4$  m/s. The ions are accelerated to very high velocities using the electrostatic field.

### **Example 10.2** Electromagnetic force:

A steady stream of charged cesium ions is traveling at a mean velocity of 20 m/s orthogonal to a magnetic field of strength  $0.5 \times 10^{-3}$  Tesla (which is about 10 times stronger than the Earth's magnetic field). The cesium ions have an average charge of  $10^4$  Coulomb. Determine the force exerted by the magnetic field on the moving charge.

$$\begin{aligned} \text{Solution: Electromagnetic force} &= q\vec{v} \times \vec{B} = (10^4) (20) (0.5 \times 10^{-3}) \text{ C} \times \text{m/s} \times T \\ &= 10^2 \text{ Cm/s} \text{ Ns/Cm} = 100 \text{ N} \end{aligned}$$

Powerful magnetic fields are required to generate significant forces.

### **Example 10.3** Ion thruster using grids:

A steady stream of propellant xenon interacts with electrons in an ionization chamber to generate positively charged ions of xenon at an average charge density of  $2 \times 10^4$  Coulomb/kg. The ions are captured in an extractor grid and thereafter accelerated to high velocities using an acceleration voltage of 3 kV. The current due to the flow of ions is 0.25 Ampere. Determine:

- (i) The exit velocity of the ions
- (ii) Thrust generated.



**Solution:** (i) Exit velocity of ions:

$$\text{Charge density} = 2 \times 10^4 \text{ Coulomb/kg}$$

$$\text{Current due to charge} = 0.25 \text{ A} = 0.25 \text{ Coulomb/s}$$

$$\text{Hence mass flow rate of the charge } \dot{m} = \frac{0.25}{2 \times 10^4} = 12.5 \times 10^{-6} \text{ kg/s}$$

$$\text{Potential difference accelerating the charge} = 3000 \text{ V}$$

$$\text{Power accelerating the charge} = \text{Current} \times \text{Voltage} = 0.25 \times 3000 \text{ W}$$

This is equal to rate of kinetic energy increase of the charge

$$= \frac{d}{dt} \left( \frac{1}{2} m V_J^2 \right) = \frac{1}{2} \dot{m} V_J^2$$

$$\therefore \frac{\dot{m} V_J^2}{2} = 0.25 \times 3000, \text{ giving}$$

$$V_J = 10,950 \text{ m/s}$$

(ii) Thrust generated:

$$\text{Thrust} \quad F = \dot{m} V_J = 12.5 \times 10^{-6} \times 10950 = 0.137 \text{ N}$$

**Example 10.4** Limiting current density, beam diameter:

Determine the minimum beam diameter of an ion rocket, generating a thrust of 0.5 N, using xenon as the propellant. The potential difference between the extractor grid and the accelerator grid of the ion thruster is 3 kV and the gap between these grids is 1 mm. The permittivity of free space is  $8.85 \times 10^{-12} \text{ C}^2/\text{Nm}^2$ .

**Solution:** For the limiting current density using Child-Langmuir relation, the thrust per unit area is:

$$\frac{F}{A} = \frac{8}{9} \epsilon_0 \frac{V^2}{L^2} = \frac{8}{9} \times 8.85 \times 10^{-12} \times \frac{3000^2}{(10^{-3})^2} = 70.5 \text{ N/m}^2$$

Thrust of the ion rocket = 0.5 N

$$\text{Minimum beam area of the ions} = \frac{0.5}{70.5} = 7.1 \times 10^{-3} \text{ m}^2$$

Diameter of beam current = 0.095 m.

**Example 10.5** Thrust:

An electrical rocket operates at an efficiency of 85% when the input power level is 1.5 kW. If the specific impulse of the rocket is 20,000 Ns/kg, determine the thrust.

**Solution:** Effective jet velocity  $V_J = I_{sp} = 20,000 \text{ m/s}$

Input electrical power  $P = 1500 \text{ W}$

Since  $F = \dot{m} V_J$  and power of the jet =  $\eta P = \frac{1}{2} \dot{m} V_J^2$  we have:

$$F = \frac{2\eta P}{V_J} = \frac{2 \times 0.85 \times 1500}{20,000} = 0.1275 \text{ N}$$

The thrust generated by the rocket = 0.1275 N.



**Example 10.6** Optimum specific impulse for a given mission, propellant requirement:

- (i) A space capsule is to be electrically propelled in deep space using the electrical power generated by a nuclear power plant that is carried by the capsule. The nuclear power plant works on the principle of radioactive isotope decay. The mission in deep space calls for an incremental velocity  $\Delta V$  of 5 km/s to be provided in 60 days by continuous operation of the electrical rocket. The specific mass of the system comprising the space capsule, power plant, electrical power processing unit and the rocket is 100 kg/kW. Assuming the efficiency of the electrical rocket as 85%, determine the specific impulse for which the rocket is to be designed in order to obtain the maximum payload mass.
- (ii) What is the maximum payload ratio? If the mass of the useful payload is 1000 kg and the power plant has a rating of 15 kW, determine the mass of propellant required for the mission.

**Solution:** (i) Optimum specific impulse:

The payload fraction from eq. 10.27 is:

$$\frac{M_U}{M_i} = \left(1 + \frac{\chi V_J^2}{2\eta t}\right) e^{-\Delta V V_J} - \frac{\chi V_J^2}{2\eta t}$$

Denoting  $\frac{\chi}{2\eta t} = a$  and  $\Delta V = b$ , the equation reduces to:

$$\frac{M_U}{M_i} = (1 + aV_J^2) e^{-bV_J} - aV_J^2$$

For maximum payload:  $\frac{d}{dV_J} \left( \frac{M_U}{M_i} \right) = 0$ . This gives:

$$\frac{b}{V_J^2} (1 + aV_J^2) + 2aV_J - 2aV_J e^{-bV_J} = 0$$

This can be written as:  $\frac{b}{V_J^2} (1 + aV_J^2) + 2aV_J (1 - e^{-bV_J}) = 0$

Solving the above equation iteratively for  $V_J$  for values of  $a$  and  $b$  given by:

$$a = \frac{100 \times 10^{-3}}{2 \times 0.85 \times 60 \times 24 \times 3600} = 1.134 \times 10^{-8}$$

$b = 5000$ , we get:

$$V_J = 6710 \text{ m/s}$$

The optimum specific impulse for the mission is 6710 m/s.

(ii) Useful payload and mass of propellant:

The above specific impulse corresponds to the maximum payload ratio. The payload ratio is given by:

$$\begin{aligned} \frac{M_U}{M_i} &= (1 + 1.134 \times 10^{-8} \times 6710^2) e^{-5000/6710} - 1.134 \times 10^{-8} \times 6710^2 \\ &= 0.207. \end{aligned}$$



The useful payload ratio is 0.207.

Since the useful payload mass = 1000 kg, the initial mass is  $\frac{1000}{0.207} = 4831$  kg.

However, the mass of the structure, inert and power plant mass ( $M_S + M_{PP}$ ) is

$$M_S + M_{PP} = \chi P = (100 \times 10^{-3}) \text{ kg/W} \times (15 \times 10^3) \text{ W} = 1500 \text{ kg}$$

Initial mass  $M_i = M_U + M_S + M_{PP} + M_P$ . This gives the mass of propellant  $M_P$  to be  $4831 - (1000 + 1500) = 2331$  kg.

The mass of propellant = 2331 kg.

## Nomenclature

$B$ :	Magnetic field (Tesla)
$C_0$ :	Velocity of light in vacuum ( $3 \times 10^8$ m/s)
$E$ :	Electric field (Volts/m)
$F$ :	Thrust (N)
$I$ :	Current (A)
$L$ :	Distance; Spacing between extractor grid and accelerator grid (m)
$M, m$ :	Mass (kg)
$\dot{m}$ :	Mass flow rate (kg/s)
$P$ :	Power (Watts)
$q$ :	Charge (C)
$r$ :	Distance (m)
$R$ :	Aspect ratio of current beam (diameter/length)
$t$ :	Time (s)
$V$ :	Potential difference (Volts)
$V_J$ :	Efflux velocity (m/s)
$\Delta V$ :	Incremental velocity (m/s)
$\chi$ :	Specific mass of power unit (kg/W)
$\epsilon$ :	Permittivity of medium (Farads/m)
$\epsilon_0$ :	Permittivity of free space ( $8.852 \times 10^{-12}$ Farads/m)
$\eta$ :	Efficiency
$\mu$ :	Permeability (Henry/m)
$\mu_0$ :	Permeability of free space ( $1.257 \times 10^{-6}$ Henry/m)
$\Delta$ :	Increment

## Subscripts

$f$  : Final

$i$  : Initial



- $P$  : Propellant  
 $PP$  : Power plant  
 $S$  : Structure  
 $U$  : Payload

## EXERCISES

1. A resistojet uses propellant helium heated to 1000 K at a pressure of 1.5 MPa. The heated helium is exhausted through a convergent divergent nozzle having a throat diameter of 0.2 mm and exit diameter of 3 mm. Determine the characteristic velocity, mass flow rate of helium, specific impulse and the thrust generated. Helium has a molecular mass of 4 kg/kmole and a specific heat ratio of 1.67.
2. Determine the acceleration voltage to be provided in an ion thruster of specific impulse 20000 Ns/kg in which the propellant is charged to  $5 \times 10^4$  C/kg? What is the thrust to power ratio of the thruster?
3. A combination of a cold ammonia gas and a hot ammonia gas resistojet seems to be a viable option for thrusters for attitude and orbit control and station keeping of a geosynchronous satellite. The hot ammonia resistojet is required to generate a specific impulse of 2200 Ns/kg at a thrust of 10 N. The expansion ratio of the nozzle is 80. If the pressure at which ammonia is heated is 0.5 MPa, determine the electrical power to be supplied to the resistojet assuming the efficiency of the electrical heating of ammonia to be 75%. You can neglect the decomposition of ammonia. The specific heat ratio of ammonia ( $\text{NH}_3$ ) is 1.31. The ambient pressure at the geosynchronous altitude would be zero.  
What is the change in specific impulse if ammonia dissociates into nitrogen and hydrogen? The standard heat of formation of ammonia is -46 kJ/mole.
4. (i) An arc jet thruster using hydrogen gas as the propellant operates in deep space. The hydrogen is heated to a temperature of 5000 K by the arc at a pressure of 100 kPa and the heated hydrogen is expanded in a convergent divergent nozzle of area ratio 100. Assuming the throat diameter to be 3 mm and no dissociation of hydrogen and frozen flow in the nozzle, determine the specific impulse of the thruster. The specific heat ratio of hydrogen can be assumed as 1.4.  
(ii) In practice the hydrogen gas dissociates. If the equilibrium constant  $K_p$  (discussed in Chapter 4) for dissociation of hydrogen to monatomic hydrogen ( $\text{H}_2 \rightarrow 2\text{H}$ ) is given as  $\ln(K_p) = 14.9 - 55,870/T$ , and the average specific heats at constant pressure of  $\text{H}_2$  and  $\text{H}$  are 20 and 35 kJ/(kmole K) in the temperature range of interest, what is the fractional change in the specific impulse due to the dissociation? The flow in the nozzle can be assumed to be frozen. Ionization of hydrogen can be neglected. The specific heat ratio of monatomic hydrogen is 1.67. The temperature of the heated gases, as in the earlier problem is 5000 K. The standard heat of formation of monatomic hydrogen  $\Delta H_f^\circ$  is +217.5 kJ/mole.
5. A satellite of mass 800 kg is required to be propelled from a Low Earth Orbit (LEO) to a Geo-Stationary Orbit (GSO) using electrical propulsion. The mass of the satellite includes the mass of the useful payload, the satellite structure, electrical power plant, propellant storage devices and the rocket hard-ware. The mission from LEO to GSO is to be achieved in 150 days by continuous firing of the electrical rockets. The incremental velocity required for this mission is 6 km/s. The electrical rocket has an efflux velocity of 40 km/s and the efficiency of operation is 90%. The available electrical power is 10 kW, the specific mass of the system being 20 kg/kW. Determine the mass of propellant required for the mission?
6. In the above problem, what is the thrust generated by the electrical rocket?



- 
7. Determine the payload ratio for a space vehicle which achieves a velocity increment of 4 km/s by operating an electric propulsion unit in a continuous mode over a period of 8 days. The specific impulse of the electrical rocket is 20 kNs/kg and the specific mass of the space capsule is 0.09 kg/W. The efficiency of the electric propulsion system is 90%. The power supplied to the electrical thrusters is 10 kW.
  8. If the mass of useful payload in the above problem is 500 kg, determine the mass of propellant required for the mission?

## References

1. Fearn, D.G., *Ion propulsion*, Spaceflight, vol. 34, 1992, pp. 324-326.
2. Funke, R.C., *Electric Propulsion and its Application to Space Missions*, Progress in Astronautics and Aeronautics, vol. 79, AIAA Inc., Washington, 1981.
3. Hill, P.G. and Peterson, C.R, *Mechanics and Thermodynamics of Propulsion*, ed. II, Addison Wesley Publishing Company, Reading, Massachusetts, 1992.
4. Myers, R.M, Oleson S.R., McGuire, M, Meckel, N.J. and R.J., Cassady, *Pulsed Plasma Technology for Small Satellite Mission*, NASA Cr 198427, NASA, Nov. 1965.
5. Langmuir, D.B., Stuhlinger E. and Sellen Jr. J.M, *Electrostatic propulsion*, Progress in Astronautics and Aeronautics, vol. 5, Academic Press, New York, 1961.
6. Ramamurthi, K. and Madhavan Nair, G, *Evolution and Growth of Spacecraft Propulsion Systems*, J. Spacecraft Technology, vol. 8, 1998, pp. 1-22.
7. Stuhlinger, E., *Electric Propulsion Development*, Progress in Astronautics and Aeronautics, vol. 9, Academic Press, New York, 1963.
8. Sutton, G.P. and Biblarz, O., *Rocket Propulsion Elements*, 7th Ed., Wiley Interscience Publications, New York, 2001.
9. Tajmar, M., *Advanced Space Propulsion Systems*, Springer, Wein, 2003.

## Glossary

Augmented electro-thermal hydrazine thruster: Increasing temperature of products of dissociation of hydrazine in a rocket with electrical resistive heating and expanding the hot gases in a nozzle

Bombardment ion thruster: Ion thruster using ions generated by field emission viz., bombarding surfaces with electrons and ions

Charge limited current density: Threshold value of current density in the ion beam above which is not possible to extract ions and accelerate them; given by Child Langmuir law

Colloidal propulsion: Charging droplets and accelerating in electrostatic field to generate thrust

Electric field: Region said to have an electric field if an electric charge, placed in the region, experiences a force. The unit of electric field is Volts/m.

Electromagnetic thruster: A rocket in which charged particles are accelerated to high velocities by a magnetic field.

Electro-thermal thruster: Rockets in which propellants are heated either resistively or by arc discharge to high temperatures and the hot gases expanded in a nozzle

Hall Effect: Interaction of a magnetic field at right angles to the flow of current induces voltage perpendicular to both



---

**310** *Rocket Propulsion*

Hall Effect thruster: Electrostatic thruster using Hall Effect to generate ions and ejecting ions at high velocities

Ion thruster: Achieving high efflux velocities by accelerating ions in an electric field

Magnetic field: If an electric charge moving in a region experiences a force but does not experience a force when at rest in the region, the region is said to have a magnetic field. The unit of magnetic field is Tesla

Magneto Plasma Dynamic Thruster: Electromagnetic thruster in which the flow of charge induces the electromagnetic field

Neutralization: Injection of electrons in the efflux stream of ions leaving the thruster

Permeability: Ability of a medium to magnetize in a magnetic field. Unit is Henry/m.

Permittivity: Ability of the medium to store electrical energy and permit an electric field. Unit is Farad/m.

Plasma: Hot gases containing electrically charged particles

Pulsed plasma thruster: Pulses of plasma accelerated by magnetic field

Radio frequency thruster: Ions generated by radio frequencies in the ion thruster

Specific mass of electrical power unit: Mass of power unit (including the associated structural mass) per unit power (kg/W)

## Chapter 11

### Nuclear Rockets and Advanced Rockets

*The fundamental point in fabricating a chain reacting machine is of course to see to it that each fission produces a certain number of neutrons and some of these neutrons will again produce fission.*

*Enrico Fermi, Renowned physicist*

*Numerous authors made a man travel from star to star a subject of fiction....No one has ever thought to seek the physical requirements and the orders of magnitude of the relevant phenomenon necessary for the realization of this idea.*

*Robert Esnault Pelterie, a pioneer of Aviation and Astronautics.  
He proposed in 1913 the use of nuclear energy (400 kg of radium)  
for interplanetary travel.*

We have discussed the different types of rockets, such as chemical rockets and electrical rockets. The chemical rockets comprised solid propellant rockets, liquid bi-propellant and mono-propellant rockets and hybrid rockets. The electrical rockets consisted of electrothermal, electrostatic and electromagnetic thrusters. The principle was to accelerate either the propellants or the combustion products of the propellants to high velocities.

Nuclear energy has also been employed for heating a propellant and generating thrust by expanding the heated propellant in a nozzle or for producing electrical power for electrical rockets. Such rockets, using nuclear energy, are known as nuclear rockets. Work on nuclear rockets was initiated some fifty years ago. Considering the problem of radiation and the shielding required and safety, nuclear rockets have not been flown so far. Nuclear energy has, however, been used in spacecrafts for generating electric power.



In chemical propulsion, the use of two liquid fuels, one with low molecular mass and the other having higher molecular mass, referred to as tri-propellant, offers some advantages over the conventional propellants. The number of stages in a satellite launch vehicle could be brought down with the use of a tri-propellant rocket. Perhaps, a Single Stage To Orbit (SSTO) launch vehicle would become viable. We briefly deal with nuclear rockets and tri-propellant rockets and point out some other advanced modes of rocket propulsion in this chapter.



## 11.1 NUCLEAR ROCKETS

Nuclear reactions like chemical reactions generate heat and are used to heat a low molecular mass gas such as hydrogen to generate thrust in nuclear rockets. The nucleus of an atom consists of protons and neutrons, the total number of which is the mass of the atom or its atomic mass. The number of protons in the nucleus (which equals the number of electrons in an uncharged atom) is the atomic number. The atomic number characterizes a given element. Elements having the same atomic number (number of protons) but of different mass (corresponding to total number of protons and neutrons) are known as isotopes.

Nuclear reactions are very different from chemical reactions which involve a fuel and oxidizer to form products of combustion discussed in chemical rockets. While in a chemical reaction the number of atoms of each of the elements in the reactant and in the product remain the same or is conserved, in a nuclear reaction the number of protons and neutrons in the nuclei are conserved. New elements can be formed in a nuclear reaction since the balance is for the total number of protons and neutrons.

There are three types of nuclear reactions. In the first case, when an unstable isotope of an element tends to form a relatively stable element i.e., it tends towards a state of equilibrium, it emits energy. The change or the associated reaction involving the change is said to be one of radioactive decay since long wavelength waves are formed in the process. In the second type of nuclear reactions, the nucleus could be broken up and neutrons emitted in which case the reaction is termed as nuclear fission. The third type of nuclear reaction involves the fusing of neutrons in a given nucleus in which case it is termed as nuclear fusion.

We shall deal with the above three types of reactions involving the nuclei of atoms and address their suitability for nuclear rockets.



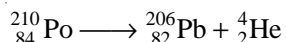
## 11.2 RADIOACTIVE DECAY

When a relatively unstable isotope changes to a more stable isotope, it releases energy. The release of energy is generally very slow and could stretch over several hundreds of years. As an example, consider the isotope Polonium having an atomic number 84 and having 126 neutrons in its nucleus. It is denoted by  $^{210}_{84}\text{Po}$ , where Po denotes the element Polonium, 210 denotes the total number of protons and neutrons in its nucleus while 84 denotes the number of protons in its nucleus. The element was discovered by the Nobel Laureate Marie Curie in 1898 and the element Polonium has been known to have 35 isotopes. For each of the isotopes, the number 210 signifying the total number of



protons and neutrons in its nucleus would vary. However, the number 84 will always be the same as it signifies the element Polonium.

The isotope  $^{210}_{84}\text{Po}$  is a naturally occurring isotope and is also generated by the decay of Uranium. The Polonium  $^{210}_{84}\text{Po}$  decays to stable lead with an atomic number of 82 with 206 protons and neutrons as per the reaction:



In the above decay, the total number of protons and neutrons are balanced. Lead of atomic number 82 with 124 neutrons and helium (2 protons and 2 neutrons in its nucleus) are formed in the nuclear decay. Energy is released in the process of the decay.

The decay process continues for a long time. We define the time taken for the concentration of  $^{210}_{84}\text{Po}$  to decay to half its original value as half the life time of the reaction and this is about 128 days. The rate of energy release is slow.

The emission of particles from the atomic nucleus as it disintegrates is known as radioactivity. The decay process, also therefore known as radioactive decay, is associated with the formation of (i) alpha particles with the helium,  $^4_2\text{He}$  (ii) beta particles which are high energy electrons and (iii) gamma rays which are short wavelength electromagnetic radiation. The alpha emission coming from the expulsion of the helium gives rise to thermal energy. It is this thermal energy which could be used for heating.

Considering the very low rate of decay, the rate of release of thermal energy is not adequate to generate any viable thrust for nuclear rockets. It has, however, been used to generate small quantities of power in spacecrafts. The thermal energy is converted to electric power using the thermoelectric principle of generating electricity from heat. Here the principle is one of Seebeck effect viz., obtaining electromotive force (emf) from junctions of two dissimilar materials at different temperatures. The emf depends on the dissimilar materials used and the amount of heating i.e., the relative temperature difference. Power generation devices for spacecrafts using the radioactive isotope decay are known as Radioactive isotope Thermo-electric power Generators (RTG).

In addition to Polonium  $^{210}_{84}\text{Po}$ , isotopes Thorium  $^{232}_{90}\text{Th}$ , Uranium  $^{235}_{92}\text{U}$  and  $^{238}_{92}\text{U}$  radioactively decay to ultimately form lead. The half life of the decay of Uranium  $^{238}_{92}\text{U}$  is 4.5 billion years.



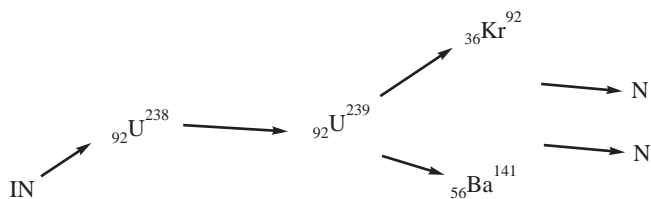
### 11.3 NUCLEAR FISSION

Massive isotopes like Uranium, Thorium and Plutonium have large number of protons and neutrons in their nucleus. The protons and neutrons are held together by nuclear forces which are very strong forces. The large number of protons in the nucleus makes it unstable and in general isotopes having atomic number greater than 83 have somewhat unstable nucleus.

When a heavy isotope is hit strongly with a neutron, the nucleus absorbs the neutron and thereafter breaks up and releases neutrons which further break up the nuclei of the other elements formed. In



this way a large number of neutrons are cumulatively formed as a chain reaction process so long as sufficient mass of the parent isotope is available. The break up of the nucleus and the subsequent release of neutrons in a cascading process is referred to as nuclear fission. As a typical example, isotope Uranium  $^{238}_{92}\text{U}$  absorbs a neutron to form Uranium  $^{239}_{92}\text{U}$ . The nucleus of  $^{239}_{92}\text{U}$  releases neutrons to form Barium  $^{141}_{56}\text{Ba}$  and Krypton  $^{92}_{36}\text{Kr}$ . The neutrons generated in the process further fission the Uranium. The fission process can be written as  $^{239}_{92}\text{U} \longrightarrow ^{141}_{56}\text{Ba} + ^{92}_{36}\text{Kr}$  and is shown schematically in the figure below:



The formation of an avalanche of neutrons leads to an ever increasing number of neutrons as the fission process progresses so long as sufficient mass of Uranium is available.

Low molecular mass substances like water or an element such as carbon absorb the neutrons and can be introduced to control the reaction. In a fusion reactor therefore such low molecular mass substances known as moderators are introduced to control the rate of release of neutrons. However, too much of absorption can lead to a fall in the neutrons generated and it may be necessary to reflect off the neutrons back into the reactor. Reflectors made of Beryllium of atomic mass 4 which is a very light solid are used to bounce back the neutrons. By suitably tailoring the fission process with adequate absorption by moderators and reflection back into the fission process by reflectors, it is possible to generate a steady rate of generation of neutrons.

A nuclear fission reactor would therefore comprise of a fissionable substance, a moderator and a reflector. When the spiraling rate of generation of neutrons in the chain process of fission is made to reach a steady state value by suitably absorbing the excess neutrons by moderators and in case of too much of absorption by suitably reflecting the neutrons back into the fission process, the reactor is said to be critical. When the neutron generation rate in the reactor exceeds the loss it is referred to as supercritical while if the losses of neutrons exceed the rate of its generation in the fission process, it is said to be subcritical.

Neutrons have kinetic energy and a steady state release of neutrons in a fission reactor can be made use for nuclear rockets.

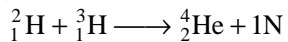


## 11.4 NUCLEAR FUSION

The nuclei of isotopes having small mass could be fused if brought together at very high pressures with sufficient energy levels. Consider the three isotopes of Hydrogen. Hydrogen occurs most abundantly as  $^1_1\text{H}$  containing one proton in its nucleus. The other two isotopes are Deuterium  $^2_1\text{H}$  containing one proton and one neutron in its nucleus and Tritium  $^3_1\text{H}$  containing one proton and two



neutrons in its nucleus. If Deuterium and Tritium are brought together at extremely pressures, the nuclei are in close contact and if the temperatures are very high they could fuse as per the nuclear reaction:



The nuclear force binding the nucleus is released and it is possible to use the energy of fusion to heat up gaseous hydrogen to generate thrust. However, the requirement of extremely high values of pressure and temperature for the nuclear fusion has been a deterrent and it has not been applied for nuclear rockets.



## 11.5 NUCLEAR ELECTRIC AND NUCLEAR THERMAL PROPULSION

The nuclear fission process has been used for nuclear rockets compared to the radioactive decay and nuclear fusion. The thermal energy of the high velocity neutrons generated in the fission reactor is transferred to gaseous hydrogen and the resulting high enthalpy hydrogen is expanded in a nozzle to generate thrust. A schematic of the arrangement is shown in Fig. 11.1 and is referred to Nuclear Thermal Propulsion. Here hydrogen gas is heated to high temperatures in a fission reactor. Rockets have been developed using this principle and tested and are known as Nuclear Thermal Rockets (NTR). A typical development is the NERVA (Nuclear Energy for Rocket Vehicle Applications) rocket in USA.

It is also possible to convert the nuclear energy from the fission process to electrical power and use it for electrical rockets such as electrostatic or electromagnetic thrusters. The use of electrical power from nuclear reactors for rockets is spoken of as Nuclear Electric Propulsion (NEP). The necessity of high electrical power for the electromagnetic thrusters justifies the use of nuclear fission reactors. However, rockets using Nuclear Electric Propulsion have not been developed till date.

### 11.5.1 Nuclear Thermal Rocket

The nuclear thermal rocket consists of a reactor in which hydrogen gas is heated to high temperatures in a reactor. The hydrogen gas is stored as a liquid in propellant tanks and pumped at high pressures as a gas into the fission reactor. The configuration of the fission reactor is first considered before reviewing the feed system for liquid hydrogen.

#### A. Solid core fission reactor

Pellets of isotope uranium are contained in tubes and a series of such tubes are bundled together to form a cluster. A number of such clusters are assembled together to form the solid core in which fission of uranium isotope takes place.

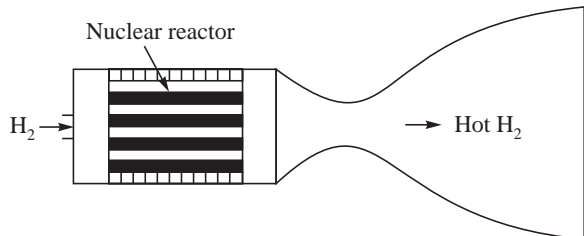


Fig. 11.1 Nuclear Thermal Rocket



A large number of straight axially oriented holes are made in each of the tubes containing the isotope uranium for heating hydrogen gas to high temperatures. A schematic of the reactor is shown in Fig.11.2.

The fission of uranium in the tubes is initiated by sending in neutrons from an auxiliary chamber. The core is surrounded by reflectors made of Beryllium to prevent the escape of neutrons from the reactor core. Moderators, comprising of carbon rods or boron carbide coated drums are used for absorbing the neutrons from the fission process. The placement of the reflective beryllium mirrors and the absorbing rods or drums is so varied such that adequate neutrons are either reflected back into the reactor or are lost from the reactor so as to keep the generation of neutrons at a steady state i.e., fission process in reactor being critical.

The flow of hydrogen through the holes in the reactor rods meets with the high velocity neutrons generated in it and gets heated as in a heat exchanger. The residence time of hydrogen through the reactor is not significant and the efficiency of heating is therefore not very high. The heated hydrogen gas is expanded in a convergent divergent nozzle. A specific impulse about twice the value obtained in cryogenic propellant rockets (using liquid hydrogen and liquid oxygen) is achieved in this nuclear rocket.

The hydrogen before being admitted into the reactor is used to cool the reactor walls and the mirrors used for focusing the neutrons back into the reactor. In this way the waste heat is used to enhance the enthalpy of hydrogen supplied to the reactor.

### B. Particle bed fission reactor

The disadvantage of smaller values of residence time in the solid core reactor is overcome by passing hydrogen through a porous bed of fine particles of the isotope uranium. The porous bed is contained in an annulus between an inner and outer cylindrical chamber. The walls of these two tubular chambers are porous. Hydrogen gas is introduced through the outer tube and passes through the fission reactor bed and exits through a nozzle connected to the inner cylindrical tube. A schematic of the particle bed fission reactor for heating hydrogen gas is shown in Fig. 11.3.

Considering the close contact between the isotope particles and the flowing hydrogen gas, the heat transfer process is much more efficient than in the solid core fission reactor. The residence time of hydrogen in the reactor is also considerably enhanced.

Uniformity of hydrogen flow in the different parts of the particle bed of uranium undergoing the fission process cannot however be assured. The hydrogen gas takes the path of least resistance and the temperatures shoots up to abnormally high values in the

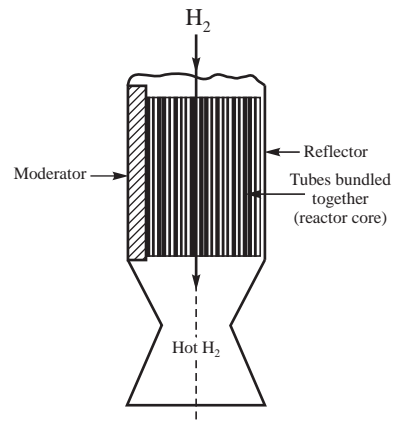


**Fig. 11.2** Solid Core Fission Reactor

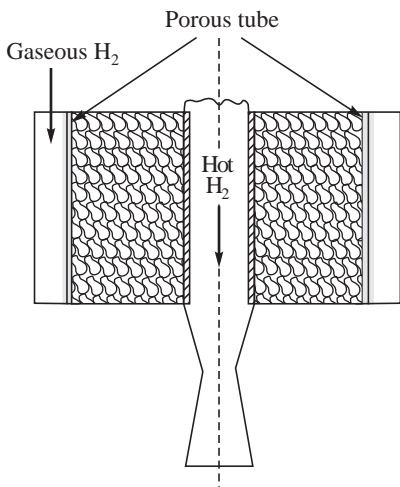


**Fig. 11.3** Particle Bed Fission Reactor



portions not cooled by hydrogen. As a result thermal instability sets in and is undesirable. It becomes essential to ensure uniform flow of hydrogen gas in the annulus containing the particles undergoing fission.



## 11.6 FEED SYSTEM CYCLES

Liquid hydrogen is stored in liquid phase in tanks. The thrust of nuclear rockets is generally designed to be very large and hence a pump-fed feed system becomes necessary. The feed system cycle for hydrogen gas is similar to that used in liquid propellant rockets except that a gas generator or a pre-combustion chamber cannot be used since we need additional oxygen for the burning. Only the expander cycle can be applied.

### 11.6.1 Expander Cycle

In the expander cycle feed system, the liquid hydrogen, heated in a regenerative mode by the walls of the reactor, is supplied to run a turbine. The energy developed by the turbine is used to drive the pump. The warm hydrogen gas from the turbine exhaust is heated to high temperatures in the reactor. A schematic of the expander cycle for use in nuclear thermal rockets is shown in Fig. 11.4.

The different processes taking part in the nuclear rocket using the expander cycle are shown in the temperature entropy plot in Fig. 11.5. Liquid hydrogen and gaseous hydrogen would coexist in the region within the dome comprising the saturated liquid line and saturated vapor line. The critical pressure of hydrogen is 1.33 MPa and the critical temperature is 133 K. Beyond the critical pressure and temperature, it is not possible to distinguish between the liquid and gas phase. The process of pressurizing liquid hydrogen by the pump is shown by AB in Fig. 11.5. Since the process is not isentropic the entropy increases during the process of compression. The heat addition to liquid hydrogen during the regenerative cooling of the warm reactor walls is shown by the constant pressure process BC. The expansion of the hydrogen gas in the turbine to the lower pressure in the reactor with an increase of entropy is shown by CD. Hydrogen enters the reactor at state D and is heated at constant pressure to a high temperature by the neutrons generated in the fission process to E. The expansion of the heated hydrogen gas in the nozzle is shown by EF.

Denoting the enthalpy per unit mass of hydrogen by  $h$ , the work done by the pump per unit time  $\dot{W}_P$  is given by:

$$\dot{W}_P = (\dot{m}_H / \rho_H) \Delta P = \dot{m}_H (h_B - h_A)$$

Here  $\dot{m}_H$  denotes the mass flow rate of hydrogen,  $\Delta P$  is the pressure rise in the pump and  $\rho_H$  is the density of liquid hydrogen.  $h_B$  and  $h_A$  denote the specific enthalpy at states A and B respectively in Fig. 11.5.

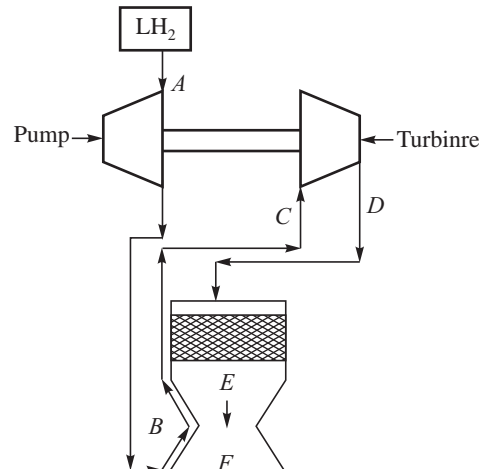
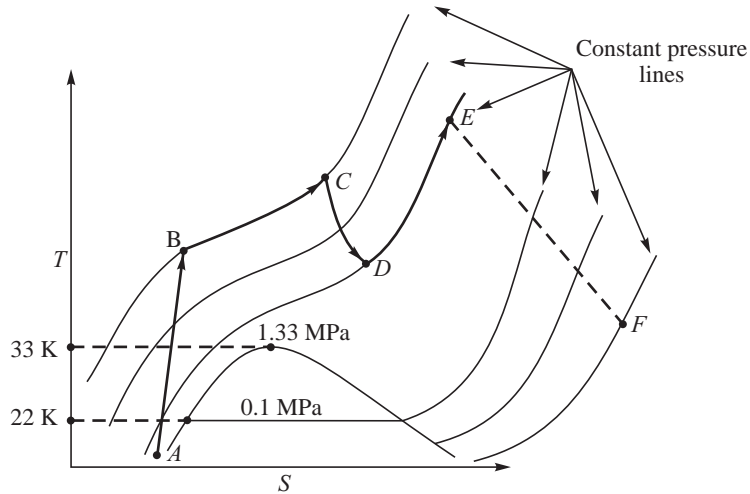


Fig. 11.4 Expander Cycle for Feeding Hydrogen to the Reactor



**Fig. 11.5** Processes in the Expander Cycle on the T-s Diagram

The work done by the turbine  $\dot{W}_T$  per unit time is given by:

$$\dot{W}_T = \dot{m}_H (h_C - h_D)$$

where  $h_C$  and  $h_D$  denote the specific enthalpy at states C and D respectively in Fig. 11.5. If the mechanical efficiency of the pump is  $\eta_P$  and the mechanical efficiency of the turbine is  $\eta_T$ , the work output by the pump must be able to supply the work required for the pump. We therefore have:

$$\dot{W}_P / \eta_P = \dot{W}_T \times \eta_T$$

The exhaust jet velocity  $V_J$  of the nuclear rocket can be determined from the drop in the specific enthalpy across the nozzle viz., from  $h_E$  to  $h_F$  to give:

$$V_J = \sqrt{2(h_E - h_F)}$$

The states at the different points in the process and the specific impulse of the rocket are thereby determined.

The temperature at the outlet of the regenerative cooling arrangement is not sufficient to generate the high power requirements of pumps if the liquid hydrogen supply is required at high pressures. The exhaust or outlet pressure of the turbine would also not be adequate for it to be supplied to the chamber. As a result the expander cycle is not a desired option for a high pressure nuclear rocket. Cold bleed and hot bleed cycles become essential.

### 11.6.2 Cold Bleed Cycle

The cold bleed cycle corresponds to the split expander cycle used in liquid propellant rockets except that the exhaust from the turbine is not fed into the reactor. It is let out through an auxiliary nozzle since the pressure at the turbine outlet is low. Part of the hydrogen gas heated in the regenerative cooling of the reactor walls is expanded in the turbine while the remaining part of it is supplied to the fission reactor. A schematic of the feed system cycle is shown in Fig. 11.6.



The different processes for the cold bleed cycle are shown in the Temperature entropy diagram in Fig. 11.7. The major difference from the expander cycle of Fig. 11.5 is in the turbine expansion CD to a lower pressure (higher pressure ratio) and the constant pressure heating of hydrogen in the reactor CE at a higher value of temperature (instead of DE in the expander cycle) and in the larger expansion ratio EF in the nozzle. The mass flow rate of hydrogen through the reactor is lower than the net hydrogen supplied by the pump.

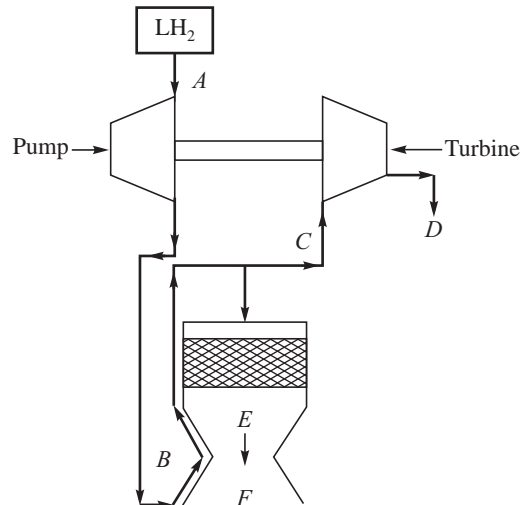


Fig. 11.6 Schematic of the Cold Bleed Cycle

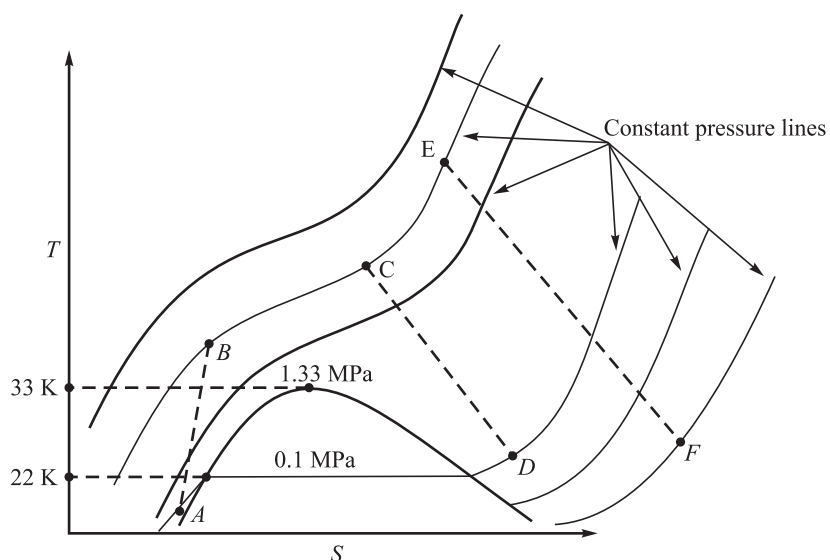


Fig. 11.7 Processes on the Cold Bleed Cycle on the T-s Diagram

### 11.6.3 Hot Bleed Cycle

The enthalpy available at the entry to the turbine is constrained by the amount of heating of hydrogen in the regenerative cooling of the walls of the reactor and the mirrors. When the hydrogen flow rate is large, such as in the case of a large thrust nuclear rocket, the enthalpy at the entry to the turbine in the expander cycle and in the cold bleed cycle is not adequate to generate sufficient work in the turbine capable of driving the pump. It becomes essential to enhance the enthalpy at the entry to the turbine using the principle of the combustion tap-off cycle discussed in liquid propellant rockets.



A small fraction of the hydrogen that is heated in the reactor is bled from the reactor and mixed with part of the hydrogen after regenerative cooling. This mixture is fed to the turbine for generating the necessary work for the pump. The bleed rates are very small and the reduction in the net specific impulse due to the loss of effective impulse in the turbine exhaust is a minimum. However, the bleed lines and components in the bleed line have to be designed for handling the higher temperatures of hydrogen. A schematic of the hot bleed cycle is shown in Fig. 11.8.

The processes taking part in the hot bleed cycle are shown in temperature entropy diagram of Fig. 11.9. It may be noted that the temperature at the inlet to the turbine has increases from point C in the expander and cold bleed cycle (Figs. 11.5 and 11.7) to  $C'$  in Fig. 11.9 due to mixing with the hot hydrogen from the reactor. The expansion ratio in the turbine is also much larger.

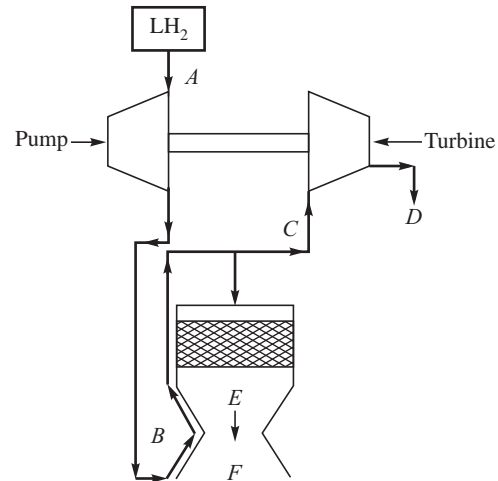


**Fig. 11.8** Schematic of Hot Bleed Cycle

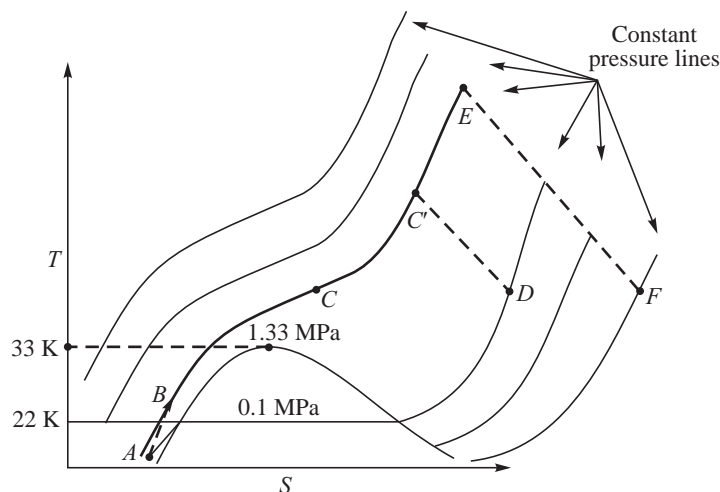


**Fig. 11.9** Processes on the Hot Bleed Cycle on the T-s Diagram

The hot bleed cycle is to be preferred for large thrust nuclear thermal rockets.



## 11.7 STATUS OF NUCLEAR ROCKETS

Nuclear thermal rockets have high performance with specific impulse of the order of 8000 N s/kg. They can generate high values of thrust of several MN and was claimed to be a better substitute for the large boosters used in the Saturn Moon Rocket. The high performance in the nuclear thermal rocket is essentially derived from the low molecular mass of hydrogen that is heated to high temperatures in the fission reactor. Though the temperatures are only about 30% higher than in the



cryogenic rocket burning hydrogen and oxygen, the molecular mass of the gases being expanded in the nozzle is around 2 g/mole in the nuclear rocket compared to about 18 g/mole for a stoichiometric combination of hydrogen and oxygen in the cryogenic liquid propellant rocket. The reduction in the molecular mass gives rise to an increase of specific impulse by about a factor of 3. The major factor contributing to the higher specific impulse is from the very low molecular mass of the hydrogen.

The Nuclear thermal rocket is limited by the power and not by energy considerations as in a chemical rocket. The limitation arises from the rate at which the neutrons are able to transfer the thermal energy to heat up the hydrogen in the reactor. There is also a limit on the temperature to which the pellets of the radioactive material used for the fission process can be heated by the neutrons. Considering the rate of energy transfer is a constraint, the nuclear thermal rocket is limited by power like an electrical rocket.

Nuclear Electric Propulsion holds promise for deep space and planetary missions. The incident solar flux drops off in our solar system beyond Jupiter and a nuclear electric rocket based on a fission or fusion reactor appears feasible. As the nuclear power increases, the specific mass of the power unit dealt with in electrical rocket decreases and makes the electrical rocket viable.

Nuclear fusion process demands high temperatures and pressures and appears more difficult to use than the nuclear fission process. Radioactive decay is of interest as power source for satellites. The RTGs and power generated in fission process are essential for satellites in deep space missions. However, radiation from radioactive fragments in case of launch failures, accidental re-entry into the Earth's atmosphere and collisions with the debris in space is a major cause of concern. Nuclear propulsion and nuclear power generation for satellites in Low Earth Orbit is not to be recommended. The radiation from reactors, unless shielded, is disruptive for the sensors carried in the satellite and the other satellites and could be tolerated only for deep space missions.



## 11.8 PULSED NUCLEAR ROCKETS

A series of directed nuclear explosions, if organized to impact on a steel base plate attached to a space vehicle, would generate an impulse and propel the vehicle. Suitable mechanism could be improvised between the base plate and the spacecraft for absorbing the shock loads. The space vehicle carries the nuclear bombs and drops them in the vicinity of the base plate and detonates it. The pulsed nuclear propulsion is also referred to as bomb propulsion.



## 11.9 POWER GENERATION IN SPACECRAFTS

A number of spacecrafts have used the radioactive decay of isotopes for power generation. No radiation problem has been reported. A radar ocean reconnaissance satellite Cosmos-954, which had an on-board nuclear reactor to power its radar system, did not create any adverse radiation when it re-entered the Earth's atmosphere and disintegrated in 1978. The power generation using the radio-active decay is referred to as Radio-isotope Thermo-electric Generator (RTG).



## 11.10 TRI-PROPELLANT ROCKETS

We had seen in Chapter 2 that the density specific impulse ( $\rho I_{sp}$ ) rather than the specific impulse ( $I_{sp}$ ) influences the incremental velocity ( $\Delta V$ ) provided by the rocket when the mass of the rocket is large such as during take off. The density specific impulse is a figure of merit of a booster rocket compared to specific impulse for the upper stage rocket. If a single rocket is to provide the required  $\Delta V$  for a mission (instead of obtaining the  $\Delta V$  through two or three rocket stages), the initial operation of the rocket must preferentially give high values of  $\rho I_{sp}$  compared to high values of  $I_{sp}$  required later during the mission. This is done by choosing the liquid propellant rocket to initially burn a heavy hydrocarbon fuel such as kerosene with liquid oxygen ( $LO_2$ ) to provide high  $\rho I_{sp}$  and later on in the mission change over to a cryogenic propellant combination of liquid hydrogen and liquid oxygen for obtaining larger values of  $I_{sp}$ . In essence two fuels one heavy and the other light are used with an oxidizer, three propellants in all in the liquid propellant rocket. The rocket is called a tri-propellant rocket.

If small quantities of hydrogen are added to the dense hydrocarbon-oxygen propellant combination, the specific impulse is enhanced since combustion products of lower molecular mass are generated. Hydrogen being more reactive also inhibits the occurrence of combustion instability by bringing down the combustion delay. In the initial phase of operation with heavy hydrocarbon fuels, small quantities of hydrogen are therefore added to the hydrocarbon oxygen mixture. The operation of the rocket, in this case, is truly with three propellants. This phase of operation is followed by using propellants  $LH_2$  and  $LO_2$ . The specific impulse averaged over the trajectory is lower than that obtained with propellants  $LH_2$  and  $LO_2$ . However, the advantages are that higher density impulses are initially obtained and a lower propellant volume, associated with the dense propellants contributes to a reduction of the mass of the tanks and turbo-pumps.

The principle of operation and materials of construction of a tri-propellant rocket are similar to those of a bi-propellant rockets except that two fuels (hydrocarbon and hydrogen) are initially burnt with liquid oxygen and this transits to the use of cryogenic propellant ( $LH_2$  and  $LO_2$ ) later. The injector is configured to efficiently atomize different proportions of the liquid fuels and the oxidizer and distribute them adequately in the combustion chamber. Like impinging injectors and coaxial swirl injectors, dealt with in Chapter 6, have been experimented with.

The use of liquid propane or liquid methane as the hydrocarbon fuel in place of kerosene gives higher performance. This is essentially from the smaller negative value of the heat of formation of methane and propane as compared to kerosene. Tri-propellant rockets with extendible nozzles and self adapting nozzles, as detailed in Chapter 3, would also contribute to reduce the number of rocket stages; however, they have not been adequately developed and applied.



## 11.11 PULSED DETONATION ROCKETS

High pressure and high temperature gases are generated in liquid propellant rockets by burning the liquid fuel and liquid oxidizer contained in propellant tanks in the combustion chamber and thereafter expanding these gases in a convergent divergent nozzle. The burning process consisted of mixing



together of the fuel and oxidizer vapors followed by chemical reaction to generate the high temperature products. Liquid propellant rockets could also be operated in a pulsed mode by periodically injecting the propellant into the combustion chamber.

The vapor of fuel and oxidizer mixed in the chamber could be detonated instead of being burnt as in the liquid propellant rockets. A detonation is different from burning in that the combustion is induced by a shock wave. The shock wave compresses the gases to a high value of temperature at which chemical reactions occur spontaneously. The energy released from the spontaneous chemical reactions pushes the shock wave or rather drives it. A shock wave which is driven by the energy release from the chemical reactions induced by it is known as a detonation. The shock wave couples with the energy release from the chemical reactions and this strongly coupled shock-cum-combustion front travels at a steady supersonic velocity known as Chapman Jouguet velocity. The Chapman Jouguet velocity is a constant for a given fuel and oxidizer mixture. A Chapman Jouguet detonation can be propagated in the medium of the gaseous fuel and oxidizer.

The pressure rises across a detonation due to the compression nature of the shock wave. The pressure rise is between 15 to 20 times the initial value of pressure of the unburned gas mixture. The increased pressure across a detonation is converted to thrust in a pulse detonation rocket.

### 11.11.1 Principle of Operation

A mixture of the vapor of fuel and oxidizer, used for the propellants, is formed at about atmospheric pressures in a tube or a pipe known as the detonation tube. A steady detonation is made to propagate at the Chapman Jouguet speed in this vapor mixture. Gaseous propellants, if used, can more readily mix compared to vapor of the liquid fuels and oxidizers. This is because the liquid has to first vaporize and vaporization is much slower than the processes of mixing and chemical reactions. However, the storing of the gaseous fuels in a rocket is not to be suggested since the volume of the tanks would be large and the mass of the tanks would adversely influence the useful payload mass and the velocity provided to the payload by the rocket. Liquid fuels and oxidizers are therefore to be preferred.

Hydrocarbon fuels, which are readily storables, like kerosene or jet mix products (JP fuel) used in the aviation industry, have been experimented with. Air available in the atmosphere has been proposed to be used for the oxidizer for flight through the atmosphere. In the absence of stored oxidizer in tanks, the pulse detonation device is known as a “Pulse Detonation Engine”.

The liquid hydrocarbon fuel is either injected as droplets into the detonation tube by an injector or it is heated and made to flash vaporize in the detonation tube. Air is also admitted through valves and a mixture of hydrocarbon air mixture is formed in the detonation tube. Alternatively, a premixed mixture of hydrocarbon air mixture is formed in a carburetion system as in the two stroke spark ignition internal combustion engines. An electrical spark is used to initiate the detonation of the hydrocarbon air mixture. Figure 11.10 shows a schematic of the detonation tube, the feed system and the igniting spark.

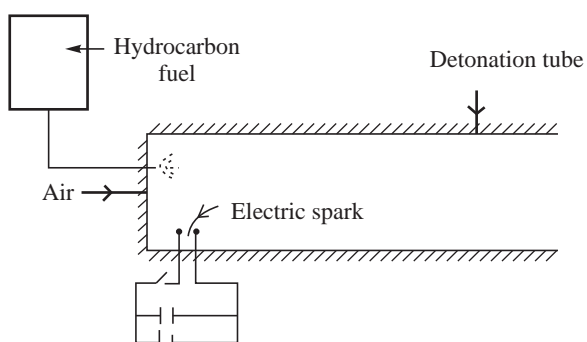


Fig. 11.10 Detonation Tube



Initiation of a detonation in the hydrocarbon oxidizer mixture by an electric spark, or otherwise, requires very large energy levels of the order of several hundred kilojoules or a few Mega joules. It is not possible to provide for such huge energy sources in the pulse detonation engine. The only alternative is to form a flame in the mixture by the spark and then convert the flame into a detonation. The initiation of a flame requires energy of only a few milli-joules. The flame, formed by the ignition source, at the injection head of the detonation tube, pushes the unburned gas mixture ahead of it just like a solid piston surface pushes the gas ahead of it. The unburned gas, ahead of the flame, reaches high velocities and becomes turbulent. The flame thereafter propagates in the turbulent flow of unburned gas as a turbulent flame. The turbulent flame has much higher burning velocities. The turbulent flame causes the unburned gas ahead of it to move with yet higher velocities and the cascading influence of flame acceleration progresses and causes a shock wave to be formed in the unburned gas mixture.

Rough surfaces over the inner surface of the detonation tube or blockages, if placed within it, further contributes to promote turbulence in the unburned gases ahead and formation of shock waves in the flow. In essence, it appears possible to create a precursor shock by the accelerating flame especially in the presences of blockages. The precursor shock can form a detonation. This process of transition of a flame to a detonation is spoken of as Deflagration to Detonation transition (DDT).

The distance traveled by a flame before it turns to a detonation is known as the “Run-up Distance”. All pulse detonation engines make use of DDT. They make use of blockages in the form of a coil called as Schelkin’s spiral which is inserted in the detonation tube. The diameter of the spiral  $D$ , the thickness of the wire  $d$  and the pitch of the spiral  $p$  are parameters influencing its performance which is to promote the formation of detonation. A sketch of a detonation tube with a Schelkin’s spiral is illustrated in Fig. 11.11.

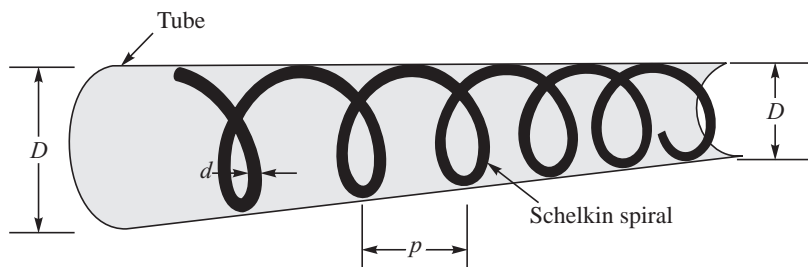


**Fig. 11.11** Schelkin Spiral

As the run-up distance for forming a detonation increases, the pressure at the closed end of the detonation tube decreases and the thrust therefore drops. It becomes necessary to ensure that the transition to a detonation takes place in the detonation tube as early as possible.

### 11.11.2 Pseudo-Detonation

The detonation tubes used in practice are a few centimeters in diameter. In order to achieve a steadily propagating detonation wave traveling at the Chapman Jouguet speed in the hydrocarbon-air mixture, the diameter of the tube is required to be more than an order of magnitude greater at about a few meters. In the smaller diameter tubes, the precursor shock wave forms a detonation traveling at sub Chapman Jouguet speed with much smaller pressure rise across it. These detonations are known as



pseudo detonations. Considering the smaller values of pressure rise across them, they cannot effectively be used in a pulse detonation engine to generate sufficient thrust.

### 11.11.3 Processes in Pulse Detonation Engine and Sequence of Operation

A detonation tube is first filled with the fuel air mixture. The mixture is ignited at the injection end and a flame is formed which transits to a detonation. The higher values of pressure behind the detonation generate the thrust. After the detonation exits the tube, the products of the detonation are flushed out of the tube by admitting air into the tube. After the purging is over, the cycle of events commence again with the filling of the detonation tube by the hydrocarbon air mixture. The sequence of events, which are idealized, is shown in Fig. 11.12. The processes of filling, travel of the flame and detonation in the tube and purging require some time. If these are represented by  $t_f$ ,  $t_o$  and  $t_p$  respectively, the time required for one pulse of operation is  $t_f + t_o + t_p$ . The maximum frequency of operation of the detonation tube is  $1/(t_f + t_o + t_p)$ .

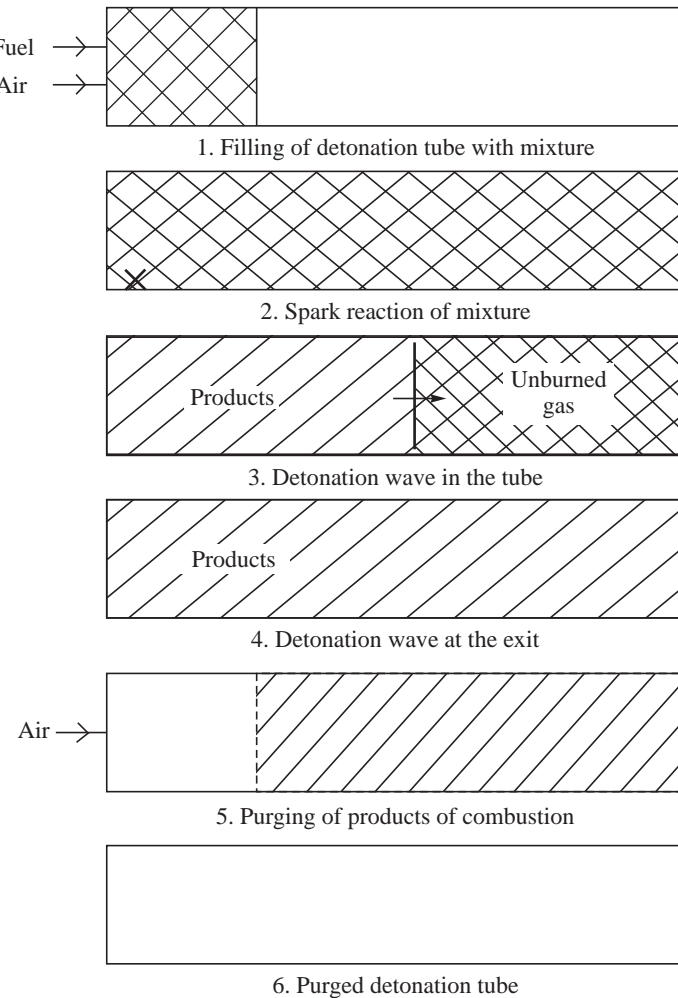


Fig. 11.12 Sequence of Events in a Pulse Detonation Engine



#### 11.11.4 Multiple Detonation Tubes in a Pulse Detonation Engine

The maximum frequency of operation of a single detonation tube is about 50 Hz based on the time required for filling, detonation wave travel and purging. If a number of detonation tubes can be clustered together as shown in Fig. 11.13, the number of pulses of thrust generated per unit time can be increased. This is done by operating the tubes successively one after the other. A common mixture preparation chamber feeds the different tubes; however, each one has its own ignition source. With a large number of detonation tubes, the thrust generated becomes almost continuous or steady instead of discrete pulses of thrust generated in a single detonation tube.

A nozzle is sometimes provided to enhance the thrust.

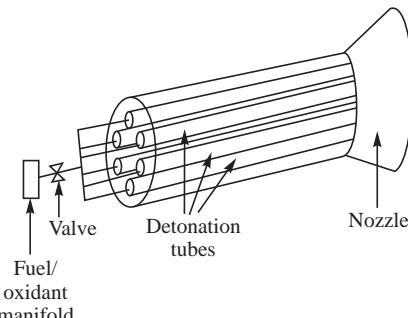


**Fig. 11.13** Multiple Detonation Tubes

#### 11.11.5 Salient Features of Pulse Detonation Engines

A high pressure fuel pump, as in liquid propellant rockets, is not required for the pulse detonation engines since the fuel-oxidizer mixture is filled in the detonation tubes at pressures around 100 kPa. The net heat release from the detonation is at constant volume and constant volume heat addition is more efficient than the constant pressure heat addition in a liquid propellant rocket.

The elements of the pulse detonation engine comprise of propellant tank, air intake, inlet valves, detonation tubes and electric spark system with the blockages to form the detonation. The construction is simple without any moving parts. However, formation of a Chapman Jouguet detonation in the small diameter detonation tubes is difficult and a large value of the run up distance leads to a significant loss in thrust. The placement of blockages in the detonation tube also causes pressure losses leading to loss of thrust. The filling of the fuel-oxidant vapor mixture over the length of the detonation tube at constant value of mixture ratio, well within the limits of detonation which are quite narrow, in the detonation tubes and its purging after the detonation wave travels in it calls for further developments to be carried out before the pulse detonation engine becomes a reality.



#### 11.12 BEAMED ROCKETS AND SAIL PROPULSION

Laser beams or microwave radiation from the Sun, if focused on an ablating surface, causes mass release and provides thrust. Coherent beams can also be used without an ablation material by impinging the beams over solid surfaces or screens and generating the thrust from the impact of the photons in the beam. Large surface areas may be required for generating thrust. The use of coherent beams for generating thrust is known as beamed propulsion. The mechanism is similar to the sail which provides motion to a boat from the wind and the mode of propulsion is referred to as sail propulsion.

Different strategies and innovative methods can be thought of for generating thrust and moving in space. Methods of propelling in space are endless. Robert Goddard, one of the greatest of the rocket pioneers, said “I have learned to use the word ‘impossible’ with the greatest of caution.”



## SOLVED EXAMPLES

**Example 11.1** MEMS vapourising micro-thruster:

A micro resistojet for satellite applications was developed using MEMS (Micro Electrical Mechanical Systems) technology. In this water was vaporised to generate small amount of thrust. A resistor, vapourising chamber, nozzle and micro-channels for feeding water to the vapourising chamber were all etched in silicon wafers. The water was vaporised by electrical heating using the resistor. The nozzle terminated at the throat. The throat had a square cross-section.

Determine the throat dimension and the thrust generated in such a vapourising water micro-thruster when the power dissipated in the resistor is 20 W and the water flow rate is 5 mg/s. The efficiency of the heating is 79%. The pressure in the vapourising chamber is 0.20 MPa. The thruster was developed for operation in deep space.

**Solution:** The temperature of steam formed by heating the water has to be first determined. If  $\dot{m}$  is the flow rate of water injected into the vaporiser and  $\dot{q}$  is the heat transferred to the water, the enthalpy  $h_s$  of the steam formed is obtained from the energy balance:

$$\dot{m}(h_s - h_w) = \dot{q}$$

The saturation temperature of water at 0.2 MPa is 120.23°C. The enthalpy of the injected water  $h_w$ , if assumed to be at 30°C, using steam tables is  $\frac{30}{120.23} \times 504.6 = 125.9$  kJ/kg. Here 504.6 is the enthalpy of water at the saturation temperature of 120.23°C. The enthalpy of steam formed after addition of heat is:

$$h_s = \frac{\dot{q}}{\dot{m}} + h_w = \left( \frac{20 \times 0.79}{5 \times 10^{-6}} + 125.9 \times 10^3 \right) \text{ J/kg} = 3.286 \times 10^6 \text{ J/kg} = 3286 \text{ kJ/kg}$$

From steam tables, the above value of enthalpy at 0.2 MPa pressure is seen to correspond to a superheat of 400°C.

Assuming the superheated steam as a perfect gas and taking its  $C_p = 58$  J/mole K, the value of the specific heat ratio  $\gamma$  is obtained from the relation:

$$C_P = \frac{\gamma R_0}{\gamma - 1}$$

Substituting the value of gas constant  $R_0$  [= 8.314 J/(mole K)] in the above, we get  $\gamma = 1.17$ . The characteristic velocity of the thruster is determined as:

$$C^* = \frac{1}{\Gamma} \sqrt{\frac{R_0 T}{\mathfrak{M}}} \quad \text{where } \Gamma = \sqrt{\gamma} \left( \frac{2}{\gamma + 1} \right)^{\frac{\gamma + 1}{2(\gamma - 1)}}$$

For  $\gamma = 1.17$ ,  $\Gamma = 0.64$  and

$$C^* = \frac{1}{0.69} \sqrt{\frac{8.314 \times 10^3 \times (400 + 273)}{18}} = 871 \text{ m/s}$$



Since  $\dot{m} = \frac{p_c A_t}{C^*}$ , we obtain on substituting the above value of  $C^*$ ,  $p_c = 0.2 \times 10^6$  Pa and  $\dot{m} = 5 \times 10^{-6}$  kg/s, the throat area as:

$$A_t = \frac{808 \times 5 \times 10^{-6}}{0.2 \times 10^6} = 21.8 \times 10^{-9} \text{ m}^2$$

The throat is of square cross-section. The dimensions of the throat =  $\sqrt{21.8 \times 10^{-9}}$  m<sup>2</sup>  
 $= 147 \mu\text{m} \times 147 \mu\text{m}$

The pressure at the throat  $p_t = \left(\frac{2}{\gamma+1}\right)^{\frac{\gamma}{\gamma-1}} p_c = 0.572 \times 0.2 \text{ MPa} = 0.114 \text{ MPa}$ .

Substituting this value in the equation for jet velocity, we have:

$$V_J = \sqrt{\frac{2\gamma R_0 T}{(\gamma-1)\mathfrak{M}} \left\{ 1 - \left( \frac{p_e}{p_c} \right)^{\frac{\gamma}{\gamma-1}} \right\}} = \sqrt{\frac{2 \times 1.17 \times 8314 \times (400 + 273)}{0.17 \times 18} \left\{ 1 - \left( \frac{0.114}{0.2} \right)^{\frac{0.17}{1.17}} \right\}} = 579 \text{ m/s}$$

Net thrust  $F = \dot{m} V_J + (p_t - p_a)A_t$ . With ambient pressure  $p_a$  being zero:

$$F = 5 \times 10^{-6} \times 579 + 0.114 \times 10^6 \times 21.8 \times 10^{-9} = 5.34 \times 10^{-3} \text{ N} = 5.34 \text{ mN}$$

### Example 11.2 Nuclear thermal rocket

A nuclear thermal rocket operating in a hot gas bleed cycle generates a thrust of 800 kN. In this rocket, liquid hydrogen is stored in tanks at a temperature of 20 K and a pressure of 0.2 MPa. It is pumped using a turbo-pump to a high pressure of 8 MPa. The high pressure liquid hydrogen from the pump is supplied to the coolant channels surrounding the nuclear reactor. The temperature of hydrogen at the outlet of the coolant channels is 400 K. The temperature of hydrogen at the reactor exit is 4000 K. The warm hydrogen from the exit of the coolant channels is mixed with the hot hydrogen gas bled from the reactor exit in the ratio 5:1 and is used to drive the turbine.

The temperature of the gases at the exit of the nozzle of the nuclear reactor is 250 K. The turbine outlet temperature is 350 K.

The critical temperature and pressure for hydrogen are 33 K and 1.33 MPa respectively. The specific heat of hydrogen gas at constant pressure can be assumed to be the same at all temperatures and equal to 14.5 kJ/(kg K). The density of liquid hydrogen is 71 kg/m<sup>3</sup>.

- (a) Determine the specific impulse of the nuclear rocket neglecting the contribution from the turbine exhaust and assuming no dissociation of hydrogen.
- (b) What is the mass flow rate of hydrogen in kg/s through the reactor?
- (c) If the efficiency of the turbine is 0.8 and the efficiency of the pump is 0.7, determine fraction of the total mass flow rate of hydrogen through the turbine?
- (d) What is the mass flow rate of hydrogen in kg/s through the turbine?

**Solution:** (a) Let us assume that the pressure at the exit of the nozzle is the same as the ambient pressure. In this case the magnitude of the exit jet velocity is the same as the specific impulse.



The exit jet velocity  $V_J$  is given by:

$$\frac{V_J^2}{2} = \Delta h \text{ across the nozzle}$$

$$V_J = \sqrt{2C_p\Delta T} = \sqrt{2 \times 14500 \times (400 - 250)} = 10,428 \text{ m/s}$$

$$I_{sp} = 10,428 \text{ Ns/kg}$$

(b) Mass flow rate of hydrogen through the reactor

$$= \dot{m}_R = \frac{F}{I_{sp}} = \frac{800 \times 10^3}{10428} = 76.72 \text{ kg/s}$$

(c) Work balance for the turbo-pump unit is:

$$\frac{(\dot{m}_{Total}/\rho)\Delta P}{\eta_P} = \eta_T \dot{m}_{Turb} C_P (\Delta T)_{Turb}$$

The drop in temperature across the turbine = Inlet temperature – outlet temperature

$$\text{Inlet temperature at the turbine} = \frac{5 \times 400 + 4000}{6} = 1000\text{K}$$

Outlet turbine temperature = 350 K

Substituting the values in the equation for work balance we get:

$$\frac{\dot{m}_{Turb}}{\dot{m}_{Total}} = 0.021$$

Fraction of the total mass flow rate through the turbine is 0.021

(d) The total mass flow rate is given as

$$\dot{m}_{Total} = \dot{m}_R + \dot{m}_{Turb}$$

$$\text{However } \dot{m}_R = 76.72 \text{ kg/s and } \dot{m}_{Turb} = 0.021(\dot{m}_R + \dot{m}_{Turb})$$

$$\therefore \dot{m}_R + \dot{m}_{Turb} = \dot{m}_R + 0.021(\dot{m}_R + \dot{m}_{Turb})$$

Substituting in  $\frac{\dot{m}_{Turb}}{\dot{m}_{Total}} = 0.021$ , we have:

$$\dot{m}_{Turb} = \frac{0.021 \times 76.7}{0.979} = 1.65 \text{ kg/s}$$

Mass flow rate of hydrogen through the turbine is 1.65 kg/s.

## References

1. Bekey, I., SSTO Rockets: A Practical Possibility, Aerospace America, July 1994, pp. 32-37.
2. Bussard, R.W., and Delauer R.D., Nuclear Rocket Propulsion, McGraw Hill Book Company, New York, 1965.



3. Kammash, T., *Fusion Energy in Space Propulsion*, Progress in Astronautics and Aeronautics, vol. 167, AIAA Inc., Washington, 1995.
4. Johnson, L., James B., Bagget R. and Montgomery E.E., *NASA's In-space Propulsion Technology Program: A Step towards Interstellar Exploration*, J. British Interplanetary Society, vol. 59, Is. 3-4, 2006, pp. 99-103.
5. Manski, D. and Martin, J.A., *Optimization of Propulsion Cycles for Advanced Shuttles*, Part 2: Performance Model Methodology, AIAA 90-2436, 26th Joint Propulsion Conference, Orlando, July, 1990.
6. Martin, J.A., Vongpaseuth T. and Venkatasubramanyam G., Russian RD-704 for Single Stage Vehicle, J. Spacecraft and rockets, Vol. 33. 1996, pp. 309-311.
7. Pedersen, E.S., *Nuclear Energy in Space*, Prentice Hall, Inc., Englewood Cliffs, 1964.
8. Roy, G.D., Frotov S.M., Borisov A.A. and Netzer D.W., *Pulse Detonation Propulsion: Challenges, Current Status and Future Perspective*, Progress Energy Combustion Science, vol. 30, 2004, pp. 545-672.

## Glossary

Bomb propulsion: Directing nuclear explosions external to a spaceship for propelling it; known also as pulsed nuclear propulsion

Detonation: High speed combustion associated with explosive release of energy

Nuclear electric propulsion: Electricity generated in a nuclear power plant housed in the rocket and the electric power used for electrical rockets

Nuclear thermal rocket: Heating of low molecular mass propellant by nuclear reactions and expansion of the heated gas in a nozzle

Pulsed detonation rocket: A rocket using pulses of detonation for generating thrust

Radioactive decay: The process of change of an unstable atomic nucleus over a prolonged period during which it emits radiation in the form of alpha, beta and gamma rays. The radioactive decay produces heat

Solar sail: A thin opaque film stretched to form a large surface area to provide a force under the influence of solar radiation pressure incident on it

Tri-propellant rocket: A liquid propellant rocket using a combination of a low performance dense hydrocarbon fuel with a high performance hydrogen fuel

## Annexure A

### Shape of Nozzles and Plumes



#### A.1 DESIGN OF CONICAL AND CONTOUR NOZZLES

The discussions of conical and contour nozzles were based on the assumption of steady one dimensional isentropic flow taking place through them. The throat diameter of the nozzle and its exit diameter were obtained based on isentropic flow. The velocity at the exit of the nozzle was related to the nozzle area ratio ( $\epsilon$ ). The two dimensional effects in the axisymmetric nozzle were introduced as a correction factor for divergence and the performance of the nozzle was determined.

The variations of the nozzle cross-sectional area along the length of the nozzle *i.e.*,  $A(x) = f(x)$  where  $x$  is the distance along the length of the nozzle and  $A(x)$  is the cross-sectional area at  $x$  is required to configure the nozzle. The variation of  $A(x)$  with  $x$  is discussed in the following for conical and contour nozzles.

##### A.1.1 Conical Nozzle

Based on the acceptable level of divergence loss and the acceptable mass of the nozzle discussed in Section 3.5, a semi-divergence angle of  $15^\circ$  for the divergence part of the conical nozzle was found to be reasonable. This angle  $\theta_d = 15^\circ$  could be used for determining the variation of area ratio  $A(x)$  in the divergent starting from the throat. Figure A.1 shows a conical divergent with the half cone angle of  $15^\circ$  and a throat diameter of  $d_t$  and the exit diameter of  $d_e$ .

In the convergent part of the nozzle for which the flow is subsonic and accelerates to sonic condition at the throat, the rate of expansion –  $dA(x)/dx$  can be very much greater than in the divergent. This is because flow separation and shocks from adverse pressure gradients are not possible as the pressure is still high in this region and the Mach number is less than unity. The convergent part of the nozzle

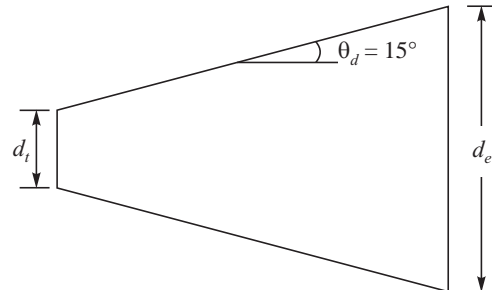


**Fig. A.1** Shape of the Divergent Part of Conical Nozzle



is therefore provided with a somewhat rapid change in the value of  $-dA(x)/dx$ . When the convergent is in the form of a cone, the half cone angle ( $\theta_c$ ) can be as high as  $60^\circ$ , which is very much higher than the value of  $15^\circ$  for the divergent. A conical convergent is sketched in Fig. A.2. Here  $d_i$  denotes the diameter of the rocket chamber.

The convergent and divergent parts, shown in Figs A.2 and A.1 are put together as shown in Fig. A.3 at the throat  $d_t$  to form the convergent divergent nozzle.

An abrupt change is observed in Fig. A.3 at the throat wherein the decreasing area with distance in the convergent portion is arrested and the area begins to increase again in the divergent. It is not possible to configure a nozzle with abrupt changes in its dimensions as shocks and flow separation would take place downstream of the abrupt expansion. A circular arc with a radius  $R_t$  equal to between 0.1 and 0.4 times the radius of the throat  $r_t$  ( $= d_t/2$ ) is provided connecting the convergent and divergent conical portions. A sketch of the conical nozzle with a smooth profile at the throat is shown in Fig. A.4.

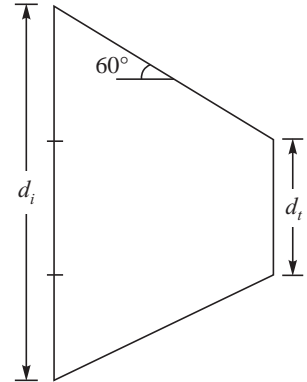


**Fig. A.2** Convergent Portion of Conical Nozzle

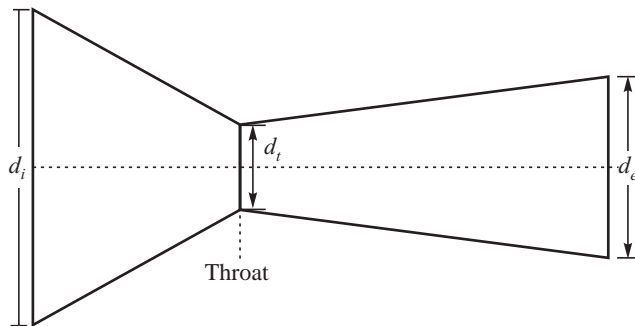


**Fig. A.3** Conical Nozzle Shape

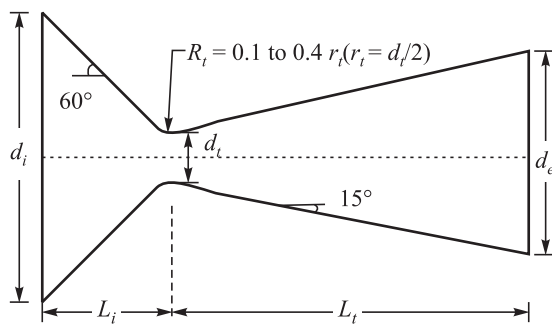


**Fig. A.4** Curvature at Throat

The length of the convergent portion  $L_c$  is seen from Fig. A.4 to be:

$$L_c = (d_i/2 - d_t/2) \cot \theta_c$$

The length of the diverging part of the nozzle is:

$$L_d = (d_e/2 - d_t/2) \cot \theta_d$$



It may be recalled that the contraction ratio  $A_i/A_t$  gives sonic conditions at the throat  $A_t$ . The contraction ratio is generally about three or greater. The contraction ratio denoted by  $\chi$  is:

$$\chi = A_i/A_t \geq 3$$

We will observe, while studying combustion instabilities, that a gradually tapering nozzle with a small convergent angle  $\theta_c$  is desirable so that the tendency for the formation of standing waves by the reflection of acoustic waves at the throat is reduced. However, the ratio  $\chi$  must provide sonic condition at the nozzle throat.

Instead of a conical convergent, a curved profile is generally provided till the throat. This is shown in Fig. A.5. The curve upstream of the throat is given a circular radius  $R = d_t$ . This radius is linked to the diameter of the chamber  $d_i$  along streamlines of the flow. The flow being sub-sonic in this region adapts to the curved wall contour.

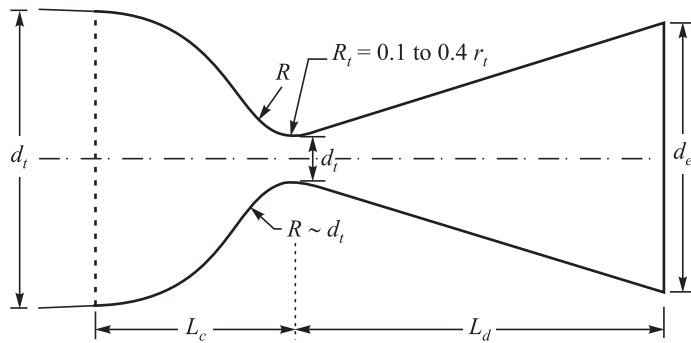


Fig. A.5 Shape of Conical Divergent with Shaped Convergent

### A.1.2 Contour Nozzle

The shape of the convergent and throat regions corresponding to subsonic and sonic flow remains the same as for the conical diverging nozzle given in Fig. A.5.

For the divergent part, a contour in the form of a bell is used instead of a cone. As pointed out in Section 3.6, a fraction  $f$  of the length  $L_d$  of the  $15^\circ$  conical nozzle is chosen for the contour nozzle. This fraction  $f$  could vary between 0.7 and 0.95 and accordingly we said that it is a 70% bell to a 95% bell nozzle. A shorter length is possible for the contour divergent since the flow can be more readily expanded immediately downstream of the throat where the pressure is still high for which condition flow separation and formation of shocks will not take place.

The divergent part of the contour nozzle therefore has a large value of the initial wall angle  $\theta_m$  at  $x = x_i$  and this is specified. A very small value of the exit wall angle  $\theta_e$  is provided at the nozzle exit to reduce the divergence loss. For the given length of the divergent  $L = f \cdot L_d$  and values of  $\theta_m$  and  $\theta_e$  and diameters  $d_t$  and  $d_e$ , a parabolic shape which provides a larger turning angle  $\theta_m$  initially and a small  $\theta_e$  at the exit is chosen. The profile of the contour nozzle is illustrated in Fig. A.6. A second order parabola of form  $y = ax^2 + bxy + cx + d$  where  $a, b, c, d$  are constants fits the values of  $\theta_m, \theta_e, L, d_t$  and  $d_e$ . The constants  $a, b, c$  and  $d$  are obtained from the conditions:

1. At  $x = x_i : y = d_t/2$
2. At  $x = x_i : \theta = \theta_m$  (specified)

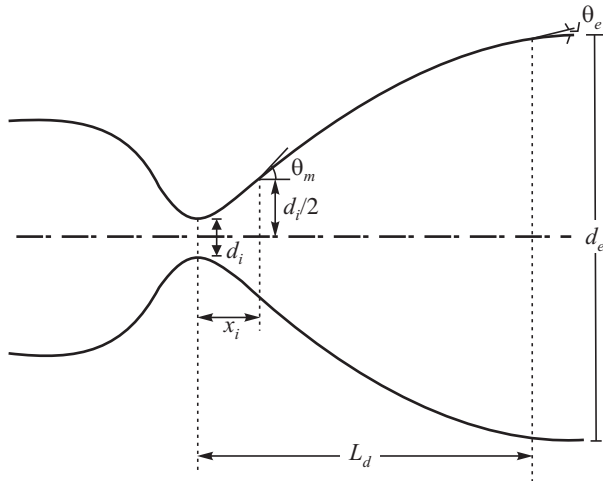


**Fig. A.6** Contour Nozzle Profile

3. At  $x = L_d$ :  $y = d_e/2$
4. At  $x = L_d$ :  $\theta = \text{between } 1 \text{ and } 3.5^\circ$

The choice of values  $\theta_m$  and  $\theta_e$  depend on the area ratio  $\varepsilon$  of the nozzle and is a function of the chamber pressure and the ambient pressure. For large area ratio nozzles,  $\theta_e$  tends to a limit of about  $1^\circ$  whereas values of  $\theta_m$  are between  $35$  and  $40^\circ$ . For small values of area ratios,  $\theta_e$  is somewhat higher at values between  $3$  to  $5^\circ$  while  $\theta_m$  retains the high values between  $35$  and  $40^\circ$ .

We shall in the following deal with a procedure for determining the performance of a contour nozzle. The flow in the divergent is assumed to be two dimensional in the  $x, y$  coordinate system rather than axisymmetric coordinates  $x, r$  to illustrate the method. A two dimensional coordinate system with distance along the axis  $x$  starting from the throat and a lateral distance  $y$  from the centre line along the nozzle is used. The velocity at any point  $(x, y)$  is represented by the vector  $\vec{V}(x, y)$ . The axial and radial components of this velocity are  $u(x, y)$  and  $v(x, y)$ . A steady potential flow is assumed. However, this 2-d steady potential flow cannot be solved for the contour nozzle using analytical methods i.e., a simple closed form solution is not possible. Numerical methods such as Method of Characteristics (MOC) and Computational Fluid Dynamic (CFD) methods become necessary. We shall choose the simple MOC method to illustrate the analysis.



## A.2 METHOD OF CHARACTERISTIC APPLIED TO CONTOUR NOZZLE DIVERGENT

### (a) Background of the Method

The flow in the divergent is supersonic and therefore can be felt only downstream. A point  $O$  traveling at the supersonic velocity  $V$  along the axial direction would occupy positions  $A$ ,  $B$ , and  $C$  at time  $t$ ,  $2t$  and  $3t$  such that  $OA = Vt$ ,  $OB = 2Vt$  and  $OC = 3Vt$ . If the velocity of sound in the medium is denoted by  $a$ , the region over which the disturbances originating from the point  $O$  as it moves along  $x$  to a



point  $A$  in a time  $t$  is given by a circle of radius  $at$ . When the point  $O$  is at  $B$  at time  $2t$ , the disturbances are felt over a circle of radius  $2at$  in a time  $2t$ . Similarly the region of influence over a time  $3t$  such as when the point is at  $C$  is a circle of radius  $3at$  with its center at  $C$ . The region of influence of  $O$ , as it moves at speed  $V$  with  $V > a$ , is therefore bound by two lines tangent to the circles at  $A'$ ,  $B'$ ,  $C'$  and  $A''$ ,  $B''$  and  $C''$ . This is because the effects of flow are perceived by disturbances traveling at the speed of sound. The region of the cone bound by the two limiting lines  $OA'B'C'$  and  $OA''B''C''$  contain the information about the supersonic flow. The angle that the limiting lines make with the direction of the flow  $OABC$  is  $\mu = \sin^{-1} 1/M$  (Fig. A.7). These two lines  $OA'B'C'$  and  $OA''B''C''$  are known as Mach lines.

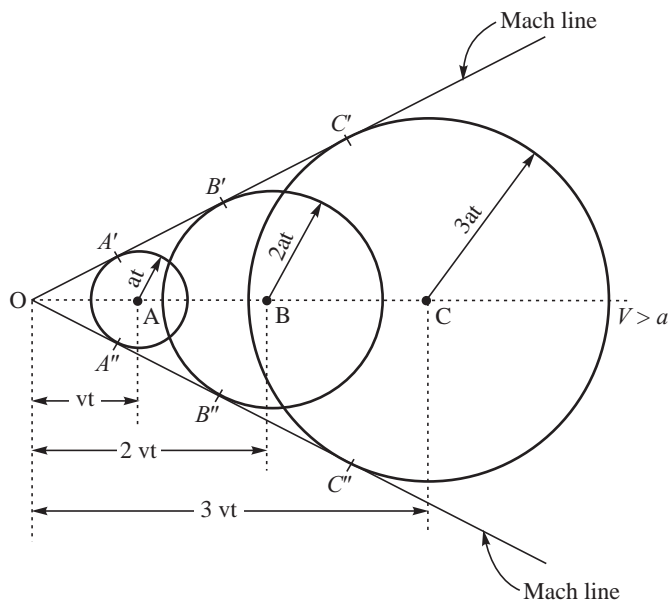


**Fig. A.7** Mach Cone and Mach Lines in Supersonic Flow in the Inertial Frame of Reference

The supersonic flow in a nozzle divergent can be resolved along the two Mach lines within which alone the expansion effects of the wall are felt by the flow. We deal with the method in the following.

#### (b) Sudden Divergence of Contour after the Nozzle Throat

Let us consider a two dimensional nozzle as shown in Fig. A.8. The Mach number at the throat is sonic ( $M = 1$ ) and becomes supersonic in the divergent. If there is a sudden divergence after the throat, as shown in Fig. A.8, the flow downstream of the throat at  $B$  gets expanded. If we restrict our attention to the lower half of the nozzle and presume that the Mach number just after the throat at  $B$  is slightly greater than one and equal to  $M_1$  and that this supersonic flow at Mach  $M_1$  is parallel to the wall  $AB$ , the sudden divergence of the wall at  $B$  would expand the flow. The final flow at the wall region has got to be along the wall  $BC$ . A Mach line  $BD$  at an angle  $\mu_1 = \sin^{-1} (1/M_1)$  to the direction of flow along  $AB$  is generated at the point  $B$  due to the expansion signal or disturbance at the point  $B$ . The flow increases in Mach number and gets deflected towards the wall. However, the deflection of the flow which is possible across the Mach line  $BD$  is not sufficient to bend the flow parallel to  $BC$ .

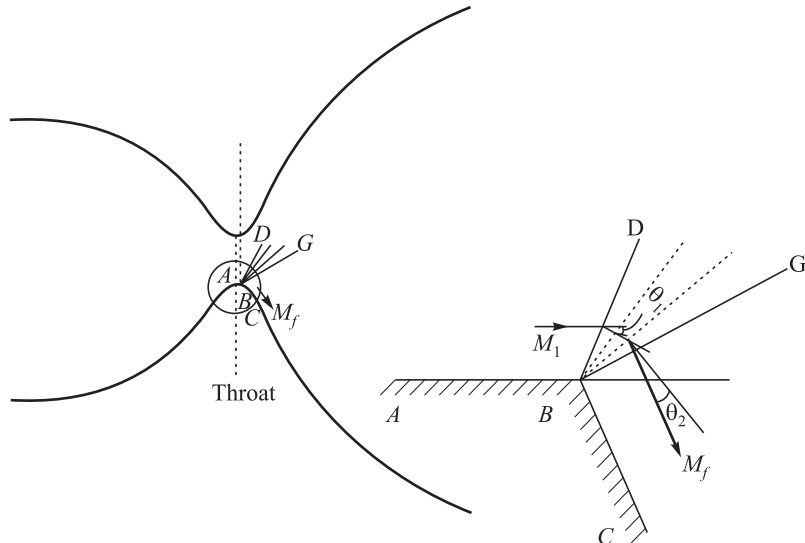


**Fig. A.8** Sudden Expansion at Throat

A series of Mach lines very much like a fan centered at  $B$  is necessary to make the final flow align itself along the wall. Each Mach line in the fan expands and bends the flow further until the flow becomes parallel to  $BC$ . The expansion thus progresses through a series of such Mach lines until the terminal Mach line  $BG$  accelerates the flow to Mach  $M_f$  and parallel to  $BC$ . If the Mach number of the stream upstream of the terminal Mach line is  $M_2$ , the angle made by this Mach line ( $BG$ ) to the stream at Mach  $M_2$  is  $\mu_2 = \sin^{-1}(1/M_2)$ . As the value of Mach number increases progressively, the value of  $\mu$  decreases. It may be noted that the angle  $\mu$  of the Mach line is with respect to the incoming direction of the flow and this causes the Mach lines centered at the point  $B$  to diverge out as shown. This centered expansion fan is termed as Prandtl Mayer expansion.

The flow bends by angle  $\theta_1$  at the first Mach line  $BD$  and by  $\theta_2$  at the terminal Mach line  $BG$ . The supersonic flow, initially at Mach  $M_1$  expands through a series of diverging Mach lines in the Prandtl Mayer fan though not explicitly shown in Fig. A.8. The expansion process can be assumed as isentropic since the flow is expanded through a series of small angles.

Though the flow can be expanded by the sudden divergence, the viscous effects in the flow will result in a boundary layer at the wall and its separation at the walls. A shear layer is also formed separating the recirculation regions downstream of the sudden expansion from the rapidly expanded regions. The expansion fan comprising the Mach lines on interacting with the shear layer are reflected as compression waves and these compression waves coalesce to form shock waves. The pressure rises across a shock while the flow velocity reduces across it and these result in a serious loss of performance of the nozzle. A sudden divergence of flow in a Contour nozzle is therefore not desirable.

### (c) Gradual Divergence of Contour after the Nozzle Throat

When the expansion is not sudden but is gradual and continuous, a series of Mach lines are formed along the expanding contour. This is shown in Fig. A.9 for the lower portion of a two dimensional nozzle. The gradual curvature at the wall ensures that at each Mach line the flow in the wall region bends along the wall. Three typical Mach lines  $BD$ ,  $EF$  and  $GH$  are shown which make angles  $\mu_1$ ,  $\mu_2$  and  $\mu_3$  with the incident flow and deflect the flow by  $\theta_1$ ,  $\theta_2$  and  $\theta_3$  respectively.

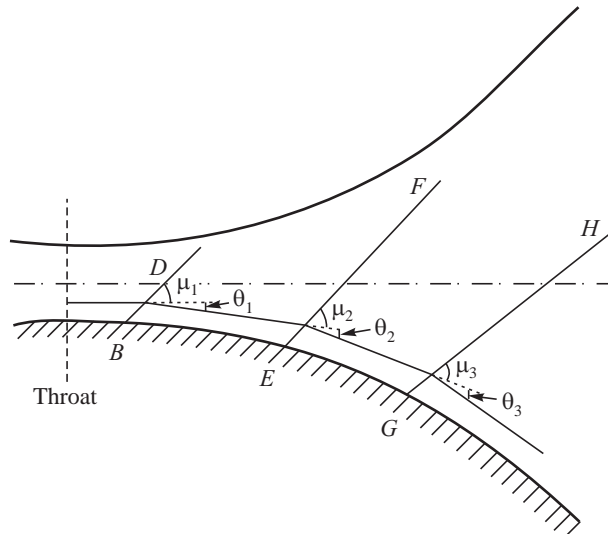


Fig. A.9 Gradual Expansion after the Throat

In practice, a gradually increasing curvature is initially provided after the throat and this curvature is subsequently reduced to provide near axial flow at the nozzle exit. Figure A.10 gives a schematic of the divergent in a two dimensional contour nozzle with the wall angle increasing from 0 at the throat to a maximum value of  $\theta_m$  over a distance  $X_m$  and thereafter getting reduced to a negligibly small value  $\theta_e$  over a distance  $X_e$  at which the nozzle exit is reached.

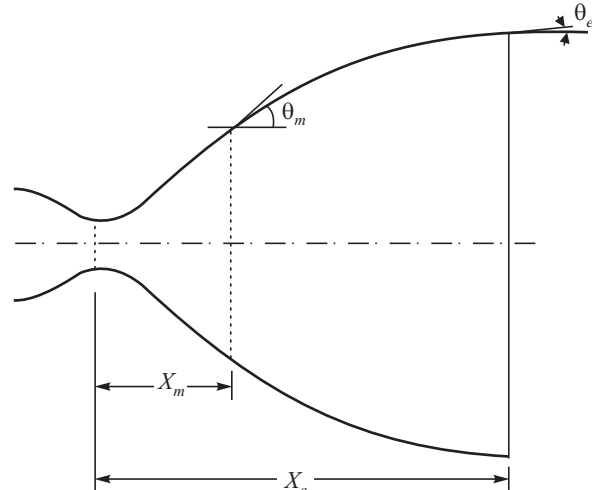


Fig. A.10 Nozzle Divergent Contour



### A.3 CONTOUR NOZZLE ANALYSIS

#### (a) Simple and Non-simple Regions of Flow

The uniform axial flow of an inviscid fluid, at a Mach number slightly greater than one, can be assumed to enter the divergent contour at section AA' which is very close to the throat in Fig. A.11. The expansion takes place across a series of Mach lines which are shown by A'C and AC, D'E' and DE, F'G' and FG and G'H' and GH corresponding to the lower and upper half respectively of the two dimensional nozzle. These Mach lines are also denoted as right running and left running waves and termed as Characteristics "C". The characteristics from the lower wall appear to move along the flow



and are called as  $C^+$  characteristics or right running waves whereas those from the upper wall appear to move opposite to the flow and are called as  $C^-$  characteristics or left running waves.

The  $C^+$  characteristic from the wall point  $A'$ , in Fig. A.11, meets the  $C^-$  characteristic from point  $A$  at point  $C$ . The point  $C$  is on the center line which is symmetric with respect to the upper and lower contours. If we further extend these two characteristics beyond the point  $C$ , the  $C^+$  will not meet the incident parallel flow at Mach number  $M_1$ , but would meet the accelerated flow at Mach number  $M_2$  downstream of the characteristic line  $AC$  because of the expansion from the wall  $AD$  which is not parallel to the nozzle axis. It would therefore bend from its original path to  $CE$ . This process would continue as the Mach number of the incident flow on to the characteristic  $C^+$  increases and the flow bends further to deviate the characteristic along  $EG$ ,  $GH$  and  $HB$ . The  $C^+$  characteristic along  $CB$  will no longer be a straight line but would comprise of a series of discrete lines bending at its intersections with the family of  $C^-$  characteristic from the upper wall. Similarly we would have the characteristic line  $C^-$  from the point  $A$  bending whenever it meets a  $C^+$  characteristic from the lower wall. Considering the symmetry of the upper and lower contours, the characteristics would be symmetrical about the center line.

The above line of reasoning applies to  $C^+$  and  $C^-$  characteristics emanating from points  $A$  and  $A'$  to the points  $I$  and  $I'$  for which the wall angle is a maximum at  $\theta_m$ . Beyond point  $I$ , the wall angle decreases. No expansion takes place at the wall region and the wall only guides the flow.  $IOX$  and  $I'OX'$  show these regions in Fig. A.11 and characteristics of a single family either  $C^+$  or  $C^-$  are present in this region. These two regions  $ACI$  and  $A'C'I'$ , which comprise of only one family of characteristics are known as simple regions. In the region  $IC'I'O$ , the  $C^+$  and  $C^-$  characteristics intersect and the directions of the characteristics change. This region of flow is known as a non-simple region. The flow is uniform and parallel to the center line in the region  $XOX'$ .

### (b) Analysis for the Simple Region

Only one family of characteristics is present in this region. The properties ahead and downstream of the characteristic would therefore be constant. Let us illustrate this case with a flow across a characteristic line  $A'C$  when the lower wall turns the flow, initially at Mach  $M_1$  by a small angle  $\delta\theta$ . Figure A.12 illustrates the flow turning by angle  $\delta\theta$  and increasing its Mach number due to the small expansion process to  $M_1 + \delta M_1$ .

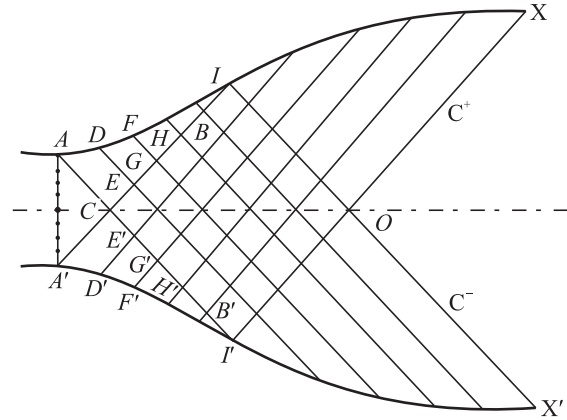


**Fig. A.11** Simple, Non-simple and Uniform Regions of Flow

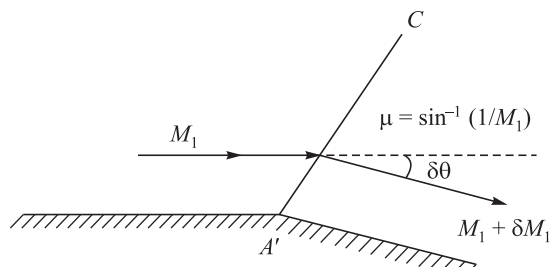


**Fig. A.12** Mach Wave and Flow Turning due to Sudden Expansion



The angle made by the characteristic to the direction of  $M_1$  is given by  $\mu = \sin^{-1}(1/M_1)$ . Across the characteristic, the velocity increases from  $\vec{U}$  to  $\vec{U} + d\vec{U}$  as shown in Fig. A.13 by deflecting through the angle  $d\theta$ . There cannot be a velocity along the characteristic since it only separates the two states. The resulting change has to be normal to the characteristic. If we can resolve the resultant velocity  $d\vec{U}$  in terms of the axial(x)  $du$  and vertical(y)  $dv$  components, we have for the flow bending by angle  $d\theta$  and the resultant velocity normal to the characteristic as shown in Fig. A.13, the following relations.

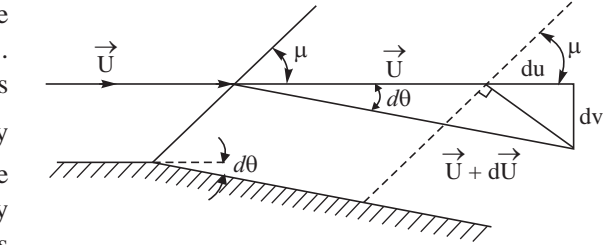


**Fig. A.13** Analysis in Simple Region (Velocity Parallel to Mach line is zero)

$$\frac{du}{dv} = \tan \mu \quad (\text{A.1})$$

$$\text{However } dv = u d\theta \quad (\text{A.2})$$

$$\text{Hence } \frac{du}{ud\theta} = \tan \mu \quad (\text{A.3})$$

From relation  $\mu = \sin^{-1}(1/M_1)$ , we get:

$$\tan \mu = \frac{1}{\sqrt{M_1^2 - 1}} \quad (\text{A.4})$$

$$\text{This gives: } \frac{du}{u} = \frac{d\theta}{\sqrt{M_1^2 - 1}} \quad (\text{A.5})$$

$$\text{The sound speed is given by } a_0^2 = \gamma RT \text{ so that } u^2 = M_1^2 \gamma RT \quad (\text{A.6})$$

Writing the temperature in terms of the stagnation temperature  $T_0$ , which for the isentropic expansion process is constant, we have:

$$u^2 = M_1^2 \gamma R \frac{T}{T_0} T_0 = \frac{M_1^2 \gamma R T_0}{1 + \frac{\gamma - 1}{2} M_1^2} \quad (\text{A.7})$$

On differentiating we get:

$$2u \frac{du}{dM_1^2} = \frac{\gamma R T_0 M_1^2}{\left(1 + \frac{\gamma - 1}{2} M_1^2\right)^2} \times \frac{1}{M_1^2} \quad (\text{A.8})$$

$$\text{This gives: } \frac{du}{u} = \frac{1}{2 M_1^2} \frac{dM_1^2}{1 + \frac{\gamma - 1}{2} M_1^2} \quad (\text{A.9})$$

Combining the above expression with  $\frac{du}{u} = \frac{d\theta}{\sqrt{M_1^2 - 1}}$ , we get:



$$dM_1^2 = \frac{2M_1^2 \{1 + (\gamma - 1)M_1^2/2\}}{\sqrt{M_1^2 - 1}} d\theta \quad (\text{A.10})$$

The Mach number change is therefore related to the change of angle of the flow due to the wall. Once the Mach number change is known, the changes in all the other properties such as temperature  $T$ , density  $\rho$  and pressure  $p$  can be determined from the change in  $dM_1^2$ . We can write for the changes in temperature, density and pressure:

$$\frac{dT}{T} = -\frac{\gamma - 1}{2} \times \frac{dM_1^2}{1 + \{(\gamma - 1)/2\} M_1^2} \quad (\text{A.11})$$

$$\frac{d\rho}{\rho} = -\frac{1}{2} \times \frac{dM_1^2}{1 + \{(\gamma - 1)/2\} M_1^2} \quad (\text{A.12})$$

$$\frac{dp}{p} = -\frac{\gamma}{2} \times \frac{dM_1^2}{1 + \{(\gamma - 1)/2\} M_1^2} \quad (\text{A.13})$$

The curved wall is replaced by a series of straight segments and using relations A.5, and A.10-A.13, the properties of velocity, Mach number, temperature, density and pressure in the simple region which has only one family of characteristics is obtained.

### (c) Analysis for the Non-simple Region

In this region the characteristics  $C^+$  and  $C^-$  cross each other and the conditions downstream of a given characteristic is no longer a constant. The region is illustrated in Fig. A.14 where the  $C^+$  characteristic  $AO$  and  $OB$  intersects with the  $C^-$  characteristic  $DO$  and  $OE$  at  $O$ . The incident Mach number upstream of characteristics  $AO$  and  $DO$  is the same and is taken to be  $M$ . Let the Mach number change from a value of  $M$  to  $M + \delta M_1$  on crossing the characteristic  $AO$  and the Mach number change from  $M$  to  $M + \delta M_3$  on crossing characteristic  $DO$ . The direction of the flow which was same upstream of these characteristics is now different and is shown by  $\delta\theta_1$  and  $\delta\theta_3$  respectively in Fig. A.14.

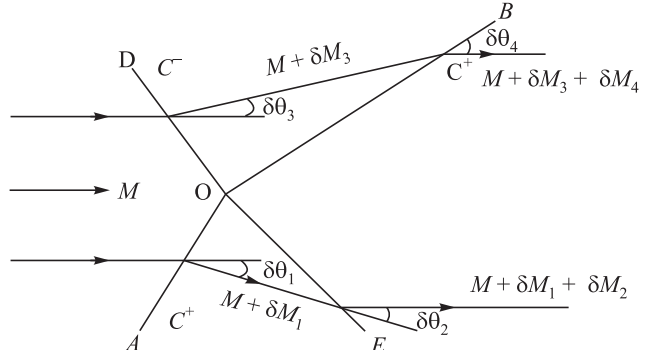


**Fig. A.14** Analysis in Non-simple Region

The streams in the region  $BOE$  must have the same Mach number and the same direction. If the characteristic  $OE$  bends the upstream flow at Mach  $M + \delta M_1$  by angle  $\delta\theta_2$  to Mach  $M + \delta M_1 + \delta M_2$  and the characteristic  $OB$  bends the upstream flow at Mach  $M + \delta M_3$  by angle  $\delta\theta_4$  to  $M + \delta M_3 + \delta M_4$ , Mach, we have (see Fig. A.14):

$$\delta\theta_1 - \delta\theta_2 = \delta\theta_3 - \delta\theta_4 \quad (\text{A.14})$$

$$\delta M_1 + \delta M_2 = \delta M_3 + \delta M_4 \quad (\text{A.15})$$

However, the equation linking the change in  $M^2$  i.e.,  $dM^2$  with the bending of the flow across a characteristic is given by Eq. A.10 viz.,



$$dM^2 = \frac{2M^2 \{1 + (\gamma - 1)M^2/2\}}{\sqrt{M^2 - 1}} d\theta$$

Taking a finite difference approximation for  $\delta M$ , we can write:

$$\delta M = \frac{M \{1 + (\gamma - 1)M^2/2\}}{\sqrt{M^2 - 1}} d\theta \quad (\text{A.16})$$

We can therefore write:

$$\delta\theta_2 = m_1 \delta M_2 \quad (\text{A.17})$$

$$\delta\theta_4 = m_3 \delta M_4 \quad (\text{A.18})$$

where  $m_1$  and  $m_2$  are given by:

$$m_1 = \frac{\sqrt{(M + \delta M_1)^2 - 1}}{(M + \delta M_1) \{1 + (\gamma - 1)(M + \delta M_1)^2/2\}} \quad (\text{A.19})$$

$$m_3 = \frac{\sqrt{(M + \delta M_3)^2 - 1}}{(M + \delta M_3) \{1 + (\gamma - 1)(M + \delta M_3)^2/2\}} \quad (\text{A.20})$$

Equations A.14, A.15, A.17 and A.18 can be solved for  $\delta\theta_2$ ,  $\delta\theta_4$ ,  $\delta M_2$  and  $\delta M_4$  as follows:

From Equations A.14, A.17 and A.18, we have:

$$m_1 \delta M_2 - m_3 \delta M_4 = \delta\theta_1 - \delta\theta_3 \quad (\text{A.21})$$

From Equation A.15, we have:

$$\delta M_2 - \delta M_4 = \delta M_3 - \delta M_1 \quad (\text{A.22})$$

We can solve the above two equations for  $\delta M_2$  and  $\delta M_4$  to give:

$$\delta M_2 = \frac{(\delta\theta_3 - \delta\theta_1) - m_3 (\delta M_1 - \delta M_3)}{m_3 - m_1} \quad (\text{A.23})$$

$$\delta M_4 = \frac{(\delta\theta_3 - \delta\theta_1) - m_1 (\delta M_1 - \delta M_3)}{m_3 - m_1} \quad (\text{A.24})$$

As  $\delta\theta_1$ ,  $\delta\theta_3$ ,  $\delta M_1$  and  $\delta M_3$  are known, the values of  $\delta M_2$  and  $\delta M_4$  are determined and we know the Mach number in the region BOE. Substituting the values of  $\delta M_2$  and  $\delta M_4$  in Equations A.17 and A.18 respectively, the values of  $\delta\theta_2$  and  $\delta\theta_4$  are determined. In this manner the non-simple region of flow is analyzed.

#### (d) Divergent Design using 2-d MOC

The exit diameter and Mach number are based on the area ratio ( $\epsilon$ ) and the throat diameter while the length of the divergent is determined from the fractional length of a  $15^\circ$  conical nozzle. The nozzle is divided into three regions comprising:

(i) **Non-simple region:** This region corresponds to increasing values of the wall angle ( $\theta_w$ ) of the nozzle till a maximum  $\theta_{w,\max}$  at the inflection point A in Fig. A.15. The characteristics  $C^+$  and  $C^-$  originating downstream of the throat region are reflected from the walls. The characteristics intersect with each other leading to the  $C^+$  and  $C^-$  characteristics with a curved shape. This is the



expansion region and is termed as a non-simple region since the family of  $C^+$  and  $C^-$  characteristics interact.

(ii) **Simple region:** The characteristics  $C^+$  and  $C^-$  on interaction with the wall get cancelled in the region between  $\theta_{w, \text{max}}$  and  $\theta_e$  as no expansion takes place at the wall and the flow is guided along the wall.  $ADB$  and  $A'DB'$  in Fig. A.15 show the region. The region  $ADB$  consists of  $C^+$  characteristics while region  $A'DB'$  consists only  $C^-$  characteristics. The regions are simple regions as they are covered with characteristics of only a single family either  $C^+$  or  $C^-$ .

(iii) **Uniform flow region:** The region is shown by  $BDB'$  in Fig. A.15. There are no characteristics in this region and the flow is uniform along the axis of the nozzle.

The analysis is therefore done for the simple and non-simple regions following the procedure given earlier and the velocity at the exit is determined. The properties pressure, temperature and density are also determined based on the equations derived for the simple and non-simple regions. In summary, the region of increasing wall angles, starting from the throat to  $ADA'$  in Fig A.15 for which expansion waves are generated is traversed by  $C^+$  and  $C^-$  characteristics. After this the wall angle decreases and only one family of characteristics exist in the region  $ADB$  and  $A'DB'$ . The flow is uniform in the region thereafter *i.e.*, downstream of the region corresponding to the  $C^+$  and  $C^-$  characteristics passing through the exit (region  $BDB'$  in Fig. A.15). The entire flow characteristics are thus determined for the divergent. With sufficiently small steps at the walls, accurate predictions for flow are possible.

The analysis is done starting just downstream of the sonic throat. The sonic line at the throat region is generally curved and depends on the streamlines of flow in the convergent and the shape of the throat region. The initial line at which the analysis starts could be assumed to be a straight immediately downstream of the throat. A curved line could be chosen based on experiments or a perturbation analysis of the conditions upstream of the throat. The initial assumption will not drastically influence the results.

Considering the symmetric nature of the characteristics about the two dimensional nozzle axis, only the upper or lower half of the nozzle is analyzed. The  $C^-$  characteristic reflects symmetrically from the center line as a  $C^+$  characteristic and vice versa.

#### (e) Perfect Contour Divergent

A perfect contour could be generated using this method instead of arbitrarily choosing a large initial expansion with a maximum wall angle at a given downstream distance from the throat and then fitting a contour to bring down the exit angle to a minimum. Starting from the initial line at a Mach number slightly greater than one and an initial small part of the contour, the procedure is used to determine the  $C^+$  and  $C^-$  characteristics. This is shown in Fig. A.16. As the marching proceeds through

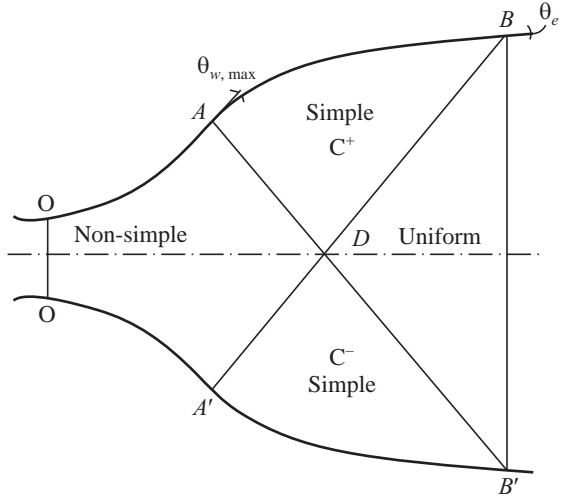


**Fig. A.15** Analysis of the Contour Divergent in the Different Regions



the non-simple region, a point is reached on the nozzle axis at which the desired exit Mach number  $M_e$  is reached. The flow is axial thereafter and the terminal  $C^+$  characteristic would be from this point. This is shown by point  $D$  and the terminal characteristic by  $DB$  in Fig. A.16. Downstream of  $DB$ , the flow is axial and flow properties do not change subsequently. The angle  $\mu_e$  of this characteristic is known ( $= \sin^{-1}(1/M_e)$ ) and at all points along this characteristic the fluid properties are all constant and known being the properties at the exit Mach number  $M_e$ .

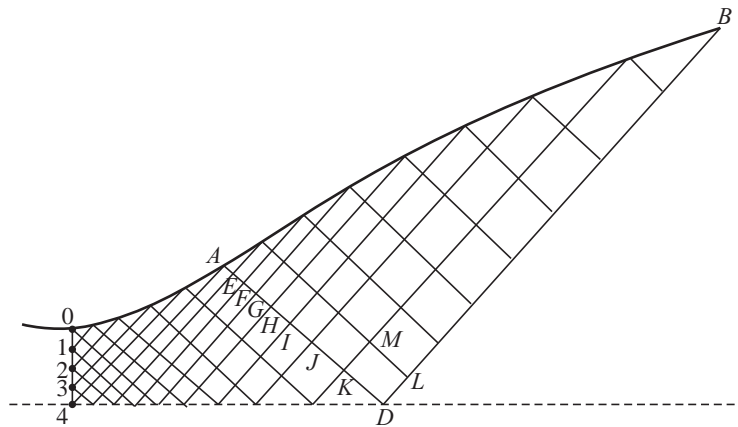


**Fig. A.16** Determining a Perfect Contour Nozzle

A solution for the non-simple region from the initial line  $O4$  for the initially assumed wall region  $OA$  is determined by the method cited earlier. Downstream of  $A$ , the wall contours are determined by the known properties at  $A, E, F, G, H, I$ , and  $K$  and properties on the terminal characteristics  $DB$ . This is shown in Fig. A.16. We therefore obtain the meshes e.g., point  $M$  from known points  $L$  and  $D$ . Once the meshes are known, the streamlines are drawn in the wall region. The streamline  $AB$  passing through  $A$  is the required wall contour.

This perfect contour nozzle has a long length and gives rise to a heavy nozzle. Towards the exit, the wall angle is very nearly zero. The exit portions are therefore removed and an optimum contour with a small divergence angle is used.

#### (f) Minimum Length Nozzle

Nozzles generally have a gently curved expansion section. For very rapid expansion, a Prandtl Mayer expansion at the sharp throat corner is used. Here, only the simple region of expansion plays a role with the expansion section (interaction of  $C^+$  and  $C^-$  characteristics) being replaced by the corner point. The wall angle at the throat is the maximum value  $\theta_{w, \text{max}}$ . The process is illustrated in Fig. A.17.

The  $C^+$  characteristics starting at point  $B$  and  $C^-$  characteristics starting from point  $A$  in the throat region do not interact with each other except along the axis wherein the flow is axial. This is shown by the point  $C$  in Fig. A.17.

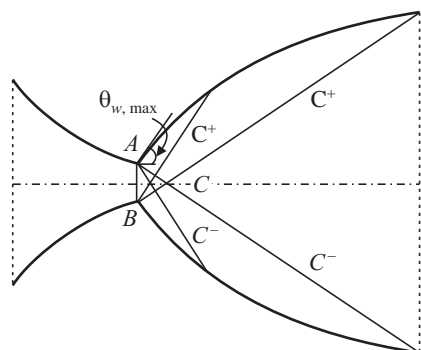


**Fig. A.17** Minimum Length Divergent



### (g) Axi-symmetric Nozzle Divergent

The treatment of the method of characteristics in the above sections was for two dimensional flows. In the case of axially symmetric flows such as in the cylindrically divergent nozzle, the computations become more involved due to the divergence in the radial direction. The coordinates are  $(x, r)$ , with  $x$  being the distance along the axis of the nozzle and  $r$  along the radius. The characteristics are curved lines. The flow is symmetric in the tangential direction.

The method of characteristics has been extended to rotational flows and non-adiabatic flows.

The constraint in a rocket nozzle is its length and with smaller lengths the exit flow is not uniform and parallel. G. V. R. Rao has described a computational procedure using the method of calculus of variations for determining the nozzle contour for a specified thrust. ("Exhaust Nozzle Contour for Maximum Thrust", Jet Propulsion, vol. 28, June 1958, pp. 377-382)



## A.4 PLUMES FROM UNDER-EXPANDED AND OVER-EXPANDED NOZZLES

The shape of the jet issuing from the nozzle depends the pressure at the nozzle exit ( $p_e$ ) and the ambient pressure ( $p_a$ ). When  $p_e > p_a$ , there would be a sudden expansion at the nozzle exit; however, if  $p_e < p_a$ , a shock wave is required to bring about a matching of the lower exit pressure  $p_e$  with the ambient pressure  $p_a$  as the flow at the nozzle exit is supersonic. The plumes from under-expanded and over-expanded nozzles have different features and are discussed in the following. A two dimensional coordinate system is considered as in the case of contour nozzles.

### A.4.1 Expansion and Compression Waves

We had studied Mach lines, also known as Mach waves or expansion waves, in supersonic flows and the angle made by these Mach lines (Mach angle) with respect to the direction of the flow ( $\mu$ ) while dealing with the contour shapes of the nozzle divergent. The information of the expansion process induced by the wall was communicated within the Mach angle in the supersonic flow and the expansion waves deflected the flow along the wall. When the expansion requires a large deflection of the flow as compared to the small deflection provided by the expansion wave, a single Mach wave could not meet the flow deflection and a series of expansion waves are required. This becomes necessary as the expansion wave makes an angle of  $\mu = \sin^{-1}(1/M)$  with respect to the incident flow. Here  $M$  is the Mach number of the upstream supersonic flow. The flow turns by a small angle with the Mach number downstream of the expansion wave being  $M_1$  with  $M_1 > M$ . Since the flow bent by the expansion wave, is not along the wall, another expansion wave is formed which further bends the flow and increase the Mach number to  $M_2$ . The

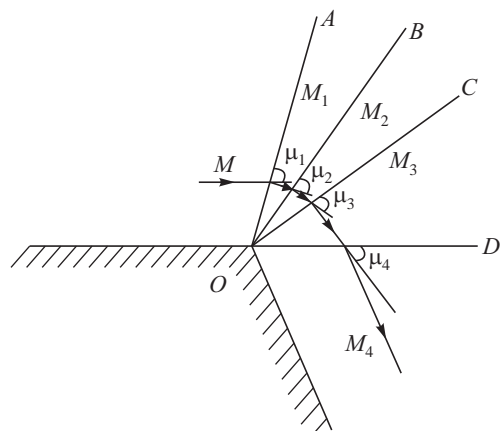


**Fig. A.18** Expansion Fan



process continues until the flow is expanded as per the requirement of the wall. Figure A.18 is a schematic of a series of expansion waves  $OA, OB, OC$  and  $OD$  which make angles of  $\mu_1, \mu_2, \mu_3$  and  $\mu_4$  with the incident flow at Mach numbers  $M, M_1, M_2$  and  $M_4$  on the successive expansion waves. The Mach numbers  $M_1 > M, M_2 > M_1$  and  $M_4 > M_3$ . The angles  $\mu_2 < \mu_1, \mu_3 < \mu_2$  and  $\mu_4 < \mu_3$  since  $\mu = \sin^{-1}(1/M)$ . As a result, the expansion waves diverge and the series of expansion waves is termed as an expansion fan.

If instead of expansion, the supersonic flow is compressed, a series of compression waves are formed as shown in Fig. A.19. Here the Mach number of the flow progressively reduces due to the compression with  $M_1 < M, M_2 < M_1$  and  $M_4 < M_3$ . The angle  $\mu$  now progressively increases to give  $\mu_2 > \mu_1, \mu_3 > \mu_2$  and  $\mu_4 > \mu_3$ . The compression waves converge unlike the expansion waves. They coalesce to form a single strong compression wave or an oblique shock wave.

When a compression wave or an oblique shock wave strikes a solid surface, it gets reflected as a compression wave. If instead of a solid boundary, the boundary represents the interface between two gases of different densities, the compression wave passing through a gas of higher density to lower density gets reflected at the interface as expansion waves due to yielding at the interface of the two gases. The interaction of the oblique shock waves with a solid boundary and a gas-gas interface is schematically shown in Fig. A.20 and Fig. A.21.

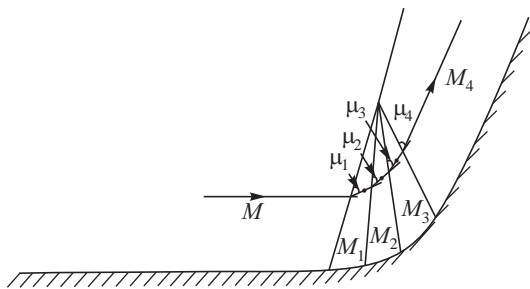


Fig. A.19 Compression Waves

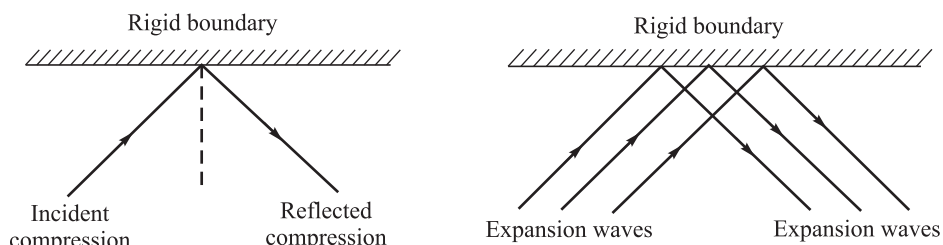


Fig. A.20 Interaction of Waves with a Rigid Boundary

Similar to a compression wave, an expansion fan is reflected at a solid boundary as an expansion fan and as compression waves from a gas-gas interface. Figure A.20 and A.21 show the interaction of expansion fan with a solid boundary and a gas-gas interface. Gas 2 has lower density than Gas 1 in Fig. A.21. In reality, instead of gas densities, we should be considering the acoustic impedance of the gases which is the product of the density of the gas and the sound speed in it.

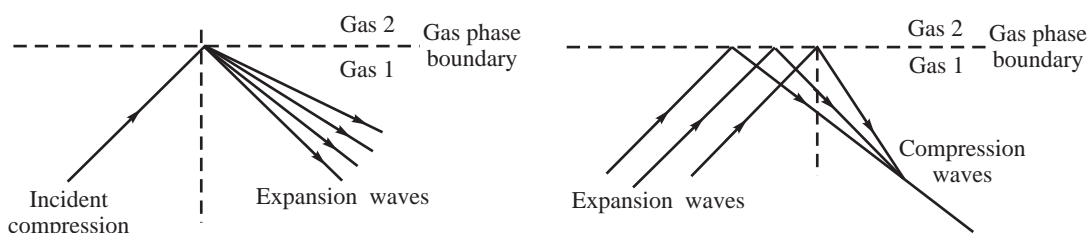
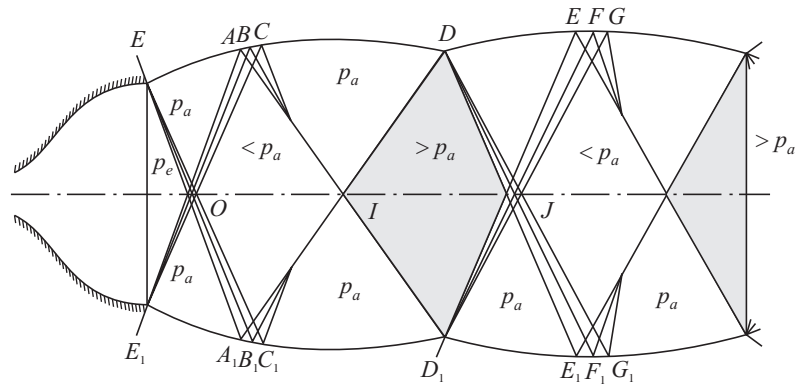


Fig. A.21 Interaction of Waves with a Boundary Separating Gases



#### A.4.2 Plume from an Under-expanded Nozzle

In an under-expanded nozzle  $p_e > p_a$  consequent to which the plume expands further on leaving the nozzle as shown in Fig. A.22. At the nozzle exit, a series of expansion waves are formed to reduce the pressure from  $p_e$  to  $p_a$ . These expansion waves diverge out as  $EA_1$ ,  $EB_1$  and  $EC_1$  and  $E_1A$ ,  $E_1B$  and  $E_1C$  respectively. These waves further process the gases at pressure  $p_a$  and reduce their pressure to a value less than  $p_a$  in the region downstream of  $COC_1$ .



**Fig. A.22** Shape of Under-expanded Plume

The diverging expansion waves interact with the plume surface and are reflected back as compression waves; these compression waves converge and coalesce to form oblique shock waves respectively as shown in Fig. A.22. The pressure in the plume downstream of the compression/oblique shock waves increase to the ambient pressure  $p_a$  and the plume contracts in view of the increase of the pressure. The oblique shock waves intersect the axis at  $I$ . Downstream of this region beyond  $I$ , the pressure increases from the compression by the oblique shocks to values greater than  $p_a$ .

The oblique shocks intersect the plume surface at  $D$  and  $D_1$  respectively and are reflected as a family of expansion waves  $DE_1$ ,  $DF_1$  and  $DG_1$  and  $D_1E$ ,  $D_1F$  and  $D_1G$  respectively. The plume pressure falls to  $p_a$  and the plume diverges. Downstream of this region of pressure  $p_a$  the pressure reduces to a value less than  $p_a$  in the region beyond  $J$ . The interaction of the expansion waves with the plume surface at  $E$ ,  $F$  and  $G$  and at  $E_1$ ,  $F_1$  and  $G_1$  results in compression waves and oblique shock waves as at  $A$ ,  $B$  and  $C$  and  $A_1$ ,  $B_1$  and  $C_1$  respectively and the cycle of processes as at  $A$ ,  $B$  and  $C$  and  $A_1$ ,  $B_1$  and  $C_1$  continue. Alternate regions starting with pressures less than  $p_a$  and followed by those having pressures greater than  $p_a$  are formed. The regions of higher pressures have higher temperatures and are therefore more luminous and are readily observed in the plume.

#### A.4.3 Plume from an Over-expanded Nozzle

The shape of the plume is sketched in Fig. A.23. Since the pressure in the nozzle falls to pressures less than  $p_a$ , an oblique shock is formed inside the nozzle to compress the gases to the higher value of the ambient pressure  $p_a$ . The plume converges as the pressure increases  $p_a$ .  $EOA_1$  and  $E_1OA$  represent the two oblique shocks in the two dimensional nozzle.  $EOE_1$  is the region having pressure less than  $p_a$  while regions  $EOA$  and  $E_1OA_1$  have pressure equal to  $p_a$ . Part of the oblique shocks  $OA$  and  $OA_1$  increase the pressure from  $p_a$  to a value higher than  $p_a$  in region  $AOA_1$ .

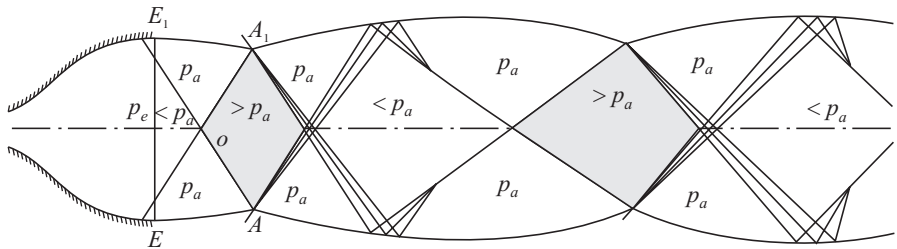


**Fig. A.23** Shape of Over-expanded Plume

The oblique shocks interact with the plume boundary at  $A$  and  $A_1$ . Expansion waves are formed from this interaction and these expansion fans reduce the pressure downstream of region  $OA_1$  to  $p_a$  as shown. The reduction in pressure causes the plume boundary to widen.

Downstream of the expansion fan, the pressure falls below  $p_a$ . The cycle of the interaction of the expansion fan with the plume boundary now continues in the same cyclical process as discussed with the expansion fans forming at the exit of the under-expanded nozzle.

The major difference in the plume between an under-expanded and over-expanded nozzle is that the first high pressure region is formed closer to the nozzle exit when the nozzle is over-expanded.

#### A.4.4 Shock Diamonds and Mach Diamonds

The shape of the luminous zones in a plume is in the form of diamonds and is in regions of higher pressures formed by the oblique shocks. These luminous zones are therefore often spoken of as shock diamonds.

In practice when oblique shock waves interact, they do not undergo regular reflection if the angle between them exceeds some threshold value. During the interaction a strong shock known as Mach stem shock and a reflected shock wave are generated. Figure A.24 shows a typical Mach stem shock formed by oblique shocks and the shape of the diamond pattern. The shock diamonds are also known as Mach diamonds.

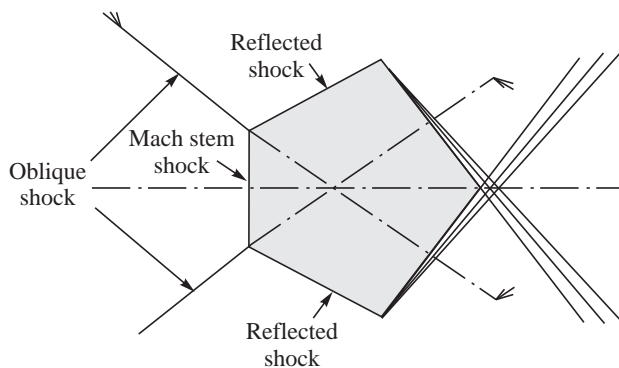


**Fig. A.24** Mach Waves and Shape of the Shock Diamond

#### A.4.5 Heat Transfer in Nozzles

Starting from low subsonic Mach numbers at the entrance to the nozzle, the gas flow accelerates to the sonic velocity at the throat and to supersonic velocities in the divergent. The accelerating flow of



the hot gases transfers heat by convection to the nozzle walls. The heat transferred by this forced convection requires knowledge of the boundary layer growth along the nozzle walls due to the high speed gas flow.

An adiabatic wall temperature or the recovery temperature at the wall, which drives the heat transfer due to the boundary layer, is first defined. It is the temperature experienced by the wall due to the moving high speed stream of hot gas when there is no heat transfer at the wall. Figure A.25 shows a schematic of the adiabatic wall brought out by the slowing down of the gas stream in the boundary layer. The zero temperature gradient in the direction normal to the stream flow brings about the adiabatic condition at the wall. If the temperature of the wall is denoted by  $T_W$  and the adiabatic wall temperature is denoted by  $T_{AW}$ , the heat flux transferred by the high speed flow of accelerating gases is:

$$\dot{Q}'' = h_g (T_{AW} - T_W)$$

where " $h_g$ " is the heat transfer coefficient.

The adiabatic wall temperature is related to the free stream temperature  $T_\infty$  outside the boundary layer and the free stream velocity  $U_\infty$  by:

$$T_{AW} = T_\infty + R \frac{U_\infty^2}{2C_P}$$

In the above expression  $R$  is the recovery coefficient which depends on whether the flow is laminar or turbulent and the thermal properties of the medium. If the Prandl number of the flowing gas stream is represented by  $Pr$ , the recovery coefficient is given for laminar and turbulent flow as  $(Pr)^{1/2}$  and  $(Pr)^{1/3}$  respectively.

The determination of the heat transfer coefficient " $h_g$ " also requires a knowledge of the boundary layer growth along the nozzle walls. It is assumed that the skin friction coefficient and the Stanton number for the accelerating flow is the same as for the flow over a flat plate at the same free stream condition and the same boundary layer thickness. The boundary layer equations are solved preferably in the integral form and the displacement, momentum and energy thicknesses are determined. The skin friction coefficient is based on the Reynolds number defined with the momentum thickness as the characteristic length scale. The Stanton number is related to the skin friction coefficient by either the Colburn or von Karman form of the Reynolds analogy dealing with the similarity of the momentum and energy equations. Here corrections for the difference between the energy thickness and the momentum thickness are applied. The Stanton number is determined along the length of the nozzle. Details of the method are given in the Technical report on "Calculation of Turbulent Boundary Layer Growth in Axisymmetric Nozzles" by D. G. Elliot, D. R. Bartz and S. Silver (Jet Propulsion Lab., Feb. 1963). Based on the heat transfer coefficient deduced from the boundary layer development, the following dimensional correlation for the forced heat transfer coefficient  $h_g$  was determined in this method:

$$h_g = \left( \frac{0.1087 \times 10^4}{D_t^{0.2}} \right) \left( \frac{\mu^{0.2} C_P}{Pr^{0.6}} \right) \left( \frac{p_C g_c}{C^*} \right)^{0.8} \left( \frac{D_t}{R} \right)^{0.1} \left( \frac{A_t}{A} \right)^{0.9} \sigma$$

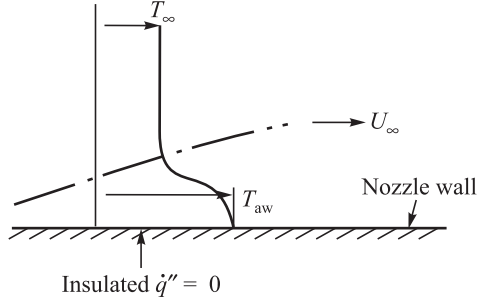


**Fig. A.25** Adiabatic Wall Temperature



Here  $h_g$  is expressed in  $\text{W}/(\text{m}^2\text{K})$ . The throat diameter  $D_t$  and the radius of curvature of the throat  $R$  are in cm, the characteristic velocity  $C^*$  is in m/s and the chamber pressure  $p_C$  is in  $\text{kg}/\text{cm}^2$ . The viscosity  $\mu$  and specific heat of the hot products of combustion  $C_P$  are expressed in  $\text{g}/(\text{cm s})$  and  $\text{cal}/(\text{g K})$  respectively. Since  $p_C$  is expressed in  $\text{kg}/\text{cm}^2$ , the value of  $g_c$  as  $981 \text{ cm/s}^2$  is required in the expression for  $p_C/C^*$ . The parameter  $\sigma$  is a correction factor for property variations across the boundary layer and varies between 1.4 and 1.6 depending on the temperature ratio between the wall and the gas, the ratio of specific heats and the Mach number of the flow.

If the mean properties are evaluated at the film temperature  $T_f$  which is the mean of the free stream and the wall temperatures, and since the mass flow rate could be expressed as a function  $p_C g_c A_t / C^*$ , the above expression is simplified to give the heat transfer coefficient as a function of the mass flux  $G$  as:

$$h_g = 0.1087 \times 10^4 \left( \frac{G^{0.8}}{D_t^{0.2}} \right) \left( \frac{\mu^{0.2} C_P}{Pr^{0.6}} \right) \left( \frac{T_0}{T_f} \right)^{0.68}$$

A non-dimensional correlation with the properties evaluated at the film temperature is also given in the form:

$$Nu_f = 0.026 \ Re_f^{0.8} \ Pr_f^{0.4}$$

Here  $Nu$  is the Nusselt's number while  $Re$  is the Reynolds number.

The heat transfer coefficient is seen to be a maximum at the region where the mass flux is a maximum viz., at the throat. The boundary layer is also a minimum at the throat.

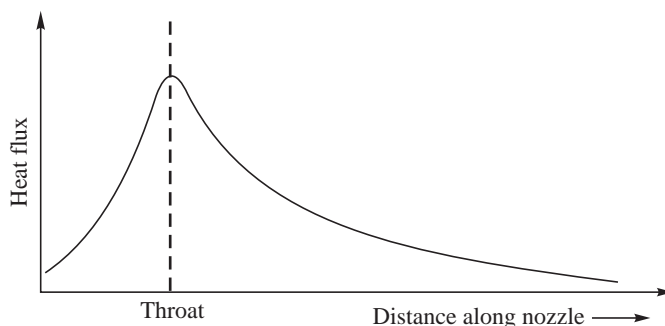


**Fig. A.26** Heat Flux Distribution along the Length of the Nozzle Walls

The heat flux is determined using the above value of the heat transfer coefficient and its product with the difference between adiabatic wall temperature and the wall temperature. The maximum heat flux is obtained in the throat. The pattern of the heat flux distribution along the length of the nozzle is given in Fig. A.26. Maximum values of heat flux could, for high chamber pressure rockets, reach values of about  $15 \text{ kW/cm}^2$ . Special materials of construction for the nozzles and specific cooling methods are required for the nozzle to withstand the high heat flux especially in the throat region. These aspects are considered in the chapter on Liquid Propellant Rockets.



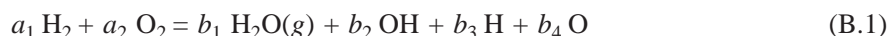
## References

1. Anderson, John, D. Jr., Modern Compressible Flow, McGraw Hill, New York, 2<sup>nd</sup> Edition, 1990.
2. Bartz, D. R., "Survey of relationships between theory and experiment for convective heat transfer from rocket combustion gases" p. 291, Advances in Tactical Rocket Propulsion, AGARD Conference, August 1968.
3. Elliot, D. G., Bartz, D. R. and Silver, S., "Calculation of Turbulent Boundary Layer Growth in Axisymmetric Nozzles" Jet Propulsion Lab. Report, Feb. 1963
4. Hill, P. and Peterson, C., Mechanics and Thermodynamics of Propulsion, Addison Wesley Publishing Company, Reading, 2<sup>nd</sup> Edition, 1992.
5. Liepmann, H. W. and Roshko, A., Elements of Gas Dynamics, Dover Publications Inc, New York, 1957.

## Annexure B

### Dissociation of Gases: Frozen and Shifting Equilibrium

At high temperatures, the completely oxidized products of combustion like H<sub>2</sub>O and CO<sub>2</sub> dissociate into OH, H, O and CO. The dissociation is favored at lower pressures as there is less resistance to the breaking up from the neighboring molecules. As an example, the dissociation of products in the reaction of  $a_1$  moles of hydrogen with  $a_2$  moles of oxygen, would result in:



Here OH, H and O are the dissociated products. The dissociation of H<sub>2</sub>O into OH, H and O absorbs heat and the temperature of the combustion products reduces. It also decreases the molecular mass of the products. In this Annexure, the thermodynamic equilibrium procedure for computing the dissociated products and their temperatures is given using equilibrium constants and Gibbs Free Energy. The methods of assessing the performance of a rocket in the presence of dissociation are also discussed.



#### B.1 GIBBS FREE ENERGY AND EQUILIBRIUM

Thermodynamics is not constrained to heat and energy applications. It can be used to determine the equilibrium of a number of chemical species coexisting with each other in a chemical reaction. The thermodynamic property Gibbs Free Energy  $G$ , which provides a measure of the maximum amount of work obtainable from a system at constant pressure  $p$  and temperature  $T$ , is used for determining the equilibrium of a chemical reaction and the equilibrium constants.  $G$  for a single component gas is defined as:

$$G = U + pV - TS \quad (\text{B.2})$$

Here  $U$  is the internal energy,  $V$  is the volume and  $S$  is the entropy. In a differential form:

$$dG = dU + pdV + Vdp - TdS - SdT \quad (\text{B.3})$$

From the first law of thermodynamics,  $dU = -pdV + dQ + d\xi$ , where  $d\xi$  designates work done on the system other than pressure volume work.  $dG$  therefore becomes:

$$dG = Vdp - SdT + d\xi \text{ since } TdS = dU + pdV \quad (\text{B.4})$$

At constant temperature  $T$  and pressure  $p$ ,  $dG = d\xi$ . If  $dG$  is positive, work is done on the system at constant temperature  $T$  and pressure  $p$ . When  $dG = 0$ , no useful work is done at constant pressure



and temperature and the system is in equilibrium. The change in Gibbs Free Energy  $G$  is therefore an indication of the direction of a process at a given pressure and temperature. It is useful for determining equilibrium conditions for a reacting system at a given temperature and pressure.

### B.1.1 Equilibrium in a Chemical Reaction and Equilibrium Constants

When we have a number of species in products, we need to incorporate all of them to determine the change in Gibbs Free Energy. If in a generalized way, we define the number of species to be  $i = 1, \dots, N$  and their number of moles  $n_j$  with  $j = 1, \dots, N$ , the value of  $dG$  resulting from changes in the number of moles  $dn_j$  from Eq. B.4 is given by:

$$dG = Vdp - SdT + \left( \frac{\partial G}{\partial n_i} \right)_{T, p, n_j, j \neq i} dn_1 + \dots + \left( \frac{\partial G}{\partial n_i} \right)_{T, p, n_j, j \neq i} dn_i + \dots \quad (\text{B.5})$$

The quantity  $\left( \frac{\partial G}{\partial n_i} \right)_{T, p, n_j, j \neq i}$  represents the increase in Gibbs Free Energy when 1 mole of component  $i$  is added to an infinitely large quantity of the mixture so that it does not significantly change the overall composition. It is known as the chemical potential ( $\mu_i$ ) and represents the driving tendency of chemical systems to equilibrium. The change in Gibbs Free Energy is written as:

$$dG = Vdp - SdT + \sum \mu_i dn_i \quad (\text{B.6})$$

The Gibbs Free Energy is given by:

$$G = U + PV - TS + \sum \mu_i n_i \quad (\text{B.7})$$

If we consider a reaction taking place at constant temperature and pressure wherein specie  $A$  changes to specie  $B$ :



the reduction in the number of moles of  $A$  equals the number of moles of  $B$  formed. Denoting the change of moles by  $d\chi$ , we have:

$$dn_A = dn_B = d\chi \quad (\text{B.8})$$

where  $dn_A$  moles  $A$  are converted to  $dn_B$  moles  $B$ . We have the change in Gibbs Free Energy at constant temperature and pressure as:

$$dG = \mu_B dn_B - \mu_A dn_A \quad (\text{B.9})$$

giving

$$dG = (\mu_B - \mu_A) d\chi$$

The progress of the reaction is given by:

$$(dG/d\chi)_{T, p} = \mu_B - \mu_A \quad (\text{B.10})$$

When  $dG$  becomes zero, no further change is possible and the species  $A$  and  $B$  are in equilibrium. This is given by:

$$dG/d\chi = 0 \text{ or } \mu_A = \mu_B. \quad (\text{B.11})$$

The reaction  $A = B$  proceeds until  $G$  reaches the minimum value for which  $dG/d\xi = 0$ , giving  $\mu_A = \mu_B$ .



For a single component system

$$dG = Vdp - SdT \quad (\text{B.12})$$

or  $(dG/dp)_T = V \quad (\text{B.13})$

Assuming ideal gas, we have  $pV = nR_0T$ , so that

$$(dG/dp)_T = nR_0T/p \quad (\text{B.14})$$

giving on integration  $G = G^\circ + nR_0T \ln p$

$G^\circ$  is the value of  $G$  under standard reference conditions of 1 atmosphere pressure. For a multi-component system, if the different species follow the perfect gas law, we can similarly write:

$$\mu_i = \mu_i^\circ + R_0T \ln p_i \quad (\text{B.15})$$

where  $p_i$  is the partial pressure of component  $i$  and  $\mu_i^\circ$  is the chemical potential under standard conditions. The progress of the reaction  $A = B$  can therefore be written as:

$$(dG/d\chi)_{T,p} = \mu_B^\circ - \mu_A^\circ + R_0T \ln(p_B/p_A) = \Delta G^\circ + R_0T \ln(p_B/p_A) \quad (\text{B.16})$$

Here,  $p_B$  and  $p_A$  are the partial pressures of  $B$  and  $A$  respectively.

The reaction proceeds with Free Energy changes under conditions specified by  $p_B$  and  $p_A$ . The term  $-(dG/d\chi)_{T,p}$  is called affinity of the reaction and is indicated by the ratio  $(p_B/p_A)$ . At equilibrium for which  $(dG/d\chi)_{T,p} = 0$ , we get

$$\Delta G^\circ = -R_0T \ln(p_B/p_A) \quad (\text{B.17})$$

The value of  $p_B/p_A$  at equilibrium is known as equilibrium constant for the reaction and is denoted by  $K_P$ , giving

$$\Delta G^\circ = -R_0T \ln(K_P) \quad (\text{B.18})$$

The above equation tells us that if  $\Delta G^\circ$  is negative,  $\ln(K_P) > 0$  giving  $p_B > p_A$  and hence more products of  $B$  are formed.

From the definition of Gibbs Free Energy for a single component system:

$$\begin{aligned} G &= U + pV - TS \\ dG/dT &= -S \end{aligned} \quad (\text{B.19})$$

and

$$G = U + pV + T(dG/dT) \quad (\text{B.20})$$

Writing  $U + pV = H$ , where  $H$  is enthalpy and dividing by  $T^2$ , we get

$$G/T^2 = H/T^2 + (1/T)(dG/dT)$$

or  $(d/dT)(G/T)_p = -H/T^2 \quad (\text{B.21})$

For an ideal gas enthalpy is only a function of temperature and the right hand side of the above equation is independent of pressure. Equation B.21 can also be written as

$$(d/dT)(\Delta G/T) = -\Delta H/T^2. \quad (\text{B.22})$$

From Eq. B.18,

$$\Delta G^\circ = -R_0T \ln(K_P), \text{ giving}$$

$$d/dT \ln(K_P) = -\Delta H^\circ/R_0T^2 \quad (\text{B.23})$$

The equilibrium constant is independent of the total pressure and is seen to be function of only the temperature. Tables of the equilibrium constants are available for chemical equilibrium of different



reactions in standard text books on combustion. They are easily calculated from Eq. B.18 using the values of the Standard Gibbs Free Energy of the different species at the required temperature.



## B.2 USE OF EQUILIBRIUM CONSTANTS TO DETERMINE COMPOSITION AT A GIVEN TEMPERATURE

Let us consider a problem in which hydrogen gas is heated to a high temperature of 4000 K in a rocket chamber by electrical heating or otherwise. The hydrogen gas at the high temperature partially dissociates into H atom according to the reaction  $H_2 \rightarrow H + H$ . Let the pressure in the chamber be 10 atm. We need to determine the fraction of H atom and  $H_2$  when in equilibrium at the temperature of 4000 K, and pressure of 10 atmospheres.

At equilibrium at 4000 K,  $H_2$  and H must coexist as per the equation  $H_2 \leftrightarrow 2H$  for which the equilibrium constant  $K_{eq}$  is:

$$K_{eq} = \frac{p_H^2}{p_{H_2}} \quad (B.24)$$

The value of the equilibrium constant in terms of the change in the standard Gibbs Free Energy  $\Delta G^\circ$  for the reaction  $H_2 \leftrightarrow 2H$  is:

$$\ln K_{eq} = -\frac{\Delta G^\circ}{R_0 T} \quad (B.25)$$

with  $\Delta G^\circ = 2 \times G_H^\circ - G_{H_2}^\circ$

From thermodynamic tables of standard Gibbs Free Energy (standard pressure of 1 atm.) the value of  $G_H^\circ$  and  $G_{H_2}^\circ$  at 4000 K is  $-15.299$  kJ/mole and 0 kJ/mole respectively.

The value of equilibrium constant at 4000 K is therefore given by:

$$\ln K_{eq} = +\frac{2 \times 15.299 \times 1000}{8.314 \times 4000} = 0.92 \quad (B.26)$$

Substituting in Eq. B.24, we get:

$$\frac{p_H^2}{p_{H_2}} = e^{0.92} = 2.51 \quad (B.27)$$

Since the total pressure in the chamber is 10 atm:

$$p_H + p_{H_2} = 10 \quad (B.28)$$

thus giving:  $p_H^2 + 2.51p_H = 10 \quad (B.29)$

The solution of the above quadratic equation gives:

$$p_H = 3.91 \text{ atm}$$

and

$$p_{H_2} = 6.09 \text{ atm} \quad (B.30)$$

The fraction of H and  $H_2$  is therefore 0.391 and 0.609 respectively.

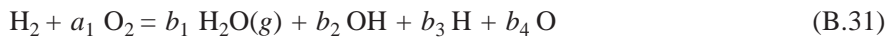


It should be noted that as the temperature increases, the value of  $G^\circ$  for H becomes more negative whereas the value of  $G^\circ$  for  $\text{H}_2$  is zero. At 5000 K,  $G_H^\circ = -77.103 \text{ kJ/mole}$  compared to  $-15.299 \text{ kJ/mole}$  at 4000 K. The value of  $\ln K_{eq}$  therefore increases giving a much larger fraction of H as the temperature increases.



### B.3 USE OF EQUILIBRIUM CONSTANTS TO DETERMINE COMPOSITION IN PRESENCE OF DISSOCIATION AND TEMPERATURE OF THE DISSOCIATED PRODUCTS

The use of the equilibrium constant for determining the products of dissociation and the temperature of the dissociated products is illustrated by an example. Consider the reaction between hydrogen and oxygen in which the water formed partly dissociates. Let the equilibrium composition be given such as in Eq. B.1 by



The value of  $a_1$  is known and is obtained from the specified value of mixture ratio. There are four unknowns  $b_1$ ,  $b_2$ ,  $b_3$  and  $b_4$  in Eq. B.31. The atom conservation equations give:

$$2 = 2b_1 + b_2 + b_3 \quad (\text{for H atom}) \quad (\text{B.32})$$

$$2a_1 = b_1 + b_2 + b_4 \quad (\text{for O atom}) \quad (\text{B.33})$$

Two more equations are therefore required to determine the composition of the dissociated products.

Consider the following two reactions which consider the equilibrium between products  $\text{H}_2\text{O}(g)$ ,  $\text{OH}$ ,  $\text{H}$  and  $\text{O}$ :



for which the equilibrium constant  $K_{P1} = p_{\text{H}} \times p_{\text{OH}} / p_{\text{H}_2\text{O}(g)}$

$$\text{or} \quad p_{\text{H}_2\text{O}(g)} = p_{\text{H}} p_{\text{OH}} / K_{P1} \quad (\text{B.35})$$

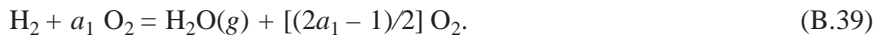


for which the equilibrium constant  $K_{P2} = p_{\text{O}} p_{\text{H}} / p_{\text{OH}}$  (B.37)

$$\text{or} \quad p_{\text{O}} = K_{P2} p_{\text{OH}} / p_{\text{H}} \quad (\text{B.38})$$

We now have the two additional equations Eqs. B.35 and B.38. However,  $b_1$ ,  $b_2$ ,  $b_3$  and  $b_4$  in the atom conservation equations are in terms of moles whereas  $p_{\text{H}}$ ,  $p_{\text{OH}}$ ,  $p_{\text{O}}$  and  $p_{\text{H}_2\text{O}}$  from the equilibrium constant relations are in terms of partial pressures. We need to convert partial pressures into moles. For this purpose, if the total number of moles in the products is given as  $n_t$ , the number of moles of  $j^{\text{th}}$  specie  $n_j$  whose partial pressure is  $p_j$  is given by  $n_j/n_t = p_j/p$ , where  $p$  is the total pressure.

The total number of moles  $n_t$  is, however, not known. But it does not differ very significantly from the stoichiometric value. It could be assumed to be equal to  $(a_1 + 1/2)$  to begin with and corrected subsequently through a series of iterations. Since the stoichiometric reaction is:



the total number of moles of the products is  $(a_1 + 1/2)$ . This gives



$$b_1 = p_{\text{H}_2\text{O}} (a_1 + 1/2)/p \quad (\text{B.40})$$

$$b_2 = p_{\text{OH}} (a_1 + 1/2)/p \quad (\text{B.41})$$

$$b_3 = p_{\text{H}} (a_1 + 1/2)/p \quad (\text{B.42})$$

$$b_4 = p_{\text{O}} (a_1 + 1/2)/p \quad (\text{B.43})$$

Substituting in the atom balance equations, we have:

$$2p_{\text{H}_2\text{O}} + p_{\text{OH}} + p_{\text{H}} = [2a_1/(a_1 + 1/2)]p \quad (\text{B.44})$$

$$p_{\text{H}_2\text{O}} + p_{\text{OH}} + p_{\text{O}} = [2a_1/(a_1 + 1/2)]p \quad (\text{B.45})$$

The other two equations are (Eq. B.35 and Eq. B.38):

$$p_{\text{H}_2\text{O}(g)} = \frac{p_{\text{H}} p_{\text{HO}}}{K_{p1}} \quad (\text{B.46})$$

and  $p_{\text{O}} = \frac{K_{p2} p_{\text{OH}}}{P_{\text{H}}} \quad (\text{B.47})$

The values of  $p_{\text{H}}$ ,  $p_{\text{OH}}$ ,  $p_{\text{O}}$  and  $p_{\text{H}_2\text{O}}$  can be determined from the above four equations [Eqs. B.44 - B.47] provided the values of  $K_{p1}$  and  $K_{p2}$  are known. In order to be able to determine  $K_{p1}$  and  $K_{p2}$  we need to know the temperature of the products which is not known a priori. We therefore assume a value of temperature of products and calculate for Eqs. B.34 and B.36, the values of  $K_{p1}$  and  $K_{p2}$ .  $b_1$ ,  $b_2$ ,  $b_3$  and  $b_4$  can be found from the relations between moles and partial pressures (Eq. B.40-B.43).

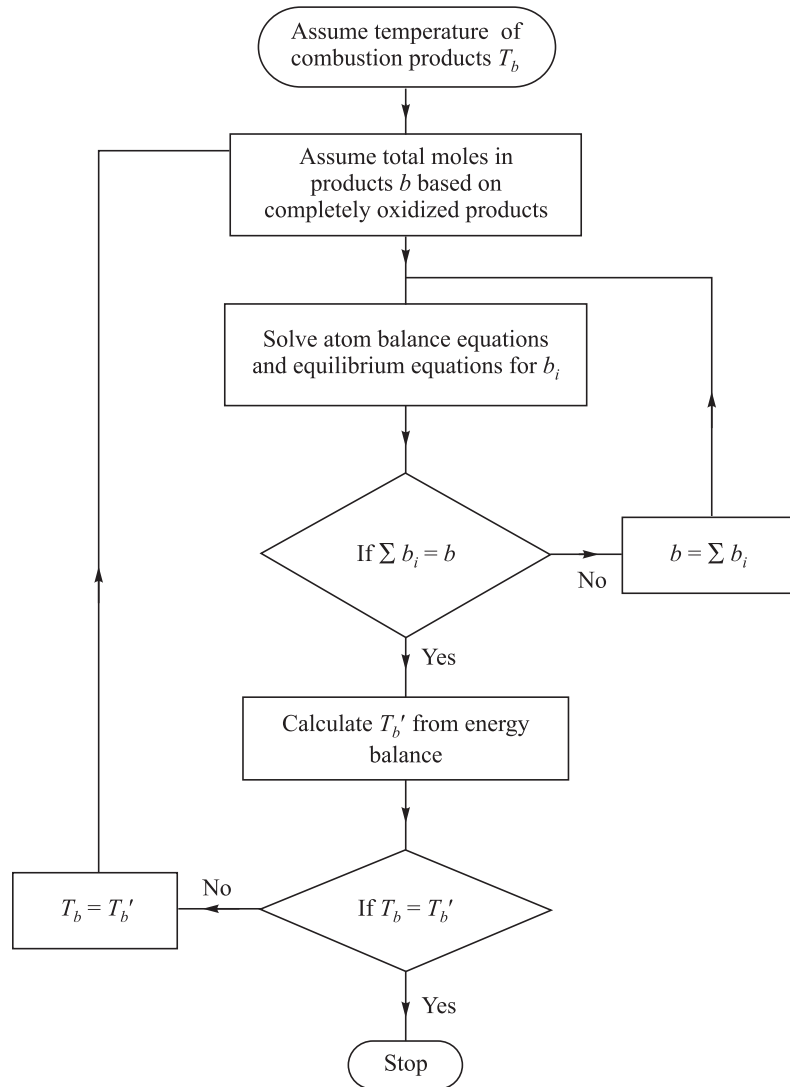
Once the number of moles  $b_1$ ,  $b_2$ ,  $b_3$  and  $b_4$  are determined, the atom balance equation is verified to see if  $2 = 2b_1 + b_2 + b_3$  and  $2a_1 = b_1 + b_2 + b_4$  (atom balance Eq. B.32 and B.33). If this is not satisfied,  $n_t$  is taken equal to  $b_1 + b_2 + b_3 + b_4$  and the process repeated till the atom balance is achieved. The products of combustion when dissociation takes place are determined in the above manner.

The moles  $b_1$ ,  $b_2$ ,  $b_3$  and  $b_4$  of the products are determined at the assumed value of temperature. The enthalpy balance equation is then checked using the heats of formation by:

$$\begin{aligned} &[b_1 \Delta H_f^{\text{O}}_{\text{H}_2\text{O}} + b_2 \Delta H_f^{\text{O}}_{\text{OH}} + b_3 \Delta H_f^{\text{O}}_{\text{H}} + b_4 \Delta H_f^{\text{O}}_{\text{O}}] - [\Delta H_f^{\text{O}}_{\text{H}_2} + a_1 \Delta H_f^{\text{O}}_{\text{O}_2}] + \\ &[H_{\text{H}_2} + a_1 H_{\text{O}_2}]_{(T_i - 298)} + [b_1 H_{\text{H}_2\text{O}} + b_2 H_{\text{OH}} + b_3 H_{\text{H}} + b_4 H_{\text{O}}]_{(T_f - 298)} = 0 \quad (\text{B.48}) \end{aligned}$$

Here  $T_f$  is the assumed temperature of the combustion products and  $T_i$  is the temperature of the reactants.  $H$  denotes the enthalpy which includes the sensible heat ( $C_p T$ ) and the latent heat where applicable.  $\Delta H_f^{\text{O}}$  is the standard heat of formation. If the assumed value of temperature  $T_f$  is not correct, the above equation will not be satisfied. A new value of temperature is assumed, equilibrium constants at the new temperature calculated, the moles  $b_1$ ,  $b_2$ ,  $b_3$  and  $b_4$  determined and the enthalpy balance checked. The procedure is repeated till two successive iterations give values of temperature within a prescribed accuracy.

The iterative procedure is sketched in the Flow Chart given on next page.



#### B.4 MINIMIZATION OF GIBBS FREE ENERGY

We had seen that the equilibrium conditions for a reaction correspond to minimum of Gibbs Free Energy. At a given temperature and pressure, the Gibbs Free Energy for a N species system is:

$$G = \sum_{j=1}^N n_j \mu_j \quad (B.49)$$

The values of  $n_j, j = 1, \dots, N$  are to be determined under chemical equilibrium conditions for which  $G$  is a minimum.



The minimization of  $G$  is subject to the constraint that the atoms of all elements taking part in the chemical reaction are conserved and gives the moles of the dissociated products. The temperature is determined using the procedure outlined in the last section. Computer codes such as NASA SP273 and COSMIC use this minimization method.



## B.5 EQUILIBRIUM AND FROZEN ASSUMPTIONS FOR PERFORMANCE PREDICTION

The composition of the combustion products and the temperature considering the dissociation were obtained in this Annexure assuming chemical equilibrium conditions to prevail *i.e.*, the chemical reactions have gone to completion. This is to be expected in the combustion chamber wherein the residence times are sufficiently large.

The expansion of the hot gases in the nozzle is associated with a decrease in temperature and pressure. The equations derived in Chapter 3 for the performance of chemical rockets assumed no change in the composition of the hot gases flowing in the nozzle viz., a “frozen” composition. However, as temperature of the hot gas reduces during the expansion process, the equilibrium constant changes and the composition would vary. The amount of the dissociated species would decrease and energy would be released during this process. The equilibrium composition during the expansion process and the associated energy release can be determined by method of equilibrium constants or the minimization of Gibbs Free Energy. As expansion occurs there is a shift in the composition corresponding to the equilibrium corresponding to the lower temperatures.

If the gases are assumed to expand under chemical equilibrium conditions, there is change in the composition of the products and the process of expansion is referred to take place under “shifting equilibrium” conditions. The energy release during the expansion under “shifting equilibrium” conditions will contribute to a higher value of specific impulse than obtained under “frozen” conditions.

Chemical reactions, however, take some finite time to be completed. Instantaneous achievement of chemical equilibrium is not possible in the nozzle flow. The actual performance of the rocket would therefore be in between the values obtained under frozen and shifting equilibrium assumptions.

In the convergent portion of the nozzle, wherein the flow velocities are subsonic, the residence time is relatively larger and shifting equilibrium may be assumed. In the divergent supersonic flow regions, wherein the residence times are smaller, the frozen flow assumption is more reasonable. Predictions using shifting equilibrium flow till the nozzle throat and frozen flow in the divergent give more reasonable estimates of specific impulse than the assumption of frozen or equilibrium flow over the entire nozzle.

## Annexure C

# Cryogenic Propellant Rockets



## C.1 INTRODUCTION

The word cryogenics relates to very low temperatures and liquid propellants whose normal boiling temperatures (at atmospheric pressure) are less than about - 150°C (123K) are known as cryogenic propellants. Hydrogen and oxygen, which exist in gas phase in nature, could be converted to liquids if cooled down to very low temperatures of about 20K and 90K respectively at atmospheric pressure. These low temperature liquids could be stored in tanks at the cryogenic temperatures and used in a pump fed system in the liquid propellant rockets dealt with in chapter 6. The low temperatures introduce distinct difficulties in the operation of the rockets and special procedures are required to store them and supply them to the thrust chamber. Special materials of construction are also required to withstand the low temperatures. We shall deal with these issues in this chapter.

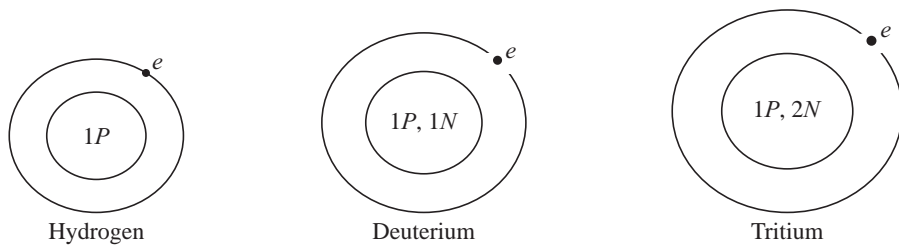


## C.2 CRYOGENIC PROPELLANTS

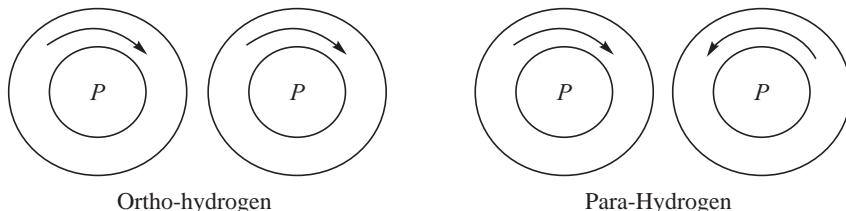
### (a) *Cryogenic Fuels*

Liquid hydrogen and liquid methane have a normal boiling temperature of 20 K and 112 K respectively and are therefore liquid fuels only at cryogenic temperatures. They are therefore termed as cryogenic liquid fuels. Natural hydrogen is a mixture of two isotopes; molecular hydrogen and molecular deuterium. They comprise of Hydrogen ( $^1H$ ) atom and Deuterium ( $^2H$ ) atom respectively. While the hydrogen atom has one proton in its nucleus, the deuterium atom has a proton and a neutron in its nucleus. Tritium ( $^3H$ ) is a rare radioactive isotope of the hydrogen atom with 2 neutrons and one proton in its nucleus with an atomic mass of 3. The configuration of the Hydrogen, Deuterium and Tritium atoms are sketched in Fig. C.1.

Hydrogen gas exists in two different molecular forms: Ortho-hydrogen ( $o-H_2$ ) in a higher energy state wherein the spin of the two atoms of hydrogen are in the same direction. It may be recalled that the hydrogen molecule consists of two atoms of hydrogen atom joined together in a covalent bond. The other form is Para-hydrogen ( $p-H_2$ ) at a lower energy state in which the spin axis of the two atoms is in opposite directions. The Ortho and Para hydrogen are shown in Fig. C.2.



**Fig. C.1** Hydrogen, Deuterium and Tritium atoms



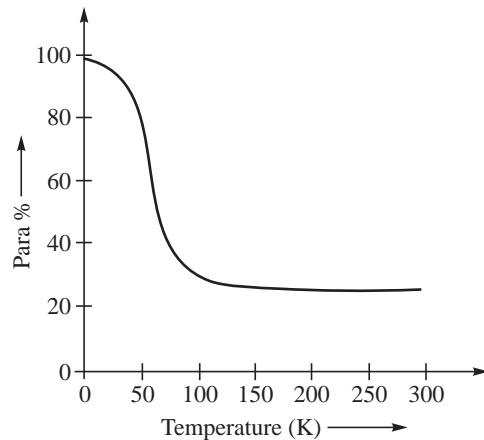
**Fig. C.2** Ortho and Para hydrogen

Figure 3 shows the percentage of Para hydrogen in a mixture of Para and Ortho hydrogen at the different temperatures when in equilibrium. At the ambient temperature of about 30°C, 25% of hydrogen exists under equilibrium conditions as Para-hydrogen with the remaining 75% being Ortho-hydrogen. At the normal boiling temperature of liquid hydrogen of 20.2 K, almost the entire mass of hydrogen (99.79%) exists under equilibrium conditions as Para-hydrogen. As a result, when gaseous hydrogen is liquefied from room temperature, wherein it has a large percentage of Ortho-hydrogen, it would invariably continue to comprise of this larger fraction of Ortho-hydrogen till equilibrium condition are reached at the lower temperature of the liquid hydrogen. When equilibrium is attained, the liquid hydrogen is essentially Para-hydrogen. However, the equilibration rates are very slow at the low temperatures with the result that the transition from Ortho to the Para form progresses rather slowly. When hydrogen is liquefied, the excess energy of the Ortho over the Para form is therefore gradually released in the liquid state. The energy release associated with the Ortho to Para conversion is 0.702 kJ/kg and this exceeds the latent heat of vaporization of liquid hydrogen of 0.454 kJ/kg. The heat of the transition due to the change from Ortho to Para form will therefore boil off the liquid hydrogen being liquefied.

Temperature (K)	Para %
0	100
25	50
50	30
100	25
200	25
300	25

**Fig. C.3** Variation of the Percent of Para Hydrogen when in Equilibrium with Ortho Hydrogen at the different Temperatures

The energy from the conversion of the Ortho to Para states is therefore removed from the liquid hydrogen as it is liquefied. During the liquefaction process, therefore, liquid nitrogen is used to absorb part of this heat at a temperature of about 67 K. The equilibrium concentration of Para-hydrogen at 67 K is 60% (Fig. C.3). Catalysts such as hydrous ferric oxide, chromic oxide on alumina particles



**Fig. C.3** Variation of the Percent of Para Hydrogen when in Equilibrium with Ortho Hydrogen at the different Temperatures



and nickel silicate are used to speed up the conversion process at 67 K. In this way a significant part of the energy release during the Ortho to Para conversion is removed during the liquefaction process itself.

Liquid hydrogen has a very low density of 70.8 kg/m<sup>3</sup> at its normal boiling temperature. It behaves as a quantum fluid *i.e.*, it has a relatively large zero point energy (835 J/mole) compared to the inter-atomic forces (lattice energy of 1670 J/mole). As a consequence, the zero point energy effectively counteracts part of the attractive forces giving larger atomic spacing. Solid hydrogen, formed by cooling the liquid hydrogen to 14.01 K, therefore behaves as a liquid. The density of solid hydrogen is 86 kg/m<sup>3</sup> and it is the lowest density solid. Slush hydrogen is a combination of liquid and solid hydrogen obtained by bringing down the temperature of the liquid hydrogen to the solidification temperature of 14 K. The density increase of about 16 to 20% for the slush hydrogen compared to liquid hydrogen and higher cooling capacity of slush hydrogen coupled with its liquid like characteristics makes it attractive as a fuel for rockets.

The cryogenic fuel liquid methane with the normal boiling temperature of 112 K, density of 425 kg/m<sup>3</sup> and latent heat of vaporization of 511.5 kJ/kg, has not been applied for liquid propellant rockets. It is readily available as Liquid Natural Gas (LNG). Its higher density coupled with its non-toxic and non-corrosive properties, however, makes it attractive for liquid bi-propellant and liquid tri-propellant rockets.

#### (b) Cryogenic Oxidizers

Liquid Oxygen and liquid Fluorine are the two cryogenic oxidizers. Oxygen, as it occurs in nature, consists of three stable isotopes with atomic masses of 16, 17 and 18 in the proportion 10,000:4:20. It condenses to a light blue liquid of density 1140 kg/m<sup>3</sup> at the normal boiling point of 90.18 K. Liquid oxygen is slightly magnetic with a paramagnetic susceptibility of 1.003. It freezes to a solid at 54.5 K.

Oxygen is reactive even at the low temperatures and it is necessary to keep the surfaces of the storage devices and lines coming in contact with oxygen very clean. Cotton soaked in liquid oxygen is an explosive. Reactive materials such as aluminium and titanium should be used cautiously. Use of carbon steel in the handling of oxygen is to be avoided since carbon can react with gaseous oxygen. The maximum velocity of oxygen flow in carbon steel pipelines is about 30 m/s at a pressure of about 10 atmospheres. The bends and elbows are to be made of steel to prevent hot spots and ignition. Copper, brass and stainless steel pipes are recommended for use with oxygen.

Fluorine has an atomic mass of 18.998. It condenses as a yellow liquid at the normal boiling temperature of 85.3 K. It is a very dense cryogenic liquid having a density of 1504.3 kg/m<sup>3</sup>. Liquid Fluorine freezes to a yellow solid at 53.5 K and when sub-cooled to 45.6 K, turns into a white solid. The nearness of the boiling temperature, freezing temperature and densities of liquid oxygen and liquid fluorine allows a mixture of these two cryogenic liquids known as FLOX, to be used as oxidizer.

Fluorine reacts with almost all materials. Metals are passivated by passing fluorine gas slowly in order to build up a layer of passive fluoride on its surfaces before using them with liquid and gaseous fluorine.

Liquid Fluorine is hypergolic with hydrogen. The very high reactivity of fluorine with almost anything that it comes across has been a deterrent in its application as a cryogenic oxidizer.



### (c) Choice of Cryogenic Propellants

The choice of cryogenic propellants therefore narrows down to liquid oxygen for the oxidizer and liquid hydrogen for the fuel. Though Liquid Methane is being proposed from considerations of its higher density, the molecular mass of combustion products with oxygen is higher than for hydrogen. The standard heat of formation of methane is – 74.9 kJ/mole, compared to zero for hydrogen, and leads to lower energy release for the methane-oxygen reaction. These two factors add up to give a lower value of specific impulse for the methane-oxygen system of propellants. The cryogenic propellant combination consisting of Liquid hydrogen and Liquid Oxygen has alone been commercially applied for rockets.



## C.3 PROPELLANT TANKS AND PROPELLANT SUPPLY SYSTEM

Liquid hydrogen and liquid oxygen are required to be stored at low temperature of 20 K and 90 K respectively if the storage pressure is atmospheric pressure. At higher values of storage pressures, the boiling temperatures of liquid hydrogen and liquid oxygen would increase thus bringing down the lower limit of temperatures at which the propellants have got to be stored. However, with increase in storage pressures, the mass of the tanks will increase and the low density of hydrogen does call for large storage volumes. The practice therefore is to store the cryogenic propellants at pressure slightly greater than the atmospheric pressure. Booster pumps are used for increasing the supply pressure of the hydrogen and oxygen to the turbo-pumps. The requirement of somewhat higher pressure at the turbo-pump inlet is from considerations of preventing cavitation in turbo-pumps. The minimum threshold value of the Net Positive Suction Head (NPSH) depends on the temperature of liquid oxygen and liquid hydrogen and the speed of operation of the turbo pump.

The large temperature difference between the ambient and the liquid hydrogen or oxygen contained in the tanks will lead to substantial heat transfer or heat-in-leaks from the ambient into the cryogenic liquids. The low temperatures of the tanks will also lead to its contraction from the original dimensions of the tank at the ambient temperature. The same would be true for all lines and components which come into contact with the low temperature fluids. These two aspects viz., heat transfer and thermal contraction are dealt with below:

### C.3.1 Heat-in-Leak and Stratification in Tanks

The heat transfer from the surroundings into the low temperature fluids is spoken of as heat-in-leak. The heat transfer is dominantly through the vertical walls of cylindrical tanks as shown in Fig. C.4. The liquid hydrogen or liquid oxygen, when heated by the heat exchange at the walls, locally increases in its temperature and becomes relatively more volatile. It rises to the top and in the process causes convective currents and non-equilibrium processes within the stored liquid. A warmer liquid at a temperature higher than the bulk temperature of the stored liquid collects at the surface. The temperature therefore varies along the height of the liquid with the warmer liquid at the top and this process of temperature variation with height of the liquid is known as thermal stratification.

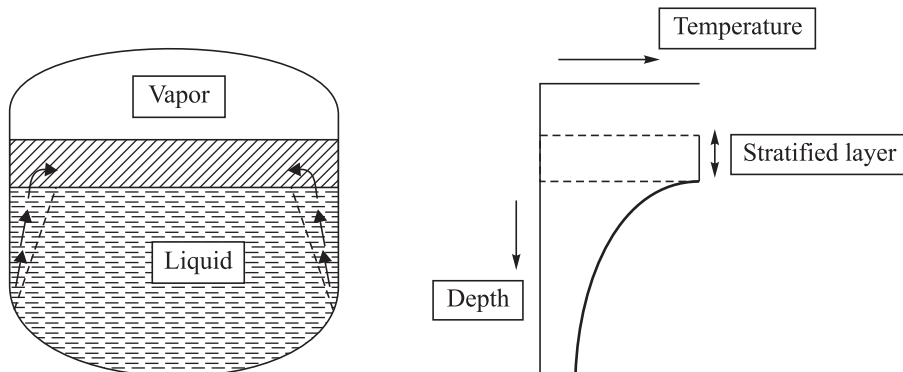


**Fig. C.4** Thermal Stratification

#### C.3.1.1 Venting of Vapor to maintain Uniformity of Temperature

The warmer liquid at the liquid vapor interface results in evaporation of the liquid when the interface temperature exceeds the equilibrium boiling temperature at the pressure at which the liquid is stored. The pressure of the vapor therefore increases and in order to prevent the higher values of pressures in the tank it becomes necessary to vent off the vapor. The warmer liquid on entering the pump towards the end of the depletion process, could also result in cavitation and stalling of the pumps. It becomes necessary to maintain uniform temperature of the liquid propellants in the tank to the extent possible.

The pressure of the vapor above the liquid surface decreases due to the expansion process when the vapor is vented out of the tank. The saturation temperature of the liquid decreases as the pressure to which it is subjected to decreases. This trend of change of saturated liquid temperature with the saturation pressure is shown in Fig. C.5. The fall in pressure of the vapor results in a lowering of the saturation temperature of the liquid and consequently a drop in the liquid surface temperature. This lower temperature layer being heavier now diffuses into the bulk of the liquid through the stratified layer till equilibrium is reached in the liquid column.

#### C.3.1.2 Spraying Liquid in the Vapor Column

Liquid hydrogen has a thermal diffusivity of  $2.23 \times 10^{-7} \text{ m}^2/\text{s}$  [thermal conductivity =  $0.152 \text{ W}/(\text{m K})$ , density =  $71.3 \text{ kg/m}^3$  and specific heat =  $9560 \text{ J}/(\text{kg K})$ ] while the thermal diffusivity of liquid oxygen is  $5.32 \times 10^{-8} \text{ m}^2/\text{s}$  [thermal conductivity =  $0.1033 \text{ W}/(\text{m K})$ , density =  $1142 \text{ kg/m}^3$  and specific heat =  $1700 \text{ J}/(\text{kg K})$ ]. The low thermal diffusivity of liquid oxygen compared to hydrogen does not allow equilibration of temperature to take place swiftly in it from the venting operation in a liquid oxygen tank as in the case of a liquid hydrogen tank. Further reduction of the liquid oxygen surface temperature is sometimes done by spraying liquid oxygen in the volume of the oxygen vapor. The absorption of latent heat from the evaporation of the spray of liquid oxygen further brings down the temperature of

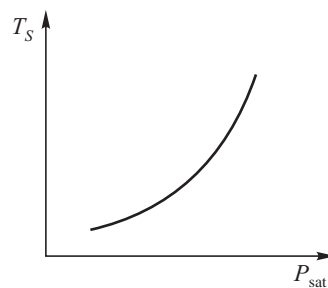


**Fig. C.5** Variation of Saturation Temperature of the Liquid with Pressure



liquid oxygen at the surface. This low temperature liquid being denser gravitates down and helps in homogenizing the temperatures in the liquid oxygen column. A schematic of the spraying process is shown in Fig. C.6. This spraying process of controlling stratification of the liquid oxygen tank is spoken of as thermal conditioning system.

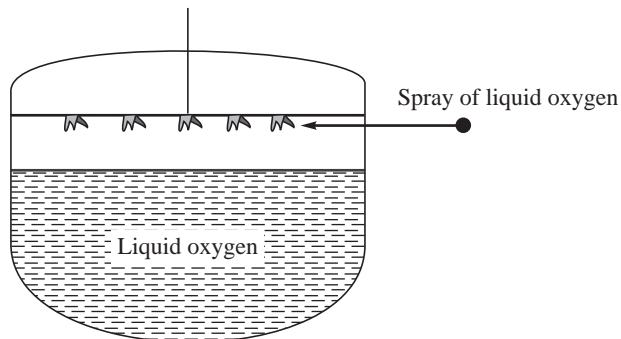


**Fig. C.6** Spray of Liquid oxygen for de-stratification

### C.3.2 Choice of Materials for Propellant Tanks

At the lower range of temperatures, metals and alloys having a body centered cubic (BCC) structure such as carbon steels become brittle. Below the temperature of transition at which the material becomes brittle, it can no longer be used for tanks and structural load bearing members. Plastics and rubber also become brittle when cooled below a specified value of the transition temperature. The brittle 'O' rings in the Solid Rocket Booster of Space Shuttle at the sub-zero temperatures on the day of the launch resulted in gas leakage through it and failure of the Space Shuttle mission Challenger in January 1986 (chapter 5). Notable exceptions to the plastic materials becoming brittle are Teflon and Kel-F.

Metal alloys with Face Centered Cubic (FCC) structure such as Copper, Aluminium alloys and Austenitic Stabilized Steels do not exhibit the ductile to brittle transition and are used for application at cryogenic temperatures. Figure C.7 shows the onset of the ductile to brittle transition at about 100 K, as characterized by the percentage elongation, in carbon steel while the transition is not present in aluminium and stainless steel.

The ultimate tensile strength however increases as the temperature decreases and this trend is shown for stainless steel, carbon steel and aluminium alloy in Fig. C.8. The thermal conductivity also decreases below a certain cryogenic temperatures for stainless steel, carbon steel and aluminium alloy.

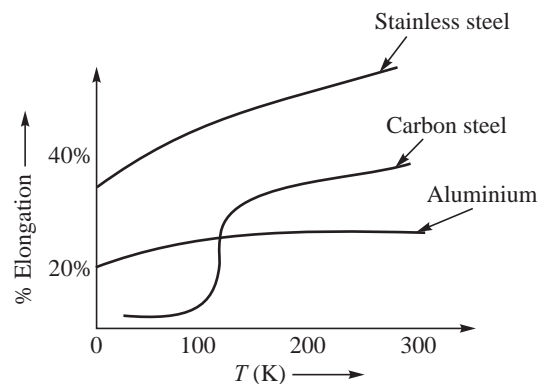


**Fig. C.7** Percentage Elongation indicating Ductile to Brittle Transition at Low Temperatures in Body Centered Cubic Materials of Construction viz., Mild Steel

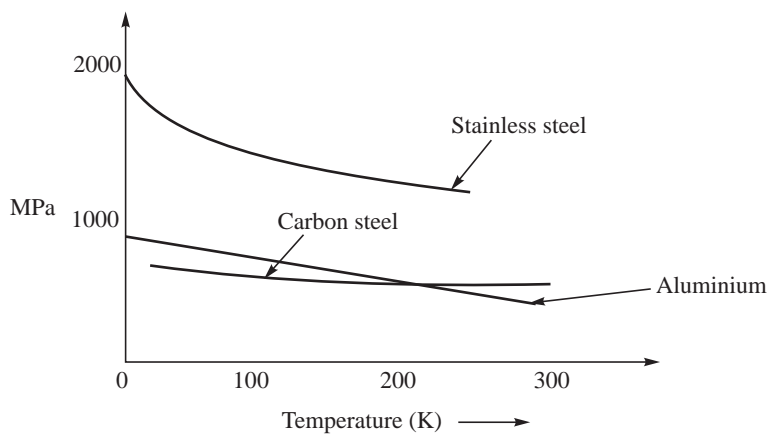


Fig. C.8 Variation in Ultimate Tensile Strength at the Low Temperatures



## C.4 INSULATION

The heat transfer to the cryogenic liquids is brought down by isolating the tank walls and the lines and components from the ambient. The insulating material reduces the conduction, convection and radiation heat transfer from the ambient to the liquid column. Different types of insulations are used, the simplest being foam.

### C.4.1 Foam Insulation

The low conductivity of the foam material reduces heat conduction. The small isolated gas cells in the foam material increases the path length of the conduction and effectively gives rise to a major reduction in the heat transfer. Conduction of moisture at the interface of the metal wall and insulation and ingress of moisture in the pores lead to the formation of ice bridges thus lowering the effectiveness of the insulation. It becomes necessary to wrap the outer surface of the foam insulation with a layer which would prevent the ingress of moisture into the foam. The ease of processing the foam, the low cost and the ease of support for positioning the foam makes it attractive. Poly isocyanurate foams are generally used.

Foam materials have coefficient of thermal expansion between 2 to 3 times greater than the aluminium or steel tanks on which they are coated. Reinforcing threads, expansion joints and addition of fibers are usually incorporated to take care of the differential contraction. The larger thermal stress from the enhanced contraction when the cryogenic propellants are loaded in the tanks causes cracks and voids are developed. Humid air would enter the voids and cracks and form ice thereby reducing the effectiveness of the insulation. A layer of non-impermeable coating is therefore applied over the external surfaces of the foam insulation to prevent ingress of moisture. An electrical conductive coating is also provided on the external surfaces to avoid accumulation of static electricity.

The thickness of insulation is essentially to maintain the temperatures of liquid oxygen and liquid hydrogen in the tanks within permissible limits such that boil-off of the propellants is controlled. Since an increase in the mass of the tanks adversely influences the performance of the rocket, a compromise between the thickness of insulation and boil off losses is adopted.



#### C.4.2 Vacuum Jacketing of Feed-lines and Components

The use of vacuum jackets drastically reduces the heat-in-leak and is used for the feed lines conveying the cryogenic liquids. A reduced pressure in the jacket of about 0.1 Torr ( $1.3 \times 10^{-4}$  atm) essentially removes the heat conduction and convection component and thereby decreases the heat in leak by an order of magnitude or greater. Incorporation of powder insulation, in particular opacified powder or else opacified copper or aluminium flakes further reduce the radiation component of heat transfer. The annular jacketing technique cannot be adopted for the tanks since they have to withstand a collapsing pressure differential equal to the ambient pressure.

The vacuum jacketed methods are preferred for lines; however, suitable supports and spacers for supporting the inner and outer lines are required. Expansion bellows, U bends and specific joints such as Bayonet joint become necessary to take care of the problem of thermal contraction.

#### C.4.3 Polyimide Pipes

The differential contractions from the different parts being subjected to different temperatures calls for a system to compensate for differential contractions as discussed in the last section. Polyimide pipes have insulating capability and low stiffness. The later property, which makes them capable of absorbing the differential expansion and contraction, makes them attractive for use for lines and joints. They act as thermal compensators. Polyimide plumb lines with metallic end fittings are used.

The thermal contraction of tanks is also to be accounted for in design with suitable joints using spherical bearings and polyimide lines.

#### C.4.4 Multi Layer Insulation

Use of evacuated multilayer insulation with multiple layers of reflecting materials (such as aluminized mylar or aluminium foils) separated by insulating sheets of fiber glass or nylon net bring down the heat in leak by a factor of about 30 compared to the evacuated powder insulation. The reflecting surfaces reduce the radiation while the insulating layer reduces the conduction heat transfer.

The multilayer insulation is very widely used and it is possible to store liquid hydrogen in sealed containers using multi layer insulation without venting for about 10 days. The high compressibility liquid hydrogen, due to it being a quantum fluid, aids in the zero venting requirement.

The multilayer insulation can be also used to reduce the heat in leak from the ambient to the different components which handle the cryogenic liquids.



### C.5 CHILL DOWN OF TANKS, LINES AND COMPONENTS BEFORE CONTACT WITH CRYOGENIC PROPELLANTS

If the low temperature liquid hydrogen or liquid oxygen were to be directly introduced in a tank or a pipeline at the ambient temperature, it would immediately flash into vapor. This is clearly not acceptable as the explosive release of vapor would not only create a surge in pressure but also prevent the flow of the liquid in the pipeline. All parts of the cryogenic rocket such as tanks, valves, transfer lines and plumb lines, pump system , injectors and combustion chamber are required to be cooled down to the



liquid hydrogen or liquid oxygen temperature with which they come in contact. This process of cooling down is known as chill down.

If we were to supply cryogenic propellants to chill down a line initially at the ambient temperature, the propellant would immediately vaporize on contact with the warm surface of the line bringing down its temperature. A two-phase flow starts off with vapor bubbles formed at the surface. This is known as bubbly flow. As more of the liquid is admitted for chill-down, the increased volume of the bubbles collects into plugs of vapor and is known as plug flow. The flow of liquid and vapor and the difference in velocity between them cause the interface between the liquid and the vapor to become wavy and this type of flow is called as wavy flow. The wavy nature of flow develops further filling the entire cross section of the pipe to give rise to slugs of liquid being formed. This slug flow could develop further into an annular flow with liquid film at the walls. During the process of chill-down, different regimes of flow such as bubbly flow, plug flow, wavy flow, slug flow and annular flow each with a distinctly different heat transfer coefficient at the surface takes place. These regimes of flow are shown in Fig. C.9. It would be necessary to consider these modes of flow to determine the quantity of the propellant required for the chill-down and the time required for the chill-down process.

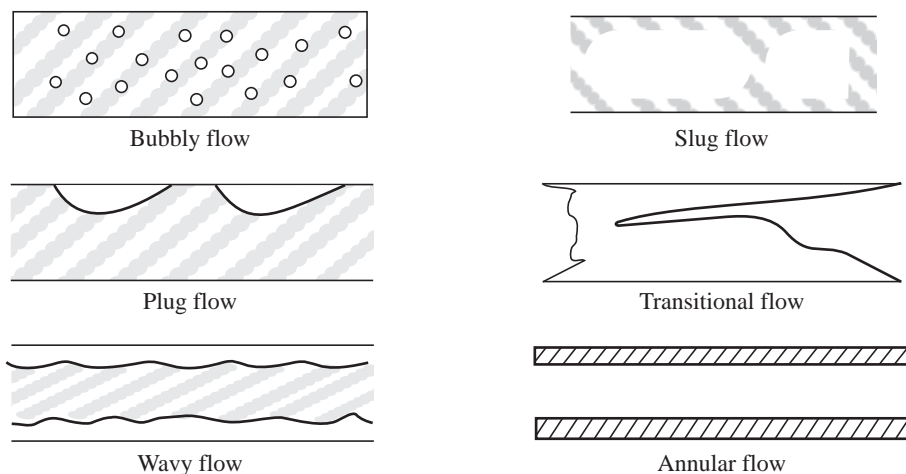


**Fig. C.9** Regimes of Flow during Chill-down

During the chilling of the tanks, lines and components, the heat transfer coefficient at the walls would be continually varying with the different types of flows between bubbly and annular. However, a major reduction in the temperature would be achieved with the low temperature vapor from the vaporized mass of liquid. At the start of the chill-down, the liquid flashes into vapor and it is this cold vapor which effectively contributes to the cooling and leaves the system at a temperature between the saturated vapor temperature and the initial temperature of the hardware. As further chill-down continues, the liquid moves further down until it fills the system.

### C.5.1 Low and High Flow Rate Chilling

If we draw the saturation curve on a plot of Temperature vs. Specific Volume for any pure liquid, we obtain a dome shape curve as shown in Fig. C.10. The left side boundary corresponds to the saturated liquid line and separates the liquid phase from the liquid and vapor phase. The right side boundary



corresponding to the saturated vapor line denotes the condition beyond which only superheated vapor is possible. The two curves meet at the critical point. The constant pressure lines have a constant value of temperature (saturation temperature) within the dome in the two phase region. The latent heat of vaporization decreases as the saturation pressure increases and reaches a value of zero at the critical pressure.

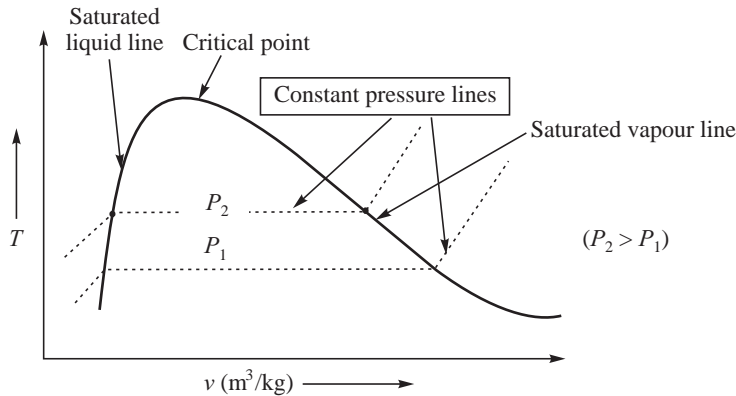


**Fig. C.10** Saturation Curve for a Pure Liquid

A low pressure liquid would be able to cool the system better since it has a higher value of latent heat of vaporization. The vapor formed is also at low temperature corresponding to the saturation temperature at the corresponding pressure. Low pressure cooling of the lines and components is initially resorted to in practice to bring down the temperatures. The mass flow rates of the liquid propellants are small during this phase of cooling. Thereafter chilling is done at high flow rates of the propellant corresponding to higher pressures so as to remove the entire vapor and fill the concerned system with the low temperature fluid. Oscillations occur in flow rates, pressure and velocities during the chill-down process till liquid propellant completely fills it viz. chill-down is completed.

### C.5.2 Time Required for Chill-down

An order of magnitude of the time and the quantity of propellants required for chill-down could be estimated by the procedure outlined by R. F. Barron in the book on “Cryogenic Systems”. Here the object to be chilled is treated as a control volume and the first law of thermodynamics is applied to this control volume. In this section we derive the time for chill-down and the quantity of propellants required.

Let the total time required for chill-down be denoted by  $t_C$ . Before the commencement of chilling, the temperature of the object is the ambient temperature  $T_0$ . At the end of the chilling operation, the temperature is  $T_C$ . If  $u_0$  is the internal energy of the fluid of mass  $m_0$  contained in the control volume before chilling and if  $u_C$  is the internal energy after completion of chill-down and the mass of fluid in it is  $m_C$ , we have by applying the 1<sup>st</sup> law of thermodynamics :

$$\begin{aligned} \Delta U &= Q - W_X + m_i h_i - m_o h_o \\ Q &= (m_C u_C - m_0 u_0) + \int_0^{t_C} \dot{m}_g h_g - \int_0^{t_C} \dot{m}_f h_f \end{aligned} \quad (C.1)$$



Here  $Q$  is the total heat transfer during the chill-down.  $\dot{m}_f$  is the rate at which the cryogenic fluid is admitted for chilling while  $\dot{m}_g$  is the rate at which the warm vapor leaves the volume being chilled.  $h_g$  is the enthalpy of the vapor while  $h_f$  is the enthalpy of the liquid being admitted. The mass balance equation for the control volume is:

$$m_C - m_0 = \int_0^{t_C} \dot{m}_f dt - \int_0^{t_C} \dot{m}_o dt \quad (\text{C.2})$$

If the average values of the mass flow rates of the cryogenic propellant entering the volume and the vapor leaving it are denoted by  $\bar{\dot{m}}_f$  and  $\bar{\dot{m}}_g$  respectively, Eq C.2 reduces to:

$$m_C - m_0 = (\bar{\dot{m}}_f - \bar{\dot{m}}_g) t_C \quad (\text{C.3})$$

The integrals  $\int_0^{t_C} \dot{m}_g h_g dt$  and  $\int_0^{t_C} \dot{m}_f h_f dt$  in Eq. C.1 can be expressed in terms of the averages as  $\bar{\dot{m}}_g \bar{h}_g t_C$  and  $\bar{\dot{m}}_f \bar{h}_f t_C$  respectively. Substituting, the value of  $\bar{\dot{m}} t_C$  obtained from Eq.C.3 as  $(m_C - m_0) + \bar{\dot{m}}_g t_C$  in Eq. C.1, we get:

$$Q = m_C u_C - m_0 u_0 + \bar{\dot{m}}_g \bar{h}_g t_C - (m_C - m_0) h_f - \bar{\dot{m}}_g t_C h_f$$

The value of  $Q$  therefore becomes:

$$Q = m_C (u_C - h_f) - m_0 (u_0 - h_f) + \bar{\dot{m}}_g (\bar{h}_g - h_f) t_C \quad (\text{C.4})$$

The heat transferred  $Q$  during the chill-down can also be written in terms of the heat-in-leak from the ambient  $\dot{Q}_L$  and the heat required to decrease the temperature of the thermal mass ( $MC$ ) from the initial temperature  $T_0$  to the final temperature  $T_C$ . Denoting the mean value of heat transfer rate as  $\dot{Q}$ , we have:

$$Q = \int_0^{t_C} \dot{Q} dt = \int_0^{t_C} \dot{Q}_L dt + \int_{T_0}^{T_C} MC dT \quad (\text{C.5})$$

If  $\dot{Q}_C$  is the steady state value of heat in leak after the chill-down process is over, the value of  $\int_0^{t_C} \dot{Q}_L dt$  in the above equation can be approximated as  $\dot{Q}_C t_C / 2$ . The value of the integral  $\int_{T_0}^{T_C} MC dT$  can also be written as:  $MC (T_0 - T_C)$ . Eq. C.5 therefore reduces to:

$$Q = \dot{Q}_C t_C / 2 + MC (T_0 - T_C) \quad (\text{C.6})$$

Equating the values of heat transferred  $Q$  determined in Equations C.4 and C.6, we get:

$$m_C (u_C - h_f) - m_0 (u_0 - h_f) + \bar{\dot{m}}_g (\bar{h}_g - h_f) t_C = \dot{Q}_C t_C / 2 + MC(T_0 - T_C)$$

The value of the chill-down time is therefore obtained as:



$$t_C = \frac{MC(T_0 - T_C) - [m_C(u_C - h_f) - m_0(u_0 - h_f)]}{\bar{m}_g(\bar{h}_g - h_f) - \dot{Q}_C/2} \quad (\text{C.7})$$

From the above Equation, we observe that if  $\bar{m}_g(\bar{h}_g - h_f) = \dot{Q}_C/2$ , the value of  $t_C$  becomes infinity, signifying that it is not possible to chill down the line. A minimum mass flow rate given by:

$$\bar{m}_g \geq \frac{\dot{Q}_C}{2(\bar{h}_g - h_f)} \quad (\text{C.8})$$

is required for the chill down. If the resistance to flow in the passages is too large and this critical value of mass flow rate cannot be achieved, it would not be possible to complete the chill-down. It may be necessary to vent the vapor at some more additional points thereby increasing the mass flow rates.

The mass of the cryogenic propellant required for the chill-down is the mass which evaporates and is vented out ( $\bar{m}_g t_C$ ) and the mass of the liquid required to fill in the space.



## C.6 MITIGATION OF HAZARDS IN THE USE OF LIQUID OXYGEN AND LIQUID HYDROGEN

A mixture of gaseous hydrogen and oxygen containing 4% by volume of hydrogen is flammable. Wide variations in the concentration of hydrogen in the hydrogen-oxygen and hydrogen-air mixtures can form flammable mixtures. The limits of flammability of these mixtures are shown in Fig. C.11. Mixtures formed between 4% and 94% by volume of hydrogen in the hydrogen–oxygen mixture can support the flame. Similarly, hydrogen–air mixtures comprising 4% to 75% by volume of hydrogen are flammable. The minimum ignition energy, which is plotted on the Y axis in Fig. C.11 is very small of the order of 0.017 mJ for hydrogen-air mixtures

and less than about 0.004 mJ for the hydrogen-oxygen mixture. Any small leak of hydrogen into the oxygen line or of oxygen into the hydrogen line can lead to a flame since the minimum ignition energies are extremely small. Similarly, leakage of hydrogen into the ambient air could result in a fire and an explosion.

Purging of lines and components is therefore required to isolate the hydrogen from the oxygen and air. The vent system which releases vapors of oxygen and hydrogen during the chill-down and during inadvertent pressurization of the tanks must suitably dispose off these gases. Any accumulation of hydrogen and oxygen from leaks which can lead to concentrations within the flammability limits need to be diluted using inert gaseous nitrogen.

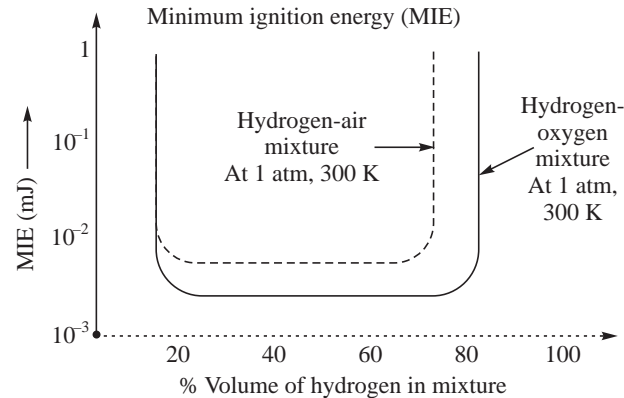


**Fig. C.11** Flammability limits of Hydrogen–Oxygen and Hydrogen–Air mixtures



The venting of hydrogen gas from the liquid hydrogen tank is not permitted during the flight of the rocket in the atmosphere.

The liquid oxygen lines are purged with nitrogen gas and the liquid hydrogen lines are purged with gaseous helium before the start of the chill-down process. Considering that the boiling temperature of liquid hydrogen is about 20 K at ambient pressure compared to the boiling temperature of liquid nitrogen (77 K), the gases in the hydrogen line are purged out using helium to prevent condensation of nitrogen or air when the unit is cooled down to temperatures less than about 77K. Gaseous helium purge system is also used to prevent the entry of hydrogen in the liquid oxygen circuit during the transients and the entry of hot gases during the shut down when the propellant flow to the combustion chamber is stopped.

After the rocket has completed its operation, the hydrogen gas from the liquid hydrogen tank is vented off in deep space so as to prevent any undue pressurization and explosion of the tank. The process is known as passivation. Similarly, the liquid oxygen tank is passivated after the operation of the rocket is over. Venting is done using pressurized helium gas for both the tanks.



## C.7 USE OF CAVITATING VENTURIES INSTEAD OF ORIFICES FOR CONTROLLING FLOW

The low boiling temperatures of the cryogenic propellants are usefully utilized by designing cavitating venturi for feeding them into the combustion chamber instead of using sharp edged orifices discussed in the chapter of liquid propellant rockets. The cavitating venturi consists of a convergent conical entry followed by a constant diameter throat and a slowly diverging conical section and is shown in Fig. C.12. The inlet cone angle is about 20° while the divergent cone angle is about 5°. The gradual shaping avoids the larger pressure drops in the flow present in sharp edged orifices and therefore gives a high value of the discharge coefficient.

If the supply pressure is so chosen that the vapor pressure of the liquid is just reached at the throat, the flow through the cavitating venturi becomes independent of the pressure at the exit. When the exit pressure decreases, the vapor cavities expand in the divergent with the result that the flow rate through the venturi remains constant irrespective of the decrease of the exit pressure. An increase of the exit pressure will decrease the pressure drop and the cavitation at the throat and thereby again maintain a constant value of the flow rate.

An increase in the value of the supply pressure will tend to increase the flow rate by suppressing the cavitation at the throat; however, the increased flow rate leads to a larger pressure drop and the associated pressure drop would essentially bring about cavitation at the throat. It would lead to a constant flow rate for different values of exit pressure and would depend only on the inlet pressure. Fixed values of flow rates are thus obtained for a given value of the supply pressures.

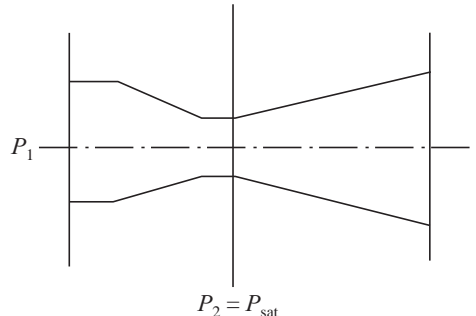


Fig. C.12 Cavitating Venturi



## C.8 CHOICE OF FEED SYSTEM CYCLES

The different feed system cycles for liquid propellant rockets were dealt with in chapter 6. The relative complexity of the issues associated with the storage, handling and use of the low temperatures liquid hydrogen and liquid oxygen and the attendant problems dealt with earlier in this chapter make the cryogenic rockets unsuitable for low thrust rockets. If the thrust levels and operating pressures of the existing cryogenic propellant rockets, developed in the different countries are examined, it is seen that there are two distinct thrust levels corresponding to booster and upper stage rockets. One cluster has thrust levels in the range between 35 and 100 kN approximately while the other has a thrust level of about 1000 to 2000 kN and is shown in Fig. C.13.

The number of rockets in the lower thrust category comprises HM7 rockets of France, RL 10 series of cryogenic rockets from USA, LE-5 of Japan and RD-56 cryogenic rocket of Russia. All these rockets use either the gas generator cycle or the expander cycle except for the RD-56 rocket which uses the staged combustion cycle. The chamber pressure of these lower thrust rockets are in the range of about 2 and 6 MPa. The relative low thrusts and the lower chamber pressures do not demand large flow rates of the propellant and higher values of pressures at the outlet of the turbo-pump, with the result that the energy required for running the pumps can generally be met from the enthalpy of the heated hydrogen in the regenerative coolant passages. The RL 10 series of engines use the expander cycle of operation. The LE5 of Japan employs a combination of the expander and gas generator cycle. The other rocket such as HM4 and HM7 use the gas generator cycle.

In the higher thrust category of about 1000 kN, wide range of chamber pressures starting from the low pressure of about 5.4 MPa for the J2 rocket to 11 MPa for the Vulcain and thereafter to about 22 MPa for SSME and RD120 rockets are observed. While the lower pressure rockets J2 and Vulcain employ the gas generator cycle, the high pressure rockets SSME and RD120 use the staged combustion cycle. The LE7 engine with a chamber pressure of 12.6 MPa also employs the staged combustion cycle.

A cryogenic rocket by name Vinci is being developed by the European Space Agency. It uses the expander cycle at a chamber pressure of 6.08 MPa and thrust level of about 180 kN and stretches the regime of operation of the expander cycle.

The different feed system cycles are seen to be used for the various cryogenic rockets developed so far irrespective of their thrust levels. However, for the lower chamber pressures, the simpler gas generator cycle or the expander cycle is seen to be preferred. The application of the expander cycle has a ceiling on the thrust level and the Vinci rocket under development corresponds to the upper limit of thrust level. In the case of very high chamber pressures and thrust levels the stage combustion cycle is invariably used in view of the advantages in specific impulse over the gas generator cycle.

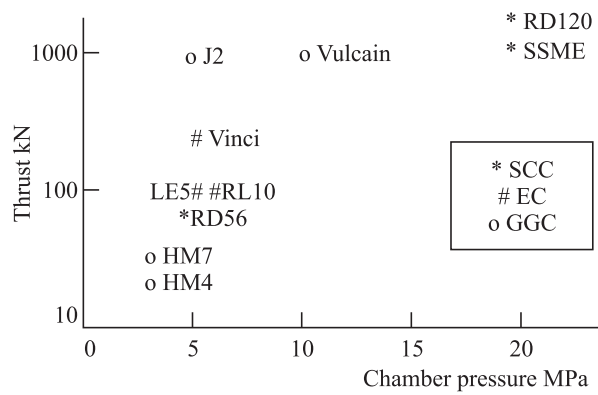


Fig. C.13 Thrust and Chamber Pressure of Different Cryogenic Rockets



## C.9 INJECTOR CONFIGURATION

Liquid hydrogen is used for regenerative cooling of the combustion chamber and by the time it enters the injection manifold it is in the gaseous phase. When the stage combustion cycle and the expander cycle is used, the expanded gases from the turbine exhaust enter the injection manifold. These consist of products of combustion of the very fuel rich mixture of hydrogen and oxygen in the case of the staged combustion cycle and the warm expanded hydrogen gas for the expander rocket. Therefore irrespective of the feed cycle, hydrogen enters the injector manifold as a gas and this gas flow is used for atomizing liquid oxygen. The injectors are known as gas assist injectors as was briefly mentioned in Chapter 6. In the following we examine these injectors meant for cryogenic propellant rockets.

### C.9.1 Coaxial Injectors

The liquid oxygen is injected through a central orifice or post while the gases are injected through a concentric annular gap surrounding the central post as shown in Fig. C.14. The ratio of the gas velocity to the liquid flow velocity is between about 10 and 15. The relative velocity at the interface between the gas flow and the liquid oxygen flow is maintained at a high value of the order of about a hundred meters per second. The high relative velocity leads to aerodynamic shear at the gas liquid interface and causes the interface to become wavy, the waviness growing until drops of liquid oxygen are pinched off from the liquid surface to form droplets of liquid oxygen.

As the liquid oxygen jet moves away from the plane of injection and the atomization proceeds, the diameter of the liquid oxygen jet decreases as shown in Fig. C.14. The length of the liquid oxygen jet corresponding to full atomization (length at which the liquid jet breaks up fully) is known as the intact core length or break-up length. The intact core length is an important parameter as it influences the length of the chamber required for complete combustion. The intact core length is a strong function of the diameter of the liquid oxygen injection diameter, the turbulence level in the liquid oxygen jet, the aspect ratio of the injection orifice and the chamber pressure and gas density. A large number of small coaxial injection elements will create a number of small diameter jets and maintain small values of the intact core length and also generate small size of the oxygen droplets. A large number of injection elements are therefore housed in the injector. This was illustrated in Fig. 6.23 for a liquid propellant rocket.

The droplets of liquid oxygen, so generated, are entrained in the high velocity jet of either gaseous hydrogen or the gaseous fuel rich products of combustion. They deform and the additional drag helps in the interface transport and mixing with the gas. Secondary breakup of the liquid oxygen droplets also takes place. The droplets of oxygen sheared off from the liquid oxygen jet during the initial phase of the jet would be smaller because of the smaller amplitude wave motion over the surfaces. These smaller droplet sizes immediately vaporize and help in the formation of a mixture suitable for combustion. A flame is therefore formed very near to the exit of the injection elements. A schematic of the flame surrounding the liquid oxygen jet is sketched in Fig. C.15.

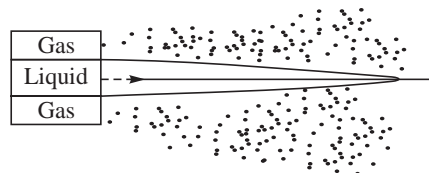
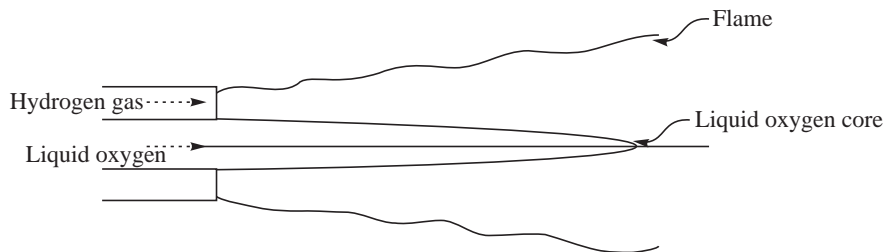
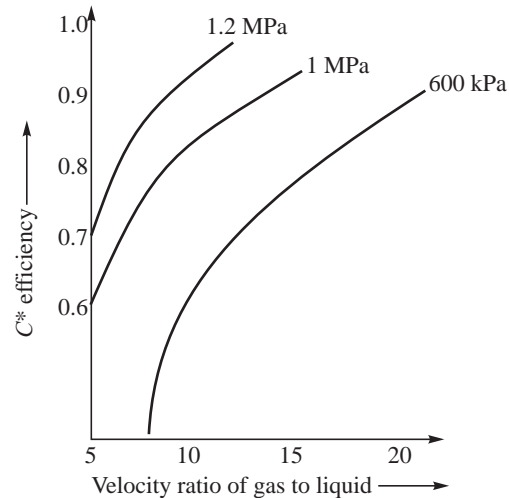


Fig. C.14 Gas Assist Coaxial Injector



**Fig. C.15** Schematic of Flame Surrounding the Liquid Oxygen Core

The  $C^*$  efficiency which is an index of the efficiency of combustion in rockets was seen in Chapter 6 to depend on the efficiency of vaporization and the efficiency of distribution. The vaporizing and mixing efficiencies are influenced by the injector configuration and the chamber pressures. Experiments show that the  $C^*$  efficiency progressively increases with increase in the velocity ratio between the gas and the liquid oxygen jet. The increase is more significant as the chamber pressure increases. Figure C.16 shows this dependence in the region of low chamber pressures. This trend is to be anticipated since a finer spray comprising of much smaller droplets are formed under these conditions of higher relative velocities and higher values of chamber pressures.



**Fig. C.16** Efficiency of Combustion with Velocity Ratio at Injection

### C.9.2 Coaxial Swirl Injectors

Though the concentric orifice elements, discussed so far for the gas assist injector, have been employed in the earliest configuration of the cryogenic engine such as RL-10, the practice of swirling the liquid oxygen jet introduces tangential velocities and improves the atomization and mixing particularly in the region near to the injector face. The later configurations of the RL10 engine used helical ribbons in the supply passages to the injection elements to generate swirl and the specific impulse of the rocket improved from 4330 N-s/kg to 4440 N-s/kg. A configuration of the swirl generated by helical

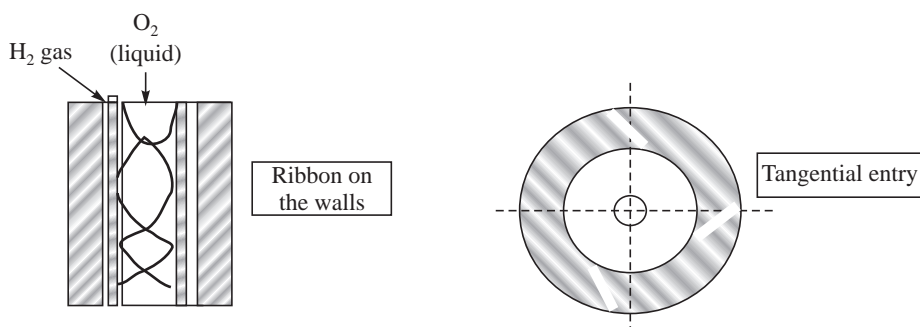


**Fig. C.17** Incorporation of Swirl in Liquid Oxygen Jet by Ribbon on Wall or Tangential Entry



ribbons placed on the walls of the liquid supply manifolds is sketched in Fig. C.17. Helical swirlers or tangential entry of the liquid oxygen (Fig. C.17) could also be used to provide the rotational velocities to the liquid oxygen jet.

### C.9.3 Gas Swirl in addition to Liquid Swirl

Gas turbine combustors provide air swirl for good mixing and better flame holding. It is possible to incorporate gas swirl in addition to liquid oxygen swirl for better mixing. Such injection elements are also used. There are a number of combinations possible in the coaxial configuration of the gas-assist injection elements.

### C.9.4 Recessing of the Liquid Oxygen Post

So far injection elements having the exit of the central liquid oxygen element and the exit of the annular gaseous element in flush with the injector face have been considered. It is possible to have the liquid oxygen element within the outer gaseous element as shown in Fig. C.18 so that the gas velocity will not relax before the atomization. This procedure of insetting the liquid oxygen element within the outer gaseous element is known as recessing of the central oxygen post.

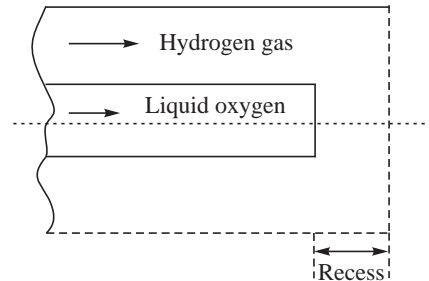


Fig. C.18 Recessing of the Central Liquid Oxygen Post

### C.9.5 Flare and Cup at the Exit of the Liquid Oxygen Post

Different shapes such as a flare or a cup at the exit of the liquid oxygen element could bring down the velocity of the liquid oxygen jet and thereby increase the velocity ratio between the annular gas jet and the liquid oxygen. Injectors of Space Shuttle Main Engine have adopted the flared liquid oxygen element with improved performance. The flared and cup arrangements of the centrally recessed liquid oxygen injection element is shown in Fig. C.19.

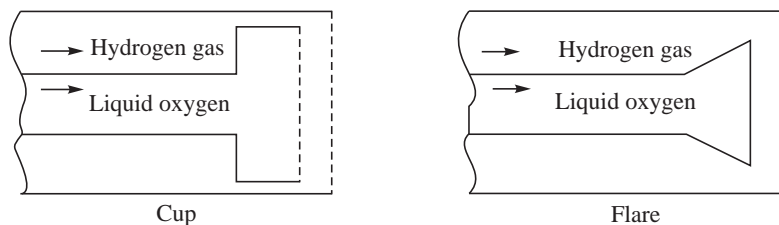


Fig. C.19 Incorporation of Cup and Flare in the Central Liquid Oxygen Element

### C.9.6 Cooling of Injector Head

The injector face runs hot because of the flame being held at the injector face. The injector face is either made of high conductivity copper alloy so that the heat can be transferred to the hydrogen gas



in the manifold. Alternatively, the injector head is made of a porous substance known as "Rigimesh" formed by sintering of fine stainless steel wire meshes. Hydrogen from the injector manifold seeps in through the pores and cools the injector head.



## C.10 COMBUSTION PROCESS

### C.10.1 Processes of Evaporation, Mixing and Chemical Heat Release

The time taken for combustion in the cryogenic propellant rocket consists of the following three events:

- (i) evaporation of liquid oxygen droplets in the spray formed by the injector,
- (ii) mixing with the hydrogen to form a flammable mixture and
- (iii) chemical reactions of this flammable gas mixture

The time for atomization is negligibly small and can be neglected. The characteristic times for evaporation, mixing and chemical reactions can be estimated readily. The evaporation time is determined from equation 6.26 in Chapter 6:

$$\tau_v = D_0^2 / \lambda = \frac{D_0^2 \rho_1}{8 \rho D_{FO} \ln(1 + B)}$$

Here  $D_0$  m denotes the mean diameter of the oxygen droplet in the spray and  $B$  is the transport number defined by following Eq. 6.28:

$$B = \frac{C_p (T_\infty - T_1)}{L}$$

It is seen from the above equation that the evaporation time can be brought down with smaller values of the droplet sizes. A reduction in the evaporation times may not be possible at enhanced values of chamber pressures since the diffusion coefficient decreases with an increase in increase of pressure. Typically, the order of vaporization time calculated for a droplet size of 100 microns is a few tens of milliseconds.

The characteristic time for mixing can be calculated from dimensional considerations viz.,

$$\tau_m = \frac{d}{V_g - V_l}$$

Here  $d$  is the diameter of the chamber or the net stream tube into which the injector element supplies the propellant.  $(V_g - V_l)$  is the mean value of the relative velocity of the gas with respect to the droplets. With the relative velocity being about 100 m/s, the characteristic time for mixing is about a millisecond considering the diameter of the stream tube as 10 cm. The relative velocity decreases downstream from the injector and the characteristic mixing time increases.

The chemical reaction time will depend on the local values of the mixture ratio in the combustion chamber and is given by:

$$t_{ch} = \frac{D_g}{S_U^2}$$



$D_g$  in the above equation denotes the diffusivity of the mixture and  $S_U$  is the characteristic flame speed. The laminar flame speeds do not change significantly with pressure while diffusivity decreases with increase of pressure. Hence the operating pressure influences the reaction times more than the mixing times and vaporization times. With the diffusivity of the mixture being about  $0.002 \text{ m}^2/\text{s}$  and the flame speed in hydrogen oxygen mixtures as  $5 \text{ m/s}$ , the characteristic chemical reaction times are typically less than a millisecond. The chemical reaction times and mixing times are very much smaller than the characteristic vaporization times and this long lead vaporization process would therefore limit the rate of the combustion process.

### C.10.2 Combustion Process under High Chamber Pressures

When the chamber pressure exceeds the critical pressure of oxygen, the distinction between the liquid and gas phase vanishes with the result that there is no phase boundary between the liquid oxygen and the gas surrounding it. Under these conditions there is no question of atomization of the liquid oxygen in the gaseous medium. There is no vaporization involved and the characteristic time of mixing and chemical reactions would therefore control the combustion rate.

The critical pressure of oxygen is  $5.04 \text{ MPa}$  and the critical temperature is  $154.6 \text{ K}$ . However, this value of critical pressure is when the liquid oxygen is in contact with only its own vapor. The critical pressure and critical temperature of liquid oxygen, in the presence of hydrogen gas in addition to its own vapor and other products such as obtained in the staged combustion cycle would depend on the equilibrium of the different phases. The equilibrium of phases between liquid oxygen and hydrogen gas can exist much above the critical pressure of  $5.04 \text{ MPa}$  as long as the critical mixing temperature is not exceeded. The critical mixing temperature varies between  $150 \text{ K}$  at  $5 \text{ MPa}$  to about  $130 \text{ K}$  at  $18 \text{ MPa}$ . When the interface temperature exceeds the above values, the surface of the liquid becomes grossly distorted and mixing would take place by the density gradients.

The feed system cycle will govern the temperature and composition of the gas surrounding the liquid oxygen jet. The temperature of the gas would be of the order of about  $800 \text{ K}$  for the staged combustion cycle while for the gas generator cycle the temperature would be about  $100 \text{ K}$ . With the expander cycle of operation, the temperatures would be even less. The choice of the feed system cycle would govern if the injection conditions are supercritical at chamber pressure in excess of  $5 \text{ MPa}$ .



### C.11 FLAME HOLDING AND STABILIZATION

The small droplets of oxygen formed in the spray at the immediate exit of the liquid oxygen post readily evaporate and forms a mixture ratio of hydrogen and oxygen within the flammability limits. An oxy-hydrogen flame is therefore anchored to the injector face plate as shown in Fig. C.20. Such flame holding by the injector has been demonstrated in controlled experiments in single element injectors with liquid oxygen being injected into co-flowing hydrogen gas.

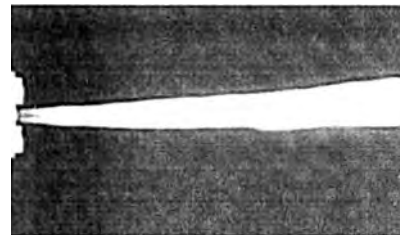


**Fig. C.20** Flame anchored to the Injector Face Plate



When the velocity of injection is increased beyond a certain threshold value, the flame gets lifted off from the injector face plate and is formed after a certain stand-off distance. A lifted flame is shown in Fig. C.21. The stand off region in the lifted flame allows the disturbances in the cold premixed regions near the injector to get incubated and grow further in the combustion zone. This makes the flame to oscillate and give variations in the chamber pressure resulting in combustion not being stable.

A decrease in the temperature of the hydrogen gas below 111 K was seen to make the combustion unstable in the RL 10 cryogenic rocket for which the injector elements were in flush with the injector face. A decrease in temperature could lead to poorer atomization of the liquid oxygen jet and the formation of mixture ratios which do not readily burn. It is also possible that the lower hydrogen temperatures lead to lower injection velocities of hydrogen giving rise to lower values of velocity ratio between the gas and liquid. These lower ratios may not allow adequate atomization near the injector face.

When the liquid oxygen post was recessed the threshold value of the hydrogen gas temperature at which the combustion became unstable was seen to be about 28 K. Recessing does not allow the gaseous hydrogen flow to relax and thereby provides better atomization of the liquid oxygen jet. A flame could be attached to the injector element for the recessed configuration of the injector element making it stable.

When the chamber pressures are much higher near to the critical pressures, the atomization is more spontaneous and the requirement of a threshold value of hydrogen gas temperature and a threshold velocity ratio may not be required.



**Fig. C.21** Flame Lifted Off from Injector Face Plate



## C.12 IGNITION SYSTEM FOR CRYOGENIC ROCKETS

Though the energy required for the ignition of a mixture of hydrogen and oxygen is small, sufficient energy is to be provided for the ignition of the flowing mixture of hydrogen and oxygen in the combustion chamber. Pyrotechnic igniters as used in solid propellant rockets, thermite igniters using metal and metal oxide reactions, solid propellant cartridges and a hypergolic slug of liquid propellants have been used. Solids and liquids retain heat unlike a gas and the use of condensed phases in the products of the igniter contributes to a better ignition system. The igniter is designed on the lines of a pilot ignition system.



## C.13 MASS OF THRUST CHAMBER

The high performance of the cryogenic engine is mainly due to the low molecular mass of products of combustion of hydrogen and oxygen. The maximum values of specific impulse are obtained when the mixture ratio is fuel-rich. The operational overall mixture ratio of the cryogenic engines depends



on the feed system cycle and the chamber pressure. At high chamber pressures, the staged combustion cycle was seen in Chapter 6 to give higher values of specific impulse at much larger values of mixture ratios than the gas generator cycle. The higher values of specific impulse came about not because of any particular improvement in combustion efficiency or otherwise in the staged combustion cycle. It was essentially due to the loss in the specific impulse in the gas generator cycle due to a larger fraction of propellants getting exhausted through the turbine. Specific impulses between 4450 and 4720 N-s/kg are obtained in the different cryogenic engines.

The mass of the rocket contributes to the performance of the mission in addition to the specific impulse. The mass of the engine should therefore be small. The mass of the hardware corresponding to combustion chamber, gas generator or pre-burner, feed system lines and components and tanks and insulation would not be significantly different for a cryogenic engine operating at a given pressure in either the gas generator or the staged combustion cycle. The pump outlet pressures would be higher in a staged combustion cycle in view of the additional pressure drop in the turbine and the requirement to feed the turbine exhaust into the main combustion chamber. The following empirical expression is representative of the ratio for the pump outlet pressure and the main chamber pressure for the staged combustion cycle and the gas generator cycle respectively. The inlet pressure to the pump is presumed to be 0.4 MPa.

$$\frac{p_{p,scc}}{p_c} = 0.0065 p_c + 1.2$$

$$\frac{p_{p,ggc}}{p_c} = 0.0022 p_c + 1.3$$

The power of the turbo-pump would be more in the staged combustion mode of operation than the gas generator mode. The mass of the turbo-pump has been compiled in literature based on the different available cryogenic engines. Figure C.22 gives the mass as a function of the power in a logarithmic plot based on the data of the existing cryogenic engines.

The mass of the turbo-pump  $M_{TP}$  may be expressed as:

$$\log_{10} M_{TP} = 0.54 \log_{10} P_{TP} + 1.68$$

The power of the turbo-pump  $P_{TP}$  in the above equation is expressed in MW and its mass  $M_{TP}$  is in kg.

The mass of the staged combustion cycle cryogenic rocket would be higher than the gas generator cycle fed rocket operating at the same turbine pressure ratio. Further as the chamber pressure increases the mass of the rocket would go up primarily due to the mass of the turbo-pump. Since the booster rockets could afford to be heavier, the high pressure cryogenic rockets using the staged combustion cycle are generally seen to be applied for the boosters and are of larger thrust levels. The expander and gas generator based engines are generally applied for upper stage rockets.

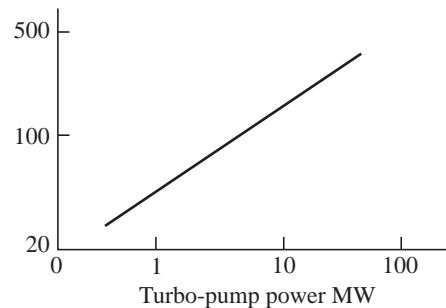


**Fig. C.22** Mass of Turbo-pumps of Different Power Levels



## C.14 THRUST CHAMBER COOLING

### C.14.1 Thermal Ratcheting

Liquid hydrogen is used for the regenerative cooling of the thruster. The formation of the bubbly flow, plug flow, wavy flow, slug flow and annular flow discussed in the chill-down of the lines as the temperature of the liquid hydrogen increases causes drastic changes in the heat transfer coefficient at the coolant-wall interface. The aspect ratio of the coolant passages is generally kept large to increase the heat transfer.

A problem known as “ratcheting” is peculiar to the cryogenic rocket and occurs due to the large temperature changes across the walls between the hot gas and the coolant hydrogen flow. The coolant channels are normally milled in oxygen free high conductivity copper (OFHC) and are closed by an electroformed layer of copper. A sketch of the channels is shown in Fig. C.23. The height “H” and width “W” of the channel would vary along the length of the channel. The high temperature of the hydrogen gas on the gas side of the coolant wall and the high pressure supply of the coolant hydrogen causes bulging and thinning of the walls. The repeated thinning after the operation of the rockets in a number of cycles causes the tensile rupture of the channel walls from the thinning. The failure is known as ratcheting and limits the number of times that the chamber can be used. The problem is not entirely due to fatigue but due to the progressive bulging and thinning of the walls. Reinforcing of the electroformed layer of copper with a material of low stiffness improves the cycle life of a milled regenerative cooled chamber.

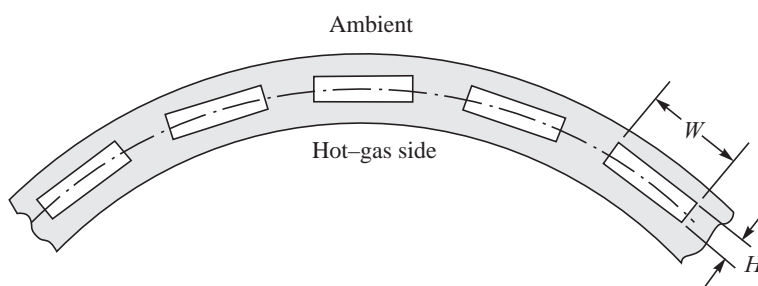


**Fig. C.23** Milled Coolant Channels in a Regenerative Cooled Chamber

A reduction in the temperature difference between the cold and hot surfaces of the channel walls also mitigates the ratcheting problem. This could be achieved by coating the hot gas side with a heat resistive barrier.

### C.14.2 Film and Transpiration Cooling with Hydrogen

The use of film cooling of the hot gas side of the chamber and nozzle follows the practice adopted in the liquid propellant rockets. The cool barrier not only reduces the heat transfer but also prevents the formation of local hot zones in between the coolant channels. Film cooling is invariably used in conjunction with regenerative cooling.



The mal-distribution of mixture ratio along the radius of the chamber arising from the film cooling results in a reduction of the specific impulse. Similarly, transpiration cooling of the injector head degrades the performance of the cryogenic rocket.



## C.15 SUMMARY

The cryogenic propellant rockets are seen to be more complex than the liquid propellant rockets using the Earth storable and Space storable propellants. The complexity arises mainly from the low temperature of the cryogenic propellants. The combustion of hydrogen and oxygen takes place readily as long as an ignition source is available. The spontaneity of the combustion process of hydrogen with oxygen and air leads to safety issues in the design and operation of the cryogenic rockets. The higher performance of the cryogenic rockets arises from the low molecular mass of the combustion products.

The use of liquid methane as a cryogenic fuel appears promising in view of its higher density compared to liquid hydrogen. The possibility of employing it in a tri-propellant mode with liquid methane and liquid hydrogen being used in the initial stages of the mission with oxidizer liquid oxygen and followed by liquid hydrogen and liquid oxygen subsequently has given some incentive towards developing a cryogenic engine with liquid methane as fuel and liquid oxygen as oxidizer.

## References

1. Barron, R.F., Cryogenic Systems, 2<sup>nd</sup> ed., Oxford University Press, New York, 1985.
2. Flynn, T. M., Cryogenic Engineering, Marcel Dekker, New York, 2005.
3. Herding, G., Snyder, R., Scouflaire, P., Rolon, C and Candel, S., Flame stabilization in Cryogenic Propellant Combustion, Proc. 26<sup>th</sup> Int. Symposium on Combustion, pp. 2041-2047, 1996.
4. Schley, C.A., Schick, A and Krulle, G. Cryogenic High Pressure Coaxial Injection and Atomization, AIAA 95-2556, 31<sup>st</sup> AIAA Joint Propulsion Conference, July 1995.
5. Sternfield, H.J., Effect of Injector Velocity Ratio and Combustion Chamber Process on Experimental Performance of a Throttle-able LOX/GH<sub>2</sub> rocket, AIAA/SAE Joint Propulsion Conference, Dec. 1972.
6. Manski, D., Effects of Engine Cycle on Payload Delivery for Future European Launcher, IAF-85-127, 36<sup>th</sup> IAF Congress, Stockholm, Sweden, 1985.
7. Kendrick, D., Herding, G., Scouflaire, P., Rolan, C. and Candel, S., Effect of Recess on Cryogenic Flame Stabilization, Combustion and Flame, vol. 118, pp. 327-339, 1999.
8. Ramamurthi, K. and Patnaik, R.K., Noise Reduction in Non-Premixed Lifted Jet Flames, Flow, Turbulence and Combustion, vol. 72, pp. 49-67, 2004.

# Index

- Ablative cooling, 186, 187f  
Acceleration, 4, 6–7  
Action time  
    solid propellant grains, 150, 150f  
Adapted nozzles, 77  
Aerozine, 105  
Aluminium powder, 129  
Ammonia decomposition, 219  
Ammonium Perchlorate (AP), 100, 143  
Angular velocity, 11, 13  
Aniline ( $C_6H_7N$ ), 104  
Apogee, 17, 17f  
Applied Field MPD thruster, 296  
Arc breakdown voltage, 289  
Ariane V satellite launch vehicle, 41, 42f, 201  
Astronomical unit (AU), 3  
Atomization, 163  
    of swirled liquid sheet, 176, 176f  
Augmented Electrothermal Hydrazine Thruster (AEHT), 290  
Augmented Satellite Launch Vehicle (ASLV), 41, 41f
- Barrier cooling, 185, 186  
Bell Nozzle *See* Contour Nozzle  
Bell rocket belt, 225  
Binder *See* Polymeric fuel  
Black powder, 143  
Blow-down cold-gas pressurization, 164  
Bombardier beetle, 164, 164f
- Bombardment ion thrusters, 293  
Bond energy, 91  
Boundary layer combustion, 231f  
Burn rate  
    enhancement with acceleration, 151  
    of propellant strands, 150  
    variations  
        due to rocket size, 151  
        rocket vs strands, 150  
Burn rate constant, 184  
Burn rate law, 132  
Burn time  
    hollow cylindrical grains, 138  
    solid propellant grains, 150  
Burning surface, surface acoustic admittance of, 266  
Burning surface parameter, 271
- $C^*$  efficiency, 76, 181  
 $C^*$  *See* Characteristic velocity  
Carboxy Terminated Poly Butadiene (CTPB), 101  
    *See also* Hydroxy terminated Poly Butadiene  
Catalyst bed loading, 218  
Cavitation, 171, 194  
CMDB *See* Composite modified double-base propellant  
Centrifugal force, 9–11  
Centripetal force, 10  
 $C_F$  *See* Thrust coefficient  
Characteristic length ( $L^*$ ), 182



- Characteristic velocity ( $C^*$ ), 72, 87  
for fuel-rich mixture ratio, 180, 181, 180f 181f  
larger values of  
    ideal conditions, 87
- Chemical arc jet thruster, 290
- Chemical propellants, 86
- Chemical rockets, 43, 86  
    power density, 237
- Child–Langmuir law, 292
- Chuffs, 253
- Clarke orbit, 14
- Clustering  
    of rockets, 40–3
- Coaxial injectors, 175–177
- Cold-gas rocket, 42
- Colloidal propulsion, 291
- Combustion chamber  
    cylindrical cavity, 243  
    standing waves, 242–245  
    velocity perturbations, 244  
    wave modes, 255–265
- Combustion instability, 238  
    bulk modes, 238–242  
    non-linear instabilities, 274  
    process-induced, 274  
    suppression and control, 277  
    wave modes, 245–246, 253
- Combustion process  
    disturbances or fluctuations, 237  
    end-burning solid propellant rocket, 245  
    fuel-rich, 91, 94, 97
- Combustion product  
    aluminium oxide, 102  
    determination of, 94  
    heat of formation, 96, 96f  
    temperature variations, 97, 97f  
    with lower molecular mass, 96
- Composite modified double-base propellant, 103
- Composite propellants, 100  
    burn rate variations, 131f, 131  
    burning process, 125
- heterogeneity of, 275  
processing of, 102–103
- Conical divergent nozzle, 77, 78f
- Conical nozzles  
    performance loss, 65–66
- Conocyl grains, 139
- Contour nozzle, 68
- Control volume  
    containing a stationary rocket, 73, 74f  
    burn rate analysis, 126
- Convergent-divergent nozzles, 61, 62–63, 62f
- Coulomb's law, 286–287
- Crawford bomb, 150
- Cryogenic propellant rocket, 201
- Cyclotetramethylene tetranitramine (HMX), 96
- Cyclotrimethylene trinitramine (RDX), 96
- Cylindrical grains  
    burning surface, 140
- Damkohler number (Da), 273
- Dark zone, 126
- De Laval nozzles, 61
- Detuning, 273
- Dissociation, 97
- Double-base propellants, 99, 125  
    burn rate, 126–129  
    variations, 128, 128f  
    burning mechanism, 125  
    burning process, 125–129  
    combustion zones, 125, 125f
- Doublet impinging jets, 172–174
- Dribble volume, 178
- Dual bell nozzle, 69, 70f
- Earth-storable propellants, 107
- Efficiency factor *see C\* efficiency*
- Efflux velocity  
    nozzle shape, influence of, 58  
    of expanding gases, 55  
        variations, 56, 61, 56f, 57f, 58f, 60f, 61f  
    of rockets, 39, 40, 54
- Electric field, 286–287



- Electrical rockets, 286
  - applications, 303
  - choice of jet velocity ( $V_j$ ), 299–302
- Electromagnetic force, 287–288
- Electromagnetic thruster, 296–298
- Electrostatic force, 288
- Electrostatic thruster, 43, 290–296
  - neutralization of, 293
- Electro-thermal thrusters, 43, 289–290
- End burning grains
  - burning surface, 140
- Entropy waves, 275
- Erosive burning
  - long propellant grains, 151
- Escape velocity, 19, 19f
- Evaporation constant, 182, 183, 184
- Expander cycle rockets, 201
- Expansion deflection nozzle, 70–73, 70f
- Explosives, 86
- Extractor and acceleration grids
  - accelerated flow of the charge, 292–293
- Field emission electric propulsion (FEEP), 296
- Film cooling, 185, 186f
- Finocyl grains, 139
- First radial mode, 262f
- First tangential mode, 259f
- Fizz zone, 125
  - energy balance, 126, 126f
- Flame spread, 145
- Flex nozzles, 152
- Flow energy equation
  - of control volume, 55
- Foam zone, 125
- Freely falling bodies, 19–20
- Fuel hydrazine ( $N_2H_4$ ), 105
- Fuel kerosene, 105
- Fuel
  - aluminium powder, 102
  - heat of formation, 96, 96f
  - molecular mass, 96
- stability, 99
- Fuel-rich mixture, 94–95
  - ratio, 98
- Gain stabilization, 273
- Gas generator cycle (GGC), 187–192
- Gas requirements, draining of, 195–196
- Gas-assist injectors, 177–178
- Geostationary orbit, 13–14, 14f,
- Geosynchronous altitude, 13
- Geo-synchronous Launch Vehicle (GSLV), 41, 42f
- Geosynchronous orbit, 13–14, 17f
- Geosynchronous transfer orbit, 17
- Glycidyl Azide Polymer (GAP), 102
- Gravitational field, 8–9
- Gridded ion thruster, 292
- Hall effect thruster/ Stationary plasma thrusters (SPT), 294–296, 303
- Heat of combustion, 92–93
- Heat of formation, 90–92
- Heat sink chambers, 187
- Her Majesty's Explosive, 103
  - See also* hybrid propellants
- High-energy propellants, 106, 106f
  - See also* Low-energy propellants; Medium-energy propellants
- HMX *See* Her Majesty's Explosive
- Hollow cylindrical grains
  - burn time, 138–139
  - chamber pressure, variations of, 136–137, 137f
- Homentropic flow, 255
- Hybrid propellant combination, 108
- Hybrid propellants, 108, 228–230
  - See also* High energy oxidizer FLOX; Solid propellants; Liquid propellants
- Hybrid rockets, 228
- Hydraulic flip, 171
- Hydrazine ( $N_2H_4$ ), 96, 105, 215–216
  - decomposition of, 216–218
  - heat of formation, 96



- Hydrazine monopropellant rockets, 216–218  
Hydrogen peroxide monopropellant rockets, 225  
Hydroxy Terminated Poly Butadiene (HTPB), 101–102  
*See also* Carboxy terminated Poly Butadiene  
Hypergolic propellants, 107–108
- Ideal thrust coefficient ( $C_F$ ), 74  
Ignition spike, 147, 147f  
Impinging coaxial injectors, 175, 175f  
Impinging jet injectors, 172  
Impulse, 5–6  
    of rocket, 38, 54  
    to mass ratio, 39  
Inertial frame of reference, 4–5, 5f  
Inhibited red fuming nitric acid (IRFNA), 105  
Inhibitors, 139  
Injection pressure drop, 250  
Ion thrusters, 303  
    use in communication satellites, 303
- Jet velocity *See* Efflux velocity
- Kepler's laws, 3, 3f  
Kerosene, 105–106
- $L^*$  burner, 253  
 $L^*$  instability, 253  
Large amplitude oscillations, 237  
Large propellant grain, 275  
Linear burn rate, 125  
Linear momentum, 4  
Linear nozzles, 71  
Liquid droplets  
    combustion, 184, 184f  
    formation of, 172, 172f  
        near-injection region, 179  
    in hot gas, 185  
    motion of, 179  
    vapourisation, 182  
Liquid fluorine (LF), 106
- Liquid fuel, 163–164  
Liquid hydrogen ( $LH_2$ ), 106  
Liquid monopropellant rockets, 215–218  
    catalyst loss and poisoning, 220  
    performance and applications, 219  
Liquid oxidizer, 163–164  
Liquid propellant rocket(s), 43, 163, 164f *See also*  
    Solid propellant rockets  
    combustion chamber, 179–185, 179f  
        combustion in, 179  
        vapourisation, 181  
    combustion instability, bulk modes, 246–251  
    complexities, 198–200  
    cycle choice, influence of, 169  
    development trends, 200–201  
    injection elements, 178  
    nozzle, 179  
    propellant feed system, 164–170  
    propellant tank structure, 275–277  
    thrust chamber, 163, 170–187  
        characteristic length, 182  
        cooling of, 185–187  
        injectors, 170  
    wave mode instability, 272–273
- Liquid propellants, 104–108  
*See also* Solid propellants; Hybrid propellants  
Low Earth Orbit (LEO), 40, 303  
Low-energy propellants, 104–106, 106f  
*See also* High-energy propellants; Medium-energy propellants  
Luminous fizz zone, 126
- Mach number, 59, 61, 62  
    at nozzle exit ( $M_e$ ), 62  
    at throat ( $M_t$ ), 71
- Magnetic field, 287–288  
Magneto plasma dynamic (MPD) thruster, 296  
Manifolds, 178
- Mass efflux  
    of rocket, 36, 37f



- Mass, 6  
 initial  
   of multistage rocket, 40  
   of electrical power unit, 299  
 of propellant, 36  
 of rocket, 31–33, 32f  
 payload, 34  
 unit of, 4
- Maximum thrust coefficient, 73–75
- Medium-energy propellants, 106, 106f  
*See also* Low-energy propellants; High-energy propellants
- MEMS (Micro electrical mechanical systems) technology, 327
- Mesa-burning propellant, 129, 129f
- Microgravity conditions, draining of, 196–198
- Mixture ratio (MR), 89–90
- Mole fraction, 89–90
- Molecular mass  
   combustion products, 86, 87, 108
- Moles, 89–90
- Molniya orbit, 16
- Momentum, 4  
   change of, 5–6, 5f, 6f  
   of rocket, 33  
   of sled, 28, 29
- Mono-methyl hydrazine (MMH), 96, 105
- Monopropellant rockets, 290
- Motion in space  
   frame of reference, 4–5, 9,  
   parameters, 4–7  
   requirements, 9–13,  
   of squid, 30, 31, 31f
- Motor case, 151–152
- Multi-element coaxial injector, 177, 177f
- Multi-pointed star grain, 139, 139f  
   burning surface, 140–141, 141f
- Net positive suction head (NPSH), 195
- Neutral burning, 135, 136f  
*See also* Progressive burning; Regressive burning
- Newton's Laws of Motion, 6–7
- Nitramine propellants, 103–104  
   burning process, 129
- Non-hypergolic propellants, 107
- Non-impinging coaxial injectors, 175, 175f
- Non-uniform mixture ratios, 180, 180f
- Nozzle, 54  
   control volume, 55, 55f  
   characteristic velocity, 72  
   choking of, 62, 62f  
   closure disc, 148, 148f  
   construction material, 77  
   flow separation, 66–68  
   gas expansion through, 55, 55f, 56  
   gas flow  
     parameter variations, 57–62, 58f  
   mass flow rate, 71–73  
   shape, 58–63  
   size, 77  
   throat area, 137
- Nozzle area ratio, 62–64  
   in contour nozzles, 68–69  
   pressure ratio, variations with, 64, 64f
- Nuclear reactions, 312
- Nuclear rockets, 312
- Optimum thrust coefficient ( $C_F^0$ ), 75
- Orbit, 9, 11–13  
   eccentricity, 14–15  
   energy and velocity requirements, 17–18  
   inclination of, 15–16  
   time period of revolution, 12, 13f
- Orbital  
   flight, 19–20  
   period, 11–13  
   velocity, 11–13, 12f
- Orifice, 170–171, 170f, 171f  
   discharge coefficient ( $C_d$ ), 177  
   mass flow rate, 171
- Over-expanded nozzles, 66, 67, 67f



- Oxidisers, 100  
heat of formation, 95, 95f, 96  
stability, 99  
toxicity, 99
- Oxygen-rich mixture, 94
- Payload mass fractions, 34  
variations, 34, 35f
- Pentad impinging jets, 172
- Perigee, 17
- Permeability, 288
- Planets, 2, 7  
diameter, 2, 2f  
distance from Sun, 2–3, 3f  
mass, 2, 2f  
motion, 3  
orbital period, 2, 3f
- Plateau-burning propellant, 128, 129f
- Plug nozzle, 70, 70f
- Pogo corrector, 277
- Pogo instability, 276
- Pogo stick, 276
- Polar orbit, 16, 16f
- Polar Satellite Launch Vehicle, 41, 41f
- Polybutadiene chain structure, 101
- Polybutadienes, 101
- Polymeric fuel, 100–101
- Polyurethanes, 102
- Polyvinyl chloride (PVC), 102
- Popping instability, 275
- Port volume, 139
- Positive expulsion system, 197, 197f
- Power processing unit (PPU), 299
- Premixed flame, 130
- Pressure atomizing injectors, 170
- Progressive burning, 136, 136f  
*See also* Regressive burning; Neutral burning  
for cylindrical grains, 136–137, 137f
- Propellant acquisition vanes, 198, 198f
- Propellant grains, 124, 124f  
configurations, 139–143
- Propellant mass fractions, 34
- Propellants  
burn rate law, 132  
burn rate of  
factors influencing, 150–151  
temperature influence, 132  
chemicals used as, 86  
choice criteria, 95–99  
combinations, 96–98  
corrosiveness, 99  
density, 99  
energy content, 104  
energy release, 88–95  
flow rate, 188  
flow  
in injector manifolds, 178  
fuel-rich, 94  
ionization of, 293  
pyrolysis, 145  
sea-level specific impulse, 98, 98f  
storage, 99, 107  
temperature distribution, 127, 127f  
use of nuclear energy, 311
- Pseudo force, 9–11, 10f
- Pulse detonation rocket (PDR), 322
- Pulsed nuclear rockets, 321
- Pulsed plasma electromagnetic thrusters, 303
- Pump-fed liquid propellant rocket, 166, 166f
- Pump-fed pressurization, 165–170  
combustion tap-off cycle, 169, 169f  
expander cycle, 168, 168f  
gas generator cycle, 166, 167f  
split expander cycle, 169  
staged combustion cycle, 166, 167f
- Pure kerosene, 105
- Quadruplet impinging jets, 174, 175f
- Quasars, 2
- R&D explosive (RDX), 103
- Radio frequency ion thrusters (RIT), 293
- Rayleigh criterion, 254–255
- RDX *See* R&D explosive



- Reaction, 7  
     Liquid oxidizer, 229  
 Red fuming nitric acid (RFNA), 229  
 Regenerative cooling, 186, 186f  
 Regressive burning, 136, 136f  
     *See also* Progressive burning; Neutral burning  
 Regulated Cold-gas pressurization, 164, 165f  
 Relative permittivity, 288  
 Resistojets, 289, 289f  
 Retrograde equatorial orbit, 15–16  
 Reynolds number (Re), 273  
 Rocket assisted take off (RATO), 152  
 Rocket equation, 31–32  
 Rocket propellant, 104, 106  
 Rockets, 27, 42  
     area ratios, 64  
     classification of, 42–43  
     clustering of, 39–42  
     mass efflux rate, 36, 37f  
     mass ratio of, 33–34  
     performance parameters, 38–39  
     propulsive efficiency, 36–38  
         variations, 37, 37f  
     staging of, 39–42  
     thrust developed by *See* Thrust coefficient  
     with small propellant mass fractions, 35–36  
     working principle, 30, 31–33  
 Rotational frame of reference, 9–10  
     in rotating body, 11, 11f  
  
 Sail propulsion, 326  
 Saint Roberts' law, 128  
 Satellite launch vehicles, 39  
 Saturated hydrocarbons, 100  
 Saturn V rocket, 47, 47f, 200  
 Sea-level specific impulse ( $I_{sp,SL}$ ), 98  
 Second luminous flame zone, 126  
 Secondary injection thrust vector control (SITVC),  
     77  
 Segmented grain, 275  
 Shock, 67  
  
 Short take off and landing (STOL), 152  
 Showerhead injectors, 170, 170f  
 Single stage to orbit (SSTO) vehicle, 41  
 Sintin, 106  
 Sleds—28  
     frictionless surface, motion over, 28  
 Sliver, 141, 141f  
 Slotted grain, 139, 139f  
 Solar rockets, 43  
 Solar system, 2, 7  
 Solid oxidisers, 96  
 Solid polymeric fuels  
     with liquid oxidizers, 228  
 Solid propellant blocks, 124  
 Solid propellant rockets  
     *See also* Liquid propellant rockets  
     combustion instability, bulk modes, 251  
     components, 151–152, 152f  
     growth constant, evaluation and application  
         using T  
     burner, 268  
     igniters, 143, 144f  
     ignition, 143–149  
         mass, 148  
         pressure rise, 148  
         processes, 145, 146f  
     index choice, 133–135, 135f  
     pressure decay, 149, 149f  
     pyrogen igniters, 144, 144f  
     thrust, 136  
     vortex shedding, 275  
     wave mode instability, 266  
 Solid propellants grains  
     burn time, 150  
     configuration of, 135–143  
 Solid propellants, 99–104 *See also* Liquid propellants;  
     combustion of, 124  
 Solid rocket booster (SRB), 152  
 Sound wave  
     propagation of, in a medium, 58, 58f  
 Space shuttle main engine (SSME), 201



- 
- Spacecrafts, 9, 27
    - power generation, 321
  - Space-storable propellants, 107
  - Specific diameter ( $d_s$ ), 194
  - Specific heat, 87, 88f
  - Specific heat ratio, 56, 87
    - in propellants, 87
    - mixture ratio, chamber pressure, variations, 98, 98f
    - of combustion products
    - variations, 98, 98f
  - Specific impulse
    - correlation with  $C^*$  and  $C_F$ , 76
    - of combustion products
    - variations, 98, 98f
    - of liquid propellant rocket, 190
    - of rocket, 38
  - Specific speed ( $N_s$ ), 194
  - Splash plate injectors, 175
  - Spray fan, 172, 172f, 174f
    - formation, 172, 172f
    - liquid, 175
    - mixing, influences, 173
    - orientation, 173, 173f
  - Staged Combustion Cycle (SCC), 187
  - Standing wave modes
    - identification of, 255
  - Standing waves with nodes and antinodes, 257
  - Stoichiometric chemical reaction, 89
  - Stoichiometric combustion, 89
  - Stoichiometric mixture ratio, 97
  - Stoichiometry, 89
  - Strap-on rockets, 41
  - Structural mass fractions, 34
  - Sub-orbital flight, 19–20
  - Summerfield criterion, 68, 81
  - Sun-synchronous orbit, 16
  - Surface tension expulsion system, 197–198
  - Swirled liquid sheet, 176
  - Synchronous orbit, 14
  - T burner, 268
  - Tangential and radial frequencies, 258
  - Temperatures
    - chemical propellants, 86, 87
    - in propellants, 87
    - of combustion products, 92, 93
    - for propellant combination, 93
    - mixture ratio, variations with, 97, 97f
    - sensitivity parameter, 132
  - The milky way, 1, 2
  - Thermionic emission, 293
  - Thin-web propellants, 145, 145f
  - Throat, 59, 61
  - Thrust
    - of rocket, 38
    - of solid propellant rocket, 133, 135
    - to mass ratio, 39
  - Thrust coefficient, 73–76
    - dependence on  $P_e/P_c$ , 75, 75f
    - solid propellant rocket, 135
    - variations, 75f
  - Thrust correction coefficient, 76
  - Transfer orbit, 17, 17f
  - Transpiration cooling, 187
  - Transport number, 185
  - Triplet impinging jets, 174, 190
  - Tri-propellant rockets, 322
  - Turbo pumps, 193
  - Two stage to orbit (TSTO) launch vehicle, 41
  - Ullage volume, 164
  - Unconventional nozzles, 69
  - Under-expanded nozzles, 66, 67f
  - Unified propulsion system, 223
  - Universal Law of Gravitation, 3, 7–8, 7f, 8f, 9
  - Unlike triplet impinging jets, 174, 174f
  - Unrestricted burning grain, 139, 139f



- Vapours  
mixing of, 170, 172, 163, 179  
time, 185
- Velocity, 4  
at throat, 62  
for rocket staging, 39, 40  
of the rocket, 32, 32f, 33, 35  
of sled, 28, 29
- Vena contracta, 170
- Vielle's law, 128
- Volume  
of propellant, 36
- Vortex shedding, 275
- Vulcain, 201
- Water rocket, 42
- Web burning, 141, 141f
- Weightlessness, 20
- White fuming nitric acid (WFNA), 105
- Xylidine ( $C_8H_{11}N$ ), 104
- Zero g conditions, 20, 196, 198



# ROCKET PROPULSION



## ABOUT THE BOOK

This book deals with the fundamental aspects of rockets and the current trends in rocket propulsion. The book starts with a description of motion in space, the requirements of rockets for placing spacecrafts in different orbits about the Earth and escaping from the gravitational pull of celestial bodies. The rocket equation is subsequently formulated, following examples of the motion of a sled from change of momentum and movement of giant squid in deep seas. The operating principles, performance prediction procedures, design aspects and problem areas of the different types of rockets are discussed in detail. Practical examples and exercises are provided in each chapter to aid in understanding the concepts. Some of the salient features of the book are:

- Terms employed in practice for defining the characteristic features of rockets are derived from basics and are illustrated with examples.
- Selection of propellants for rockets is debated and a simplified analytical method is given for evaluating propellants used in solid, liquid and hybrid propellant rockets.
- An exhaustive description and analysis of the cycles of operation of liquid propellant and cryogenic propellant rockets is provided.
- An entire chapter is devoted to the problem of combustion instability, often encountered in the development of solid and liquid propellant rockets. The factors causing the instability are deduced. Detuning and gain stabilization methods of overcoming combustion instability are discussed.
- The principles governing the operation of electrical rockets and the limitations arising from power and associated mass are deduced.
- A brief on advanced rockets such as nuclear rockets, tri-propellant rockets, pulse detonation rockets is also provided.

## ABOUT THE AUTHOR

**Professor K Ramamurthi** obtained his Ph.D. in Mechanical Engineering from McGill University, Montreal. He worked for about 35 years on the development of solid propellant rockets, liquid propellant rockets and spacecraft propulsion in the Indian Space Research Organisation before joining the Mechanical Engineering Department of the Indian Institute of Technology, Madras. He taught undergraduate and postgraduate courses on thermodynamics, air-breathing engines, rocket propulsion and explosions and safety at the Indian Institute of Technology, Madras and carried out both fundamental and applied research in combustion, explosion and propulsion. He has served on several committees and panels on combustion and propulsion and is currently Chairman of the Combustion, Detonics and Shock Wave Panel of the Armament Research Board.



An Imprint of Laxmi Publications Pvt. Ltd.  
An ISO 9001:2008 Company

